ANNUAL REPORT 2018-2019

Published by:
Inter-University Accelerator Centre, New Delhi

Layout & Printed by:
Neelkanth Printers, New Delhi

For comments/suggestions, please write to:
editorial@iuac.res.in

Available online at:
http://www.iuac.res.in/reports/index.html

DIRECTOR'S REPORT

This report showcases the many ways in which we support research work at country and global level to turn the aims of the IUAC into results for a wide range of researchers working in universities, institutes and colleges to realize their potentials and build resilience. This annual report is for the period of April 2018 – March 2019 and during this period many major initiatives have been initiated in the area of academic as well as in administrative front.

Building a scientific community has been one of IUAC's key aims since its foundation. Excellent scientific practice and value-based care can only be driven forward by the very best and brightest minds. This mission is rooted in the fundamental understanding that interdisciplinary exchange is essential to successful translational research. Event formats such as the Schools/Workshops/ Lectures by visiting national/international scientists and the subject experts furthermore strengthened scientific exchange – both at the discipline-specific and interdisciplinary level. These events were regularly attended by many participants. Additionally, we have pushed on the development of scientific-technological platforms and taken a challenge of having indigenous MRI magnet.

Centre embarked into High Current Injector (HCI) project. This project has been prioritized to ensure timely commissioning. This once commissioned will not only ease pressure from our work horse Pelletron but will also help in reducing the pending beam shifts due to large currents HCI can provide.

IUAC is in the process of establishing a national facility for Geochronology funded by Ministry of Earth Sciences, Govt of India. The facility will comprise of sophisticated equipment such as AMS system for heavy and medium mass radionuclides, High Resolution Secondary Ion Mass Spectrometry (HRSIMS), Optical dating systems, Thermal ionization mass spectrometry (TIMS), Laser Ablation (LA) Multi Collector Inductively Coupled Mass Spectrometry (MC-ICPMS) as well as sample characterization facilities, such as the Scanning Electron Microscope (SEM), Electron Probe Micro Analyzer (EPMA), X-ray diffraction (XRD), X-ray florescence (XRF) etc. The intended research areas include high resolution paleo-climatology on terrestrial and marine settings, erosion rates in Himalaya and their relation to tectonics and climate, dating of seismic events via river incision/fault surfaces, strath terraces, erosion rates of mountain and sediment fluxes in rivers, quantitative earth surface processes studies, glaciations of the past and estimation of Equilibrium line altitude (ELA) depressions/elevation through time, studies on monsoon using deep sea cores, studies on ocean circulation etc.

It was felt in recent past that there is a growing demand of intense and coherent photon beams in India to conduct experimental research in the multidisciplinary fields. So it was decided that an accelerator based photon source will be developed at IUAC to provide an experimental photon facility to the vast research community of India to be used in various multidisciplinary areas. A compact, pre-bunched Free Electron Laser facility, Delhi Light Source (DLS), being developed at IUAC. Once operational, the facility will produce intense THz radiation (0.18 to 3 THz) and low emittance electron beams (<8 MeV). Various subsystems of the facility e.g. electron gun with photocathode, High Power RF device including klystron and modulator, solenoid magnet, Beam Position Monitor, various beam line components, etc. are being commissioned. Other devices like the Fibre laser system, photocathode deposition system, undulator, Faraday cups, electromagnets, etc. are in the final stage of developments/procurement and will start getting installed from the beginning of 2020.

Major thrust was given to streamline and create transparency in the process beam time requests submission process by the accelerator user. The whole process is now online from 67th AUC onwards. Users are required to register through online portal and submit the proposals for obtaining beam time. All the proposals are evaluated online / offline by internal and external reviewers.

A new organizational chart was made based on Group of Functional Activities & Classification with the objective that every staff member will be part of a specific/support group, to avoid person dependency, to create human resource pool, equitable distribution of Manpower to name a few. Each and every device / facility is assigned to a group to ensure accountability and multilayer trained manpower for operation, service & repair.

Process has been initiated to have Annual Performance Appraisal Reports (APAR) fully online. A module is under development and is expected to be installed by February 2010. IUAC has also expedited the efforts to revamp the in-house developed Enterprise Resource Planning (ERP) package to make in CERT compliance so that our email system along with ERP can be migrated to NIC server.

Centre has started preparation of the new audit-compliant CMS based website as per GOI Guidelines. The website will be bilingual (English/Hindi) having role based content workflow. Website and applications will be developed in open source platform/technology with PHP technology & PostgreSQL Database and all the contents from existing website will be migrated to new website. Website/Application will be integrated with email/SMS gateway for notification at required stages.

I trust that you will enjoy reading this account of IUAC's activities in 2018-19 and that it will provide you with new insights into the work of various programs of our Centre.

Avinash Chandra

(Avinash Chandra Pandey)
Director

1. ACCELERATOR

1.1 PELLETRON

1.1.1 Operational Summary

G Raturi, J Singh, Pranav Singh, S Kumar, S Mohan, N S Panwar, M P Singh, R Kumar, J Prasad, V P Patel, R P Sharma, Deeksha, G Umapathy, Rajveer, P Baghel, K Devarani, M Sota, Ambuj Mishra, Abhilash, A Kothari, P Barua, D Kabiraj, S Ojha, S Gargari, R Joshi and S Chopra

Performance of 15 UD Pelletron accelerator was quite satisfactory from 1st April 2018 to 31st March 2019. Few problems were also encountered which were resolved properly. There was only one scheduled tank opening maintenance during the mentioned period. The details of the tank opening maintenance are mentioned in maintenance section. The operational summary of the accelerator from April 2018 to March 2019 is mentioned below.

Total No. of Chain Hours	=	7086 Hours
Total Beam utilization	=	5042 Hours
Machine breakdown	=	0244 Hours
Accelerator Conditioning	=	0500 Hours
Beam Change Time	=	0014 Hours
Tank opening maintenance	=	1054 Hours
Beam tuning time	=	0267 Hours
Experimental setup time	=	0094 Hours
Accelerator set up time after maintenance	=	0065 Hours

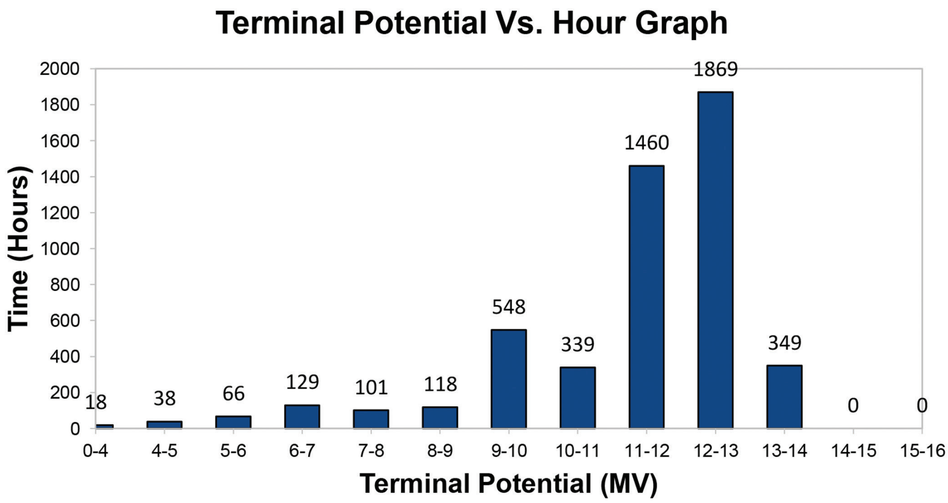

Figure 1.

Total number of 631 shifts were used for experiment during mentioned period, 130 shifts were for pulsed beam and 501 for DC beam. The machine up time for this period was 96.56% and the beam utilization was 71.15%. Figure 1 shows voltage distribution graph of Terminal Potential used for beam runs for the mentioned period. ^{28}Si, 9^+, 140 MeV dc beam at maximum terminal potential 13.99 MV and ^{7}Li, 3^+, 15 MeV dc beam at the minimum terminal potential of 3.7 MV were delivered to users. Maximum terminal voltage achieved during conditioning in this year was 15.3 MV. Figure 2 shows the Chain hours utilization for the mentioned period.

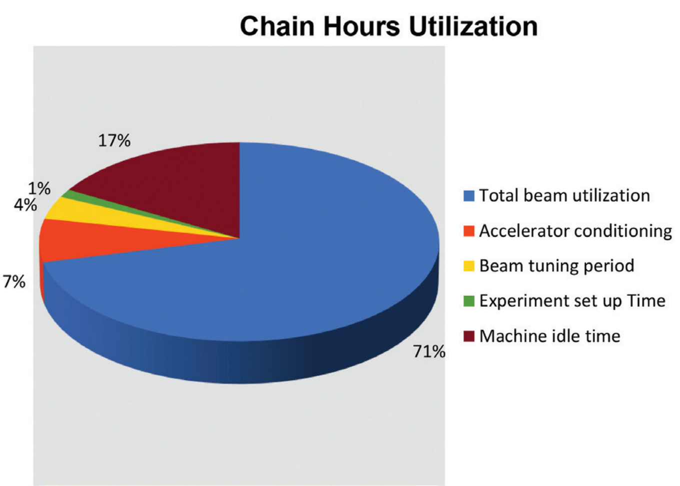

Figure 2.

Duration of beam run time in percentage, for different ions species, is shown in table 1.

Beam Delivered	Utilization (%age of total time)
^{6}Li	0.79%
^{7}Li	7.41%
^{9}Be	4.01%
^{12}C	7.35%
^{13}C	4.28%
^{14}N	0.97%
^{16}O	14.41%
^{18}O	13.87%
^{19}F	3.66%
^{28}Si	12.44%
^{32}S	3.36%

Beam Delivered	Utilization (%age of total time)
^{35}Cl	0.09%
^{37}Cl	1.70%
^{48}Ti	1.21%
^{56}Fe	1.22%
^{58}Ni	4.45%
^{63}Cu	0.31%
^{79}Br	0.14%
^{107}Ag	11.06%
^{109}Ag	0.45%
^{197}Au	6.81%

Pi- chart in figure 3 shows the distribution of delivered beam species during beam run from 1st April 2018 to 31st March 2019.

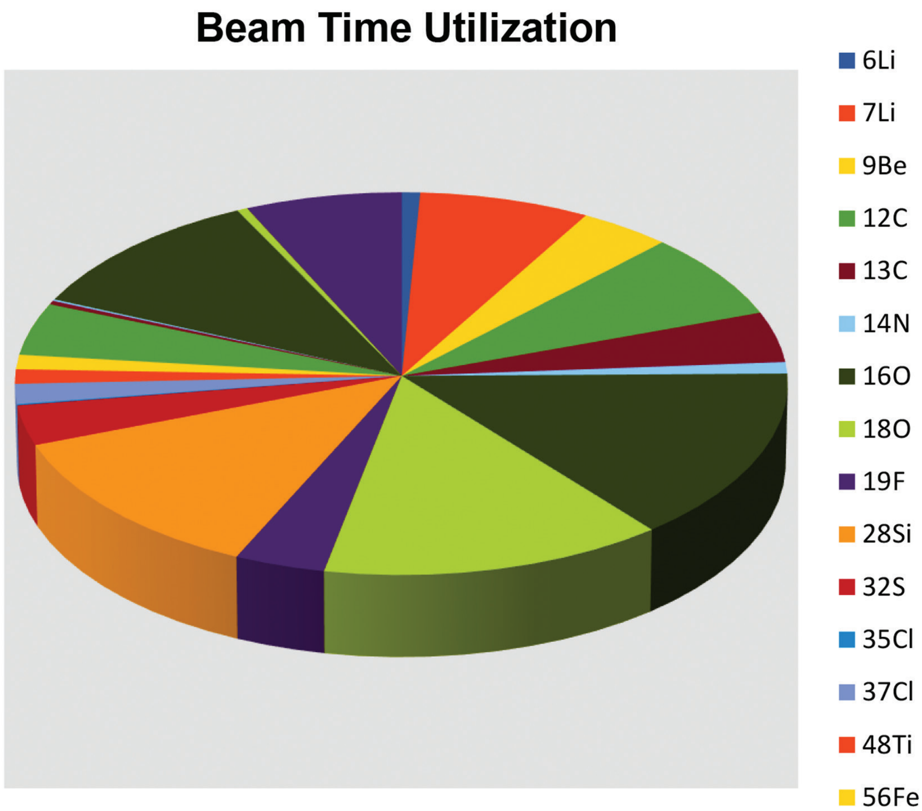

Figure 3.

1.1.2 Maintenance and Development Activities

There was only one scheduled tank opening maintenance. Detail of this maintenance is mentioned below.

Tank opening maintenance (scheduled)

There was only one scheduled tank opening maintenance in this academic year. 15 UD Pelletron was operated successfully for the users' experiment up to 30th July 2018. Thereafter, it was taken for scheduled maintenance from 1st August 2018 to 15th September 2018.

1) Jobs before tank opening

a) Testing of charging currents of both the charging chains

Condition of both the charging chains was accessed just before maintenance. Terminal of 15 UD was shorted to ground by using shorting rods. Both the charging chains were operated and their charging currents were observed at different Charging Power Supply (CPS) values. It was observed that current carrying capacity of chain #1 is better than chain #2 at a given CPS value. Charging chain #1 was able to carry ~51 mA at the CPS of 22 kV and its current started fluctuating at CPS values beyond 22 kV. Whereas, charging chain #2 was able to carry ~46 mA at the CPS of 22 kV and ~68 mA at the CPS of 32 kV. Charging current of chain #2 started fluctuating at CPS values beyond 32 kV. Fluctuation in charging chain #1 was higher as compared to chain #2.

b) Dew point measurement of SF_6 gas

Dew point of SF_6gas, stored inside Pelletron Accelerator Tank (PAT) was measured and found to be ~-27.5 deg C.

c) Testing of Earthquake RAMs (EQ RAMs)

The functioning of EQ RAMs was tested before tank opening at actual conditions. The EQ RAMs were pressurized at ~260 psi with SF_6 gas. Both the chain motors, both the rotating shafts and blower motor were put ON. TP was set equal to 12.023 MV at CPS = 9.6 kV with corona probe in for TP stabilization in AUTO / GVM mode. The earth quake sensor box, in control room, was hammered very lightly, with a mallet, to generate the effect of earth quake. As soon as it was hammered, the EQ sensor generated signal and EQ RAMs got fired and RAMs traveled towards terminal. A tank spark was generated and both the chains and both rotating shafts were tripped off. SF_6 gas pressure in EQ RAMs dropped down to ~230 psi. The EQ sensor was then reset from control room and EQ RAMs were retracted. After retraction of RAMs both the chains and both the rotating shafts were put ON to confirm the retraction of EQ RAMs. This test confirms the satisfactory working of EQ RAMs.

Major jobs performed during scheduled tank opening maintenance:

1. Charging system maintenance

Terminal was grounded, so that terminal should not accumulate any charge if chains are running. Condition of both the charging systems was checked. Total six idler wheels were replaced for charging system #1. Lots of vibrations were noticed in chain #1. After proper investigation, it was found that chain #1 got elongated, hence one pellet of chain #1 was cut. All the idler wheels of charging system #1 were aligned and its counter weight was adjusted for proper tension on chain #1.Both the chains ran and condition of all idler wheels for both the charging systems was checked in running condition which was satisfactory. Condition of nylon links for both the charging chains was inspected also for cracks and no crack was found. Performance of both the charging systems was checked electrically at different CPS from 2 kV to 7 kV and it was satisfactory. Both the chains were cleaned. Both the charging systems were kept ON for ten hours overnights to check its mechanical performance which was satisfactory. All the nuts and bolts for both the charging systems, in terminal area and at tank bottom, were checked and tightened, where required. Semiconducting rim of all the pulleys of both the charging systems were oiled with TP oil to reduce the friction between pulley and chain. Pillow blocks and chain motors of both the charging systems were properly greased. The ground connection of terminal was disconnected. This completed the charging system maintenance.

2. Maintenance of Rotating parts inside accelerator tank

Thorough maintenance of all the rotating parts, such as charging chain motors, rotating shaft motors, separator box assemblies for rotating shafts and blower motor was done. Bearings of total number of twenty two separator boxes were replaced, ten in low energy side and twelve in high energy side. Bearings of these assemblies were replaced with new ones. All the repaired separator box assemblies were installed back and aligned after maintenance. In all five tank motors (2 chain motors, 2 rotating shaft motors and a blower motor) were also greased properly.

3. Stripper foil loading in terminal

Fresh stripper foils were loaded in terminal; 154 stripper foils of IUAC make and 15 Diamond Like Carbon (DLC) type (micrometer make) foils.

4. Repairing of Column Support Post (CSP) gaps

To ensure that the condition of all CSP gaps is good, they were checked thoroughly. This is important for stable operation of tandem accelerator. If condition of even a single CSP gap or accelerating tube gap, is bad, machine cannot handle the rated high voltage and field will collapse. This may also lead to instability in beam.

Multiple vertical cracks were observed across gap #11 in unit #22 and its resistance was measured to be ~3.5 G ohms. This gap was shorted. Now, the total number of 36 CSP gaps have been shorted; 17 in LES and 19 in HES.

5. Hoop Screws maintenance

Equipotential rings, also known as Hoops, are mounted on every accelerating units of tandem accelerator and are responsible of proper field distribution. Hoop screws are the screws which hold the Hoops at the mounting position on Column Support Posts. Resistance between hoop screw and equi-potential rings ideally should be zero. But this resistance value varies from few ohms to Mega ohms and even open due to deposition of by-products of SF_6 gas.

Resistance measurement between Hoop screws and equi-potential rings was done for 14 units. The Hoop screw which shows more than 1 kilo ohm value, were changed.

6. Corona probe maintenance

The condition of all seven corona probe needles was good. Therefore, none of the corona needles were replaced.

7. Vacuum read problem for IP T-2 pump

There was no vacuum read from IP T-2. After proper investigation, it was found that a 6 channel ORA card in LL box at tank bottom, was faulty. This card was replaced to solve the problem.

8. Movement problem in Foil Stripper in HEDS

FS D2-1 was moving in INC mode but not in DEC mode. A dry solder point was located in the relay bases. Re-soldering of the bases of relays was carried out. This solved the problem and FS D2-1 started working in both INC and DEC mode.

Other maintenance outside Pelletron Accelerator tank

1. Maintenance of Vacuum related components

Routine maintenance of all ion pumps and sublimator pumps along with their controllers was done and required repair work was done where ever required.

2. Maintenance of different devices

The routine checkup and breakdown maintenance of different devices, such as Beam Line Valves (BLVs), Faraday Cup controller, a power supply, CAMAC control system etc., was also done.

1.1.3 Ion Source Activities

Operation

The operation and ion beam delivery of MC-SNIC ion source has been excellent during April 2018 to March 2019. Routinely, energized ion beam of various ion species in the energy range, 130 to 230 keV were extracted from the ion source. The ion source ran to its high capacity to provide pulsed ion beam. Other than routinely delivered ion beam, various enriched isotope ion beam, ^{6}Li, ^{13}C, ^{18}O and ^{37}Cl were produced. In regular interval, varieties of cathode samples were prepared as per users' requirement and loaded to the cathode wheel as and when required.

Maintenance

1. Preventive Maintenances

The source was opened in the month of September 2018 for routine maintenance. All the electrical connections of ion source were removed and the source was vented. The cesium was kept in Argon environment. The source was dismantled and all of its parts were cleaned thoroughly. The source was assembled, aligned and installed back after cleaning. New cesium was not loaded, rather we continued with the old cesium.

Apart from routine maintenance work a major maintenance work to replace the gate valve was also taken up. The gate valve is extensively used during every cathode loading process. The purpose of the valve is to isolate the cesium from the air This valve developed a through leak and due to this failure the cesium was contaminating. Therefore, this valve was replaced by new valve.

2. Breakdown Maintenances

During this year the MC-SNICS was opened once for break down maintenance work in the month of April 2018. The source was highly contaminated by the over flow of cesium. The Einzel lens assembly was unable to hold any potential and the ceramic surface got shorted from inside. Einzel lens focus power supply also went bad. The MC-SNICS source was vented with argon and opened. It was noticed that the ceramic studs holding the immersion lens had a layer of cesium on the surface and the Ionizer was also shorted. It was observed that whole source body was full of cesium. So all the ceramic parts were replaced with the new spares. The source body and the other components were cleaned properly. The source was assembled back and aligned. The Einzel lens assembly and ionizer were replaced with the new one. The source was installed back on the HV deck and new fresh Cesium was loaded. The cathode wheel was loaded with fresh cathodes and source was tested for regular operation. The damaged focus power supply was also repaired later.

Following breakdown maintenance related to electronics of ion source (MC-SNICS) was also carried out during the mentioned period:

1) Extractor power supply was not operating properly and beam could not be tuned properly. Power supply was replaced and repaired later.
2) During one of the user beam run, there was no beam current from the ion source. Connection from cathode power supply output to cathode broke from cathode side. This connection was restored to get the beam from ion source.
3) All the read back parameters from ion source were fluctuating due to failure of -15 Vdc bias supply in the LL box kept at ground potential. -15 Vdc was restored back to take care of the fluctuations.
4) Read back of HV power supply was fluctuating from -6 kV to -206 kV but the beam from ion source was stable. Investigated that temperature in ion source room was high due to problem in dehumidifier. The problem was taken care by placing an external cooling fan and later the dehumidifier was repaired. Now temperature is better than 25 deg. C and RH is better than 45%.

3. Developmental activities

Guide Rail Assembly for ion source

A development work related to the mounting of MC-SNICS source was also carried out. During a routine run, it was noticed that beam was getting steered in both X and Y axes in BPM #1 profile as and when immersion lens value was changed. This resulted due to misalignment in source mounting, which results in beam extraction at an angle from the source. A new mounting arrangement, with proper alignment, was developed and installed in ion source HV deck. The ion source, after maintenance, installed back by using this new mounting arrangement to ensure its proper alignment. This solved the steering problem of beam.

Thorough cleaning of HV deck, multiplier stack and filter stack of HV power supply was also carried out. Apart from this, Conditioning of HV deck was also done.

1.1.4 Beam Pulsing System

Operation

130 shifts of beam time was used for pulsed beam runs using Multi Harmonic Buncher (MHB) along with low energy chopper. Traveling Wave Deflector (TWD) was also used whenever different repetition rates of pulsed beam, other than 250 ns, is required. All the pulsed beams, were utilized by users to perform their experiments in different experimental lines. All 130 shiftss were utilized using Pelletron only and the beams bunched were ^{12}C, ^{13}C, ^{16}O, ^{18}O and ^{35}Cl.

There was no beam run using LINAC facility during the mentioned period.

All the pulsed beam runs were quite stable.

Maintenance

a) Chopper maintenance

Routine maintenance of chopper was carried out. Tuning of output stage of 100W, 4 MHz. With 50 Ω pure resistive dummy load was checked which was satisfactory. The output of this amplifier was then disconnected from dummy load and connected to tank circuit of chopper. Chopper tank circuit was then tuned for maximum power transfer from chopper amplifier. The chopper tank circuit could be tuned to get maximum forward power of ~20 W with reflected power of ~0.5 W. The chopper amplifier was kept ON for two days and its stability was satisfactory.

b) Traveling Wave Deflector (TWD) maintenance

In routine maintenance of TWD, all the control electronics and switching amplifier electronics were checked. The performance of TWD electronics was satisfactory.

During a beam run in January 2019, TWD stopped working. Plate voltage to tetrode valve got tripped off due to failure of 4^{th} channel. Problem was the failure of its driver circuit. The driver circuit was repaired to solve the problem. Thereafter, TWD worked satisfactorily.

1.1.5 Low Energy Negative Ion Implanter Facility

1. Operation

The operational status and ion beam delivery of the implanter facility had been excellent during the academic year (2018-2019). About 30 users from different colleges, universities and institutes availed the beam time from April, 2018 to March, 2019. Altogether, there were 31 runs. The sanctioned beam times up to AUC 65 as well as few beam times approved by Director, IUAC, were being successfully performed. The particulars about the implantation experiment performed during this period are given below:

1. No. of users: 30
2. Number of beam run: 31
3. Total time of machine run other than beam on the target = 320hrs
4. Total number of shifts utilized/beam on the target: 110
5. Total number of samples implanted: 1097
6. Ion fluencies used: 1x1012 to 5x1017 ions/cm2
7. Ion species utilized: ^{7}Li, ^{11}B, ^{12}C, ^{16}O, $^{24}C_2$, ^{27}Al, ^{28}Si, ^{31}P, ^{32}S, ^{40}MgO, ^{48}Ti, ^{56}Fe, Ge, ^{58}Ni, ^{59}Co, ^{63}Cu, ^{107}Ag, ^{197}Au
8. Energy range utilized : 20 to 200 KeV

2. Maintenance and development activities

The implanter accelerator system had a smooth run except for few breakdowns in control system and ion source injector systems. However, in regular interval, the operation had to stop for cathode sample loadings as well as for preventive maintenances. The ion source had run smoothly for almost one and half year without any maintenance. Therefore, in the month of May, 2018, after performing the break down maintenance, the preventive maintenance was carried out. It was mainly for cleaning three components of injector system i.e. a) ion source assembly, b) Einzel lens assembly and c) Accelerating column (General Purpose Accelerating tubes).

In mid-April, 2018, ion source failed to function. The problem was investigated and solved as mentioned below.

1. The frequent failure of DAC in IMAC placed on HV deck of Negative Ion Implanter during HV spark or glitch. Source could not be operated. Grounding connection related HV deck was modified. After proper grounding and grounding modification work, DAC is working fine.
2. Output voltage of Extractor power supply was ~130Vdc even if control voltage from control console is zero. Problem investigated and found that actual voltage at the control input of extractor power supply was 0.065Vdc with zero control input from "Control Console" which make the power supply output ~130 Vdc. The analog ground of DAC was connected to chassis ground to solve the problem.
3. Whenever the HV deck voltage was increased to 200kV, the extractor power supply read back increases to ~5.5 kV without any control voltage input to extractor power supply. Value of the resistor, connected

between extractor power supply and ground, got increased. This resistance was replaced to solve the problem.

4. Relative Humidity (RH) of high voltage room raised up to 86% while its room temperature was lying low around 22^{0}C. This caused discharge paths all over the insulation surfaces of accelerating tubes, lenses and Teflon insulation gaps that isolate ion source assembly, Einzel lens and GP tubes from High Voltage deck. New insulation gaps were designed and fabricated in IUAC workshop. They replaced the old ones without disturbing alignment of beam line. Higher load current, due to high RH value, was observed from deck HV supply. The RH value is now controlled to ~54% to solve the problem.

5. There was another failure of CAMAC control system for the beam line. it was rectified by replacing the damaged card.

From July, 2018 onwards, energized ion beams were delivered to users for their experiment. The radiation monitor was replaced with a new calibrated one. Apart from operation and helping users for their experiment, efforts were made to develop new beams as per users' request.

1.1.6 Utilization of Beam Runs using 15 UD Pelletron Accelerator from 1st April 2018 to 31st March 2019

The utilization of beam time by different users, using facility at IUAC, New Delhi is mentioned below. Field wise utilization and user wise utilization of beam time are shown in figure 4 and figure 5 respectively. List of users from different universities, colleges, IITs etc. are tabulated in table 2.

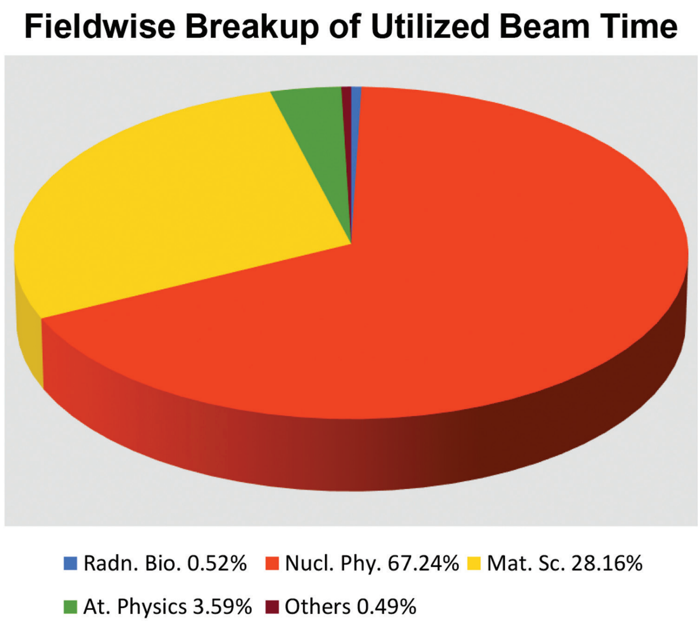

Figure 4.

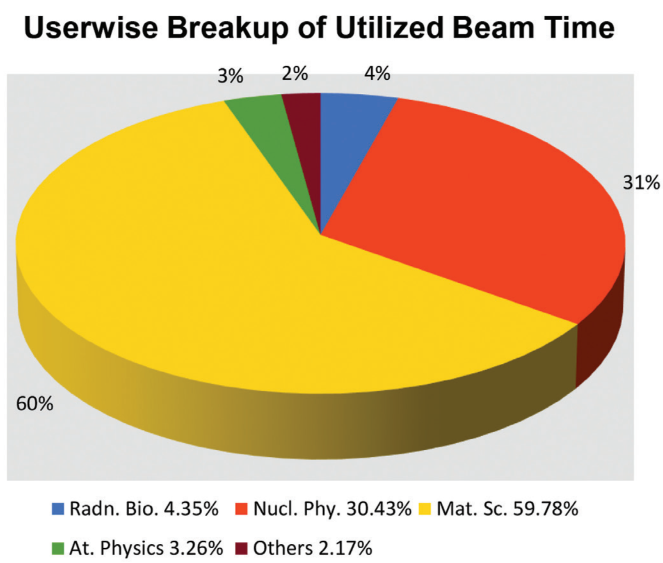

Figure 5.

Table 2. User List : April 2018 to March 2019

Sr. No.	University / Institute / College	Shift Utilized
1.	Aligarh Muslim University	39
2.	Amity University, Noida	3
3.	Andhra University	14
4.	Banaras Hindu University, Varanasi	48
5.	BARC, Mumbai	4
6.	BCAS & C Kalyan	3
7.	Bharathiar University	3
8.	Central University of Jharkhand, Ranchi	20
9.	Central University of Kerala	12
10.	Central University of Punjab, Bhatinda	1
11.	Central University of Rajasthan	9
12.	DA Vishwavidyalaya, Indore	6
13.	DAE CSR, Kolkata	32
14.	DAV College, Amritsar	3
15.	Doon University, Dehradun	9
16.	Dr. B.A.M University, Aurangabad	5
17.	Dr. B.A.R.N.I.T, Jalandhar	2
18.	G.B.P.U.A.T, Pant Nagar	3
19.	Gauhati University	15
20.	GGSI University, New Delhi	10
21.	GGD University, Bilaspur	4
22.	GNDU Amritsar	3
23.	Gautam Buddha University, Greater Noida	1
24.	Gujrat University, Ahmedabad	3
25.	HP University Shimla	20
26.	IGCAR, Kalpakkam	3
27.	IISER, Mohali	1
28.	IIT, Roorkee	8
29.	IIT, Ropar	18
30.	IIT, Jodhpur	9
31.	IIT, Kharagpur	6
32.	ISRO, Bengaluru	11
33.	IUAC (Student), New Delhi	3
34.	IUAC, New Delhi	42
35.	Jamia Milia Islamia, New Delhi	1
36.	JNU, New Delhi	1
37.	KA&S College, Coimbatore	2
38.	Kalindi College, New Delhi	21
39.	Kanya Mahavidyalaya, Punjab	3
40.	Karnataka University, Dharwad	16

41.	KIIT University, Bhubaneswar	2
42.	Kyoto University, Japan	3
43.	M.S.U. of Baroda, Vadodara	19
44.	MNIT Jaipur	11
45.	Nirmal University, Gujrat	4
46.	NIT, Srinagar	1
47.	Panjab University, Chandigarh	25
48.	RTMN University, Maharashtra	3
49.	Shiv Nadar University, Greater Noida	1
50.	Sikkim University	3
51.	SINP, Kolkata	21
52.	SLIET, Longowal	6
53.	UCEA, Tamil Nadu	3
54.	Kalyani University, Kalyani	21
55.	University of Calicut, Kerala	13
56.	Delhi University, Delhi	29
57.	University of Hyderabad	6
58.	University of Mysore	3
59.	Tripura University	3
60.	Visva Bharti Shantiniketan	36
61.	VTU, Mangaluru	1

1.2 LINAC

B.K.Sahu, R.Ahuja, J.Antony, S.Babu, G.K.Chaudhari, A.Chowdhary, T.S.Datta, R.N.Dutt, S.Ghosh, R.Joshi, S.Kar, J.Karmakar, B.Karmakar, M.Kumar, R.Kumar, D.S.Mathuria, K.K.Mistri, A.Pandey, P.Patra, P.N.Prakash, A.Rai, S.K.Sahu, A.Sarkar, A.Sharma, K. Singh, P. Singh, S.S.K.Sonti, S.K.Suman

1.2.1 Status of the Superconducting Linac

The superconducting (SC) linac working as the energy booster for the Pelletron accelerator consists of five cryostats containing twenty seven quarter wave resonators. Twenty four resonators are used to accelerate the ion beam and the remaing three are responsible for longitudinal focussing or defocussing (only for Rebuncher) of the beam. As previously reported there was an extened beam run of linac for user experiments for more than 5 months duration during year 2017-18. During the beam acceleration, an energy gain of about 9 MeV/q had been demonstrated. In order to achieve higher energy gain, steps were taken subsequently. As the performance of most of the resonators in Linac-III cryostat was found to be less than the desired value, steps were taken to improve the performance of resonators in Linac III. Based on the past history of the resonators, four resonators out of eight were electropolished and all the resonators were rinsed with high pressure (~80 bar) 18 MΩ-cm deionized water along with their couplers, slow tuner bellows and pickups inside class-100 clean room. The resonators were also assembled in the same clean room before loading them in the cryostat inside a class-5000 clean room. An Offline test of Linac III was done to evaluate the performance of the resonators post the surface treatment. Significant improvement in the performance of all the resonators except one was observed as compared to the last linac operation. During the beam acceleration in 2017-18, the time bunching of the beam at the user's scattering chamber was supposed to be accomplished by the two resonators of the re-buncher (RB). As reported in last year's annual report, this was completely avoided for the extensive use of optimum phase focusing (OPF), for each and every scheduled experiment. The RB resonators are now planned to be used in accelerating mode and phase optimization for the same is being worked out with optimum phase focusing (OPF) using an in house developed program. Three cases have been studied where OPF has been applied along with RB as accelerating QWRs. The ΔE at LINAC exit, after RB and the Δt at NAND experimental area for the three cases is tabulated in table1 below. The results will be verified experimentally during linac oper`ation.

Table 1: OPF case studies with RB as accelerating QWRs

Case	ΔE @ LINAC exit	ΔE @ RB exit	Δt @ NAND area
Case1: OPF of all 26 QWRs optimized @ NAND	~ 0.75 MeV	~ 0.2 MeV	~ 0.430 ns
Case2: OPF of 24 QWRs optimized @ RB + OPF of 2 RB QWRs optimized @ NAND	~ 0.6 MeV	~ 0.68 MeV	~ 0.360 ns
Case3: OPF of 24 QWRs optimized @ NAND + OPF of 2 RB QWRs optimized @ NAND	~ 0.325 MeV	~ 0.6 MeV	~ 0.190 ns

1.2.2 Developmental activities accomplished to Improve the Linac Operational Efficiency

A. Implementation of PWM based frequency tuning scheme for super-buncher and rebuncher.

The super buncher, Re-buncher and first accelerating module of linac use pneumatic helium gas operated tuners for phase locking of the resonators. The control scheme of the gas operated tuners of first linac module were improved with a pulse width modulation (PWM) based control mechanism and the same was successfully tested to phase lock all the resonators of linac 1 during last linac acceleration for more than five months. It can correct the slow drifts in frequency at a faster rate thereby making the resonators less prone from frequency unlocking and reducing the RF power requirement. Implementation of the PWM based tuner control mechanism on the resonators of the super buncher (SB) cryostat and re-buncher cryostat is completed this year for better operational efficiency. For both super-buncher and re-buncher, the mechanical assembly is similar to the linac cryostat 1 with two channels operating on each pot assembly. Two channel Helium gas flow system was tested with independent electronics modules (two channels). In Superbuncher set up the second channel has been kept as spare whereas an additional two channel spare assembly was made for rebuncher

B. Remote RF drive control for resonators during Linac operation

When the resonators produce high accelerating fields, especially at the time of high Power Pulse conditioning, access is often restricted due to the presence of X-rays. In order to avoid exposure to radiation during high power pulse conditioning, prototype remote movement of the drive couplers of the resonators were tested earlier along with software interface for pulse conditioning of the resonators from existing Pelletron-Linac control room. Dedicated electronic modules consisting of remote control system using incremental encoders for closed loop position control of the power couplers to couple power in to the superconducting resonators is developed. The electronics module control the stepper and monitors the exact coupler position. The actual position sensed by the encoder is calibrated and displayed on a local display. The system design uses a serial network type architecture to enable control of RF power coupler motors of the resonators with a serial networked backbone based on the RS485 standard to integrate 8 channel motor position control units. While the RS485 backbone is implemented with the help of unshielded twisted pair (UTP) wiring with proper end terminations, the coupler motor controllers act as the control nodes. The motor, constrained by the limit stoppers, rotates in response to commands sent by the local keypad. When one of the endpoint limits is reached, micro-switch based limit sensors get actuated, causing immediate stopping of the motor.

The system is responsible to control of the 27 RF power couplers from the control room. High Power RF conditioning of all the resonators of the three accelerating modules of the superconducting linac is planned from the control room. During the forthcoming operation of linac, the remote drive control mechanism will be extensively used for all the resonators of linac.

C. Dedicated Electronics module for Energy and time measurement of Linac beam.

Surface barrier detectors are routinely being used to measure the energy and timing in the Diagnostic box. The processing of the timing and energy signals from the pre amplifier are processed using various commercial nuclear electronics modules such as spectroscopy amplifiers, Timing filter Amplifier (TFA), Constant fraction discriminators (CFD), Gate and Delay generator (GDG), Time to Amplitude converter (TAC). In order to avoid using these expensive imported modules and to ease the requirement of interconnections among the modules, a dedicated module combining the specific requirements of energy and timing signals from pre amplifier is designed. The module takes energy and timing signal from the pre amplifier of the detector and gives analog output and strobe signal for pulse sensing ADC for digitization. The module is under the final stage of development and planned to be tested during linac operation.

1.2.3 Superconducting Niobium Resonators

P.N. Prakash, A. Rai, S.S.K. Sonti and K.K. Mistri

The construction of six spare quarter wave resonators (QWRs) and additional slow tuner bellows for the superconducting linac has progressed further. The two SSR1 resonators with their outer helium vessel installed, were sent to Fermilab. IUAC had attached the Nb-SS brazed transition rings on the SSR1 resonators prior to the installation of the helium vessel by BARC, Mumbai. One of the resonators that has performed exceedingly well has been installed in the SSR1 cryomodule for the PIP-2IT injector experiment. For carrying forward the studies on improving the accelerating gradient and quality factor in quarter wave resonators, a resonator that had been set aside due to its high resonance frequency, is being readied. The 2nd prototype low beta resonator is also being completed.

1.2.3.1 Construction of Spare QWRs and Slow Tuners for Linac

Construction of the six spare QWRs for the superconducting linac has progressed further. The QWRs and slow tuner bellows are being built as spares for the Linac as well as for conducting other offline development works. Several parts / sub-assemblies for the resonators, e.g. components for the drift tubes, transition flange assemblies and slow tuner bellows, have been completed. In figure1, several parts/assemblies are shown.

Figure 1: Clockwise from top-left: (i) niobium housings, (ii) end caps and upper caps, (iii) welded niobium leaves for the slow tuner bellows, (iv) transition flange assemblies.

1.2.3.2 SSR1 Single Spoke Resonators

The two SSR1 niobium single spoke resonators which had come back from Fermilab after the VTS tests for the installation of the outer helium vessel, were sent back to Fermilab after completing the work. IUAC had attached the Nb-SS brazed transition rings on the SSR1 resonators before the helium vessel was installed by BARC, Mumbai. In 2K tests of the dressed cavity in the spoke test cryostat (horizontal test stand) the first resonator S104 performed exceedingly well. In fact the performance of this resonator is one of the best among the resonators installed in the SSR1 cryomodule for the PIP-2IT injector experiment. In figure 2, the performance of SSR1 S104 at 2K is shown.

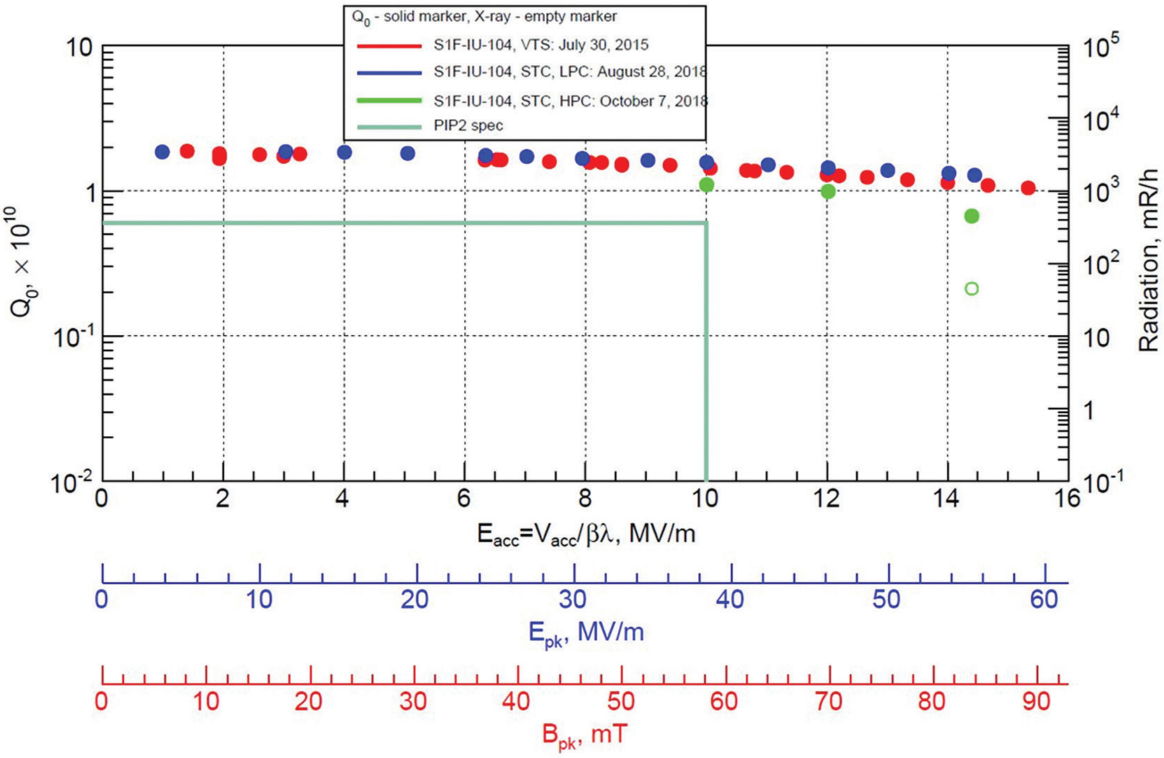

Figure 2: 2K Test Result of dressed SSR1 S104 single spoke resonator tested at Fermilab. The box shows the PIP-II design specification.

1.2.3.3 Reworking of QWR-I11

Systematic studies have been conducted to improve the achievable accelerating gradient and associated quality factor in QWRs using several different techniques [1]. In order to continue these studies, a QWR (QWR-I11) which had been kept aside due to its low resonance frequency, is now being completed. The resonator has been cut open and its central conductor has been shortened to the correct size to obtain the desired frequency. This resonator is now ready after the reworking, electropolishing and heat treatment, for the installation of the outer helium vessel. After completion, initially it will be tested for a baseline test (at 4K) before subjecting to further processing to study the improvement in its accelerating gradient and quality factor through various techniques which will include nitrogen doping and infusion.

1.2.3.4 Completion of 2nd Prototype Low Beta Resonator

The first prototype low beta resonator has performed exceedingly well; very easily achieving the design goal of 6 MV/m accelerating gradient at 4 W of RF Power. In order to validate the various processing techniques that have been systematically studied [1], performing the tests on a low beta resonator provides further credence to them. Some of the tests have been already applied. In order to expedite the turn-around time for processing and testing of various resonators, it is essential to have additional resonators available in hand. In view of this the 2nd low beta resonator is being completed. The resonator is ready for electropolishing which will be followed by heat treatment. Thereafter it will proceed for the installation of the outer helium vessel. We feel that the resonator will be available for cold tests in the next 3-4 months.

REFERENCE:

[1] A. Rai et al., accepted for publication in Superconductor Science and Technology, in press, https://doi.org/10.1088/1361-6668/ab2794

1.3 PARAS (1.7 MV PELLETRON ACCELERATOR AND RBS ENDSTATION)

1.3.1 Operation

The 1.7 MV Pelletron accelerator for Rutherford backscattering facility was in regular operation all year round. Total 2015 measurements of 73 users from 40 Universities/colleges/institutes were performed. Around 40 Publications and 10 conference proceedings came out of measurements carried out ustilizing the facility.

RBS, Channeling, Resonance RBS for Oxygen and Nitrogen energies were routinely performed. Elastic Recoil Detection Analysis (ERDA) to assess the hydrogen content in the sample was also performed for couple of users. RBS is one of the popular methods of ion beam analyses performed for different types of samples including thin films on substrates, free standing, carbon supported grown by different techniques such as thermal evaporation, RF sputtering, MBE and PLD. The ion implanted and irradiated single crystals, thin films and bulk samples are also characterized using RBS and Channeling. Ion channeling is very accurate method for probing defects caused by implantation.

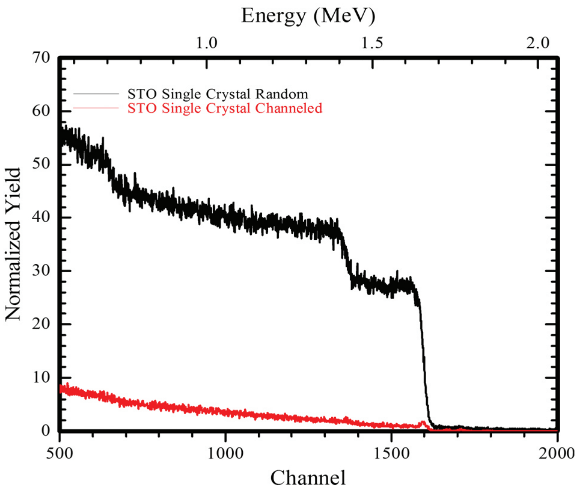

Fig 2A: RBS Random and Channeled spectra of STO single crystal with χ min = 3.45%

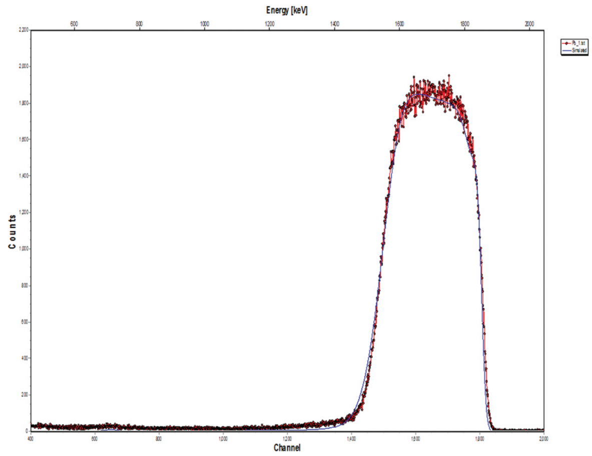

Fig 2B: RBS spectra of self-supported Pb target (red) deposited by thermal evaporation with simulation (Blue).

Resonance backscattering 16O(α,α)16O at 3.045 MeV, 14N(α,α) 14N at 3.69 Mev commonly referred Resonance RBS as has been used for oxygen and Nitrogen depth profiling in various thin oxide films, implanted and processed materials respectively.

ERDA setup at IUAC is suitable for hydrogen estimation up to depth 0.5–1µ. Measurements are performed with 2.7- 3.045 MeV alpha projectiles impinging over 75° to surface normal. Forward recoiled protons at round 30° are detected by detector with a stopper foil to stop scattered alpha particle.

1.3.2 Maintenance

1.3.2.1 Ion Source Maintenance

Ion source maintenance was performed during November 2018. The source got chocked due to deposition of Rubidium all around, preventing helium beam from coming out. The source was opened, cleaned and reassembled back. Rubidium was loaded in argon atmosphere. Two ampules of 5 grams each is loaded for smooth operation of source. It has been observed that, once loaded, the source runs for 700-800 hours. On conditioning the source for few hours, continuous and stable He- beam was achieved.

Interlock circuitry of ion source hanged because of malfunctioning of one of the 24 V power supply. A supply was installed with the help of Beam Transport Lab to solve the problem.

1.3.2.2 5SDH2 Pelletron Accelerator and Endstation Maintenance

No major maintenance of Pelletron accelerator was carried out. The accelerator operated smoothly with highest terminal potential around 1.2 MV. Control system of RBS endstation stopped working as one data file got corrupted. The new data file was generated and control system was made operational at the earliest.

1.4 AMS AND GEOCHRONOLOGY FACILITIES

1.4.1 Accelerator Mass Spectrometry

Deeksha Khandelwal, Umapathy G R, R. Sharma, Soumya Prakash Dhal, Chinmaya Maharana, Pankaj Kumar, S. Ojha, S. Gargari, R. Joshi, S. Chopra and D. Kanjilal

An Accelerator Mass Spectrometry facility for the measurement of ^{14}C, ^{10}Be and ^{26}Al, based on a dedicated 500kV ion accelerator is in operation since March 2015. The 500 kV accelerator is of tandem type and procured from National Electrostatic Corp. (NEC), USA. Carbon sample processing and graphitization are performed in a comprehensive graphitization laboratory and ^{10}Be and ^{26}Al samples are processed in a clean chemistry laboratory.

1.4.1.1 Graphitization Laboratory

Graphitization laboratory is equipped with all the equipment required for the sample pre-treatment and graphitization. Charcoal, wood, macrofossils, plant remains, sediment and carbonate samples (shells, foraminifera) are processed routinely in this laboratory. Different pre-treatment methods, depending upon the type of samples, are followed. This laboratory is equipped with three Automated Graphitization Equipment (AGE) coupled with elemental analysers for the graphitization of organic samples. Out of these three AGE, one AGE is also coupled with carbonate handling system (CHS) for the graphitization of carbonate samples. During April 2018-March, 2019, about 850 samples have been pre-treated and graphitized by 25 users from different universities and institutes for their research work.

1.4.1.2 Graphitization of small size samples using AGE

AGE is utilized to graphitize samples having various sample sizes which produces 200 µg to 1000 µg of CO_2. This sample size range covers most of the radiocarbon dating applications. However, there are certain applications where even smaller sample sizes are available to graphitize. For example: radiocarbon measurement of particulate matter, DNA, compound specific radiocarbon dating etc. Therefore, we tried to graphitize OXII, IAEA radiocarbon standards and Ph blank samples in different sizes to produce 20-200 µg of CO_2 using AGE. To observe the effect of temperature, we have also performed graphitization reaction for these samples at different graphitization temperatures, 450, 500, 550, 580 and 600 °C. To observe the effect of size of reaction tube, we have performed graphitization of these small samples in two different tubes having length 8 cm (tube used for regular size samples) and 5 cm. Tube used for regular size samples have been cut down to 5 cm length.

We have found in this study that samples having size up to 60 µg can be graphitized using AGE. We have found best results at 580 °C temperature using reaction tube having length 8 cm. But graphitization yield for theses sample was very less, so current observed in ion source was also less in comparison to regular size samples. Also higher background values were observed for small size samples. All these shortfalls can be improved if we can improve vacuum in graphitization system and water absorption during graphitization reaction.

1.4.1.3 Use of iron nano size powder as a catalyst in graphitization reaction

Iron powder is used as a catalyst in graphitization reaction. Particle size of iron powder used for this purpose is in micron range. What happen if we use iron nano powder for this purpose? To investigate this, we first synthesized iron oxide nano powder using green route. We dissolved iron chloride in water and then green tea extract was mixed into this solution. A black color solution was obtained and it was centrifuged and resultant iron oxide was freeze dried. XRD and SEM analysis confirmed that the obtained powder was Iron oxide with particle size in 40 – 50 nm range. Further, Iron oxide nano powder was conditioned in AGE by treating it with hydrogen gas. Conditioned Iron oxide was also analyzed with XRD and SEM and it was found that the iron oxide nano powder was converted into iron nano powder. OXII and Ph blank samples were prepared with AGE system using iron nano powder as catalyst.

In comparison to normal (micron size) iron powder, following three points were observed in graphitization with iron nano powder:

- Longer reaction time (150 minutes) is needed for complete graphitization in comparison to normal iron powder (120 Min.).
- Lower background values.
- Lesser amount (0.8 – 1 mg) of iron powder is required in comparison to normal size iron powder (4-5mg).

1.4.1.4 Training to the Birbal Sahni Institute of Palaeosciences (BSIP) Radiocarbon laboratory staff

BSIP, Lucknow has procured automated graphitization equipment (AGE) and Carbonate handling system (CHS) for radiocarbon AMS sample preparation. BSIP radiocarbon laboratory staff was trained by our group in the field of pretreatment and graphitization of samples using above two instruments. Total 35 samples (some of them were graphitized in BSIP lab) have been prepared and measured in this exercise.

1.4.1.5 Clean chemistry lab for ^{10}Be and ^{26}Al sample preparation

After renovation activities this laboratory was used to prepare 160 ^{10}Be and 31 ^{26}Al samples by 5 different users.

Beryllium was extracted from 130 sediment samples by following users:

- Sediment samples from Mahanadi Basin, Bay of Bengal – 35 samples (NIO, Goa)
- Antarctic & Arctic Lakes, -65 samples (Goa Univ)
- Sediment samples from Chillika and Anshupa lake – 30 samples (IIT Roorkee)

Beryllium and aluminium were extracted from 31 quartize samples by following users:

- Quartz samples from Kashmir Valley – 15 samples (Kashmir University).
- Quartzite rock samples from Sikkim – 16 samples (BSIP/BHU).

Twenty standard samples were also prepared from SRM 4325 (treated for Boron reduction) and SRM, 3105a.

1.4.1.6 XCAMS facility

The AMS system at IUAC is designated as XCAMS i.e. Compact ^{14}C Accelerator Mass Spectrometer eXtended for ^{10}Be and ^{26}Al. This system is routinely utilized for the measurement of ^{14}C, ^{10}Be and ^{26}Al. Total 1100 graphite (^{14}C) samples and 44 ^{10}Be samples have been measured this year. 37 users from different institutes have been utilized this facility for their research work.

Maintenance

Following maintenance activities were carried out in this facility.

- 134 MC SNICS source was opened for routine maintenance in February and October. This source was also opened in April for breakdown maintenance and Ionizer was replaced.
- 40 MC SNICS was opened for routine maintenance in July. Ionizer and other parts were cleaned. This source was also opened in March (2019) for breakdown maintenance. The reason for breakdown maintenance was that the immersion lens voltage was following the cathode voltage. Source was opened, cleaned, re-assembled and brought back to operation.
- Accelerator tank was opened for breakdown maintenance in March. It was found that the varistor is faulty in the circuit used for providing power to rotating shaft of Pelletron. Same problem was also occurred in October but problem was fixed without opening the tank.
- Channel 2 of pixie was not working. However, channel 3 of pixie was empty and also working fine. Therefore, pre amplifier signal (dE2) was fed to channel 3. This new configuration was also updated in AccelNet software for smooth data collection.

1.4.2 National Geochronology facility

Deeksha Khandelwal, Umapathy G R, R. Sharma, Soumya Prakash Dhal, Chinmaya Maharana, Pankaj Kumar, S. Ojha, S. Gargari, R. Joshi, S. Chopra and D. Kanjilal

The objective of the project is to develop a comprehensive Geochronology facility at IUAC that will permit measurement of quality isotopic data for Geochronological purposes including relevant characterization at the highest international level. The dedicated geochronology facility at IUAC will enable researchers from Indian Universities and research institutes to study different aspects related to Earth Sciences. The proposed geochronology facility will enhance the research capabilities in the country with the following objectives:

- Carrying out various research studies in the field of climate change, palaeo-climate studies, global carbon cycle, oceanographic parameters, Antarctica research programs, archaeology, biomedicine and history of art etc.

- Capacity building: Initiation of new PhD programs using the facility for universities and research institutions.
- Generating geochronological data that shall be of interest to Earth Scientists, which require precise geochronology.

Following instrumentation have been commissioned and being utilized under this project:

Quadrupole- Inductively coupled plasma mass spectrometry (Q-ICPMS)

Q-ICPMS (Model: iCAPQ) procured from Thermo Fisher Scientific has been operational since early 2018. Fig 1 shows the Q-ICPMS installed with auto-sampler. This has been used for the trace element and rare earth element (REE) analysis of the water samples and digested rock and sediment samples. The samples are introduced by the peristaltic pump to the nebulizer where the fine aerosols of the sample are generated. Argon plasma is ignited in the ICP torch by coupling the RF energy with argon gas. The sample aerosol is introduced to the plasma and the positive ions of the components of the aerosol are formed. These positive ions are passed to the quadrupole which acts as a mass filter and selects a particular m/z at one time. Ions of a given m/z are counted by the detector which gives the measurable electronic signal corresponding to the number of incident ions. The detector system is of secondary electron multiplier (SEM) type, in which the ions incident on the first dynode of the detector produces electrons. These electrons strike the surface of the second dynode and more electrons are produced. The signal is amplified until a measurable signal is detected. Q-ICPMS provides a dynamic working range from ppb to percent. An auto sampler procured from Teledyne CETAC Technologies has been coupled to the Q-ICPMS. At a time 180 samples can be loaded for the sequential measurement.

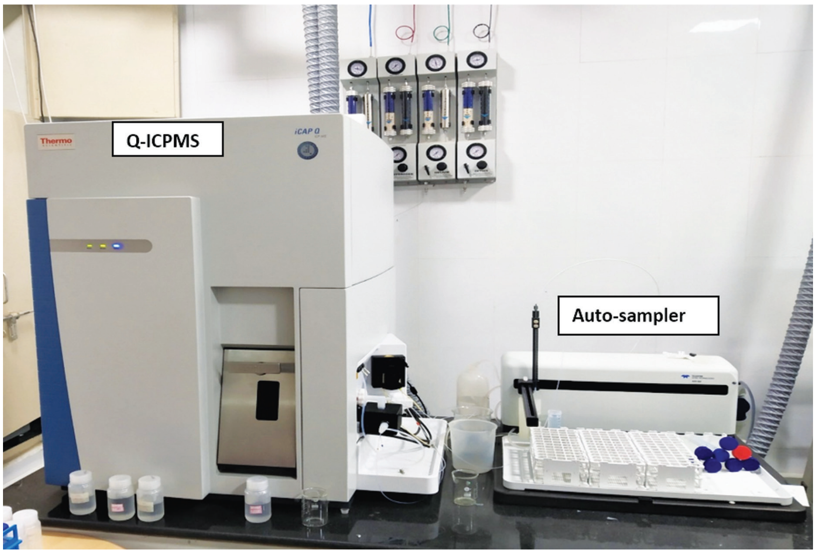

Fig 1: Q-ICPMS installed with Auto-sampler

Q-ICPMS has regularly been used by the users from several universities and institutions for determining the trace and REE metal concentration. During April-2018 to March-2019, trace metal and rare earth element (REE) analysis of 560 samples of 7 users from 4 different universities has been done using Q-ICPMS. Brief scientific motivation of the studies performed are the reconstruction of the paleo-climate and paleo-environment, to understand the controls on ground water geochemistry (Central University of Punjab, Bhatinda), to study the elemental mobilization process during granite weathering (JNU/IUAC), to assess ground water quality in the coastal region of Kerala (JNU), to reconstruct the quaternary climatic variability and sediment provenance of the little Rann of Kutch (MSU, Baroda/JNU), quantification of metals in aerosol collected from Agra region (DEI Agra) and concentration of heavy metals in soil and water samples from Chamba district of Himachal Pradesh to study their effects on the growth of the crops as well as the human health (LPU, Jalandhar).

Femto second laser ablated high resolution- inductively coupled plasma mass spectrometry (Fs-LA-HR-ICPMS)

HR-ICPMS (model: ELEMENT-XR) procured from Thermo Fisher Scientific is now operational. This ICPMS is equipped with the auto sampler and syringe driven inline dilution system procured from Teledyne CETAC

Technologies and ESI prepFAST respectively. Fig 2 shows the HR-ICPMS installed with laser, auto-sampler and auto-dilution system. The samples are introduced by the peristaltic pump to the nebulizer where the fine aerosols of the sample are generated. Argon plasma is ignited in the ICP torch by coupling the RF energy with argon gas. The sample aerosol is introduced to the plasma and the positive ions of the components of the aerosol are formed. The positive ions are passed through a high resolution magnetic sector. This magnet selects the ions based on the ME/q^2 of the incident ions. The detection system consists of a combination of dual mode secondary mass spectrometer (SEM) with a Faraday detector. HR-ICPMS has several advantages over Q-ICPMS. Magnetic sector field in place of quadrupole, removes most of the interferences. The high resolution of ELEMENT XR makes it suitable for the measurement of isotopic ratio measurement. Using the dual detection mode, the dynamic range is increased by three orders of magnitude and count rates of the order of 10^{12} cps can be handled. Element XR at IUAC has been interfaced with a Teledyne femto second laser. Nd:YAG (neodymium-doped yttrium aluminum garnet; Nd:$Y_3Al_5O_{12}$) is the crystal that has been used as a lasing medium in Teledyne laser. The system can be configured for 1028 nm, 257 nm or 206 nm wavelengths. U-Pb dating of different phases of minerals can be done with ELEMENT-XR.

Liquid solutions or solid samples (via laser ablation) can be analyzed with the help of ICPMS. The technique finds the application for trace element analysis and in the field of geology, environmental sciences, pharmaceuticals, food analysis, clinical, and forensic sciences.

Fig 2: HR-ICPMS installed with Femto-second laser, auto-sampler and auto-dilution system

Wave length Dispersive X-Ray fluorescence and X-Ray Diffraction:

X rays fluorescence spectrometry is utilized for non-destructive elemental analysis of rocks, mineral, sediments and fluids for geological applications. This XRF facillity has been operational since 2018. A sequential wavelength dispersive X-rays fluorescence spectrometer along with necessary standards has been installed. A fuse bead machine, pellet press and vibratory cup mill have been installed for the sample preparation required for XRF measurements. XRF calibration curves have been made using the available standards. From April-2018 to March-2019, XRF measurements of 904 samples from 7 users from 3 different universities and one institution has been done. The analysis helped the users to do OSL dose rate calculation, geochemical analysis and identification of surface processes of Earth.

X rays diffractometry is used for studying lattice structure to determine minerology of different geological samples i.e. clay, sediments etc. This XRD facility has been operational since 2017. X rays diffractometer has been installed and utilized routinely by users for characterization of their samples. From April-2018 to March-2019, 2081 samples of 28 users from 12 different universities and 3 institutes, were measured using XRD. These analyses helped the users to understand past climatic changes, depositional environment, Earth surface processes. Fig. 3 (a) and (b) shows the XRF and XRD instruments, respectively.

Fig. 3 (a) WD XRF and 3(b) XRD

2. ACCELERATOR AUGMENTATION

2.1 HIGH CURRENT INJECTOR

The High Current Injector (HCI) Project will accelerate the ion beam from ECR source using normal temperature Radio-Frequency Quadrupole (RFQ), and IH type Drift Tube Linac (DTL) to match the input velocity at our existing superconducting linear accelerator. This year beam was successfully accelerated (A/Q=3 & 2) through RFQ and first DTL cavity to achieve the design energy output of 325 keV/amu.

2.1.1 18 GHz HTS ECR Ion Source, PKDELIS and LEBT

G. Rodrigues, P. S. Lakshmy, Y. Mathur, Sarvesh Kumar, U. K. Rao & A. Sarkar

(a) Ion Source Operation and Measured Radiation Levels

The low energy beam transport section (LEBT) after the HTS ECR ion source was modified due to huge beam loss caused by the large distance between ion source and the analyzer magnet. The ion Source was shifted towards the magnet by removing the existing Faraday cup and beam profile monitor. The water cooled extraction system was replaced with an air cooled extraction system. The small HV platform for housing the bias power supply was re-positioned and refurbished by placing it on a rail close to the ion source. The extracted beam intensities improved by a factor of 10 after the LEBT modification. Various gaseous beams like Ar, Ne, N_2, O_2, He etc. were developed. However, due to radiation shielding issues around the ion source, we could not run at relatively higher levels of RF power.

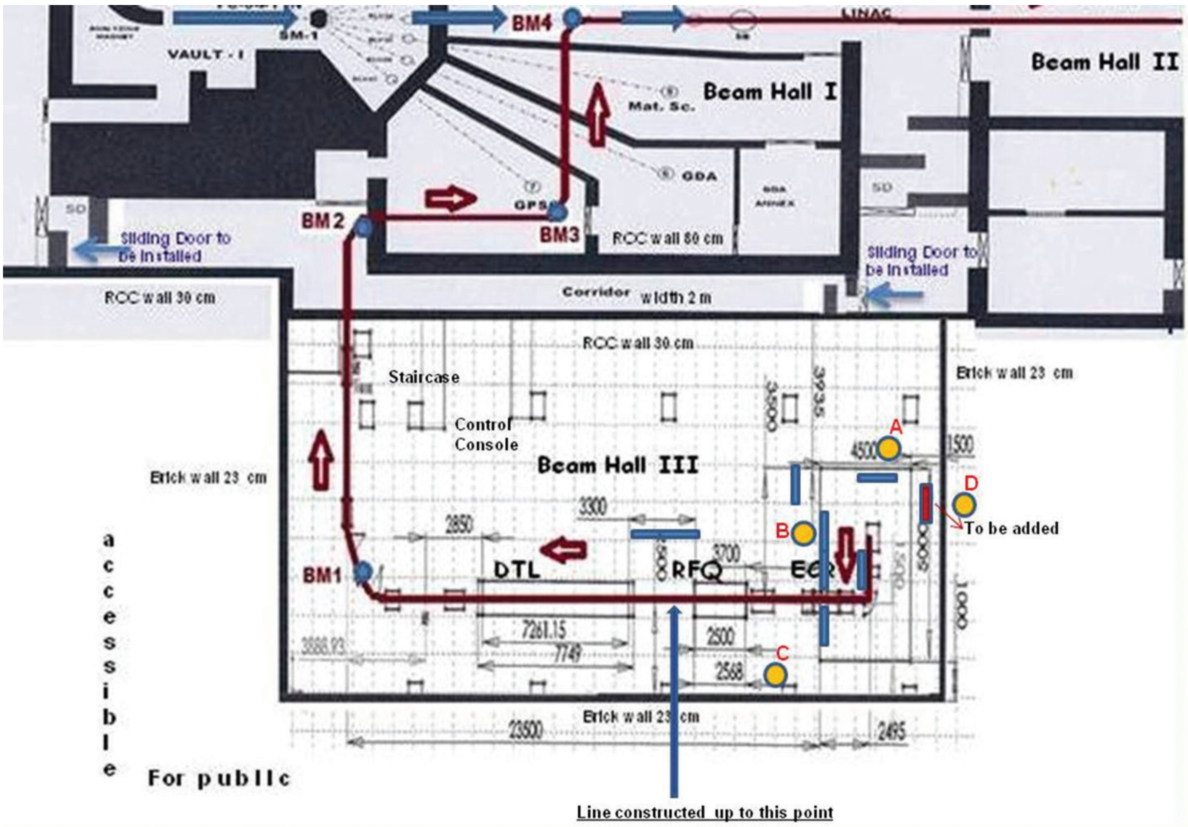

Fig.1. Radiation survey around beam hall III when the ion source was powered at various levels of RF power

Beam Hall III was surveyed thoroughly, with four RF power levels 100, 400,700 and 920 Watt (Fig.1). The whole area was thoroughly monitored. The staircase area (downstairs from the control/data room) and the control console area were completely safe from radiation point of view (<50 μR/hr, even with maximum power). The points A, B, C marked in the picture were the radiation-wise most hot points in the beam hall, but still they did not cross 350 μR/hr with maximum power (permissible for radiation workers is 1000 μR/hr). Point D behind the glass back door of the cage however showed non permissible radiation level, which can be brought down to safe level by using a movable lead shield covering the glass door. (While surveying this, movable lead shield was not in position, but will be put back in place). Hence, with all lead shields in proper position (as per figure 1.), the HCI Beam Hall is completely safe for a radiation worker outside the source cage. No extra shielding is found necessary. However, entry of non radiation workers should be restricted. The average radiation level even with maximum power is well below the permissible limit. But radiation workers should ensure using radiation badges as a compulsory measure.

(b) Failure of 18 GHz Klystron and Water Chiller

The RF generator for the ion source has been running over 16 years and its functioning and operation has been deteriorating. This has resulted in downtime of the ion source. We have had problems with the water chiller which is generally being used for cooling the cryo-coolers. This has also resulted in the downtime of the ion source. Efforts are underway to minimize these problems with both these systems.

(c) Beam Acceleration Tests

Ion source was in continuous operation for beam acceleration tests of HCI during last academic year. The energy measurement from RFQ and DTL#1 was carried out using a newly installed beam line consists of spiral buncher, DTL, quadrupoles, steerers, beam diagnostic elements etc. after RFQ, along with the 45^0 bending magnet (Figure 2.). Beam acceleration tests for DTL#1 was carried out using Ne^{8+} and N^{5+} DC beams. The boosted energy from RFQ and DTL#1 were 188 keV/amu and 137 keV/amu respectively. Spiral buncher was tested with Ne^{8+} (bunched beam). The bunch width at fast Faraday cup was measured to be 2.42 ns. The maximum DC beam transmission achieved upto fast Faraday cup was 75%. Efforts have been made to look into the reasons for DC as well as bunched beam transmission loss after RFQ and DTL#1 in a stepwise manner and different methods were tried to streamline the beam tuning process for optimum transmission.

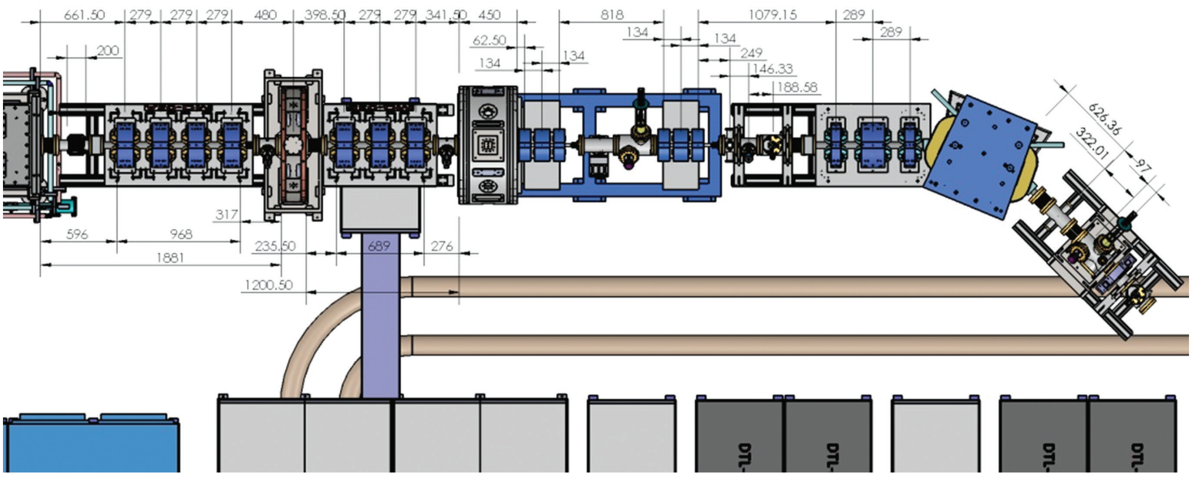

Fig.2. New test layout for DTL, spiral buncher and first cavity of DTL

(d) Multi-harmonic Buncher Test

Multi harmonic buncher tests were carried out to obtain optimum bunch width. The buncher tests were carried out with O^{6+} beam and the bunch width was measured using a fast Faraday cup. Ion source was optimized to have a stable beam. LEBT parameters and buncher parameters were optimized to obtain a stable bunch of 1.6 ns measured using a 4 GHz oscilloscope, which was desirable for maximum transmission through RFQ. A 3 mm collimator was installed close to the entrance of the buncher to minimize the rf defocusing. An improved collimation of the beam close to the entrance of the buncher as per the designed optics would improve the bunched width of the beam measured at the fast Faraday cup. Beam current of 2.8 µA was injected into the MHB. Stability of the beam bunch was also checked. Fig.3 shows the preamplifier signal from the fast Faraday cup using a 600MHz oscilloscope.

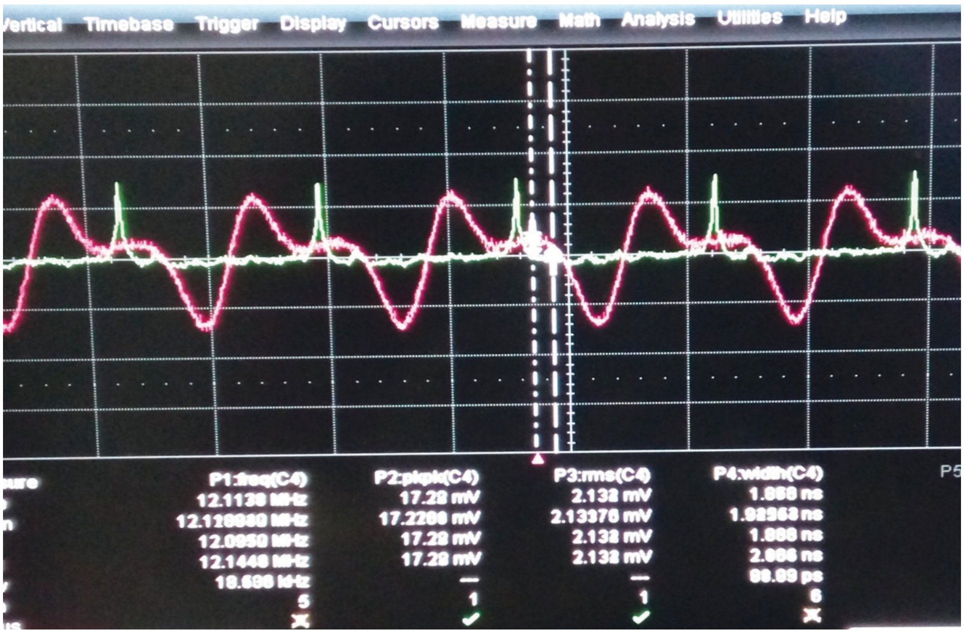

Fig.3 Bunch width measured using a 600MHz oscilloscope

2.1.2 Status of the Multi-Harmonic Buncher for the High Current Injector

A Sarkar, Sarvesh Kumar, Rajesh Kumar, R Ahuja, S K Suman, Y Mathur, P Barua, A Kothari, A J Malyadri, V V V Satyanarayana, B P Ajithkumar

A fully indigenously developed multi-harmonic buncher (MHB) was fabricated and commissioned in the beamline for the high current injector (HCI) at IUAC, New Delhi. The entire control electronics along with an RF power amplifier was integrated with the tank circuits connected to the bunching girds. Since beginning of 2017 it is operational and several beams from the ECR source have been bunched successfully using this system. Oxygen, Nitrogen, Helium and Neon beams have been bunched. The best FWHM observed was 2.5 ns as measured by the signal from a Fast Faraday Cup (FFC) on a 500 MHz oscilloscope. It was observed that an FWHM of 2.5 ns when measured on a 500 MHz oscilloscope measures 1.5ns on a 4 GHz oscilloscope. It was also observed that the beam convergence and divergence play a major role in the bunch width. Different A/q beams were bunched and it was observed that these scale linearly with the bunching voltage across the grids. Some of the results showing the bunched beam (FFC signals) and saw-tooth pick-up voltage (differentiated signal) as seen on the 500 MHz oscilloscope are shown in the following figures.

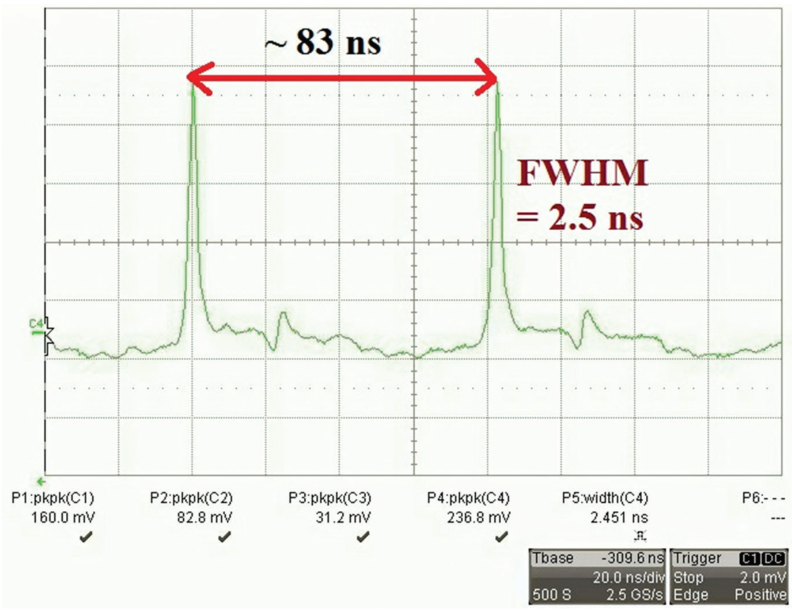

Fig.4 Bunch width measurment for O^{6+} ion beam

2.1.3 High Power RF Tests and Beam Test on Radio Frequency Quadrupole

Sugam Kumar, R. Ahuja, A. Kothari, C.P. Safvan

(a) Power Coupler and High Power Conditioning

To power the RFQ cavity we have designed a new prototype L-shaped water-cooled coupler. The newly designed RF coupler is based on a 6-1/8" coaxial waveguide, and its water-cooled inductive loop has to withstand up to 80kW power in CW operation at 48.5MHz. The coupling factor of the RF coupler insertion and rotation inside the coupling cell have been analyzed for different effective loop areas. The shape of the loop has been adopted in order to increase the coupling coefficient. The loop is made of two concentric copper pipes one of with diameter 12mm and other of 6mm. The loop has several bends which were introduced in order to optimize the coupling coefficient.

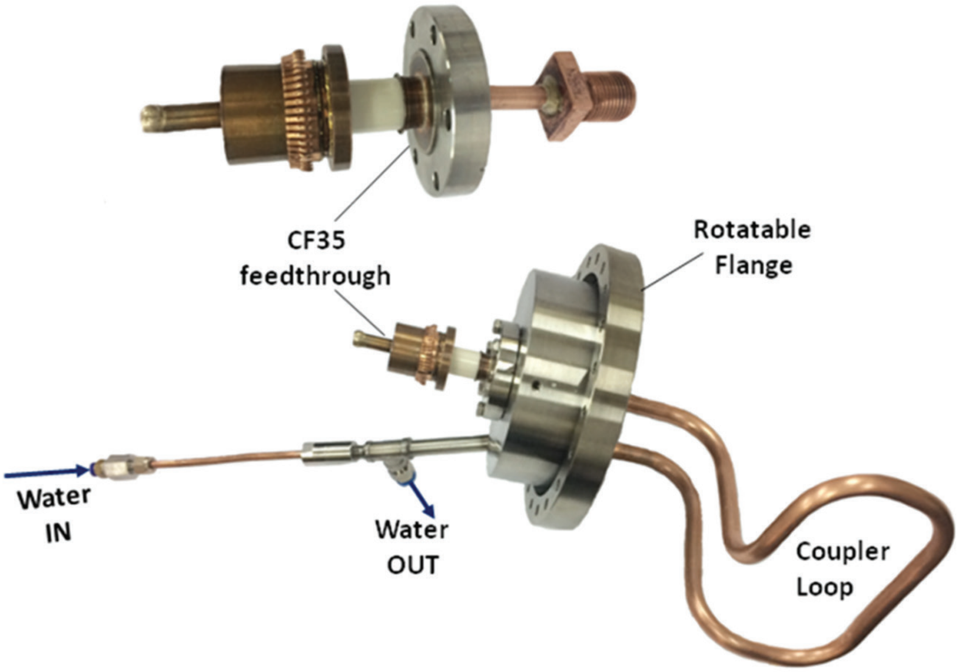

Figure 1: Assembled photo of the rotatable water-cooled L-shaped rf power coupler, a commercial alumina ceramic CF-35 feedthrough is used as a RF-window

A commercially available Alumina ceramic based CF-35 feedthrough is used as an RF vacuum window. The feedthrough is screwed with stainless-steel custom-made CF 150 flange, which also has a water channel to cool the inductive loop. The central conductor of the 6-1/8" coaxial rigid line connected to the feedthrough with the help of Cu-Be finger strips. The outer conductor of the 6-1/8" coaxial line also connected to the CF 150 through Cu-Be finger strips. The one end of the inductive loop is then brazed to the central conductor of the feedthrough and another end is brazed on the rotatable CF150 flange of the coupling cell of the coupled RFQ cavity. Inside the loop and the feedthrough water flowing at maximum, 2 liters/min is used for the cooling of the loop surface as well as ceramic.

The purpose of high power rf tests were to check the rf and temperature stability of the RFQ also to survey both the RF and X-ray leaks from the RFQ cavity. The conditioning was started with an input power of 1 kW while carefully monitoring the cavity vacuum pressure and checking reflected power for signs of sparking. Slowly we reached to the 38kW forward power without any losing RF contacts. The RFQ was than conditioned at the 38kW power for few hours. We encounter a few major sparking or vacuum degradation in the cavity in the power range of 14-16kW, but above this power level cavity was performing reasonably well. After 6 hours of conditioning, the vacuum pressure in the cavity was 7.5×10^{-8} mbar at 38kW forward power. We observed marginal rise in the water temperature from 19^0C to 22^0C at the 38kW power.

(b) Beam Acceleration Test

The beam acceleration test setup was adopted and installed after the RFQ. The background pressure was maintained at around 5.65 x 10^{-7} mbar along the whole system. For the energy measurement of the accelerated beam, a 45^0 bending magnet is installed after the RFQ. Two Faradays cups were installed just downstream the beam before the 45^0 bending magnet and another faraday cup system along with the BPM installed at the end of the diagnostic chamber to measure the current and the beam profile of the accelerated beam. The input current was measured with the fast faradays cup installed upstream the RFQ.

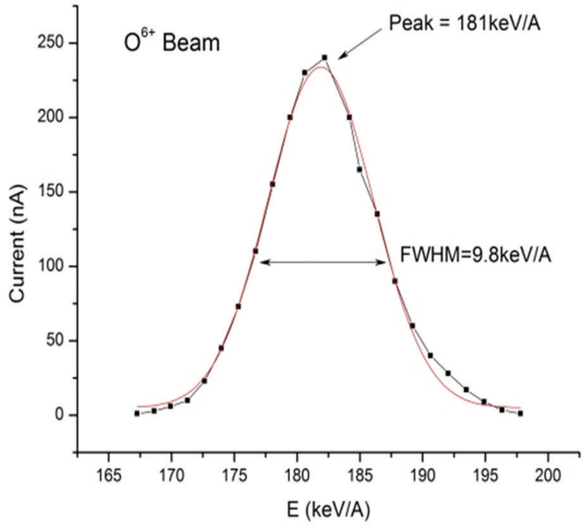

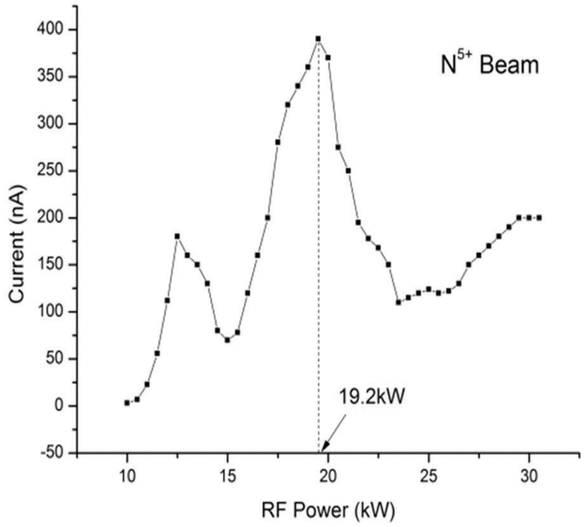

He^{2+}, 128keV of the O^{6+} and 112keV of the N^{5+} ion beam into the RFQ. The output beam energy is estimated from the momentum spectrum of the beam, which was taken with the 450-bending magnet. The input and output beam currents were measured with the faraday cups. The estimated output energy of He^{2+}, Ne^{8+}, O^{6+} and N^{5+} and other parameters are shown in the table 1.

Table 1: Accelerated parameters for He^{2+}, Ne^{8+}, O^{6+} and N^{5+} from 8keV/u to 180keV/u.

Beam	A/q	Ein(keV)	Eout(keV)	Cavity Pickup (mV)	Peak Power (kW)
He^{2+}	2.0	32	707 ± 3.0	38.2	13.2
Ne^{8+}	2.5	160	3640 ± 2.8	43.0	18.0
O^{6+}	2.67	128	2896 ± 2.7	43.5	18.3
N^{5+}	2.8	112	2520 ± 2.5	44.8	19.2

Successful acceleration of ion beams from 8keV/u to 180keV/u validates the design of RFQ modulation. It is just a matter of time and we should be able to accelerate the ions beam of A/q = 6 also from 8keV/u to 180keV/u. We are planning to accelerate bunched beam through the RFQ.

2.1.4 DRIFT TUBE LINAC RESONATOR

The role of the room temperature DTL in HCI is to accelerate the 180keV/u beam from the RFQ to 1.8 MeV/u. The DTL consists of 6 multiple gap IH type cavity resonators, operating at 97 MHz. The transverse focusing is done by compact quadrupole triplets, placed in between the resonator tanks. The design of the DTL incorporates bunching sections inside the cavity to take care of the longitudinal focusing. All the resonators are different with length ranging from 38 cm to 94 cm and power ranging from 5kW to 25kW.

Out of the six resonators, the first one has been installed and tested with beam. The energy gain has been verified. The second resonator assembly has been completed and powered up to 6kW. Resonator #3 and #6 are kept ready for power test. The power coupler and slow tuner assembly for the five resonators are progressing. All the components have been fabricated. The cavities will be power conditioned and assembled soon. An inside view of resonator #6 is shown below.

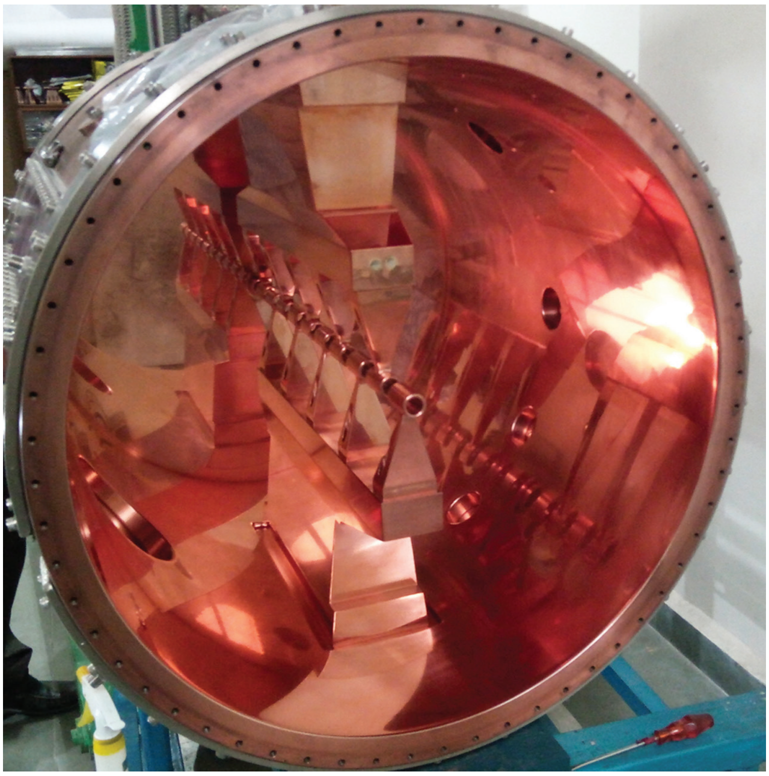

2.1.5 Travelling Wave Chopper

S Kedia, Rajesh Kumar and R Mehta

Chopping and Deflecting System (CDS) has been proposed to provide the chopped beam with various repetitions rates to the IUAC experimental facilities. The CDS has been designed, fabricated, assembled and tested with DC electronics.

The CDS has been installed in the Low Energy Ion Beam Facility (LEIBF). The test setup in LEIBF was configured to simulate actual layout of LEBT section (figure 1). Since the energy in the LEBT section is 8 keV/amu we have selected ion beam of Oxygen, Nitrogen, and Argon with various charge state to have energy of 8 keV/amu. A DC power supply has been developed indigenously and connected to the deflecting plates of the CDS. The DC power supply is capable of providing the voltage of 0 V to 1000 V. The CDS was tested with. The amount of deflection, at a distance of 750 mm, was measured for the various beams and different values of A/q. The measured and analytically calculated voltage matches closely, as presented in the table.

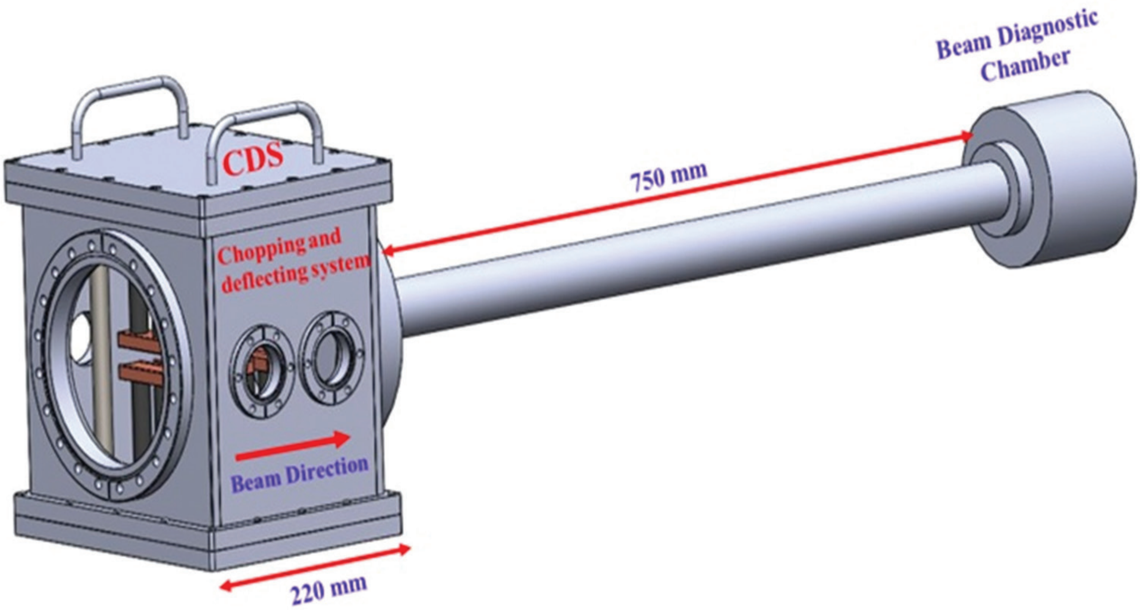

Figure 1. Schematic setup of CDS setup installed in the Low Energy Ion Beam Facility.

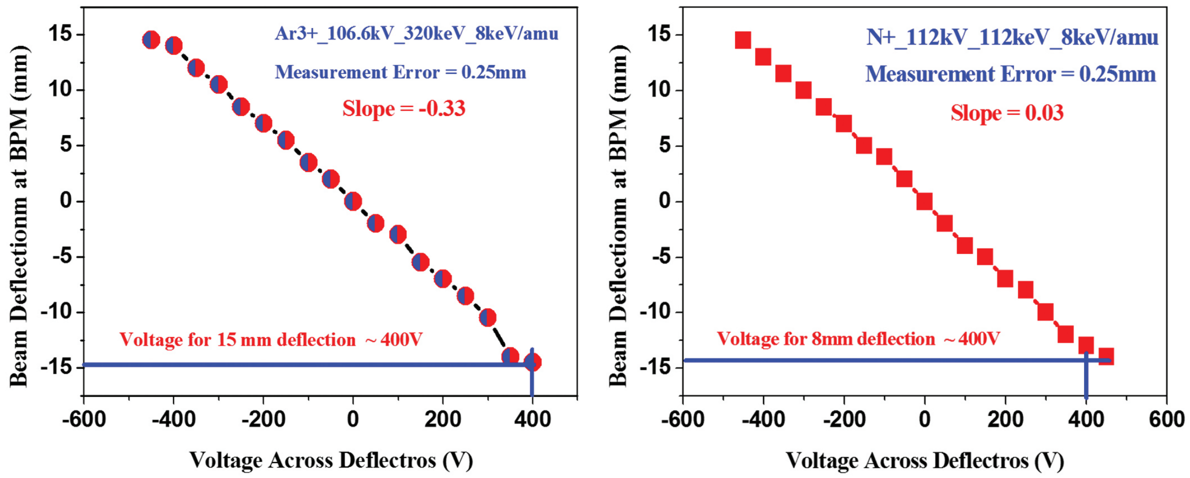

Figure 1. Schematic setup of CDS setup installed in the Low Energy Ion Beam Facility.

Voltage required for 15 mm deflection at 750 mm from CDS		
Theoretically Calculated Voltage	**CST Simulations**	**Experimentally Measured Voltage**
~350 V	330 V	~400 V

The experimentally measured voltage to deflect undesired charged particles match closely with the analytical value and CST simulated value. The measurement error is ~ ±0.5 mm because of instability and fluctuation in deck power supply.

2.1.6 HIGH POWER TEST OF 48.5 MHz SPIRAL BUNCHER FOR MEBT SECTION OF HCI

R Mehta, S Kedia, R V Hariwal, R Ahuja

A 48.5 MHz spiral buncher has been installed in the MEBT section of HCI beamline to provide the longitudinal beam matching at the entrance of the Drift Tube Linac (DTL) after successfully validating the design. The cylindrical chamber was fabricated of copper plated stainless-steel, while OFHC copper was used for the inner components. The measured quality factor, shunt impedance, resonance frequency, electric field profile and power requirement matches very well with simulated value. The bead-pull technique has been used to validate the electric field profile and to determine the various low-level RF parameters. A fine tuner has been developed and employed to correct the frequency shift during the high-power operations in the phase and amplitude lock condition. The cavity has been tested up to the full power of 1 kW to produce 27 kV across each gap.

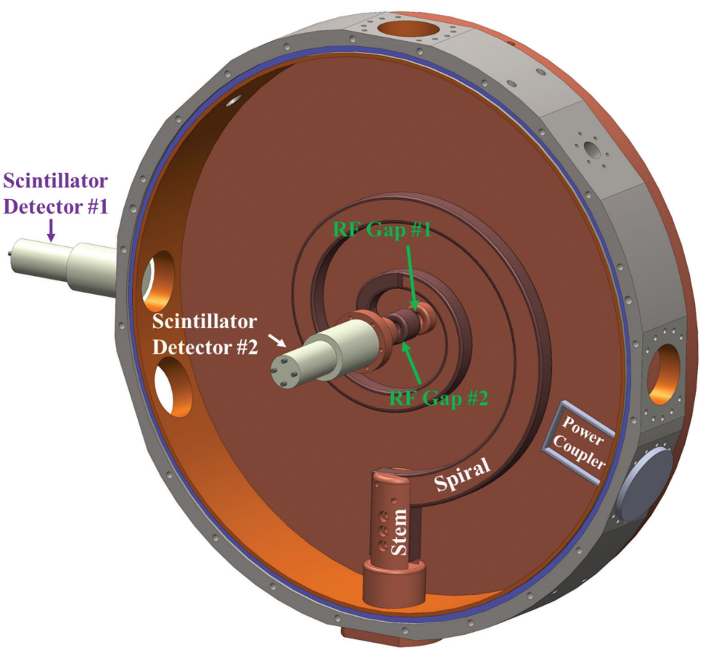

The X-ray energy spectroscopy method was used to measure the gap voltage experimentally. The data analysis was carried out to find out the end point of the Bremsstrahlung spectrums. The endpoint of the Bremsstrahlung spectrum provides the information of maximum gap voltage across the drift tube. The various X-ray spectrums were fitted using a standard Bremsstrahlung equation at different power level. The error between analytically calculated and experimentally measured gap voltage is ~5%. The cavity has been successfully tested with the beam. The bunched beam was accelerated through DTL #1 to get designed energy gain of 325 kev/amu, with spiral buncher (SB) off. After optimizing the beam transmission through DTL #1 the SB was powered and tuned. The measured current was increased by factor of two indicating bunching effect. The cause of low transmission through DTL #1 was large bunched width at the entrance of the SB, ~7 ns. Since the acceptance of the SB is 2-3 ns, SB cannot provide efficient longitudinal matching at the DTL #1 entrance. The bunch length could not measure after spiral buncher since there is no longitudinal diagnostic device is available, in the MEBT section of HCI.

2.1.7 DEVELOPMENT OF COMPACT BEAM DIAGNOSTIC SYSTEM FOR HCI

R. V. Hariwal

(a) Development and Test of Compact Beam Diagnostic System (CBDS) for DTL-1 in HCI

Indigenously designed and developed Compact Beam Diagnostic System (CBDS) have been installed after the 450 bending magnet downstream to RFQ in the High Current Injector (HCI) at Inter-University Accelerator Centre (IUAC). The ultimate vacuum near the CBDS was observed to be ~1x10^{-7} mbar which shows that the separate pumping may not be required in the diagnostic box. The design validation of various diagnostic elements namely Faraday Cup, Slit scanner and electronic modules have been carried out by performing online test with 100 keV O^{6+} beam in the HCI beam line. Various operational aspects of a Python programmable logic controller (PLC) based electronic module and Graphical User Interface (GUI) have also been validated during this test. The installed CBDS-1 in HCI is shown in Fig.1.

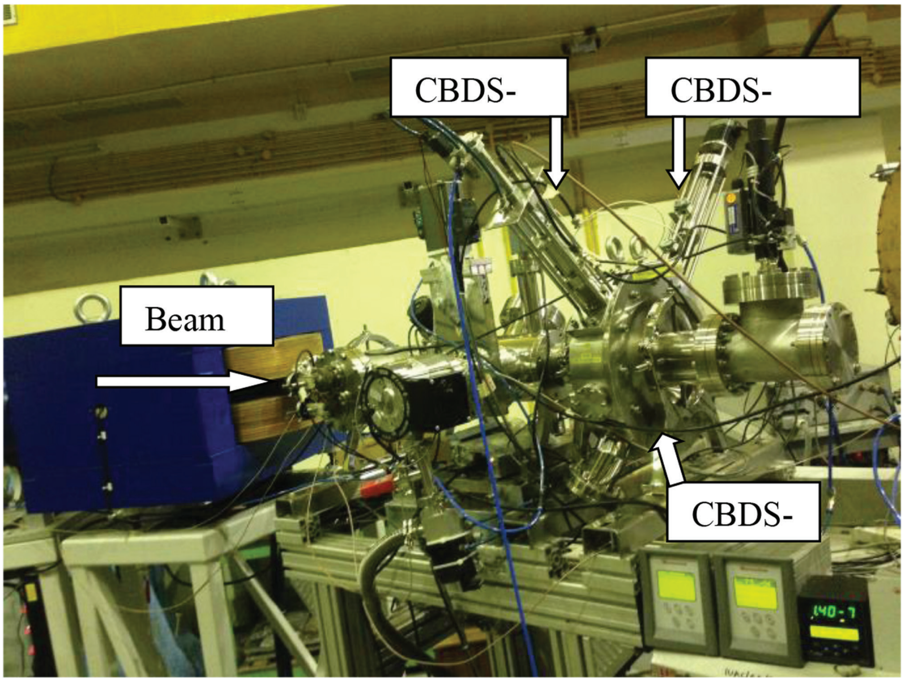

Fig.2.1.16: Modified 3D design of FC, SSC, CDB, CBDS and CBDS with DTL

Current measurements were performed in CBDS FC and NEC, USA made FC simultaneously to compare the magnitude of currents. It was observed that the currents measured in the CBDS FC are perfectly matching with the current measured in NEC FC. The beam current results are presented in Table 1.

Sr. No.	Beam 100 keV	Current in NEC FC	Current in CBDS FC	Results
1	16 O6+	154 nA	154 nA	Match
2	16 O6+	100 nA	100 nA	Match
3	16 O6+	70 nA	70 nA	Match
4	16 O6+	160 nA	160 nA	Match

The beam profiles in various tuning conditions are also checked and compared in the CBDS BPM (slit scanner) and NEC BPM (wire scanner). The result is discussed and shown in the Fig. 2.

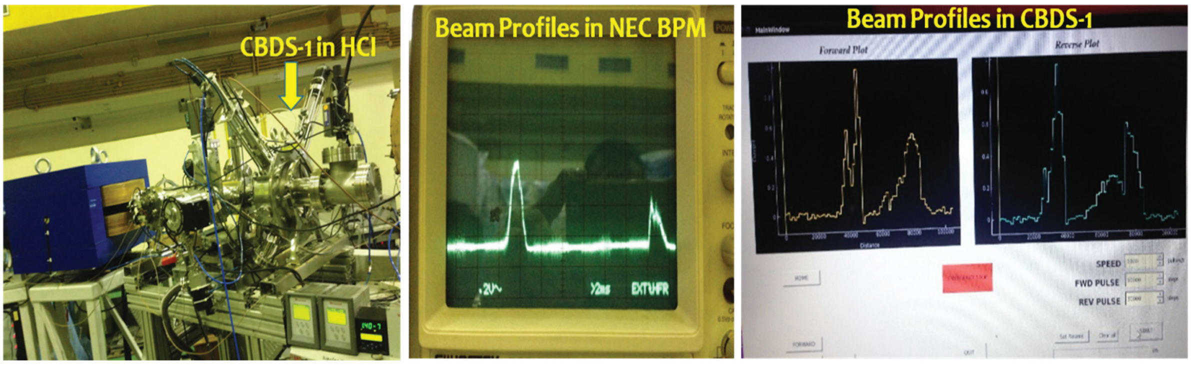

Fig. 2: Comparison of Beam profile in NEC BPM and CBDS BPM

Various currents and beam profiles have been checked in the CBDS-1 and it was found that the currents and profiles are perfectly matching with the currents and profiles measured in the standard NEC FC and BPM. The GUI and electronic module (PLC based stepper motor) for data acquisition has also been verified. These results validated the design, mechanical fabrication, electrical design and operation of various components of CBDS.

(b) Development of CBDS for DTL-2 to DTL-6 Cavities in HCI

The successful results of these tests lead to further develop the excellence, state-of-art design, robust and quality product of CBDS for DTL-2 to DTL-6 cavities in HCI. The present design needs further modifications to make it more professional and fail-safe from the operational aspects. The design modifications of the diagnostic box (DB), Faraday cup (FC) and Beam Profile Monitor (BPM) have been performed to fit them with DTL-2 cavities onwards. The 3D design and various assemblies have been made in the 3D-solid works. A prototype of newly designed elements like DB, FC and BPM are fabricated at IUAC. The PCD reduction from 300 mm (in DTL-1) to 180 mm of the DTL-2 entrance flange, made the design really critical and even more compact. Some important modification like electrical connections and water cooling techniques have also been carried out in this CBDS. This time, it was decided to use the Aluminum materials for the fabrication of DBs instead of stainless steel which reduces its weight significantly. One set of CBDS consisting of one diagnostic box, one FC and one BPM assembly are made successfully as per the modified design. This system is now compatible to DTL-2 to DTL-6 cavities in HCI. After the successful development of CBDS for DTL-2 cavity, it has been decided further to develop six more diagnostic boxes for HCI. The processes of six numbers of CBDS fabrications having uniform design for DTL-2 to DTL-6 are started. The procurement of the items to fabricate the eight numbers of FC, eight numbers of BPM and six numbers of DBs have also been initiated.

2.2 A COMPACT FREE ELECTRON LASER FACILITY TO PRODUCE INTENSE THz RADIATION

S. Ghosh[1], B. K. Sahu[1], P. Patra[1], S. R. Abhilash[1], J. Karmakar[1], B. Karmakar[1], D. Kabiraj[1], S. Tripathi[1], A. Sharma[1], V. Joshi[1], S. K. Saini[1], A. Pandey[1], P. Barua[1], A. Kothari[1], S. Kumar[1], G. O. Rodrigues[1], R. Kumar[1], S. K. Suman[1], J. Urakawa[2], A. Aryshev[2], V. Naik[3], N. Madhavan[1], T. Rao[4], M. Tischer[5], R. K. Bhandari[1] and A. C. Pandey[1]

[1]Inter University Accelerator Centre (IUAC), Aruna Asaf Ali Marg, New Delhi, India
[2]High Energy Accelerator Research Organization, KEK, Tsukuba, Japan
[3]Variable Energy Cyclotron Center, Kolkata, India
[4]Brookhaven National Laboratory,USA
[5]Deutsches Elektronen-Synchrotron, Germany

2.2.1 INTRODUCTION

A compact pre-bunched Free Electron Laser facility named as Delhi Light Source (DLS) is under construction at IUAC since last five years [1]. A low emittance electron beam will be produced by a photocathode based normal conducting RF gun. The electron beam will be injected into a compact undulator magnet to produce intense THz radiation in the frequency range 0.18 – 3 THz. It is planned to produce electron beam initially from copper photocathode and subsequently from the semiconductor photocathode whose deposition system is in the final stage of fabrication. The commissioning of the FEL beam line has been started. The developmental status of the major subsystem is described below.

2.2.2 DEVELOPMENT OF VARIOUS SUBSYSTEMS OF PHASE-I OF DLS

The developments in the major areas of the Phase - I are listed in the following sections:

2.2.2.1 The Copper Cavity as the Electron Gun

The copper cavity along with the copper photocathode was fabricated and tested in the past and kept under vacuum at IUAC. Now the cavity and the solenoid have been installed and aligned in the beamline [figure 1(a)]. The copper photocathode along with the RF spring contact and the insertion chamber to insert the copper photocathode into the RF cavity are shown in figure 1(b) and 1 (c) respectively.

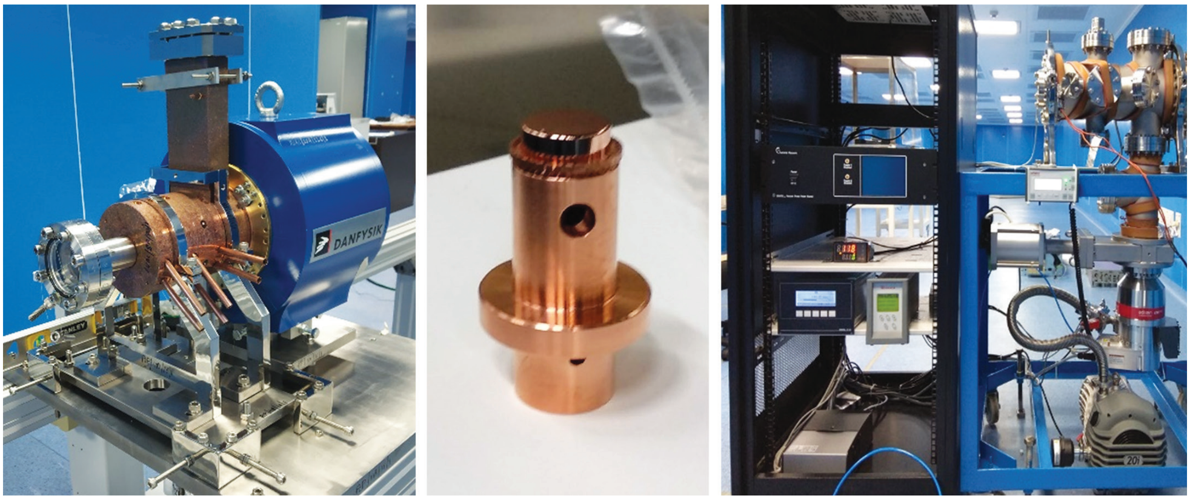

(a) (b) (c)

Figure 1. (a) Copper cavity as electron gun is installed with the solenoid magnet, (b) the copper photocathode plug with the RF contact spring, (c) the insertion chamber to insert the photocathode plug in to the electron gun.

2.2.2.2 The High Power RF System (Klystron, Modulator, Waveguide, Circulator, etc.)

The High Power RF system consists of Klystron, Modulator, vacuum based waveguide and vacuum Circulator, etc. The purchase order for the complete device was placed to Scandinova and the Factory Acceptance Test (FAT) has been conducted successfully at the site of the company. The required specifications mentioned in the tender documents have been achieved during the factory acceptance test. Now the device has arrived at IUAC and is waiting to be installed in its designated area of FEL. The schematic of the device and the arrangement during FAT are shown in figure 2.

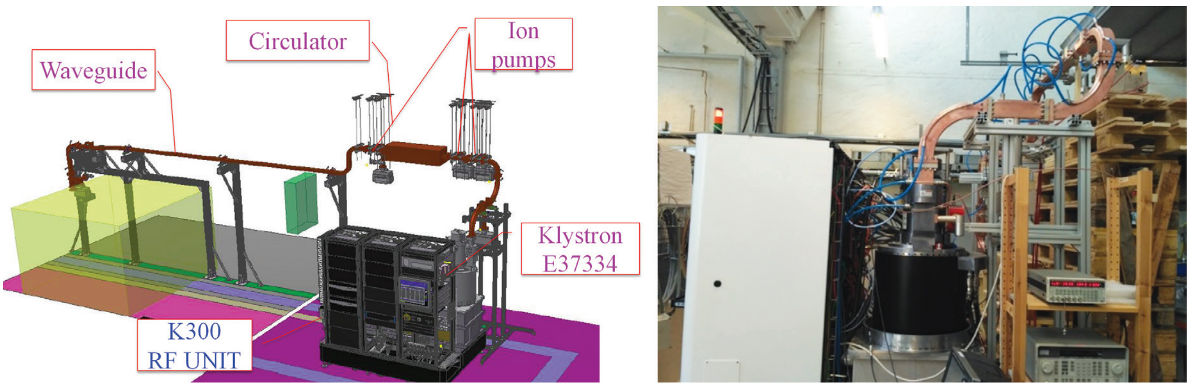

Figure 2. The schematic of the RF device and its arrangement during FAT at Scandinova, Sweeden.

2.2.2.3 Laser System to Produce Electron Beam from Photocathode

The main laser system for the free electron facility will be an Yb doped fiber laser system to produce multi micro bunch electron pulses from photocathode. Current design has been shown in the figure 3.

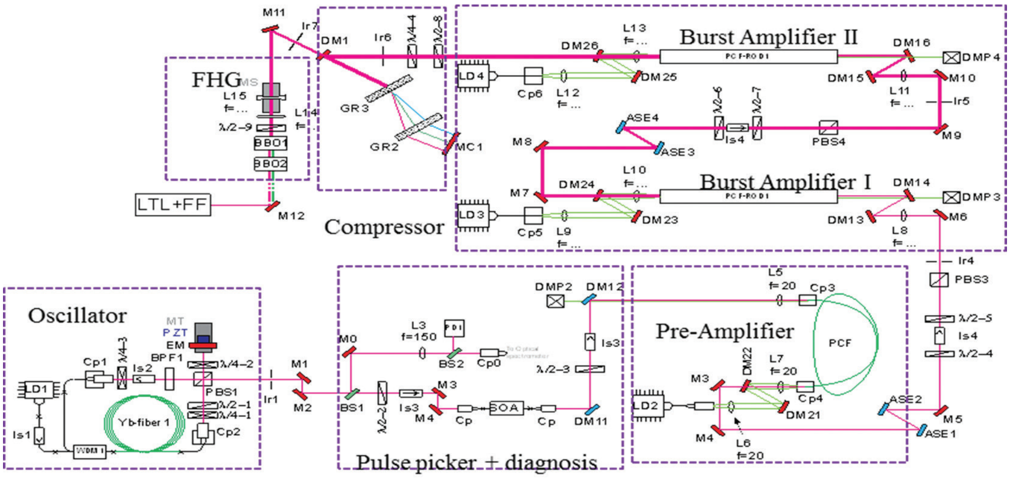

Figure 3. Fiber laser system latest design

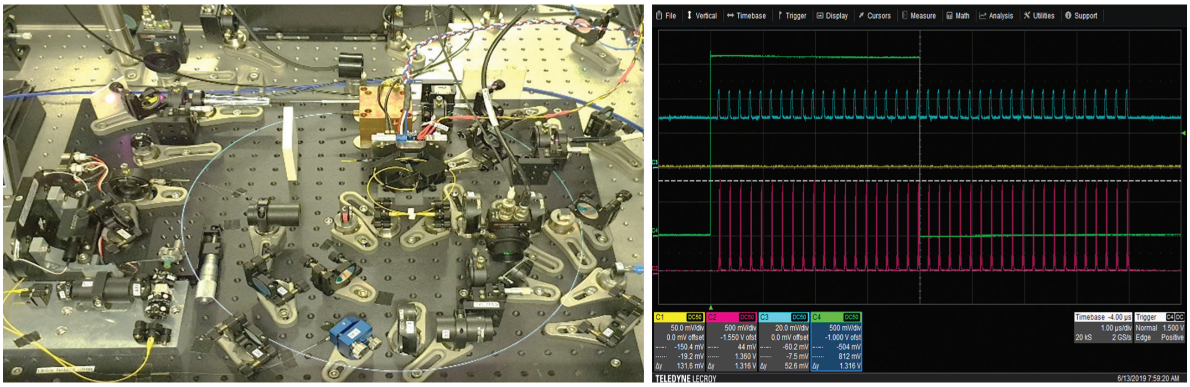

(a) (b)

Figure 4. Oscillator+Pulse picker+preamplifer and its output with pulse seeding

As per the plan the total system is being assembled at KEK and later it will be shifted to IUAC. The main oscillator frequency will be 130 MHz which is the integer division of the main master clock (1300 MHz). The main oscillator is an Yb doped fiber to produce 1030 nm as fundamental which will be synchronized with the master clock that will drive the electron gun and klystron. The oscillator output is passed through a SOA based pulse picker to pick up the pulses at 5 MHz rep rate inside ~4 microsecond RF window with 3.125/6.25/12.5 Hz machine rate. So it will be a multibunch structure at 3.125/6.25/12.5 Hz rep rate with 200 ns separation between two bunches and then it is amplified by passing through a PCF fiber. The following is the oscillator+pulse picker+ pre amplifier system [Figure 4(a)] and its output [Figure 4(b)] assembled at KEK.

After this, two burst amplifiers (PCF ROD) are being added to increase the pulse energy. The splitting mechanism will split each laser into 1-16 pulses. The actual position of the splitting mechanism is still under consideration. It can be placed before or after amplification. Then finally after fourth harmonic conversion, the UV laser will be delivered to the photocathode using telescope system to produce multi-microbunch electron pulses. With 0.1 uJ/pulse we can produce maximum of 200 pC charge from Cs2Te photocathode. The average current can go upto ~24nA for 6pC charge/mircobunch for 20×16 multi-microbunch structure with 12.5 Hz rep rate.

2.2.2.4 Undulator

The design of the compact hybrid undulator magnet has been finalised with the code RADIA [2] to produce the radiation between 0.18 to 3.0 THz. When the procurement process for the undulator was started, IUAC was offered a spare Undulator for use by BESSY, Germany. Fortunately the parameters of BESSY's undulator was found to be very close to the designed parameters of IUAC's undulator and the comparison table is shown in Table-2. The beam optics and radiation simulation calculation [3] are performed again for the spare undulator of BESSY and the results are found to be same for both the designed one as well as BESSY's undulators.

Table: 1. Parameter Comparison of the Undulator

	Undulator designed for FEL project of IUAC	BESSY's Undulator to be used at IUAC's FEL
TechnologyHybrid planar	Planar	
Period length 50 mm	48mm	
Device length ~1.5 m	~ 1.7 m	
No of Periods28 (Full)	34 (Full)	
Magnetic gap 20 - 45 (mm)	17-42 (mm)	
Magnetic field0.62 - 0.11 (T)	0.62 - 0.11 (T)	
Undulator parameter (K)	2.89 - 0.61	2.73 -0.52
Wavelength0.18 - 3.0 (THz)	0.18 - 3.0 (THz)	
Beam Line Height	1.1m	1.5m

To validate the performance of BESSY's undulator (to be donated to IUAC), a detailed measurement of magnetic fields and remnant activation level was performed at BESSY. The magnetic measurement was found to be alright which validated the usability of the undulator at the FEL project of IUAC. After incorporating a few modifications and refurbishments, the undulator will be shipped to IUAC by the end of 2019 and is expected to be installed in the beam line in the beginning of 2020.

2.2.2.5 Beamline Commissioning

The commissioning of the beam line is presently going on. The RF cavity to be used as the electron gun has been installed and aligned along with the solenoid magnet. The insertion chamber along with the copper photocathode plug is waiting to be connected at the back side of the RF cavity. The high power RF device along with the waveguide are about to be commissioned and then the RF conditioning of the cavity will be started. The other components of the beam line are either procured or under the process of procurement. The various holding and alignment fixtures are designed and getting fabricated. The electromagnets e.g. quadrupoles, dipoles and steering magnets are already designed and being procured. The power supplies of all the electromagnets will be developed at IUAC.

2.2.3 Conclusion

The compact Free Electron Laser facility of IUAC is at the beginning stage of commissioning at IUAC. The important components of the facility e.g. the RF cavity, Copper photocathode, High Power RF device, the fibre laser system, solenoid magnet, etc. are either installed and will be installed in next few months. The Undulator to produce THz radiation will be installed at the beam line by the beginning of next year. It is expected that the electron beam and the THz radiation will be demonstrated by 2019 and 2020 respectively.

Reference

[1] S.Ghosh et al. Nuclear Instruments and Methods in Physics Research – B 402, (2017), page 358-363.
[2] RADIA, Online. Available: http://www.esrf.eu/ Accelerators/groups/Insertion Devices/Software/Radia.
[3] V.Joshi, et al., Nuclear Instruments and Methods in Physics Research – A 913, (2019), page 28-39.

2.3 2.45 GHz MICROWAVE ION SOURCE BASED FACILITY

G.Rodrigues, Y.Mathur, Narender Kumar, Gajendra Singh, U.K.Rao, R.N.Dutt, R.Ahuja, Ruby Shanthi, V.V.V Satyanarayana, D.Kanjilal, Avinash C.Pandey

2.3.1 X-RAYS MEASUREMENTS

A 2.45 GHz microwave ion source based high flux system has been operational since the year 2017. The facility is frequently used for carrying out experiments in the fields of Materials Science and Plasma Physics. In the academic year 2018-19, plasma characterization with the help of X-ray measurements using NaI(Tl) detector was again carried out for oxygen plasma. The results have shown that X-rays in the energy range of 10 keV to 50 keV are being produced using RF power up to 100 W. This energy signature directly relates to the electron energy distribution function (EEDF) inside the plasma and are unusually high in this kind of ion sources.

PIC simulations are undergoing investigations to study the effect of ambipolar and non-ambiploar diffusion mechanisms by looking into the effects of insulators placed inside the plasma chamber. These information can be useful to extract intense ion beams. The aim is to compare the simulations with recent experimental observations in plasmas exhibiting ambipolar and non-ambipolar diffusion mechanisms.

2.3.2 ATOMIC SPECTROSCOPY USING ECR PLASMA

Spectroscopy is a standard diagnostic technique for astrophysical and laboratory plasmas, the electron cyclotron resonance (ECR) ion sources are excellent tool to carry out such diagnostics. These studies include calibration of density diagnostics, x-ray production by charge exchange, line identifications and accurate wavelength measurements, and benchmark data for ionization balance calculations. In the present work context, our main focus will be on measurements of relative line intensities in the vacuum ultraviolet spectral range (VUV) to visible range, and if possible some other important line spectra in X-ray region.

In VUV to visible region we can investigate the relative line intensities of the 2s2p ^3P-2p^2 ^3P and 2s^2 ^1S-2s2p ^2P transitions for C III, O V, Ne VII and other partially ionised atoms as a function of different ion source parameters [1]. For complete Collision – Radiative modelling of fusion devices the diagnostic lines from impurities like H_2, D_2, O_2, N_2, Ar and He is very indispensable to identify. For instance the ratio of 728.13 nm He-line to 750.39 nm Ar-line is used to determine electron temperature and ratio of 587.76 nm He-line to 706.52 nm Ar-line is sensitive to electron density [2]. In X-ray region closed shell, such helium-like or neon-like ions, which radiates predominantly in the X-ray range. This radiation can be used to diagnose the plasma conditions, such as the electron temperature, electron density, ion temperature, ion transport and diffusion, and bulk plasma motion. The radiation from highly charged ions contributes to the overall power loss of the plasma, and the associated radiative power loss can be severe and prevent ignition and burn, if the plasma contains too many heavy ions [3].

Ar ions, which happen to be the most abundant impurities in fusion plasma device, can serve as a great candidate for plasma parameter diagnosis in colder region. Apart from magnetic fusion plasma, the spectral lines of Ar I, Ar II and Ar III ions are indispensably required for ongoing development of plasma thrusters' diagnostics where Ar gas is used as propellant [4,5].

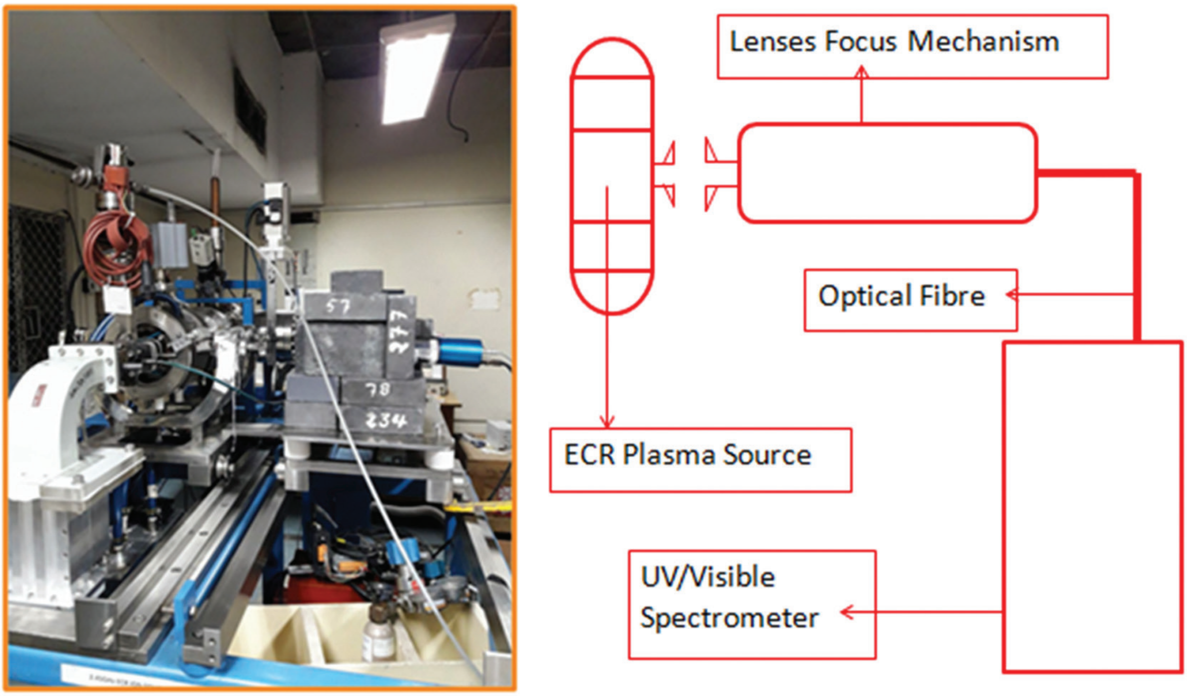

2.45 GHz ECR Ion source lab — Planned experimental Setup

Fig 1: Experimental Setup

All the above studies of magnetic fusion plasmas and plasma thrusters also consume a large amount of atomic data, especially in order to develop new spectral diagnostics. So along with experimental line identification work as mentioned above we will be working on the computation of reliable atomic data by the most advance and ab-initio calculations based on Multiconfiguration Dirac-Fock (MCDF) calculations [6]. These calculations will include the relativistic calculations of accurate energy levels, transition probabilities, wavelengths and oscillator strengths of the ions under study.

References:

[1] W. Pöffel et.al. Review of Scientific Instruments 61, 613 (1990); doi: 10.1063/1.1141934
[2] W.B. Wu et.al. AIP Conference Proceedings 2011, 020004 (2018); doi: 10.1063/1.5053246
[3] P Beiersdorfer, J. Phys. B: At. Mol. Opt. Phys. 43 (2010) 144008; doi:10.1088/0953-4075/43/14/144008
[4] K. Katsonis, 32nd International Electric Propulsion Conference (IEPC-2011-169); Germany
[5] T. Nandi et. al. Journal of Quantitative Spectroscopy & Radiative Transfer 112 (2011) 2771–2778
[6] Gajendra Singh et.al. J. Phys. B: At. Mol. Opt. Phys 49 (2016) 205002; doi:10.1088/0953-4075/49/20/205002

3. RESEARCH SUPPORT FACILITIES

3.1 SUPPORT LABORATORIES

3.1.1 High vacuum laboratory

Chandra Pal, A. Kothari, P. Barua, S. Chopra

High vacuum laboratory is primarily responsible for maintaining vacuum and vacuum systems in beamlines and experimental facilities. It provides support to different labs and users in vacuum related problems. Vacuum lab is also involved in the installation and commissioning of various beamlines, experimental and accelerator facilities at IUAC. High Current Injector [HCI] installation is in progress and installation of Spiral Buncher and DTL-I along with testing set-up was completed. All the beamline devices in this experiment set up have been interfaced with VME control system and can be controlled remotely by control console.

3.1.1.1 Installation of High Current Injector (HCI) Components (Spiral Buncher, DTL, Quadrupoles, etc.) with Half-Achromat and Diagnostics in Beam Hall III:

Chandra Pal, Ashok Kothari, P. Barua, DK Munda, Kundan Singh, Prem Kumar Verma, Mukesh Kumar, S K Suman, Thomas Varughese, Rajeev Ahuja

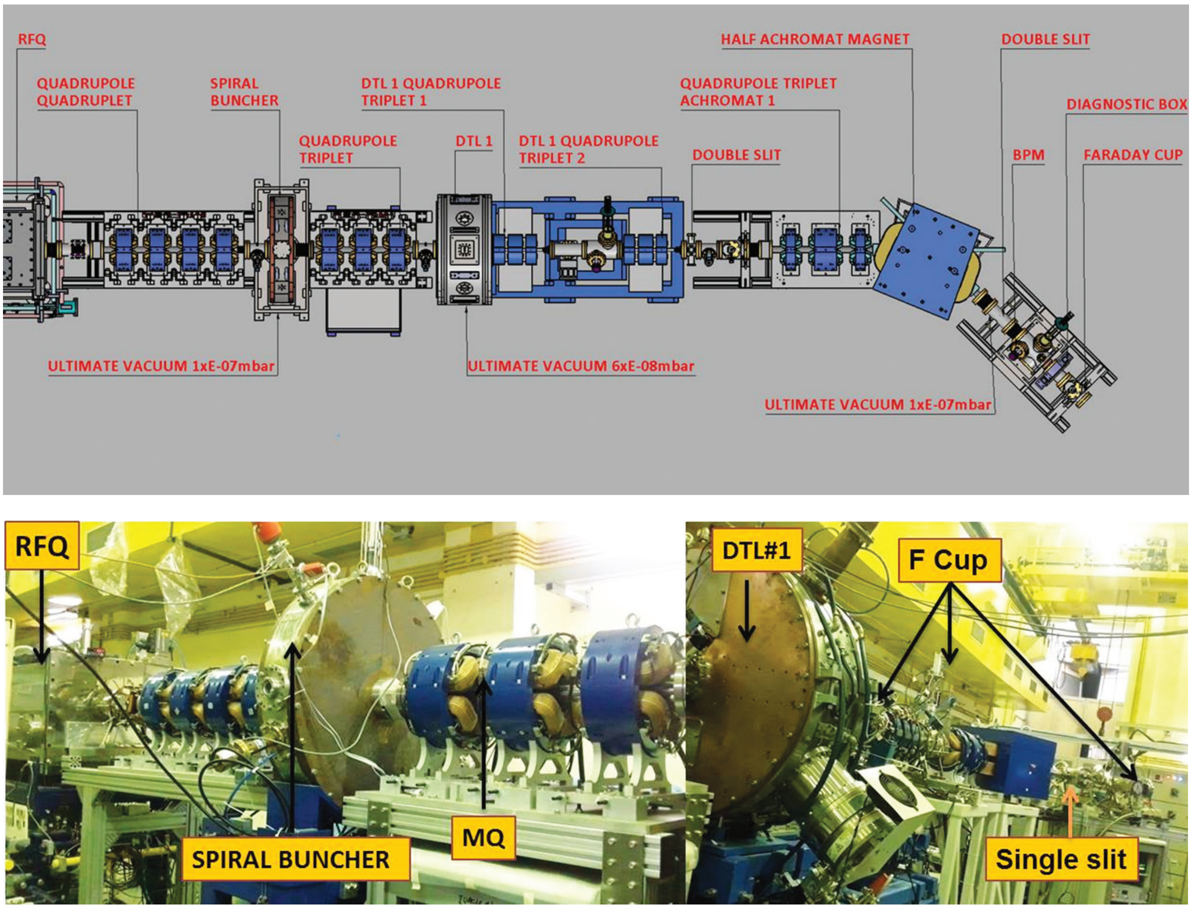

Figure 1: Layout and Installed Beamline for Testing Setup for HCI MEBT Components

The existing beam energy measurement setup was dismantled beyond four quadruplets section and Spiral Buncher -1 and DTL - 1 cavity have been installed in the HCI beamline as per final layout scheme of HCI. In the present configuration, DTL-2 cavity can be installed later without disturbing other installed components. The two DTL quadrupole triplets and beam diagnostics at required positions are also installed. The half Achromat section along with analyzed beam measurement set up have been shifted accordingly as per beam optics for this new configuration. Beam defining slits are also installed before and after the magnet. All the cavities and beam diagnostic elements are aligned within 50 microns of beam axis. All the beamline devices are interfaced with VME control crate for remote operation of devices. Four turbo based pumping stations with necessary interlocks are also installed and ~6 E-08 mbar of ultimate vacuum was achieved. The layout and the installed components are shown in figure 1.

3.1.1.2 LEIBF Maintenance and ECR Source re-Alignment

There was a major maintenance work in New LEIBF. The ECR source had some alignment problem. Dismantling of vacuum and other components like Einzel lens, vacuum pumps, vacuum valves and vacuum gauges etc. was done from the high voltage deck for maintenance purpose. Alignment of the source within 1 mm accuracy about the beam axis was done using theodolite with respect to available references and installed back all the components after completion of alignment work. Alignment of material science chamber and target ladder was checked and correction of both were done using available references. All log amps for diagnostic devices were tested for their proper operation and calibration was done for entire usable range using source meter. After completion of all the maintenance work, evacuation was done for ion source as well as beam line in proper phase and ultimate vacuum in the range of 5.10E-8 mbar was achieved.

3.1.1.3 Modification of GDA Beamline for DTL (Drift Tube Linac) Testing

To test DTL cavity with Pelletron beam in phase I, GDA beamline was modified, as per approved plan. Beam optics was carried out (by Dr. Rodrigues) and requirement of an additional quadrupole was seen as per optics. As per the new optics, layout of the beamline was modified with provision for additional quadrupole and DTL tank was position at the end. It was also ensured that regular GDA experiments would not be hampered due to this modification. The beamline was dismantled and fresh reference for beam axis was taken from switching magnet I. It was noticed that beamline quadrupole was off from beam axis and it required adjustment in alignment. We fabricated packing plates and realigned the quadrupole. The beam axis reference points were also transferred on the floor, wall and valves for future reference. The modification was completed and old position for GDA experiments was restored.

3.1.1.4 Design, Fabrication and Installation of Guide Rail Mechanism for Pelletron Ion Source.

Chandra Pal, A. Kothari, P. Barua, Rakesh Kumar, Jagdish Prasad

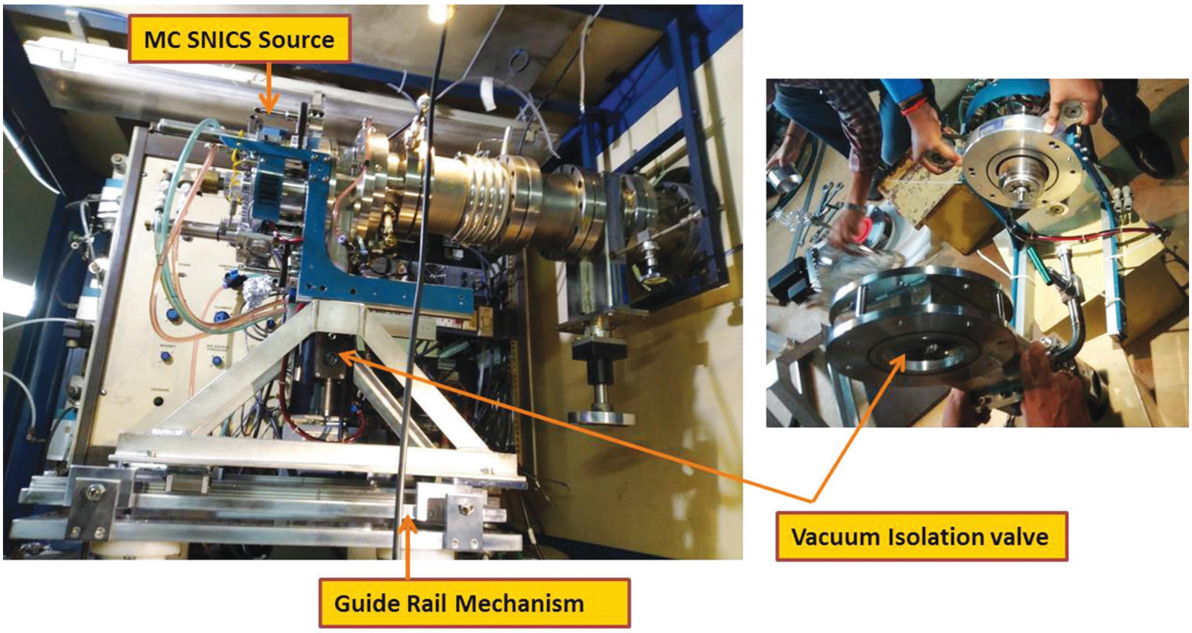

Figure 2: Ion Source with guide rail mechanism

Ion source of Pelletron is required to be opened for maintenance and in absence of proper fixtures rejoining it back with the system becomes very cumbersome. A guide rail mechanism for easy maintenance was designed, fabricated and installed for the same. The Ion source and other associated components were dismantled from the high voltage deck and the new guide rail mechanism was installed. After that the source and other components were installed and aligned within 0.2 mm of mating flange. The existing vacuum isolation valve was also replaced with a new one as the existing one was leaky. Tilting in Base plate of High voltage deck was observed during installation. After measurement nylon insulator was machined and installed on the deck plate. After installing the guide rail mechanism (as shown in figure 2), it is now quite easy to disengage the source for maintenance and can be easily connected back without any change in alignment.

3.1.1.5 Layout Design of FEL Beamline Test set up and Design of Components

Layout design of Initial part of FEL setup was done to finalize how the different components would assemble, their installation and holding fixture, alignment possibilities, etc. A 3-dimensional model of this beamline along with FEL components, brackets, stands, etc. was made. Photocathode chamber procured from vendor was vacuum tested for vacuum leak and ultimate vacuum. For this chamber new brackets were designed and fabricated for holding. Installation of vacuum pumps was done and thorough baking continued for few days to achieve 2×10^{-10} mbar vacuum. Design of mounting and alignment fixture for solenoid and cavity has been completed. Design of Laser Insertion chamber, Mirror mounting fixture and other necessary beam joining components was also completed.

3.1.1.6 Maintenance Activities

- Turbo Pumps failures and replacement work: The Turbo Pumps (5 nos.) installed on the Re-buncher, Super buncher, LEIBF switching magnet, HCI ECR source and spiral buncher were replaced due to bearing failure. A Varian make turbo pump (about 25 year old) installed on HIRA failed and stopped working. It was replaced with a turbo pump having pumping speed of 600 l/s. Turbo electronics failure happened in LINAC II and LINAC III so, alternate interlocks for operation of gate valve was made for normal operation. In due course of time these modules were procured and replaced.

- Vacuum problem due to Helium Leak in HYRA: Ion Pump 12-1 frequently tripped due to helium gas leak from experiment chamber side and Ion pump could not handle high helium load. So an additional turbo pumping station was connected to support the ion pump and beam run was completed.

- Thorough maintenance of GPSC Diffusion pump (2000 l/s) and rotary pump (175 m^3/hr) was done. Both the pumps were dismantled, necessary seals were replaced and all parts were properly cleaned. As existing pirani gauge (very old) had gone bad, so the interlocking logic in existing vacuum interlocking system for backing vacuum and gate valve was modified as per new gauge. After reassembly and integration of pump with the system, ultimate vacuum of 1.2 E-06 mbar was achieved.

- Getter Pump of 05 areas was cleaned and its cartridges were replaced. Ion pump of 05 areas got shorted, so new spare pump was installed. Ion Pump installed in material science beamline got shorted, so a new pump was installed, baked and then the magnet was installed after baking. During testing of the pump it was found that the controller of the Ion pump had also gone bad. It was replaced with a spare controller. Now the pump and controller are working fine.

- In Vault-1 area, through leak problem was observed in BLVL-02-1(AMS beam line). It was dismantled and repaired by changing the sealing sheet of internal bellow and installed back in the beam line and tested for through leak. No through leak observed.

- The existing beam line vacuum valve (30 yrs. old NEC make) of material science was not sealing properly. A series 48 all metal valve has been installed in its place and a PCB power box was fabricated and placed for its operation.

- IP 04 got contaminated. It was replaced with regenerated pump, followed by proper baking and leak testing procedures, required for vacuum.

3.1.2 Cryogenics Laboratory

Anup Choudhury, Joby Antony, Suresh Babu, Manoj Kumar, Soumen Kar, Santosh Sahu, Rajesh Nirdoshi and T.S.Datta

3.1.2.1 Developemental Activities

Anup Choudhury, Santosh Sahu, Suresh Babu and Manoj Kumar

(1) Oxford cryostat modification:-

There is a PPMS system from Oxford Instuments at IUAC whose measured liquid helium evaporation load is ~14 litres per day(lpd). It is planned to incorporate a cryocooler liquefier (developed at IUAC) to run the system which can make the system to be a stand alone facility. To reduce the static heat load of the Oxford cryostat, a new modified helium vessel was designed and fabricated with an additional nitrogen vessel attached to it, which will be later be integrated to the indigenously developed helium liquefier with GM Cryocooler. The new cold vessel has been tested and the evaporation of the liquid helium has been found to be 8 lpd. The measured evaporation rate of liquid nitrogen vessel is ~20 liters per day.

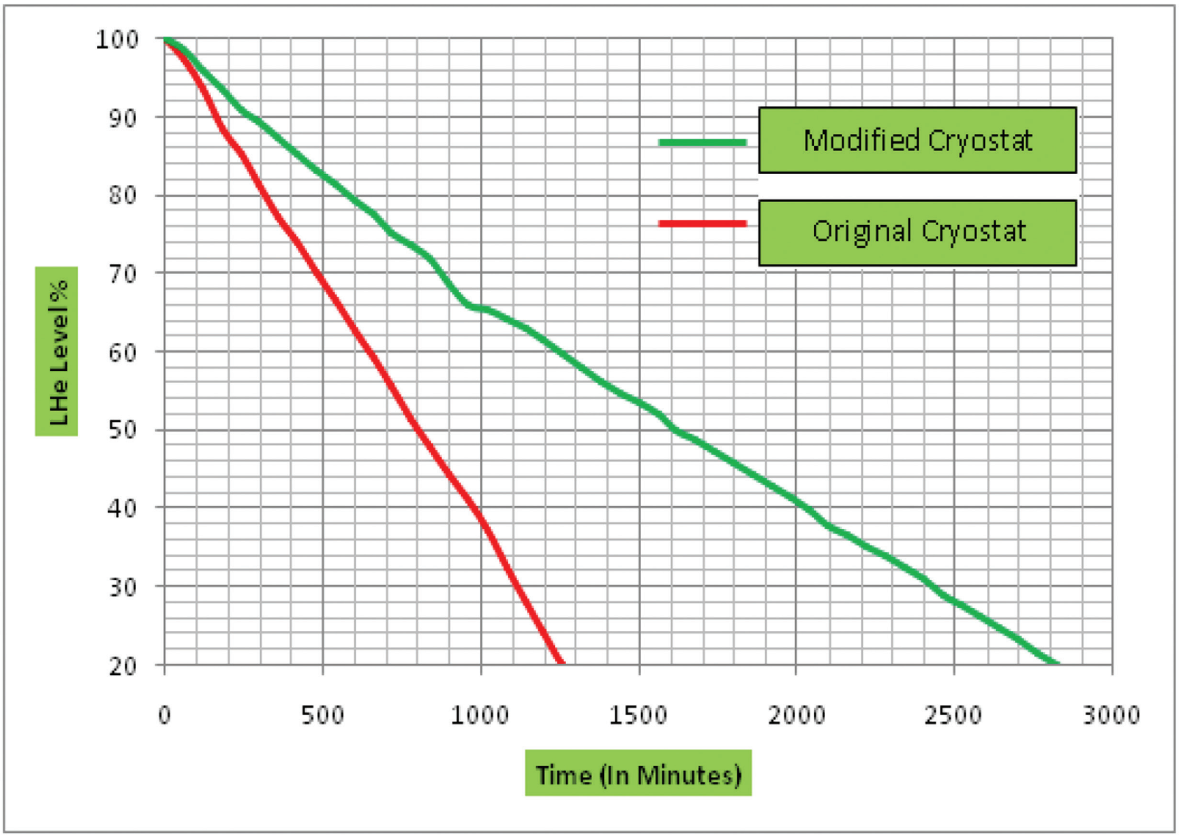

(2) Cryocooler helium liquefier with thermo-siphon :-

A helium liquefier study setup using a 1.5 watt at 4.2K Gifford Mac Mohan (GM) cryocooler has been developed at IUAC for understanding the heat transfer mechanism between the gas and the cryocooler surface at all the four stages of cooling. A thermo-siphon loop is added to the liquefier bottom with a heater to know the precise liquefaction rate under various study conditions. Inclusion of thermo-siphon loop reduces the consumption of helium gas by utilizing the evaporated gas in a controlled manner. The study setup has other capabilities to measure the liquefaction rate under various conditions such as varied pressure, with or without heat exchanger at both cooling stages, and with or without nylon shroud in the regenerator regions etc. The experimental setup is successfully put in place and preliminary experimental results have started coming in. A liquefaction rate of 17.4 liters per day (lpd) has been measured with the basic configuration.

3.1.2.2 Activities on Applied Superconductivity

A. Development of a whole-body 1.5T Superconducting MRI magnet system (MeitY-Project)

Soumen Kar, Navneet Suman, Vijay Soni, Sankar Ram Theketthil, Ajit Nandwadekar Rajesh Kumar, Santosh Sahu, Joby Antony, S. K Saini, Suresh Babu, Manoj Kumar, R.G. Sharma and T.S. Datta

Ministry of Electronics and Information Technology (MeitY), Govt. of India has initiated a multi-institutional project to develop a 1.5T superconducting MRI scanner in India. SAMEER, Mumbai is the nodal agency of the project. IUAC is one of the partner institutes for the project on indigenous development of the 1.5T superconducting MRI scanner. IUAC-MRI team is primarily responsible for the development of 1.5T superconducting magnet and ever-cooled or zero-boil off (ZBO) cryostat for the MRI scanner.

MRI magnet Bobbin

The mechanical design of the bobbin for the optimized EM design of the multi-coil MRI magnet has been completed with desired tolerances and surface finish for the winding pack of each coil. The weight of the bobbin has been optimized to ~ 600kg considering the electro-mechanical forces on the magnet during its operation. Figure 3.1.2.2.1 shows the integrated bobbin structure which is under fabrication presently.

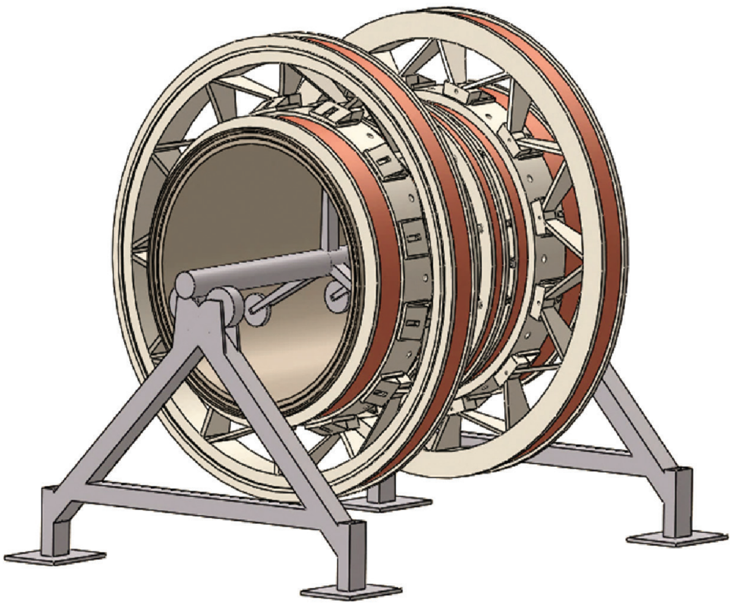

Figure 3.1.2.2.1 Integrated bobbin structure of 1.5T whole-body MRI magnet.

Helium Recondenser

The MRI magnet to be housed in a cryocooler based Zero-Boil-Off (ZBO) helium cryostat. ZBO is achieved by recondensation of the evaporated helium inside the MRI cryostat using a fin-based heat exchanger (HX) integrated with 4.2K GM cryocooler. A fin-based heat exchanger has been developed for characterizing the zero-boil-off technique to be used in MRI cryostat. Figure 3.1.2.2.2 shows the helium recondenser and its associated test rig. The ZBO performance of the HX has been tested up to 6 psi of operating pressure as shown in Figure 3.1.2.2.2(a).

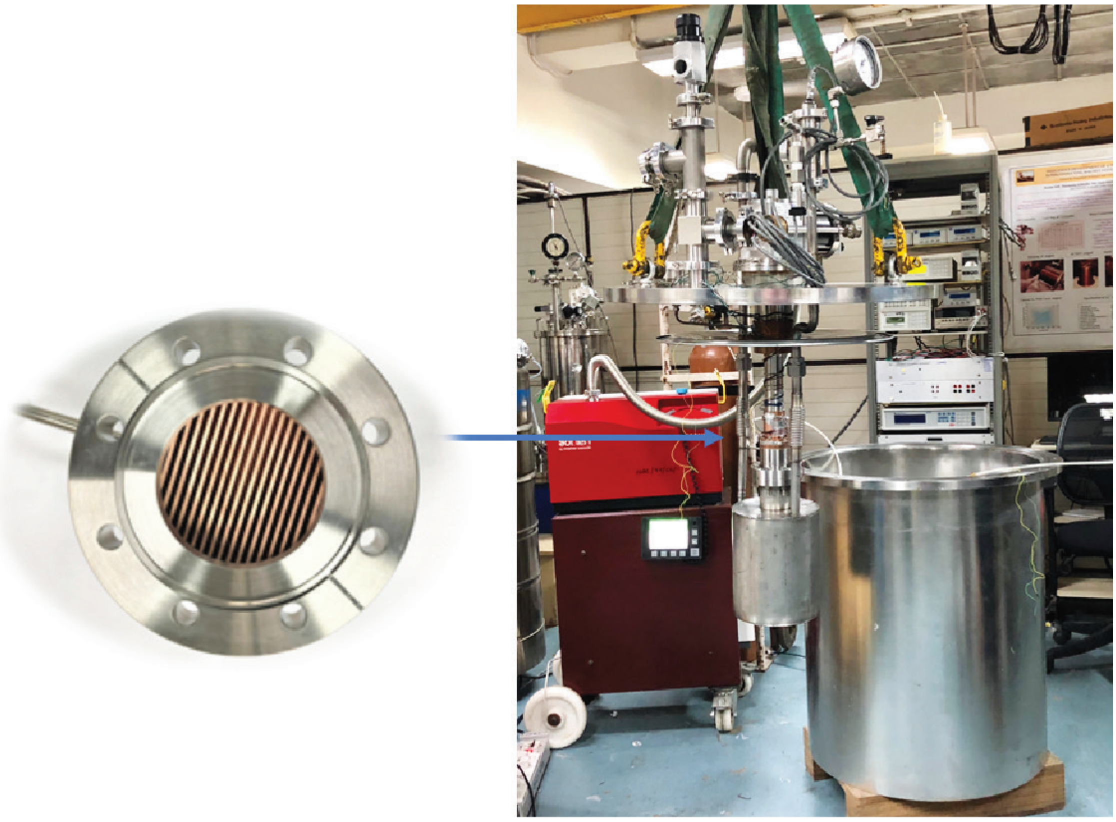

(a) (b)

Figure 3.1.2.2.1 (a) Fin based helium recondenser for Zero-boil-off MRI cryostat, (b) helium recondenser integrated bobbin to the cryocooler based test rig.

The pressure inside the helium bath of the MRI cryostat needs to maintain around the operating pressure of the MRI magnet. A PID based helium bath pressure stabilization scheme has been developed and tested in the cryocooler based test rig. Fluctuation around the set pressure of 1psi has also been studied as shown in figure 3.1.2.2.2(b). The fluctuation is found to be of the order of ± 0.03psi.

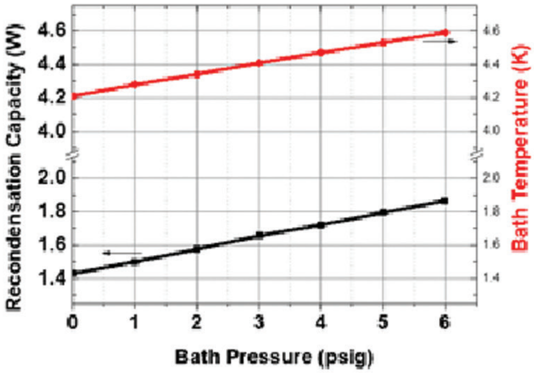

(a)

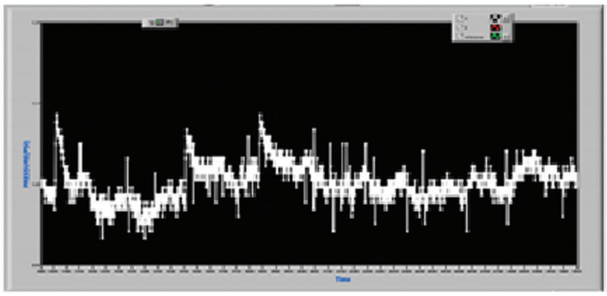

(b)

Figure 3.1.2.2.2 (a) Recondensation capacity of the fin-based helium heat exchanger, (b) fluctuation of helium bath pressure at 1 psi set pressure using PID based pressure stabilization scheme.

Persistent Current Switch (PCS)

The Persistent current switch or superconducting switch plays a very crucial role in the persistent operation of the MRI magnet. A superconducting switch of capacity 500A has been developed using CuNi-NbTi conductor for the main MRI magnet. Figure 3.1.2.2.3(a) shows the superconducting switches developed for the MRI magnet. The current carrying capacity and the switching performance of the PCS have extensively been studied using an in-house developed 4K test rig. Figure 3.1.2.2.3(b) shows the switching performance of the PCS. The transition time for the PCS is measured to be less than 10s.

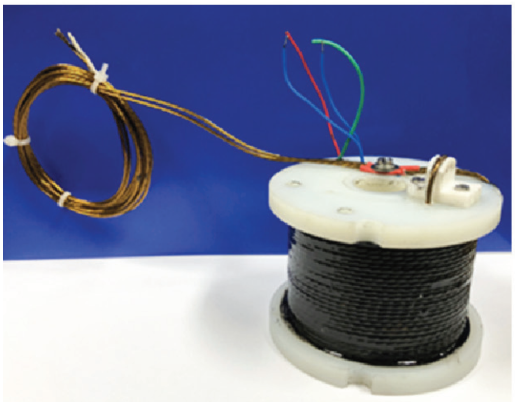

(a)

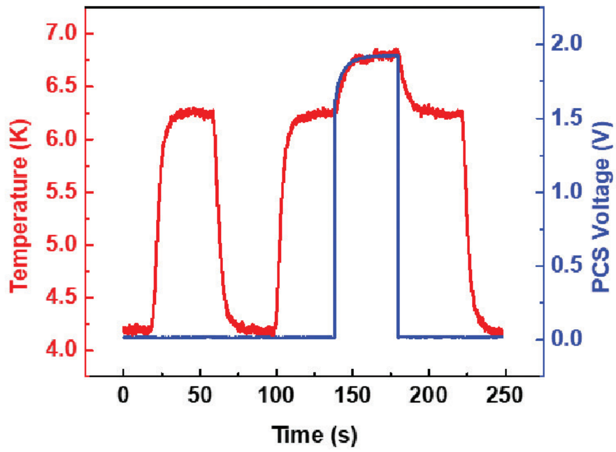

(b)

Figure 3.1.2.2.3 (a) Superconducting persistent switch developed for MRI magnet, (b) switching performance of the PCS.

Retraceable Current Lead (RCL)

Vapour cooled retraceable current lead is a crucial component of the MRI magnet. In an MRI magnet, the current leads are taken out after energizing the magnet at its operating current and park the magnet in persistent mode. A pair of vapour cooled RCL of capacity 500A has been developed using multi-lam based current contacts as shown in Figure 3.1.2.2.4 (a). The retractable mechanism and the current carrying capacity of the RCL have been tested at 77K in liquid nitrogen using an indigenous DC power supply (600A/10V). The electrical joint resistance of each multi-lam contact is measured to be 55 at 77K which corresponds 23mV voltage drop across each lead at 420A of operating current of the MRI magnet.


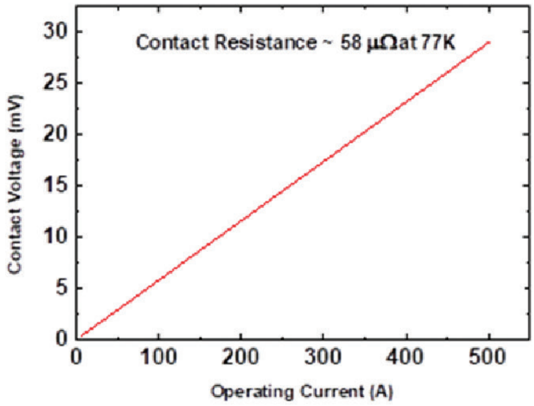

(a) (b)

Figure 3.1.2.2.4 (a) Multi-lam based retraceable current lead of capacity 500A,
(b) the I-V curve of the retraceable current contact (up to 500A current) at 77K .

Quench Protection Diodes

High power cold diodes play an important role in the quench protection system and quench propagation circuit for the MRI magnet. Selection of proper diode having current (forward) carrying capacity more than 500A is a crucial task during designing of the quench protection system using finite element analysis based OPERA-QUENCH code. V-I characteristics have been done for various types of high power diodes at RT, 77K, and 4.2K. Figure 3.1.2.2.5 (a) shows the V-I characteristics at RT and 77K. Figure 3.1.2.2.6 shows the V-I characteristics of cold diode at 4.2K. The forward voltage is measured to be 7.9V at 4.2K as shown in figure 3.1.2.2.6.

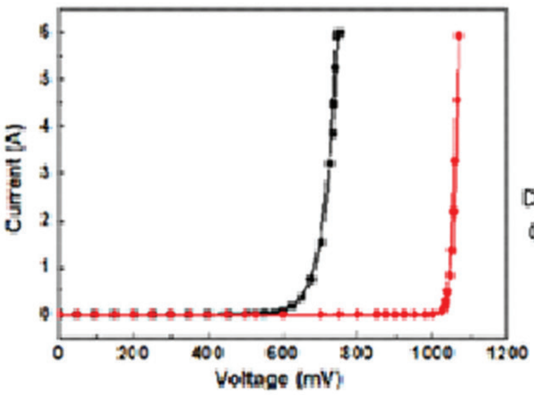

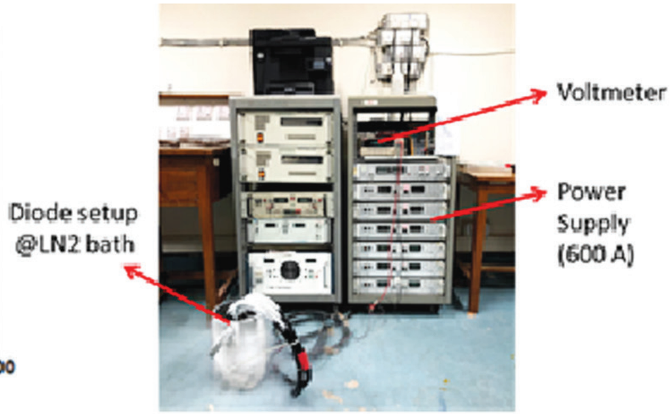

(a) (b)

Figure 3.1.2.2.5 (a) V-I characteristics of the cold diode at RT and 77K,
(b) test rig for characterizing the diodes with 500A at 77K.

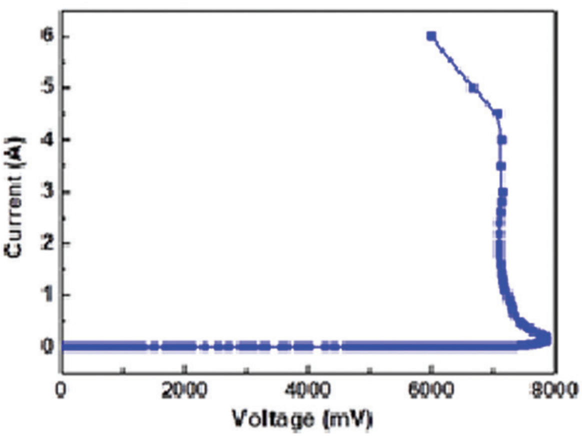

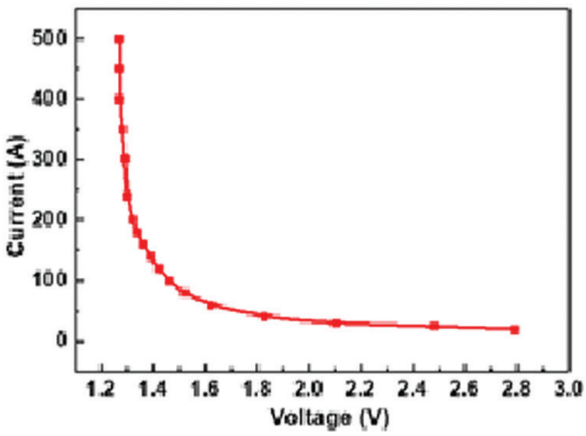

(a) (b)

Figure 3.1.2.2.6 (a) Forward voltage characteristics of high power cold diodes at 4.2K,
(b) the forward voltage characteristics of high power cold diode at higher operating current (up to 500A) at 4.2K.

B. Characterization of 2G High-temperature Superconducting tape for Modular Superconducting FCL application (CPRI-Project)

Soumen Kar, Reetu Bharti, Rajesh Kumar & T.S.Datta

A R&D project on "Characterization of 2G high temperature superconducting (HTS) tape for modular superconducting fault current (SFCL) application" funded by CPRI, Bengaluru is at the final stage of completion. An electrical test rig has been developed using a 60V/300A transformer and an indigenously developed fault generator and controller. The schematic of the experimental set up is shown in figure 3.1.2.2.7(a). The fault generator is developed using high-power thyristor having capability of generating fault up to 12 cycles. The maximum fault current has been generated up to 4kA at 60V_{rms}. The resistive load of the circuit determines the nominal current through the SFCL during normal operation. Various configuration of modular unit has been developed, as shown in figure3.1.2.2.7(b), for their electrical characterization as modular unit.

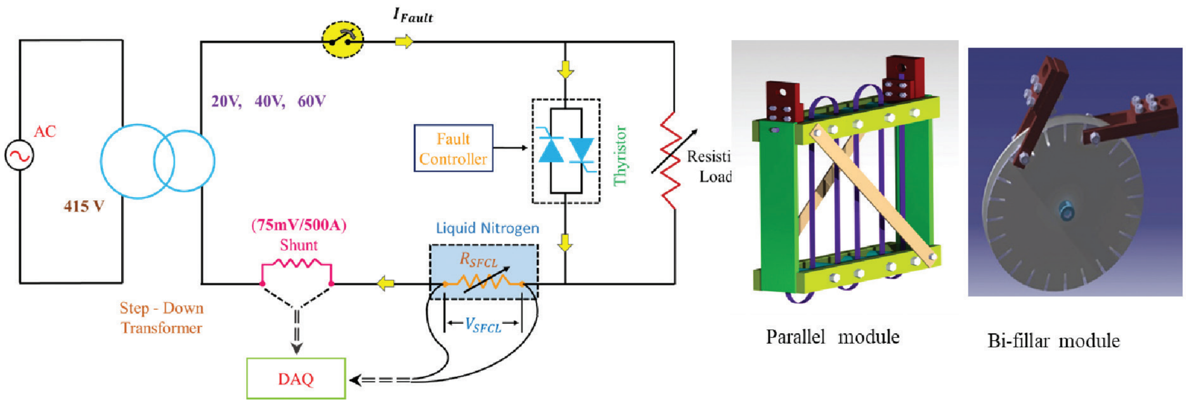

(a) (b)

Figure 3.1.2.2.7 (a) The schematic of the test rig for characterizing modular SFCL units at 77K, (b) Various configuration of modular SFCL unit; parallel module and bi-filler module.

SFCL modular unit has been tested with two types of 2G HTS (YBCO) tapes: copper laminated HTS tape and SS-laminated HTS tape. Figure 3.1.2.2.8(a) shows the current limiting capability of the modular SFCL unit with copper laminated HTS tape at 20, 40 and 60V_{rms} for five cycles (100ms). The perspective peak fault currents (without SFCL) are 1.8kA, 2.8kA, and 4kA respectively for 20, 40 and 60V_{rms}. During fault, the voltage growth across the SFCL is shown in figure 3.1.2.2.8(b).

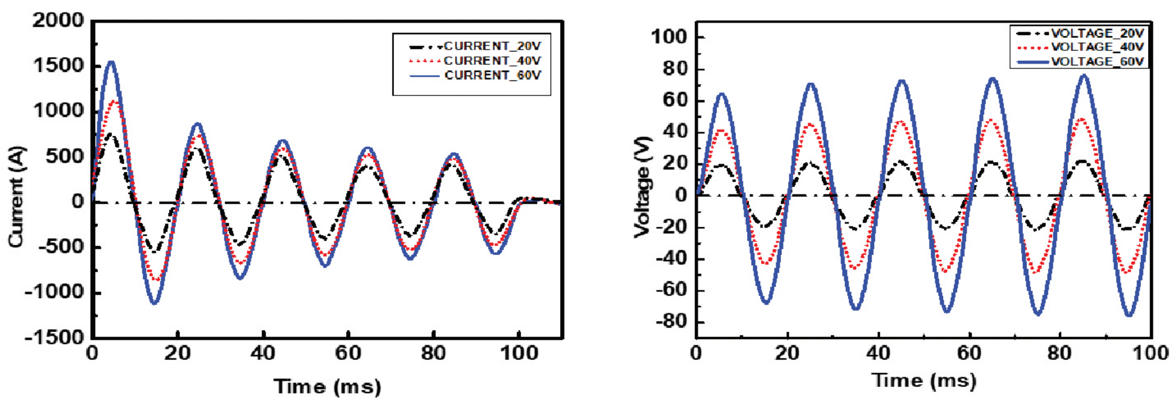

a e

Figure 3.1.2.2.8 (a) Fault limiting behavior of modular SFCL unit made of copper laminated 2G HTS tape, (b) the voltage growth across SFCL unit during fault at 20, 40 and 60V_{rms}.

The perspective peak fault currents (without SFCL) are 1.8kA, 2.8kA, and 4kA respectively for 20, 40 and 60V_{rms}. During fault, the voltage growth across the SFCL is shown in Figure 3.1.2.2.8(b). The thermal profile of the HTS tapes has been studied during fault and recovery stage as shown in Figure 3.1.2.2.9(a). It takes ~ 1.8s to recover its normal operation after fault as shown in its thermal and voltage profile (figure 3.1.2.2.9).

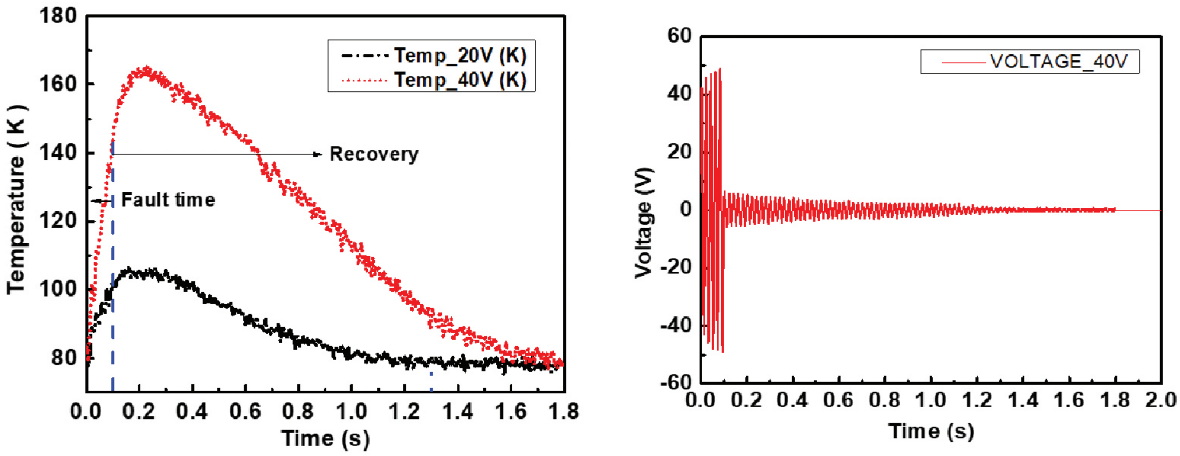

(a) (b)

Figure 3.1.2.2.9 (a) The thermal profile of the copper laminated 2G HTS tape in a modular SFCL unit, (b) The voltage recovery curve.

Similar characterization has also been done with SS-laminated 2G HTS tape in modular SFCL unit. Figure 3.1.2.2.10 (a) shows the fault limiting behavior of the SS-laminated 2G HTS tapes at 40V_{rms} for various length of the superconductor. Post-fault recovery is much longer (~ 8s) as shown in Figure 3.1.2.2.10 (b). This recover is under-load condition.

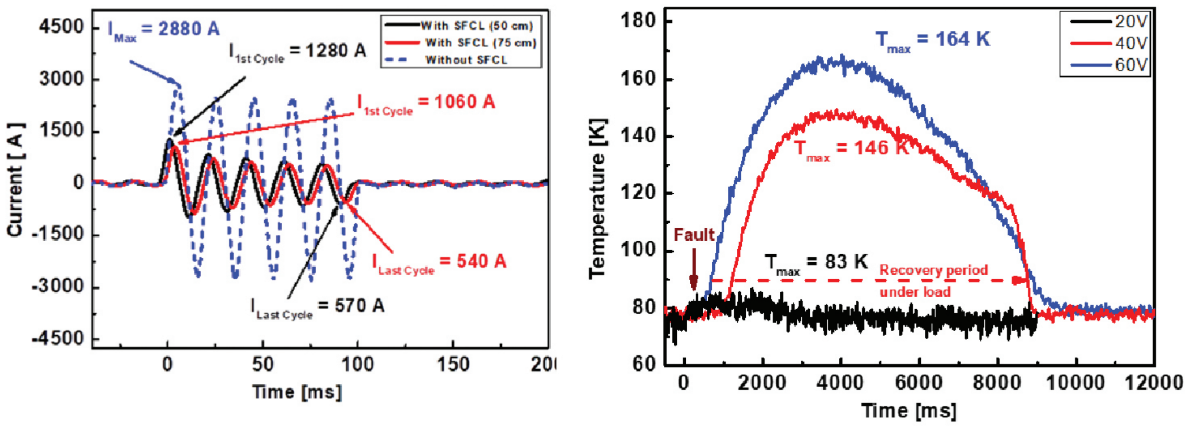

(a) (b)

Figure 3.1.2.2.10 (a) Fault limiting behavior of modular SFCL unit made of SS-laminated 2G HTS tape, (b) thermal profile of SS-laminated 2G HTS tape in modular SFCL unit during fault and recovery.

3.1.2.3 Electronics for Cryogenics and LINAC: Lab activities

Joby Antony, Rajesh Nirdoshi, Anup Choudhury, Manoj Kumar, Suresh Babu, Soumen Kar and T.S.Datta

a) CRYOGENIC CONTROL SYSTEMS

The IUAC Cryogenics control room has been operational in continuous working mode. The control systems were used this year mainly for the off-line LINAC test runs. At present, the control room has the following computer control systems in place .

i) CADS

CADS is the Ethernet based Crate-less model of completely indigenous Cryogenic control system with indigenously built cryogenic meters and control hardware (together called device-servers) built for LINAC Cryogenic distribution systems. This system has in-house designed intelligent Cryogenic device-servers/ instruments (i.e. Cryogenic sensor nodes and actuator nodes) which is designed with a total of 72 embedded device-servers (on-chip HTTP servers), interconnected over Ethernet (LAN). The networked distributed control system survived to work for the closed loop control operations of Cryogenic distribution system components where the control loops run every second for PID & data logging and control operations. Based on the operational experience, in-situ modifications are planned for next year while considering the hardware redundancy.

i-a) FIRST PHASE UPGRADE OF CADS FOR REDUNDANCY

It has been decided to build a parallel low cost redundant commercial version of hardware, in additional to the indigenous ones, only for the critical LHe and LN_2 refill systems. This has 10 channels of PID controllers switched using PID Switcher Unit. The unit can select between any one of the indigenous IUAC make devices or commercial meters in case of emergency. This can save time due to hardware failures during an experimental run. Therefore the upgrade is planned in two steps. The first phase upgrade consisted of procuring ten such commercial PID controllers which completely suits to our linac refill needs and interconnect them to build remote control & DA software over Modbus protocol. Our team tried out two different low cost microprocessor based PID controllers from the market. The first one is Honeywell make DC1040CL30200BE model and the second one is Fuji make PXF9AEY2FVM00 model. Both these controllers were initially tested for the suitability with our off-line LINAC application which used our own home-built software specially made for this application. The control GUIs and back-end control programs were developed in-house using Labview. After thorough online and offline mode tests, Honeywell make DC1040CL30200BE model was rejected due to lack of remote changeover options from manual to auto in critical situations. Therefore Fuji PXF9AEY2FVM00 device has been chosen for 5 LN_2 and 5 LHe devices. This year we restricted the control GUI development for one single channel (figure 1). We will take up the 10 channels version with multi dropped RS485 via Modbus for control & DA GUI development next year. The basic functional block diagram is shown in figure 2.

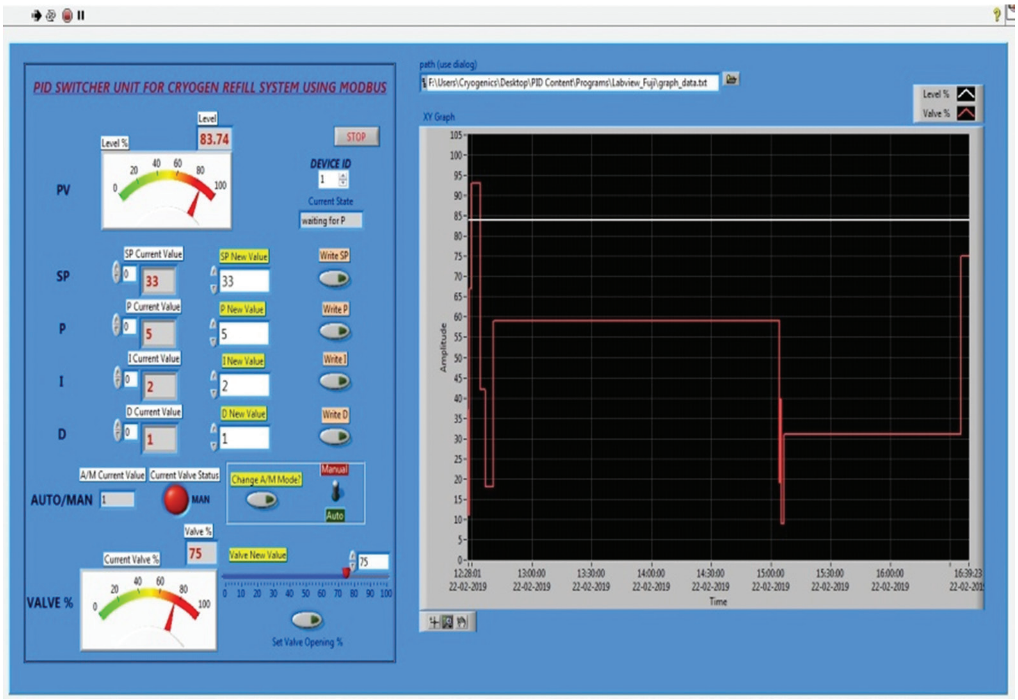

Fig 1: Single channel GUI system tried out using Modbus protocol of PID controllers

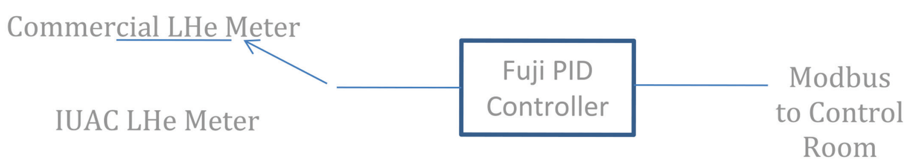

Fig 2: Block diagram of single channel switcher unit

ii) CRYO-DACS

The second control system, CRYO-DACS, is a VME system which was installed in the year 2002, currently running only for all the LINAC temperature monitoring and logging operations. Considering aging risk of this VME CPU and systems, a second phase upgrade is planned to replace VME system with low cost crate-less technology.

ii-a) SECOND PHASE UPGRADE OF CRYO-DACS

It has been decided to take up the second phase later this year to replace CRYO-DACS system (VME + software) by indigenous temperature meters with RS232 interface as well as commercial Lakeshore meters together (one to one replaceable with IUAC temperature meters) with compatible RS232 command set. This means that there is a requirement to newly design a large number of cryogenic monitors (up to 4.2K) which have the similar command set of RS232. So, hardware and firmware design process has been initiated and would need at least 10 new temperature monitors compatible to Lakeshore but each with 5 channels. This will help to interconnect these meters and eliminate expensive VME crate to control room. All the first and second phase upgrades would need a lot of firmware and software developments as we need to build our own devices compatible with commercial ones.

b) DEVELOPMENTAL ACTIVITIES

i) LV FPGA based Fast DAQ System for MRI Project

A fast RT FPGA based fast data acquisition system is developed this year for the undergoing MRI project. The work involved fast data acquisition and logging for MRI monitoring and controls. The control hardware includes fast differential ADC, DAC, Digital I/Os, RS232 modules etc. The first level version 1.0 of software development is completed. The system used NI cRIO backplane with Labview FPGA as the base development system. The RT scanning will be at the rate of 1 millisecond per channel and the data storage will account to huge GBs per day.

The block diagram of the system is shown in figure 3.

The following are some of the required features of the fast DA system that can capture and record various fast activities inside MRI.

Time resolution of each data monitored & recorded has to be 1 millisecond

- Analog inputs can go to 1mS high voltage spikes (+/- 2000 Volts inside)
- cRIO FPGA Platform (figure 4) is used, Programming language is Real Time Labview®
- cRIO (Compact RIO) has an FPGA which can be programmed to make a final bit file similar to other FPGA technologies.
- RT Labview with FPGA library can use VHDL inside. All Xilinx tools are inside.
- 24 bit fast ADCs can connect to Blank FPGA backplane but Blank FPGA has to be programmed to create a digitizer, similar to other languages.
- FPGA is programmed to create a program which runs on a remote target – for fast digitizers

MRI Fast Data Acquisition System has been developed for multichannel digitizers with 1 millisecond time resolution. Following are the specifications of the hardware used.

✓ NI cRIO-9035 (Embedded Compact RIO Controller with Real-Time Processor and Reconfigurable FPGA)

✓ C-Series Modules: NI 9229 (4 AI, ±60V, 24 Bit, 50 kS/s/ch Simultaneous), NI 9375 (16 DI/16 DO, 30VDC)

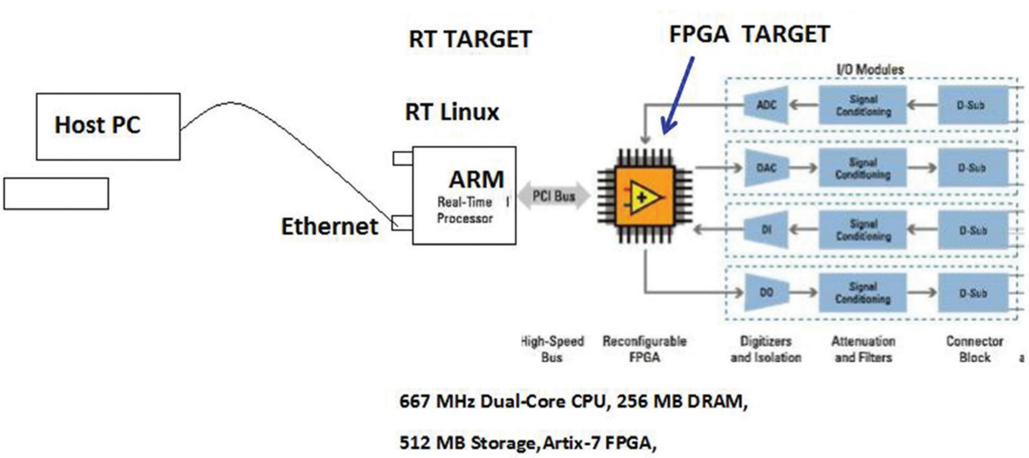

Fig 3: The internal architecture of cRIO based system

Fig 4: The FPGA based cRIO hardware for fast MRI DA system

The main signals of MRI system are:

a) Fast quench high voltages across coils (1 millisecond resolution)
b) Many low temperatures (> 4.2K)
c) Pressures
d) Cryogen Levels
e) Vacuum, fast interlocks

The GUI of MRI fast DA system is shown in figure 5.

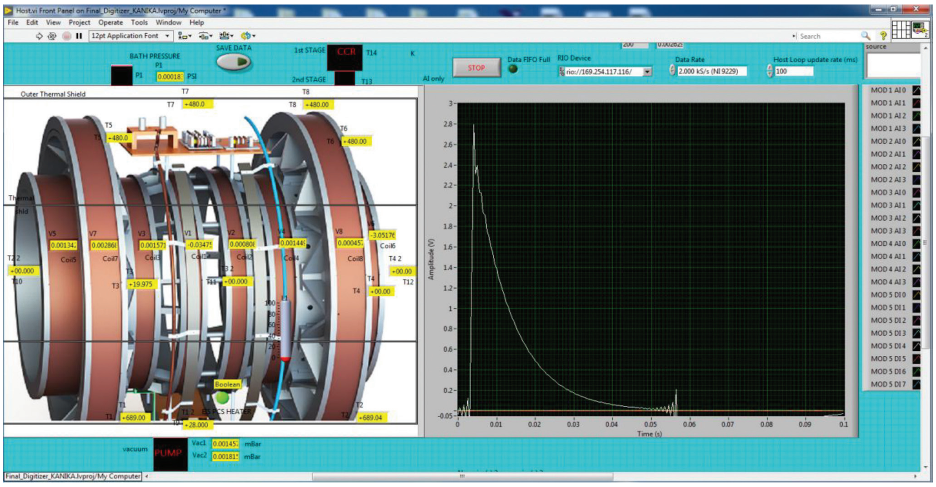

Fig 5: The GUI of MRI system

The simulated sampled/captured data of one of the 40 channels of MRI (One channel off-line test using a function generator) is shown below in figure 6.

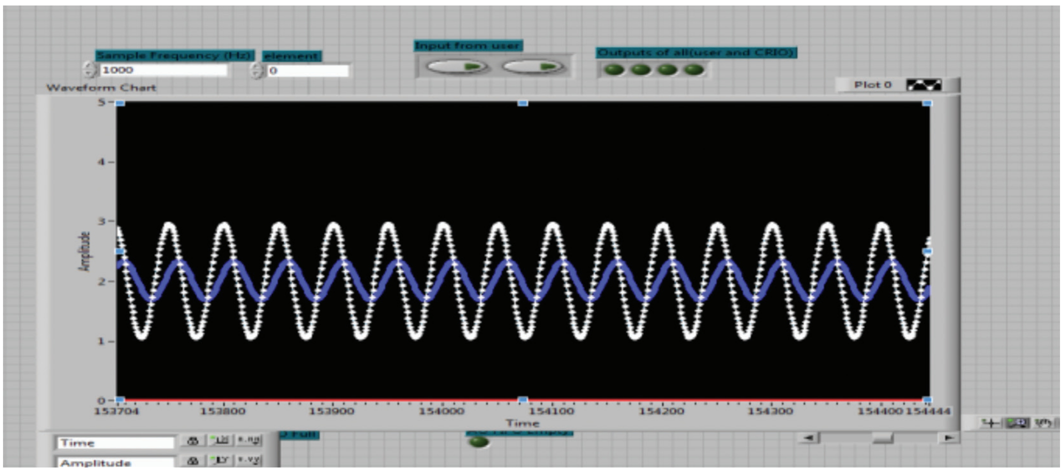

Fig 6: The fast sampled signals at the quench inputs reproduced on PC screens

ii) MRI Chamber-Constant Pressure PID Regulator using IUAC PID DEVICE

In order to maintain constant pressure within the MRI chamber, an indigenous device called "MRI PRESSURE REGULATOR with USB" has been designed (figure 7) and developed in-house to test and study the MRI pressure regulation in a simulated chamber. The USB data logger logged the data with respect to time. The following is the block diagram, data regulation test results at 1.5 PSI, 2.0 PSI and 3 PSI which achieved +/- 0.05 PSI stabilization. The figure 8 and 9 demonstrates some test results.

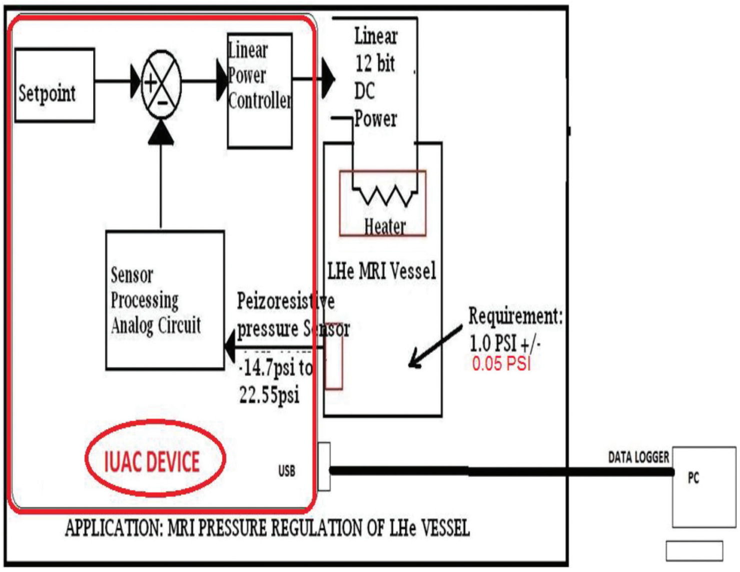

Fig 7: The indigenous MRI Pressure regulator meter system with interface

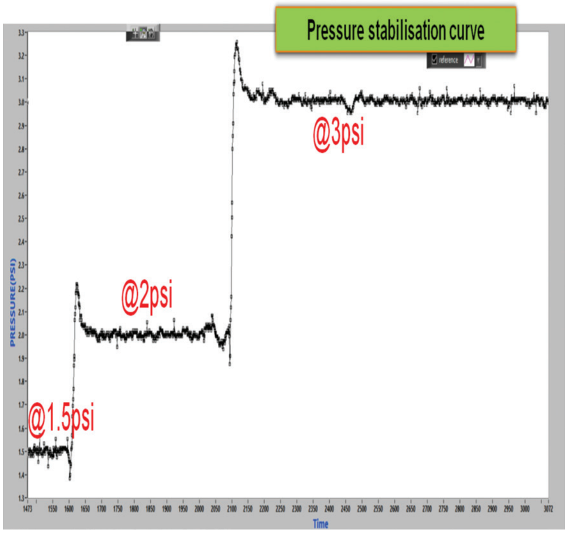

Fig 8: The indigenous MRI Pressure regulator regulated MRI chamber pressure in ramp up mode

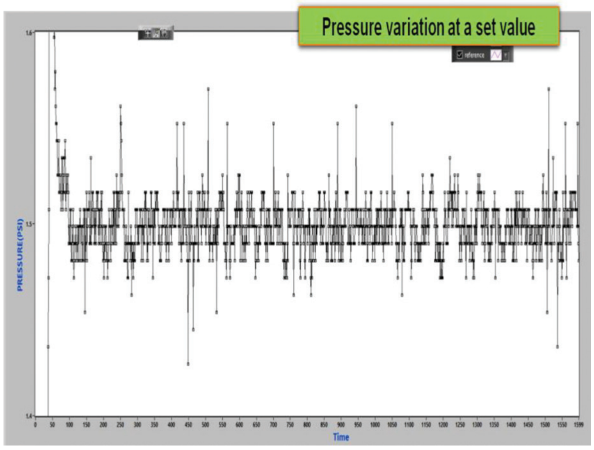

Fig 9: The PID regulation test results within +/-50mK

All the above hardware designs were based on an IUAC 32 bit MCU board (figure 10) which is designed indigenously using ARM processor.

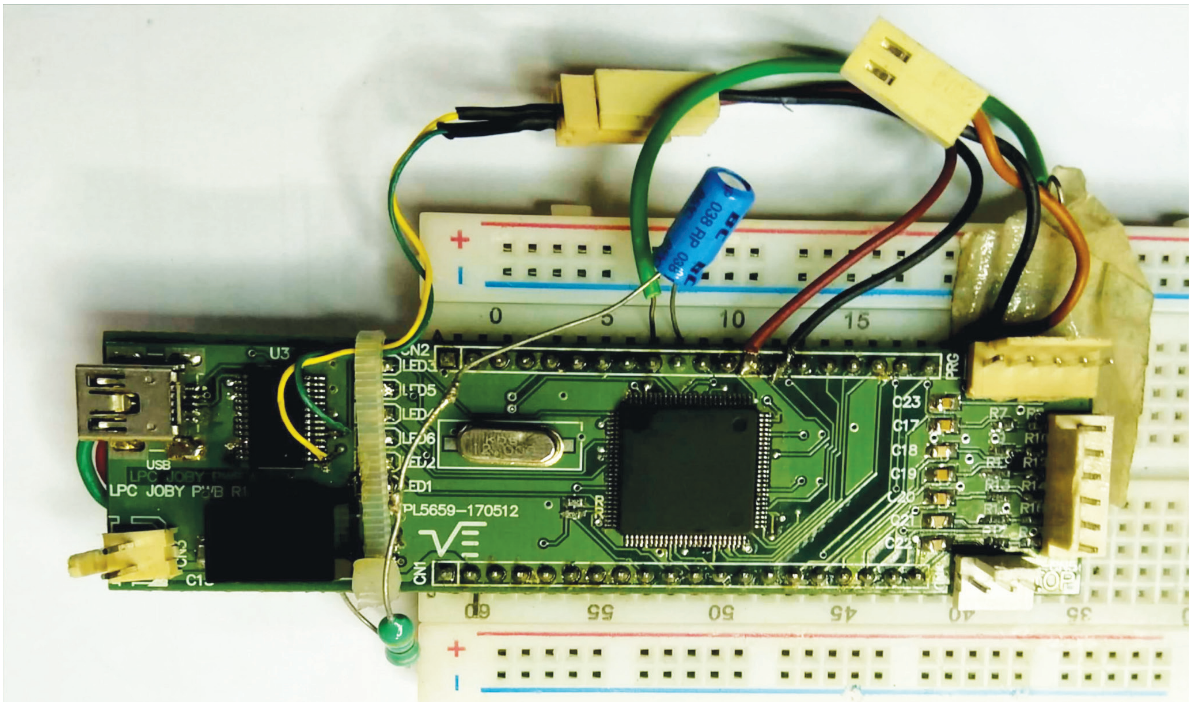

Fig 10: The IUAC MCU board designed for all developments using ARM processor

iii) PID based TEMPERATURE CONTROLLERS DEVELOPMENT

Device made for	Requirement	Range	sensor	Till now measured/achieved	Comment	Data logger in USB
MRI	**+/- 0.1 Bar**	**+-1 Bar to +3 bar**	**peizo resistive**	**+/- 50 mBar**	**Full range measured**	**USB Yes**
Low Temp Lab	**+/- 0.1 K or better**	**40K to 350K**	**Pt100**	**+/- 1K**	**Partial range measured**	**USB Yes**
Photoluminescence	**+/- 1 K**	**77K to 350K**	**Si diode**	**+/- 1K**	**Partial range measured**	**Ethernet software needed extra, not yet done**
NAND	**+/- 1 millibar**	**1-100 mBar**	**inbuilt**	**+/- 1 millibar**	**Full range measured**	**USB(win) version done, Ethernet interface with linux Qt not yet done**

Fig 11: Comparison of instrument calibrations

A number of low cost, low precision PID based temperature controllers with dc power outputs have been built to regulate Pressure, Temperature, Photoluminescence setup, NAND etc. where the requirements were different. However, since every device used PID for regulation, a comparison has been made based on test results of instrument-only-calibrations which are listed below. An online instrument calibration will be done in the future to verify the results in figure 11.

iv) An AC Susceptometer demonstrations on National Science day and at University

Joby Antony, A.K. Rastogi and K. Asokan

A prototype AC Susceptometer built at IUAC was demonstrated to various students at IUAC on National Science day and also at a conference at Cochin university of Science and Technology.

The AC susceptometer is used to study the magnetization induced in various magnetic materials in response to AC magnetic fields inside a driven solenoid. The indigenous list of parts for this experiment include LN_2, AC function generator, AC current source, two-phase lock-in amplifier, embedded Pt100 temperature sensor, computer data acquisition system with YBCO and Gadolinium samples. The major difficulty faced in the development of such a system is the noise contained in measurement, as the noise is approximately 1000 times more than the signal because of which we used digital DSP lock-in amplifier techniques to extract the AC signal.

In the second successfully tested experiment with our indigenous device, when YBCO sample is cooled to LN_2 temperature, the device gives negative diamagnetic signal and when temperature of the sample rises above 93 Kelvin, diamagnetic signal becomes zero.

v) An additional Gas Flow Processor hardware for NAND:

Joby Antony, Rajesh Nirdoshi, R. Saneesh, P. Sugathan

Regulated gas flow through a detector system (0.0 to 99.99 Torr) with an accuracy of the order of +/- 1 milliTorr was made last year and has been duplicated as a spare piece this year using this indigenous device. The remote control software development requirement using USB will be taken up next year.

c) IFR (INDIGENOUS FABRICATION OF RESONATORS) RELATED ACTIVITIES

Joby Antony, Rajesh Nirdoshi, Kishore Mistri and P. N. Prakash

This set of people are responsible for the complete maintenance of the electronics in the facilities used for fabricating SCRF resonators indigenously. This includes the Electron Beam Welding machine (EBW), Surface preparation lab automation and high vaccum furnace.

This year there were two issues related to EBW machine
i) Electrical cabinet FAN failure issue
ii) Pumping system valve sensor failure

The first issue was solved by replacing the failed FAN with a new one and second issue was solved by repairing the sensor contacts which got stuck.

d) OTHER ACTIVITIES

Other activities of the lab include the regular Electronics Apprentice training and management, conducting regular exams, evaluations (at present 3 electronic apprentices), B.Tech summer internship projects etc.

3.1.3 Beam Transport System (BTS) Group

The Beam Transport System (BTS) group is a central support group, which is responsible for the upkeep of the BTS Magnet Power Supplies (MPS) and associated instruments of all the accelerator facilities at IUAC. More than 100 numbers of current regulated high stability magnet power supplies are in round-the-clock operation. The group performs yearly scheduledpreventive maintenance of all the BTS instruments to ensure breakdown-free operation with optimum performance every year. During beam operations the group members are available 24x7 (on-call) to investigate the causes (if any) for beam trips due any BTS instrument. As an additional responsibility, the group also performs the preventive maintenance and repairs of Detector Bias HV power supplies, a large number of which are used in the experimental facilities. Besides maintenance and repair activities, the group is also involved in design and fabrication of BTS-MPS power supplies and LLRF based control instrumentation for the upcoming High Current Injector (HCI) Facility. The yearly activities related to BTS maintenance and development are summarised below.

OperationalStatus Report of Beam Transport System

The overall uptime of the beam transport system magnet power supplies has been recorded to be more than 99% this year. All the power supplieshave met the required expectation in terms of stability. There has been no major breakdown which may result in considerable loss of beam time. However, there were random trips of the power supplies due to corrosion in the fuse holders of the transistor banks. In some occasions the power supplies have failed or have been down due to problems in the associated systems such as water, electricity and remote control. Failure logs of the power supplies have been maintained over the period to decide upon the required actions to be taken during scheduled preventive maintenance. The beam line selection system (motorised electromechanical switches) has been out of operation due to corrosion since the last few years. Presently the beam line selection is done manually connecting the magnets of the selected beam line to the corresponding power supplies. Purchase of new motorised switches to replace the corroded ones has not been initiated until the problem of corrosion is completely resolved.

Preventive Maintenance

Maintenance Schedules: The BTS at IUAC consists of large number of high performance and high current power supplies along with other BTS associated instruments. It is not possible with the limited manpower to conclude preventive maintenance of such a large system in one month (annual schedule). The effects of corrosion on the stability and performance of power supplies has also been observed in the last few years. Because of corrosion, preventive maintenance has become more intense and time-consuming.

To allot enough time for each instrument for ensuringreliable service, maintenance activities have been spread throughout the year. The total BTS has been divided in zones. The Pelletron zone is maintained during scheduled maintenance of the Pelletron. Maintenance of other zones (Linac, HIRA-HYRA, Low Energy, RBS, HCI) are scheduled as per availability of access any time of the year. At present (till the HCI is operational), all the facilities are not working simultaneously. So it is possible to maintain all the facilities throughout the year.

Maintenance Activities: Proven maintenance procedures, which have been finalized on the basis of past experience, are followed to standardise the activity and in turn to ensure high quality of service. A few corrosive components in the power supplies have resulted in reduced reliability. The silver alloy coated fuse holders are the worst affected parts. These were replaced with the new silver alloy coated fuse holders in some of the power supplies two years ago. But the problem has resurfaced. It has now been decided to replace the silver alloy coated fuse holders with nickel coated fuse holders, as nickel is less reactive. The fuse holders of all the Pelletron-BTS power supplies have been replaced this year.

Repair of Faulty Power Supply Modules: The faulty electronic modules, which are identified and taken out during preventive and break-down maintenance schedules, are repaired at the BTS lab. Instead of importing spare power supplies, the faulty modules are repaired in-house to replenish the stock. The effort has reduced the running costs of the BTS system drastically. For the instruments developed in-house, the spares are also fabricated in-house. The following electronic modules have been repaired this year:

- Power supply control module: 04 nos.
- Auxiliary power supply module: 02 nos.
- Regulation module: 01 nos.
- IGOR interface module: 03 nos.

Procedures of Preventive Maintenance: The power supplies undergo high level of examination, monitoring and maintenance procedures. Test Report Proforma (TRP), containing the maintenance procedures, have been prepared for every type of power supplies to standardize the maintenance procedures. Before initiating the preventive maintenance, the condition of each power supply has been assessed by noting down the following in the TRP – visual inspection, AC/DC voltage measurement of different test points and measurement of temperature. Analysis of these data helps to conclude the required actions for preventive maintenance.

Preventive Maintenance and Repairs of Detector HV Bias Supplies

Under the yearly maintenance activity, the detector HV bias supplies of the following experimental facilities have been serviced and tested for optimum performance and safe operation:

Indian National Gamma Array (INGA): A total of 60 bias supplies of three types (5 kV, 3 kv and pre-amplifier) have been cleaned, serviced and tested at the BTS Lab. These power supplies were developed by the BTS Group in 2006 and have been in operation since then in the INGA experimental facility. These power supplies have been immersed in ultrasonic bath using LR grade alcohol which has been proved to be very effective. The racks housing the detector bias supplies in the beam hall have also been repositioned to have better access for monitoring and servicing.

National Array of Neutron Detectors (NAND): All the neutron detectors of the NAND experimental facility are biased using power supplies developed in-house. All these power supplies have also been serviced and tested in the lab to ensure optimum performance and trouble-free operation during experiments.

Steps Taken to Improve the Functioning and Preparedness of the Laboratory

Breakdown repair is always accorded the highest priority (round the clock) to ensure minimum loss of beam time. The following steps have been taken to ensure quality of preventive maintenance and to improve the in-situ repair capabilities of the available manpower:

- All the service manuals of in-operation instruments have been kept updated and revised.
- A test proforma has been prepared for each type of BTS instrument to standardise the maintenance procedures.
- The laboratory has been rearranged to maximize the working area for maintenance activities.
- Critical maintenance processes and implicit knowledge has been identified and documented.
- Jigs and set-ups have been developed to repair faulty modules which are kept ready for future use.
- Limited quantities of spare cards have been stocked.
- Spare parts have been stored in designated places for easy and fast access.

Academic Support Activities

The BTS group has provided / participated in the following academic support activities this year:

1. Developed a HV (3 kV / 100 mA) power supplyfor HCI-ECR source extractor.
2. Developed a HV (2 kV / 5 mA) power supply for HCI-fast Faraday cup biasing.
3. Participated in designing the low impedance grounding scheme for the HCI facility.
4. Participated in designing the cooling water layout for the instruments and RF cavities of the HCI facility.
5. Repaired power supplies for other labs of IUAC and other institutes:
    - Vacuum deposition unit e-gun power supply (6 kV / 1 A) of Target Development Lab. of IUAC.
    - Super-conducting magnet power supply of SQUID-Magnetometer of IIT Delhi.
    - Vacuum Tube based RF Amplifier of HCI-RF cavities of IUAC.
6. The BTS group is actively involved in the development of MRI magnet with the Applied Superconductivity Group and has participated in the following works:
    - Provided high current sources (500 A) and helped in setting-up test set-ups to characterise quench protection components, superconducting joints and persistent switches at 4.2 K.
    - Designed and delivered a controller for MRI-EIS coil persistent switch.
    - Participated in the design of MRI magnet quench protection schemes and magnet powering sequences and protections.

In-house Development of Power Supplies

If all the BTS magnet power supplies are imported, there will be large number of different types and makes of power supplies. To maintain different designs of power supplies, it needs different spares inventory and trained manpower for each type, which is not feasible. In order to streamline upkeep of the power supplies, the type and make are minimised by taking up in-house development. The single type of power supplies which is used in large quantity has been developed and assembled in-house whenever needed. The steerer and scanner magnets power supplies are the largest number of one type, constituting approximately 50% of the total BTS magnet power supplies. The BTS Group has been designing and assembling such power supplies since 1998. At present, 100% steerer and scanner magnets are being operated with power suppliesmade in-house.

This has helped to have complete control on maintenance / manpower training and resulted in approximately 100% uptime of the beam transport system at IUAC, though the variation in load values (current rating) is large. The power supplies for these magnets are true bipolar (class A output) current regulated power supplies with current rating up to ±10 A and wattage up to 500 W. To minimise the type of power supplies for different load values, the in-house made power supplies are designed with flexibility for output currents and voltages to meet all the load requirements within ±10 A. Linear transistorised design is adopted for simplicity and ease of maintenance. Common control electronics for power supplies with varying ratings is designed with the goal to simplify maintenance, personnel training and to reduce the types of spares. Presently the BTS group is assembling 70 such power supplies for the upcoming HCI facility. It has also agreed to supply approximately 20 such power supplies for the upcoming FEL facility.

Power Supplies for FEL- Beam Transport System Magnets

Approximately 20 power supplies will be needed for the FEL-BTS magnets. There will be 2 power supplies (10 A / 5 V / 25 ppm) for dipole magnets, 7 power supplies for quadrupole magnets (10 A / 5 V / 50 ppm) and 10 bipolar power supplies for steerer magnets (±4 A / 8 V / 100 ppm). For steerer and quadrupole magnets the existing design (same as in HCI facility) of power supplies will be modified to match the current and load ratings. This process has already been started. For the power supplies with stability of 25 ppm, the design will be modified with temperature compensation techniques and DCCT as the feedback element to achieve the required stability.

True Bipolar Power Supply Development Activity

To meet the technological needs for future power supplies, the BTS group has been making continuous efforts. Efforts are being made for developing bipolar power supplies which are used in large quantity in accelerators and other offline set-ups to generate bipolar magnetic fields. The development is aimed to have a simple technique of "class-AB" configuration which will give "class-A" output without any zero crossover distortion. In the presently used technique, additional feedback loops and accurately matched shunts are used to set-up a quiescent current in the push-pull stage in order have class AB bias. This technique has a major limitation, as it depends on the current gain of the BJTs, which decreases drastically at high output current.

A relatively simple technique was developed last year in which MOSFETs were used in place of BJTs and the quiescent currents were set by simply providing an offset voltage to MOSFET gates. As MOSFETs have high input impedance and constant current gain over a wide current range, no additional feedback loops are required to control the quiescent current. To validate the design of the new technique, a ±100 A / 50 Vtrue bipolar power supply was assembled. The group is presently working on different class AB bias schemes with an objective to increase the bandwidth and to provide a thermally stable bias point in passive biasing schemes.

3.1.4 Detector Laboratory

Mohit Kumar, Akhil Jhingan

Detector Laboratory at IUAC provides experimental support to various users in setting up charged particle detectors and readout electronics. New detectors and electronics have been designed and developed, and are used in various user experiments in HIRA, HYRA, GDA, GPSC and NAND facilities. Detector lab provided training on experimental activities for Scientist Trainees, JRF, M.Tech., B.Sc. and M.Sc. students.

MWPC for GPSC/NAND

A new two-dimensional position sensitive MWPC (fig.1), developed with the aim of detecting low energy heavy ions at angles ranging from 2 -10 degrees was installed in GPSC and tested in-beam using 90 MeV ^{16}O on ^{197}Au and ^{64}Zn. The detector was used to detect low energy fusion ERs, deep inelastic events, fission fragments, projectile-like elastics etc. These events were tagged with neutrons and light charged particles detected in liquid scintillator and CsI detector respectively. The MWPC has been prepared using a four electrode geometry, three wire frames and one PCB frames with strips for position information in vertical direction. Such a design will be useful in detecting low energy ERs. The active area of the detector is 10 × 5 cm^2. Off-line measurements were also performed using ^{241}Am

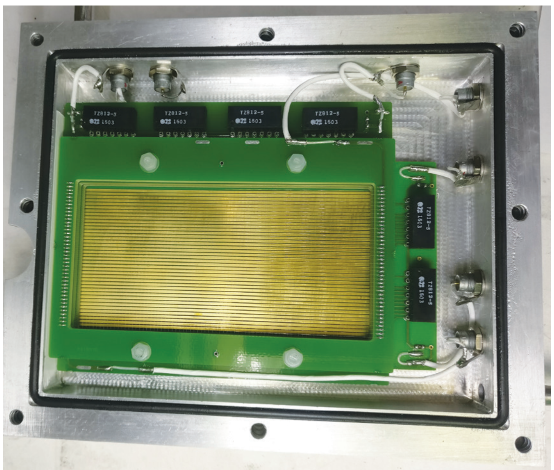

Fig.1: MWPC for ER detection

alpha source and ^{252}Cf fission source. At very forward angles, the detector is expected to be exposed to particle count rates as high as 10^6 pps. The survival and long term stability of the MWPC at such high rates needs is being established. It was observed that 3 electrode operation had higher count rate handling capability as compared to the 4 electrode as detector breakdowns were observed at high count rates.

HYTAR in GPSC

HYTAR detector system was used in GPSC for performing quasi-elastic scattering measurements using accelerated beams from the Pelletron. The detectors were placed in 3 groups of different angles. Three different gas handling systems were installed for the same so as to operate them at different pressures depending upon the energy of the reaction product to be detected. Experiments were performed with beams such as oxygen, silicon and lithium. For the detection of light ions, efforts were made to operate HYTAR at higher pressures (150-250 mbar). For the same, new foil flange were prepared with circular opening of 10 mm diameter and foil thickness of 2 µm. It was found that during prolonged operations, channels developed in the foil, resulting in leaks. For measurements with lithium beam, detector was operated at pressures as low as 20 mbar, and separation between low energy lithium isotopes was observed which may have been due to scattering from oxygen impurity in tin target.

TEGIC Detector for NUSTAR collaboration

IUAC – Delhi Univ. - Panjab Univ. (Chandigarh) – GSI (Germany)

Developmental activities for the fabrication of TEGIC detector were initiated. Detector mechanical housing of cuboid shape was designed and machined using aluminum sheets. The electrode material for the detector were procured. These are made out of FR4 printed circuit boards. There are 21 stacked electrodes (10 anodes, 11 cathodes) prepared by stretching aluminized mylar foil of 2 µm thickness. Inter-electrode gap is 2 cm and active area is 20×8 cm^2. These electrodes will be tilted at an angle of 30 degrees (fig.2) with respect to the normal to the beam direction. Ten charge sensitive preamplifier units, with differential readouts, were also developed for anode readout. Gains are 90 mV/MeV (Si equi.) with decay time constant of 10 µs. Shorter decay times will enhance high count rate handling capability. The CSPA units have been tested with silicon PIPS detector as well as axial field gas ionization chamber (from HYTAR) with 0.4 µs shaping time constants. Performance achieved is as per design goals. A custom designed gas distribution system for pressure uniformity inside TEGIC chamber is currently under development. The detector is proposed to be commissioned, in last quarter of 2019, at the exit of FRS for initial phase of NUSTAR campaigns from 2020-2022.

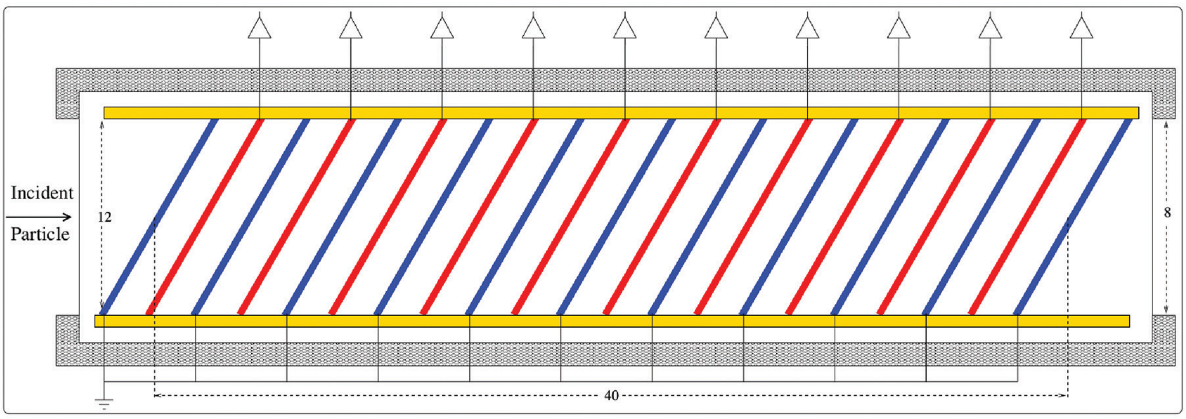

Fig.2: Schematic layout of TEGIC detector.

Development of CSPA and FTA units

New charge sensitive preamplifier (CSPA) and fast timing amplifier (FTA) units were developed for detector signal processing as per requirements of the future experiments. 12 units of CSPA with gains 10 mV/MeV were developed for 6 silicon detector telescopes used to study the breakup effects in lithium induced reaction in molybdenum. Efforts are also on to develop high gain versions for the detection of low energy heavy ions at LEIBF and table top accelerator facility. Development has been initiated to develop dedicated 8 channel FTA unit for the signal processing of position sensitive MCP signals.

3.1.5 Target Development Activities

Abhilash S R, Ambuj Mishra and D Kabiraj

Target Development for Accelerator Users

The primary responsibilities of target lab are operation and maintenance of instruments in Target Development Laboratory (TDL) for developing and delivering the targets and thin films for accelerator users. Several research scholars are trained in the operation of thin film deposition techniques during the target and thin film development. Most of the instruments in TDL were well–utilized in this year. Man-machine utilization in target development laboratory is shown in the bar chart and table given below.

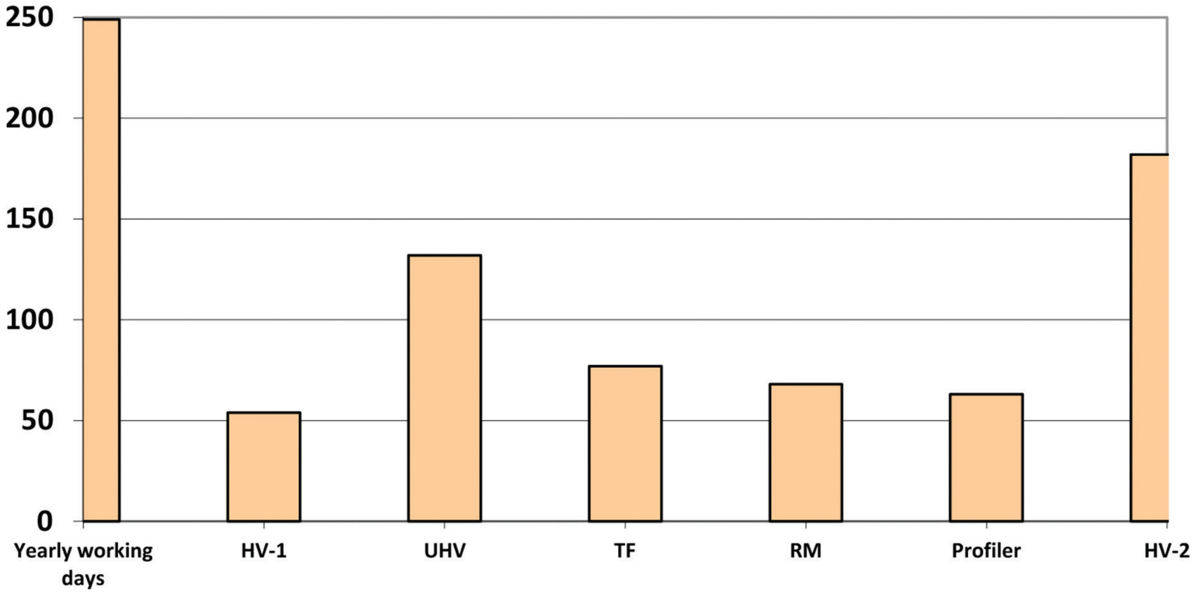

Caption ....

Facility	No of attempts
High Vacuum Evaporator-I (HV-1)	54
Ultra- High Vacuum Evaporator (UHV)	66
Tubular furnace (TF)	77
Rolling Machine (RM)	62
Profilo Meter	63
High Vacuum Evaporator-II (HV-2)	91

Table.1-Utilizatation of facilities

This indicates that more than two facilities of TDL have been used every day in this year. More than 250 attempts were made for target fabrication in different systems for the completion of target requests of more than 41 users of various streams viz., materials science, nuclear physics and atomic physics. TDL has successfully delivered more than 140 targets for various nuclear physics experiments in this year. Target development in IUAC is reported in many national symposia and peer reviewed journals in this year as listed below:

REFERENCES:

[1] R. Mahajan et al. Vacuum 150 (2018) 203-206
[2] N.K. Deb, et al. Vacuum 163 (2019) 148–157
[3] M.M. Hosamani et al 2019 JINST 14 P01007
[4] A Banerjee et al. NIM A 887 (2018) 34–39
[5] Divya Arora et al., Proceedings of the DAE Symp. on Nucl. Phys. 63 (2018)
[6] N. K. Rai. et al., Proceedings of the DAE Symp. on Nucl. Phys. 63 (2018)
[7] Nabendu Kumar Deb et al., Proceedings of the DAE Symp. on Nucl. Phys. 63 (2018)
[8] Nabendu Kumar Deb. et al., Proceedings of the DAE Symp. on Nucl. Phys. 63 (2018)
[9] D. Kumar et al., Proceedings of the DAE Symp. on Nucl. Phys. 63 (2018)
[10] Banerjee et al., Proceedings of the DAE Symp. on Nucl. Phys. 63 (2018)

[11] R Umapathy et al., Proceedings of the DAE Symp. on Nucl. Phys. 63 (2018)
[12] C.Joshi et al., Proceedings of the DAE Symp. on Nucl. Phys. 63 (2018)
[13] Suhail A. Tali et al., Proceedings of the DAE Symp. on Nucl. Phys. 63 (2018)
[14] S Ghosh et al., Book of Abstract, InPAC-2018,
[15] Abhilash S R et al., Book of Abstract, InPAC-2018.

Recent highlights in Isotopic Target development

Approximately 80% of the time is being utilized for the fabrication of isotopic targets. List of isotopic targets developed in the last year is shown in Table 2. Few of them are first-time-development. Targets are fabricated by physical vapour deposition and cold rolling techniques.

Sl. No.	Description of target	No of targets	Thickness
1.	^{116}Sn	>12	~200-600 μg/cm^2
2.	^{118}Sn	>44	~200-600 μg/cm^2
3.	^{148}Nd	>25	~600 μg/cm^2
4.	^{146}Nd	>24	~600 μg/cm^2
5.	^{142}Nd	>25	~600 μg/cm^2
6.	^{122}Sn	2	~2000 μg/cm^2
7.	^{124}Sn	2	~2000 μg/cm^2
8.	^{61}Ni	>14	~150 μg/cm^2
9.	^{62}Ni	>18	~150 μg/cm^2
10.	^{144}Sm	>10	~200μg/cm^2
11.	^{154}Sm	>10	200μg/cm^2
12.	^{92}Mo	>8	150μg/cm^2
13.	^{100}Mo	>8	150μg/cm^2
14.	^{148}Nd	3	~900μg/cm^2

Table 2: List of few isotopic targets developed in 2018-19

Preparation of targets of oxidizing elements and its preservation

The TDL laboratory is continuously working on fabrication and preservation of oxidizing targets with minimum material consumption. In previous years, TDL has successfully delivered several targets of lanthanides and other oxidizing materials with various specifications. Minimizing the exposure of target surface to atmosphere plays the most significant role in target preparation of oxidizing elements. Protecting the target surface by sandwiching it between stable materials (e.g. C and Au) is more effective. Releasing agent also has crucial role in minimizing the contamination on target surface. The level of contamination with various releasing agents was also studied in detail during this year.

Fabrication of ^{150}Nd and ^{142}Nd targets of 150 μg/cm^2 with thin carbon backing is one of the targets developed recently. Neodymium, a rare-earth metal, one of the more reactive lanthanide rare-earth elements, quickly oxidizes in air. The oxide layer which peels off after the oxide layer formation exposes the metal to further oxidation. Neodymium metal tarnishes slowly in air and it reacts slowly with cold water. However it reacts quickly with hot water to form Neodymium (III) hydroxide. So the preservation of either Nd target material or Nd targets in metallic form is a difficult task.

The melting point and boiling point of Nd 1024 °C and 3074 °C respectively. Since the boiling point is very high, the Nd is usually evaporated by electron beam bombardment technique. However, to explore the possibility of Nd evaporation by thermal evaporation, initially few attempts were done in thermal evaporation set-up. As the results were not satisfactory, the Nd targets were finally fabricated by e-beam bombardment. To start with, the carbon backing foils for Nd targets were fabricated by e-gun bombardment. After annealing the carbon coated glass slides at 250 °C, it was again loaded in the vacuum chamber as backing foil. The isotopic Nd was evaporated on carbon foil by electron gun using the parameters which were optimized during the evaporation of natural Nd. A protective layer of carbon of 5 μg/cm^2 was then deposited for protecting the Nd surface from surrounding. After the deposition, the Nd film in carbon sandwich was again annealed at 250 °C for relieving the stress. Finally the film was floated in cold water and subsequently it was fixed on a stainless steel target frame. More than 15 targets of ~150 μg /cm^2 were successfully fabricated by this method using 30 mg of material. The targets were characterized by Energy Dispersive X-ray Spectroscopy technique and no unwanted impurities were traced in the analysis. The targets were successfully used for an experiment in IUAC Pelletron Accelerator.

In addition, few targets of ^{148}Nd of 900 μg/cm^2 thickness with thick gold backing were also developed in this year using the above mentioned method. For achieving 900 μg/cm^2, only 100 mg material was consumed. A tantalum crucible was used as the evaporation source to improve the collection efficiency of the evaporation [1].

Fabrication of ^{144}Sm and ^{154}Sm targets is another recent target development for a nuclear physics experiment in IUAC for measuring the quasi-elastic cross-section. The requirement of the user was for Isotopic Sm targets of ~200 μg/cm^2 thickness with a thin carbon backing. Thin

Sm target are generally fabricated by thermal evaporation and e-beam techniques. TDL has already reported fabrication of many Sm targets of various specifications.

Freshly prepared samarium film has a silvery luster. In air, it slowly oxidizes at room temperature. Samarium reacts slowly with cold water and quickly with hot water to form samarium hydroxide. Even when stored under mineral oil, samarium gradually oxidizes and develops a grayish-yellow powder of the oxide-hydroxide mixture at the surface. Minimizing the exposure to air and moisture is the most important challenging task during the fabrication of targets of materials like Sm. For longer life, after the fabrication the target surface is protected by sealing it under an inert gas such as argon.

Due to oxidizing nature of Sm, possibility of forming self-supporting thin targets is completely ruled out. Therefore, very thin C-foil was chosen as the backing material. To facilitate the removal of C film from the glass slide KCl was used as the parting agent [2]. Prior to final deposition, many trials were performed with natural Sm to optimize different parameters of deposition such as current, thickness and evaporation geometry to evaporate the Sm from tantalum boat which is used as source. The Ta boat containing Sm material was placed at a distance of 12 cm below the carbon coated glass slides. Once the vacuum level reached to 2×10^{-6} mbar, Sm was deposited by thermal evaporation method. After the deposition of Sm, Sm coated glass slides were shifted to e-gun source for carbon evaporation. The shifting of substrate is done through a rotatable feed through which is capable of imparting rotary and linear motion to the substrate holder [3]. After placing the Sm coated glass slide over the e-beam source, capping of C of thickness 10-15 μg/cm^2 was deposited by e-beam bombardment. After this, the chamber was left for 7-8 hours to cool down to room temperature. Before proceeding to final deposition ofenriched Sm, thickness of natural Sm film which was prepared during trial run was verified with profilometer and was found to be 140-150μg/cm^2 and that of C capping was 20 μg/cm^2. Before floating, the Sm film under carbon sandwich was annealed in argon at 200oC temperature. The annealing is done for easy separation of films from glass slides during floating. Few Sm targets were also characterized by EDX measurement for studying the impurity level in the targets. The targets were successfully used in a recent nuclear physics experiment in IUAC.

Preparation of self-supporting Sn targets

This laboratory has delivered many self-supporting targets of isotopically enriched Sn in this year. The requirement of the experiment was for ^{116}Sn and ^{118}Sn self-supporting targets of thickness varying from 200μg/cm^2 to 800μg /cm^2. Since the number of targets required by the user was approximately 44, several trial evaporations were performed with natural Sn for optimizing the parameters of evaporation for maximum yield with minimum material consumption. Various releasing agents, viz; $BaCl_2$, NaCl and KCl were also tried using various evaporation sources for this purpose [1].

Finally, the Sn isotopes were evaporated by thermal evaporation technique using Ta tubular boat. About 50mg material was evaporated on KCl coated glass slide which was placed at 9 cm distance from the source. The KCl film of 100nm was deposited by e-beam bombardment technique prior to Sn evaporation. The Sn films were separated from glass slide by floating them in the warm water. After mounting the films on the target frame, the thickness of each targets were measured by alpha-transmission method. The films were also characterized by Rutherford Back Scattering (RBS) technique and no major contamination was observed in the analysis.

New Electron beam deposition facility

Carbon thin films of various thicknesses are regularly fabricated in this laboratory. Carbon thin films are used as a backing target in many reaction experiments in IUAC. In addition, we also fabricate more than 400 carbon films every year for use as stripper foils in the Pelletron accelerator. The new system is designed to have oil-free high vacuum environment with the provision for thermal heating source and electron gun. The salient features of the facility are vacuum chamber with leak rate of better than 1×10^{-10} mbar-liter/sec, substrate heater with radiant heating, quartz crystal thickness monitor, electron gun and two thermal evaporation heating sources. The facility was recently installed in target lab and it is available for users (Figure1).

Figure1: Electron beam deposition facility

Efficiency in evaporation technique

Target development with minimum material consumption is very important as isotopes are highly expensive. TDL has already established several techniques to minimize the material consumption. Controlling the solid angle of evaporation plays significant role in increasing the efficiency of evaporation. We have successfully fabricated 26 targets of 0.7 mg/cm2 of Sm using 100 mg of Sm in indigenously developed Ta crucible [1].

Fabrication, Inspection and Loading of stripper foils

More than 400 stripper foils of carbon of ~4 $\mu g/cm^2$ were fabricated in this year. 13 evaporations of carbon were done in high vacuum chamber for the stripper foil. TDL has already established a consistent method for the fabrication and loading of the stripper foils [4, 5]. We have also initiated the work for minimizing the human intervention in applying the releasing agent and in floating the foils. Application of machine will improve the uniformity of releasing agent and minimize the damage of films during floating.

Upgradation of Turbo based deposition facility

The turbo pump based deposition facility which was added in the last year is in regular use for e-beam evaporation. A thermal evaporation set-up was added recently to this facility. Since the solid angle of evaporation can be controlled effectively in thermal evaporation, expensive and rarely available materials having low melting points are evaporated by thermal evaporation to minimize the material consumption.

In the modified set-up, the thermal evaporation electrodes are fixed beside the electron gun source. This set-up will enable us to perform sequential evaporation and co-evaporation of materials using both the technique. Sm and Nd were evaporated successfully by thermal evaporation during the testing of the facility.

Thin Film/ Target Thickness Measurement Facility

(1) Alpha Energy Loss Target Thickness Measurement Setup

After preparing the thin films it is essential to measure their thickness. In case of free-standing thin films which are mostly used for experiments of Nuclear Physics, the thickness is measured by *Alpha Energy Loss* Target *Thickness Measurement Setup*. In this academic year, thickness of around 514 free standing nuclear targets of 8 users from different Universities/ Institutes have been measured using this facility.

In this setup at a time 5 targets can be loaded on a target ladder, which is mounted on a linear motion feedthrough. The alpha radiation source, generally Am^{241} is used, is mounted in bottom and SBD detector is mounted in top flange. In the side flanges, vacuum pumping and a view-port are installed. Alpha particles of the initial energy of

5.486 MeV are detected on the SBD detector after losing their energy through target. Alpha particle energy loss is measured using 4K MCA with Linux based MCA software. Then using SRIM calculated energy loss per unit thickness (in keV/Å or in keV/(mg/cm2)), actual thickness of the target can be calculated.

(2) Stylus Profiler

In case of thin films deposited on thick substrates, alpha energy loss target thickness measurement method is not effective. Thickness is measured using *Stylus Surface Profiler,* Model: Bruker DektakXT. For this a shadow mask is used to establish a step between substrate and the thin film. Following is the features of *Stylus Surface Profiler* at IUAC:

- Stylus Force: 1 – 15 mg, 0.3 – 15 mg (N-Lite)
- Scan Length: 55 mm.
- Vertical Range: 1 mm
- Vertical Resolution: 1 Å
- Max. Sample Thickness: 50 mm

During this academic year, thickness of around 132 thin film samples of 32 users from different Universities/ Institutes have been measured using this facility.

REFERENCES:

[1] R. Mahajan et al. / Vacuum 150 (2018) 203-206
[2] M.M. Hosamani et al 2019 JINST 14 P01007
[3] K.K. Rajesh et al. / Vacuum 141 (2017) 230-234
[4] D.K Avasthi et al. / NIM A 303 (1991) 43-45
[5] D. Kabiraj et al. / NIM A 521 (2004) 183–186

3.1.6 RF and Electronics Laboratory

Arti Gupta, Bhuban Kumar Sahu, Deepak Kumar Munda, Kundan Singh, Mamta Jain, Parmanand Singh, Prem Kumar Verma, S.Venkataramanan, Ajith Kumar B.P

Pre-amplifiers for multi-wire proportional counters

We have developed a compact pre-amplifier unit to meet front end electronics requirement of multi-wire proportional counter (MWPC) detector. This unit accommodates different types of pre-amplifiers (up to 7 nos.), including two independent channels of charge sensitive pre-amplifier (CSPA) and five channels of wideband pre-amplifier to process the energy and fast timing signals originating from MWPC electrodes respectively.

The wideband pre-amplifier design is a transistorized (BJT) type, wherein multiple common emitter amplifier stages are cascaded depending upon polarity required, to achieve the required bandwidth and gain. There are 4 nos. of inverting type and 1 no. of non-inverting type wideband amplifiers are assembled with required gain of ~250. The bandwidth achieved by suitable component selection is measured to be ~350MHz (-3dB). These amplifiers are assembled on a common high quality RF type PCB with continuous ground plane, in turn flush mount on die-cast aluminium box top cover, which acts as a heat sink. To reduce cross talk, the pre-amplifiers are shielded with a thin copper sheet. SMA type connectors are used for input and output connections to preserve the rise time of the signal.

The charge-sensitive pre-amplifier design is a transistorised type with JFET front end along with optional front end protection circuit. The charge conversion gain is ~ -44 mV/MeV (Si equ.) with ~100 µS decay time. The preamplifier has two independent outputs (Energy & Timing) for energy and timing spectroscopy respectively. All the pre-amplifiers are mounted inside a die-cast aluminium box.

The wide band pre-amplifiers were tested for long term stability over a period of ~120 hrs and observed gain variation was < ±0.15%. They were tested with alpha source ^{241}Am at the focal plane of HIRA beam line. Position resolutions of ~2 mm and ~2.4 mm were obtained in X and Y positions, respectively which is comparable with the existing set up. Five such preamplifier boxes have been assembled, tested and delivered to the user.

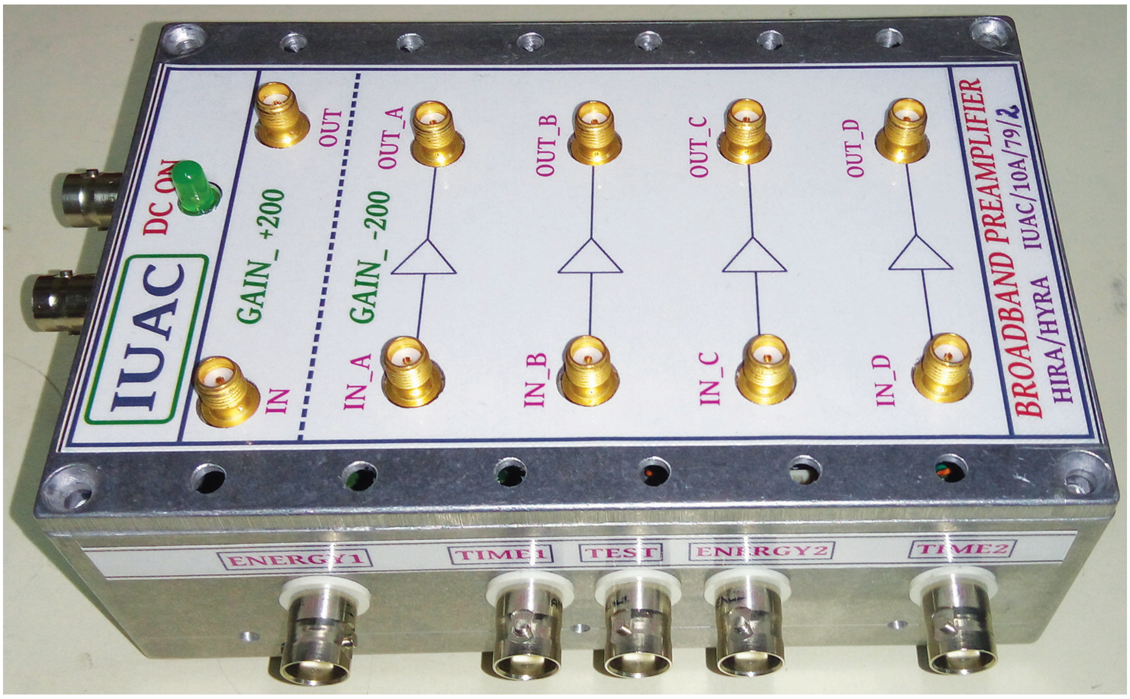

Figure: View of MWPC Pre-amplifier unit

MWPC Fission detector Electronics module

This front end electronics module processes Multi Wire Proportional Counter (MWPC) signals coming through pre-amplifier unit. The single width NIM module accommodates a Shaping amplifier for energy spectroscopy and Constant Fraction Discriminators (CFD) of MWPC of 5 electrode geometry. This year five modules were fabricated, assembled, tested and handed over to the user. The details of this module is discussed in earlier IUAC Annual report of year 2010, pg: 56-57.

Quad channel Level adapter module

A Quad Level Adapter is a general purpose single width NIM module to cater the need of logic translation from TTL to Fast NIM & vice-versa. This NIM module accommodates four identical and independent channels of level translators while each channel accepts either of the two inputs, Fast NIM or TTL and convert it into direct and complementary TTL and Fast NIM logic signals. The module has been developed successfully and duplicated (2 nos.) that are being used regularly with experimental facilities at IUAC.

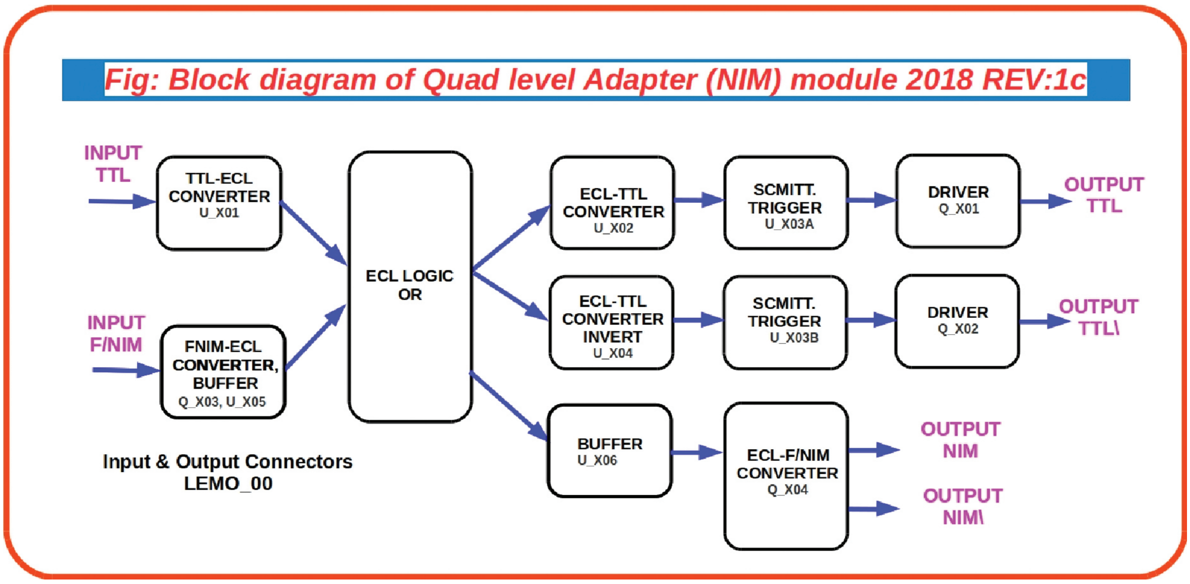

Block diagram of Quad Level Adapter (NIM) module

Multi-TAC NIM module

As reported in the IUAC Annual Report 2017-18 page 66-67, the module was further refined as per the user requirements. The modifications made are in TAC Range: 100 / 200 / 300 nS corresponding to 0-10 V output. The performance tests were conducted to measure its resolution, linearity and long term stability to compare with commercially available Ortec 566 TAC module. We have used Ortec make Time calibrator module model: 462 for linearity and resolution measurements. The module was further subjected to live test with NAND type detector (STOP) and BaF_2 type detector (START) with Co-60 radiation source for duration of ~ 54 hours to study its long term stability. We have observed its resolution is about ±0.25% of full scale at 100nS range. The long term stability is measured to be ±0.03%, when tested with Co-60, which are comparable with Ortec 566 TAC. All the three channels of the module match within ±3.5% with respect to its TAC range.

VME SDAC64 Module Implementation

In this year we have completed the in-house development of high density (64-channels) scanning ADC (analog-to-digital converter) module for VME bus architecture. Last year, four layer printed circuit board (PCB) was designed in-house and populated with FPGA (Field programmable gate array) and discrete electronics components. The firmware (which contains the core functionality of the module) for FPGA device is written in industrial standard hardware description language, VHDL. The major components of firmware constitute, board selection, VME bus Slave interface, free running sequencer for analog circuitry and data steering logic. There are generic in-built registers which contains module information such as firmware revision, board ID, control and status register etc. The solid works design files are made and supplied to the vendor for front panel precision cutting (wire-cut) in local market. The full board assembly is completed in-house and FPGA is configured with newly developed firmware. The board is calibrated and rigorously tested for functionality and stability of the output of each independent channel. The firmware is implemented on Xilinx Spartan3 FPGA. One of the commercial scanning ADC module is replaced with indigenously developed module in HCI (high current injector) beam line for in-beam testing of the board. The module performance is at par with the commercial board.

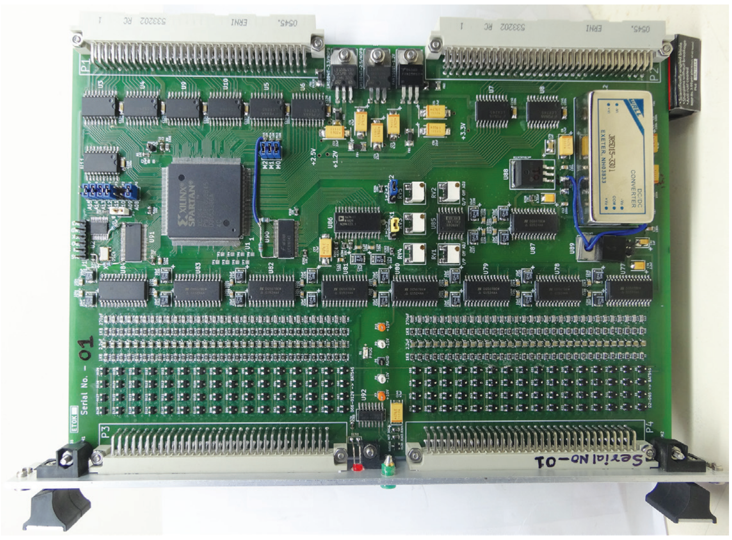

Fig: Top view of VME SDAC64 Module

VME Input Gate/Output Register module (IGOR)

In accelerator control system hardware we are slowly migrating from CAMAC bus based servers to VME bus servers in a phased manner in the older facilities, viz. Pelletron and LINAC accelerators. The transition, especially in Pelletron, has put up a requirement of developing customized VME module to control magnet power supplies. These older magnet power supplies (e.g. analyzing magnet or switcher magnet) has customized remote control feature which need special boards to control remotely. In the continuation of our in-house control system instrumentation development we have designed two channels of IGOR module (in 6U single width VME board space) which can control two power supplies independently. The four-layer PCB has been designed using open source KiCAD PCB design software. The firmware for board functionality will be written in hardware description language, VHDL.

3.1.7 Health Physics

Debashish Sen & Birendra Singh

The radiation safety aspect of IUAC is taken care of by the Health physics group. Besides this, radiation safety related research and development work is also carried out by users from different

Universities & Institutes. Routine maintenance of interlock system and radiation monitors is done regularly to keep a vigil on the overall radiation safety.

A few university faculties and research scholars are using the existing Health Physics Lab facilities (gamma irradiation chamber, TLD reader, electrochemical work station, furnace etc.) maintained and updated by this group. Some research scholars have completed their Ph.D. using the facilities and a few research scholars are continuing to do so. Many of the AUC approved projects require these off line facilities throughout the year. Users are from Delhi University, Jawaharlal Nehru University, IIT Delhi, Shiv Nadar University, Indra Prastha University, AIIMS, Amity University, NIT Jalandhar, Anna University, Nagpur University, Kolhapur University etc. Regular status reports for the Gamma irradiation chamber, Pelletron accelerator and RBS facility is being sent to AERB. Renewal of licence of existing radiation facilities has been taken from AERB. All dose records are maintained and are also available online. Facility wise RSO re-nomination and renewal of licence was also done using the eLORA facilty.

Few of the Gamma/X ray monitors/ surveymeters/ pocket dosimeters have been calibrated this year. Also some of the door interlock systems underwent thorough repair. Some monitors were replaced, and some were installed in new strategic locations (as new facilities are coming up in the centre).

3.1.7.1 e-LORA facility of AERB

Debashish Sen & Birendra Singh

Electronic **L**icensing **O**f **R**adiation **A**pplications (eLORA) System is an e-Governance initiative by AERB. It is a basically a web-based application for automation of regulatory processes for various Radiation Facilities in India. The system is aimed at achieving paperless licensing of Radiation Facilities. The objective of the project is to enhance efficiency and transparency in the regulatory processes of AERB.
Following procedures has been carried out using the **e-LORA facility:**

- Submission of siting, design & construction request of a radiation facility
- Renewing license of a radiation facility
- Informing safety status of radiation facilities at regular intervals
- Providing details of the radiation monitors used in the facility along with their calibration dates and other details
- Providing details of radiation sources in custody of IUAC
- Procurement of new radiation sources
- Non-compliance of any safety measures and its rectification
- Renewal of tenure of IUAC Radiation Safety Officers.

3.1.7.2 AERB correspondence for different upcoming radiation facilities of IUAC (regarding radiation safety aspects)

Debashish Sen

A. Modification of HCI beam line in beam Hall 1

The Site approval has been sanctioned. The final design of the facility/beam line/ shielding layout need some modifications. Shielding calculations are also in the final stages.

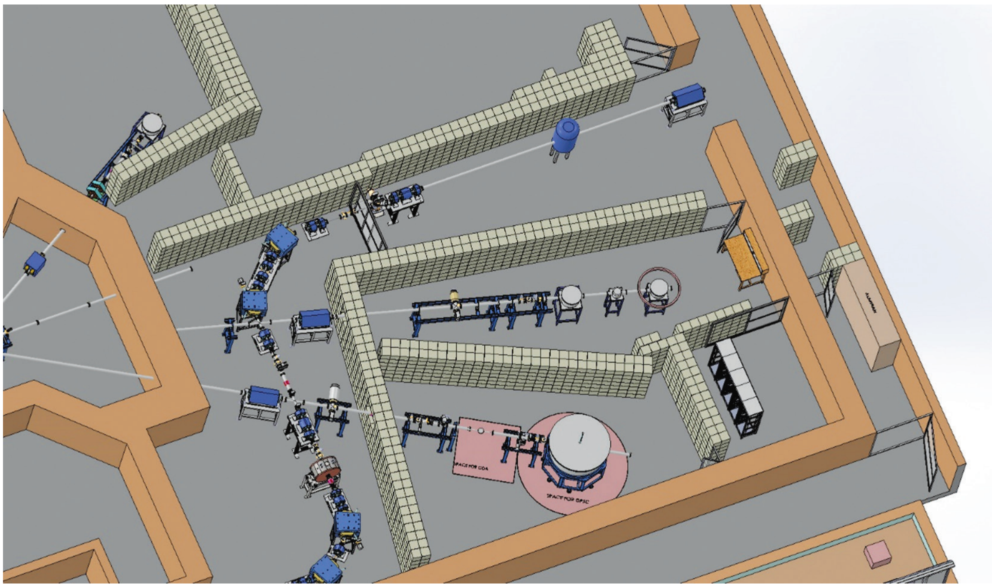

Fig 1: Proposed beam line of HCI (in beam hall I) and necessary shielding modifications (proposed)

The latter part of HCI beam line is to be built in Beam Hall I, which will merge into the zero degree beamline of the Pelletron accelerator. Hence, the original approved shielding layout has to be modified so that the beam lines of GPSC and Materials Science remains operational and accessible even when the HCI beam is ON. Fig. 1 shows the proposed beam line of HCI in beam hall I merging with zero degree line and the necessary shielding modifications required thereafter.

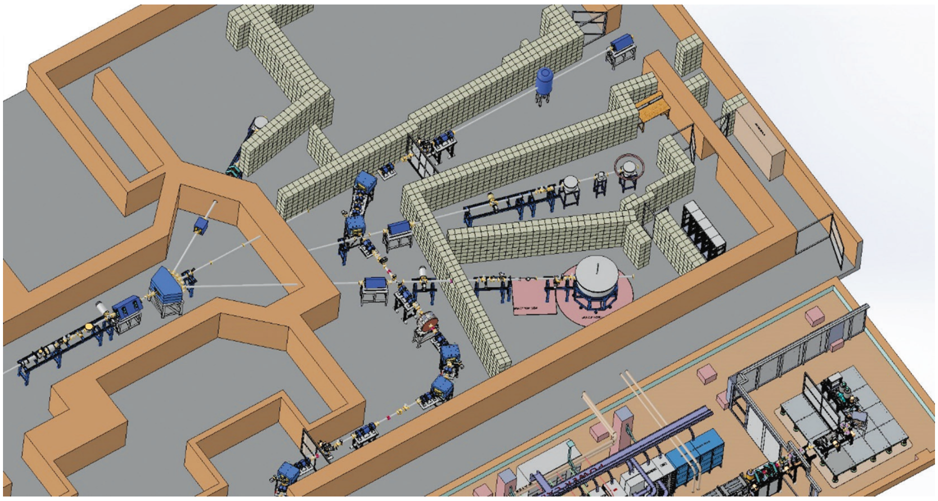

Fig 2: Proposed layout modifications of Beam Hall I with a new entrance (adjacent to the GDA cabin)

Under these circumstances, the entrance to the Materials Science beamline from the zero degree line has to be closed, and no access from that side will be allowed as per radiation safety rules. This requires a new door opening, from the corridor adjacent to GDA cabin area so as to access the GPSC and Materials Science beam line when HCI is ON. The feasibility of opening such a door (along with associated shielding lay out changes) is under consideration. The adjacent corridors also need new shielding set ups (to take care of the radiation safety when HCI is running). All these modifications are being planned at this stage and will be implanted only after obtaining necessary approvals from AERB.

B. Revival of proton run facility in the original LIBR line

The existing AMS line in beam Hall I was originally used to deliver proton beams to the users. But later very light ion (e.g proton, deuteron) beam runs were suspended. The Centre is planning to revive this facility as demand for proton runs from the users is increasing. Hence, the beam line needs to be modified as per new requirements, and, most importantly, a beam dump has to be built at the end of this line to take care of the radiation safety. High neutron radiation level may damage the ASPIRE chamber components (at the end of adjacent BIO line). Hence an extra shielding wall has been proposed (between the ASPIRE chamber & Beam Dump) to protect it from any radiation damage). All these modifications are being planned at this stage and will be implanted only after AERB approval is obtained.

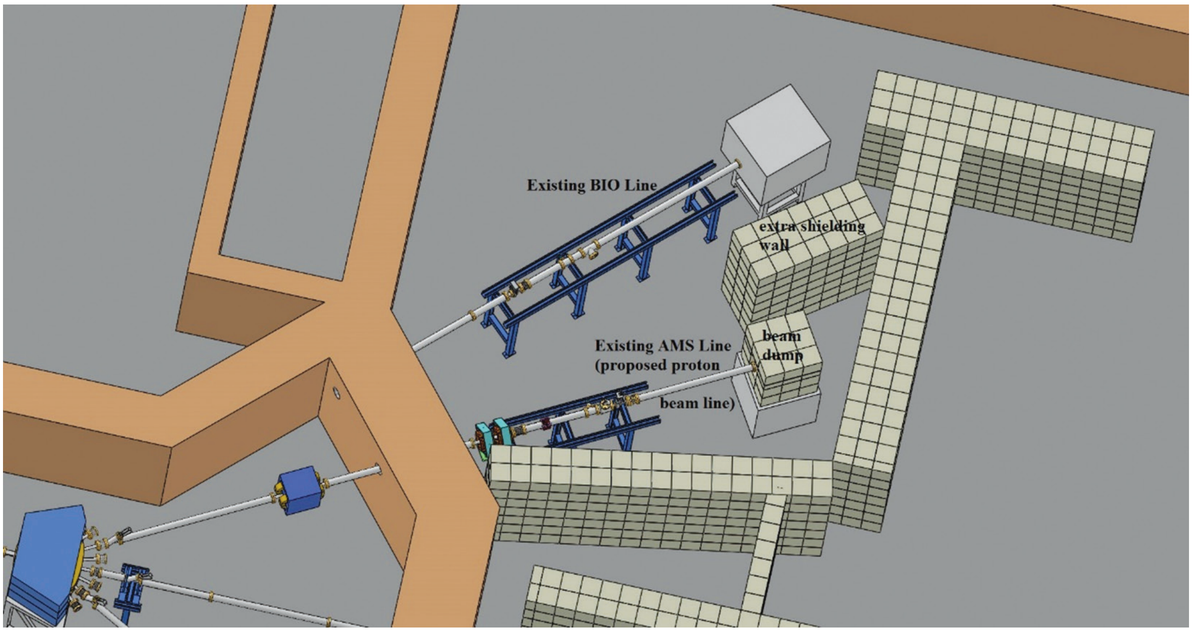

C. Free Electron Laser (FEL) Facility

The Site approval has been sanctioned. The design & construction approval application needs some extra clarifications. Shielding calculations are also in the final stages.

D. Accelerator Mass Spectroscopy (AMS) Facility

Final approval will be obtained after submission of the Quality assurance manual & detailed Acceptance test Report.

E. License to procure & operate X-ray diffractometer & X-ray fluorescent device (cabinet type) was obtained.

F. Preliminary site layout information related to upcoming Geochronology facility (Ministry of Earth Sciences) and ISRO electron Accelerator Facility (Dept. of Space) has been conveyed to AERB.

3.1.7.3 Investigating the Thermoluminescent Properties of Nano-crystalline $K_2Ca_2(SO_4)3$:Eu,Cu and CaF_2:Tm

Anant Pandey[1], Chirag Malik[1], Kanika Sharma[1], Pratik Kumar[2], Birendra Singh[3] and Debashish Sen[3]

[1]Department of Physics, Sri Venkateswara College, University of Delhi, New Delhi
[2]Medical Physics Unit, IRCH, AIIMS, New Delhi
[3]Health Physics Lab, IUAC, New Delhi

The effect of co-doping and change in dopant concentration on thermoluminescence (TL) properties of $K_2Ca2(SO_4)_3$:Eu,Cu has been studied by varying the concentration of the two dopants europium and copper (0.05, 0.10, 0.20, 0.30 and 0.40 mol% equally divided between Eu and Cu). Chemical co-precipitation technique was used to prepare the co-doped phosphor $K_2Ca_2(SO_4)_3$:Eu,Cu. Using Williamson-Hall plot in the X-ray diffraction pattern of the phosphor, the size of the crystallites was estimated to be around 51.3–73.6 nm. Maximum TL sensitivity was obtained for 0.2 mol% concentration (0.1 mol% Eu and 0.1 mol% Cu). The co-doped phosphor was compared for its TL sensitivity with that of the singly doped phosphors $K_2Ca_2(SO_4)_3$:Eu, and $K_2Ca_2(SO_4)_3$:Cu and the standard TL dosimeter LiF:Mg,Ti (TLD-100). Higher TL peak intensity of co-doped phosphor compared to the singly doped phosphors $K_2Ca_2(SO_4)_3$:Eu and $K_2Ca_2(SO_4)_3$:Cu has been explained on the basis of energy transfer between the dopants. Photoluminescence studies of the co-doped and the singly doped samples confirm a positive energy transfer from Cu^{2+} to Eu^{2+}. A linear TL response curve over a wide range of doses (10 Gy to 1 kGy) is a key factor that makes the present phosphor quite capable for dosimetric purposes.

Further, chemical co-precipitation technique was used to initially prepare nano-particles of CaF_2 which were later activated by thulium (0.1 mol%) by the use of the combustion technique. X-Ray diffraction (XRD) and transmission electron microscopy (TEM) were used to characterize and confirm the preparation of the desired salt. 1.25 MeV of gamma radiation and 65 MeV of carbon (C^{6+}) ion beam were used to irradiate the samples. A major peak is evident at around 169 °C and two small humps at 223 °C and 295 °C in case of gamma radiation. Further, the salt at hand exhibited a linear TL response for the complete range of studied doses i.e. 10 Gy to 2000 Gy. Moreover, when the nanophosphor was exposed with 65 MeV of C6+ ion beam its glow curve exhibited a major TL peak at around 161 °C and a small shoulder at about 237 °C and the nanophosphor displayed a linear TL response for the entire range of studied fluences i.e. $5x10^{10}$ ions/cm^2 to $1x10^{12}$ ions/cm^2. Finally, a variety of tests like batch homogeneity and reproducibility were also performed in order to define the final product. Thus, co-precipitation method followed by combustion technique was successful in producing a dosimetric grade CaF_2:Tm for dosimetry of gamma radiation as well as carbon (C^{6+}) ion beam.

This work has been presented in the 22nd Asia-Australasia Conference of Radiological Technologists (AACRT 2019) in conjunction with the Australian Society of Medical Imaging and Radiation Therapy's 14th National Conference (ASMIRT 2019), held at Adelaide Convention Centre, from 28-31 March 2019 in Australia [2]. All of the above mentioned works have been performed at the Health Physics Lab, IUAC, New Delhi under the projects: BTR No. 57301, **BTR No. 63201 and BTR No. 63203.**

REFERENCES:

[1] Malik C, Katoch A, Singh B, and Pandey A, "Effect of co-activation on the thermoluminescence and photoluminescence properties of nano-crystalline K2Ca2(SO4)3:Eu,Cu" 2019 Journal of Luminescence 207 526-533.

[2] Pandey A, Sharma K, Singh B, and Kumar P, "CaF2:Tm nanophosphor as gamma radiation and carbon beam dosimeter for radiotherapy" 22nd Asia-Australasia Conference of Radiological Technologists (AACRT 2019) in conjunction with the Australian Society of Medical Imaging and Radiation Therapy's 14th National Conference (ASMIRT 2019), 28th-31st March 2019, Organized by the Australian Society of Medical Imaging and Radiation Therapy, held at Adelaide Convention Centre, Adelaide, Australia

3.1.7.4 Combustion synthesis and thermoluminescence response of near ultra-violet irradiated Mg2B2O5 nanophosphors

Jitender Kumar[1], Birendra Singh[2], Debashish Sen[2], Shalendra Kumar[3] and Ankush Vij[1]

1Nanophosphors Lab, Department of Applied Physics, Amity University Haryana, Gurgaon
2Health Physics Lab, Inter University Accelerator Centre, New Delhi
3Electronic Materials & Nanomagnetism Lab, Dept. of Applied Physics, Amity University Haryana, Gurgaon

Among the various kinds of metal borates, the magnesium borate has been considered to have promising luminescence properties. The synthesis techniques and conditions have a profound effect over the defect assisted luminescence properties of phosphors. We synthesized $Mg_2B_2O_5$ nanophosphors by combustion technique using urea as fuel. The formation of $Mg_2B_2O_5$ nanophosphors was investigated by X- Ray diffraction pattern, which clearly confirms the single phase triclinic structure. In order to investigate the thermoluminescence (TL) response of $Mg_2B_2O_5$ nanophosphors for near ultra-violet (UV) radiations, the samples were exposed with wavelength of 365 nm for different durations. The TL glow curve of the samples consists of two broad peaks around 425-430 K and 570-590 K, which signifies two kinds of trapping or defect sites present in the sample. With the increase in exposure time, we observed that higher temperature peak intensity increases at the expense of lower temperature peak. The analysis by using Chen's peak shape method confirms that TL glow curve comprises of complex glow peaks, thus not suitable from radiation dosimetric point of view. However the present TL results suggest that $Mg_2B_2O_5$ nanophosphors are sensitive to near-UV radiations and further synthesis optimization may be required to make $Mg_2B_2O_5$ usful for UV dosimetry.

3.1.7.5 Combustion Synthesis and Thermoluminescence Studies of Gamma Irradiated MgO Nanostructures

Savita[1,2], Birendra Singh[3] , Debashish Sen[3], Ankush Vij[4] and Anup Thakur[1]

[1]Advanced Materials Research Lab, Department of Basic and Applied Sciences, Punjabi University, Patiala
[2]Department of Physics, Punjabi University, Patiala-147 002, Punjab
[3]Health Physics Lab, Inter University Accelerator Centre, New Delhi
[4]Nanophosphors Lab, Department of Applied Physics, Amity University Haryana, Gurgaon, Haryana

Wide band gap metal oxide nanomaterials has attracted the researchers due to their excellent luminescence properties. Magnesium oxide (MgO), being a wide band gap (~7.8 eV) material, is explored for its application in radiation dosimetry. In this research, MgO nanostructures have been synthesized by solution combustion method using monoethanolamine as a fuel. A part of the sample is annealed at 950 °C to study the effect of annealing on crystallite size, and thermoluminescence behavior. The as-synthesized and annealed nanostructures are characterized by powder X-ray diffraction for phase confirmation. X-ray diffraction patterns of the nanostructures revealed the formation of single phase cubic structure in both the samples. Crystallite size of the as-synthesized and annealed samples is found to be ~20 nm and ~30 nm respectively. In order to study its thermoluminescence (TL) response, the annealed nanostrucutres were irradiated by 60 Co gamma-ray source at various radiation doses up to 10 kGy. A broad glow peak having two features at ~108 oC and ~165 0C is observed indicating the presence of various defect centers in MgO. TL glow curve intensity is found to increase with the increase in radiation dose upto 7 kGy and then saturates. Various trapping parameters viz. frequency factor, activation energy and order of kinetics were calculated from the TL glow curves.

3.1.8 Data Support Laboratory

Ruby Santhi and P. Sugathan

Data Support Laboratory at IUAC provides support to various users in setting up the required data acquisition & electronics during experiments. The lab also procures required electronic modules, co-axial connectors and cables required for user support. In data room, two CAMAC based on-line data acquisition systems are running with LINUX based FREEDOM software using CMC 100 controllers. Many nuclear reaction experiments in GPSC and HIRA facilities have been performed using the CMC100 Crate Controller based data acquisition system in data room.

3.1.8.1 VME based Data Acquisition test bench in INGA counting Room.

Ruby Santhi

A VME test bench was setup in INGA counting room for collecting signals from suppressed clover Ge detector using radio-active source. Spectrum from Europium source was collected after digitization using 32 channel VME ADC MADC-32, which is a fast, high quality 32 channel peak sensing ADC and provides 11 to 13 Bit (2 to 8 k) resolution with low differential non linearity due to sliding scale method. The ADC module also has a time stamp register. Scientific Linux software installation is no neing tried in all in one PC.

3.1.8.2 Testing of LAMPS Acquisition Software for Ethernet & USB CAMAC Controllers

Ruby Santhi and Ambar Chatterjee

Two new CAMAC controllers have been tested for data collection using LAMPS version of software. The driver parts of the controllers were modified to work for LAMPS software in Ubuntu and Scientific Linux operating systems. These are commercial controllers, Wiener CC-USB controller and CAEN Ethernet C111C controller. The Ethernet controller was procured by Dayalbagh University (Agra) user for setting up their muon measurement laboratory. After implementation of drivers and modification in LAMPS, the operating system and data acquisition software were installed in their setup at their university and sample data was collected. The setup will be used by students performing muon measurements.

3.1.9 Computer and Communications

S. Mookerjee, E.T. Subramaniam, S. Bhatnagar, A. Kumar

The major activities this year include a major overhaul of the Center's core network switching system, expansion and reorganization of the Center's local network, revamp of the internet access mechanism to a hardware firewall and UTM system, and operation and maintenance of the IUAC HPC facility. Work on swift heavy ion interaction simulations was also restarted after a hiatus of three years.

3.1.9.1. Local Area Networks

In a major upgrade, the core network switch stack, now more than ten years old and out of maintenance support, was augmented by a new single 48-port 10G switch. Five edge switches, also more than ten years old, were replaced by new gigabit Ethernet switches with 10G uplinks. The new core and edge switches were configured with full access control filters. The edge switches and associated old cabling were replaced with close to zero downtime. The new core switch is presently used as a passive standby, ready to replace the old core stack in case of failure.

Design and implementation of OFC based 10G network connectivity from IUAC core switch to auditorium network room, including all passive components and racks, was completed this year. New redundant OFC cables were laid from the network core in the IUAC data centre to the auditorium network room, with all terminations in LIU and jack panels completed in separate racks at both ends. The gigabit wired network inside the auditorium was also checked and fixed. The passive network has now been installed and tested, and is ready for active components for the auditorium network to go live.

The internet traffic load continued to increase this year, with much of the traffic being generated from the wireless LAN and mobile devices. The number of simultaneous sessions at peak times increased to about six hundred. Access to the internet by users on the local network was routed through a central Linux server running an authenticated Squid proxy server and an Iptables firewall. This server also served as a reverse proxy gateway for external access to the IUAC web page. The proxy server and firewall had to be manually configured for every change in rules, needed constant tweaking and policy changes, and had also reached performance limits. This was replaced by a hardware UTM providing firewall and web page forwarding functions, and allowing direct access to the Internet without mediation through a proxy server. The replacement involved the design of a zero-downtime migration plan, selection and purchase of a hardware firewall and UTM, reconfiguration of central servers, wireless controller and wired network switches to work through the new UTM, reconfiguration of DNS servers, migration of firewall rules, and configuration and implementation of new UTM-based internet access. Smooth migration to the new Sophos XG310 UTM was achieved with no downtime, by keeping parallel access to the old system available for a few weeks.

3.1.9.2. High Performance Computing Facility

In 2008, the Department of Science and Technology sanctioned a grant of Rs. 13.54 crores to set up a high performance computing facility at the Inter University Accelerator Centre. The purpose of the grant was to provide a major computing facility for faculty and students of universities and colleges across the country. The facility was operational since 2010, and served more than four hundred users from a hundred and fifty research groups in colleges, universities and institutes across the country.

The HPC facility consisted, at the beginning of the academic year, of a Infiniband-based MPI cluster comprising 2880 Xeon cores across 180 compute nodes. with a total of more than four hundred users from a hundred and forty groups. Maintenance of compute, storage and interconnect hardware and software, and addition and administration of the user pool, was done in-house.

While another fifty users in twenty groups were added during the year, and software problem resolution was speeded up, hardware problems multiplied and the number of usable cores came down to 1700 by January 2019. Hardware problems with master node and storage were resolved for some time by reconfiguring compute nodes as master and metadata nodes, and using parts from nodes already down to repair other nodes. However, the cluster was working with reduced node and core counts and reduced reliability. After March 2019, no more new user requests could be entertained. Multiple hardware failures across nodes and storage continued. The fact that the systems were six years old and at the end of useful life, coupled with lack of hardware maintenance support, finally led to an unacceptable loss of nodes and reliability. An attempt is now being made to revive a skeletal system to enable users to transfer data to their home institutions and enable a graceful shutdown.

3.1.9.3. New Generation Instrumentation and Acquisition System

E.T. Subramaniam, Kusum Rani, Mamta Jain

The defining direction of data acquisition system development work this year was towards the design and implementation of the next generation VME-based data acquisition system. Significant progress was made in putting together the associated hardware and software required for the development effort:

- The existing net boot 32 bit tiny LINUX OS was adapted to cater to the need of the VME SDK which would be required for the new data acquisition system.
- Feasibility study of VME based DAQ system was completed. The SDK and the driver available from the crate controller manufacturer appears to be incompatible with the recent 64 bit systems. So a user level driver was developed to communicate with the commercial VME crate controller through the built-in VME API of LINUX systems. The NiasOS (Tiny Linux) was modified to have provisions for the same. A text user interface (TUI) based client was also developed.
- Universal serial bus based interface was envisaged to cater to the needs of the upcoming DAQ requirements. The necessary middle ware and TUI based interface were designed and developed.
- Design, development and implementation of VME interface hardware and middleware was started.
- Design, development and implementation of unified event identification module with cascaded time stamp for multi strobe acquisition systems was completed.

3.2 UTILITY SYSTEMS

3.2.1 Electrical Group Activities

U. G. Naik and Raj Kumar

This group is primarily responsible for maintaining the electrical installations of IUAC and also to develop adequate electrical infrastructure for the new scientific projects. The uptime achieved for electrical systems was close to 100%. This was possible with judicious maintenance schedules and monitoring arrangements. The group has also successfully completed the projects and works envisaged for the year F.Y. 2018-2019.

PROJECT WORKS:

11 kVA Compact Substation

A Compact electrical substation with transformer of 11 kV/433 V, 1600 KVA has been Commissioned and put into operation after planning, designing, procurement, execution. Necessary approvals from the Electrical Inspectorate, CEA have also been obtained. Substation is in use since its commissioning on 28th march 2019.

Auditorium Works

All the works related to the auditorium have been completed and the auditorium is put into use. On completion of all works at Auditorium, application to Delhi Fire service was made by IUAC requesting for fire clearance. Fire inspector on his visit made observations and suggested certain changes to be made as per relevant BBL 1985. All the necessary modifications were carried out in record time of 30 days and NOC was obtained from Delhi Fire service to operate and use the Auditorium. In February IUAC organized the AFAD-2019 Workshop in the new auditorium.

UPS-SITC of 3 nos. of 60 KVA UPS

A 3x60 kVA On-line UPS System consisting of 3 units of 60 kVA UPS in load sharing N+1 configuration complete with AC, DC cabling etc. on turn-key basis was planned and procured after removal of existing 2x60 kVA UPS System. Five year Comprehensive AMC charges after expiry of warranty period are also part of the purchase order.

Maintenance Activities

Maintenance of Electrical Installations of Substation, Office Blocks and Residential Colony

Maintenance of electrical installations is managed through the AMC with external agency, however all the consumables required are supplied by IUAC. M/s KBS Electricals was engaged for AMC during financial year 2017-18, who have carried out the maintenance.

There was not even a single event occurred for the transformers or any switch gears related to transformer HT and LT.

Dehydration of transformer oil for 7 Transformers- (4500ltrs)

- Periodic maintenance of LT panels, Distribution boards and other accessories, Lighting, Fixtures, lighting and power circuits.
- Maintenance of street lighting and earthing.

Captive Power Installations

IUAC had a captive power base of 2500 kVA. Three DG Sets of 750 kVA are synchronized to power 15UD Pelletron, He Plant and HPC Data Centre. The group has shown ever readiness in running the systems round the clock O&M activities within short period if need arose.

Synchronisation panel and the PLC is subjected to the ambient temperature of >45 °C in summer on its successful service of 5 years it has failed for the first time and has been replaced. Fresh programming also has been done and put in to service.

Batteries are periodically changed once in 2 years or on failure whichever is earlier. Servicing (B-check) is carried out by Engine manufacturer once a year with Cummins genuine parts.

These 3nos of 750KVA DG sets were procured in year 2012 through M/s NCE Jaipur. Installation was completed by M/s H N Traders, New Delhi in 2014. However we were informed at that point of time that the approval of Electrical inspectorate was not mandatory. Now we have come to know that the approvals are needed and accordingly action initiated. On rigorous pursuation with Electrical inspectorate, CEA.

And on complying to their observation the installations stands approved by Electrical inspectorate, CEA.

Roof Top Solar System for IUAC

Roof top grid interactive 2×50 kWp solar power generation plant is functioning successfully and is operational. Peak power generated in any particular day has reached 650 KVAH units. Average generation is 500 units. Periodical cleaning of the panels is done to get maximum power output.

UPS Installations

IUAC has 10×60 kVA UPS, 3×300 kVA, 4×200 kVA, UPS systems maintained by electrical group. These are under supervision and control of this group. Although the day to day operations are carried out by electrical group, the comprehensive AMC order has been placed on the manufacturer for all the sets out of warrantee period. Under AMC, routine preventive maintenance is carried out by AMC agency once in every quarter.

Power Factor Compensation

Electrical group is pleased to state that yet again average power factor of >0.98 lag was achieved for the year. Our system power factor without correction was around 0.85, and by raising it we have saved > Rs.162 lakhs through the year from energy saving.

Fire Detection and Alarm System

Electrical group has been maintaining fire detection & alarm system covering whole lab complex and new guesthouse. This system has been extended to Beam Hall-II stores areas. Renovation of fire detection system has been done in Beam Hall-III as this system was giving lots of troubles. All parts of the system were maintained in good health throughout the year. This year scope has increased due to addition of Lab Block 2nd floor and Auditorium Block.

3.2.2 Air Conditioning, Water System and Cooling Equipments

A. J. Malyadri, Bishamber Kumar, P. Gupta

AC System

IUAC's central air conditioning / low temperature cooling system of Phase-1, consisting of 400 TR Central AC plant, performed with 100% uptime. Maintenance ensured that the safety record of the plant was maintained at 100% and the power consumption kept at optimum level. 2×200 TR chillers installed in 2013 have run 28000 hours each. Other rotary equipment have logged 2,15,500 continuous run hours. It is relevant to note that the Indian industrial norms specify a life of ~25,000 run-hours for compressors and ~50000 hours for other rotating equipment.

The Phase-II & III screw chiller based central AC plants performed to an uptime of 100%.

The highlight of the operation and maintenance of the above systems was the in-house supervision provided to the contracts, which affected significant savings.

The hook-up of AC plants ensured optimum power consumption.

The equipment being into their twenty-ninth year of sustained operations have far outlived their economic lives, yet have high operational reliability.

WATER SYSTEM

IUAC's centralized water system of Phase-I feeding low temperature cooling water having a total heat removal capacity of 115 TR performed to an operational uptime of 100%. This is due to the stringent maintenance practices which have been followed over the years. The system has overshot 1,70,000 hours from its expected life span.

IUAC's centralized water system of Phase-II & III feeding low temperature cooling water also performed to an uptime of 100%.

A strict monitoring on the water quality has ensured that the flow paths are in healthy condition. The maintenance costs were kept significantly low as compared to world class bench mark values.

150 KLD Sewage Treatment Plant (STP) performed satisfactorily.

COOLING SYSTEM

Availability of equipment was recorded at 99%.

WORKS CARRIED OUT DURING THE YEAR:

- Installation, Testing & Commissioning of 5 KW Process Chiller for FEL
- Installation of 30 KW Process Chiller for FEL
- Laying of SS Water Headers from Beam Hall#III Basement to Chiller Room for FEL
- Extension of SS Process Water Headers to MRI room from Beam Hall#III
- Replacement of leaking GI Pipes at various locations
- Provision of 6 nos. of process water tap-off connections from the main headers in Beam Hall#III for HCI
- Installation of RO Water Purifier in Parijat#1
- Replacement of 5 TR compressor in Beam Hall#II store extension ductable unit
- Overhauling of 3 nos. of Softeners of Ph-1, 2 & 3 AC Plants
- Planning & processing of renovation/repair of Workshop & LHe Compressor room Air-Washers
- Auditorium Air-Conditioning system was commissioned and taken over by IUAC in the month of July 2018.

3.2.3 Mechanical Workshop (MG-III Gr.)

Rajeev Ahuja, Sanjay Kumar Saini, Bipin Bihari Choudhary and Davinder Kumar Prabhakar

Machine Shop

Welding Shop

The prime responsibility of the workshop group is to take care of the machine shop activities. IUAC workshop is well equipped with *tool room type* modern machines and welding facilities.

The major facilities in the workshop are Machine shop and Welding shop.

Machine Shop is equipped with a five axis Vertical Machining Centre and a CNC Lathe machine, four conventional Lathe machines, two Milling machines and a Radial Drilling machine, one cylindrical grinder, one tool and cutter grinder, one horizontal and one vertical Band Saw machine, catering to different types of jobs. Most of these machines are of renowned makes HMT, Batliboi, BFW.

Welding shop is having high quality TIG welding machine and other equipments. Some of the TIG welding machines can give pulsed arc for thin sections welding. Air plasma cutter with a capacity to cut up to 40 mm thickness of stainless steel is extensively used. Oxy-acetylene cutting and brazing set ups are also available.

Workshop has Solid Works CAD facility for design and drafting purpose. It also has VISI CAM for the CAM support for the Vertical Machining Centre and CNC Lathe. A portable CMM, with 1.8 m inspection area with 40 µm accuracy is also part of Workshop for highly accurate measurement and assembly.

We cater to a large community of users and researchers from different labs of IUAC related with the development and experimental activities, right from inception of an idea till final fabrication and even installation. For most of the jobs, the users discuss with Workshop personnel regarding their requirements. Then it is designed, drawings are prepared and the job gets done under our supervision either in-house or from outside eligible vendors (if it is not possible to do in our workshop). Before delivering the job to the users or lab staff, the job is inspected to ensure that it is fabricated as per the required specifications. If required, we assemble and install it also at the site.

This year we had received and fabricated around 350 jobs of different nature in the workshop.

IUAC workshop is providing Apprentice Training for the ITI passed students in both welding shop as well as in machine shop. Basic workshop training is provided for the scientist trainees and Ph.D. students enrolled in IUAC.

Apart from the above mentioned regular activities, MG-III group members were also involved in some of the on going major development projects and experiments related research and development activities. Some of them are mentioned below:

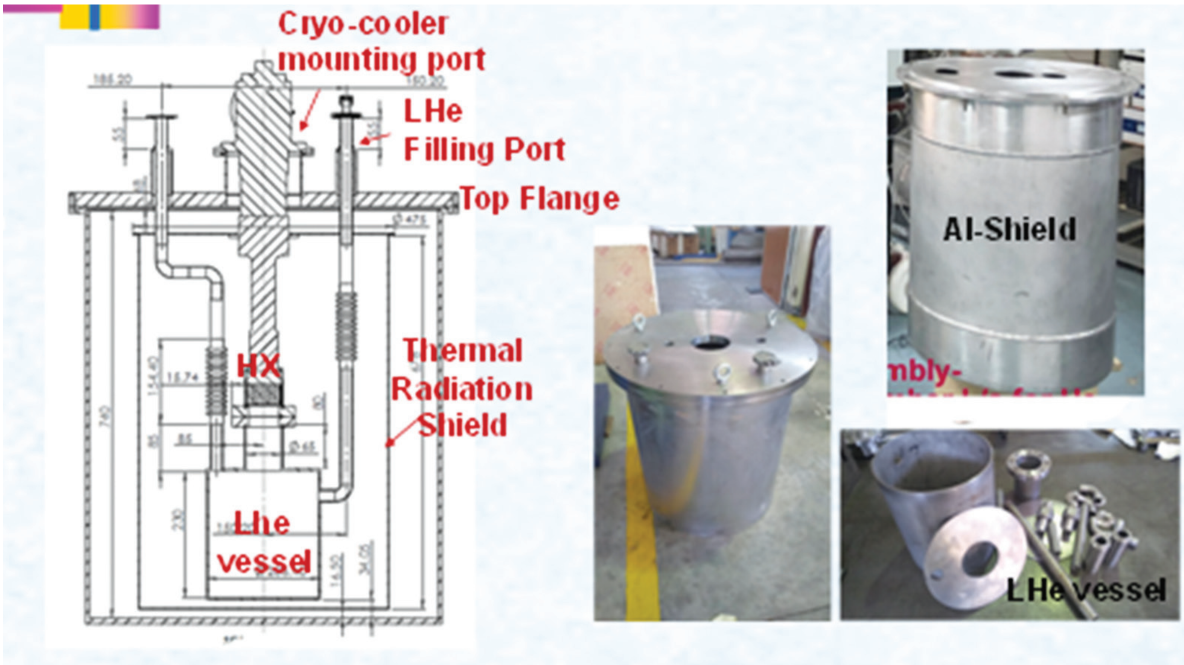

Cryo cooler based test cryostat for MRI development Project

- Radio Frequency Quadrupole, RFQ
- Drift tube Linac, DTL
- MEBT Spiral Buncher
- One meter diameter Vertical Scattering Chamber for LEIBF
- TEGIC related works
- MRI development program
- FEL related works
- Fabrication of Mezzanine platform for LINAC control room

Mezzanine platform for LINAC control room

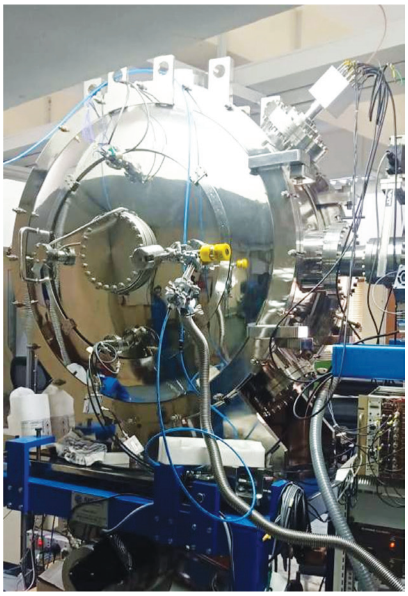

Vertical Scattering Chamber for LEIBF

3.2.4 Civil Works

Harshwardhan, A.J Malyadri, M.K. Gupta

Works under Civil Section:

- Major Projects (right now under process /planning for renovation of housing and Lab Building Construction by CPWD under deposit mode)
- Minor Projects
- Minor works
- Civil Maintenance (from day to day basis under AMC (Civil)
- External cleaning of Campus
- Liaison with outside agencies for statutory approvals and various civic problems

Important Civil Activities undertaken during the year 2018-19

Following important civil works were undertaken during the year 2018-19 in addition to routine civil maintenance and minor works:

- P/F M.S Frame for vertical wall garden in front of Old Guest House's Entry wall.
- Supply of epoxy material for repair of floor in Room No. 308 in Engineering Building.
- Addition /alterations in waste pipes & rain water pipes on beam hall –I roof due to recent waterproofing.
- Cleaning of sewage effluent tank (1 no.) in housing area.
- Construction of room for water chiller for FEL project near south-side entrance of BH-III.
- Misc. civil works & wooden partitions in Spectroscopy, UV –Vis-NIR & FTIR lab (R. No. 348), 2nd floor, Main Lab Building.
- P/A External & Internal Painting of Parijat -1 (Director Residence) at IUAC.
- P/F new vinyl flooring (of 2 mm thickness) tough grade in R. No. 110 A, Main Lab Building.
- P/F EWC (European type water closet) in Parijat -1.
- Renovation of tea pantry near Room No. 212, 1st floor, Main Lab Building in IUAC.
- Misc. wooden work for Room No. 341 (Nuclear Target Lab), 2nd floor, Main Lab Building.

- P/F small glass partition for 3 nos. toilet in Auditorium & Main Lab Building.
- Waterproofing and re-sloping of Beam hall-I roof.
- Supply of painting related material for civil maintenance work at IUAC.
- Making enclosures outside Beam Hall –III on south-side for protection of BH-III Equipment.
- P/A painting of workshop area and corridor area in Engineering. Building.
- Waterproofing work on roof of canteen building, BH III Side terrace & Low Temp. Lab near BH-II.
- Construction of ramps at various places in phase –I housing area for facilitating elderly person for access to phase-I housing block.
- Civil work for making a central junk yard near AC plant III in IUAC.
- Misc. Civil works in IUAC Campus (I) Renovations of gent's toilet near Old Guest House & G.F Main Lab Bldg. (II) Renovations of visitor room near old guest house.
- P/F M.S Railing on existing parapet wall of 2^{nd} floor, Main Lab Bldg.
- Misc. painting work in IUAC Campus (painting of material store, steel staircase & VIP Guest Dining hall etc.).
- P/A painting of 5 nos. flats in IUAC housing area.
- Misc. painting (under annual preventive maintenance) of outdoor location in IUAC.
- Civil works for TEM installation in Room No. 101, Main Lab Bldg., IUAC.
- Civil work for making vertical garden in front of flat let area in IUAC.

3.2.5 COMPRESSED AIR SYSTEM AND MATERIAL HANDLING EQUIPMENTS

K.K. Soni and Bishamber Kumar (MG I)

Our Group is associated in the following activities:

i) **Compressed Air System:** Compressed air plant (Ph-I&II) consisting of three nos. of screw compressors each of $115M^3$/hr capacity, 4 nos. of air dryers, pre/fine/oil removal filters with capacity of 3000 lpm @ 9.00 Kg/cm^2, Storage Tank of 25 cum have maintained uninterrupted air supply to various labs within IUAC round the clock throughout the year. Pneumatic connections are provided to different labs / area / instruments as and when required.

ii) **Laboratory Gases:** Indigenous / imported various industrial / lab purity gases / cylinders / regulators have been made available as per the requirement in different labs from time to time.

iii) **Elevator:** Proper maintenance is carried out so that elevator operates safely without fail.

iv) **Material Handling System :** Periodic maintenance / servicing of more than 14 nos. E.O.T cranes and electric hoists of various capacities varying from 1 Ton to 7.5 Tons are being carried out periodically to ensure there smooth, uninterrupted and safe operation.

v) **Fire Safety :** Annual refilling and periodic maintenance of all the fire extinguishers are carried out. Demonstration for use of Fire extinguishers have been arranged and all the users and IUAC employees are trained to use the fire extinguishers.

Fire extinguishers have been installed in the newly built II Floor of Lab Building. For Fire safety purpose pressurized water hydrant system, including underground Water tank, electric / diesel engine water pumps have been installed. With this, continuous water pressure is maintained in the water hydrant line. Wet risers, down comers, hose reels, hose pipes, boxes, hydrant branches have been provided in and around different buildings i.e. Material Science building, Engineering Building, New Guest house and Auditorium.

4. EXPERIMENTAL FACILITIES IN BEAM HALL

4.1 NEUTRON DETECTOR ARRAY FACILITY (NAND) & GENERAL PURPOSE SCATTERING CHAMBER (GPSC)

N. Saneesh, K.S. Golda, Mohit Kumar, A. Jhingan & P. Sugathan

During the last year we have scheduled many student's thesis experiments and completed all of them successfully. Students from Banaras Hindu University, Panjab University, MSU of Baroda,Visva-Bharati University and Andhra University performed multiple experiments using NAND and GPSC facilities.

Experiment in NAND facility measured fission mass distribution for symmetric and asymmetric fission modes in Thorium compound nucleus and investigation of role of entrance channel nuclear dissipation on neutron multiplicity. 50 liquid scintillators are used to detect neutrons in coincidence with fission fragments detected in pair of large area multi wire proportional counters (MWPC). Pulsed beams from Pelletron accelerator were used in experiments. Fragments velocity distribution and neutron time of flight were recorded online using VME multi parameter data acquisition system. The pre- and post-scission neutron multiplicities were extracted for the reaction $^{18}O+^{186}W$ at different excitation energies populating the compound nucleus ^{204}Pb to investigate the entrance channel effect on the nuclear dissipation involved in the heavy ion fusion-fission dynamics. The reaction $^{18}O+^{186}W$ have entrance channel mass asymmetry similar to the reaction $^{16}O+^{181}Ta$ studied earlier expecting similar behavior from both the systems against the nuclear dissipation. The detailed analysis and results are reported in a recent publication in Phy. Rev. C.

Other experiments performed in GPSC facility aimed to extract barrier distribution using quasi-elastic measurements and influence of breakup like process in weakly bound projectiles. Following experiments have been completed.

1) Quasi-elastic scattering measurements for ^{16}O, ^{28}Si + ^{144} Sm, the thesis experiment of Ms Kavita Rani, Panjab University.
2) Thesis experiment of Mr Saumyajit Biswas, Visva-Bharati University. The experiment measured quasi-elastic scattering using ^{16}O and ^{28}Si beams at Pelletron energies.
3) Thesis experiment of Ms Arshya Sood, I.I.T Ropar. The experiment was performed to explore the effect of breakup channel on fusion around barrier energies using ^{7}Li, beam.
4) Ms Chhavi Joshi, MSU of Baroda performed experiment to study the effect of breakup on the elastic scattering and fusion mechanism of weakly bound projectiles using ^{7}Li beam.

All these experiment used array of gas-Silicon Hybrid detector telescopes mounted inside GPSC chamber and its multi-channel readout electronics. To measure the quasi-elastic back-scattering events four telescopes were mounted in cone geometry at back angle of 173°. The online data collected using CAMAC based Freedom data acquisition software installed in Data room machines.

The preliminary results from some of these experiments are reported in later section of this annual report.

4.2 GAMMA DETECTOR ARRAYS : GDA AND INGA

Yashraj, R.K. Gurjar, Indu Bala, Kusum Rani, R. Kumar, S. Muralithar and R. P. Singh

4.2.1 Indian National Gamma Array (INGA)

In the last academic year about ten experiments were performed to study the structure of nuclei at high excitation energy and angular momentum. A total of about 200 shifts of beam time was utilised for these experiments. To enhance the efficiency of the array two more clover detectors were added to the setup. Eleven clover detectors were annealed and outgassed with the annealing setup at IUAC to restore the high resolution of the detectors. Order is also placed for two more Anti-Compton Shield (ACS) BGO detectors to add to the INGA setup. A five day school on “Modern techniques of γ-ray spectroscopy for nuclear structure studies” was organised in IUAC and more than thirty research scholars participated in this school.

4.2.2 LN_2 Filling System

R. K. Gurjar, R.N. Dutt, Kusum Rani, Yashraj, Indu Bala, S. Muralithar and R. P. Singh

New LN_2 sensors (PT100) were installed at the outlet of clover detectors. A new LN_2 control system using industrial modules based on MODBUS standard and RS485 serial back plane for communication was tested. The test system incorporates Graphic user interface (GUI) based on LabView software for control and automation of the filling system. The pilot system has been used successfully for automated filling of 3 clover detectors in the INGA setup.

4.2.3 Gamma Detector Array (GDA)

GDA setup was used for eight experiments (groups from University of Delhi, AMU, Central University of Jharkhand) in the last academic year. Experiments used the HPGe detectors for study of incomplete fusion reactions with heavy ions and in one of the experiments (IUAC) one HPGe detector was used at the focal plane of HIRA spectrometer.

4.2.4 Perturbed Angular Distribution (PAD) setup

R. Kumar, P. Barua, R P Singh and S Muralithar

The coils for the PAD setup in GDA beam line were refurbished to work with higher magnetic field. The setup is moved to 45º beamline and GPSC is shifted to GDA beamline in the earlier position of PAD setup.

4.2.5 New Charged Particle Detector Array

R. Kumar, Arti Gupta, T. Varughese , S. Venkataramanan and R. P. Singh

Eleven CsI detectors for light charge particles were mounted and tested with alpha and gamma sources for detector resolution. Figure below shows a picture of the array. A project to supplement the array with more detectors and the processing electronics was submitted to SERB for funding.

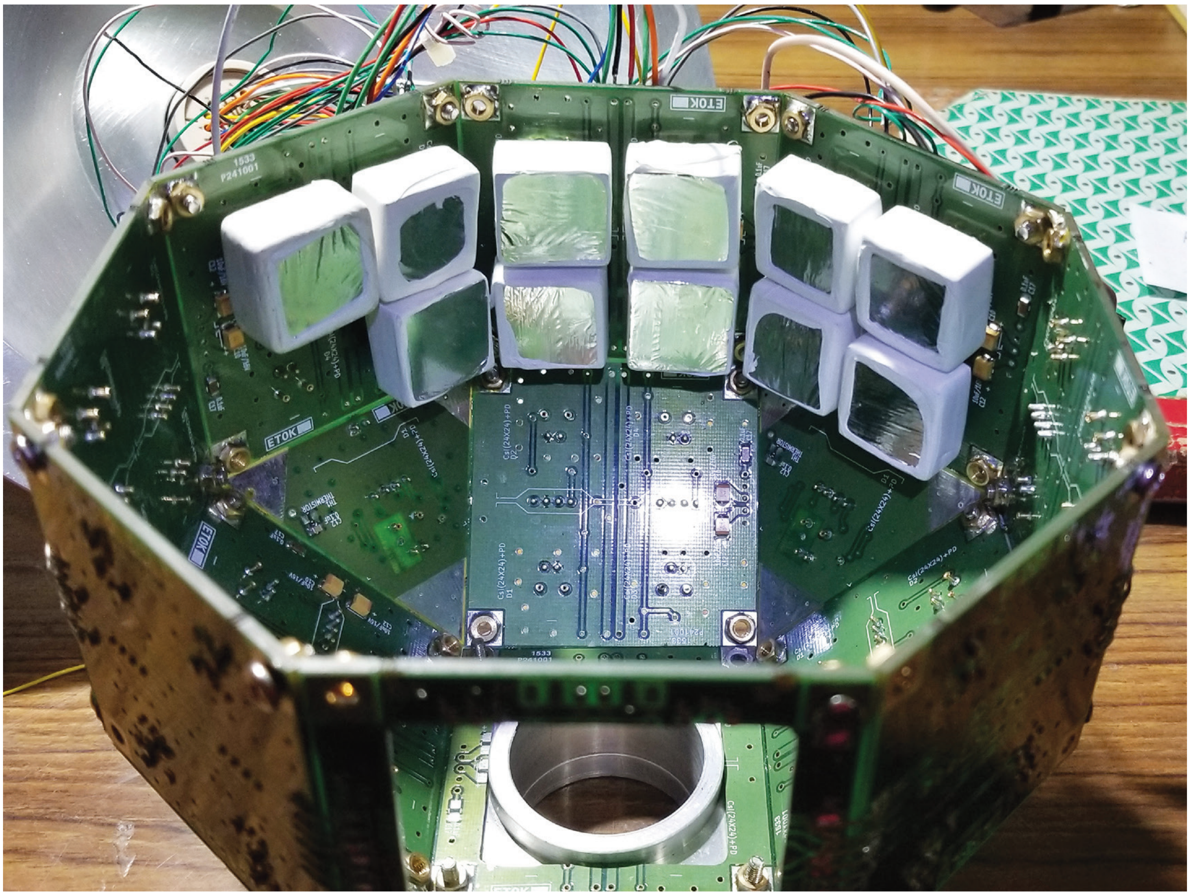

4.3 RECOIL MASS SPECTROMETERS

4.3.1 Heavy Ion Reaction Analyzer (HIRA)

S. Nath, J. Gehlot, Gonika, T. Varughese, A. Jhingan, N. Madhavan

Last year HIRA was used in five user experiments all of which were related to thesis work and two facility tests were taken up by IUAC personnel.

Measurement of Evaporation Residue (ER) and quasi-elastic backscattering cross-sections in $^{12,13}C$ + ^{197}Au reaction were carried out (Naba K. Ghosh et al., Calcutta University) to study the Collective Enhancement of Level Density (CELD) effects. Survival of ERs as a function of entrance channel mass asymmetry and neutron numbers in colliding partners was studied (P. Jisha et al., Calicut University) by measuring ER excitation function for $^{16,18}O$ + $^{182,184,186}W$ systems. Barrier distribution through ER excitation function was studied (Nabhendu K Deb et al., Guwahati University) for the systems $^{16,18}O$ + $^{61,62}Ni$,^{106}Sn) to understand transfer channel coupling in sub-barrier cross-section enhancement. Measurement of evaporation residue (ER) cross sections for ^{16}O + $^{142,150}Nd$ were carried out (A. Vishakh et al., Central University of Kerala) above and below the Coulomb barrier in order to study fusion reactions forming medium heavy compound systems and the role of target deformation. ER cross sections for the reaction ^{37}Cl + ^{68}Zn were measured (Amit Chauhan et al., IIT-Roorkee) above and below the Coulomb barrier, for studying production optimisation of neutron deficient radio-nuclides of noble metals in low energy reactions. Sub-barrier fusion in ^{37}Cl + ^{130}Te system, for which data was collected in the preceding year, has been published in Physical Review C.

In the facility tests, ER cross-section measurement deep below the one-dimensional barrier in ^{19}F + ^{181}Ta system was attempted (S. Nath, et al., IUAC) through detection of characteristic online gamma rays from the ERs using a germanium clover detector and mass distribution of fission fragments from the fusion of ^{12}C + ^{235}U was undertaken with encouraging results.

Electronics laboratory, IUAC has developed electronic modules such as Time to Amplitude Converter (TAC), multi channel fast pre-amplifiers to be used with the multi-wire proportional counters. These electronic modules were tested for their functioning with the detectors, as and when they were fabricated. Ms. Gonika won one of three prizes for best presentation in SERB School on Nuclear Astrophysics at SINP, Kolkata. Two research scholars, who used HIRA for their experiments earlier, obtained their Ph. D. degrees during this period.

4.3.2 HYbrid Recoil mass Analyzer (HYRA)

N. Madhavan, S. Nath, J. Gehlot, T. Varughese, Gonika, A. Jhingan

As the SC-LINAC accelerator did not operate during the past year, only two experiments which needed Pelletron beam energies were taken up using HYRA. ER excitation function and angular momentum distributions were measured (M. M. Hosamani et al., Karnatak University) for ^{16}O + ^{208}Pb and ^{18}O + ^{206}Pb, both leading to same compound nucleus (CN) $^{224}Th^*$, to study entrance channel effects in fission hindrance. The analysis of experimental data have been completed. In the other experiment, ER excitation function were measured for ^{16}O + $^{204,206}Pb$ and ^{18}O + $^{204,208}Pb$ systems (P. Sandya Devi et al., Andhra University) from near barrier energy upwards. Earlier, in mid-2017, the higher energy points for these experiments had been measured using Pelletron + SC-LINAC beams. The pending experiments in HYRA are planned to be taken up when SC-LINAC beams are available which is expected to be during the last quarter of 2019.

The new focal plane detector chamber for the planned isomer decay setup, to be used with gas-filled mode of HYRA, has been designed and fabricated. It will allow up to seven germanium clover detectors to be installed close to the silicon detector in which ERs will be implanted. The final flange and the chamber wall have been machined to be thin enough to minimise gamma attenuation in the direction of the longitudinal and the six radial detectors, respectively. Servicing of the MWPC detector cab be done from the front-end after isolating the chamber from HYRA while the silicon detector can be accessed from behind after removing the detector in the longitudinal direction. The compact MWPC detector is being fabricated. All electrode frames have been made and fabrication of wire frames will begin shortly.

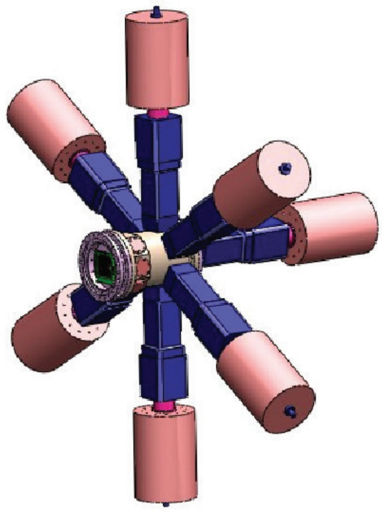

Design of new focal plane detector chamber and seven clover germanium detectors

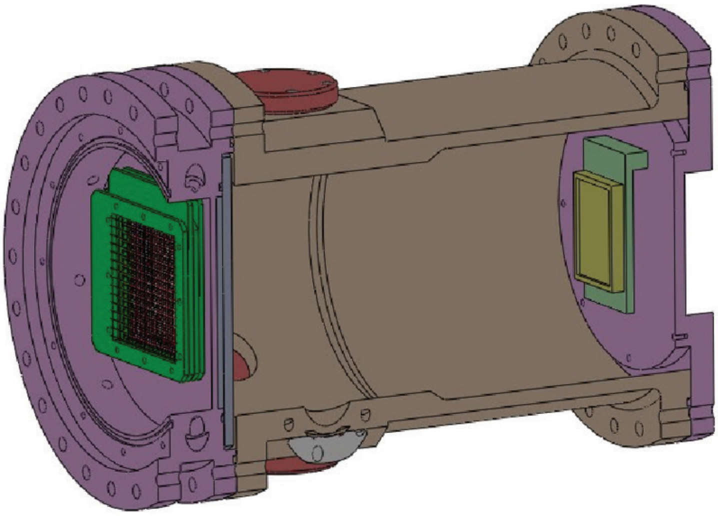

View of the planned MWPC detector and the silicon detector for detection of ERs

Two research scholars, who used HYRA for their theses experiments earlier, have obtained their doctorate degree during the past year and three more are in the process of submitting their theses. Analysis of the experiment to look for Pairing Vs. Clustering of two neutrons in ^{18}O, by using the vacuum momentum achromat mode of HYRA, has been completed and manuscript has been finalised. Experimental observations on ER excitation function in ^{16}O + ^{203,205}Tl systems have been published in Physical review C and two manuscripts based on experiments using HYRA are being communicated.

4.4 MATERIALS SCIENCE FACILITY

A. Tripathi, K. Asokan, V.V. Sivakumar, Fouran Singh, S.A. Khan, P. K. Kulriya, I. Sulania and R.C. Meena

The materials science facilities continue to support research programmes of a large number of users from different universities and institutions. This year there were a total of 63 user experiments spread over 202 shifts and were performed without any major beam time loss due to facility break down in materials science beamline in beamhall I. BTA experiments associated with students' Ph.D. programmes continued to get priority with 18 runs spread over 53 shifts. Though the swift heavy ion (SHI) irradiation and related experiments mostly utilize irradiation chamber in the materials science beamlines in beamhall-I, one experiment was performed in the materials science beamline in beamhall-II. Besides this, 5 experiments of 23 shifts requiring low fluence irradiation were performed in GPSC beamline. The details of the experiments being done in areas of SHI induced materials modification and characterization are given in Section 5.2.

Besides irradiation facilities, materials science group is also providing many materials synthesis and characterization facilities such as XRD, AFM, SEM, Raman, UV-Vis, I-V, Hall measurement etc and these are heavily utilized by users. This year more than 2100 samples were characterized.

4.4.1 Maintenance of Irradiation Chamber in Beam Hall I

S. A. Khan, R. C. Meena, A. Tripathi,

The beamline with low and high temperature irradiation and in-situ measurement facilities was used by a large number of materials science users and 57 experiments of 178 shifts were performed in this chamber. There were no breakdowns this year and a faulty ion pump was replaced without any loss of user beamtime.

4.4.2 Scanning Probe Microscope

Indra Sulania, A. Tripathi

The SPM has been running without any major problem this year. The two very old CRT computer monitors associated with the system developed a problem and were replaced.

The monitor associated with the microscope, for initial viewing of the sample, was also changed. The settings for balancing the vibration isolation table had got disturbed after a nitrogen cylinder change and the same was restored.

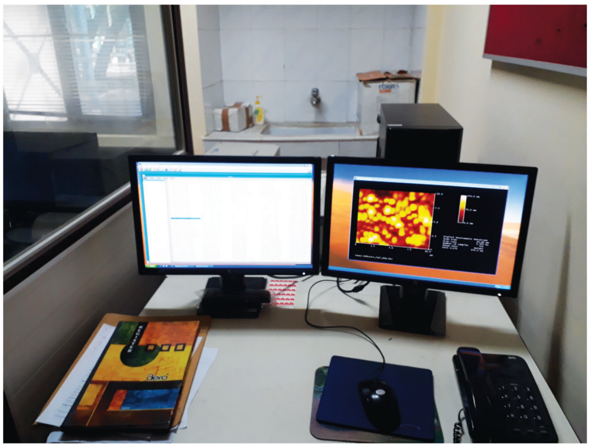

Figure 1: SPM monitors

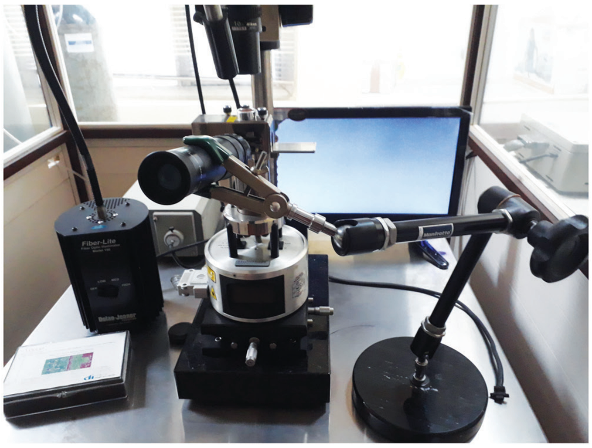

Figure 2: SPM set-up with Optical Microscope for sample viewing

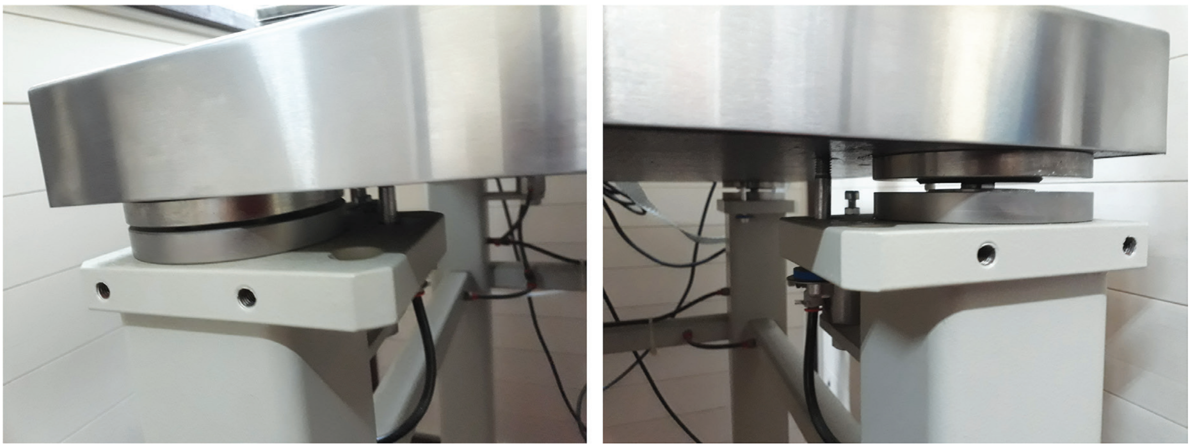

Figure 3: Vibration Isolation Table with adjusting screws

4.4.3 Tescan MIRA II FE-SEM with Oxford INCA PentaFETx3 EDS

S.A. Khan, A. Tripathi

Tescan MIRA II FE-SEM *with* Oxford INCA PentaFETx3 EDS is under regular operation after a new electron emitter (Denka TFE) was installed in Feburary, 2017 (after ~75000 hrs of operation). Last year (Feb 2018), the computer which had gone bad was procured from TESCAN Brno and was replaced. It has since been working without any major problem. This year new batteries (12V,18Ah,4 nos) were also procured. After replacement of computer, 331 samples of 56 users were characterized. Above numbers are for the period August 17 to July 18. Additionally, 300 samples from 69 users were analyzed between August 2018 to March 2019.

4.4.3.1 Q150T-S HV Sputter Coater

Q150T-S HV Sputter Coater system is working fine and 315 samples from 46 users were coated for SEM measurement for the period August 17 to July 18. Additionally, 152 samples from 28 users were analyzed between August 2018 to March 2019.

4.4.4. RF Sputtering System, DC Sputtering System and Ball Milling System

V. V. Siva Kumar.

The RF parallel plate diode sputtering system was maintained in proper working condition. A substrate heater was installed and tested. The system was used for thin film deposition work of copper oxide (25 films, IGU, Rewari) and zinc oxide (48 films, Dayalbagh Educational Institute, Agra). The DC sputtering system was used for deposition of thin films of CuO (10 films, IGU, Rewari), Ti (15 films, Kurukshetra university), pure and Al doped $ZnSnN_2$ (~100 films), MgO (5 films) and Cu-Cu_2O (4 films, GGSIPU, Delhi). The pure and Al doped $ZnSnN_2$ films were grown by the user from Bharathiar University, Coimbatore, with different deposition conditions for two different ion beam studies involving Al ion implantation and Ni ion irradiation while Cu-Cu_2O films were grown for gamma irradiation work. The images of plasma formed due to Cu and Zn-Sn sputtering are shown in Fig. The ball milling system was used to pulverize thermo-luminescent materials by user from University of Delhi and LiF and MgF_2 material by user from AIIMS, Delhi (11 times).

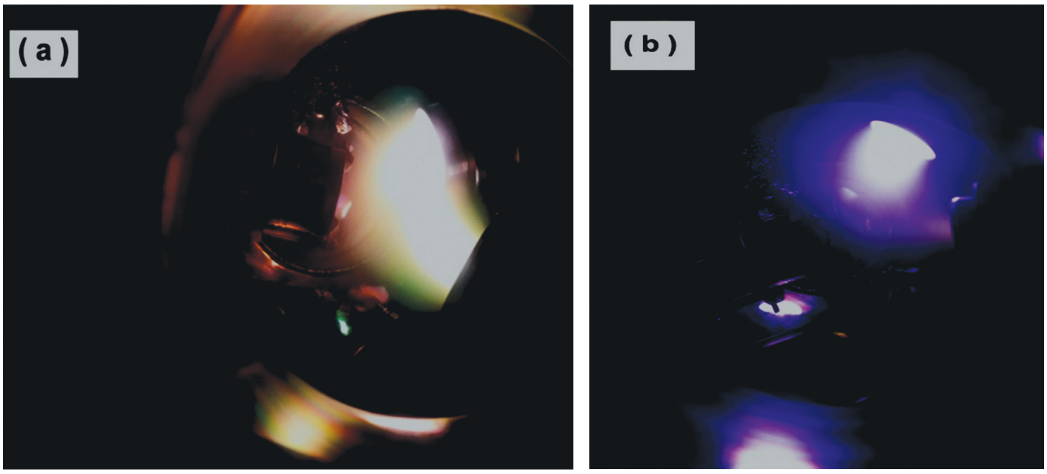

Figure: Images of plasma formed due to (a)Cu sputtering and (b) Sn , Zn sputtering.

4.4.5 Structure and Spectroscopy Laboratory

Pawan K. Kulriya and Fouran Singh

There have been several experiments besides regular upkeep and utilization of the structure and spectroscopy facilities for research in materials science. In-situ x-ray diffraction (XRD) facility has been extensively used for structural characterization of materials. This year offline XRD system has been used for characterization of around 400 samples. Last year, X-ray generator stopped functioning due to problem in its electronic circuit which was not repairable. Therefore, a new X-ray generator was procured and replaced old generator with new one. Similarly, we have also replaced scintillation detector with new detector. An in-situ experiment, in which structural characterization was carried out during ion irradiation, was also performed. Another facility namely high-temperature irradiation setup also exists in the same beamline and one experiment were performed by keeping the target at elevated temperature during swift heavy ion irradiation.

Micro-Raman facility is another heavily utilized facility for the materials characterizations. This facility operates in two modes as ex-situ and in-situ modes. About 670 spectra were measured for large number users across the country in ex-situ mode. Presently, laser is out of order and order of the procurement of new laser has been placed and probably facility will be operational after the installation of new laser for regular experiments. The other facilities such as UV-photoluminescence and ionoluminescence are also operation and being utilized for regular experiments. About 188 PL spectra were measured on various types of samples pre- and post irradiation of samples. UV-Vis-NIR facility is also got operational for regular experiments, which was down for some time. Solar simulator facility for the characterizations of solar cells and photo diodes is also operational. RF sputtering setup is being in regular operation and about 28 depositions have been carried out by various users. We are happy to inform that few new facilities has been implemented such FTIR, e-gun evaporation and high temperature furnace

4.4.6 High Temperature Furnace and Electron Beam Evaporator System

P.K. Kulriya

Two new research facilities: (a) high-temperature furnace and (b) electron beam evaporator system for the preparation of the thin films (Figure 1) were established this year. Electron beam based thin films evaporator unit is consisting of (a) high vacuum chamber equipped with Pfeiffer (Hipace 700) turbo molecular pump and Alcatel ACP dry pump, (c) substrate holder cum heater with PID controller for 500 oC (d) Inificon quartz crystal thickness monitor and (e) evaporator electrode assembly for the evaporation of two materials.

Figure 1. Photograph of the Electron beam based thin films evaporation system (a) water chiller (b) Control unit and (c) thin film coating setup.

Another facility is a high-temperature furnace which can be used to carry out sintering of the materials up to a temperature of 1700ºC in the ambient condition. Both systems were successfully installed, commissioned and are being used extensively.

4.4.7 Electrical Transport and Low Temperature Laboratory

Ramcharan Meena, Anha Massarat, Anuradha Bhogra, Razia Nongjai, Ashish Kumar, K. Asokan

There are various experimental facilities available in the transport lab that allows one to measure room temperature as well as temperature dependent physical properties of materials. The major facilities are listed below along with their working temperature range and the method of measurements.

Sr No.	Measurement Facility	Temp Range	Method of measurement
1	Resistivity Measurement (Ohm-Giga Ohm Range)	10 K -450 K	2-Probe. 4-Probe
2	Dielectric Measurement	10 K -450 K	Capacitance Method
3	Seebeck Effect	85K- 450 K	Differential Method
4	Hall Effect	300K& 80K	Hall effect Method
5	I-V, V-I	10 K -450 K	Pressure probe Method
6	A.C. Susceptibility	10 K -300 K	Induction Method
7	C-V	85K- 450 K	Capacitance Method
8	High temperature dielectric	300K-1100 K	Capacitance Method

Above mentioned facilities are routinely used by mainly university users and also in house experiments. Last year approx. over 100 users have utilized these facilities. Apart from the above, there are three furnaces that can operate in the temperature range up to 1250 ˚C and other minor facilities that are used for sample preparation. One of these furnaces can be used for the purpose of vacuum annealing having pressure of the order of $3*10^{-2}$ mbar.

A dedicated Rapid thermal annealing set up operating in the temperature range up to 1000 ˚C is also operational. The ramping rate can be up to 60-80 ˚C/S. There are four medium available for the annealing (Vacuum, O_2, N_2, Ar_2). The pressure of the gas can be varied up to range 0-1000 SCCM. In last year, RTA has been used by 15 users.

This lab also supports the in-situ measurements in the Materials Science Beamline and in last year there were 4 *in-situ* temperature dependent electrical transport measurements: I-V, C-V, and R-T.

4.5 STATUS OF THE RESEARCH WORK DONE IN THE RADIATION BIOLOGY FACILITY

A. Sarma, IUAC, New Delhi

The Radiation Biology experiments involving accelerated heavy ions are carried out at the dedicated Radiation Biology Beam line of IUAC and utilizing the **ASPIRE** [Automated sample positioning and irradiation system for radiation biology experiments] system. In this system the irradiation of cells by accelerated heavy ions can be done at atmospheric pressure with a set of preset doses. The system is characterized by the dose uniformity over a field of 40 mm diameter within 2 % standard deviation. The mean fluence is within 1 % of the electronically measured value at the centre of the field. The characterization of the system has also been done using irradiating SSNTD [CN 85].

The radiation biology laboratory is having the following equipment to facilitate the sample preparation and post irradiation treatments.

1. Two CO_2 incubators, Two biosafety cabinets, one small laminar flow bench for cell culture
2. Field Inversion Gel electrophoresis, Normal gel electrophoresis, protein gel electrophoresis set up
3. Image based cell counter Countess [Invitrogen] which also gives information about cell viability and Beckman-Coulter Z2 cell counter
4. PCR machine, a crude gel documentation system, UV-Vis Spectrophotometer and a Fluorescence microscope.
5. Perkin Elmer Multimode Plate Reader, Eppendorf and Plastocraft Refrigerated Centrifuge and a Biotek micro-plate washer.

Apart from that, LN_2 Dewars, -80C ultra freezer, -20 deep freezer and other refrigerators serve as the storage facilities. The laboratory section has independent Split AC supply isolated from the central AC system. Regular work is going on in the laboratory on Analytical procedures involving gene expression studies using PCR, Western Blot, Fluorescence Immunostaining studies etc by the University Users

The following are the projects which are undertaken at present

(1) Investigation of DNA Repair Pathways and cross talk between PARP-1 and P53 after C ion irradiation of cultured human cells, [Dr. Utpal Ghosh, Priyanka Choudhury BTA, Kalyani University]

(2) Signaling pathways of activation and secretion of Matrix Metalloproteinases from human lung carcinoma cells after irradiation with carbon ion beam, Payel Dey, Kalyani University

(3) Radiosensitization of human cancer cells using G-quadruplex ligands. Sourav Ghosh, Kalyani University

(4) Carbon nanomaterials as cell radiosensitizors in therapeutics, M. Mukherjee, Amity University.

(5) Evaluation of Radio-protective property of 2,4 di nitrophenol in cellular model against particle radiation. Anant Narayan Bhatt, INMAS.

(6) Chromosomal damage induced by High LET Carbon beam radiation in comparison to gamma radiation in human peripheral blood lymphocytes/ Chinese hamster fibroblast (V79) cells and the effect of Diclofenac sodium in modulating it. Amit Alok, INMAS

(7) DNA damage repair kinetics by a potential countermeasure agent using γ-H2AX/comet assay. Paban K Agrawala, INMAS

4.6 ATOMIC AND MOLECULAR PHYSICS

4.6.1 Modification of Vacuum Chamber at 75º Beam Line in LEIBF

D. K. Swami[1], Shashank Singh[2], S.K. Saini[1] and T. Nandi[1]

[1]Inter University Accelerator Centre, Aruna Asaf Ali Marg, New Delhi-110067, India.
[2] Physics Department, Panjab University Chandigarh, 160014, India

Several experiments have been approved line in LEIBF. For example: One experiment is based on mean charge state measurement using a very simple but novel method [1]. In this experiment, mean charge state will be measured for highly ionized atoms passing through thin bilayer targets made up of metal and insulator. Here, aluminized mylar foil will be used as a target. The purpose of this experiment is to find the dependency of mean charge state on ordering of the target. Another experiment is based on the study of heavy ion solid collision processes in the inverse kinematics so that so that we can study isotopic effect on ionization cross section precisely compared to that with direct kinematics where impurity problem in target is difficult to avoid. For these experiments, some modifications were required in vacuum chamber at 750 beam line. One circular disk with M6 tapped holes place at the bottom of the chamber was designed and fabricated in order to mount the two Faraday cups one in front (penetrable) and other at back of the target along the beam axis. This system acts as beam collimation along with mean charge state measurements [1]. Once the Faraday cups are made aligned, the surface plate is fixed using a certain arrangement. For the angular motion of the targets, one rotatable axis-360° adjustable stage is mounted at the top of the lid and a multi target holding ladder on it. This arrangement will let us keep either metal or insulator of the bilayer target at the exit side.

Penetrable Faraday cup

Target Manipulator

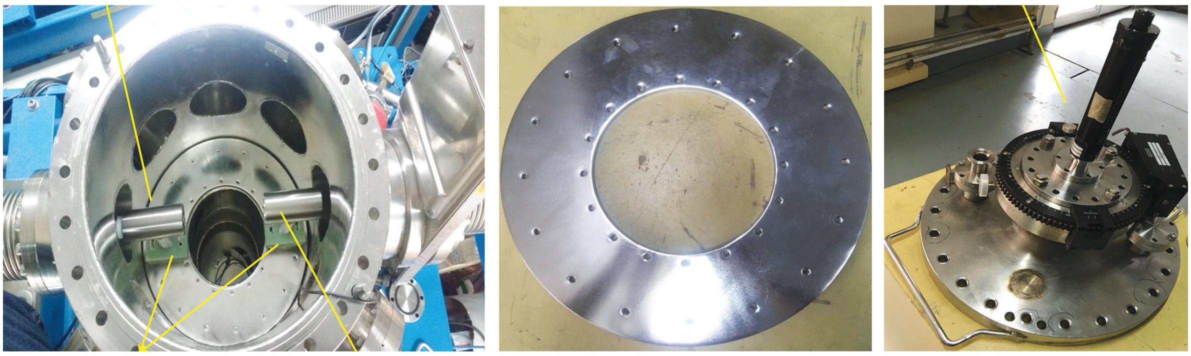

(a)
G10 for insulation Faraday cup

(b)
Surface plate

(c)
Rotatable axis-360° adjustable stage

Fig 1: (a) Both the Faraday cups inside vacuum chamber are mounted on the surface plate, (b) surface plate and (c) target manipulator on a rotatable axis-3600 adjustable stage.

REFFERENCE

1. Xianming Zhou et. al., Nucl. Instr. Meth. Phys. Res. B 299, 61 (2013).

4.6.2 Design of Ion Trap Facility for the Life Time Measurement of The Atomic Metastable States

Sugam Kumar, C.P. Safvan and Lekha Nair

An ion trap facility is under development in the Low Energy Ion Beam Facility (LEIBF) at IUAC for the measurement of the life time of the metastable states in the atomic and molecular system. The highly charged ions will be selectively captured and trapped in their metastable states from the ECR ion source. The decay of the metastable state is measured in isolation at low energy, without any active cooling. The ion trap is designed to accept externally produced ions of all species and charge states. The proposed experimental user facility will allow to benchmark corresponding radiative life time measurements with high significance and with broad range of ions species.

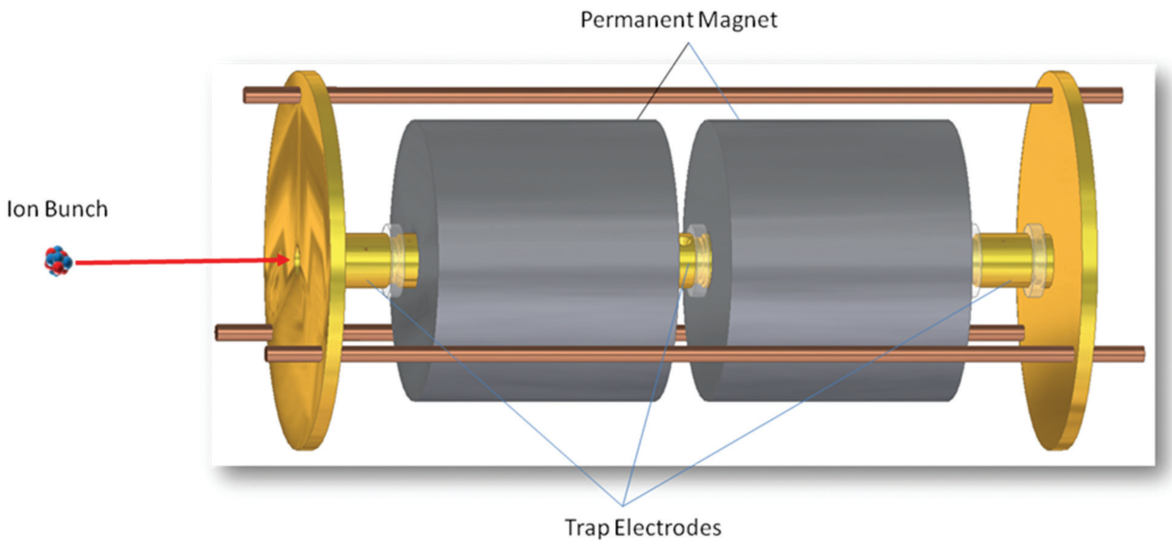

Figure 1: Schematic of the ion trap electrodes assembly with permanent magnet.

A mixture of charge state is extracted from the ECRIS and ejected in an ion pulse. An analyzing magnet in the beam line selects out the desired ions of specific *m/q*. The selected ions are of high kinetic energy and cannot be trapped into the Penning trap, to slow down the ions they are passed through a decelerating system which is already installed in the LEIBF beam line. The energy of the ions is reduced to few eV from few keV, which makes them idea to be captured 'on the fly' into the Penning trap. The transit time over the $\approx$ 20 m beam line from the ECR ion source to the Penning trap would < 50 μs for most of the highly charged ions, much shorter than the radiative lifetime to be measured which is of the order of $\approx 10^{-3}$ s. The ECRIS in combination with the analyzing magnet and decelerating system enable to select the desired charge state of the ions and capture them into the Penning trap with a few eV energy distributions without any active cooling scheme. The lower energy contributes to reduction of systematic errors in the lifetime measurement. The highly charged ions in the metastable states emits photons when they undergo either, M1, E2, M2 etc. transitions. For the ions of our interest the emitted photons lie in the visible range of the whole electromagnetic spectrum. The emitted photons are collected by the lens system and detected by a photomultiplier tube (PMT) or detected directly by an array of photodiodes known as silicon photomultiplier (SiPM) which is an array of few thousand photodiodes on a chip. The advantage of SiPM is that they can be directly mounted on the holes of the Penning trap ring-electrode for the higher collection efficiency. The life time of the forbidden transition is measured by counting the photons falling on the detector and fitting resultant exponential decay curve.

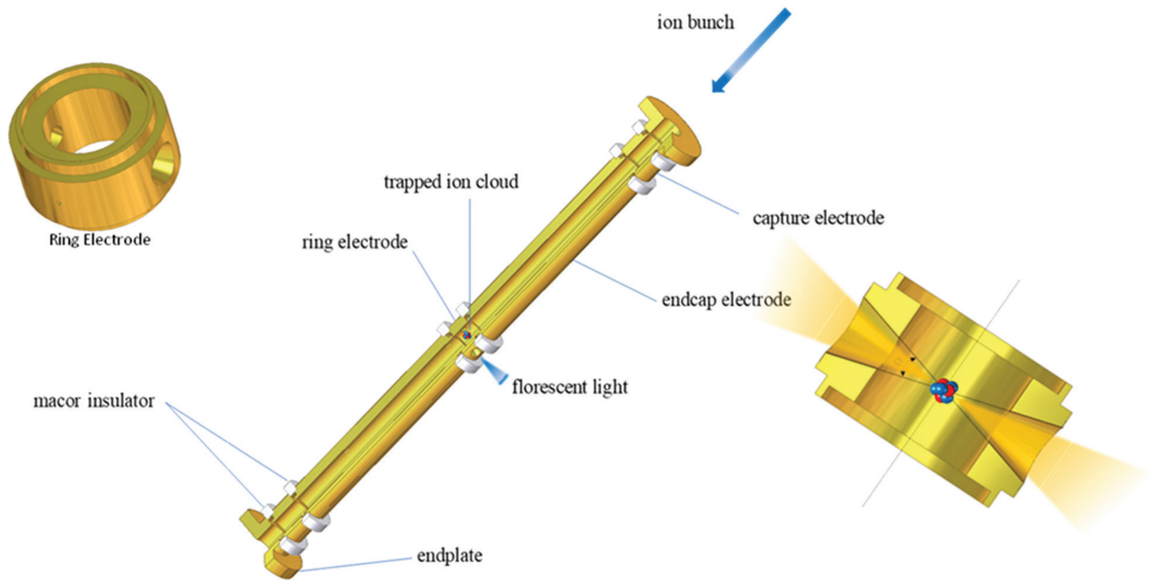

Figure 2: Section view of the ion trap electrodes assembly and ring electrode

The experiment is centered around the Penning trap arrangement inside the homogeneous field region of a 0.8T permanent magnet as shown in figure 1. The trap is a cylindrical open-endcap three-pole Penning trap with an additional capture electrode on either end. It confines the ions radially by the permanent magnet's axial field and axially by an electrostatic potential well created by appropriate voltages applied to the trap electrodes. These consist of oxygen-free copper and are gold-plated to avoid oxidization and to minimize electrostatic patch effects. The electrical insulation is guaranteed by Macor rings and sapphire blocks in between electrodes. One of the endcap electrodes is split into two segments to allow magnetron cooling and also for ion cyclotron frequency detection, ion. Ring segment is equipped with a two, diametrically opposite 3.5 mm holes for detection of fluorescence light and are located 4.5mm away from the main trap axis. This diameter was chosen as the maximum size that does not compromise the stability of the electrode segments. They define a solid angle of 0.475 sr, which is a fraction of $3.7*10^{-2}$ out of the total solid angle of 4π as shown in figure 2. The holes offer 100% transmission for photons and create a negligible loss in the harmonicity of the potential.

The trap electronics include, filters for all signal lines going towards the trap electrodes and pre-amplifiers for axial and cyclotron frequency signals going from the trap electrodes. The trap and its electronics are designed for maximum acceptance with respect to capture, storage, cooling and electronic detection of ions. The experimental cycle including ion creation in the ECRIS, transport, deceleration and capture is defined by a control and data acquisition software based on LabVIEW, which uses, amongst others, two digital delay generators and three synthesized function generators to provide the trap electrode triggers, the frequencies for the system clock, ion excitation and laser scan, and controls the SR430 multichannel scalar used for time-of-flight measurements. The trap itself and its cryo-electronics are cooled to liquid helium temperature by the He Cryo-cooler which maintains the 10 K at the magnet, magnet bore and with it the trap and the attached electronics.

The refurbished 0.8T permanent magnet has been acquired from GSI, Germany. The electrostatic simulation and CAD design of the trap electrodes are completed. The manufacturing of the trap electrodes is under process. The assembly and initial testing will be carried out by the next year.

4.6.3 Effect of Tuner on Reflection Coefficient of 10 GHz Nanogan ECR Ion Source Cavity

Kedar Mal

There are several techniques to improve the performance of ECR ion sources, one of the most efficient technique is frequency tuning. A set of measurements with 10 GHz Nanogan ECR ion source has been carried out to investigate the effect of tuner on reflection coefficient and different excited modes of evacuated cavity. In these measurements, the tuner position was varied from 10mm to 15mm in steps of 0.5mm. At each tuner position, the microwave frequency swept in a range of frequency from 7.5 to 10.6 GHz in steps of 2MHz. The dc bias tube was kept out during measurements. Each peak in reflection coefficient graph shows an excited mode either hybrid or TE and TM. To find out different excited modes, frequency domain solver of CST Studio was used to simulate the evacuated cavity. In the simulation, the plasma lens, all parts of rf cube were included. Figure 1 shows measured reflection coefficient at different tuner position. The simulations of cavity at different tuner position are going on.

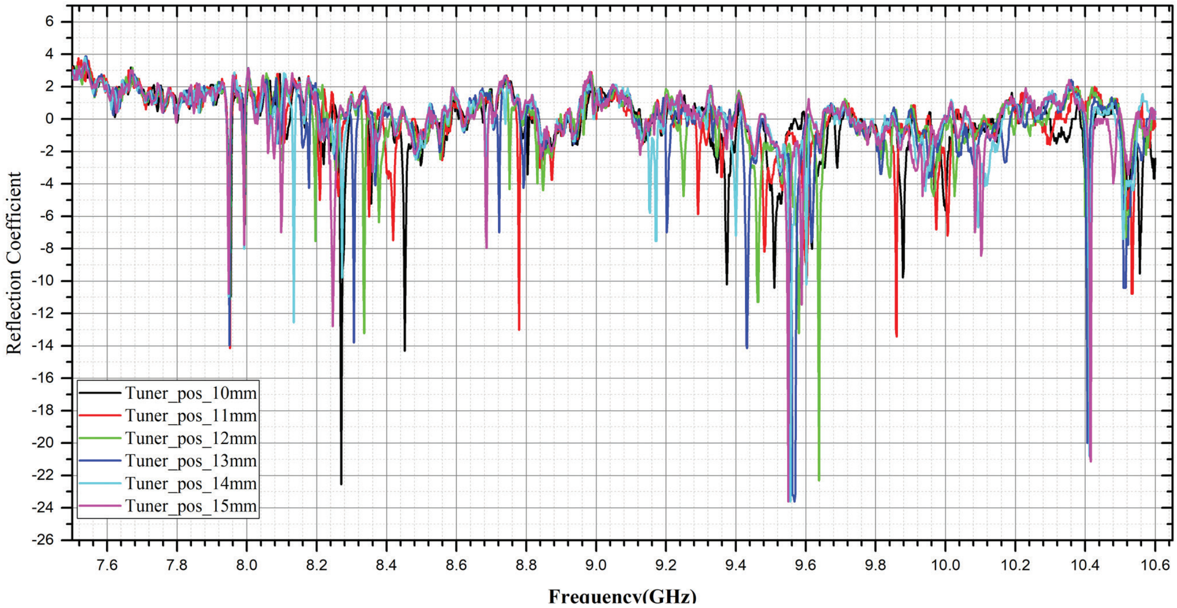

Figure 1: Reflection Coefficient at different tuner position of evacuated cavity

4.6.4 Developmental Work and Experiments Conducted at LEIBF in Atomic and Molecular Physics:

Pragya Bhatt and C P Safvan

(1) A new experimental setup is installed recently in the 105º beam line in LEIBF to study ion induced molecular dissociation. To improve the vacuum of this system, two additional turbo molecular pumps have been installed; one in the beam line and the other in the main experimental chamber. Further, a new provision for heating the chamber has been made. These two additions have helped in improving the vacuum of the beam line and the chamber by one order of magnitude.

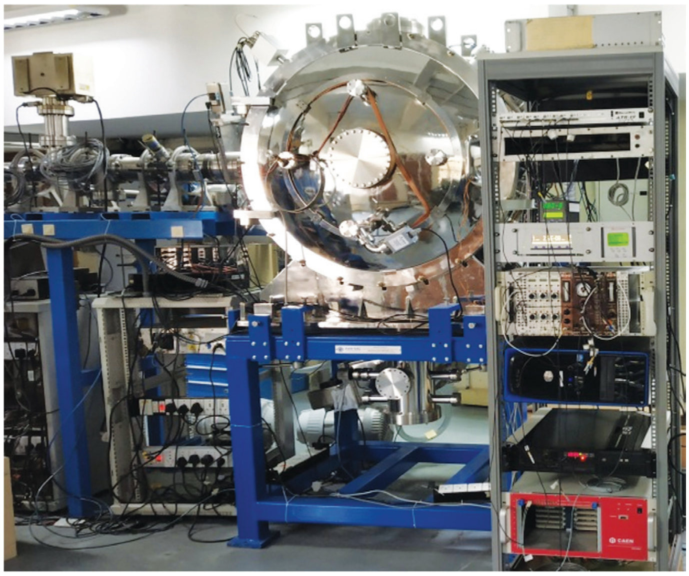

Figure 1: Photograph of the newly developed experimental setup

(2) To study the electron capture by the target gas molecules, a new position sensitive dual-micro channel plate detector has been installed at the exit port of the chamber. The projectile ions interact with an effusive jet of the target gas. One or more electrons from the projectile ion may get captured by a target molecule. An electrostatic energy analyzer is used to deflect these projectile ions according to their energies and charge states after interacting with the target. These are termed as post collision projectile ions. Due to the electron capture process, a number of charge states of the projectile ions are observed at the detector.

A test result for 450 keV Ar^{9+} ion beam interacting with neutral Ar molecules is shown in Figure 2. The different charge states of the Ar^{9+} projectile after a few electrons are captured by the target are clearly visible in this figure.

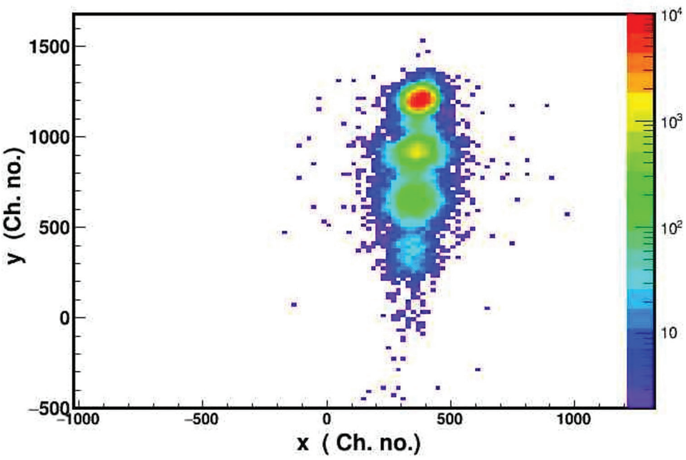

Figure 2: Position spectrum of the post collision ions in 450 keV Ar^{9+} interactions with Ar

(3) The experiments on the interaction of 50 and 200 kV/q Ar^{9+} ions with the Acetylene (C_2H_2) gas targets are performed using the ion momentum mapping spectrometer installed in the above mentioned chamber. The analysis of the acquired data is underway. A typical time of flight spectrum and a double ion coincidence spectrum of the recoil ions generated from C_2H_2 in these collisions in capture and/or ionization events are shown as below:

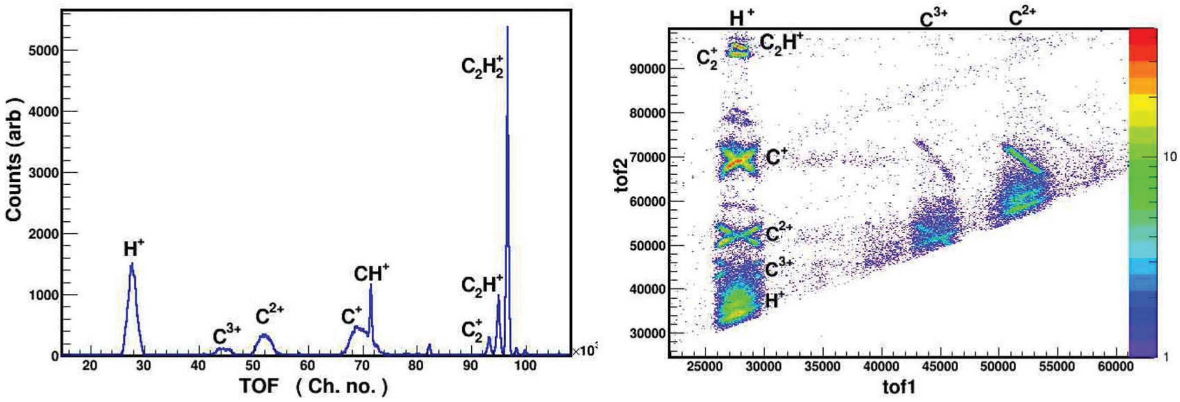

Figure 3: Time of flight spectrum (left) and double ion coincidence spectrum (right) generated in 1.8 MeV Ar^{9+} impact on C_2H_2

5 RESEARCH ACTIVITIES

5.1 NUCLEAR PHYSICS

S. Muralithar, N. Madhavan and P. Sugathan

More than 20 Nuclear Physics experiments were performed using beams from Pelletron accelerator in 2018-2019, most of which were Ph.D. thesis related experiments. Of these, ten were in nuclear spectroscopy using INGA facility looking for high spin states in unstable nuclei and a few were lifetime measurements using Dopple-Shift Attenuation Method (DSAM) technique. The nuclear reaction experiments were carried out in HIRA (5), GPSC (4), HYRA (2) and NAND (1). As HYRA and NAND experiments usually require high energy, heavier projectiles from Pelletron + LINAC accelerator combination, the non-availability of LINAC beams during the year resulted in lesser number experiments in those two facilities.

Experiments in HIRA concentrated on sub- and near-barrier fusion reactions probing transfer and other channel coupling effects, effect of deformation and/or shell closure in colliding partners and quasi-elastic back-scattering measurements were also carried out in one case. Experiments in GPSC involved quasi-elastic back-scattering measurements and/or deciphering the effect of projectile break-up on elastic scattering and fusion cross-sections. HYRA experiments involved measurement of evaporation residue (ER) cross-sections just above the barrier in heavy systems with ^{16,18}O projectiles and ^{204,206,208}Pb targets. NAND was used to extract pre- and post-scission neutron multiplicities in ^{18}O + ^{186}W system by detecting neutrons using 50 liquid scintillation detectors in coincidence with either fission fragment.

Efforts are on to shift the GPSC facility beyond GDA structure (30 degree beam-line) from the existing 45 degree beam-line in beam hall I to make room for setting up of HCI beam transport components. There is a plan to upgrade to VME-based Data Acquisition System (DAS) using indigenous development from the existing CAMAC-based DAS in most of the nuclear physics facilities. A proposal has been submitted to SERB to realise a Charged Particle Detector Array for particle-gated gamma measurements using INGA facility at IUAC. Clover and ACS (BGO) detectors have been procured using IUAC grants to increase the efficiency of the array.

Based on results from earlier years' experiments, several articles have been published in reputed journals and a few research scholars have been awarded doctorate degrees.

A five-day school on "Modern techniques of γ-ray spectroscopy for nuclear structure studies" was organised in IUAC which was attended by more than thirty research scholars.

Ms. Gonika (Scientist Trainee) won one of three prizes for best presentation and Mr. Rohan Biswas (JRF) won a special prize, both in SERB School on Nuclear Astrophysics at SINP, Kolkata.

5.1.1 High spin spectroscopy of ^{153}Eu

K. Mandal[1,8], A. K. Mondal[1], A. Chakraborty[1], U. S. Ghosh[1], A. Dey[1], S. Rai[1,10], S. Biswas[1,9], K. Katre[2], Yasraj[2], Indu Bala[2], R. K. Gurjar[2], R. Kumar[2], R. P. Singh[2], S. Muralithar[2], A. Sharma[3], Saket Suman[4], S. K. Tandel[4], G. Mukherjee[5], B. Mukherjee[1], R. Raut[6], S. S. Ghugre[6] and A. K. Sinha[7]

[1]Department of Physics, Siksha Bhavana, Visva-Bharati, Santiniketan, West Bengal 731235, India
[2]Inter-University Accelerator Centre, Aruna Asaf Ali Marg, New Delhi 110067, India
[3]Department of Physics, Himachal Pradesh University, Shimla 171005, India
[4]UM-DAE Centre of Excellence in Basic Sciences, Mumbai 400098, India
[5]Variable Energy Cyclotron Centre, 1/AF, Bidhan Nagar, Kolkata 700064, India
[6]UGC-DAE-Consortium for Scientific Research, Kolkata 700098, India
[7]UGC-DAE Consortium for Scientific Research, Indore 452017, India
[8]Chandidas Mahavidyalaya, Khujutipara, Birbhum, West Bengal 731215, India
[9]Murshidabad College of Engineering and Technology, Berhampore, West Bengal 742102, India
[10]Department of Physics, Salesian College, Siliguri Campus, Siliguri 734001, India

The level structure of ^{153}Eu at high spin has been investigated. The purpose was to look for the missing parity doublet bands built on $[\pi d_{5/2}]3/2^+$ and $[\pi h_{11/2}]3/2^-$ orbitals [1] and to settle the debate related to reflection symmetric versus reflection asymmetric behavior for the ground state parity doublet band built on $[\pi d_{5/2}]5/2^+$ and $[\pi h_{11/2}]5/2^-$ orbitals [2,3].

The experiment was carried out using the fusion evaporation reaction ^{150}Nd(^{7}Li, 4n). The 38 MeV ^{7}Li beam was delivered by the 15UD Pelletron of IUAC. A thin foil made of enriched ^{150}Nd (thickness ~ 3mg/cm^2), with mylar backing, was used as the target. De-excited gamma rays were detected by the Indian National Gamma Array (INGA) comprising of sixteen Clover detectors and two LEPS. Six Clover detectors were placed at 90º relative to the beam axis. Arrangement of the other detectors was as follows: four at 148º, two at 123º, three at 32º and one at 57º. The two LEPS were at 119º and 61º. Detailed off-line analysis of the acquired data is in progress. A representative coincidence spectrum, with the gate on 151 keV ground state feeding transition of ^{153}Eu, is shown in Fig. 5.1.1.1.

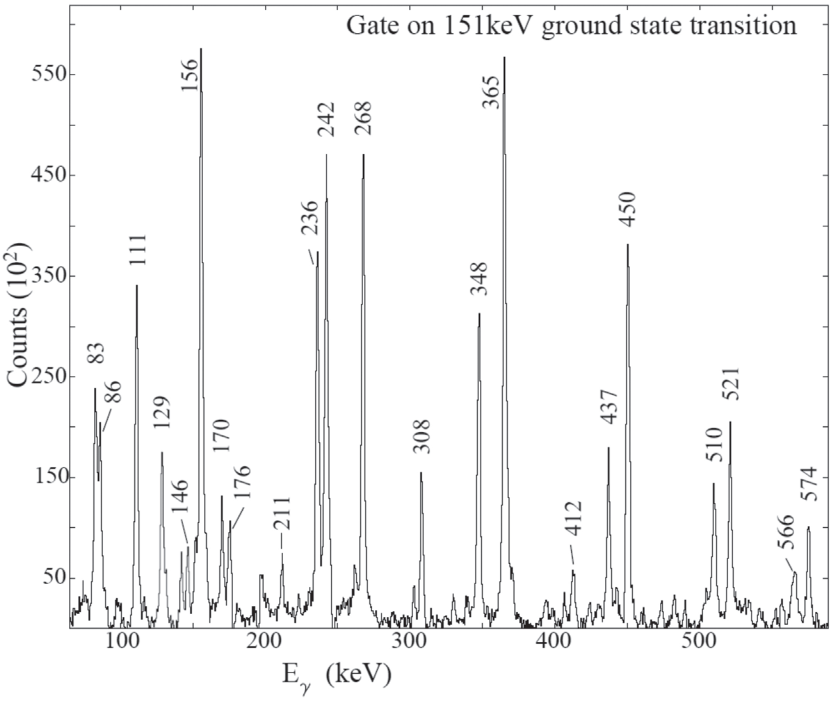

Fig. 5.1.1.1: A coincidence spectrum, gated with 151 keV ground state feeding transition of ^{153}Eu. The peaks labeled with their energies belong to ^{153}Eu.

REFERENCES:

[1] C. J. Pearson *et al.,* Phys. Rev. C **49**, R1239 (1994).

[2] D. Nosek *et al.,* Z. Phys. A **344**, 277 (1993).

[3] Somapriya Basu *et al.,* Phys. Rev. C **56**, 1756 (1997).

5.1.2 Quasi-elastic scattering measurements for ^{16}O,^{28}Si+^{144}Sm

Kavita Rani[1], B. R. Behera[1], A. Jhingan[4], G. Kaur[4], Saneesh N.[4], R. Mahajan[1], H. Arora[1], M. Kumar[4], D. Arora[2], S. Narang[1], D. Kaur[1], Kavita[2], Subodh[1], C. Sharma[1], Amit[1], A. Rani[3], K. Chakraborty[3], K. S. Golda[4], H. Singh[2] and P. Sugathan[4]

[1]Department of Physics, Panjab University, Chandigarh 160014, India
[2]Department of Physics, Kurukshetra University, Kurukshetra 136119, India
[3]Department of Physics and Astrophysics, University of Delhi, Delhi 110007, India
[4]Inter-University Accelerator Centre, Aruna Asaf Ali Marg, New Delhi 110067, India

The study of channel coupling in heavy-ion collisions has been a topic of interest for several years now. The enhancement in fusion reactions at sub-barrier energies is a result of this channel coupling which cannot be accounted by single potential model. The single potential barrier (V_b) splits into a distribution of barriers as a result of coupling of the relative motion between the colliding nuclei to their intrinsic motions as well as direct reaction channels. The barrier distribution (BD) formed due to this coupling acts as fingerprint for any reaction. Understanding the coupling schemes in any reaction is vital as it has a greater influence on the formation probability of compound nuclei [1-7]. The BD can be experimentally studied by the measurement of fusion excitation function $\sigma_{fus}(E)$ using the relation $D_{fus} = d2(E\sigma_{fus})/dE$ [2] and the quasi-elastic (QE) excitation function using $D_{qel} = -d\,(d\sigma_{qel} / d\sigma_R)/dE$ [4]. Theoretically, coupled-channel calculation scheme is used [6]. In the present work, we have performed an experiment for the QE-measurements for the systems ^{16}O, ^{28}Si+ ^{144}Sm. The aim is to extract information about the fusion barrier from experimental BD and study the role of nuclear structure as well as transfer channels in the reaction dynamics by comparing with the already existing results for ^{28}Si+ ^{154}Sm (having deformed target and positive neutron transfer reaction channels unlike in ^{28}Si+ ^{144}Sm) and ^{16}O+^{144}Sm.

The measurements have been performed in the General Purpose Scattering Chamber (GPSC) using the HYTAR [7] detection facility. Beam energy has been varied in steps of 5 MeV ranging from the barrier down to 25% below the barrier and in steps of 4 MeV ranging from the barrier up to 12% above the barrier for ^{28}Si. In case of ^{16}O, beam energy has been varied in steps of 3 MeV ranging from 20% below the barrier up to 10% above the barrier. Particle identification has been obtained with gas ionization chamber as ΔE detector and PIPS as E detector. Four telescope detectors, two in plane and two out of plane, each at an angle of 173º have been arranged in a symmetrical cone geometry. Nine telescopes, six at angles from +60º to +160º with angular separation of 20◦ and three at angles -30º, -42º and -54º, have been placed on rotatable arms of the GPSC. Two monitor detectors of thickness 300 μm have been placed at ±10º for normalization. Isotopic targets of samarium were prepared at the Target Development Laboratory of IUAC. Particle identification spectra obtained in the measurements have been shown in Fig. 5.1.2.1.

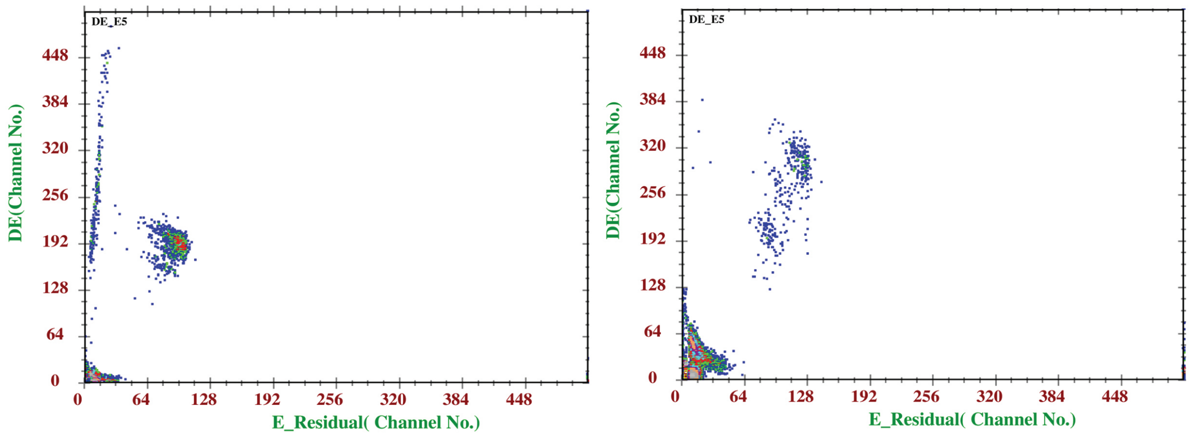

Fig. 5.1.2.1: Particle identification (E-ΔE) spectra for $^{28}Si+^{144}Sm$ at beam energy 132 MeV (left panel) and for $^{16}O+^{144}Sm$ at beam energy 76 MeV (right panel) at 140º, respectively.

The angular distributions of the QE events, for $^{28}Si+^{144}Sm$ (in the range 90 - 140 MeV) and for $^{16}O+^{144}Sm$ (in the range 60 - 82 MeV), have been measured. Fig. 5.1.2.2 shows the excitation functions extracted as a function of $E_{eff,}$ where $E_{eff} = 2E_{c.m.}/(1+\mathrm{cosec}\,(\theta_{c.m.}/2))$ corrects for centrifugal effects. The measured QE events will be used to extract the experimental BD for both the systems.

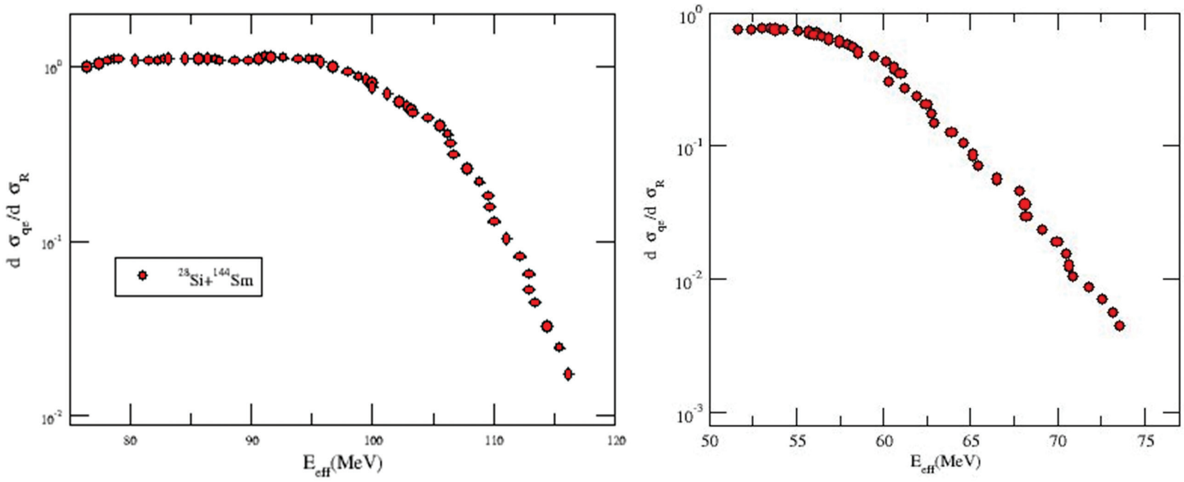

Fig. 5.1.2.2: Quasi-elastic excitation functions for $^{28}Si+^{144}Sm$ (left panel) and $^{16}O+^{144}Sm$ (right panel).

REFERENCES:

[1] G. Kaur et al., Phys. Rev. C **94**, 034613 (2016).
[2] Md. Moin Shaikh et al., Phys. Rev. C **91**, 034615 (2015).
[3] N. Rowley, G. R. Satchler, and P. H. Stelson, Phys. Lett. B **254**, 25 (1991).
[4] M. Dasgupta et al., Annu. Rev. Nucl. Part. Sci. **48**, 401 (1998).
[5] H. Timmers et al., Nucl. Phys. A **584**, 190 (1995).
[6] K. Hagino, N. Rowley, and A. T. Kruppa, Comput. Phys. Commun. **123**, 143 (1999).
[7] A. Jhingan et al., Nucl. Instrum. Methods A **903**, 326 (2018).

5.1.3 Role of positive transfer Q values in fusion evaporation residue cross-sections for $^{18}O+^{182,184,186}W$ reactions

P. Jisha[1], A. M. Vinodkumar[1], B. R. S Babu[1], S. Nath[2], N. Madhavan[2], J. Gehlot[2], S. Sanila[1], K. Arjun[1], A. Parihari[2], A. Vinayak[3] and Amit Raj[4]

[1]Department of Physics, Calicut University, Calicut 673635, India
[2]Inter-University Accelerator Centre, Aruna Asaf Ali Marg, New Delhi 110067, India
[3]Department of Physics, Karnataka University, Dharwad 580003, India
[4]Department of Physics, Panjab University, Chandigarh 160014, India

Study of fusion dynamics in the sub barrier energy region is interesting due to the well-established fact that fusion cross-sections are greatly enhanced when compared with predictions of 1D barrier penetration model (1D BPM) [1,2]. The coupling of the relative motion of colliding nuclei to the internal degrees of freedom plays an important role in describing sub-barrier fusion enhancement. The vibration of the nuclear surface and the rotation of deformed nuclei are used to explain many of the experimental results [3-6] for heavy nuclei. Also, Sargsyan et al. [7] suggested the role of transfer or transfer induced neutron rearrangement as reasons for fusion enhancement in the sub-barrier region. The change in the magnitude of the capture cross-section after the neutron transfer is suggested as an indirect effect of the quadrupole deformation. In order to study the effect of positive transfer Q-value, we performed an experiment to study the reactions $^{18}O+^{182,184,186}W$, which has positive 2n transfers Q values. One of the main objectives of this work was to compare the evaporation residue (ER) cross-section with nearby systems, namely $^{16}O+^{182,184,186}W$, with negative transfer Q values for 2n channels.

The experiment was performed using the Heavy Ion Reaction Analyzer (HIRA) at IUAC. HIRA was kept at 0^o with respect to the beam direction with 10 mSr entrance aperture. A pulsed beam of ^{18}O with 4 μs pulse separation was used to bombard the enriched $^{182,184,186}W$ targets of thickness ≈ 70 μg/cm², 200 μg/cm² and 100 μg/cm², respectively. ERs were measured from E_{lab} = 104 MeV to 68 MeV (35% above to 15% below the fusion barrier) in steps of 2- 4 MeV. A Multi-Wire Proportional Counter (MWPC) was placed at the focal plane of HIRA for the detection of the ERs. Two silicon surface barrier detectors (SSBD) were placed inside the target chamber at an angle of ±15° with respect to beam direction for normalization of cross-sections. A time of flight (TOF) was set up between anode signal of MWPC and RF signal to separate the beam-like particles from ERs. A two-dimensional spectrum between energy loss in MWPC and TOF is shown in Fig. 5.1.3.1. The preliminary results are shown in Fig. 5.1.3.2. A detailed analysis using a statistical model and CCFULL are in progress.

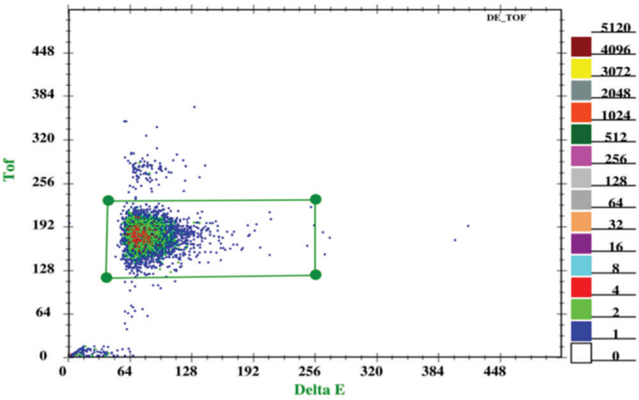

Fig. 5.1.3.1: Energy loss vs TOF spectrum for $^{18}O+^{182}W$ at E_{lab} = 84 MeV.

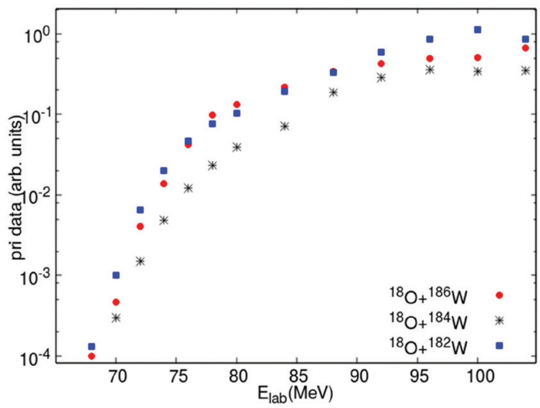

Fig. 5.1.3.2: Preliminary ER excitation functions for the reactions $^{18}O+^{182,184,186}W$.

REFERENCES:

[1] M. Beckerman, Phys. Rep. **129,** 145 (1985).
[2] M. Beckerman, Rep. Prog. Phys. **51,** 1047 (1988).
[3] J. X. Wei *et al.,* Phys. Rev. Lett. **67,** 3368 (1991).
[4] A. M. Stefanini *et al.,* Phys. Rev. Lett. **74,** 864 (1995).
[5] M. Trotta *et al.* Phys. Rev. C **65,** 011601 (2001).
[6] V. I. Zagrebaev *et al.* , Phys. Rev. C **64,** 034606 (2001).
[7] V. V. Sargsyan, Phys. Rev. C **85,** 024616 (2012).

5.1.4 Study of reaction dynamics involving weakly bound projectile and medium mass nuclei

Chhavi Joshi[1], N. L. Singh[1], H. Kumawat[2], R. K. Singh[1], S. D. Sharma[3], A. Parihari[4], K. Arora[5], J. Acharya[1], Ishtiaq Ahmed[4], P. K. Giri[6], Sushil Kumar[4], G. Kaur[4], K. S. Golda[4], Saneesh N.[4], Mohit Kumar[4], A. Jingan[4] and P. Sugathan[4]

[1]Department of Physics, The M. S. University of Baroda, Vadodara 390002, India
[2]Nuclear Physics Division, Bhabha Atomic Research Centre, Mumbai 400085, India
[3]Department of Physics, Aligarh Muslim University, Aligarh 202002, India
[4]Inter-University Accelerator Centre, Aruna Asaf Ali Marg, New Delhi 110067, India
[5]Department of Physics, Panjab University, Chandigarh 160014, India
[6]Centre for Applied Physics, Central University of Jharkhand, Ranchi 835205, Jharkhand, India

We performed an experiment to measure cross sections for elastic scattering, alpha production and fusion using the General Purpose Scattering Chamber (GPSC) at IUAC. The beams of weakly bounded projectiles were bombarded on two isotopes of molybdenum (^{92,100}Mo). Both the targets were prepared at the Target Development Laboratory of IUAC. Around 20 targets of ^{92}Mo and ^{100}Mo each, with thickness ~ 217 μg/cm^2 and 305 μg/cm^2 respectively, were prepared using the physical vapor deposition (PVD) technique [1]. In order to fabricate sustainable thin films of molybdenum, natural carbon was used as backing material.

In the experiment, ^{6,7}Li beams were used in the energy range 15 – 30 MeV. Both the beams are weakly bound and thus show interesting reaction dynamics around the barrier. The beam current was kept between 2 to 5 pnA. Silicon surface barrier detectors were mounted on rotatable arms inside the scattering chamber to cover wide range of angles. One High Purity Germanium (HPGe) detector was used to capture gamma-radiations produced in the experiment. Part of the analyzed data for elastic scattering angular distribution is presented in the Fig. 5.1.4.1.

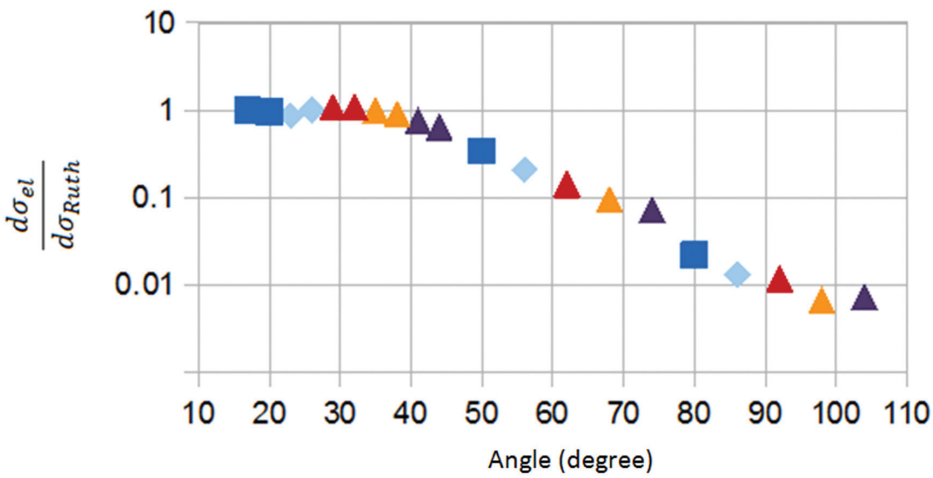

Fig 5.1.4.1: Angular distribution for the system ^{7}Li+^{100}Mo at E_{lab} = 30 MeV with inter detector normalization.

REFERENCE:

[1] C. Joshi *et al.,* Proc. DAE Symp. Nucl. Phys. **63**, 1210 (2018).

5.1.5 Lifetime of 6023 keV state in ^{104}Pd

C. Majumder[1], H. P. Sharma[1], S. Chakraborty[1], S. S. Tiwary[1], R. P. Singh[2], S. Muralithar[2], Indu Bala[2], S. S. Bhattacharjee[2], R. Garg[2], Neelam[3], S. Das[4], S. Samanta[4], S. S. Ghugre[4], A. Sharma[5], P. V. Madhusudhana Rao[6], R. Palit[7] and U. Garg[8]

[1]Department of Physics, Institute of Science, Banaras Hindu University, Varanasi 221005, India
[2]Nuclear Physics Group, Inter-University Accelerator Centre, Aruna Asaf Ali Marg, New Delhi 110067, India
[3]Department of Physics and Astrophysics, University of Delhi, Delhi 110007, India
[4]UGC-DAE Consortium for Scientific Research, Kolkata Centre, Kolkata 700098, India
[5]Department of Physics, Himachal Pradesh University, Shimla 171005, India

[6]Department of Physics, Andhra University, Visakhapatnam 530003, India
[7]Department of Nuclear and Atomic Physics, Tata Institute of Fundamental Research, Mumbai 400005, India
[8]Department of Physics, University of Notre Dame, Notre Dame, Indiana 46556, USA

Various structural effects were observed in the nuclei belonging to mass A ≈ 100 region, close to N = Z = 50 shell closures. In Pd isotopes, having four proton holes below Z = 50 shell gap and a number of neutron particles above N = 50 closed shell, a number of collective phenomena have been observed. The evolution of collectivity in these bands can be explained by the change of transition quadrupole moment. One of the ways to deduce the transition quadrupole moment (Qt) is measurement of lifetime of the states of a band. The lifetime of a number of states has been deduced by Doppler Shift Attenuation Method (DSAM). Lifetime of 6023 keV state, reported in Ref. [1], has been shown in this work.

High spin states of ^{104}Pd were populated via ^{94}Zr(^{13}C, 3n) fusion-evaporation reaction at a beam energy of 55 MeV at IUAC [2,3]. The target was ~1 mg/cm^2 thick with ~10 mg/cm^2 gold backing. The γ-rays were detected in the Indian National Gamma Array (INGA) [4] facility having eighteen Compton suppressed Clover detectors. To investigate the nucleus and deduce the lifetime of the states INGASort [5] and LINESHAPE [6] programs were used.

Table I: Summary of the experimental results, extracted from the present work.

E_γ(keV)	E_{ex} (keV)	I^π h	Q_t eb	τ (ps)	β_2	B(E2) e^2b^2	B(E2) W.u.
1059	6023	15	2.76 (7)	0.23 (1)	0.23	0.26 (.02)	90 (4)

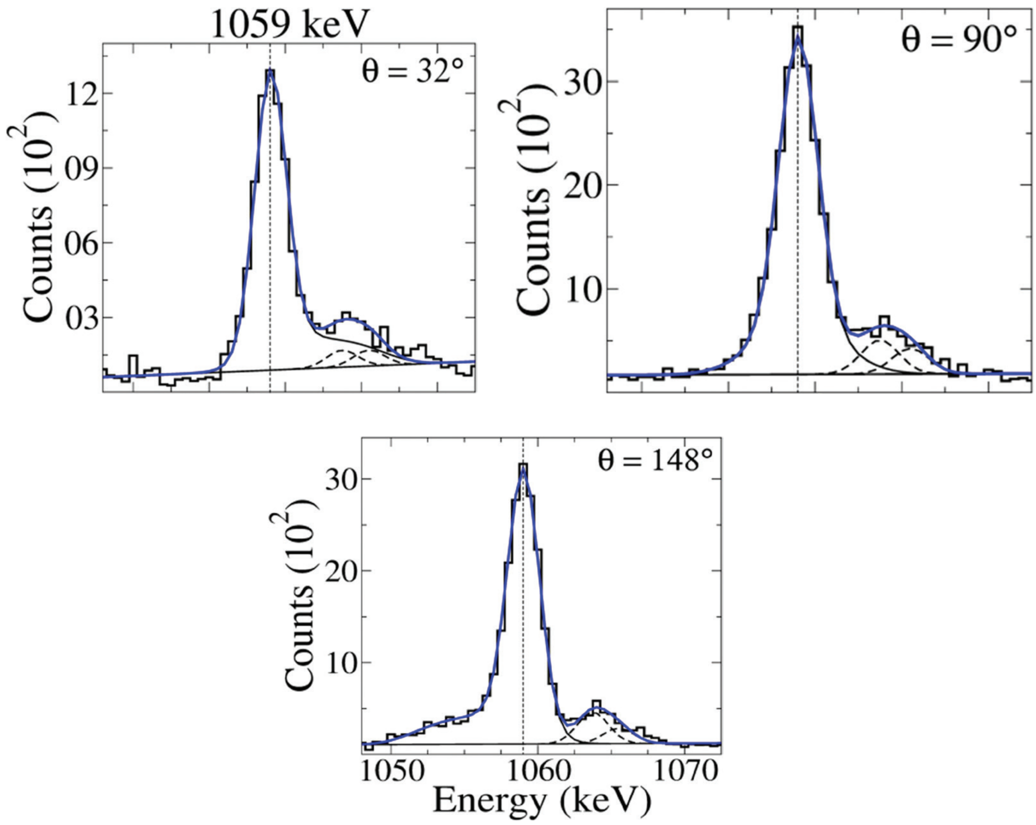

Fig. 5.1.5.1: Doppler shift attenuation spectra for the 1059 keV γ-ray at θ = 32°, 90° and 148°.

The quadrupole moment shows a moderate deformation of the state of the band. Lifetime of the other states is also measured and the work is underway.

REFERENCES:

[1] D. Sohler et al., Phys. Rev. C **85,** 044303 (2012).
[2] G. K. Mehta et al., Nucl. Instrum. Methods A **268,** 334 (1988).
[3] D. Kanjilal et al., Nucl. Instrum. Methods A **328,** 97 (1993).
[4] S. Muralithar et al., Nucl. Instrum. Methods A **622,** 281 (2010).
[5] R. K. Bhowmik, Proc. DAE Symp. Nucl. Phys. **44B,** 422 (2001).
[6] J. C. Wells et al., Tech. Rep. (1991).

5.1.6 Spectroscopy of ^{145}Gd

C. Majumder[1], H. P. Sharma[1], S. Chakraborty[1], S. S. Tiwary[1], S. Muralithar[2], R. P. Singh[2], Indu Bala[2], Yash Raj[2], K. Katre[2], B. Rohila[3], A. Kumar[3], Anuj[4], S. Kumar[4], R. Bhusan[4], S. K. Chamoli[4], A. Sharma[5] and T. Trivedi[6]

[1]Department of Physics, Banaras Hindu University, Varanasi 221005, India
[2]Inter-University Accelerator Centre, Aruna Asaf Ali Marg, New Delhi 110067, India
[3]Department of Physics, Panjab University, Chandigarh 160014, India
[4]Department of Physics and Astrophysics, University of Delhi, Delhi 110007, India
[5]Department of Physics, Himachal Pradesh University, Shimla 171005, India
[6]Department of Physics, Guru Ghasidas Vishwavidyalaya, Bilashpur 495009, India

^{145}Gd is a spherical nucleus, with Z = 64 sub-shell gap and one neutron hole below the N = 82 shell closure. A number of non-collective states have been reported at lower angular momentum [1,2]. The spin or parity of states is not firmly defined in the literature at higher angular momentum. The nucleus has been revisited and mostly all the de-excited gamma-rays, that are previously reported [1] have been seen in this investigation. A number of symmetric and asymmetric (angle dependent) matrices have been formed to study the γ-γ coincidence relationship and also to determine their multi-polarity. Some important energy-gated γ-spectra have been shown in Fig. 5.1.6.1. The value of correction factor $a(E_\gamma)$ of some of the detectors having three or four crystals are shown in Fig. 5.1.6.2. They are used for linear polarization measurements.

High spin levels of ^{145}Gd have been populated via ^{122}Sn(^{28}Si,5n) reaction at a beam energy 146 MeV at IUAC. ^{122}Sn target (99.3% enriched) has a thickness of ~1.9 mg/cm^2 with ~10.4 mg/cm^2 thick gold backing. The γ-rays have been detected in the Indian National Gamma Array (INGA) facility having sixteen Compton suppressed Clover detectors and two Low Energy Photon Spectrometers (LEPS). To investigate the nucleus, INGASort [3] program has been used.

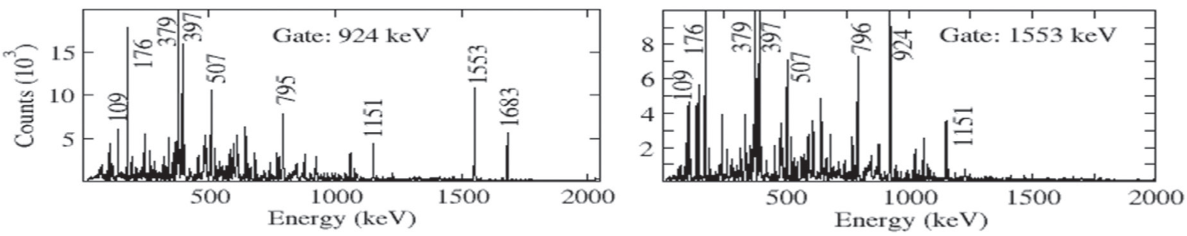

Fig. 5.1.6.1: Prompt γ-spectra gated with 924 keV (left panel) and 1553 keV (right panel) γ-line.

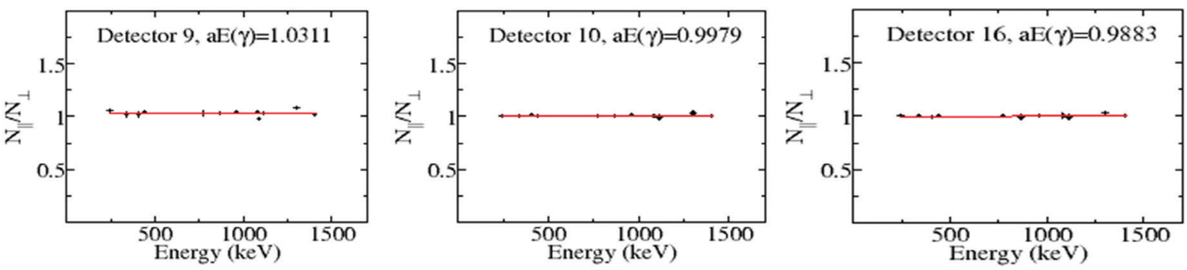

Fig. 5.1.6.2: The correction factor [$a(E_\gamma)$] for detectors 9, 10 and 16, as a function of energy.

REFERENCES:

[1] C. Schumacher, Z. Phys. A **354,** 123 (1996).
[2] A. Pakkanen, Nucl. Phys. **A373**, 237 (1982).
[3] R. K. Bhowmik, Proc. DAE Symp. Nucl. Phys., **44B,** 422 (2001).

5.1.7 Study of quasi-elastic scattering in $^{7}Li+^{116,118}Sn$ reactions

Arshiya Sood[1], Arzoo Sharma[1], Akashrup Banerjee[2], Pawan Kumar[1], Rudra N. Sahoo[1], Malika Kaushik[1], Pushpendra P. Singh[1], Kavita Rani[3], Abhishek Yadav[4], Gurpreet Kaur[5], Akhil Jhingan[5], N. Saneesh[5], Mohit Kumar[5], Manoj K. Sharma[6], K. S. Golda[5] and P. Sugathan[5]

[1]Department of Physics, Indian Institute of Technology Ropar, Punjab 140001, India
[2]Department of Physics and Astrophysics, University of Delhi, Delhi 110007, India
[3]Department of Physics, Panjab University, Chandigarh 160014, India
[4]Department of Physics, Jamia Millia Islamia , New Delhi 110025, India
[5]Inter-University Accelerator Centre, Aruna Asaf Ali Marg, New Delhi 110067, India
[6]Department of Physics, Shri Varshney College, Aligarh, Uttar Pradesh 202001, India

Heavy-ion (HI) induced reactions have inspired a great deal of efforts across the globe as they offer a radical rearrangement of nucleons in a many-body system, and have been prodigiously investigated to understand the underlying dynamics. An interesting strand of HI-reactions is the one involving weakly bound projectiles (^{6}Li, ^{7}Li, and ^{9}Be) at energies near- and below- the barrier as they offer widespread opportunities to explore different aspects of nuclear structure and reactions. There is a special interest in the field because fusion of weakly bound nuclei mimics unstable radioactive ion beams (RIBs) which have an ample relevance in astrophysical processes like nucleosynthesis and in producing new heavy and/or neutron rich isotopes [1,2]. Weakly bound nuclei are characterized by their cluster/halo structure and low breakup thresholds which makes breakup a dominant reaction process. The fusion cross-sections are sensitive to the internal structure of interacting nuclei as well as to the coupling to other reaction channels like inelastic excitations, breakup and direct nucleon transfer. This coupling essentially modifies the effective interaction potential, and leads to splitting of single, uncoupled fusion barrier into multiple barriers which results in the distribution of barriers. This distribution of barrier can be experimentally obtained by two complementary processes, *viz., fusion and large angle quasi-elastic (QEL) scattering [3,4].*

It has been observed that for strongly bound interacting partners, the distributions obtained from the foregoing two complementary approaches are similar at energies around the barrier [5,6]. However, for weakly bound projectiles, the distribution obtained from QEL has been found be to broader than that derived from fusion, and a relative shift in peak has also been observed between the two distributions indicating strong influence of breakup or breakup-like processes at energies near or below the barrier [7-9]. In this context, experiments have been performed to derive the barrier distributions from quasi-elastic back-angle scattering measurements for $^{7}Li+^{116,118}Sn$ systems.

The experiments have been performed in the General Purpose Scattering Chamber (GPSC) with beams of ^{7}Li in energy range 15-29 MeV (30% below- to above- the barrier) bombarded on self-supporting $^{116,118}Sn$ targets of thickness 430μg/cm^2 . Targets were prepared in the Target Development Laboratory of IUAC. Beam energies have been varied in steps of 2 MeV below the barrier and 3 MeV above it. To detect and identify the charged particles produced in the reaction, HYTAR detector facility was used [10]. To measure the quasi-elastic backscattering events, four telescopes were arranged in symmetrical cone geometry, two in- and out- of plane each, at an angle of 173°. Additionally, six telescopes were placed at angles +60° to +160° and three telescopes were placed at angles -36° to -60° with an angular separation of 20° and 12°, respectively. Two monitor detectors were placed at ±10° with respect to the beam direction for normalization and beam monitoring. The experimental set-up is shown in the left panel of Fig. 5.1.7.1. A typical two-dimensional ΔE-Eres spectrum obtained from the telescope at +140° for $^{7}Li+^{118}Sn$ system is presented in the right panel of Fig. 5.1.7.1.

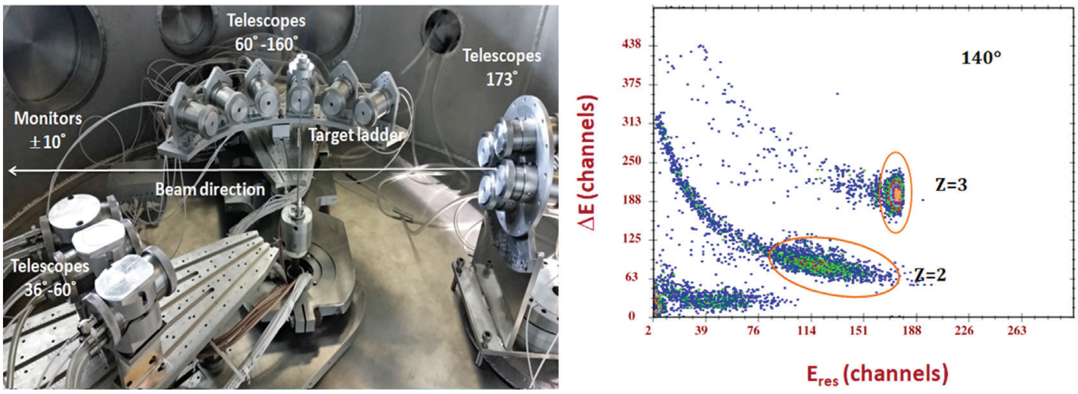

Fig. 5.1.7.1: (left) Experimental set-up for quasi-elastic scattering measurement and (right) ΔE-E_{res} spectrum at θ_{lab}= +140° for $^{7}Li+^{118}Sn$ at E_{lab} = 21 MeV.

The events corresponding to various elastic + inelastic scattering and breakup processes at E_{lab} = 21 MeV are marked in the right panel of Fig. 5.1.7.1 as Z = 3 and Z = 2, respectively. In Fig. 5.1.7.2, preliminary analysis of data for four angles *i.e.*, +120°, +140°, +160° and +173° is presented. The left panel of Fig. 5.1.7.2 shows the quasi-elastic excitation functions obtained at these angles and the right panel of the same figure shows the corresponding barrier distributions. The detailed analysis of data and its interpretation in the framework of theoretical models are underway.

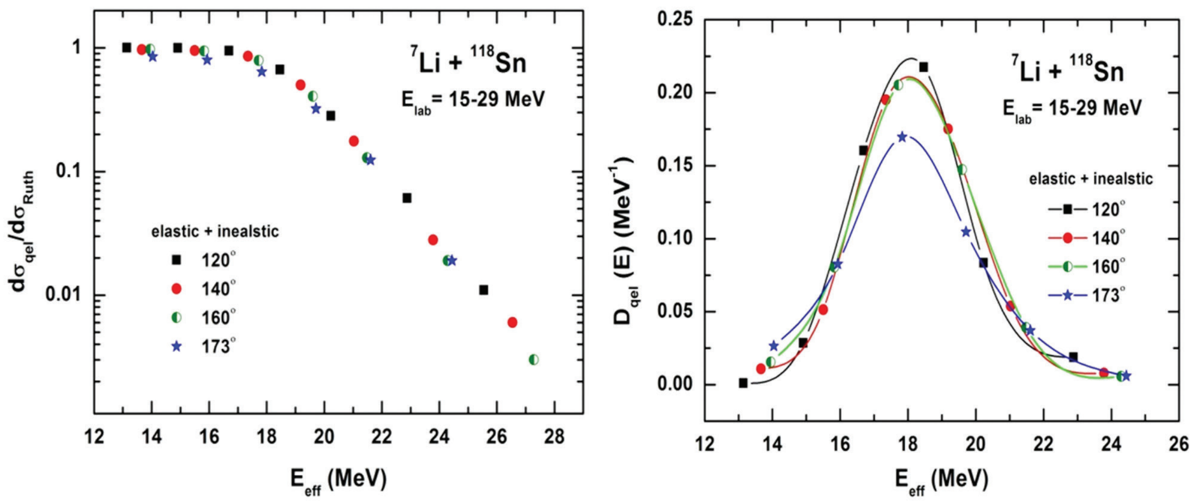

Fig. 5.1.7.2: (left) Quasi-elastic scattering excitation function and (right) corresponding barrier distribution obtained at θ_{lab}= +120° to +173° for ^{7}Li+^{118}Sn.

REFERENCES:

[1] L. F. Canto et al., Phys. Rep. **424**, 1 (2006), and references therein.
[2] V. Zagrebaev et al., Phys. Rev. C**78**, 034610 (2008).
[3] N. Rowley, G. R. Satchler and P. H. Stelson, Phys. Lett. B**254**, 25 (1991).
[4] H. Timmers et al., Nucl. Phys. A**584**, 190 (1995).
[5] M. Dasgupta et al., Annu. Rev. Nucl. Part. Sci. **48**, 401 (1998) and references therein.
[6] H. Timmers et al., Nucl. Phys. A**633**, 421 (1998).
[7] M. Zadro et al., Phys. Rev. C**87**, 054606 (2013), and references therein.
[8] C. S. Palshetkar et al., Phys. Rev. C**89**, 024607 (2014).
[9] Md. Moin Shaikh et al., Phys. Rev. C**91**, 034615 (2015).
10] A. Jhingan et al., Nucl. Instrum. Methods A **903**, 326 (2018).

5.1.8 Gamma-ray spectroscopy of ^{70}As

A. Biswas[1,2], U. S. Ghosh[1], B. Mukherjee[1], S. Rai[1,3], K. Mondal[1], A. Chakraborty[1], A. Sharma[4], S. Muralithar[5], R. P. Singh[5] and U. Dutta[6]

[1]Department of Physics, Siksha-Bhavana, Visva-Bharati, Santiniketan, Bolpur 731235, India
[2]Department of Physics, A. M. College, Jhalda, Purulia 723202, India
[3]Department of Physics, Salesian College, Siliguri Campus, Siliguri 734001, India
[4]Department of Physics, Himachal Pradesh University, Shimla 171005, India
[5]Inter-University Accelerator Centre, Aruna Asaf Ali Marg, New Delhi 110067, India
[6]Saha institute of Nuclear Physics, Kolkata 700064, India

The nuclei in A≈70 region exhibit various kinds of excitations, both single particle and collective, with different shapes, namely prolate, oblate and triaxial. Structures of the odd-odd nuclei in this region attract more attention. At low spins, properties of the nuclei are governed by $1f_{5/2}$, $2p_{3/2}$ and $2p_{1/2}$ spherical shell model orbitals. However, at higher spins and excitation energies, the particle-hole excitation from the $1f_{7/2}$ and $1g_{9/2}$ high-j intruder orbitals are important. In the odd-odd nucleus ^{70}As, the low lying states are similar to ^{72}As and were experimentally well investigated by Brink et al. [1] and Filevich *et al.* [2] using proton, alpha and light-ions as projectiles. The study of the high spin states of these nuclei, using heavy projectile was done by Badika *et al.* [3], using ^{16}O as the projectile. They could populate up to 11^+ and tentatively up to the 13^+ state at 4.076 MeV. The lifetime measurements of 11^+ and 13^+ levels, by Garcia Bermudez *et al.* [4] indicated an enhancement in B(E2) values of the 981 keV and 1343 keV. The work by Mukherjee *et al.* [5], using HIRA+GDA at IUAC extended the level scheme up to 8.9 MeV with tentative spin parity 19^+. Authors had reported three rotational bands, with two positive parity bands which were the signature partners of each other. However the signature partner of the negative parity band could not be established in this work. To get more information about the nuclear structure of ^{70}As, an experiment was performed using the INGA array at IUAC.

Excited states in ^{70}As were populated through in-beam γ-ray spectroscopic techniques using the ^{48}Cr(^{28}Si, αpn) fusion-evaporation reaction at a beam energy of 100 MeV. Emitted γ-rays of excited nuclei were detected in the γ-γ coincidence mode using 16 Compton suppressed Ge Clover detectors of the Indian National Gamma Array (INGA).

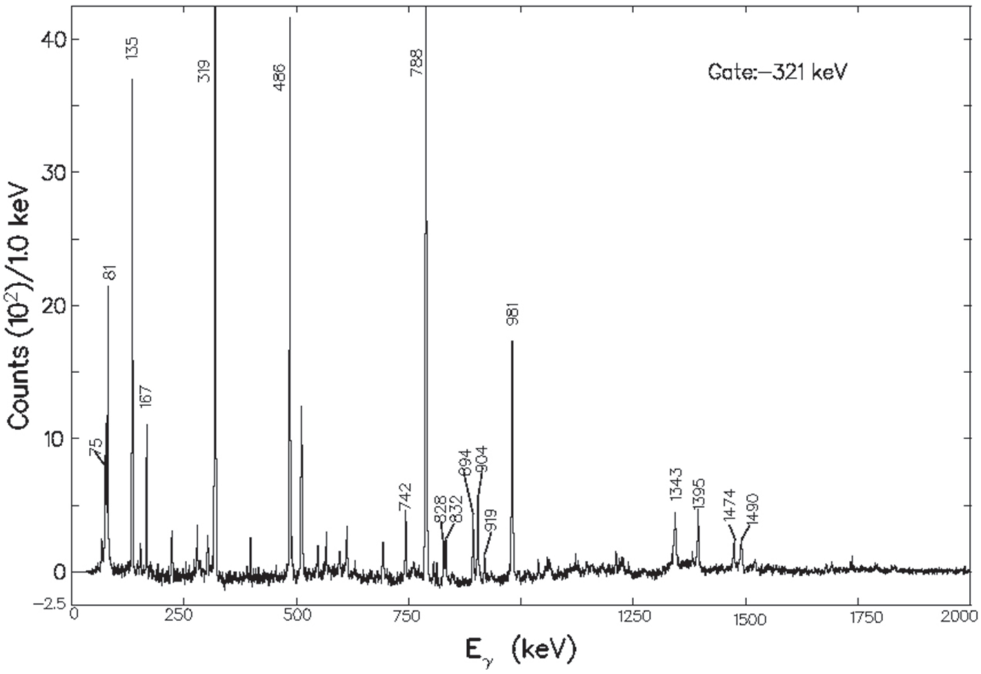

Fig. 5.1.8.1: Background subtracted γ-γ coincidence spectra for ^{70}As gated on 321 keV (7- → 5-) transition.

Data analysis is in progress. In Fig. 5.1.8.1 we have shown a 321 keV gated spectra of ^{70}As. Here, almost all the strong transitions are labelled. New results, in details, will be published as soon as the analysis is completed.

We acknowledge Abhilash S. R. for target preparation and the Pelletron staff of IUAC for providing excellent beam.

REFERENCES:

[1] B. O. Ten Brink, J. Akkermans and H. Verheul, Nucl. Phys. A**330**, 409 (1979).
[2] A. Filevich, M. Behar, G. Garcia Bermudez and M. A. J. Mariscotti, Nucl. Phys. A**309**, 285 (1978).
[3] T. Badika, V. Cojocaru, D. Pentelica, I. Popescu and N. Scintei, Nucl. Phys. A**535**, 425 (1991).
[4] G. Garcia Bermudez, J. Döring, G. D. Johns, R. A. Kaye, M. A. Riley, S. L. Tabor, C. J. Gross et al., Phys. Rev. C **56**, 2869 (1997).
[5] B. Mukherjee et al., Acta Phys. Hung. N. S. **11**, 305 (2000).

5.1.9 Study of high Spin States in A ~ 180 mass region

A. Sharma[1], Shashi. K. Dhiman[1], Pankaj Kumar[1], S. Muralithar[2], R. P. Singh[2], Yashraj[2], K. Katre[2], R. K. Gurjar[2], S. S. Tiwary[3], Neelam[4], Anuj[4], S. Kumar[4], S. Suman[5], S. K. Tandel[5], R. Raut [6], Sutanu Bhattacharya[7], Umakant Lamani[8] and Subodh[9]

[1]Department of Physics, Himachal Pradesh University, Shimla 171005, India
[2]Inter-University Accelerator Centre, Aruna Asaf Ali Marg, New Delhi 110067, India
[3]Department of Physics, Institute of Science, Banaras Hindu University, Varanasi 221005, India
[4]Department of Physics and Astrophysics, University of Delhi, Delhi 110007, India
[5]UM-DAE Centre for Excellence in Basic Sciences, Mumbai 400098, India
[6]UGC-DAE Consortium for Scientific Research, Kolkata Centre, Kolkata 700098, India
[7]Department of Pure and Applied Physics, Guru Ghasidas Viswavidyalaya, Koni, Bilaspur 495009, India
[8]Department of Physics, Indian Institute of Technology Bombay, Powai, Mumbai 400076, India
[9]Department of Physics, Panjab University, Chandigarh 160014, India

Investigation of the structure of atomic nuclei near Z = 82 shell closure is important due to co-existence of single particle and collective excitations. The high-j orbitals, *viz.* $h_{11/2}$ and $h_{9/2,}$ lie near proton Fermi surface along with low-j $_{s1/2,}$ $d_{5/2}$ and $d_{3/2}$ orbitals, resulting in number of K-isomers in this mass region. The Iridium nuclei lie between transitional and spherical nuclei. Nuclei in this region are soft to changes in deformation. In these transitional nuclei, a complex interplay between different competing degrees of freedom was observed, and in particular, consideration of the γ-degree of freedom plays a crucial role. Besides the collective excitations, a large number of different high-K multi-quasiparticle states of different shapes have been observed in these nuclei [1]. In this region, significantly larger deformation has been observed after back-bending in Ir isotopes [2]. The change in deformation would be caused by the polarization of the Osmium core by the odd proton [3]. The present study concentrates on ^{183}Ir and is part of a systematic study of nuclei in Os-Pt region. The information on ^{183}Ir is very scarce [4,5].

High spin states of ^{183}Ir were populated via ^{169}Tm(^{18}O, 4n) fusion evaporation reaction at beam energy 94 MeV, delivered by the 15 UD Pelletron at IUAC. The Indian National Gamma Array (INGA) [9] was used for detecting two and higher fold γ-γ coincident events. A self-supporting ^{169}Tm target of 6.5 mg/cm^2 thickness was used. Offline data analysis was carried out by CANDLE [6], INGASORT [7] and RADWARE [8] computer codes. In the present study, the high spin states of ^{183}Ir were investigated. The strongly populated $\pi h_{9/2}$ band has been observed up to ~ 6.1 MeV. In Fig. 5.1.9.1 total projection spectrum from γ-γ coincidence matrix for all the Clover detectors is shown. Fig. 5.1.9.2 shows a spectrum gated with 309 keV γ-line. Further data analysis is in progress.

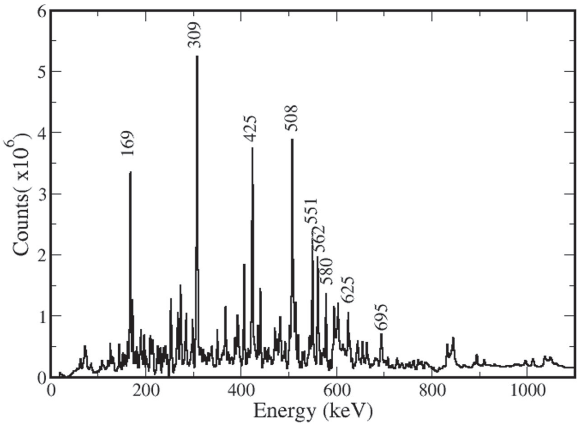

Fig. 5.1.9.1: γ-γ coincidence spectrum from the whole Clover array. Energy of the γ peaks is marked in keV.

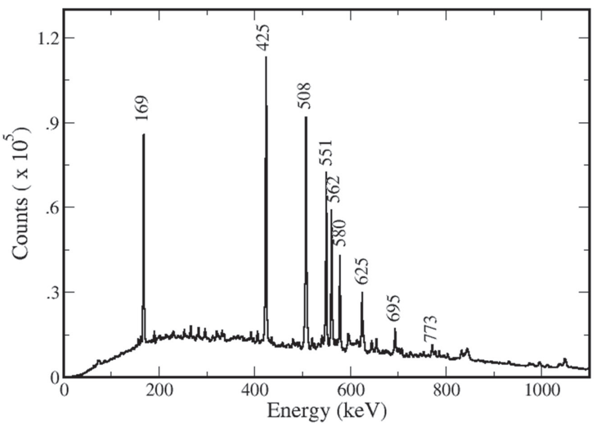

Fig. 5.1.9.2: Coincidence spectrum, gated with 309 keV γ-line of ^{183}Ir.

REFERENCES:

[1] V. Modamio *et al.,* Phys. Rev. C **81**, 054304 (2010).
[2] S. Andre *et al.,* Phys. Rev. Lett. **38**, 327 (1977).
[3] R. Kaczarowski *et al.,* Phys. Rev. C **41**, 2069 (1990).
[4] V. P. Janzen *et al.,* Phys. Rev. Lett. **61**, 2073 (1988).
[5] A. J. Kreiner *et al.,* Phys. Rev. C **42**, 878 (1990).
[6] Ajith Kumar B. P. *et al.,* Proc. DAE-BRNS Symp. Nucl. Phys. B**44**, 390 (2001).
[7] R. K. Bhowmik *et al.,* Proc. DAE-BRNS Symp. Nucl. Phys. B**44**, 422 (2001).
[8] D. C. Radford *et al.,* Nucl. Instrum. Methods A**361**, 267 (1995).
[9] S. Muralithar *et al.,* Nucl. Instrum. Methods A **622**, 281 (2010).

5.1.10 High spin states in ^{84}Sr

Naveen Kumar[1], Anuj[1], Suresh Kumar[1], Neelam[1], K. Rojeeta Devi[1], Neeraj Kumar[1], C.V. Ahmad[1], A. Banerjee[1], Aman Rohilla[1], C.K. Gupta[1], Anand Pandey[1], Ravi Bhusan[1], S. Verma[1], S. K. Chamoli[1], Unnati Gupta[1], S. K. Mandal[1], R. Garg[2], S. Bhatacharya[2], S. Muralithar[2], R. P. Singh[2], Indu Bala[2], Divya Arora[2], Vishnu Jyothi[3], Chandrani Majumder[4], H. P. Sharma[4], A. Sharma[5], S. K. Dhiman[5], Ajay Y. Deo[6] and P. C. Srivastava[6]

[1]Department of Physics and Astrophysics, University of Delhi, Delhi 110007, India
[2]Inter-University Accelerator Centre, Aruna Asaf Ali Marg, New Delhi 110067, India
[3]Department of Physics, Andhra University, Visakhapatnam 530003, India
[4]Department of Physics, Banaras Hindu University, Varanasi 221005, India
[5]Department of Physics, Himachal Pradesh University, Shimla 171005, India
[6]Department of Physics, IIT Roorkee, Roorkee 247667, India

Nuclei near the Z ≈ 40 and N < 47 falls between the deformed and spherical region. The strontium (Sr) isotopes with A ≤ 88 shows a gradual transition from the nearly doubly magic ^{88}Sr nucleus to the rotational like behaviour in ^{80}Sr nucleus. Investigation of these transitions is particularly interesting as the proton number (Z = 38 or 40) behaves like a magic one, at least when the neutron number is close to N = 50. Many collective bands have been seen in isotopes of Sr, Zr and Mo. The nucleus ^{84}Sr, which has four neutron holes in the $1g_{9/2,}$ $2p_{1/2}$ and $1f_{5/2}$ subshells, displays both collective and single particle excitations. In the present experiment, the excited states of

^{84}Sr nucleus were studied to confirm the tentatively assigned spin to various previously known states. The aim also included searching for interesting high-spin phenomena like super deformation [1,2], loss of collectivity [3,4], band termination[5], chiral rotation[6] and shape-related effects [7,8].

The excited states of ^{84}Sr was populated through the reaction $^{76}Ge(^{12}C,4n)^{84}Sr$, with a beam energy of 58 MeV which was provided by the 15UD Pelletron at IUAC. The gamma-rays were detected by the INGA spectrometer at IUAC [9] which consisted of 18 Compton- suppressed Clover detectors with four, four, six, two and two detectors placed at angles 148º, 123º, 90º, 57º and 32º, respectively, with respect to the beam direction. The distance between the target position and the detectors was 25 cm. The list mode data were collected in double and higher fold gamma-ray coincidence using a CAMAC based multi-parameter data-acquisition system along with the Collection and Analysis of Nuclear Data using Linux nEtwork (CANDLE) software. The symmetric and asymmetric matrices were generated by sorting the data with CANDLE and RADWARE [10]. The results of preliminarily analysis are shown in the Fig. 5.1.10.1 and 5.1.10.2. The analysis to obtain the RDCO and Polarization are in progress.

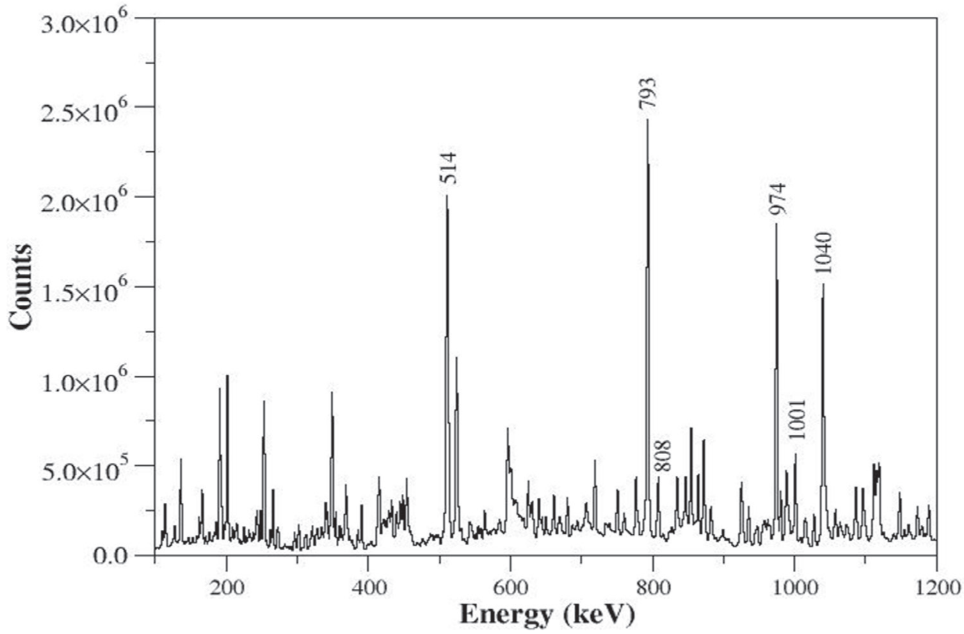

Fig. 5.1.10.1: Projection spectrum of coincidence data obtained at E_{lab} = 58 MeV.
The gamma-rays belonging to the ^{84}Sr nucleus are labelled.

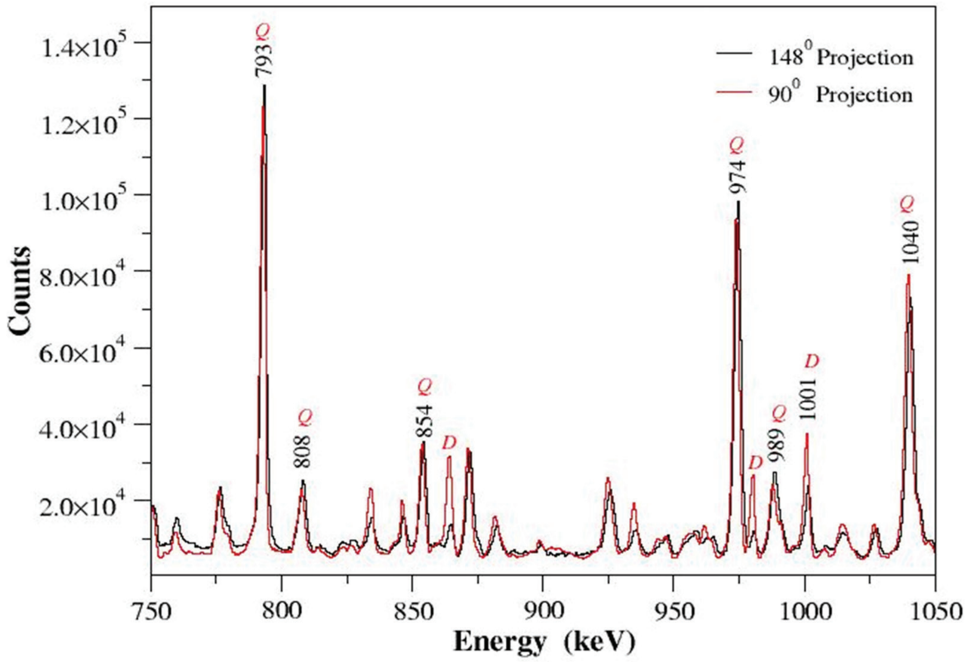

Fig. 5.1.10.2: The spectrum shows the projection of asymmetry matrix to obtain the DCO ratios – red line for 90º and black line for 148º.
The quadrupole (Q) and dipole (D) nature of the gamma-ray transition is also marked along their energy in keV.

REFERENCES:

[1] B. Singh, R. Zywina and R. B. Firestone, Nucl. Data Sheets **97,** 241 (2002).
[2] D. R. LaFosse *et al.,* Phys. Lett. B **354,** 34 (1995).
[3] R. K. Sinha *et al.,* Eur. Phys. J. A **28,** 277 (2006); 29, 253 (2006).
[4] W. Nazarewicz, J. Dudek, R. Bengtsson, T. Bengtsson and I. Ragnarsson, Nucl. Phys. A**435,** 397 (1985).
[5] M. Wiedeking *et al.,* Phys. Rev. C **67,** 034320 (2003).
[6] S. Y. Wang *et al.,* Phys. Lett. B **703,** 40 (2011).
[7] A. Dhal *et al.,* Eur. Phys. J. A **27,** 33 (2006).
[8] Ch. Winter *et al.,* Nucl. Phys. A **535,** 137 (1991).
[9] S. Muralithar *et al.,* Nucl. Instrum. Methods A **622,** 281 (2010).
[10] D. C. Radford, Nucl. Instrum. Methods A **361,** 297 (1995).

5.1.11 Measurement of the pre and post-scission neutron multiplicity for the reactions $^{18}O+^{184,186}W$

N. K. Rai[1], A. Gandhi[1], N. Saneesh[2], M. Kumar[2], G. Kaur[2], A. Parihari[2], D. Arora[2], N. K. Deb[3], A. Chakraborty[4], S. Biswas[4], T. K. Ghosh[5], Jhilam Sadhukhan[5], K. S. Golda[2], A. Jhingan[2], P. Sugathan[2], B. K. Nayak[6] and Ajay Kumar[1]

[1]Department of Physics, Banaras Hindu University, Varanasi 221005, India
[2]Inter-University Accelerator Centre, Aruna Asaf Ali Marg, New Delhi 110067, India
[3]Department of Physics, Gauhati University, Guwahati 781014, India
[4]Department of Physics, Siksha Bhawan, Visva-Bharti, Santiniketan, West Bengal 731235, India
[5]Variable Energy Cyclotron Centre, 1/AF Bidhan Nagar, Kolkata 700064, India
[6]Nuclear Physics Division, Bhabha Atomic Research Centre, Mumbai 400085, India

Heavy-ion induced fusion-fission reactions involve many complex processes, which are understood through experimental as well theoretical approach. It is well known that in a collision between two heavy nuclei there is a considerable contribution from quasi-fusion processes along with the fusion-fission processes. To investigate these processes, a number of attempts like mass distribution, mass-angle correlations, and mass-gated neutron multiplicity measurements have been done. In the recent years, nuclear dissipation has emerged as a topic of considerable interest involved in the fusion-fission process. Nuclear dissipation causes the delay in the fission process with respect to the statistical model of compound nucleus (CN) decay. The deep understanding of the nuclear dissipation is still a matter of detail study because of the complexities involved in the process. The measurement of neutron multiplicity has been done to investigate the details of the dynamical evolution of the nuclear system [1]. To understand the nuclear dissipation, evaporated neutrons are one of the preferred probes. Measurement of neutrons helps in measuring the time-scales of these processes and in understanding the mechanism of energy dissipation in heavy ion reactions. In the literature, some measurements have been reported to investigate the effect of entrance channel mass asymmetry, neutron shell closure, N/Z, etc. in the fission process [2-4]. In the present study, we have measured the neutron multiplicity for the reactions $^{18}O+^{184,186}W$ populating the compound nucleus ^{202}Pb and ^{204}Pb to understand the dissipative fission dynamics.

The experiment was performed using the National Array of Neutron Detectors (NAND) facility of IUAC. The pulsed beam of ^{18}O with a pulse separation of 250 ns, delivered from the 15UD Pelletron, was bombarded on ^{184}W and ^{186}W targets of thicknesses 770 μg/cm^2 and 637 μg/cm^2, respectively with carbon backing of 40 μg/cm^2. Neutron multiplicity measurements were performed at three energies, E_{lab} = 97, 102 and 107 MeV. The neutrons were detected in coincidence with the fission fragments using 50 organic liquid scintillators (BC 501) of 5”×5” dimensions, kept at a distance of 175 cm from the center of the target. Two Multi-Wire Proportional Counters (MWPCs) of active area 11×16 cm^2 were symmetrically placed at the folding angles, at a distance of 26 cm (35º) and 21 cm (126º) to detect the fission fragments. MWPCs were operated with the isobutene gas pressure of 4 mbar. Two Silicon Surface Barrier Detectors (SSBDs) were also placed inside the chamber at ±12.5º with respect to the beam directions to monitor the beam. Event mode data were collected using the VME based data acquisition system coupled with Linux Advanced Multi-Parameter System (LAMPS) software. The fast time signals of the MWPCs were used to obtain the time of flight of the fission fragments. The acquisition was set according to the trigger logic generated by coincidence between RF of the beam pulse and the fission detectors.

Neutron detectors are sensitive to detect neutrons as well as gamma-rays. The discrimination between neutrons and gamma was done using the time of flight (TOF) technique as well as pulse shape discrimination (PSD) based on zero – cross over method. To identify the neutron and gamma event, a two-dimensional gate was applied to the neutron spectra. The neutron TOF spectra were converted into energy spectra by considering the gamma peak as a reference line. Neutron energy spectra were gated with TOF spectra of fission fragments to ensure that neutrons are only emitted from the fusion-fission process. Experimental values of the pre- and post-scission multiplicity are shown in Fig. 5.1.11.1 and Fig. 5.1.11.2.

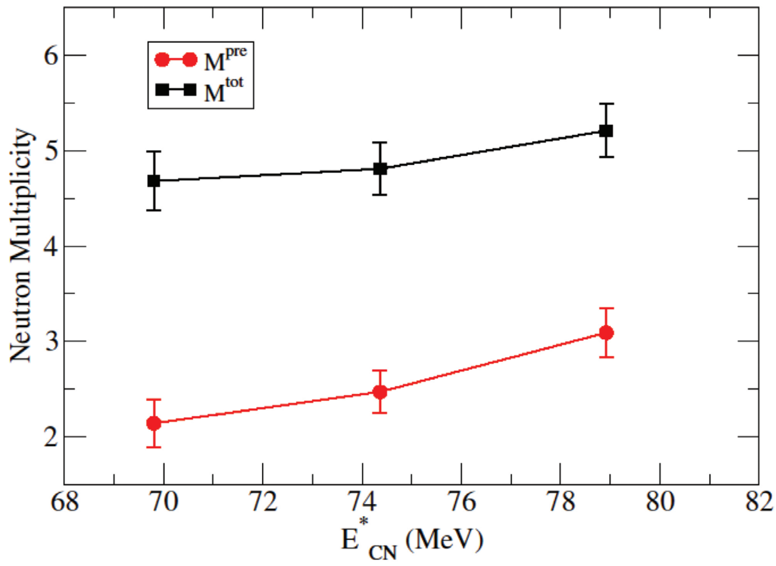

Fig. 5.1.11.1: Variation of the experimental values of pre-scission and total neutron multiplicity as a function of excitation energy for the reaction $^{18}O+^{186}W$.

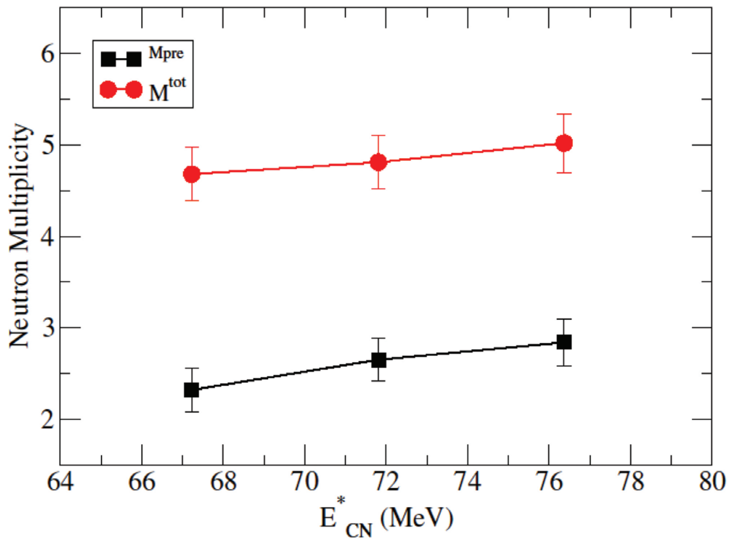

Fig. 5.1.11.2: Variation of the experimental values of pre-scission and total neutron multiplicity as a function of excitation energy for the reaction $^{18}O+^{184}W$.

REFERENCES:

[1] D. J. Hinde *et al.,* Phys. Rev. C **45,** 1229 (1992).
[2] Hardev Singh *et al.,* Phys. Rev. C **76,** 044610 (2007).
[3] V. Singh *et al.,* Phys. Rev. C **86,** 014609 (2012).
[4] Rohit Sandal *et al.,* Phys. Rev. C **87,** 014604 (2013).

5.1.12 Studying fusion in reactions forming medium heavy compound systems

A. C. Visakh[1], E. Prasad[1], S. Nath[2], N. Madhavan[2], J. Gehlot[2], Gonika[2], P. V. Laveen[1], M. Sharref[1], A. Shamlath[1], S. Sanila[3], Rohan Biswas[2], A. Parihari[2], A. M. Vinodkumar[3], B. R. S. Babu[3], K. M. Varrier[4] and S. Appannababu[5]

[1]Department of Physics, Central University of Kerala, Nileshwar 671314, India
[2]Inter-University Accelerator Centre, Aruna Asaf Ali Marg, New Delhi 110067, India
[3]Department of Physics, University of Calicut, Calicut 673635, India
[4]Department of Physics, University of Kerala, Thiruvananthapuram 695034, India
[5]Department of Nuclear Physics, Andhra University, Visakhapatnam 530003, India

Evaporation residue (ER) excitation function measurements for the reactions $^{16}O+^{142,150}Nd$ have been performed using the Heavy Ion Reaction Analyzer (HIRA) [1] at IUAC. The measurements were carried out in the beam energy range 54 - 104 MeV. Pulsed beam of ^{16}O with pulse separation of 4 μs was bombarded on isotopically enriched $^{142,150}Nd$ targets of thicknesses 140 μg/cm² and 162 μg/cm², respectively. The ERs were separated by the HIRA and were detected in the focal plane using a two-dimensional position-sensitive multi wire proportional counter (MWPC) with an active area of 150 mm × 50 mm. Two silicon surface barrier detectors were placed inside the target chamber to measure elastically scattered beam particles and to get absolute normalization of ER cross sections. A 30 μg/cm² thick carbon foil was placed 10 cm downstream from the target to reset the charge state of the ERs. The time interval between two successive pulses was slightly more than the time of flight (TOF) of ERs, from the reaction point to the focal plane of the HIRA. The ERs were selected from the two-dimensional spectrum of energy loss (ΔE) vs TOF.

The ER cross section was taken to be equal to the fusion cross section since the fission contribution in this energy region is negligible. The total ER cross section is given by

$$\sigma_{ER} = \frac{Y_{ER}}{Y_{mon}} \left(\frac{d\sigma}{d\Omega}\right)_{Ruth} \frac{\Omega_{mon}}{\epsilon_{HIRA}}$$

where, Y_{ER} and Y_{mon} are the yields of the ERs and Rutherford events respectively, $\left(\frac{d\sigma}{d\Omega}\right)_{Ruth}$ is the differential Rutherford scattering cross section in the laboratory frame, Ω_{mon} is the solid angle subtended by the monitor detector and ϵ_{HIRA} is the average transmission efficiency of the HIRA. ϵ_{HIRA} was calculated using the semi-microscopic Monte Carlo code, TERS [2, 3] for each xn-evaporation channel at all energies. The average ϵ_{HIRA} for all the ERs was obtained by taking the weighted average of the efficiency for different evaporation channels at each energy point. Relative abundance of different exit channels was estimated using the statistical model code PACE4 [4]. Preliminary ER excitation functions for the reactions studied are shown in Fig. 5.1.12.1 and Fig. 5.1.12.2. Detailed analysis is in progress.

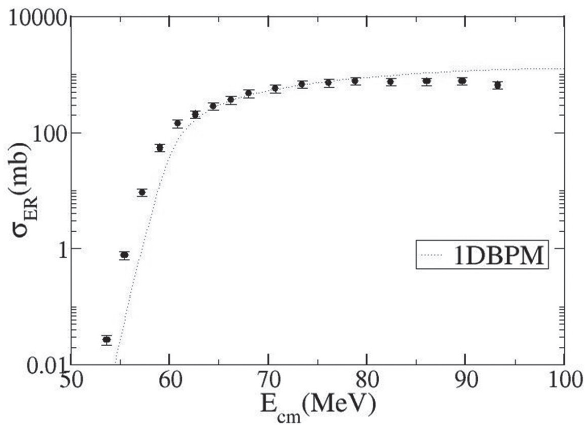

Fig. 5.1.12.1: Measured ER excitation function (preliminary) for $^{16}O+^{142}Nd$.

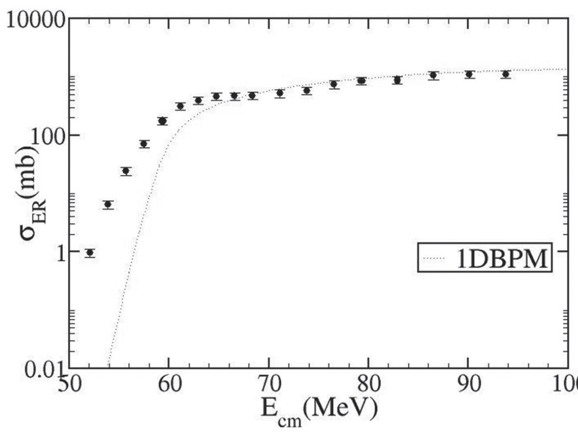

Fig. 5.1.12.2: Measured ER excitation function (preliminary) for $^{16}O+^{150}Nd$.

REFERENCES:

[1] A. K. Sinha *et al.,* Nucl. Instrum. Methods A **339,** 543 (1994).
[2] S. Nath, Comput. Phys. Commun. **180,** 2392 (2009).
[3] S. Nath, Comput. Phys. Commun. **179,** 492 (2008).
[4] A. Gavron, Phys. Rev. C **21,** 230 (1980).

5.1.13 Revisiting the level structure of ^{103}Pd

A. Sharma[1], R. P. Singh[2], S. Muralithar[2], Indu Bala[2], S. S. Bhattacharjee[2], Ritika Garg[2], S. S. Tiwary[3], Neelam[4], S. Das[5], S. Samanta[5], S. S. Ghugre[5], Gurmeet Kumar[6], P. V. Madhusudhana Rao[7], R. Palit[8], S. K. Dhiman[1] and U. Garg[9]

[1]Department of Physics, Himachal Pradesh University, Shimla 171005, India
[2]Inter-University Accelerator Centre, Aruna Asaf Ali Marg, New Delhi 110067, India
[3]Department of Physics, Institute of Science, Banaras Hindu University, Varanasi 221005, India
[4]Department of Physics and Astrophysics, University of Delhi, New Delhi 110007, India
[5]UGC-DAE Consortium for Scientific Research, Kolkata Centre, Kolkata 700098, India
[6]J.C.D.A.V College Dasuya (PU), Punjab 144205, India
[7]Department of Nuclear Physics, Andhra University, Visakhapatnam 530003, India
[8]Department of Nuclear and Atomic Physics, Tata Institute of Fundamental Research, Mumbai 400005, India
[9]Department of Physics, University of Notre Dame, Notre Dame, Indiana 46556, USA

The level structure of A~100 nuclei reveals intriguing phenomena even at low and moderate spin regimes such as vibrations and rotations built upon prolate deformed states [1,2,3]. The underlying configurations present a favorable condition for the possible observation of wobbling, even at low spins [4]. The aforementioned features provided the necessary impetus for us to revisit the level structure of ^{103}Pd, especially at moderate angular momentum spins.

The ^{94}Zr(^{13}C, 4n) reaction at an incident energy ~55 MeV was employed to populate the high spin states in ^{103}Pd. The ^{94}Zr target was ~1 mg/cm^2 thick with ~10 mg/cm^2 gold backing. The de-exciting gamma transitions were detected using the Indian National Gamma Array (INGA) at IUAC. The detectors were placed at angles of 32°, 57°, 90°, 123° and 148° with respect to the beam direction. Data analysis was carried out using CANDLE, INGASORT and RADWARE. Different set of symmetric and angle dependent matrices were made to extract information of energy, intensity, parity and multi-polarity of coincident gamma transitions. Several new transitions were observed in coincidence with 477 keV gamma transition. These transitions have not been reported in previous work. The partial level scheme of ^{103}Pd developed from the present analysis is shown in Fig 5.1.13.1.

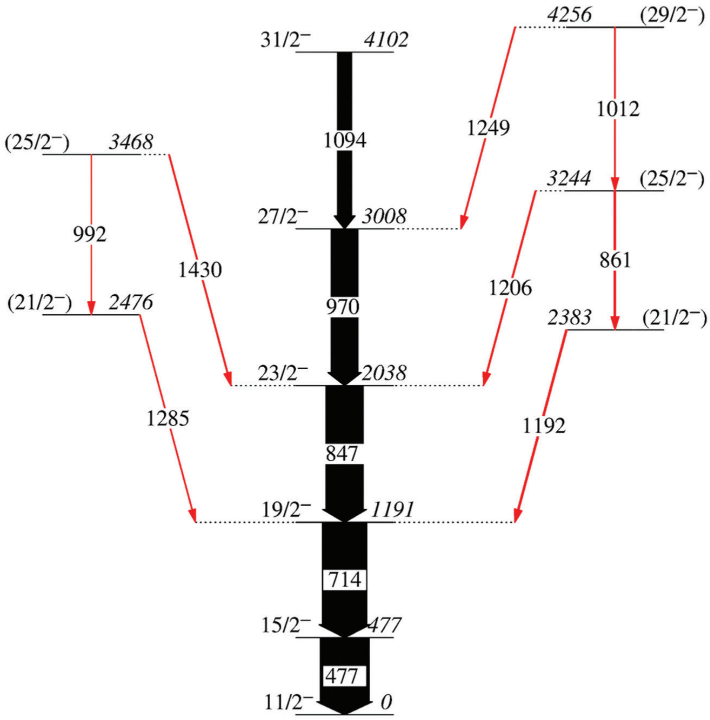

Fig. 5.1.13.1: Partial level scheme of ^{103}Pd.

REFERENCES:

[1] P. H. Regan *et al.,* J. Phys. G: Nucl. Part. Phys, **19**, L157 (1993).
[2] Dan Jerrestam *et al.,* Nucl. Phys. A**557,** 411c (1993).
[3] B. M. Nyako *et al.,* Phys. Rev. C **60,** 024307 (1999).
[4] J. T. Matta *et al.,* Phys. Rev. Lett. **114,** 082501 (2015).

5.1.14 γ-vibration in ^{124}Te

S. S. Tiwary[1], H. P. Sharma[1,*], S. Chakraborty[1], C. Majumder[1], S. Rai[2], Pragati[3], Mayank[4], S. S. Bhattacharjee[5], R. P. Singh[5], S. Muralithar[5], P. Banerjee[6], S. Ganguly[7], S. Kumar[8] and A. Kumar[9]

[1]Department of Physics, Institute of Science, Banaras Hindu University, Varanasi 221005, India
[2]Department of Physics, Visva-Bharati, Santiniketan 731235, India
[3]Department of Physics, Indian Institute of Technology Roorkee, Roorkee 247667, India
[4]Amity Institute of Nuclear Science and Technology, Amity University, Noida 201313, India
[5]Nuclear Physics Group, Inter-University Accelerator Centre, Aruna Asaf Ali Marg, New Delhi 110067, India
[6]Nuclear Physics Division, Saha Institute of Nuclear Physics, Kolkata 700064, India
[7]Department of Physics, Bethune College, Kolkata 700006, India

[8]Department of Physics and Astrophysics, University of Delhi, Delhi 110007, India
[9]Department of Physics, Panjab University, Chandigarh 160014, India

In A ~130 mass region, quasi–γ–bands were systematically reported in even-even Ba and Xe nuclei [1]. Previously, even-even Te-nuclei were considered as good examples of spherical vibrator [2], but recent studies on heavier Te-nuclei showed signatures of γ–soft behaviour [3-5]. Hence, the present work is dedicated to investigate the structural behavior of heavier Te-isotopes at low spin.

The in-beam study of ^{124}Te was carried out using ^{122}Sn(^{9}Be, α3n)^{124}Te fusion evaporation reaction at 48 MeV beam energy, obtained from the 15UD Pelletron [6,7] at IUAC. The INGA array [8] was used as the experimental setup for the present study. The array contained 14 Compton suppressed HPGe Clover detectors. The details of the experimental set-up and data analysis are discussed elsewhere [9].

Previously, the ground state band was reported up to I = 16ℏ at 5481 keV excitation energy [10-12]. In the present work, levels up to 14ħ have been confirmed on the basis of γ-γ-coincidence relationship [Fig. 5.1.14.1]. The 2483, 3038, 3549 and 4240 keV levels have been newly established in the level scheme. On the basis of decay patterns and relative excitation energy with respect to corresponding ground state band these levels are predicted to be the members of one phonon quasi–γ–band. However, further investigations are underway.

The authors are thankful to the staff of the Target Development Laboratory and the Pelletron accelerator facility of IUAC. The authors acknowledge the INGA Collaboration supported by the University Grants Commission (UGC) and the Department of Science and Technology (DST) under INGA project (IR/S2/PF-03/2003-I). The first author is thankful to the UGC for financial support-vide contract no. 23/06/2013(I)EU-V.

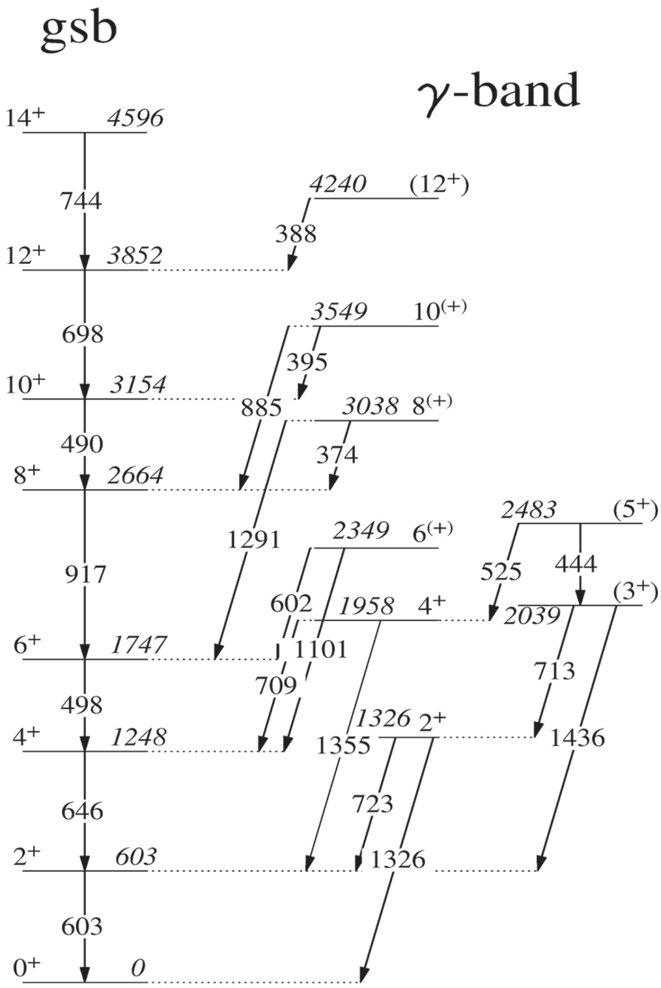

Fig. 5.1.14.1: Partial level scheme of ^{124}Te.

REFERENCES:

[1] H. Kusakari *et. al.,* Nucl. Phys. A**242,** 13 (1975).
[2] A. Kerek, Nucl. Phys. A**176,** 466 (1971).
[3] S. F. Hicks *et. al.,* Phys. Rev. C **95,** 034322 (2017).
[4] M. Saxena *et. al.,* Phys. Rev. C **90,** 024316 (2014).
[5] S. V. Jackson *et. al.,* Phys. Rev. C **15,** 1806 (1977).
[6] G. K. Mehta *et. al.,* Nucl. Instrum. Methods A **268,** 334 (1988).
[7] D. Kanjilal *et. al,* Nucl. Instrum. Methods A **328,** 97 (1993).
[8] S. Muralithar *et. al.,* Nucl. Instrum. Methods A **622,** 281 (2010).
[9] S. Chakraborty *et. al.,* Braz. J. Phys. **47,** 406 (2017).
[10] N. Warr *et. al.,* Nucl. Phys. A**636,** 379 (1998).
[11] N. Fotiades *et. al.,* Phys. Rev. C **89,** 017303 (2014).
[12] A. Astier *et. al.,* Eur. Phys. J. A **50,** 2 (2014).

5.1.15 Systematic study of low energy incomplete fusion reaction dynamics: Effect of target deformation

Suhail A. Tali[1], Harish Kumar[1], M. Afzal Ansari[1], Asif Ali[1], D. Singh[2], Rahbar Ali[3], Pankaj K. Giri[2], Sneha B. Linda[2], R. Kumar[4], Siddharth Parashari[1], R. P. Singh[4] and S. Muralithar[4]

[1]Department of Physics, Aligarh Muslim University, Aligarh 202002, India
[2]Centre for Applied Physics, Central University of Jharkhand, Ranchi 835205, India
[3]Department of Physics, G. F. (P. G.) College, Shahjhanpur 242001, India
[4]Inter-University Accelerator Centre, Aruna Asaf Ali Marg, New Delhi 110067, India

The study of heavy ion (HI) fusion reactions is of great interest for both theoretical and experimental nuclear physicists. In the energy region of ≈ 4-7 MeV/nucleon, the dominant reaction modes are complete fusion (CF) and incomplete fusion (ICF) reactions [1,2]. Many efforts are being made to comprehend the phenomenon of CF and ICF dynamics. The current interest is to understand the dependence of incomplete fusion on (a) incident projectile energy (b) projectile-target mass asymmetry (c) Coulomb effect (d) target deformation (e) projectile structure (Q_α-value) and to search some new entrance channel parameters on which ICF process may depend. Further the lack of proper theoretical model, which could reproduce the experimentally measured ICF reaction cross sections appropriately, is also a motivation for the present study [3,4]. Keeping the above points into consideration, the experiment was performed using ^{12}C (α-cluster) as the projectile and ^{165}Ho (deformed) as the target.

The experiment was performed at IUAC, New Delhi. The ^{165}Ho target foils and Al-catcher foils were prepared by using the rolling technique at the Target Development Laboratory of IUAC. The stacked foil activation technique was implemented, so as to cover a wide range of energy within limited beam time. Stacks consisting of target foils and backed by Al-foils were irradiated by the ^{12}C ion beam to cover energy above the Coulomb barrier and up to 87.4 MeV in the General Purpose Scattering Chamber (GPSC). After the irradiation, the target-catcher assembly was dismantled immediately from the GPSC and the γ-ray activities built-up in the foils were recorded by keeping them in front of a pre-calibrated High Purity Germanium (HPGe) detector. The HPGe detector was coupled to a PC through CAMAC based data acquisition system CANDLE.

When the incident projectile interacts with the target nucleus, the compound nucleus formed via CF and/or ICF process is in the highly excited state and de-excites via emission of light nuclear particles and their characteristic gamma rays. In the present work, the EFs of several ERs populated via xn, pxn, αxn, αpxn and 2αxn were measured. The experimentally measured cross sections were compared with the statistical model code PACE4, which gives only the CF cross sections. During the analysis, it was observed that the experimentally measured independent cross sections of the ERs populated via emission of xn and pxn channels were in good agreement with the PACE4 predictions with level density parameter a= $\frac{A}{10}$, MeV^{-1}, which shows that these ERs are populated via CF process. However, in case of αxn, αpxn and 2αxn emission channels, the experimentally measured independent cross sections show a significant enhancement from the PACE4 predictions with the same level density parameter a= $\frac{A}{10}$, which is attributed to the ICF process. The ICF fraction, which is defined as strength of ICF relative to total fusion i.e., FICF (%) = $\left(\frac{\sigma_{ICF}}{\sigma_{TF}}\right)\times 100$ (where $\sigma_{TF} = \sigma_{CF} + \sigma_{ICF}$), was obtained from data. In order to understand the dependence of ICF on target deformation β_2, the FICF(%) deduced for the present system $^{12}C+^{165}Ho$ is plotted in Fig. 5.1.15.1 along with the earlier studied systems at constant relative velocity (V_{rel} = 0.053c) for various projectile-target combinations. It may be seen from Fig. 5.1.15.1, that F_{ICF}(%) increases with increasing value of target deformation. But the increments are different for reactions induced by ^{12}C (α-clustered) and ^{13}C (non α-clustered) projectiles with the same target. However, a regular trend is not observed. An attempt has also been made to explore the dependence of ICF dynamics on the parameter $\mu Z_P Z_T (1-\beta_2)$ (a combination of entrance channel parameters), where μ is the mass asymmetry, $Z_P Z_T$ is the Coulomb effect and β_2 is the target deformation. F_{ICF}(%) is plotted against $\mu Z_P Z_T (1-\beta_2)$ in Fig. 5.1.15.2. It is important to mention that the systems and their symbols are the same as in Fig. 5.1.15.1. From this graph, it is clear that F_{ICF}(%) increases almost linearly. But F_{ICF}(%) is more for ^{12}C induced reactions compared to ^{13}C induced reactions with the same target. This difference may be explained on the basis of projectile Q_α value, which is simply defined as the amount of energy required to liberate an α-particle from the incident projectile. As the projectile Q_α value for ^{12}C (-7.37 MeV) is less compared to ^{13}C (-10.65 MeV), the reactions involving ^{12}C as the projectile shows more F_{ICF}(%) compared to the reactions induced by ^{13}C. Moreover, the value of ICF fraction for both $^{12,13}C+^{159}Tb$ is less and is away from the linear trend, this is probably due to the less mass asymmetry of these systems compared to others.

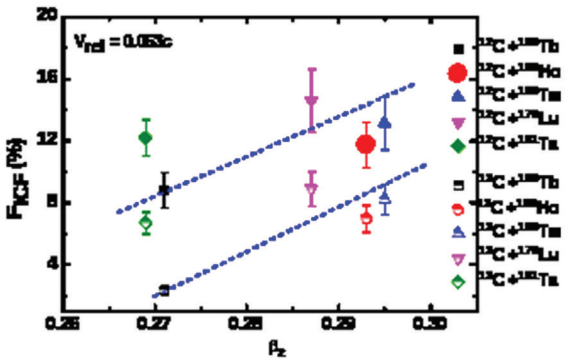

Fig. 5.1.15.1: The deduced ICF fraction F_{ICF}(%) as a function of target deformation (β2) at constant relative velocity (V_{rel} = 0.053c), for 12,13C projectile induced reactions with different targets. The dotted lines are just to guide the eyes.

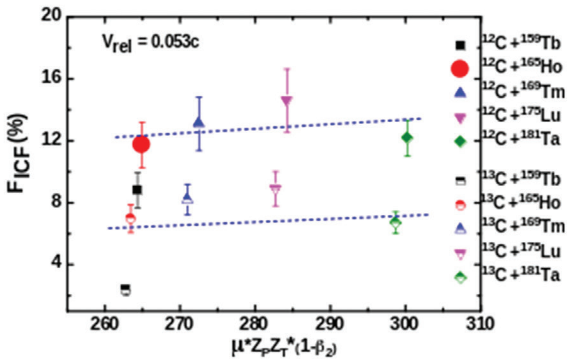

Fig. 5.1.15.2: The deduced ICF fraction FICF(%) as a function of $\mu_Z PZ_T$ $(1-\beta_2)$ at constant relative velocity (V_{rel} = 0.053c), for $^{12,13}C$ projectile induced reactions with different targets. The dotted lines are just to guide the eyes.

REFERENCES:

[1] Suhail A. Tali *et al.,* Nucl. Phys. A**970,** 208 (2018).

[2] Harish Kumar *et al.,* Phys. Rev. C **99,** 034610 (2019).

[3] Harish Kumar *et al.,* Nucl. Phys. A**960,** 53 (2017).

[4] A. Yadav *et al.,* Phys. Rev. C **96 ,** 044614 (2017).

5.1.16 Quasi-elastic scattering measurements in ^{28}Si + $^{142,150}Nd$ systems

S. Biswas[1,2], A. Chakraborty[1], P. Sugathan[3], A. Jhingan[3], D. Arora[3], B. R. Behera[4], R. Biswas[3], N. K. Deb[5], S. S. Ghugre[6], P. K. Giri[7], K. S. Golda[3], G. Kaur[3], A. Kumar[8], M. Kumar[3], B. Mukherjee[1], B. K. Nayak[9], A. Parihari[3], N. K. Rai[8], S. Rai[10], R. Raut[6], R. N. Sahu[11] and A. K. Sinha[12]

[1]Department of Physics, Siksha Bhavana, Visva-Bharati, Santiniketan 731235, India
[2]Department of Physics, Murshidabad College of Engineering and Technology, Berhampore 742102, India
[3]Inter-University Accelerator Centre, Aruna Asaf Ali Marg, New Delhi 110067, India
[4]Department of Physics, Panjab University, Chandigarh 160014, India
[5]Department of Physics, Gauhati University, Guwahati 781013, India
[6]UGC-DAE Consortium for Scientific Research, Kolkata Center, Sector III/LB-8, Bidhan Nagar, Kolkata 700098, India
[7]Department of Physics, Central University of Jharkhand, Ranchi 835205, India
[8]Department of Physics, Banaras Hindu University, Varanasi 221005, India
[9]Nuclear Physics Division, Bhabha Atomic Research Centre, Mumbai 400085, India
[10]Department of Physics, Salesian College, Siliguri 734001, India
[11]Department of Physics, Indian Institute of Technology Ropar, Punjab 140001, India
[12]UGC - DAE Consortium for Scientific Research, Indore 452017, India

An experiment was carried out for measurement of excitation functions and barrier distributions in $^{28}Si+^{142,150}Nd$ systems. The main motivation for this measurement was to study the effect of deformation of the target and projectile on the corresponding barrier distribution. The experiment was carried out in the General Purpose Scattering Chamber (GPSC) facility using ^{28}Si beam from the 15UD Pelletron at IUAC. The incident beam energy was varied from 84 to 136 MeV. The targets were ^{142}Nd and ^{150}Nd of thickness~150 μg/cm^2 with carbon capping and backing. The beam-like particles were detected at the back angles using an array of hybrid telescope detectors. A representative plot of the excitation function for $^{28}Si+^{150}Nd$ at 160^o angle is shown in Fig. 5.1.16.1. Detailed analysis of the collected data is under progress.

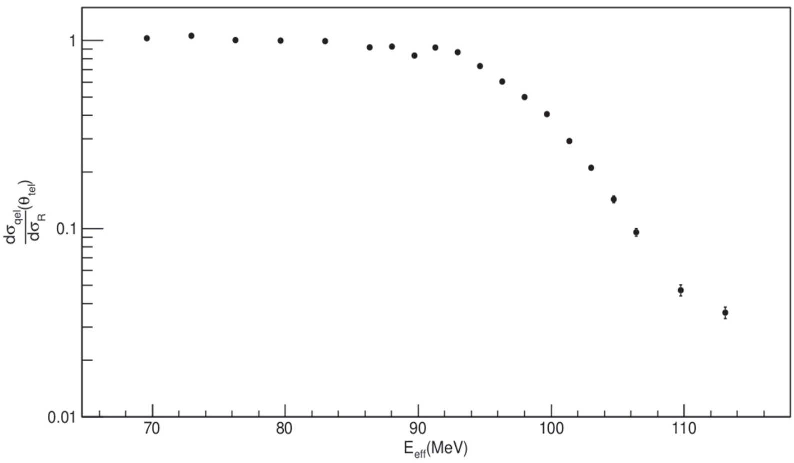

Fig. 5.1.16.1: Excitation function for $^{28}Si+^{150}Nd$ at 160^o.

5.1.17 Nuclear structure study around doubly magic ^{56}Ni-core

Saradindu Samanta[1], Soumya Das[1], Suvronil Chatterjee[1], Sajad Ali[2], Sutanu Bhattacharya[3], Shashi Shekhar Tiwary[4], Kaushik Katre[5], Anupriya Sharma[6], Rajarshi Raut[1], Sandeep S. Ghugre[1], A. K. Sinha[7], R. P. Singh[5], S. Muralithar[5] and Umesh Garg[8]

[1]UGC-DAE Consortium for Scientific Research, Kolkata Centre, Kolkata 700098, India
[2]Saha Institute of Nuclear Physics, Sector 1, AF Block, Bidhannagar 700064, Kolkata, India
[3]Guru Ghasidas Viswavidyalaya, Bilaspur 495009, Chhattisgarh, India
[4]Department of Physics, Banaras Hindu University, Varanasi 221005, Uttar Pradesh, India
[5]Inter-University Accelerator Centre, Aruna Asaf Ali Marg, New Delhi 110067, India
[6]Department of Physics, Himachal Pradesh University, Shimla 171005, Himachal Pradesh, India
[7]UGC-DAE Consortium for scientific Research, University Campus, Khandwa Road, Indore 452017, India
[8]Department of Physics, University of Notre Dame, Notre Dame, Indiana 46556, USA

Nuclei around the doubly magic nucleus ^{56}Ni are excellent candidates for the study of competition between collective and single-particle excitations. At low spins, the properties of the A~60 nuclei are governed by the particle occupancy in the $1f_{5/2,}$ $2p_{3/2,}$ and $2p_{1/2}$ orbitals. At higher excitations the possibility of deformation, and consequent observation of rotational sequences, emerges due to the occupancy of deformation driving high-j $g_{9/2}$ orbital. This structural evolution from single particle nature in the lower excitation regime to band like structure at higher excited states makes these nuclei subjects of interest. At still higher energies there is precedence of observation of core-broken states from excitations of the ^{56}Ni-core. [1]

The Nuclear Physics Group at the Kolkata Centre has embarked on a systematic investigation of the structure of these nuclei in the vicinity of the Ni-core. One of the experiments under this programme was carried out previously at the Pelletron LINAC Facility in TIFR wherein nuclei such as ^{64}Cu (Z=29, N=35) [2] and ^{61}Ni (Z=28, N=33) [3] have been investigated following their population in ^{59}Co(^{7}Li, xnyp) reaction. These studies established excitations in the fpg model space for these nuclei. However no evidence of collectivity or core broken configurations could be observed therefrom. The quest for the same has recently been pursued with heavier projectile at IUAC. The nuclei of interest are slightly more massive ones, albeit in the same region around the Ni-core. These are ^{66}Zn (Z=30, N=36), ^{66,69}Ga (Z=31, N=35, 38), ^{69}Ge (Z=32, N=37) populated through ^{59}Co(^{13}C, xnypzα) reaction at E_{lab} = 45 - 50 MeV. The INGA, stationed at IUAC and consisting of 16 Compton suppressed clover detectors was used as the detection system. A 5.2 mg/cm^2 thick ^{59}Co (on a 4 mg/cm^2 Ta backing) foil was used as the target therein. Fig. 5.1.17.1 depicts the partial projection spectrum constructed from acquired data, which is indicative of the various nuclei populated in the present experiment. These have been observed up to excitations ~ 5 MeV and 10 ħ. Further analysis is currently in progress.

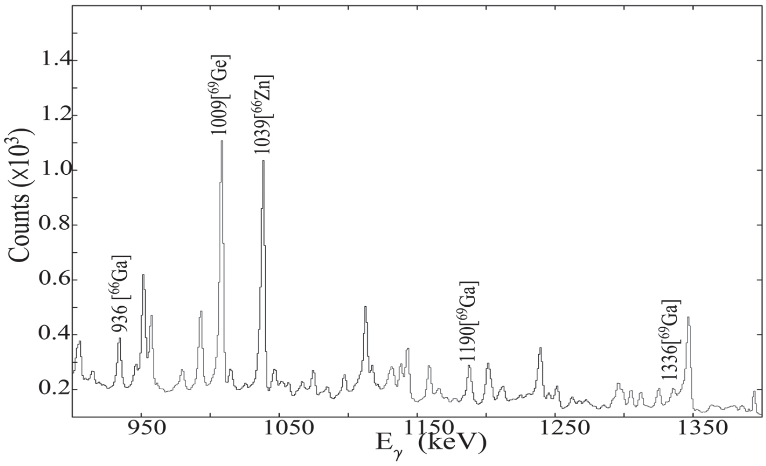

Fig. 5.1.17.1: Different nuclei populated in the present experiment.

REFERENCES:

[1] D. A. Torres *et. al.,* Phys. Rev. C **78,** 054318 (2008).
[2] S. Samanta *et. al.,* Phys. Rev. C **97,** 014319 (2018).
[3] S. Samanta *et. al.,* Phys. Rev. C **99,** 014315 (2019).

5.1.18 Level scheme of ^{127}Xe

S. Chakraborty[1], H. P. Sharma[1], S. S. Tiwary[1], C. Majumder[1], S. Rai[2], Pragati[3], Mayank[4], S. S. Bhattacharjee[5], R. P. Singh[5], S. Muralithar[5], P. Banerjee[6], S. Ganguly[7], S. Kumar[8], A. Kumar[9] and R. Palit[10]

[1]Department of Physics, Institute of Science, Banaras Hindu University, Varanasi 221005, India
[2]Department of Physics, Visva-Bharati, Santiniketan 731235, India
[3]Department of Physics, Indian Institute of Technology Roorkee, Roorkee 247667, India
[4]Amity Institute of Nuclear Science and Technology, Amity University, Noida 201313, India

[5]Nuclear Physics Group, Inter-University Accelerator Centre, Aruna Asaf Ali Marg, New Delhi 110067, India
[6]Nuclear Physics Division, Saha Institute of Nuclear Physics, Bidhannagar 700064, Kolkata, India
[7]Department of Physics, Bethune College, Kolkata 700006, India
[8]Department of Physics and Astrophysics, University of Delhi, Delhi 110007, India
[9]Department of Physics, Panjab University, Chandigarh 160014, India
[10]Department of Nuclear and Atomic Physics, Tata Institute of Fundamental Research, Mumbai 400005, India

The low lying structure of odd-A Xe nuclei in A~125 mainly consists of both positive and negative parity rotational bands based on $s_{1/2}$, $d_{3/2}$, $d_{5/2}$, $g_{7/2}$ and $h_{11/2}$ neutron orbitals, lying near the Fermi surface [1,2]. Among these, the negative parity h11/2 band was reported with the highest intensity and angular momentum. In case of positive parity bands, the population of $g_{7/2}$ band was found significant than others. However, the experimental information on this band in ^{127}Xe is very scanty. In particular, the unfavoured signature partner of this band was reported tentatively up to $I^\pi = \leq 17/2^+$ [1], whereas in lighter Xe nuclei, this band was reported up to ~$25/2^+$. This report presents a detail γ-ray spectroscopic study on $\nu g_{7/2}$ band in ^{127}Xe.

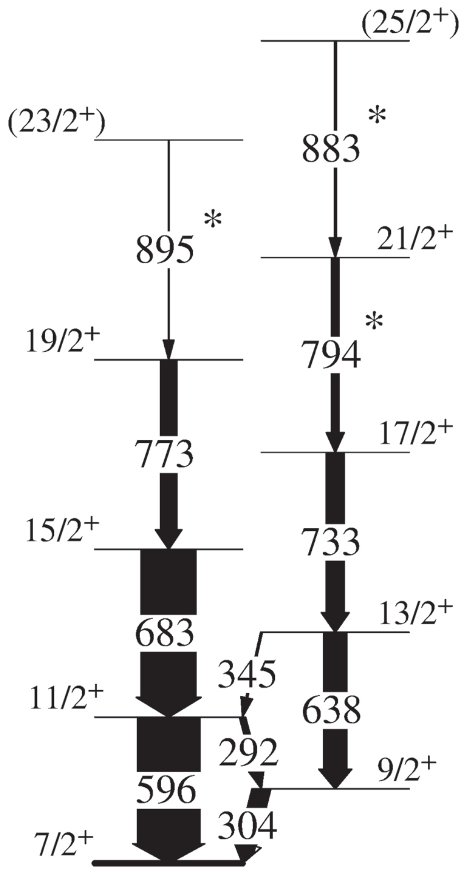

Fig. 5.1.18.1: Partial level scheme of ^{127}Xe.

Energetic ^{9}Be beam of 48 MeV, obtained from the 15UD Pelletron accelerator of IUAC, was bombarded on a 8.4 mg/cm^2 thick 99.3% isotopically enriched ^{122}Sn foil to populate the high spin states of ^{127}Xe. 14 Compton suppressed Clover detectors of INGA were used to collect the coincident γ-rays. Offline data analysis was carried out using INGAsort and RadWare computer codes. Details of the experimental set up and data analysis are available in Refs. [3, 4].

From the present experiment, alignment of two $h_{11/2}$ neutrons was reported at higher spin in negative parity band [3]. Placement of previously reported two states at 2307 keV was revised [5, 6]. A rotational band above a three quasi-neutron high-K isomer was also established with a revised half-life of the isomer [4]. A positive parity band, based on $I^\pi = 7/2^+$ state at 342 keV ($\tau_{1/2}$=36 ns) was reported up to $I^\pi = 19/2^+$ [2]. In the present work, this band has been extended up to $I^\pi = (23/2^+)$ by placing a 895 keV γ-transition, as shown in Fig. 5.1.18.1. The signature partner of this band, reported up to $I^\pi = (17/2^+)$, has also been extended up to $I^\pi = (25/2^+)$ state by placing two new γ-rays of 794 and 883 keV (Fig. 5.1.18.1). New placements are supported by the observation of the coincident γ-rays of this band in 773 and 733 energy gated spectra (Fig. 5.1.18.2). Spin and parity of several states have been assigned from present angular correlation and linear polarization measurements. Further study is underway.

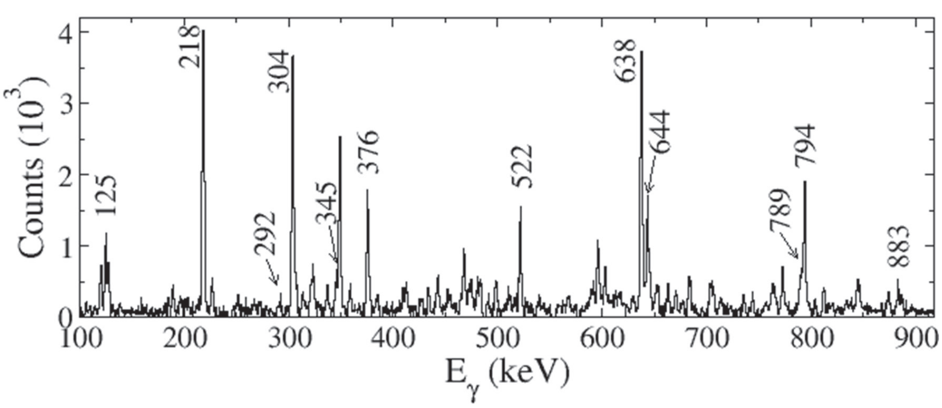

Fig.5.1.18.2: Coincidence energy gated spectrum of 733 keV.

The authors are thankful to the staff of the Target Development Laboratory and the Pelletron accelerator facility of IUAC. The INGA collaboration is duly acknowledged. The first author is also thankful to the CSIR for SRF, under file no. 9/13(662)/2017-EMR-I.

REFERENCES:

[1] W. Urban *et al.,* Z. Phys. A **320,** 327 (1985).
[2] S. Chakraborty *et al.,* Phys. Rev. C **97,** 054311 (2018).
[3] S. Chakraborty *et al.,* Braz. J. Phys. **47,** 406 (2017).
[4] S. Chakraborty *et al.,* Phys. Scr. **93,** 115302 (2018).
[5] S. Chakraborty *et al.,* Eur. Phys. Lett. **121,** 42001 (2018).
[6] I. Wiedenhöver *et al.,* Z. Phys. A **347,** 71 (1993).

5.1.19 Probing of incomplete fusion dynamics of ^{16}O interaction with ^{148}Nd

Pankaj K. Giri[1], Amritraj Mahato[1], D. Singh[1], Sneha B. Linda[1], Harish Kumar[2], Suhail A. Tali[2], Rahbar Ali[3], N. P. M. Sathik[4], M. Afzal Ansari[2], R. Kumar[5], S. Muralithar[5] and R. P. Singh[5]

[1]Department of Physics, Central University of Jharkhand, Ranchi 835205, India
[2]Department of Physics, Aligarh Muslim University, Aligarh 202002, India
[3]Department of Physics, G.F. (P.G.) College, Shahjahanpur 242001, India
[4]Department of Physics, Jamal Mohammed College, Tiruchirappalli 620020, India
[5]Inter-University Accelerator Centre, Aruna Asaf Ali Marg, New Delhi 110067, India

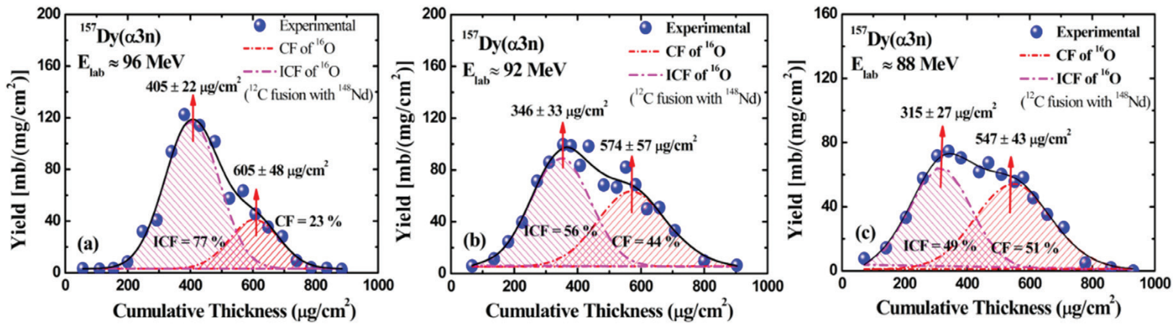

Fig. 5.1.19.1: Measured FRRDs of ER ^{157}Dy(α3n) populated in the interaction of ^{16}O with ^{148}Nd at energies ≈96, ≈92, and ≈ 88 MeV. Solid circles and dashed dotted curves represents, the measured data and Gaussian fit, respectively.

A series of offline gamma spectroscopy experiments were performed for the measurements of excitation functions (EFs) and forward recoil range distributions (FRRDs) of evaporation residues (ERs) using ^{16}O beam with ^{148}Nd target to explore the incomplete fusion (ICF) dynamics at Pelletron energy ≈ 3-7 MeV/A. Experiments were performed using the 15 UD Pelletron facility at IUAC. The enriched ^{148}Nd targets of thickness ≈ 200-700 μg/cm^2 were fabricated using high vacuum evaporation facility at the Target Development Laboratory of IUAC. The General Purpose Scattering Chamber (GPSC) was utilized for the irradiation of targets. The GPSC chamber has in vacuum target transfer facility. The irradiated stacks were taken out from the scattering chamber after buildup of sufficient activities. The ERs trapped in aluminum catcher foils were recorded by two pre-calibrated 100 cm^3 High Purity Germanium (HPGe) detectors coupled with PC through CAMAC based data acquisition system. The energy and efficiency calibration of HPGe detectors were done using standard ^{152}Eu source of known strength. The collection and analysis of data has been done by software CANDLE [1]. The detected ERs have been identified by their characteristics γ-rays and decay-curve analysis.

In the present work, FRRDs of ERs ^{159,158}Er(xn), ^{160,159}Ho(pxn), ^{157,155}Dy(αxn) and ^{155}Tb(αpxn) have been measured. The relative contributions of various ERs produced via complete fusion (CF) and/or ICF processes have been computed by fitting the measured FRRDs data using the software ORIGIN [2]. The theoretical recoil ranges have been computed using SRIM-2008 [3]. Measured FRRDs of ERs have been compared with their theoretical mean ranges. As a representative case, FRRDs of ER ^{157}Dy(α3n) at three different energies have been displayed in Fig. 5.1.19.1. From this figure, it can be seen clearly that the measured FRRDs of ER ^{157}Dy shows two peaks. The peak at larger cumulative thickness is associated with CF, while the second peak at shorter thickness can be referred to ICF of ^{16}O with ^{148}Nd. On the other hand, the peaks associated with CF and ICF channels shifted to higher cumulative thickness due to the larger momentum transfer at higher projectile energy. These FRRD results show that full and partial linear momentum transfer components are involved. It means that the ERs populated through α-emission channels are not only produced via CF, but also through ICF dynamics. The ICF fraction (F_{ICF}) has also been estimated from EFs and FRRDs and displayed in Fig. 5.1.19.2. It can be seen from this figure that the values of F_{ICF} for these measurements are in good agreement. Moreover, it can also be noticed from Fig. 5.1.19.2, that the ICF contribution increases with projectile energy. This increase in ICF contribution is due to the increase of breakup probability of projectile ^{16}O into ^{12}C and α with projectile energy.

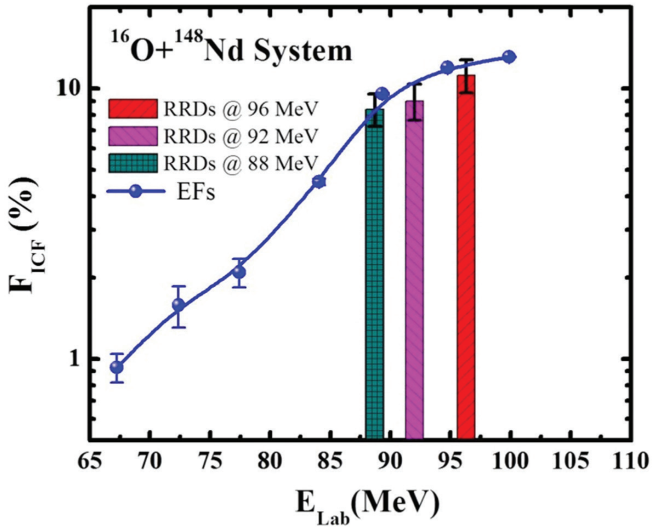

Fig. 5.1.19.2: The incomplete fusion fraction (F_{ICF}) as a function of projectile energy in the interaction of ^{16}O with ^{148}Nd.

REFERENCES:

[1] B. P. Ajith Kumar, E. T. Subramaniam, K. Singh and R. K. Bhowmik, DAE-BRNS Symp. Nucl. Phys., Kolkata, (2001); URL http://www.iuac.res.in/NIAS/.

[2] ORIGIN (OriginLab, Northampton, MA); URL http://www.originlab.com/.

[3] The Stopping and Range of Ions in Matter (SRIM-2008.04); URL: https://www.srim.org.

5.1.20 Study of transitional nuclei near N = 82 shell closure using in-beam gamma-ray spectroscopy

Neelam[1], Suresh Kumar[1], K. Rojeeta Devi[1], Anuj[1], Neeraj Kumar[1], Kajol Chakraborty[1], Anjali Rani[1], Unnati[1], S. Verma[1], S. K. Mandal[1], Madhu[2], Khamosh Yadav[2], Bharti Bhoy[2], Anil Kumar[2], Ajay Y. Deo[2], Praveen C. Srivastava[2], S. S. Tiwari[3], H. P. Sharma[3], A. Sharma[4], S. K. Dhiman[4], S. Bhatacharya[5], T. Trivedi[5], Kaushik Katre[6], Yashraj[6], Indu Bala[6], R. P. Singh[6] and S. Muralithar[6]

[1]Department of Physics and Astrophysics, University of Delhi, Delhi 110007, India
[2]Department of Physics, Indian Institute of Technology Roorkee, Roorkee 247667, India
[3]Department of Physics, Banaras Hindu University, Varanasi 221005 , India
[4]Department of Physics, Himachal Pradesh University, Shimla 171005 , India
[5]Department of Pure and Applied Physics, Guru Ghasidas University, Bilaspur 495009, India
[6]Inter-University Accelerator Center, Aruna Asaf Ali Marg, New Delhi 110067, India

The transitional nuclei in the A = 135 mass region lies near the N = 82 shell closure and are known to have γ-soft character. Many interesting high-spin phenomena such as magnetic rotation (MR), shape coexistence, chirality and bands based on the multi-quasiparticle excitations are reported in these nuclei [1-3]. In addition, the yrast 10+ isomeric states based on the $\nu[h_{11/2}]^{-2}$ configuration were also observed in the N =78 and 80 isotones [4, 5]. In the previous studies of the ^{136}Ba nucleus (N = 80) the yrast band has been studied up to spin $I^{\pi} = 10^{(+)}$ ħ and two isomeric states at spin $I^{\pi} = 10^{(+)}$ ħ and $7^{(-)}$ ħ were observed [6, 7]. Similar isomeric states were also observed in the ^{132}Xe nucleus (N = 78) at spin $I^{\pi} = (10^{+})$ ħ, $7^{(-)}$ ħ and $5^{(-)}$ ħ based on $\nu[h_{11/2}]^{-2}$, $\pi[h_{11/2}, d_{3/2}]$ and $\pi[h_{11/2}, s_{1/2}]$ configuration, respectively [8]. The structure of the ^{132}Xe nucleus has been studied up to $I^{\pi} = (16^{+})$ ħ [9].

In the present work, the excited states of ^{136}Ba and ^{132}Xe nuclei were populated using the ^{130}Te(^{9}Be, xn) reaction at 36 and 48 MeV beam energy, respectively. The ^{9}Be beam was provided by the 15UD Pelletron accelerator at IUAC. The ^{130}Te target had a thickness of 1.2 mg/cm^2 with 4.2 mg/cm^2 gold backing. The de-exciting gamma-ray transitions were detected using the Indian National Gamma Array (INGA) [10] consisting of 15 Clover detectors with 4, 2, 5, 1 and 3 detectors placed at 148º, 123º, 90º, 57º and 32º with respect to the beam direction, respectively. The list mode data was acquired using the CANDLE software. The offline data were sorted using the CANDLE and analysed using the RadWare software packages [11].

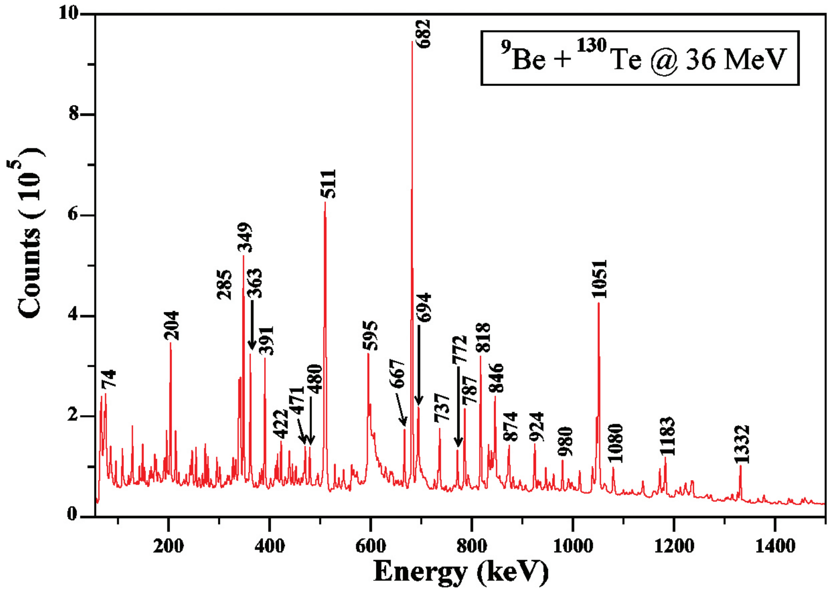

Fig. 5.1.20.1: The projection spectrum obtained in the ^{130}Te(^{9}Be, 3n) reaction at 36 MeV beam energy.

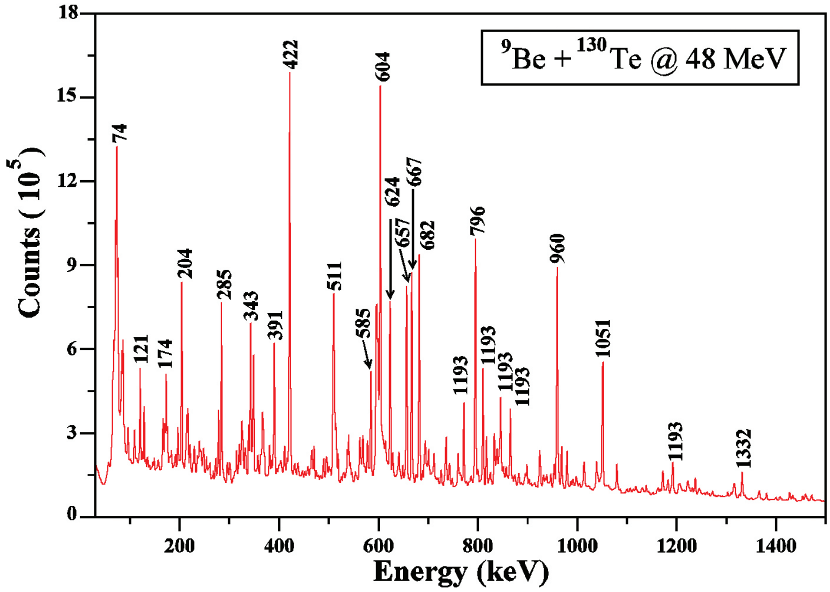

Fig. 5.1.20.2: The projection spectrum obtained in the ^{130}Te(^{9}Be, α3n) reaction at 48 MeV beam energy.

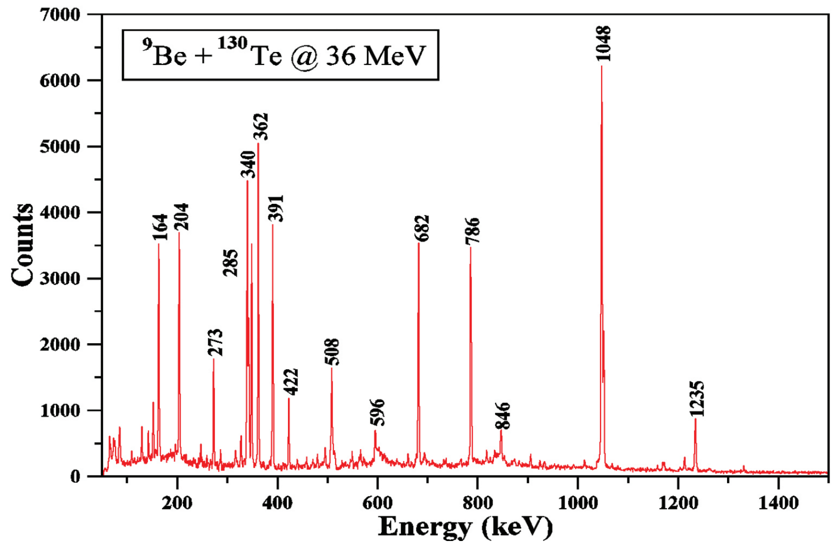

Fig. 5.1.20.3: The coincidence spectrum of the 818 keV gamma-ray transition of the ^{136}Ba nuclei obtained in the ^{130}Te(^{9}Be, 3n) reaction at 36 MeV reaction.

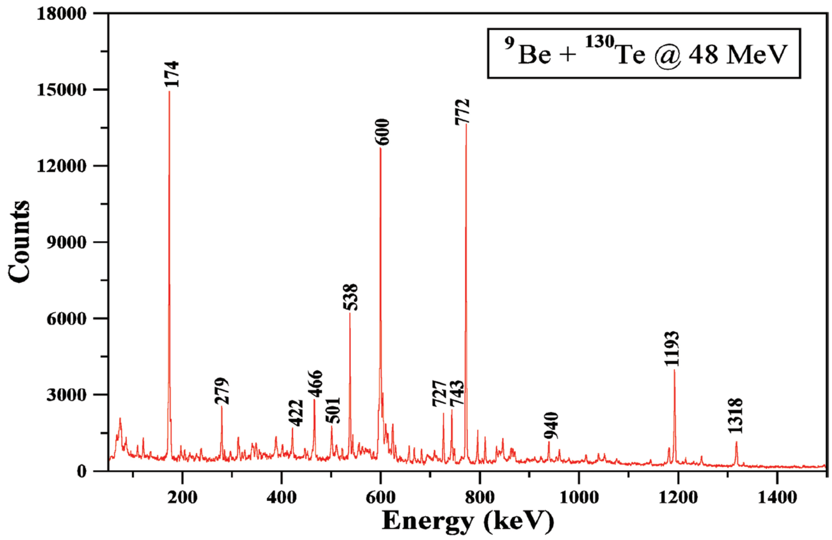

Fig. 5.1.20.4: The gated spectrum of 667 keV gamma-ray transition represents the gamma-ray transitions of the ^{132}Xe nucleus from the analysis of ^{130}Te(^{9}Be, α3n) reaction at 48 MeV beam energy.

After calibration and gain matching, the symmetric and anti-symmetric matrices were generated. The projection spectrum of the ^{130}Te(^{9}Be, xn) reaction obtained at 36 and 48 MeV beam energy are shown in Fig. 5.1.20.1 and 5.1.20.2, respectively. Fig. 5.1.20.3 and 5.1.20.4 represents the gamma-ray transitions of the ^{136}Ba and ^{132}Xe nuclei, in the gate of the 818 and 667 keV gamma-ray transitions, respectively. The previously observed gamma-ray transitions of the ^{136}Ba and ^{132}Xe nuclei were verified. The R_{DCO} and Polarization asymmetry measurements of the newly identified gamma-ray transitions are in progress.

One of the authors (Neelam), would like to acknowledge the financial assistance received from the University Grant Commission (UGC), New Delhi, via IUAC project (UFR – 51320, 62337). The financial support from the Department of Science and Technology (DST), India for the INGA project (No. IR/S2/PF-03/2003-I) is gratefully acknowledged. The supports provided by the Pelletron group, the Target Development Laboratory and the INGA group of IUAC are also gratefully acknowledged.

REFERENCES:

[1] E. S. Paul *et al.,* Phys. Rev. C **40,** 1255 (1989).
[2] S. Lakshmi *et al.,* Phys. Rev. C **69,** 014319 (2004).
[3] C. M. Petrache *et al.,* Phys. Rev. C **86,** 044321 (2012).
[4] T. Morek *et al.,* Z. Phys. A **298,** 267 (1980).
[5] J. C. Merdinger *et al.,* Nucl. Phys. A**346,** 281 (1980).
[6] J. J. Valiente-Dobón *et al.,* Phys. Rev. C **69,** 024316 (2004).
[7] T. Shizuma *et al.,* Eur. Phys. J. A **20,** 207 (2004).
[8] A. Kerek *et al.,* Nucl. Phys. A**172,** 603 (1971).
[9] A. Vogt *et al.,* Phys. Rev. C **96,** 024321 (2017).
[10] S. Muralithar *et al.,* Nucl. Instrum. Methods A **622,** 281 (2010).
[11] D. C. Radford, Nucl. Instrum. Methods. A **361,** 297 (1995).

5.1.21 Measurement of fusion excitation functions for ^{16,18}O+^{116}Sn,^{61,62}Ni

Nabendu K. Deb[1], K. Kalita[1], H. Rashid[1], S. Nath[2], N. Madhavan[2], J. Gehlot[2], Rohan Biswas[2], A. Jhingan[2], T. Varughese[2], Pankaj K. Giri[3], A. Mahato[3], R. N. Sahoo[4], N. K.Rai[5], A. Parihari[2], S. Biswas[6], B. J. Roy[7] and A. Rani[8]

[1]Department of Physics, Gauhati University, Guwahati 781014, Assam, India
[2]Nuclear Physics Group, Inter-University Accelerator Centre, Aruna Asaf Ali Marg, New Delhi 110067, India
[3]Department of Applied Physics, Central University of Jharkhand, Ranchi 835205, Jharkhand, India
[4]Department of Physics, Indian Institute of Technology Ropar, Ropar 140001, Punjab, India
[5]Department of Physics, Banaras Hindu University, Varanasi 221005, Uttar Pradesh, India
[6]Department of Physics, Visva-Bharati, Shantiniketan 731235, West Bengal, India
[7]Nuclear Physics Division, Bhabha Atomic Research Centre, Trombay 400085, Mumbai, India
[8]Department of Physics and Astrophysics, University of Delhi, Delhi 110007, India

Nuclear fusion cross section around the Coulomb barrier, reveals varieties of phenomena. One such phenomenon is the additional enhancement of the sub-barrier fusion cross sections as compared to the theoretical predictions of one dimensional barrier penetration model (1D-BPM) [1]. Such enhancement occurs due to the coupling of relative motion to internal degrees of freedom of the colliding nuclei such as deformation [2], vibration [3] and nuclear transfer channels [4] or neck formation [5]. It was observed that nuclear transfer with positive Q-values leads to fusion cross section enhancement [6]. However, the relationship between fusion enhancement in the sub-barrier region and positive Q-value neutron transfer (PQNT) is unclear [7]. Study of transfer reactions provides useful information on pairing correlation and its effect on fusion reaction mechanism. Therefore, in order to probe the PQNT effect on the sub barrier fusion cross section enhancement, experiments were performed with systems $^{18}O+^{61,62}Ni$ and $^{18}O+^{116}Sn$, around the Coulomb barrier, using the Heavy Ion Reaction Analyzer (HIRA) at IUAC [8]. All these systems favour neutron transfer due to positive Q-values for two neutron stripping. Also $^{16}O+^{61}Ni$ system was studied to investigate the enhancement in the sub-barrier region with respect to the 1D-BPM.

The experiments were performed using Pelletron beams of IUAC. Pulsed beams of $^{16,18}O$ with a pulse separation of 4 μs was used in the experiment to bombard isotopically enriched ^{61}Ni, ^{62}Ni, and ^{116}Sn targets of thickness 110 μg/cm^2, 150 μg/cm^2 [9] and 150 μg/cm^2, respectively, on thin carbon backing of 30 μg/cm^2. The fusion excitation function measurements were performed at laboratory beam energies of 34 - 53 MeV at 1 MeV for the systems with Ni targets and 54 – 84 MeV at 1 MeV steps for the systems with Sn target. Two silicon surface barrier detectors were mounted inside the target chamber at ±15.5° with respect to beam direction to measure Rutherford-scattered beam-like particles and to get absolute normalization of Evaporation Residue (ER) cross sections. A 30 μg/cm^2 carbon foil was placed downstream of the target for re-equilibration of ER charge states. At the focal plane of the HIRA, a two-dimensional position-sensitive MWPC detector with an active area of 150 mm × 50 mm was used to detect ERs. Time of flight was defined for particles reaching the focal plane with respect to RF of beam to separate multiple-scattered beam-like particles and ERs. The solid angle of acceptance for HIRA was kept 10 mSr for the measurements. A raw spectrum of data taken for $^{18}O+^{116}Sn$ is shown in the left panel of Fig. 5.1.21.1, with the energy loss (ΔE) along x-axis and the corresponding time of flight (TOF) along y-axis. All other systems displayed the similar characteristics. From the spectrum, the beam-like particles are very well separated from the ERs. The ER cross section was taken to be equal to the total fusion cross section as the fission contribution in this energy region is negligible. The transmission efficiency of HIRA was calculated by using the semi-microscopic Monte Carlo code, TERS [10] for each xn-evaporation channel at all Elab. The relative abundance of different exit channels were estimated using the statistical model code PACE4 [11].

Preliminary result of the fusion excitation functions for $^{18}O+^{116}Sn$ system is plotted in the right panel of Fig. 5.1.21.1. It is compared with the similar work done by Tripathi et al. [3] for the system $^{16}O+^{116}Sn$. The present system was found to exhibit more enhancements in the sub-barrier region which could be due to the PQNT effect. Further analysis is in progress for this system and even for the other systems. The coupled-channels calculations will be performed with a modified version of CCFULL [12] and FRESCO [13].

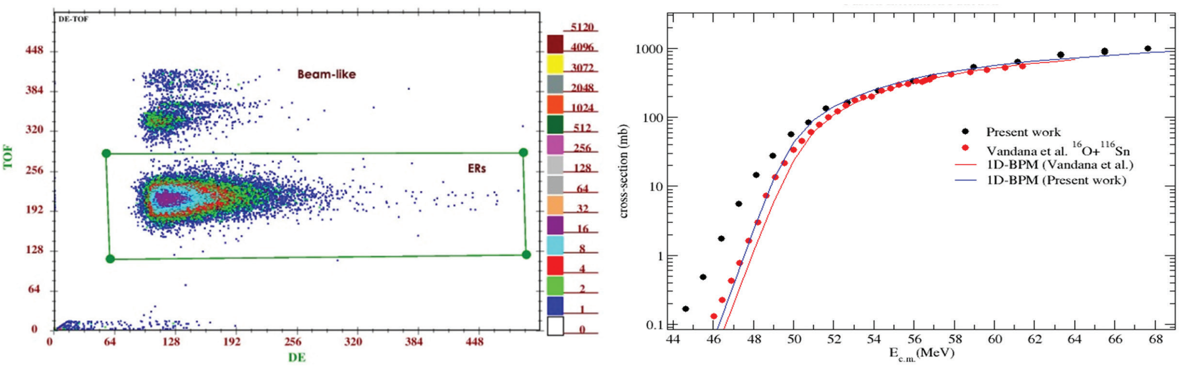

Fig. 5.1.21.1: (left) ΔE versus TOF spectrum at Elab = 66 MeV for $^{18}O+^{116}Sn$ and (right) the fusion excitation functions for $^{16,18}O+^{116}Sn$.

REFERENCES:

[1] M. Dasgupta *et al.,* Ann. Rev. Nucl. Part. Sci. **48,** 401 (1998).
[2] J. R. Leigh *et al.,* Phys. Rev. C **52,** 3151 (1995).
[3] Vandana Tripathi *et al.,* Phys. Rev. C **65,** 014614 (2001).
[4] V. I. Zagrabaev, Phys. Rev. C **67,** 061601 (2003).
[5] C. E. Aguiar, L. F. Canto and R. Donangelo, Phys., Rev. C **31,** 1969 (1985).
[6] A. M. Stefanini *et al.,* Phys. Rev. C **73,** 034606 (2006).
[7] Z. Kohley *et al.,* Phys. Rev. Lett. **107,** 202701 (2011).
[8] A. K. Sinha *et al.,* Nucl. Instrum. Methods A **339,** 543 (1994).
[9] N. K. Deb *et al.,* Vacuum **163,** 148 (2019).
[10] S. Nath, Comput. Phys. Commun. **179,** 492 (2008); 180, 2392 (2009).
[11] A. Gavron, Phys. Rev. C **21,** 230 (1980).

[12] K. Hagino, N. Rowley and A. T. Kruppa, Comput. Phys. Commun. **123,** 143 (1999).
[13] I. J. Thompson, Comp. Phy. Rep. **7,** 167 (1988).

5.1.22 Study of fusion phenomena in $^{37}Cl+^{68}Zn$ reaction around and above barrier: A route for production of Pd radionuclides

A. Chauhan[1], R. Prajapat[1], R. Kumar[1], Malvika[1], G. Sarkar[1], M. Maiti[1], Gonika[2], J. Gehlot[2], N. Madhavan[2], S. Nath[2] and A. Parihari[2]

[1]Department of Physics, Indian Institute of Technology Roorkee, Roorkee 247667, India
[2]Inter-University Accelerator Centre, Aruna Asaf Ali Marg, New Delhi 110067, India

There is a great interest in understanding the heavy ion reaction dynamics around and above the barriers energies. The enhancement in fusion cross-sections has been observed compared to 1D-BPM in the sub-barrier region that could be understood based on the different internal degrees of freedom like different inelastic couplings and deformations, etc. [1-2]. However, the explanation for such observation in the sub-barrier region for more symmetric systems is multifarious. On the other hand, the product evaporation residues (ERs) may find different applications in the field of medicine. Considering the suitable physicochemical properties of palladium isotopes for such applications, many light-ion (p, d, $^{3,4}He$) induced reactions have been reported to synthesize them [3-5]. However, heavy ion reaction data are scare. In this quest, fusion phenomena have been explored for the $^{37}Cl+^{68}Zn$ reaction over a wide energy range and the production cross-sections of ^{101}Pd, ^{101}Ag, ^{100}Pd, and ^{100}Ag radionuclides have been measured.

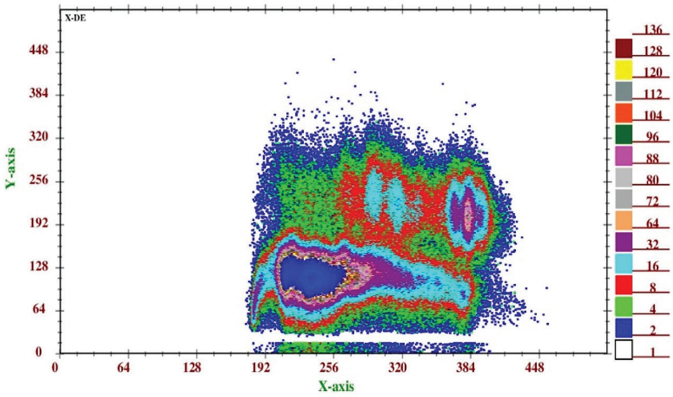

Fig. 5.1.22.1: A 2D spectrum of the energy loss (ΔE) of the product residues vs X-position at the MWPC at E_{lab} = 135 MeV. ERs with different m/q ratios and beam like particles are well separated from each other.

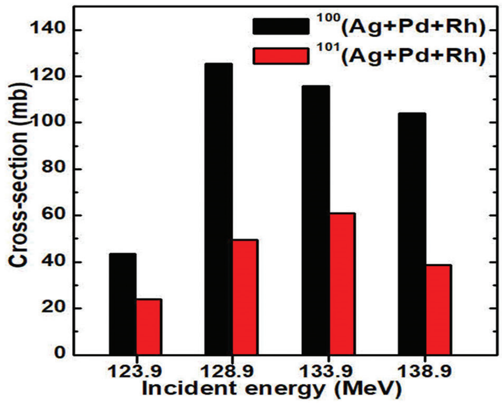

Fig. 5.1.22.2: Experimental cross-sections of ^{101,100}(Ag+Pd+Rh) at different values of E_{lab}.

The experiment was performed using the Heavy Ion Reaction Analyzer (HIRA) facility of IUAC. A pulsed ^{37}Cl beam was bombarded on ^{68}Zn in steps of 2 MeV in the range of E_{lab} = 96 - 100 MeV, and in steps of 5 MeV in the range of E_{lab} = 100 - 140 MeV. Evaporation residues were identified from the background events using a Multi-Wire Proportional Counter (MWPC) placed at the focal plane of HIRA. The ΔE vs TOF (time-of-flight) and X-ΔE spectra were recorded during the experiment. Fig. 5.1.22.1 shows an X-ΔE spectrum at E_{lab} = 135 MeV. The fusion cross-sections for $^{37}Cl+^{68}Zn$ were measured and compared with the CCFULL predictions. The fusion excitation function was found to be significantly higher than the predictions from the 1D-BPM below the barrier while the cross-sections were reproduced well in the above barrier region. The sub-barrier fusion enhancement was explained by the inclusion of inelastic couplings in the projectile as well as the target. We also measured the total cross-sections of mass 100 and 101 fractions populated through the $^{37}Cl+^{68}Zn$ reaction and found that the sum of all the residues is equal to the total fusion cross-section for a particular energy. In Fig. 5.1.22.2, the production cross-sections of ^{101,100}(Ag+Pd+Rh) are reported which shows that the ER cross-section is maximum around 128.9 MeV for mass-100, and 133.9 MeV for mass-101. This study would help to optimize the production parameters for palladium-100,101 radionuclides and to maximize the yield as short-lived $^{100,101}Ag$ decays to relatively long-lived $^{100,101}Pd$.

REFERENCES:

[1] E. Martinez-Quiroz *et al.,* Phys. Rev. C **63,** 054611 (2001).
[2] S. Kalkal *et al.,* Phys. Rev. C **81,** 044610 (2010).
[3] A. Hermanne *et al.,* Nucl. Instrum. Methods B **170,** 281 (2000).
[4] S. Sudar *et al.,* Appl. Radiat. Isotopes **56,** 821 (2002).
[5] M. S. Uddin *et al,* Appl. Radiat. Isotopes **62,** 533 (2005).

5.1.23 Deciphering the low energy incomplete fusion reactions using the recoil range distribution technique

Mohd. Shuaib[1], Ishfaq Majeed[1], Manoj Kumar Sharma[2], Abhishek Yadav[3], Vijay R. Sharma[4], Arshiya Sood[5], Rudra N. Sahoo[5], Malika Kaushik[5], Pushpendra P. Singh[5], Unnati[6], Devendra P. Singh[7], S. Muralithar[8], R. P. Singh[8], R. Kumar[8], B. P. Singh[1], and R. Prasad[1]

[1]Nuclear Physics Laboratory, Department of Physics, Aligarh Muslim University, Aligarh 202002, India
[2]Physics Department, S. V. College, Aligarh 202001, India
[3]Department of Physics, Faculty of Natural Sciences, Jamia Millia Islamia, New Delhi 110025, India
[4]Departamento de Aceleradores, Instituto Nacional de Investigaciones Nucleares, Apartado postal 18-1027, C.P. 11801, Ciudad de Mexico, Mexico
[5]Department of Physics, Indian Institute of Technology Ropar, Ropar, Punjab 140001, India
[6]Department of Physics and Astrophysics, Delhi University, Delhi 110007, India
[7]Department of Physics, University of Petroleum and Energy Studies, Dehradun 248 007, India
[8]Nuclear Physics Group, Inter-University Accelerator Centre, Aruna Asaf Ali Marg, New Delhi 110067, India

In the present work, the relative contributions of complete fusion (CF) and incomplete fusion (ICF) reactions has been studied by measuring the forward recoil range distribution (FRRD) of reaction residues using the non α-cluster beam ^{19}F bombarded on ^{169}Tm target. It may be remarked that, most of the studies of ICF reactions have been carried out using the α-cluster beams like ^{12}C, ^{16}O, ^{20}Ne etc . However, the studies using the non α-cluster beams are still limited. Therefore, for better understanding of the effect of projectile structure on ICF, it is required to extend these investigations by including the non α-cluster beams on different targets covering the periodic table. The present work is in continuation of our recent investigation on ^{19}F+^{169}Tm system [1], where measured excitation functions (EFs) have been used to understand the break-up fusion processes. The experiments have been performed at IUAC. The recoil-catcher activation technique involving off-line γ-ray spectroscopy has been employed. The CF and ICF events have been tagged by full and partial linear momentum transfer components, respectively. In forward recoil range distributions (FRRDs), nine radio-nuclides viz., ^{184}Pt (4n), ^{185}Pt (5n), ^{184}Ir (p3n), ^{185}Ir (p4n), ^{183}Os (αn), ^{181}Os (α3n), ^{179}Os (α5n), ^{177}W (2α3n), and ^{175}Ta (2αp4n) have been measured at two distinct energies ≈ 96 and 106 MeV. In the case of xn/pxn channels, only a single peak in the recoil range distribution has been observed that corresponds to the entire linear momentum transfer from projectile to the target nucleus i.e., these channels are populated via CF process. However, for α-emitting channels, the RRDs are deconvoluted into more than one Gaussian peak. The peak at the higher cumulative depth indicates the contribution due to complete LMT (complete fusion) from projectile to the target nucleus. However, the peak at lower cumulative depth corresponds to the fusion of ^{15}N (if ^{19}F breaks up into ^{15}N+α and ^{15}N fuses) with ^{169}Tm target nucleus and strongly reveals the presence of partial linear momentum component associated with the ICF processes. The experimentally measured recoil ranges of xn/pxn and αxn/2αxn/2αpxn channels obtained from the RRD data are compared with those obtained from the SRIM [2] calculations and found to be in reasonably good agreement at both the energies. As a representative case the measured ranges of ^{177}W(2α3n) residues populated via CF/ICF processes (Fig. 5.1.23.1) are compared with SRIM calculations and found to agree well at both the energies. The analysis of presently measured RRDs clearly indicates the incomplete fusion of ^{19}F projectile at energies ≈ 4-6 MeV/nucleon. Hence, on the basis of results obtained from the analysis of RRD data, it may be concluded that, the non α-cluster beam (19F) also gives a significant contribution of ICF reactions at low energies.

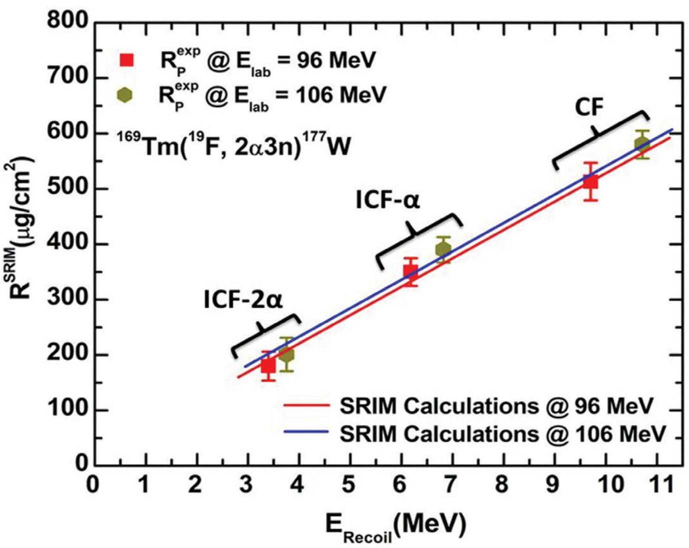

Fig. 5.1.23.1: A comparison of most probable mean ranges obtained from RRD of ^{177}W(2α3n) residues with SRIM calculations.

REFERENCES:

[1] Mohd. Shuiab, *et al.,* J. Phys. Rev. G: Nucl. Part. Phys. **44,** 105108 (2017).
[2] The Stopping and Range of Ions in Matter (SRIM-2008.04); http://www.srim.org/

5.2 MATERIALS SCIENCE

Ambuj Tripathi

The materials science facilities continue to support research programmes of a large number of users from different universities and institutions. This year there were a total of 63 user experiments spread over 202 shifts and were performed without any major beam time loss due to facility break down in materials sciences in beamhall I and II. These included 18 BTA runs spread over 53 shifts associated with students' Ph.D. programmes. Though the swift heavy ion (SHI) irradiation and related experiments mostly utilize irradiation chamber in the materials science beamlines in beamhall-I, 5 experiments of 23 shifts requiring low fluence irradiation were performed in GPSC beamline. Besides irradiation facilities, materials science group is also providing many materials synthesis and characterization facilities such as XRD, AFM, SEM, Raman, UV-Vis, I-V, Hall measurement etc and these are heavily utilized by users. Typically more than 2100 samples were characterized each year.

The materials science research programmes are being carried out in a wide range of energies varying from tens of keV to hundreds of MeV. This year there were many interesting results in the various areas of research including those on ion beams induced nanostructuring, synthesis of nanocomposites and applications, novel phase formations, etc.. Special emphasis is given to in-situ/ on-line measurements and many such experiments were performed this year. In-situ Investigation of 140 MeV Cu^{11+} and 160 MeV Br^{12+} ions induced damages in the NPN transistors showed that emitter-base (E-B) depletion region of the transistor can be effectively analyzed using Gummel characteristics. The intense energetic ions encountered in space can result in many transient and destructive single event effects (SEE) are studied with low ion fluence (~10^6 cm^{-2}) test facility at GPSC beam line and three such runs took place this year to evaluate the radiation hardness of many microelectronic devices designed and fabricated at SCL. In-situ I-V and C-V characterization studies were carried out to determine the device quality of atomic layer deposited HfO_2/SiO_2/Si-based metal oxide semiconductor devices during 120 MeV Ag ion irradiation. An increase in the oxide layer thickness due to formation of an HfSiO interlayer was observed and attributed to swift heavy ion induced intermixing, and was confirmed by X-TEM and X-ray photoelectron spectroscopy measurements. In situ X-ray diffraction measurements showed an increase in the crystallinity of the Graphene Oxide film at low fluence after irradiation with 120 MeV Au ions at fluences ranging from 10^{10} to 10^{13} ions/cm^2. The irradiated samples showed an increase in the intensity of aromatic carbon bonds by Fourier transform infrared spectroscopy which indicated the maximization of graphitic regions for lower fluences up to 3×10^{11} ions/cm^2. In-situ current-voltage (I-V) studies on Cu-ZnO/P3OT hybrid heterostructures under 80 MeV O ion irradiations was also studied. The interaction of Graphene oxide with hydrogen gas at different pressures varying from 70 mbar to 900 mbar at room temperature using in-situ Xray diffraction technique was studied. Elastic recoil detection analysis (ERDA) technique was employed to determine the concentration of hydrogen in GO film which increased from ~$1.7\text{x}10^{22}$ atoms/cc (for pristine GO) to ~ $9.5\text{x}10^{22}$ atoms/cc after exposing to 100% hydrogen environment at 900 mbar pressure, thus showing its applicability as hydrogen storage device. In situ current–voltage characteristics of Nb-doped TiO_2/p-Si-based heterojunction diode have been studied under dense electronic excitations of 84 MeV Si^{6+} ions. The diode parameters such as ideality factor, barrier height, reverse saturation current and series resistance were found to be a strong function of ion irradiation fluence. Such in situ studies on n-NTO/p-Si heterojunction diode under harsh radiation environment are very appropriate for the better understanding of heterojunction interface properties and make it suitable for use in aerospace industry and nuclear reactors. The defect induced photoluminescence studies on behavior of the Ga doped ZnO (GZO) thin films with varying doping (Ga) concentration and with energetic ion irradiation showed that violet emission might originate from zinc interstitial defects (Zni) and the concentration of Zni increases with increasing doping concentration. Electronic excitation induced modifications in the ferroelectric polarization of $BiFeO_3$ thin films have also been observed.

Apart from the studies on swift heavy ion irradiation, a large number users have published their work related to effects of low energy ion implantations and gamma irradiations in various physical properties of materials. The effect of Ni ion implantations in thermoelectric and electrical properties of $CoSb_3$ and the interface formation and magnetic properties due to 3d transition metal ion implantations have been studied. Enhancement of ferromagnetism due to ion implantations has been investigated in CeO_2, ZnO and FePt. Apart from these studies, work on solar energy, medical dosimetry, gas sensing and chemical sensing have been reported. Enhanced room temperature ferromagnetism and green photoluminescence with increase in doping in Cu doped ZnO thin flm synthesised by neutral beam sputtering was observed. It was shown that synthesised Cu doped ZnO thin flms can be used as spin LEDs and switchable spin-laser diodes. Investigations using gamma irradiation have demonstrated the enhancement of water oxidization catalytic performance in graphene oxide, multifunctionality in the same materials etc.

The International Conference on Ion Beams in materials Engineering and Characterization (IBMEC 2018) was organized by IUAC during October 9th to 12th, 2018. There were 21 invited talks (including 10 from foreigners), 15 oral presentations and 70 posters. The conference was preceded by a School on Characterization of Materials at IUAC during October 3-7, 2018 which included 5 lectures from foreigners. Another school on special topic of Ion Beams in Energy Materials was also organized by IUAC during July 12-18, 2018.

5.2.1 In situ Study of Radiation Stability and Associated Conduction Mechanisms of Nb-Doped TiO_2/p-Si Heterojunction Diode under Swift Heavy Ion Irradiation

Subodh K. Gautam[1], Jitendra Singh[1], R.G. Singh[2], Naina Gautam[3], Priyanka Trivedi[1], and Fouran Singh[1]

[1]Material Science Group, Inter University Accelerator Centre, New Delhi -110067, India
[2]Department of Physics, Bhagini Nivedita College, Delhi University, Delhi– 110043, India.
[3]Department of Electronic Science, University of Delhi South Campus, New Delhi-110023, India

The reliability of semiconductor devices in extreme environments, particularly in radiation-harsh conditions, is an important issue for applications in space, nuclear reactors, particle accelerators and military equipment [1, 2]. It is difficult to generalize whether irradiation environment causes degradation or improvement in the performance of the various types of devices. It depends on many parameters such as target material, projectile ion energy, and fluence, etc. This study reports the radiation stability and reliability of fabricated Nb-doped TiO_2 over p-Si based heterojunction diode along with the effect of secondary irradiation on various diode parameters and current conduction mechanisms. In situ current-voltage characteristics of Nb-doped TiO_2/p-Si heterojunction diode have been studied under dense electronic excitations of 84-MeV Si^{6+} ions using the 15UD Tandem Pelletron Accelerator at IUAC, New Delhi. Fig. (a) shows the schematic diagram of fabricated heterojunction diode operating under the exposure of 84-MeV Si^{6+} ion irradiation. The diode parameters such as ideality factor (η), barrier height (ϕ_B), reverse saturation current (J_s), and series resistance (R_s) are found to be a strong function of ion irradiation fluence. In Fig. (b), results show that important diode parameters such as ideality factor decrease with fluence, while barrier height shows an anomalous behaviour as first increases and then decreases as function of fluence. Similarly, J_s follows the inverse response of ϕ_B as first decreases and then increases as function of fluence. These observed unusual phenomena are understood mainly by an improvement in barrier inhomogeneity, irradiation induced-annealing of interface states. Generally, R_s plays an important current-limiting role in heterojunction based devices. It is found that R_s decreases with increasing irradiation fluence and follows a similar response as η with irradiation fluence. The improvements in η and R_s with irradiation is explained in terms of irradiation induced-structural ordering and creation of high density donor defects (oxygen vacancies (V_O) and Ti interstitials (Ti_i) and their defect complexes) induced enchantment in n-type conductivity of n-NTO later [3]. Furthermore, various current conduction mechanisms involved at different voltage ranges are discussed as a function of fluence with the help of constructed energy band diagram shown in Fig (c). It is found that trap-assisted space charge limited current conduction mechanism dominates at high voltage range and transforms to traps-free SCLC conduction at high irradiation fluence [4]. Thus, significant improvement in the diode parameters and high radiation stability makes it suitable for applications in the aerospace industry, nuclear reactors and accelerators. For details, see [Subodh K. Gautam et al. IEEE-Transactions on Electron Devices, 66 (2019) 1475].

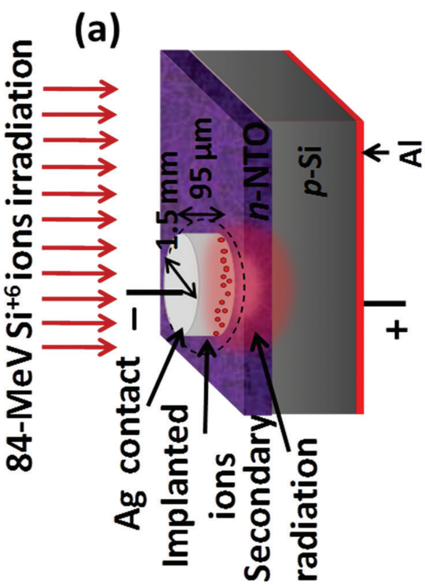

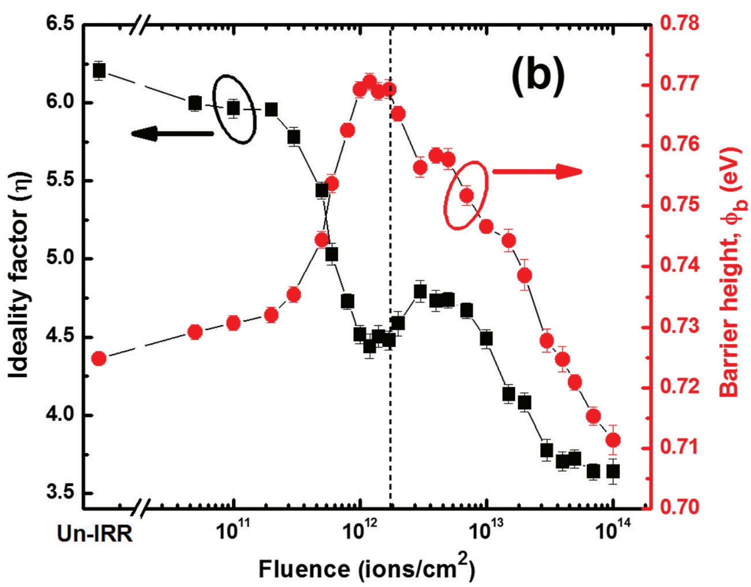

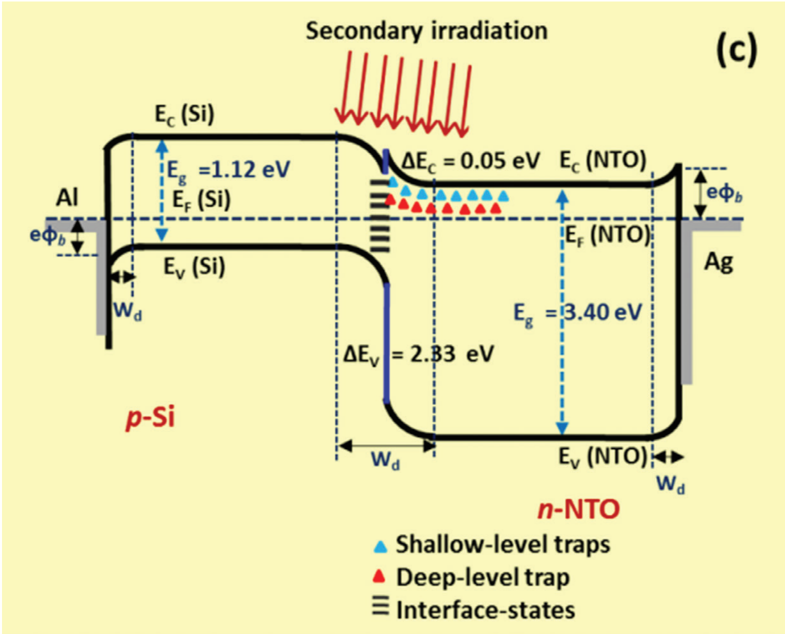

Figure: (a) Schematic diagram of fabricated heterojunction diode operating under the exposure of ion irradiation,
(b) *In situ* response of ideality factor and barrier height as a function of fluence, and
(c) energy-band diagram of irradiated n-NTO/p-Si heterojunction diode in equilibrium condition under the exposure of Si ions irradiation.

REFERENCES:

[1] C. Claeys *et al,* Radiation Effects in Advanced Semiconductor Materials and Devices, vol. **57,** Springer (2002)

[2] P. E. Dodd *et al.,* IEEE Trans. Nucl. Sci., **57** (2010) 1747

[3] Subodh K. Gautam *et al.* SSC **218** (2015) 20

[4] P. E. De Jongh *et al,* Phys. Rev. Lett., **77** (1996) 342

5.2.2 An In-situ Investigation of Bromine and Copper Ion Irradiation on NPN Transistors

T M Pradeep[1], N H Vinayakaprasanna[1], N Pushpa[2], Ambuj Tripathi[3] and A P Gnana Prakash[1*]

[1]Department of Studies in Physics, University of Mysore, Manasagangotri, Mysore-570 006, India.
[2]Department of PG Studies in Physics, JSS College, Ooty Road, Mysore-570 025, India.
[3]Inter University Accelerator Centre, Aruna Asaf Ali Marg, New Delhi-110 067, India.

The advancements in the semiconductor processing techniques have made it possible to use semiconductor devices in the instrumentations of deep space exploration spacecrafts and high energy physics experiments. However, devices operating in these applications are prone to radiation effects wherein a high density of high energy deterrent radiation exists. These radiations include energetic photons and charged particles that can cause severe degradation in the performance and operating life of the semiconductor devices [1-2]. Thus, it is very important to evaluate the radiation hardness of these devices for different radiations.

Experimental Details

The semiconductor devices investigated in the present work are silicon NPN rf power transistors (2N 3866) manufactured by Bharat Electronics Limited (BEL), India. The transistors were exposed to 160 MeV Bromine (Br^{12+}) and 140 MeV Copper (Cu^{11+}) ions using 15 UD 16 MV Pelletron Accelerator at Inter University Accelerator Centre (IUAC), New Delhi, India. The typical beam current was 0.25 p-nA and 0.5 p-nA for 160 MeV Br^{12+} and 140 MeV Cu^{11+} ions respectively. The different DC electrical characteristics such as the Gummel characteristics, excess base current (ΔI_B), dc current gain (h_{FE}), and output characteristics (I_C-V_{CE}) were studied before and after irradiation. The transistors were irradiated with different ions in the identical dose range of 1 Mrad to 100 Mrad. The ion irradiation results were compared with the ^{60}Co gamma irradiation results in the same dose range to quantify the influence of different ion irradiations on the various characteristics of transistors.

Results and Discussion

140 MeV Cu^{11+} and 160 MeV Br^{12+} ions induced damages in the emitter-base (E-B) depletion region of the transistor can be effectively analyzed using Gummel characteristics. The Gummel characteristics for 140 MeV Cu^{11+} ion irradiated transisters is shown in fig. 1 and it can be seen that IB increases with increase in the dose. The similar behavior was observed for the transistors irradiated with 160 MeV Br^{12+} ions. The increase in the IB is mainly due to the production of generation and recombination centers in the E-B depletion region. The fig. 2 shows the variation in normalized peak h_{FE} as a function of total dose for 160 MeV Br^{12+} and 140 MeV Cu^{11+} ions and ^{60}Co gamma irradiated transistors. After 100 Mrad(Si) of total dose, the peak h_{FE} is found to decreased by 99% for 160 MeV Br^{12+} and 140 MeV Cu^{11+} ions whereas 80% for ^{60}Co gamma irradiated transistors. From the fig. 2 it can be observed that the degradation in peak h_{FE} is more for 160 MeV Br^{12+} and 140 MeV Cu^{11+} when compared to ^{60}Co gamma radiation. Hence swift heavy ions (SHIs) induce more generation-recombination (G-R) trapped centers along with the point defects in the active region of the transistor when compared to ^{60}Co gamma radiation.

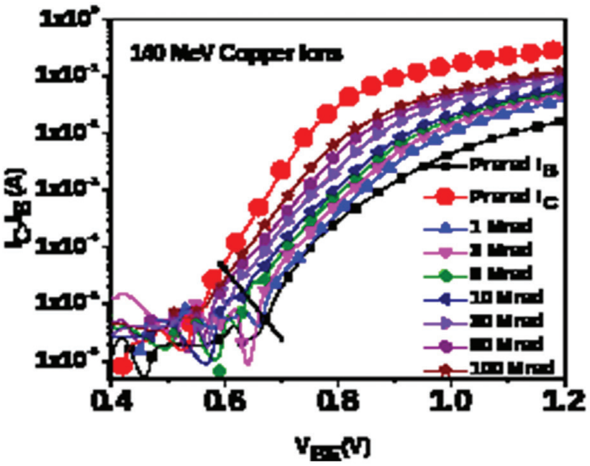

Figure 1. Gummel Characteristics of 140 MeV Copper ion irradiated transistor.

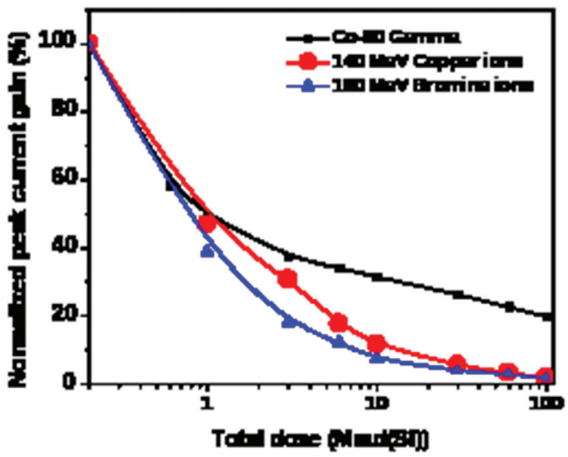

Figure 2. The variation in dc current gain after 140 MeV Copper, 160 MeV Bromine ion and ^{60}Co Gamma irradiation.

REFERENCES:

[1] A. P. Gnana Prakash, S. C. Ke and K. Siddappa, Semicond. Sci. Technol., (2004)19 1029-1039.

[2] C. Liu, X. Li, H. Geng, E. Rui, L. Guo, J.Yang, L. Xiao, Nucl. Instr. and Meth. A, (2012) 677 61-66.

5.2.3 Single Event Effects (SEE) Testing of Microelectronics for Space Applications

Kinshuk Gupta[1], Vinod Kumar[1], Raj Ramesh Babu[1], Sandhya V Kamat[1] and Saif Ahmad Khan[2]

[1]Components Management Group, U. R. Rao Satellite Centre, ISRO, Bengaluru-560017, India.
[2]Inter-University Accelerator Centre, New Delhi-110067, India.

A spacecraft encounters space radiation heavy ions of varying energies and fluxes during its lifetime in space. The heavy ions interact with spacecraft microelectronics which can lead to Single Event Effects (SEE). As the occurrence of SEE result in functional anomalies or catastrophic failures, they are a major spacecraft reliability concern for any space mission. With decreased feature size and critical charge for present day microelectronics, SEE have drawn large attention from the spacecraft radiation hardness assurance community. An assessment of the heavy ion irradiation response of susceptible spacecraft microelectronic components is indispensable and the Pelletron Facility at Inter University Accelerator Centre (IUAC) was used to test such components for assessing their usability in ISRO missions.

Experimental Details

The General Purpose Scattering Chamber (GPSC) of the Pelletron Facility at Inter University Accelerator Centre, New Delhi was used during (i)14-16 July, 2018 (ii)15-17 October, 2018 (iii)20-22 February, 2019 to obtain heavy ion beams for the SEE tests. The accelerator at this facility provided an ion current of typically 0.1 pnA (particle nano amperes). The beam was spread over an area such that the corresponding flux was about 6 x 10^8 ions/cm^2/s. However the ASTM F1192-00 (2006) standard requires the beam flux to be between 1x10^2 to 1x10^5 ions/cm^2/s. For the required low flux irradiation, the technique of scattering of direct beam was used.

There is a port at angle of 15 degree to the main port. The high energy direct ion beam is made incident on the 330 nm gold foil kept at the centre of GPSC. The flux of outgoing scattered beam in the 15 degree port is dependent on the thickness of the scatterer and the incoming ion flux, and was estimated using Surface Barrier Detector (SBD). Using this technique the required flux of $1x10^2$ to $1x10^5$ ions/cm^2/s was obtained for the SEE tests. The scattered ions are made incident on the Device Under Test (DUT) card mounted on the target ladder (Fig. 1) at the end of 15 degree port. The signals from the DUT card were terminated to the 50 pin hermetically sealed feed through connector. This was done to create a vacuum of the order of 10^{-6} mbar in the beam line so that the heavy ion beam is not attenuated by collision with air particles. The test and measurement equipment were kept near the low flux chamber.

Fig. 1: DUT card mounted on target ladder

Table 1 presents the ion beam parameters obtained at IUAC.

Table 1: Ion Beam Parameters

Heavy Ion Species	Energy (MeV)	LET (MeV-cm^2/mg)	Range (µm)	Flux (ions/cm^2/s)
Silicon	130	9.45	48.39	502
Titanium	140	22.9	29.08	582
Nickel	140	31.1	25.68	968
Silver	140	50.65	19.28	947

Results

Table 2 presents the results of SEE testing

Table 2: SEE Test Results

Microelectronic Device	Result
Application Specific Integrated Circuits	Single Event Upsets observed
Field Programmable Gate Array	Single Event Functional Interrupt observed
Hex Buffer	No SEE observed
16 bit Buffer	No SEE observed
16-Bit Transceiver	No SEE observed
Quad 2-Input NAND Gate-5V	No SEE observed
Quad 2-Input NAND Gate-3.3V	No SEE observed
Hex Schmit Trigger Inverter Inverter-5V	No SEE observed
Hex Schmit Trigger Inverter-3.3V	No SEE observed
Clock Drivers	No SEE observed

Conclusion

Microelectronic devices were tested at the Pelletron Facility, IUAC during (i) 14-16 July, 2018 (ii)15-17 October, 2018 (iii) 20-22 February, 2019. The test results indicate that some of the devices are susceptible to SEE while others are immune upto LET of 50.65 MeV-cm^2/mg. The immune devices are considered passed for on-board usage in geostationary, low earth orbit and interplanetary spacecraft missions of ISRO. Suitable mitigation techniques have been identified for the devices which have exhibited Single Event Effects.

5.2.4 Analysis of 140 MeV Copper and 160 MeV Bromine Ion Irradiation Effects on N-Channel MOSFETs

Arshiya Anjum[1], T M Pradeep[1], Vinayakprasanna N Hegde[1], N Pushpa[2], Ambuj Tripathi[3] and A P Gnana Prakash[1*]

[1]Department of Studies in Physics, University of Mysore, Manasagangotri, Mysore-570006.
[2]Department of PG Studies in Physics, JSS College, Ooty Road, Mysore-570 025, India.
[3]Inter-University Accelerator Centre, New Delhi-110067, India.

The N-channel metal oxide semiconductor field effect transistors (MOSFETs) are the key components in advanced integrated circuits and are used in space, military and other radiation harsh environments such as accelerators where high and low energy particles exist [1]. In order to use MOSFETs in radiation rich environments the devices need to withstand few krad to few Mrad of radiation [1]. Hence it is very essential to evaluate the radiation hardness of these devices from the application point of view.

Experimental Details

The MOSFETs (BEL 3N187) used in the present work were irradiated with 140 MeV Copper (Cu^{11+}) ions and 160 MeV Bromine (Br^{12+}) ions with dose ranging from 1 Mrad to 100 Mrad at Inter-University Accelerator Centre (IUAC), New Delhi using 15 UD Tandem Pelletron Accelerator. The typical beam current for 140 MeV Cu^{11+} ions and 160 MeV Br^{12+} ions is 0.5 pnA and 0.25 pnA respectively.

Results and Discussion

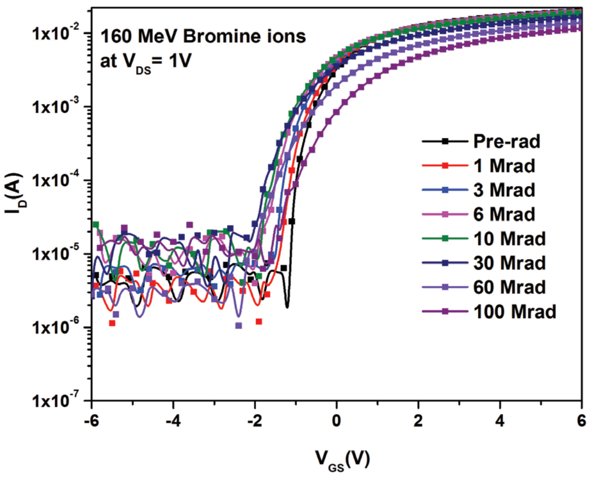

Figure 1. Transfer characteristics of 160 MeV Bromine ion irradiated MOSFET.

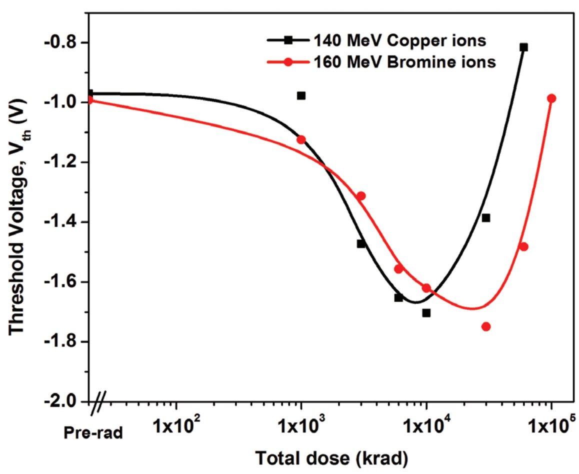

Figure 2. Variation in the V_{th} after 140 MeV Copper and 160 MeV Bromine ion irradiation.

The threshold voltage (V_{th}) is the primary degradation parameter in MOS devices and it can be determined using the subthreshold curve of MOSFETs. Fig. 1 shows the representative subthreshold curve for 160 MeV Br^{12+} ion irradiated MOSFETs. From the figure it can be seen that the subthreshold current curve shift towards negative gate voltages with slight variations in the shape of the curves as the dose increases. This is due to the fact that, the radiation induced degradation in the devices is dominated by the trapping of holes in the SiO_2 with the minimal interface states generation. The variation of V_{th} of MOSFETs with respect to dose after Cu^{11+} and Br^{12+} ion irradiations is shown in Fig. 2. It can be observed that Vth has decreased till 10 Mrad of total dose and above 10 Mrad, V_{th} was found to recover significantly which is due to the "rebound effect" or "superrecovery" [2]. It is also noticed that the degradation produced by both ion irradiations is almost identical.

REFERENCES:

[1] N. Pushpa, *et al.*, Nucl. Instr. Meth. A. **613** (2010) 280.

[2] T. P. Ma and Paul V. Dressendorfer, Ionizing Radiation Effects in MOS Devices and Circuits (1989).

5.2.5 In-situ current-voltage (I-V) studies on Cu-ZnO/P3OT hybrid heterostructures under swift heavy ion irradiations

Jitendra Singh[1], Himanshi Gupta[1], A. Kumar[1], R.G. Singh[2] and Fouran Singh[1]

[1]Materials Science Group, Inter University Accelerator Centre, Aruna Asaf Ali Marg, New Delhi-110067, India
[2]Department of Physics, Bhagini Nivedita College, Delhi University, New Delhi, 110043, India

Conducting polymer and metal-doped inorganic semiconductor based hybrid heterostructures have evoked an increasing interest to the researchers in the last few years due to their potential multifunctional applications for electronic and optoelectronic devices [1,2]. Therefore, a hybrid heterostructure (HH) (Ag/Cu-ZnO:P3OT/ITO) were prepared by depositing conducting poly (3-octylthiophene) (P3OT) polymer and Cu-doped zinc (Cu-ZnO) composites film on the indium-doped tin oxide (ITO) substrate by using sol-gel ultrasonication cast technique and the preparation details are reported in our previous study [3]. Further, the radiation stability and reliability of this HH has been tested for their possible application in the radiation harsh environments. Thusly, the in-situ current-voltage (I-V) measurements have been performed on such HH under swift heavy ion (SHI) irradiations using 80 MeV O^{6+} with increasing ion fluences from 1×10^{11} to 3×10^{13} ions/cm^2 at an applied bias voltage ± 2V as shown in Fig. 1. Interestingly, under irradiation with increasing ion fluences, the I-V characteristics of the HH reveal an insignificant changes in the forward and reverse currents which lead to the radiation hardness of HH. In this study primary incident ions effect were observed in the outer region of the HH's. However, the primary ions induced secondary charged particles radiations mostly secondary electrons effect were observed in the masked region *i.e.* near the periphery of Ag contact. Recently, a similar study has also been reported by our group to test the radiation stability and reliability of an inorganic Nb doped TiO_2/p-Si (NTO) heterojunction diode during *in-situ* I-V characteristics measurements under the influence of SHI irradiation induced secondary charged particles radiation. In that study, the I-V shows the improvements in the various diode parameters as function irradiations and reflecting the radiation hardness of NTO diode [4]. Interestingly, our study also emerges out to be very fascinating for an in-depth understanding of primary and secondary charged particles interaction process with HH. However, the detailed understanding of such phenomenon is still under progress. Thus, in-situ *I-V* studies on Ag/Cu-ZnO:P3OT/ITO HH under swift heavy ion irradiations will be very useful for the implementation of HH based devices in a variety of radiation harsh environments.

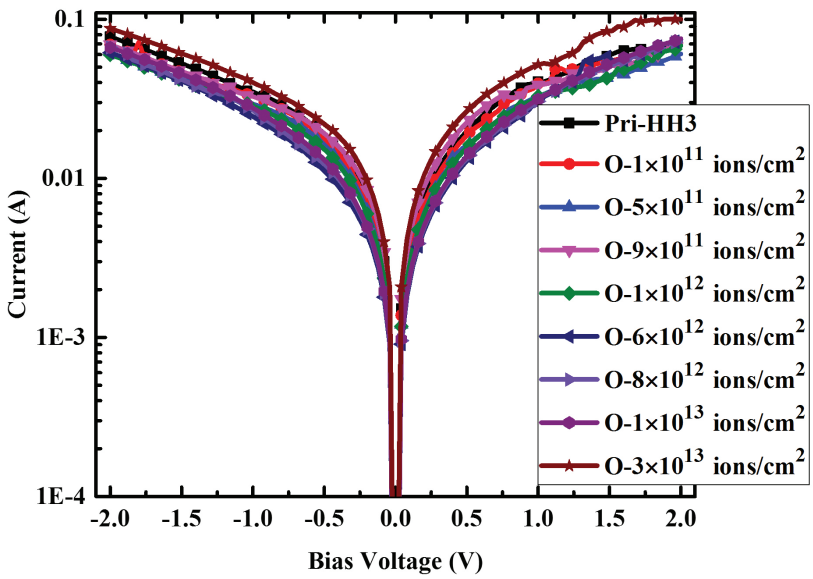

Figure 1: *In-situ* current–voltage *(I–V)* characteristics of hybrid heterostructures (HH3) under 80 MeV O^{6+} ions irradiation as function of ion fluences at an applied ± 2V bias voltage.

REFERENCES:

[1] J. Singh *et al.* J. Appl. Phys. **123** (2018) 174503.
[2] R G Singh *et al.* JRSE. **5** (2013) 033134
[3] J. Singh *et al.* Opt. Mater. (Amst). **94** (2019) 316–321.
[4] S.K. Gautam *et al.,* IEEE Trans. Electron Devices. PP (2019) 1–7.

5.2.6 Green synthesis of silver Nanoparticles and their size modulation by swift heavy ion irradiation.

Laden Sherpa[1] and Archana Tiwari[1]

[1]Department of Physics, Sikkim University, Gangtok 737102, India.

We have synthesized Ag nanoparticles (NPs) by green synthesis route. Bergenia cilliata leaves and roots are used for the synthesis. The plant extract thin films are irradiated with swift heavy ion irradiation using Ag^{15+} ions of energy 200 MeV at three different fluences, $5X10^{11}$ ions/cm^2, $1x10^{12}$ ions/cm^2 and $7x10^{12}$ ions/cm^2 . The irradiated and unirradiated plant extracts are used to synthesize the NPs and their morphologies are compared. The NPs synthesized using irradiated plant extracts are smaller in size as compared to those obtained using pristine extracts. In addition, self-assembly of NPs is also observed in some of the systems.

Experimental Details

The plants were freshly picked, washed and shade dried for a month. For the extraction, the dried plant parts were grinded in to powder. 1g of the each plant parts was taken in 10 mL of millipore water. The mixture was kept in water bath for 30 mins. The filtrate was utilized for the reduction of $AgNO_3$ and synthesis of Ag NPs. 2mL of the plant extract (drop-casted on the glass substrate for irradiation experiments) and 20ml of 1mM $AgNO_3$ were mixed and stirred for an hour using magnetic stirrer. Change in color of the solution to reddish brown was observed after about 5 mins of stirring in air and in the presence of sunlight.

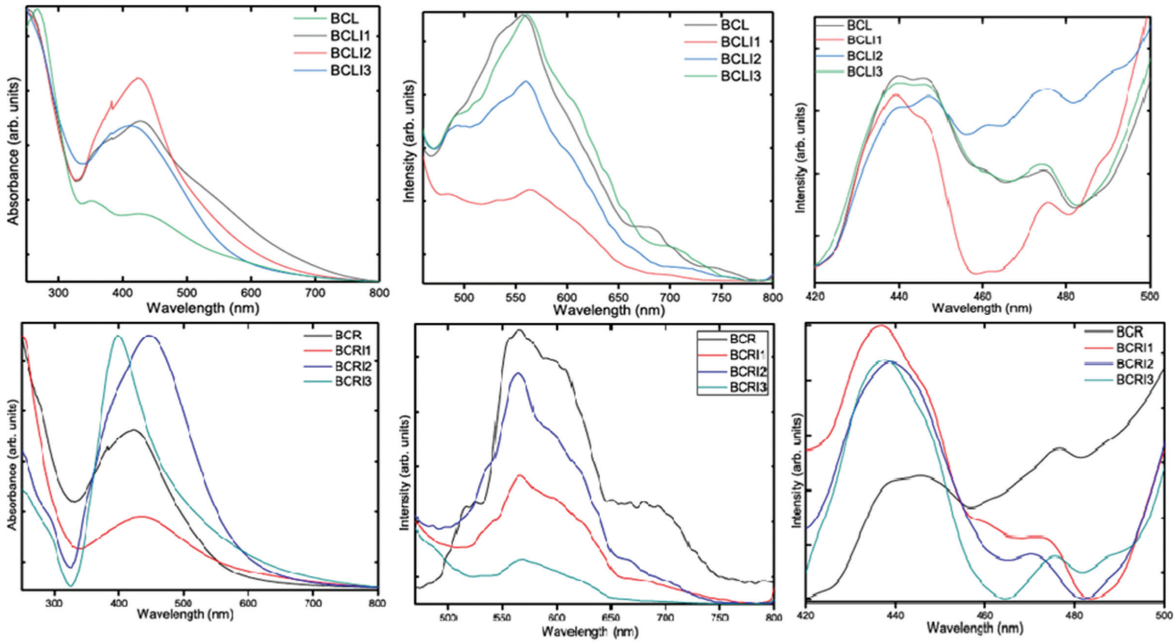

Figure 1: Absorbance spectra, Photoluminescence emission and excitation spectra of BCL and BCR Ag NPs.

Results

The synthesis of Ag NPs is confirmed by UV-vis absorption spectroscopy where the NPs synthesized using roots and leaves are labelled as BCR and BCL respectively. Signature absorption peaks centered between 400-500 nm corresponding to the surface plasmon resonance (SPR) of Ag NP are observed in all samples (Fig. 1) [1,2]. In BCR, deconvolution of luminescence spectrum (Fig. 1) shows peaks at 495 nm, 561 nm, 583 nm and 684 nm whereas in BCR the peaks are seen at 515 nm, 556 nm, 597 nm and 687 nm which are red shifted in comparison to BCL.

FTIR and XRD analysis suggest that the reduction of Ag ions and synthesis of Ag NPs are accompanied with their oxidation by hydroxyl and carbonyl groups. [3,5]. Owing to this, AgO NP crystal structure is observed at $2\theta = 29^o$ and 38^o in addition to FCC Ag NP. The effects of swift heavy ion irradiation on the sysnthesis of Ag NP is summerised in Table 1.

Table 1: Size, shape and lattice parameter data of the Ag NPs synthesized using all the plant extracts.

Reducing Agent	Irradiation (ions/cm^2)	Sample Label	Size (nm)	Shape	Lattice constant (A)
Bergenia Cilliata Leaves	Unirradiated	BCL	18.2±0.8	spherical, triangular, nanorods	4.092349
	5x10^{11}	BCLI1	18.0±0.7	spherical, oval, hexagonal	4.09121
	1x10^{12}	BCLI2	22.3±0.7	spherical, oval,	4.09525
	7x10^{12}	BCLI3	23.6±0.5	spherical, dendritic formation	4.073185
Bergenia Cilliata Roots	Unirradiated	BCR	12.0±0.5	spherical	4.049242
	5x10^{11}	BCRI1	8.3±0.1	spherical, dendritic formation	4.065
	1x10^{12}	BCRI2	19±1	spherical, hexagonal, oval, dendritic formation	4.074108
	7x10^{12}	BCRI3	11±1	spherical, dendritic formation	4.081

Dendrite like self assembly is observed upon irradiation in BCL and BCR NPs. Our research presents a simple fabrication technique for highly crystalline dendrite nanostructures of silver metals [4,6]. These dendrite structures may provide us a framework for the study of disordered systems as well as open up avenues for their applications in surface enhanced Raman spectroscopic sensors and catalysis.

REFERENCES:

[1] N. Vigneshwaran, R.P. Nachane, R.H. Balasubramanya, P.V. Varadarajan, A novel one pot 'green' synthesis of stable silver nanoparticles using soluble starch, Carbohydr. Res. 341 (2006).

[2] Kora, A., Beedu, S., & Jayaraman, A. Size-controlled green synthesis of silver nanoparticles mediated by gum ghatti (Anogeissus latifolia) and its biological activity. Organic and Medicinal Chemistry Letters, 2(1), (2012)..

[3] B. Sundararajan, G. Mahendran, R. Thamaraiselvi, B.D. Ranjitha Kumari, Biological activities of synthesized silver nanoparticles from Cardiospermum halicacabum L, Bull. Mater. Sci. 39 (2) (2016) 423–431.

[4] Partha P. Dutta, Manobjyoti Bordoloi, Kabita Gogoi, Sonali Roy, Bardwi Narzary, Dibya R. Bhattacharyya, Pradyumna K. Mohapatra, and Bhaskar Mazumder. Antimalarial silver and gold nanoparticles: Green synthesis, characterization and in vitro study. Biomed. Pharmacother., 91:567–580, 2017.

[5] Linlin Jing, Huiping Ma, Pengcheng Fan, Rongmin Gao, and Zhengping Jia. Antioxidant potential, total phenolic and total flavonoid contents of Rhododendron anthopogonoides and its protective effect on hypoxiainduced injury in PC12 cells. BMC Complement. Altern. Med., 15(1):1– 12, 2015

[6] Chen, Y., Wang, Z., He, Y., Yoon, Y. J., Jung, J., Zhang, G., & Lin, Z. Light-enabled reversible self-assembly and tunable optical properties of stable hairy nanoparticles. Proceedings of the National Academy of Sciences, 115(7), (2018).

5.2.7 Photo-absorption studies using ion-induced surface patterning of ITO thin films

G Poorani, GN Kumaraswamy

Organic Photovoltaics Laboratory, Department of Physics, Amrita Vishwa Vidyapeetham, Bengaluru-560035, India.

In organic solar cells, thin films of the transparent conducting indium tin oxide are commonly used as the top electrode. We can randomize the front surface of the cell and enhance the photo-absorption by increasing the optical path length by patterning the surface of indium tin oxide (ITO). The surface patterning of ITO was carried out using the Electron Cyclotron Resonance ion source (ECR) at the Low Energy Ion Beam Facility (LEIBF) at the Inter-University Accelerator Centre, New Delhi. Based on previous studies and its inert nature, Ar^+ ions were preferred for ion-induced surface patterning with a beam energy of 50 keV with doses varying from 10^{13} cm^{-2} to 10^{15} cm^{-2} (since the range of energy available at LEIBF is from 50 keV to 1.5 MeV for Ar ions). The ion beam angle was varied from grazing incidence to low angles (5º, 10º, 15º and 25º). The unpatterned ITO glass substrates from Ossila were used for the experiments.

Optical transmission studies of ITO samples post ion-induced patterning were done by performing UV-Vis Spectroscopy and surface studies using AFM. The ion-induced patterning of ITO increases the surface roughness of the thin films at grazing incidences, especially at 5º and 10º, sharp peaks are observed with increase in RMS roughness values. As the angle of irradiation is increased from grazing incidence to lower angles, there is a decrease in surface roughness and area of pattern formation which is confirmed by AFM images. Ripple pattern formation on thin films are well-studied and Bradley-Harper theory is widely used to study the same. According to the B-H theory there is always an interplay of smoothening versus roughening action influenced by surface diffusion, local surface curvature, sputter yield etc [2]. At 25º, the ITO surface is more exposed to the ion beam and with the highest does of irradiation, the surface roughness is observed to be less compared to other irradiated samples and the AFM image shows presence of more inhomogeneous patches (see Figure 1d) further established by the inability to measure the continuity of conductance in the thin film using multimeter. While the AFM images clearly depict the ion-induced pattern formation, the UV-Vis absorption spectroscopy performed on the samples indicate an increase in optical transmission with grazing incidence angles. As mentioned, ITO has high optical transmission in the visible range and is opaque in the UV, correspondingly its extinction coefficient in the visible range is zero, while in the UV range it is non-zero. The UV-Vis transmission spectrum of samples irradiated at 5º grazing angles with varied fluences is shown in Figure 1. It is evident that patterned ITO shows increased optical transmission over unpatterned ITO especially at lower fluences till $1x10^{14}cm^{-2}$. Above $1x10^{14}$ cm^{-2}, however there is no significant improvement in transmission compared to unpatterned ITO. Though there appeared a similar improvement for patterned ITO samples irradiated at an angle of 10º, it was not as considerable as it was for 5º and for lower doses, only a slight increase in transmission over a short range in the near UV region between 350 to 400 nm was observed. At 15º, patterning caused a decrease in transmission and was further degraded at 25º.

These results suggest low energy ion-induced pattern formation on ITO thin films might help increase the photo-absorption of solar cells, when such photovoltaic devices are fabricated over those patterned ITO substrates which exhibit a considerable improvement in optical transmission. Further studies involving the fabrication of solar cells over the patterned ITO surfaces are yet to be done, because the scaling issues involved with organic solar cell device fabrication require pixelated ITO surfaces, the patterned substrates cannot be used as is. Pixelating the ITO substrates in accordance with the desired device design involves etching of ITO, the effect of which on ion-induced patterned ITO substrates needs to be carefully examined before proceeding with device fabrication.

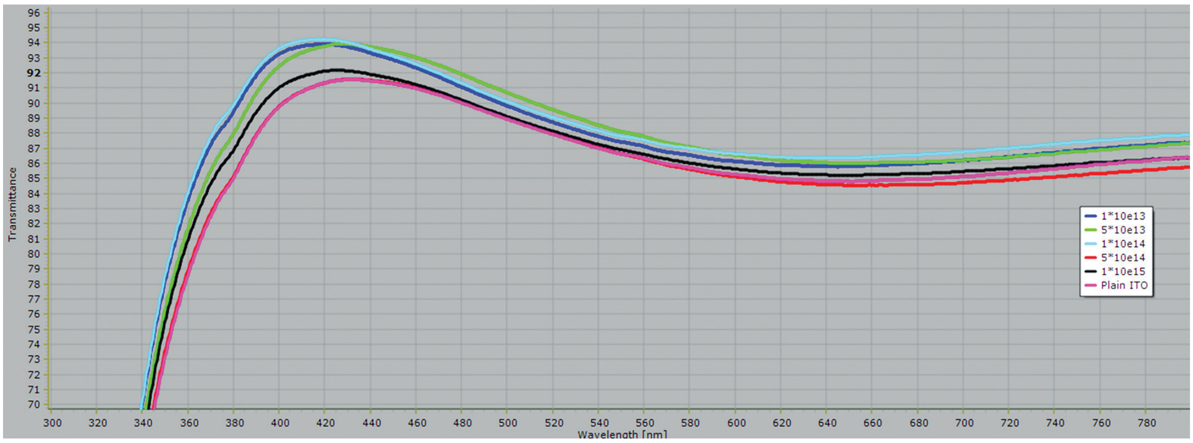

Figure 1. A comparison of UV-Vis transmission spectra of patterned ITO irradiated at a grazing angle of 5º at 5 different doses

REFERENCES:

[1] Hamberg, I., Granqvist, C. G., Berggren, K. F., Sernelius, B. E., & Engström, L, Physical Review B, 30(6) (1984): 3240.

[2] Škereň, T., Doornaert, D., Glorieux, C., Modarresi, H., Guan, T., Temst, K., Vandervorst, W. and Vantomme, A., Thin Solid Films, 589, pp.315-321 (2015)

5.2.8 Effect of patterned substrate morphology on the thin film magnetic properties

Safiul Alam Mollick[1,2], Dinakar Kanjilal[3] and Tapobrata Som[2*]

[1]Indian Association for the Cultivation of Science, Kolkata-700032, India.
[2]Institute of Physics, Bhubaneswar-751005, India.
[3]Inter-University Accelerator Centre, New Delhi-110067, India.

We have studied nanowire-like patterning by atomic manipulation using energetic Au ion beams for functional application as template for thin magnetic film. In general, highly ordered one-dimensional semiconductor nanostructures can be fabricated by self-organization methods using few tens of keV Au ions on Ge substrate. We have studied morphological and electrical properties of highly ordered nanowire-like patterned surface produced by 30 keV Au ion energy and $2x10^{13}$ ion cm^{-2} s^{-1} ion flux. These results shows good correlation with our earlier work in the ion energy range from 10 keV to 26 keV.

Experimental Details

Cleaned intrinsic Ge(100) wafer were placed in the processing chamber for ion irradiation. Ion irradiation was carried out at an oblique angle of 60° with respect to the surface normal by 30 keV Au− ions at room temperature (RT) using the negative ion implantation facility. For the present experiments, the ion flux was maintained at 2×10^{13} ions cm^{-2} s^{-1} and the fluence was 5×10^{17} ions cm^{-2}. The temporal evolution of Ge surface morphology was examined using atomic force microscopy (AFM) (Asylum Research, MFP3D), and scanning electron microscopy (SEM) (FEI, Quanta 200 FEG). The identification of phase and crystalline nature of Au-implanted samples was performed by x-ray diffraction (XRD) (Bruker, D8-Discover) under the Bragg–Brentano geometry and using the Cu-Kα radiation (λ = 0.15418 nm). Local probe-based electrical property measurements, KPFM was carried out as a non-contact local probe technique to map the work function using an Ir–Pt coated Si tip. Conductive atomic force microscopy (cAFM) measurement was employed for current mapping and I–V measurements using a conductive Pt-coated tip.

Nanowire-like Patterning on Ge

We have seen nanowire-like patterned surface fabrication doesn't depend on the incidence ion flux but only on the target projectile combination. Mollick et al [1,2] earlier reported fabrication of well ordered structure at an ion flux of 4×10^{14} ions cm^{-2} s^{-1}, here we have found similar patterning is possible at one order of lower ion flux of 2×10^{13} ions cm^{-2} s^{-1}. Figure 1(a)-(b) show AFM images of patterned substrate at two different fluences of 1×10^{17} and 5×10^{17} ions cm^{-2}. The wavelength of nanowire-like structures increases from 380 nm to 620 nm for increase of ion fluence from 1×10^{17} to 5×10^{17} ions cm^{-2}. The insets show the autocorrelation images from where the wavelength has been determined.

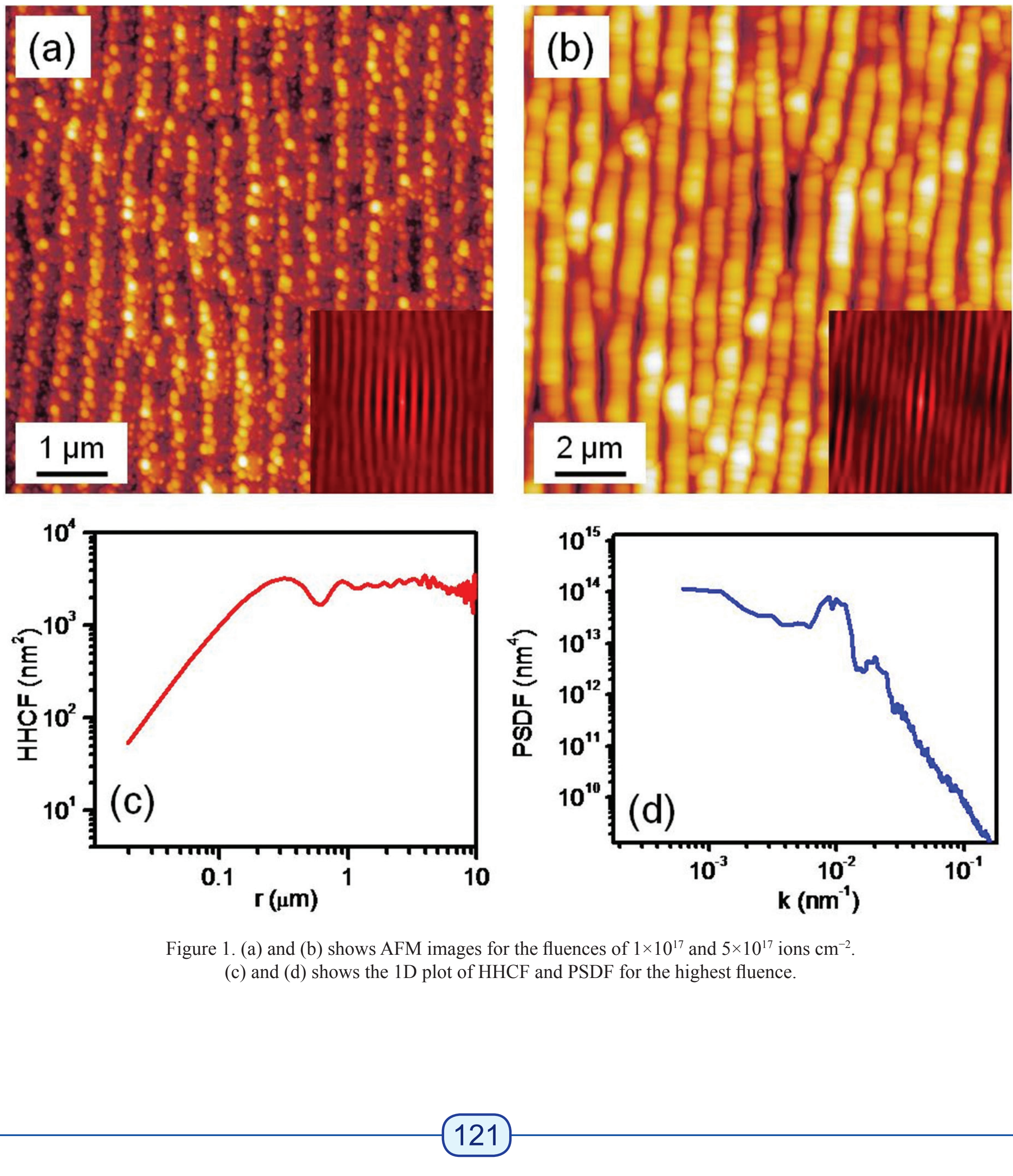

Figure 1. (a) and (b) shows AFM images for the fluences of 1×10^{17} and 5×10^{17} ions cm^{-2}.
(c) and (d) shows the 1D plot of HHCF and PSDF for the highest fluence.

The height-height correlation function (HHCF), g(r), which correlates two point heights of two different point on the surface as $g(R)=\langle[h(x.y) - h(x', y')]^2\rangle$ the pairs of points are laterally separated by $r=\sqrt{((x-x')^2-(y-y')^2}$ and ⟨⟩ denotes the ensemble average over all possible roughness configurations. The HHCF is shown in figure 1(c) from where the roughness exponent has been calculated. In our cases we found D_f varies in between 2.4 to 2.45. The scaling parameters obtained for two different fluences from HHCF is presented in Table –I

Table-I The Scaling parameters obtained from HHCF

Fluence (ions cm^{-2})	HHCF slope	Roughness exponent (α	Fractal Dimension (D=3 - α)
1×10^{17}	1.1	0.55	2.45
5×10^{17}	1.2	0.60	2.4

The statistical analysis of the surface morphology has also been performed from the scaling exponents calculated from the Power Spectral Density (PSD) gathered from the AFM topographical images using Gwyddion software, which is defined as: [3]

$$PSD(f_x, f_y) = \frac{1}{L^2} [\int\int_0^L {}_e^{i2\pi fx}\, e^{i2\pi fy} \left[h(x,y)-h'\right]dxdy\Big]^2$$

From PSD Spectrum also one can extract the roughness exponent α, correlation length ξ and fractal dimension D of the samples by fitting the power-law decay (in the linear region of the log-log plot) to

$$PSD\ (k > \xi^{-1}) = const/k^{\gamma}$$

Where γ is the slope in the linear region of the log-log plot and $\alpha=((\gamma-d')/2$, d' is dimension and in our case it is 1 for a line profile. The PSDF in Fig. 1(d) exhibit two distinct regions, (i) a plateau PSDF at low spatial frequencies and (ii) frequency-dependent decaying branch. The steeper portion of the latter is taken as the self affine range, while the high frequency range with a smaller slope is discarded since it is more affected by noise and aliasing. From the PSD obtained for the ZnPc thin film at asdeposited state and at different annealed temperature, the values of γ are obtained and fractal dimension D is also calculated from the eq.[4]

$$D= (8-\gamma))/2,$$

Table-II shows the scaling exponents obtained from the PSDF graph of the patterned samples. The fractal dimension D calculated from PSD study shows a similar trend to the one calculated from HHCF, which shows self affine characteristic of the patterned morphology.

Table-II The Scaling parameters obtained from PSDF

Fluence (ions cm^{-2})	PSDF slope (γ)	Roughness exponent (α	Fractal Dimension (D)
1×10^{17}	3.2	0.60	2.40
5×10^{17}	3.3	0.65	2.35

The functional application of these well studied surface will be done in future using the patterned substrate as template for thin film deposition.

REFERENCES:

[1] S.A. Mollick, M. Kumar, R. Singh, B. Satpati, D. Ghose, T. Som, Gold-decorated highly ordered self-organized grating-like nanostructures on Ge surface: Kelvin probe force microscopy and conductive atomic force microscopy studies, Nanotechnology. 27 (2016) 435302. doi:10.1088/0957-4484/27/43/435302.

[2] S.A. Mollick, D. Ghose, P.D. Shipman, R. Mark Bradley, Anomalous patterns and nearly defect-free ripples produced by bombarding silicon and germanium with a beam of gold ions, Appl. Phys. Lett. 104 (2014) 043103. doi:10.1063/1.4863342.

[3] F. Biscarini, P. Samorí, O. Greco, R. Zamboni, Scaling Behavior of Anisotropic Organic Thin Films Grown in High Vacuum, Phys. Rev. Lett. 78 (1997) 2389–2392. doi:10.1103/PhysRevLett.78.2389.

[4] D. Raoufi, Fractal analyses of ITO thin films: A study based on power spectral density, Phys. B Condens. Matter. 405 (2010) 451–455. doi:https://doi.org/10.1016/j.physb.2009.09.005.

5.2.9 Formation and isolation of organic nanowires via solid-state polymerization of small molecules by irradiation with swift heavy ions

Tsuneaki Sakurai[1], Kazuto Kayama[1], Koshi Kamiya[1], Shugo Sakaguchi[1], G.B.V.S. Lakshmi[2], Ambuj Tripathi[3], D.K. Avasthi[4] and Shu Seki[1*]

[1]Department of Molecular Engineering, Kyoto University, Nishikyo-ku, Kyoto 615-8510, Japan.
[2]Special Center for Nanoscience, Jawaharlal Nehru University, New Delhi 110067, India.
[3]Inter-University Accelerator Centre, New Delhi 110067, India.
[4]Amity Institute of Nanotechnology, Amity University, Noida 201313, India.

In this project, single particle-triggered linear polymerization (STLiP) method[1,2] was demonstrated, yielding wire-shaped nano-objects with controlled diameter and length by tuning the thickness of the target organic thin-films and fluence of the high-energy charged particles (ions). This is unique technique to obtain such uniform nanowires (< 10 nm in diameter) from organic materials, since "single" particle is the smallest unit as a tool to fabricate the materials. A series of π-conjugated small molecules, having particular functional groups such as ethynyl or halogen, were employed as targets. Thin films of the designed small molecular materials were fabricated on a silicon substrate by spin coating, drop casting, or vacuum deposition methods. Then, high-energy particles were irradiated at IUAC, where the fluence was set at $1 \times 10^9 \sim 1 \times 10^{11}$ cm^{-2} (~1 pnA, $1{\times}1.5$ cm^2 scan area). After the ion beam irradiation, the thin films were developed by organic solvents, and the obtained nano-objects were visualized by a series of microscopy techniques of atomic force microscopy (AFM) and scanning electron microscopy (SEM). The sublimation process instead of wet-development by solvents was tried in the present experiments, avoiding the irreversible adsorption of nanowires on the substrate. This allowed the isolation of vertically-aligned nanowires. Figure 1 shows a representative result by irradiation with 120 MeV ^{197}Au ions 1,6,7,12-tetrachloroperylene tetracarboxylic acid dianhydride (PTCAD-Cl_4). The depth of a valley observed in the AFM image Fig1(b) nearly corresponds to the initial thickness of the film (Figure 1c), which indicates the nanowires are vertically aligned, supporting the vertically aligned character of the nanowires after sublimation as visualized by a SEM image (Figure 1d).

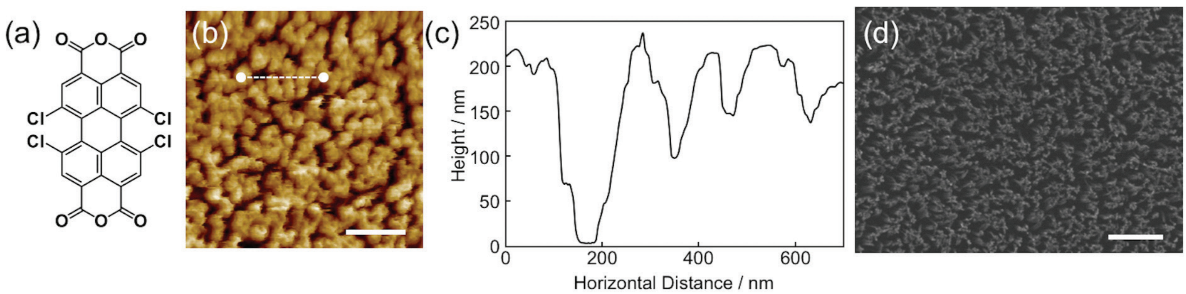

Figure 1. (a) Chemical structure of PTCAD-Cl_4. (b) AFM and (d) SEM images (top view) of nanowires from PTCAD-Cl_4 after irradiation with 120 MeV ^{197}Au at 1×10^{11} cm^{-2} and subsequent sublimation. (c) Height profile indicated as white line in (b). The thicknesses of the original film was 250 nm. Scale bars represent 500 nm.

REFERENCES:

[1] A. Horio, T. Sakurai, G.B.V.S. Lakshmi, D. K. Avasthi, M. Sugimoto, T. Yamaki, S. Seki, Nanoscale, 8 (2016) 14925.

[2] S. Sakaguchi, T. Sakurai, J. Ma, M. Sugimoto, T. Yamaki, A. Chiba, Y. Saito, S. Seki, J. Phys. Chem. B 122 (2018) 8614.

5.2.10 Electrical and optical properties of Zinc- and Strontium-Stannate thin films

Yogesh Kumar[1], Ravi Kumar[2], K Asokan[3] and A P Singh[1*]

[1]Department of Physics, Dr. B. R. Ambedkar National Institute of Technology, Jalandhar-144011, India.
[2]Centre for Material Science and Engineering, National Institute of Technology, Hamirpur -177 005, India.
[3]Inter-University Accelerator Centre, New Delhi-110067, India.

Perovskite-structured materials are one of the most technologically important materials due to their large range of physical properties varying from insulator to superconductor. In the present study, we are exploring the possibility of zinc-stannate (Zn-Sn-O) thin films thin films for transparent conducting applications. Swift heavy ion (SHI) irradiation is a very useful technique to modify the properties of materials. Zinc-stannate (Zn-Sn-O) thin films were irradiated with 120 MeV Ag^{9+} ions to study the effect of irradiation on the structural, electrical and optical properties of the thin films. The temperature dependent resistivity for pristine and irradiated thin films were studied in the range from 100 K to 400 K. The Rutherford Backscattering (RBS) Spectrometry was used to characterize the thin films thickness.

Experimental Details

Zinc-stannate (Zn-Sn-O) thin films, deposited using pulsed laser deposition (PLD) technique, were irradiated with 120 MeV Ag^{9+} ions at the fluence of 2×10^{12} ions/cm^2 using 15UD tandem pelletron accelerator, according to the beam time that had been scheduled as per letter no. IUAC/XIII.4A/63210, dated Nov. 29, 2018 on Dec. 12, 2018 at IUAC, New Delhi. Three shifts were used for the irradiation. SRIM was used to calculate the range, electronic energy loss, and nuclear energy loss of 120 MeV Ag ions. As the electronic energy loss (1.316×10^3 eV/Å) is much higher than the nuclear energy loss (6.385 eV/Å) at this energy, the modification in the film is mainly due to electronic energy loss.

Rutherford backscattering (RBS) spectrometry was used to calculate thin film thickness using 5SDH–1.7 MV Tandem accelerator at Pelletron Accelerator for RBS–AMS System (PARAS) at IUAC, Delhi. During the experiment, a pressure of the order of 10^{-6} Torr was maintained in the chamber. The intensity of helium ion beam of 2 MeV was kept constant at 10 nA and 5 μC charge was collected per spot. The RBS data was simulated and analyzed using RUMP code [1].

Results and Discussions

GIXRD patterns of the pristine and the irradiated zinc-stannate thin films is represented in fig.1. The film was found to have SnO_2 (JCPDS No. 78-1063) and Zn_2SnO_4 (JCPDS No. 74-2184) phases, as indicated in fig. 1(a). The results obtained in this work are in accordance with the observed results by Minami et. al.[2]. The crystalline to amorphous phase transformation in zinc-stannate thin film has been observed with irradiation (fig. 1(b)).

The measured RBS spectra for the pristine and the irradiated thin films are shown in black in fig. 2 (a) and (b), respectively. The calculated thicknesses are 568 nm and 534 nm for pristine and irradiated thin films, respectively.

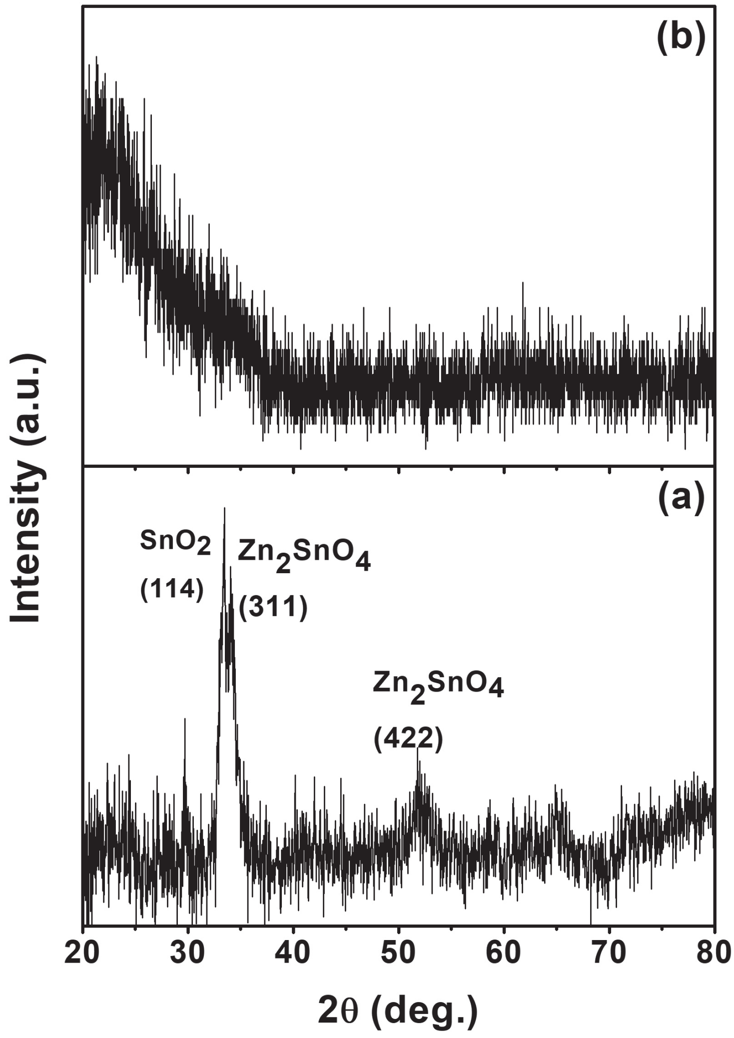

Figure 1. XRD patterns in the left are of (a) as deposited Zn-Sn-O thin films and (b) irradiated Zn-Sn-O thin films.

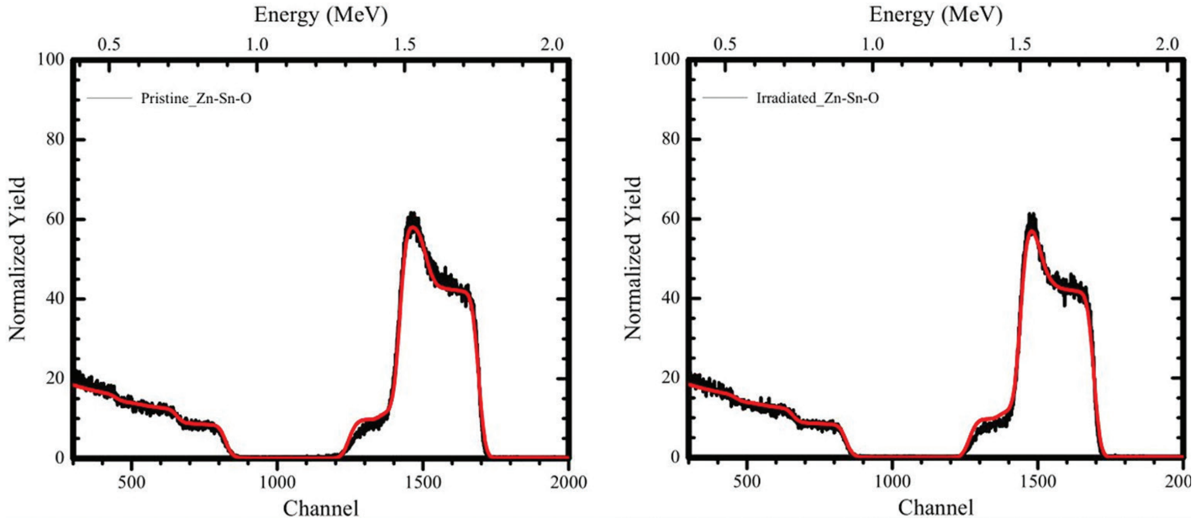

Figure 2. Representation of RBS spectrum (black color) and simulation of RBS data (red color) of (a) pristine and (b) irradiated zinc stannate thin films.

REFERENCES:

[1] Lawrence R. Doolittle. Nuclear Instruments and Methods in Physics Research Section B: Beam Interactions with Materials and Atoms, 9(3):344 – 351, 1985.

[2] T. Minami, H. Sonohara, S. Takata, and H Sato. Japanese Journal of Applied Physics, 33(Part 2, No. 12A): L1693–L1696, 1994.

5.2.11 Dielectric behavior of SHI irradiated Ba-Hexaferrite/LSMO bilayer films

Sushant Zinzuvadiya[1], Nirav C. Pandya[1], Poornima Sengunthar[1], S.A. Khan[2], A. Tripathi[2] and U.S. Joshi[1]

[1]Department of Physics, University School of Sciences, Gujarat University, Ahmedabad-380009, India

[2]Inter University Accelerator Centre, Aruna Asaf Ali Marg, New Delhi-110067

To study the defect assisted modifications in different nanostructured dielectric materials, we have irradiated different magneto dielectric materials deposited on platinized silica substrates. For the study of the effect of irradiation at heterojunction of ferroelectric and ferromagnetic thin films we chose Barium Hexaferrite(BAM)/La-Sr-Mn-O (LSMO) thin film. Frequency dependent dielectric properties and possible magneto-electric coupling are under investigations for the films irradiated with 120 MeV Au and 80 MeV Ni beams.

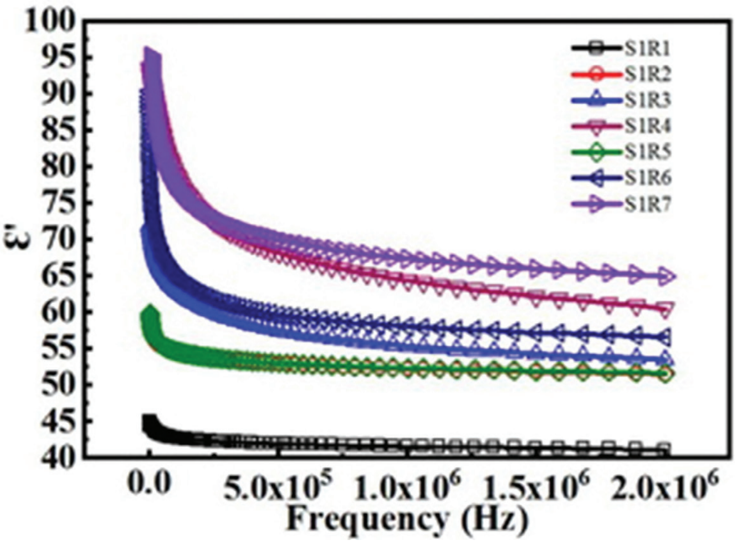

Figure. 1. Frequency dependent dielectric properties of BAM/LSMO/Pt/Si (S1R1-Pristine sample, S1R2-4- Samples irradiated with 120 MeV Au^{+9} ion, S1R5-6- Samples irradiated with 80 MeV Ni^{+5} ion)

Experimental Details

With the intention of studying the effect of irradiation caused by the SHI ion with high and medium energy respectively, Au^{+9}(120 MeV) and Ni^{+5}(80MeV) were chosen as a source of ion beam. Heterostructures of high k dielectric materials i.e. barium hexaferrite and conducting ferromagnetic material i.e. LSMO grown by PLD were irradiated for the study of the modification at the heterojunction and the variation in its electric and magnetoelectric properties.

As shown in Fig. 1, the dielectric behavior of BAM/LSMO junctions do not degrade at least upto 2 MHz frequency even after SHI irradiation using Au and Ni at different fluence values. A systematic increase in the permittivity values upon SHI irradiation is encouraging for such a system. We are investigating magneo-dielectric behavior and structural issues of the system under test.

5.2.12 100 MeV O^{7+} swift heavy ions modified molybdenum disulfide-reduced graphene oxide/ polypyrrole nanotubes ternary nanocomposite for hybrid supercapacitor electrode

Devalina Sarmah[1], P.K. Kulriya[2], Fouran Singh[2] and Ashok Kumara[*]

[1]Material Research Laboratory, Department of Physics, Tezpur University, Tezpur 784028, Assam, India
[2]Inter University Accelerator Centre (IUAC), Aruna Asaf Ali Marg, New Delhi 110067, India

Molybdenum disulfide, reduced graphene oxide and polypyrrole nanotubes (MoS_2-rGO/PPyNTs) based ternary nanocomposites have been synthesized by incorporating pre-synthesized PPyNTs in the MoS_2-GO hetero-structures followed by hydrothermal reduction of rGO without using any reducing agent. The MoS2-rGO heterostructures have been synthesized by layer-by-layer self-assembly between negatively charged GO with positively charged MoS_2 followed by hydrothermal reduction [1]. The ternary nanocomposite has been irradiated with 100 MeV O^{7+} swift heavy ions at the fluence of $3.3x10^{11}$, $1x10^{12}$, $3.3x10^{12}$ and $1x10^{13}$ ions cm^{-2}. FESEM images indicated the structural defects like folding and incision appeared in the electrode at a fluence of $3.3x10^{12}$ ions cm^{-2}. XRD spectra revealed that the polymer's crystallinity increased up to the fluence of $3.3x10^{12}$ ions cm^{-2} due to cross-linking in the polymer chain and degraded at the highest fluence $1x10^{13}$ ions cm^{-2}. MoS_2 also got crystallized at the fluence of $3.3x10^{12}$ ions cm^{-2} due to the simultaneous effects of polymer crystallinity, hammering effects from swift heavy ions and formation of periodic tracks. FTIR spectra suggest that different vibrational bands have different sensitivity towards SHI irradiation. Raman spectra revealed the increasing number of defects density in MoS2 due to the appearance of LA peak. In RAMAN spectra of rGO, the disorder parameter first decreased due to annealing and then continuously increased up to the highest fluence, indicating the increased defects or disorder in the nanocomposite. (D+D/) band was also appeared in the RAMAN spectra of the nanocomposite due to the activation of various defect states. Contact angle analysis suggests that the surface energy is mainly dominated by the vdW elements (MoS_2 and rGO) by the formation of temporary dipoles and increases with increasing SHI fluence. The GCD curve of pristine MoS_2-rGO/PPyNTs/ITO electrode showed longer discharge duration and possessed very high value of specific capacitance of 1505 F g^{-1} at 1 fold current density. The irradiated electrodes were also found to possess higher discharge period with enhanced specific capacitance for supercapacitor energy storage. The GCD curve of the electrode irradiated with fluence $3.3x10^{11}$ and $1x10^{12}$ ions cm^{-2} was found to be more linear in both charging and discharging processes (Fig. i). This might be due to the fact that, SHI irradiation widen up the pores of the electrode as observed from FESEM images. Moreover, PPyNTs got aligned and becomes crystalline as well. Therefore, the electrolyte ions can directly penetrate to the MoS_2 and rGO nanosheets and as result EDLC contribution increases after irradiation. Highest gravimetric discharge duration was observed for the electrode irradiated with $3.3x10^{12}$ ions cm^{-2} with enhanced specific capacitance. The GCD measurements for the electrode irradiated with fluence of $3.3x10^{12}$ ions cm^{-2} are performed at 1, 3, 5, 7, 9 and 11 A g^{-1} current densities and are displayed in fig. (ii). The electrode exhibits specific capacitance of 1875 F g^{-1}, 1868.5 F g^{-1}, 1678.6 F g^{-1}, 1462.5 F g^{-1}, 1099.75 F g^{-1} and 769.25 F g^{-1} at 1, 3, 5, 7, 9 and 11 A g^{-1} current densities, respectively. The pristine electrodes and the electrodes irradiated with fluence of $3.3x10^{11}$, 10^{12}, $3.3x10^{12}$ and 10^{13} ions cm^{-2} show rate capability of 46.3%, 47%, 49%, 58.6% and 46%, respectively at 9-fold of current density (Fig. iii). The pristine MoS_2-rGO/PPyNTs/ITO electrode possesses power density of 800.05 W kg^{-1} and energy density of 535.15 Wh kg^{-1} while the electrode modified with ion dose of $3.3x10^{12}$ ions cm^{-2} possesses impressive energy density of 666.72 Wh kg^{-1} maintaining almost the same power density at 1-fold current density (Fig. iv). The ternary MoS_2-rGO/PPyNTs/ITO electrode irradiated with SHI fluence of $3.3x10^{12}$ ions cm^{-2} shows power density of 8800.78 W kg^{-1} and energy density of 273.53 Wh kg^{-1} at 11-fold of current density, while the pristine electrode possesses power density of 8801.56 W kg^{-1} with energy density of 159.87 Wh kg^{-1} at of current density of 11 A g^{-1}.

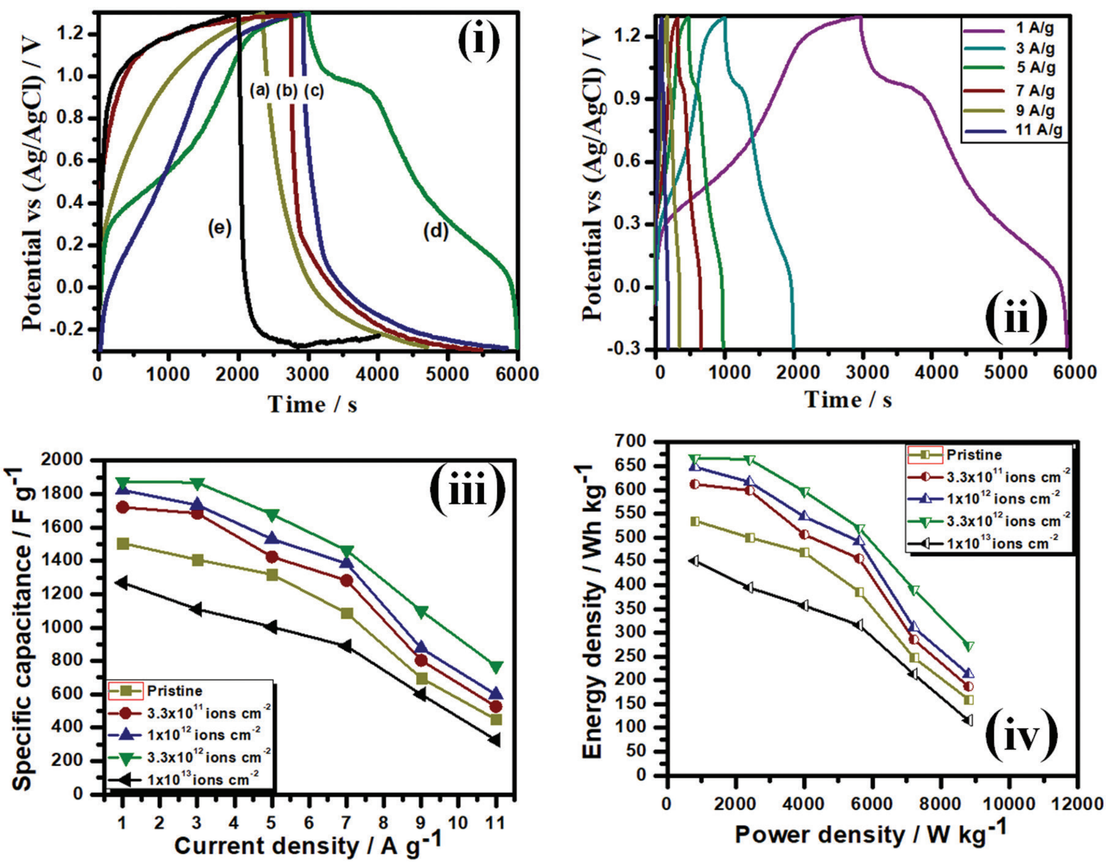

Fig.: Galvanostatic charge-discharge (GCD) measurements of (i) ternary MoS_2-rGO/PPyNTs, (a) pristine and irradiated with fluences (b) $3.3x10^{11}$, (c) $1x10^{12}$, (d) $3.3x10^{12}$, (e) $1x10^{13}$ ions cm^{-2} in 1M KCl solution in 1 A g^{-1} current density; (ii) GCD curves of $3.3x10^{12}$ ions cm^{-2} irradiated electrode at current densities of 1, 3, 5, 7, 9, 11 A g^{-1} in 1M KCl solution, (iii) rate capability of pristine and irradiated ternary MoS_2-rGO/PPyNTs electrodes and (iv) Ragone plot of pristine and irradiated ternary MoS_2-rGO/PPyNTs electrodes.

REFERENCES:

[1] Q. Li, C. Lu, C. Chen, L. Xie, Y. Liu, Y. Li, Q. Kong, H. Wang, Energy Storage Materials, 8 (2017) 59-67.

5.2.13 Defects induced photoluminescence from gallium doped zinc oxide thin films: Influence of doping and energetic ion irradiation

Himanshi Gupta[1], Jitendra Singh[1], R. N. Dutt[1], Sunil Ojha[1], Soumen Kar[1], Ravi Kumar[2], V. R. Reddy[3] and Fouran Singh[1]

[1]Department Inter University Accelerator Centre, New Delhi -110067, India.
[2]Centre of Materials Science and Engineering, National Institute of Technology, Hamirpur (H.P.) – 177005, India.
[3]UGC DAE Consortium for scientific research, Khandwa Road Indore 452017, India.

Research in ZnO remains a matter of interest due to its interesting and unique properties. Zinc oxide is an n-type semiconductor having a stable hexagonal wurtzite structure at ambient conditions. ZnO has a direct wide band gap of 3.37 eV and large exciton binding energy of 60 meV at room temperature (RT). Due to these properties, ZnO has potential applications in optoelectronics devices from LED to solar cell. [1]. So there is a great eagerness to understand the optical properties of ZnO. Moreover, ZnO exhibit a strong UV emission with a broadly visible emission [2]. The origin of the UV emission band in ZnO is well established and assigned to the exciton recombination or band to band transition. In the present report, the defect induced photoluminescence behavior of the Ga doped ZnO (GZO) thin films with varying doping (Ga) concentration and with energetic ion irradiation has been investigated. The XRD spectra reveal that all films are polycrystalline in nature with the wurtzite crystal structure. The transmittance spectra show that all of the films have high transmittance in the visible region more than 75 %. The micro-photoluminescence (μ-PL) measurements were carried out to investigate the defect-related emission with the variation of doping concentration and ion irradiation. PL spectra reveal that all films showed near band edge (NBE) emission along with a broad visible emission band consists of violet, blue, green, and yellow emission bands. The intensity of these emission bands is found to be strongly dependent on the Ga doping concentration and ion irradiation. Interestingly, a pronounced violet emission band around 2.99 eV (415 nm) observed for highly Ga doped ZnO thin film, while an irradiated film with high ion fluence exhibit a strong green emission around 2.39 eV (519 nm). The origins of all the emission bands in the visible region are identified. Comparing experimentally observed emission energy and theoretically calculated defects level energy we propose that defects responsible for violet emission, blue emission, green emission, and yellow emission are Zn_i (+2/+1), extended state of Zn_i (+1/0), singly ionized V_O (+1/0), and transition between Zn_i (+2/+1) level and singly ionized VO (+1/0) respectively. As the concentration of Zn_i increases with increasing doping concentration and the concentration of VO defects increases with increasing ion fluence. For details, see the published article **[Himanshi Gupta *et al.* Phys. Chem. Chem. Phys. 2019, DOI: 10.1039/C9CP02148E].**

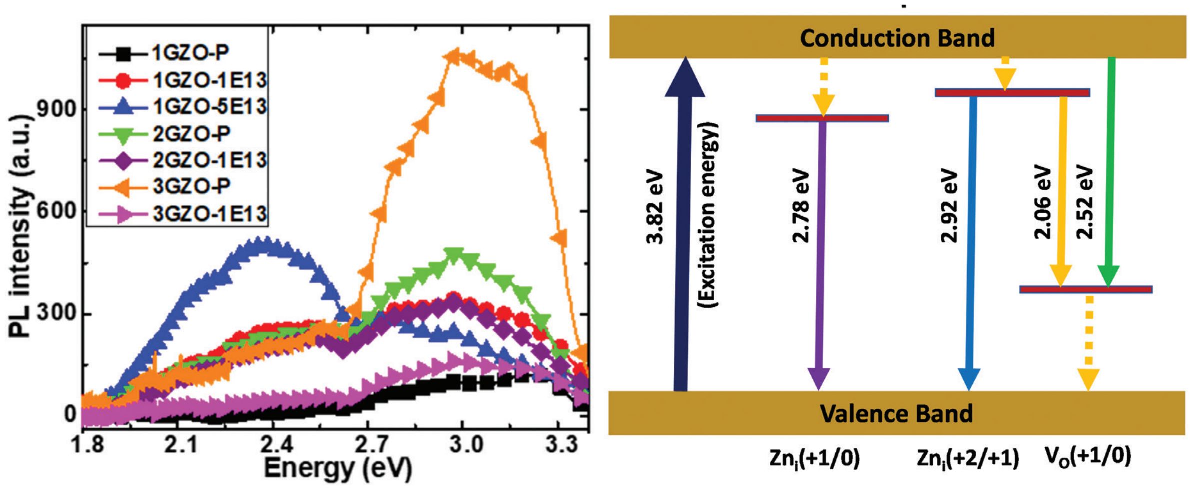

Figure: (Left) PL spectra of Ga doped ZnO thin films with varying Ga concentration and ion irradiation, (right) Schematic of defects energy levels responsible for visible emission.

REFERENCES:
[1] Ü. Ö. Hadis Morkoç, Zinc Oxide:Fundamentals,Materials and Device Technology (n.d.).
[2] W. Z. Xu *et al.,* Appl. Phys. Lett. **88,** 173506 (2006).

5.2.14 Evolution of symmetry forbidden and silent Raman modes of cadmium doped zinc oxide films activated by swift heavy ion irradiation

Naina Gautam[1], Himanshi Gupta[2], A. Kapoor[1] and Fouran Singh[2]

[1]Department of Electronic Science, University of Delhi South Campus, New Delhi-110023, India
[2]Material Science Group, Inter University Accelerator Centre, New Delhi -110067, India

In recent years wide band gap semiconductors have gained much research interest due to their potential applications in electronic and optoelectronic devices. Among which ZnO has been investigated widely for a long time. ZnO has a high band gap of 3.37 eV and high exciton energy of 60 meV at ambient conditions. Due to which it is used in a large number of applications from LED to solar cells [1]. In general optoelectronic devices gets effected by the behavior of long range longitudinal phonon modes (LO) of a material. Although there are a huge number of Raman study on ZnO yet detailed study of Raman spectra of ZnO thin films with ion irradiation is limited. Previously, effect of ion irradiation on nano-crystalline ZnO thin films were reported by our group [2]. In the present study, origin of the evolution of Raman modes from cadmium doped zinc oxide thin films are reported under swift heavy ion irradiation by performing the systematic micro-Raman investigations at various ion fluences and energy deposited into the lattices. Films were also well characterized for their structural and morphological properties. It is reported that Raman spectra of silver irradiated films show that the E_2(high) peak intensity reduces with peak broadening upon an increase in ion fluences, but not completely disappeared like in the case of undoped zinc oxide films. Evolution of intense A_1(LO) peak was also observed along with significant softening and understood by phonon localization due to a high density of defects induced by irradiation. On the other hand, irradiation by oxygen ions induces relatively strong A_1(TO) and B1(low) modes including the non-appearance of A_1(LO) mode, which were supposed to be symmetry forbidden in back-scattering and silent modes, respectively. Thus, the present study provides better experimental insights about the Raman modes for their possible implications in optoelectronic devices. For details, see the published article **[Naina Gautam *et al.* Physica B 570 (2019) 13] [3].**

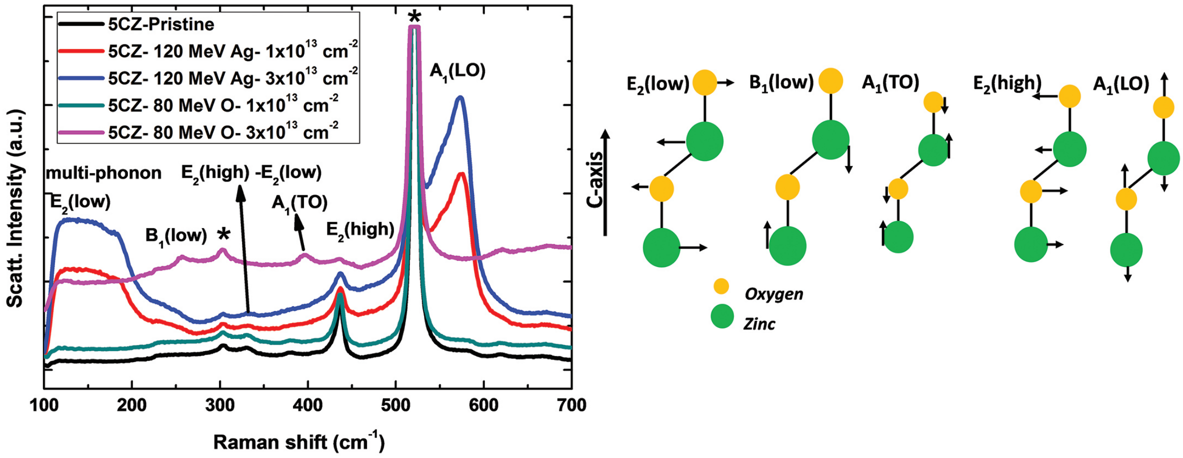

Figure: (Left) Raman spectra of pristine and irradiated thin films with 120 MeV Ag^{9+} ions and 80 MeV O^{6+} ions at varying of 1×10^{13} ions/cm^2 and 3×10^{13} ions/cm^2, (right) Schematics of the symmetry of various phonon modes of ZnO.

REFERENCES:

[1] Ü. Ö. Hadis Morkoç, Zinc Oxide:Fundamentals,Materials and Device Technology (n.d.).

[2] F. Singh, R. G. Singh, V. Kumar, S. A. Khan, and J. C. Pivin, J. Appl. Phys. **110,** 083520 (2011).

[3] N. Gautam, H. Gupta, A. Kapoor, and F. Singh, Phys. B Condens. Matter **570,** 13 (2019).

5.2.15 Tailoring dielectric properties and multiferroic behavior of nanocrystalline $BiFeO_3$ via Ni doping

Nadeem M.[1], Khan Wasi[2], Khan Shakeel[1], Husain Shahid[2] and Ansari Azizurrahaman[3]

[1]Department of Applied Physics, Z.H. College of Engineering & Technology, Aligarh Muslim University, Aligarh-202002, India.

[2]Department of Physics, Aligarh Muslim University, Aligarh-202002, India.

[3]Department of Materials Science Programme, Indian Institute of Technology Kanpur, Kanpur-208016, India.

In order to tailor the multiferroic as well as dielectric properties, we have synthesized bismuth ferrite, BiFeO3 (BFO) and Ni-doped BFO nanoparticles of composition $BiFe_{1-x}Ni_xO_3$ ($0 \leq x \leq 0.07$) via sol-gel method. [*for details, see Mater. Res. Express 5 (2018) 065506*]. The influence of Ni-doping at Fe site of $BiFeO_3$ on the structural, dielectric and multiferroic properties was investigated via various characterization techniques such as Raman spectroscopy, Vibrating sample magnetometer, polarization-electric field (P-E) loop tracer and LCR meter. The Raman spectra reveal the rhombohedral distorted perovskite structure of the samples in the R3c space group. The frequency dependent dielectric measurements at room temperature show that the dielectric constant for the pristine sample is an order of magnitude lower than the 1% Ni-doped BFO sample. It is also evident that the ac conductivity increases with the increase in frequency as well as Ni content. Further, the universal dielectric response (UDR) phenomenon is responsible for the dielectric behavior of all the samples in whole frequency range except for $BiFeO_3$ and $BiFe_{0.97}Ni_{0.03}O_3$ samples. These samples exhibit deviation from UDR phenomenon at higher frequencies. The room temperature hysteresis (M-H) loops exhibit the saturation in magnetization at higher magnetic fields. The result demonstrates a significant influence on the saturation magnetization with the Ni doing in BFO, prompting the ferromagnetic nature of the samples. The saturation magnetization of 7% Ni-doped sample is approximately six times higher than the pristine one. The saturated P-E hysteresis loops establish the ferroelectric nature of the synthesized samples that are enhanced significantly on Ni doping. Thus, the doping of Ni in $BiFeO_3$ improves the multiferroic properties of the matrix. *[for details, see J. Appl. Phys. 124 (2018) 164105].*

In order to investigate the effects of the swift heavy ion (SHI) irradiation on the structural, optical, electrical and magnetic properties of $BiFeO_3$ and Ni-doped $BiFeO_3$ thin films, we have deposited the pristine and, 1%, 3% and 5% Ni-doped $BiFeO_3$ thin films on Si (100) wafer using pulsed laser deposition (PLD) technique at UGC-DAE CSR, Indore. The distance between the target and substrate was adjusted at 5 cm and the laser energy during the deposition was 250 mJ with repetition rate of the target as 10 Hz. These films have been deposited at two different oxygen partial pressure i.e. 100 mTorr and 300 mTorr. During the deposition substrate temperature was maintained at 700 ºC and all the films were deposited for 30 minutes. After phase analysis the films were irradiated using 15 UD Pelletron tandem accelerator at Inter University Accelerator Centre (IUAC), New Delhi with 120 MeV Ag^{9+} ions at three different ion fluences i. e. 1×10^{13} ions/cm^2, 5×10^{13} ions/cm^2 and 1×10^{14} ions/cm^2.with current of 1pnA (particle nanoampere). All the films were fixed to the target ladder placed inside the high vacuum ($\sim10^{-6}$ torr) chamber during irradiation. Irradiation was performed in the direction perpendicular to the sample surface. The ion beam was focused to a spot of 10 mm diameter and then scanned over an area of 1×1 cm^2 using magnetic scanner to cover the complete sample surface for uniform irradiation. To investigate the structural changes because of the irradiation, we have carried out the XRD measurements of the irradiated thin films at room temperature at IIT Kanpur. To study the effects on optical, electrical and magnetic properties of the irradiation the other measurements and analysis are under process.

References:

[1] M. Nadeem, Wasi Khan, Shakeel Khan, Mohd Shoeb, Shahid Husain and Mohammad Mobin, Mater. Res. Express 5 (2018) 065506.

[2] M. Nadeem, Wasi Khan, Shakeel Khan, Shahid Husain and Azizurrahaman Ansari, J. Appl. Phys. 124 (2018) 164105.

5.2.16 Swift Heavy Ion Irradiation Induced Modifications in Graphitic Nanocomposites

Pankaj Singh Rawat[1], R. C. Srivastava[1], Gagan Dixit[1], G. C. Joshi[1] and K. Asokan[2].

[1]Dept. of Physics, CBS&H, G.B. Pant Univ. of Ag. & Tech. Pantnagar
[2]Inter-University Accelerator Centre, New Delhi-110067, India.

Nanocomposites derived from graphene oxide (GO), reduced grapheme oxide (rGO) and magnetic nanoparticles (ferrites) are of larger interest due to variety of possible applications such as in fabricating functional nanocomposites, waste water treatment and electromagnetic wave absorbers etc. Ferrites play useful role in many technological applications due to their high electrical resistivity and sufficiently low dielectric losses over a wide range of frequency [1-2]. The present research work is focused on synthesis and investigation of graphene oxide based nickel ferrite (GO/$NiFe_2O_4$) nanocoposites before and after SHI irradiation. X-ray diffraction (XRD), energy dispersive X-ray spectroscopy (EDX), Raman spectroscopic measurements and temperature dependent dielectric measurements of pristine samples were carried out at IUAC, New Delhi. Materials science beam-line, 15 UD Pelletron-Accelerator facility of Inter-University Accelerator Centre (IUAC), New Delhi was used to irradiated the samples by 100 MeV Au ions.

Experimental Details

XRD pattern of samples confirmed the pure phase of GO, $NiFe_2O_4$, $MnFe_2O_4$ and GO/$NiFe_2O_4$ composites. Room temperature Raman spectroscopic measurements showed the characteristic D-band at 1357 cm^{-1} attributed to the sp^3 defects in the sp^2 graphitic lattice and G-band at 1614 cm^{-1} from sp^2 carbon atoms in GO samples. EDX study confirmed the proper stoichiometry for all the samples (Ni:Fe, Mn:Fe – 1:2, C:O – 1.04 in GO and C:O – 8.09 in rGO). An increased C/O (at. wt. %) ratio (from 1.04(GO) to 8.09(RGO)) confirmed the reduction process in GO. Significantly high dielectric loss was observed in GO due to its conductivity. The dielectric constant showed a decrease when the composite is sintered at higher temperature. The dielectric constant values at 1MHz were 313, 103, 101, 68 and 39 for $NiFe_2O_4$, GO, GO/$NiFe_2O_4$, GO/$NiFe_2O_4$ (500ºC), GO/$NiFe_2O_4$ (800ºC) samples respectively [Fig.1 (a, b)]. The high dielectric loss observed in GO is due to its partially conducting nature, whereas the addition of $NiFe_2O_4$ nanoparticles lead to the reduction in electronic conductivity. The order of resistance of GO/$NiFe_2O_4$ composite (~10^3 Ohm) was found to be less than that of GO and $NiFe_2O_4$ (~10^6 Ohm) samples due to the partial reduction of GO into rGO while forming GO/$NiFe_2O_4$ composite. The partial reduction of GO into rGO in GO/$NiFe_2O_4$ composite was also confirmed in X-ray absorption spectroscopic (XAS) characterization (C-k edge, 280-315 eV and O-k edge, 520-555 eV) of the samples.

The selected samples of graphene oxide and composite were irradiated with 100 MeV Au - ions at fluences of ~ 5E11, 5E12 and 1E13 ion/cm^2. The beam current was kept constant at 1 pnA (particle-nano ampere). The energy loss, ion beam energy and projected range of ions in material were obtained using SRIM (2013) software before SHI irradiation. The optical band gap of pristine and samples irradiated at fluences of 5E11, 5E12 and 1E13 ion/cm2 was estimated from DRS spectrum using Kubelka-Munk function. A decrease in band gap from 1.64 eV for pristine $NiFe_2O_4$ to ~ 1.59 eV for irradiated $NiFe_2O_4$ samples [Fig.2 (a, b)] and from 1.67 eV for pristine GO/$NiFe_2O_4$ composite to ~1.64 eV for irradiated composite samples [Fig.3 (a, b)] was observed with an increase in fluence. This can be attributed to the introduction of defect levels by ion irradiation causing increase in charge flow in irradiated samples. Further characterization of pristine and irradiated samples and analysis of data is in underway.

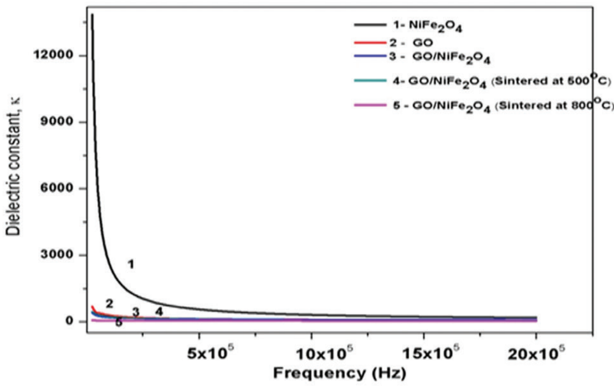

Fig.1(a)

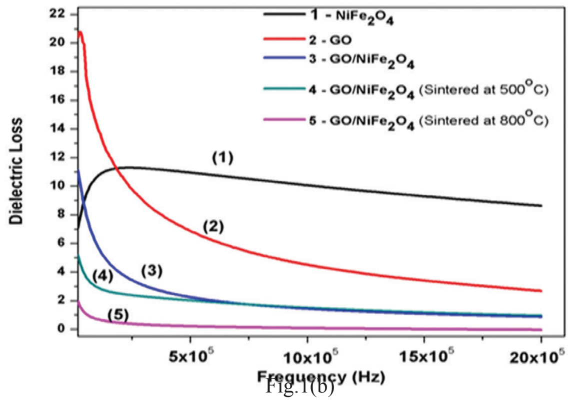

Fig.1(b)

Figure 1. (a) Dielectric constant vs Frequency (b) Dielectric loss vs Frequency of pristine samples.

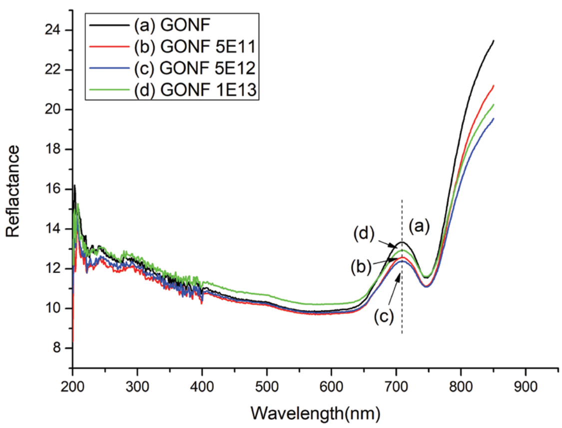

Fig.2(a)

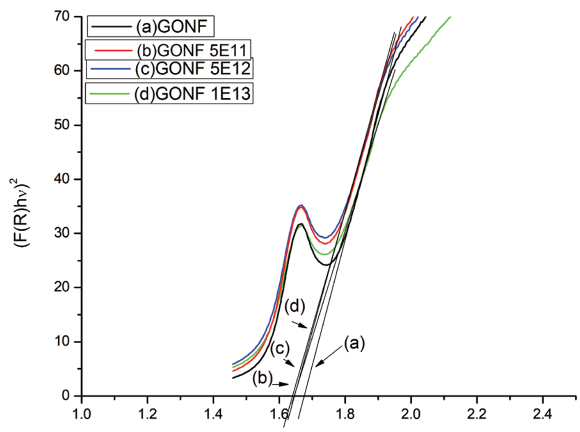

Fig.2(b)

Figure 2. (a) DRS spectrum and (b) Tauc plot of pristine and irradiated $NiFe_2O_4$ samples.

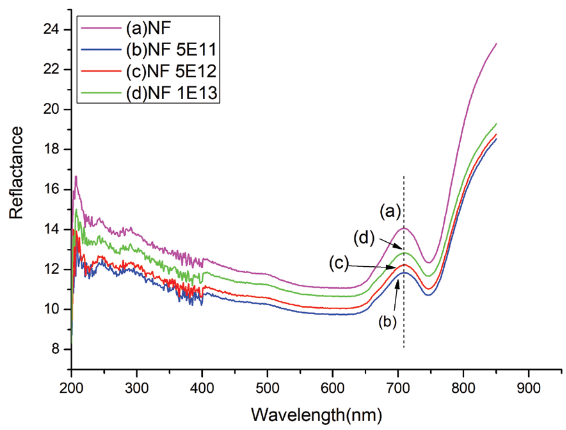

Fig.3(a)

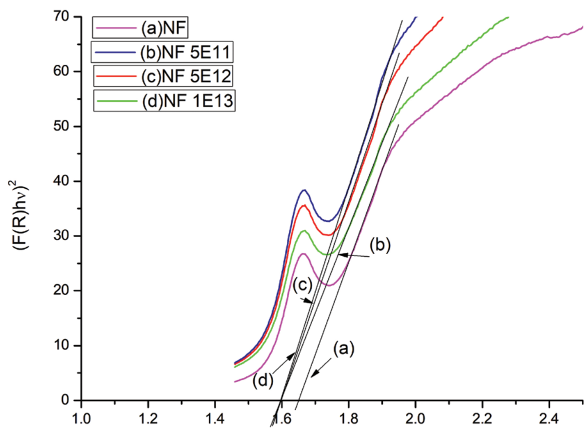

Fig.3(b)

Figure 3. (a) DRS spectrum and (b) Tauc plot of pristine and irradiated GO/$NiFe_2O_4$ samples.

REFERENCES:

[1] S. Chen *et al.,* ACS Nano. 4,2822 (2010)

[2] Y. Song *et al.,* Electrochim. Acta. 71, 58 (2012)

[3] U. Dembereldorj *et al.,* Photochem. Photobiol. 90, 659(2014)

5.2.17 Effect of Si ion irradiation on structural and optical properties of pure and Ag doped $Ge_2Sb_2Te_5$ (GST) thin films

Neetu Kanda[1], Anup Thakur[2], Fouran Singh[3], A.P. Singh[1*]

[1] Department of Physics, Dr. B. R. Ambedkar National Institute of Technology, Jalandhar-144011, India.
[2] Department of Physics, Punjabi University, Patiala, Punjab 147002, India
[3] Inter-University Accelerator Centre, New Delhi, Delhi – 110067

The most promising materials for rewritable storage are chalcogenide alloys. These materials act as active media for phase change memory devices. In our study, we study phase change materials for optical storage devices. PCM material with most favourable properties is $Ge_2Sb_2Te_5$ (GST), which is the focus of the present study. GST thin films are irradiated with Silicon ions at high energy. These high energy ions introduce defects in these films, which will ultimately change their optical and structural properties. Slight crystallization is observed for highest irradiation dose which is also indicated by the decrease in bandgap with irradiation.

Experimental Details

Bulk alloy of GST were prepared by melt quenching technique. Thin films of these samples were deposited on glass substrate by thermal evaporation technique with the help of Hind HIVAC system (Model: BC-300), at deposition rate 2-3 Å /s under the base pressure of 2.4×10^{-6} mbar. The film thickness was measured using digital thickness monitor during thermal deposition. These films were irradiated with Si^{6+} ions at different fluences at 120 MeV energy. These films are characterized using XRD, FESEM and UV-Vis-NIR spectroscopy to study the changes introduced due to ion irradiation.

Results

$Ge_2Sb_2Te_5$ is a chalcogenide alloy which is used in many phase change applications like electrical and optical non-volatile memory and photonic devices etc. [1,2,3]. This material shows drastic contrast in their optical and electrical properties while changing phase from amorphous to crystalline. These properties can be modified by swift heavy ion irradiation. In the present work, thin films of pure GST are irradiated with Si^{6+} ions with 120 MeV energy at 5×10^{11}, 1×10^{12}, 5×10^{12}, and 1×10^{13} ions/cm^2 fluences and these samples are named as G0, G5e11, G1e12, G5e12 and G1e13 respectively. The xrd spectra of G1e13 is shown in fig1. The highly irradiated film show one peak at 29.26˚ which shows the fcc phase of these films after ion irradiation. However other films do not show any phase transformation. FESEM images of G0, G5e11, G5e12 and G1e13 films are shown in fig2. It is clearly visible from fig2 that with the increase in irradiation fluence, there is generation of crystal nuclei, which ultimately leads to phase change for higher irradiation dose. Moreover, the bandgap is obtained from transmission spectra using tauc plot. Table1 shows the different values of bandgap with different fluence of irradiation. This shows that with irradiation bandgap decreases, which ensures the generation of crystal nuclei and hence crystallization with highest fluence.

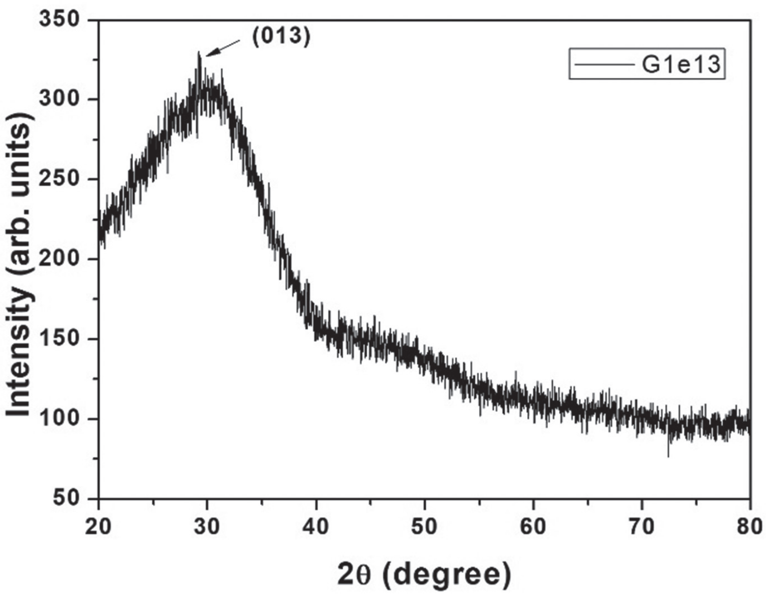

Fig1. XRD spectra of G1e13.

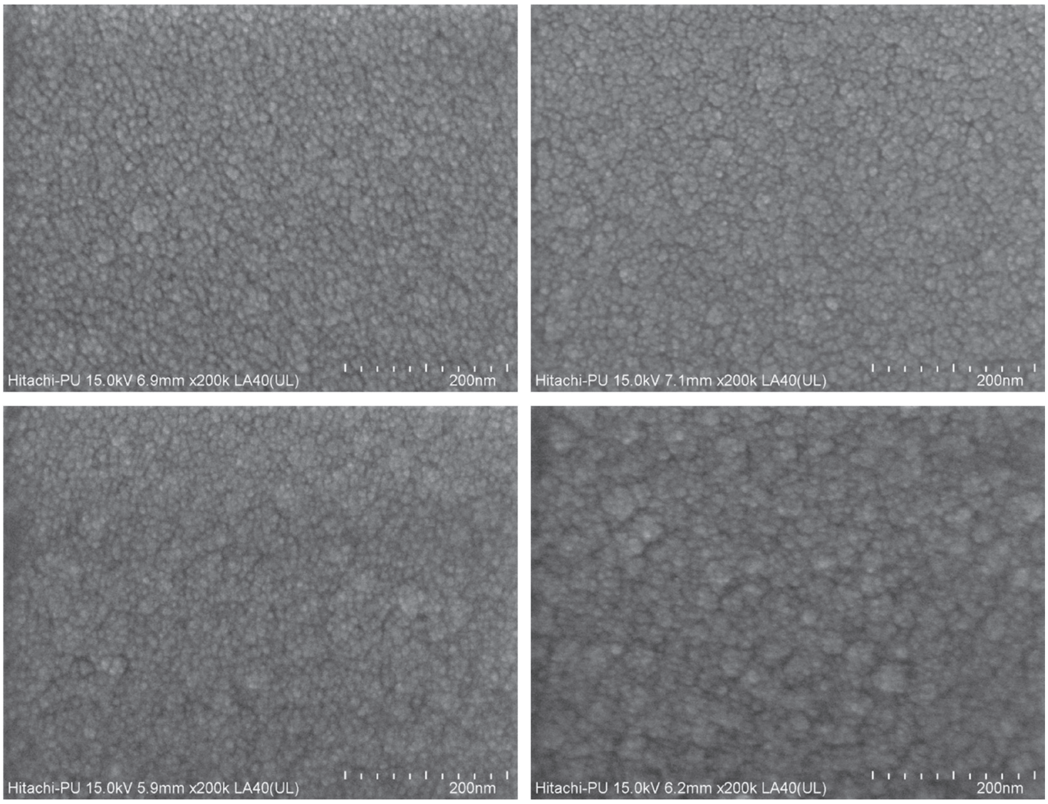

Fig2. FESEM images of G0, G5e11, G5e12 and G1e13.

Table1: bandgap of pure and irradiated thin films.

Sample	G0	G5e11	G1e12	G5e12	G1e13
Bandgap (eV)	0.65	0.64	0.64	0.58	0.55

REFERECNES

[1] G. Atwood. Phase-Change Materials for Electronic Memories. Science, 321:210, 2008.

[2] H. Lv, P. Zhou, Y. Lin, T. Tang, B. Qiao, Y. Lai, J. Feng, B. Cai, and B. Chen. Electronic properties of GST for non-volatile memory. Microelectronics Journal, 37:982, 2006.

[3] P. Singh, A. P. Singh, N. Kanda, M. Mishra, G. Gupta, and A. Thakur. High transmittance contrast in amorphous to hexagonal phase of Ge2Sb2Te5: Reversible NIR-window. Applied Physics Letters, 111:261102, 2017.

5.2.18 Enhanced thermoelectric properties of SHI irradiated metal chalcogenide thin films

P. Matheswaran[1], B. Gokul[1], R. Sathyamoorthy[1], K. Asokan[2] and D. Kanjilal[2]

[1]Department of Physics, Kongunadu Arts and Science College, Coimbatore - 641029, India
[2]Inter University Accelerator Centre, New Delhi - 110067, India

Experimental Details

The as grown $In_2(Te_{1-x}S_{ex})_3$ films were subjected to SHI irradiation ($In_2(Te_{1-x}S_{ex})_3$: 120 MeV Au, 120 MeV Ni and 120 MeV Ag) for different ion fluences (0.5 pnA) in the range 10^{12}-10^{13} ions/cm^2. The energy loss and projected range of the ions in the target was calculated with the help of SRIM-2008 simulation program.

Results and discussion

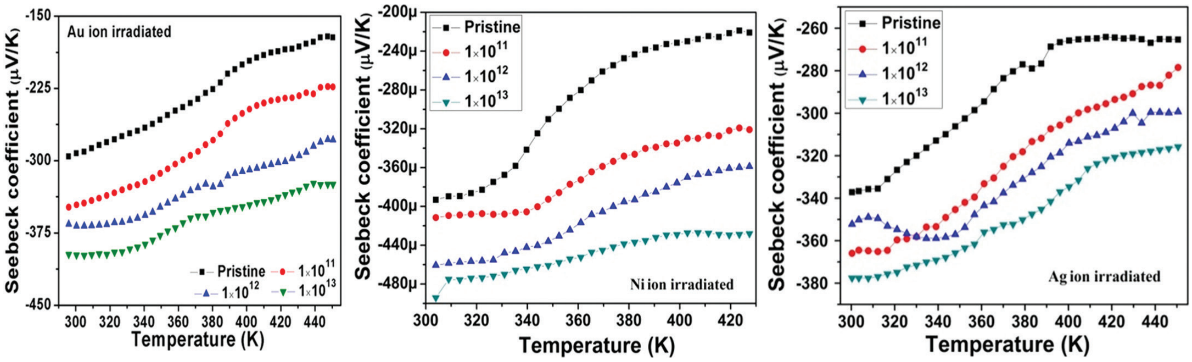

Figure.1 Seebeck coefficient (S) of all pristine and irradiated $In_2(Te_{1-x}S_{ex})_3$ thin film

XRD patterns of all the pristine and irradiated $In_2(Te_{1-x}S_{ex})_3$ thin films confirms formation of ternary In_2(Te.Se)3 phase, binary In_2Se_3 and In_2Te_3 phase (not shown here).

The FESEM image shows the uniform fragmentation of grains throughout the surface of the sample after irradiation. The negative value of Seebeck coefficient confirms the nature of n-type conductivity in the pristine and Ni ion irradiated $In_2(Te_{1-x}S_{ex})_3$ (x=0.06) samples. The Seebeck coefficient value for pristine sample is found to about ~196 μVK^{-1} and it is enhanced to ~347 μVK^{-1} at the higher fluence of 1×10^{13} ions/cm^2 at 420 K. The power factor value is about ~3.80 $\mu W/K^2m$ corresponds to sample irradiated at the fluence of 1×10^{13} ions/cm^2, shows 3 times greater as compared to pristine sample value of ~1.28 $\mu W/K^2m$ [1].

The maximum Seebeck coefficient value for the pristine $In_2(Te_{1-x}S_{ex})_3$ (x=0.02) sample is about ~221 μVK-1. At higher fluence (Au) of $1\times10_{13}$ ions/cm$_2$, the Seebeck coefficient value is found to ~427 μVK^{-1} at 400 K, shows almost 50% greater than the pristine sample value. The maximum power factor is found to ~1.23 $\mu W/K^2m$ and 4.91 $\mu W/K^2m$ are corresponding to the pristine and 1×10^{13} ions/cm^2 irradiated films. It shows irradiated sample value is 3 times greater as compared to pristine sample and hence, the enhancement to the Ni ion irradiated films. So that, charge scattering due to the grain boundary lead to significant improvement in thermoelectric properties of the irradiated films [2]. These results may find great interest in thermoelectric device applications.

Additionally, we have selected Ag^{7+} ion to enhance the thermoelectric properties of $In_2(Te_{1-x}S_{ex})_3$ (x=0.15) films. The maximum Seebeck coefficient value for the pristine sample is about ~265 μVK^{-1}. At higher fluence of 1×10^{13} ions/cm^2, the Seebeck coefficient value is found to ~335 μVK-1 at 400 K, shows almost 30% greater than the pristine sample value. All the Seebeck coefficient values are in negative shows the nature of n-type conductivity in the films. Further, the maximum power factor is found to ~1.98 $\mu W/K^2m$ and 3.48 $\mu W/K^2m$ are corresponding to the pristine and 1×10^{13} ions/cm^2 irradiated films. It shows irradiated sample value is enhanced as compared to pristine sample. Moreover, the improved thermoelectric properties of Ag ion irradiated $In_2(Te_{1-x}S_{ex})_3$

Summary

Thermoelectric performance of As grown and SHI ion (Au, Ni and Ag) irradiated $In_2(Te_{1-x}Sex)_3$ (x=0.06, 0.02 and 0.15) thin films was measured using Bridge method. The effects of SHI irradiation on structural, morphological and electrical transport properties were studied. The Seebeck coefficient and power factor values are enhanced with SHI irradiation in comparison to the as grown samples. In particular, Ni ion irradiated samples shows better thermoelectric performance and this could be due to the irradiation induced defects in the samples.

REFERENCES:

[1] J. Martin, L. Wang, L. Chen, G. S. Nolas, Phys. Rev. B - Condens. Matter Mater. Phys.79 (2009) 115311.

[2] A. Popescu, L.M. Woods, J. Martin, G.S. Nolas, Phys. Rev. B. 79 (2009) 205302.

5.2.19 Study of gas sensing behavior of 2D MoS_2 after irradiation by Au and Li ions

Rahul Kumar[1], Neeraj Goel[1], Pawan Kulriya[2] and Mahesh Kumar[1*]

[1]Department of Electrical Engineering, Indian Institute of Technology, Jodhpur-342037, India.
[2]Inter-University Accelerator Centre, New Delhi-110067, India.

We want to study of gas sensing behavior of 2D MoS_2 after irradiation by the Gold (Au) and Lithium (Li) ions. The gas sensing behavior will be investigated of the irradiated MoS_2 film by measuring the change in resistance value of the device before and after exposure the gas. The selectivity, stability aspects of the fabricated sensor from irradiated MoS_2 would also be examined. Here, we synthesized horizontally and vertically aligned MoS_2 by the conventional chemical vapor deposition process using MoO_3 and sulfur solid precursor and also fabricated the wafer scale MoS_2 through sulfurization in CVD to RF sputtering deposited Mo film on SiO_2 substrate. After irradiation the MoS_2 films of different structures, we performed the Raman and SEM experiments at room temperature. Active Raman peaks of MoS_2 show changes in its position, intensity and fwhm because of increased defects with enhanced fluence of the ions. It was also noted that surface morphology of horizontally aligned MoS_2 was also changed with high fluence. The gas sensing experiments to examine the gas sensing behavior of ion irradiated MoS_2 are in progress.

Experimental Details

2D MoS_2 flakes were synthesized using two solid precursor molybdenum trioxide (MoO_3) and sulfur (S) by three zone chemical vapor deposition (CVD) technique through kinetically controlled rapid growth processes. The substrate was put vertically away from MoO_3 in same alumina boat in the centre zone and annealed MoO_3 at 1000 ºC for 60 min at atmospheric pressure and high heating rate 50 ºC per min was used to increase the temperature. Sulfur was put in upstream heated at 180 ºC and Ar gas flow was 160 sccm through all reaction time. Finally, the furnace was turned off and the tube was cooled naturally back to room temperature. Additionaly, the MoS_2 film was also grown using a two-step process: deposition of a ~4 nm DC sputtered Mo film followed by sulfurization. During the deposition of the Mo film, the chamber pressure, DC power and Ar gas flow were maintained at 6.5×10^{-3} mbar, 40 W and 40 sccm, respectively. The sulfurization of the deposited Mo film was done using the CVD technique.

To observe the effect of SHI irradiation on gas sensing behavior of MoS_2 depsoited film, we irradiated these thin films with 100 MeV Au ions at three fluences (1×10^{11}, 1×10^{12}, and 1×10^{13} ions/cm^2) using the Pelletron accelerator at IUAC, New Delhi. Few CVD grown MoS^2 samples were also irradiated using 50 MeV Li ions at fluences of 1×10^{11}, 1×10^{12}, and 1×10^{13} ions/cm^2. The effects of ion irradiation on structural properties of MoS_2 are investigated through Raman spectroscopy. The formation of peripheral fragmentation was observed after ion irradiation, which influences the gas sensing mechanism at the surface.

5.2.20 Swift Heavy Ion (SHI) Irradiation Effects on Multiferroic BFO Thin Films

Venkatapathy Ramasamy[1], Asokan Kandasami[2], Indra Sulania[2], Devarani Devi Kshetrimayum[3] and Ramesh Kumar Gubendiran[1*]

[1]Department of Physics / UCE Arni, Anna University, Tamil Nadu -632326, India.
[2]Materials Science Division, Inter-University Accelerator Centre, New Delhi 110067, India.
[3]Pelletron and Negative Ion Implanter laboratory, IUAC, New Delhi 110067, India.
[*]E-mail: rameshvandhai@gmail.com

Thin films of Bismuth ferrite [$BiFeO_3$ - BFO] were irradiated using Ti^{7+} at various ion fluences. Upon irradiation, the multiferroic BFO thin films have been characterized using Grazing Incidence angle X-Ray Diffraction (GIXRD), UV-Vis NIR Spectroscopy, Field emission scanning electron microscopy (FESEM) and I-V measurements. Irradiation induced modifications on the structural, optical and Leakage Current properties have been studied in detail.

Results

The crystalline structure of deposited thin films of pristine and ion irradiated BFO was characterized by Grazing incidence angle x-ray diffraction (GIXRD). The GIXRD patterns of the thin films were indexed for a rhombohedral structure, and the BFO thin films grown on ITO substrate exhibited single phase perovskite with secondary phases.

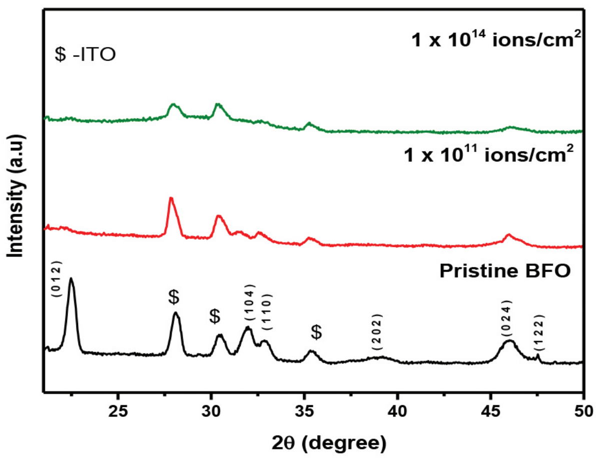

(a) GIXRD

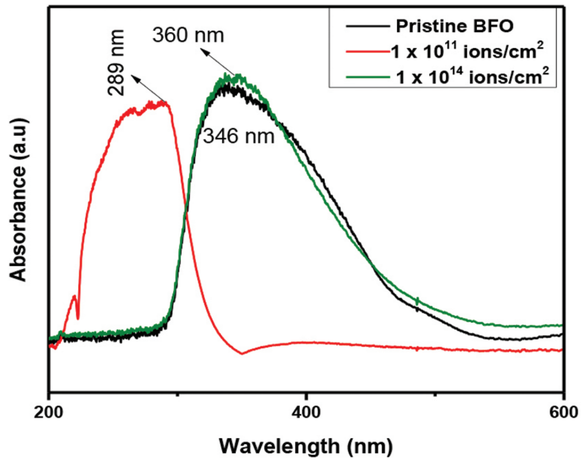

(b) UV-Vis NIR Spectroscopy

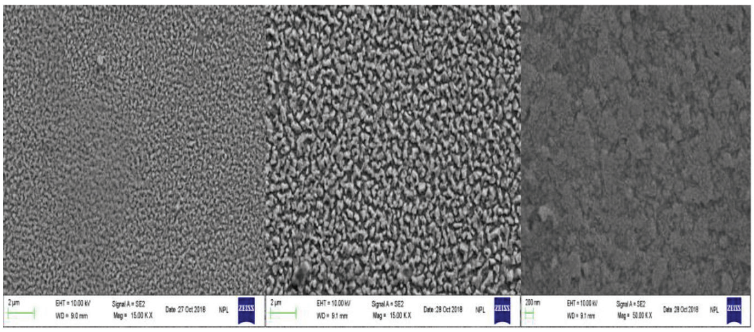

(c) FESEM

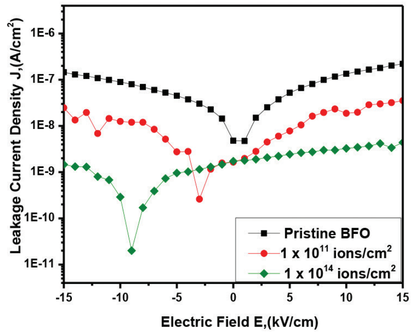

(d) I-V measurements

REFERENCES:

[1] Q.H. Jiang, C.W. Nan, journal of Amer.cera.soci. 89 (2006) 2123-2127.

[2] Dash B N, Mallick P, Dash P, Biswal R, Jai prakash, TripathI A, Kanjilal D, Mishra N C, Bull.Mate. Scie. 36 (2013) 813–818.

[3] Linlin Zhang, Jian Yu, Jour. of mater. Scie.27 (2016) 8725-8733.

5.2.21 Effect of 120 MeV Ni^{10+} and Ag^{7+} swift heavy ion irradiation on CdSe and CdS nanocrystalline thin films

Pijush Ch. Dey[1], Simi Debnath[1], Debojyoti Nath[1], Fouran Singh[2] and Ratan Das[1*]

[1]Department of Physics, Tripura University, Suryamaninagar-799022, India.
[2]Inter-University Accelerator Centre, New Delhi-110067, India.

We have prepared CdSe and CdS nanoparticles using a wet-chemical method and then deposited on silicon substrate to study the effect of swift heavy ion irradiation. The prepared CdSe and CdS nanocrystalline thin films have been irradiated with 120 MeV swift Ni^{10+} and Ag^{7+} ions having fluences of 1×10^{12} and 3×10^{13} ions/cm^2. Structural analysis of the nanocrystalline thin films has been studied before and after the irradiation, through X-Ray diffraction and Raman Study, whereas the morphological properties have been studied using SEM and TEM. Further, optical properties has been studied through UV-Vis spectrometer and Photoluminescence.

From the study of the Raman spectra of CdSe and CdS, it has been found that longitudinal optical (LO) phonons mode dominates, which may be attributed to the lattice vibration of the nanocrystals and a weaker mode arises due to second order Longitudinal optical (2LO) phonon. It has been observed that for low fluence irradiation, an increment in LO peak occurs, whereas, a drastic decrease in LO peak has been observed at maximum fluence. This variation of the intensity of LO peak may be attributed to the accumulation of defects during irradiation, as well as the associated bond distortions and tensile stress. Further, X-Ray study reveals a cubic to hexagonal phase transition for both the materials, with a different fraction of hexagonal phase depending on the electronic energy loss of the incident ion. Variation in the elastic properties of the pristine and the ion irradiated materials have been studied using Williamson-Hall, Warren-Averbach and Variance method based on the broadening of the XRD peak. It has been observed that the value of microstrain and the dislocation density also get increased after the irradiation, due to the change in the lattice structure after the irradiation. SEM and TEM analysis confirms the increase in the average particle size. Further to study the variation of the optical properties, UV-Vis and Photoluminescence analysis has been employed, which reveals an increase in PL intensity with increase in fluence with decease in the energy band. This may be attributed to the defect state formation due to SHI irradiation.

REFERENCES:

[1] Vishnu Chauhan, T. Gupta, Paramjit Singh, P.D. Sahare, N. Koratkar, Rajesh Kumar1, Physics Letters A 383 (2019) 898-907.

[2] V.V. Ison, A. Ranga Rao, V. Dutta, P.K. Kulriya, D.K. Avasthi, S. K. Tripathi J. Appl. Phys. 106, (2009) 023508

[3] S. Negi, M. P. S. Rana, F. Singh, R. C. Ramola J Sol-Gel Sci Technol (2015) 76:608–613

[4] A.Benyagoub, L.Thome, Phys.Rev.B 38 (1988) 10205.

5.2.22 Effect of 120 MeV Ag ion irradiation on gallium oxide thin films

Saurabh Yadav[1], Subhra Das[2], A. K. Patra[2], R. Singh[3] and Y. S. Katharria[1]

[1]PDPM Indian Institute of Information Technology, Design and Manufacturing, Jabalpur-482005, Madhya Pradesh
[2]Department of Physics, Central University of Rajasthan, Bandarsindri-305817, Rajasthan
[3]Department of Physics, Indian Institute of Technology Delhi, New Delhi-110016, Delhi

Gallium oxide (β-Ga_2O_3) is a wide bandgap semiconductor ($E_g \sim 4.9$ eV) which is stable both chemically and thermally, and is, thereby, suitable for operations under harsh chemical environment as well as at high temperatures [1]. It has found diverse applications in optoelectronic devices such as gas sensors, deep UV solar blind photodetectors [2], etc. The radiation hardness of β-Ga_2O_3 devices may be useful for space and military applications where issues of radiation tolerance are critical. Therefore, understanding the changes in the structural and optical properties of β-Ga_2O_3 caused by the ion irradiation effects is of critical importance. In this work, we have studied the irradiation effect of 120 MeV Ag^{9+} ions on β-Ga_2O_3 thin films.

Thin films of β-Ga_2O_3 were grown on silicon (100) and quartz substrates at room temperature using e-beam evaporation method. After deposition, the films were annealed at 900 °C for 30 min under oxygen environment to obtain stoichiometric, crystalline phase. Thereafter, swift heavy ion irradiation was carried out using 120 MeV Ag^{9+} ions with ion fluences (ϕ) of 1×10^{11}, 3×10^{11}, 5×10^{11}, 1×10^{12} and 5×10^{12} ions-cm^{-2}. X-ray diffraction (XRD) measurements were performed using a PANalytical-Empyrean system using CuK_α radiation with a wavelength of 1.5404 Å. UV-visible absorption measurements were carried out using a Hitachi U3300 dual beam spectrophotometer.

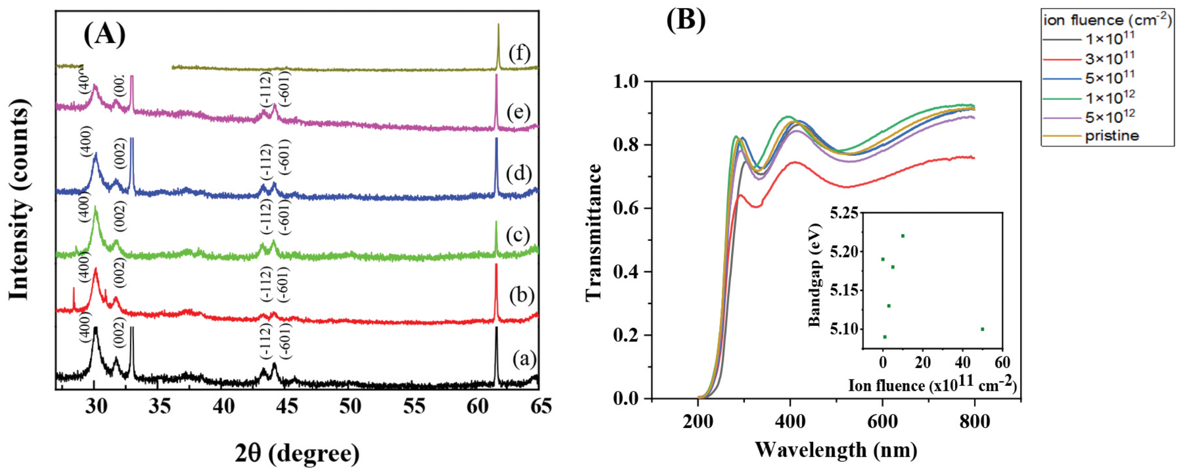

Fig.1. (A) XRD patterns; and (B) transmittance spectra of samples annealed at 900ºC, with ion fluences (ϕ), (a) $\phi = 0$, (b) $\phi = 1\times10^{11}$, (c) $\phi = 3\times10^{11}$, (d) $\phi = 5\times10^{11}$, (e) $\phi = 1\times10^{12}$, (f) $\phi = 5\times10^{12}$ ions-cm^{-2}. The inset of fig.1 (b) shows the variation of bandgap with ion fluence.

Fig.1 (A) shows XRD patterns of 120 MeV Ag^{9+} irradiated β-Ga_2O_3 thin films with ϕ varying from 1×10^{11} cm^{-2} to 5×10^{12} cm^{-2}. An increasing disorder and decrease in the crystalline size of β-Ga_2O_3 with increasing ϕ is obvious from the increasing FWHM and decreasing intensity of the peaks. Average crystallite size was ~ 13.6 nm for unirradiated thin film, and decreases to ~ 8 nm for the thin films irradiated at $\phi = 5\times10^{12}$ ions-cm^{-2}. Such a decrease in crystalline fraction under ion irradiation was also reported by Tracy et al. [3]. Fig.1 (B) shows the UV-visible absorption spectra of ion irradiated β-Ga_2O_3 thin films. For all wavelengths above 275 nm, transmittance of the films was more than 80%. The as-grown film has a sharp absorption edge at wavelength around 240 nm. This corresponds to a bandgap of ~5.19 eV. The bandgap remained almost constant within the range of 5.10 - 5.21 eV under ion irradiation suggesting the robust nature of the Ga_2O_3 against ion-irradiation and its suitability for space applications.

REFERENCES:

[1] M.A. Mastro and S.J. Pearton, ECS J. Solid State Sci. Technol. 6, P356 (2017).

[2] A. Pratiyush, S. Krishnamoorthy, and D. N. Nath, Appl. Phys. Lett. 110, 221107 (2017).

[3] C. L. Tracy, M. Lang, D. Severin, M. Bender, C. Trautmann, and R. C. Ewing, Nucl. Instrum. Meth. B 374, 40 (2016).

5.2.23 Electrocatalytic activity of ion implanted rGO/PEDOT:PSS hybrid nanocomposites towards methanol electro-oxidation

Bhagyalakhi Baruah[1], Ashok Kumar [1*], G.R. Umapathy[2] and Sunil Ojha[2]

[1]Material Research Laboratory, Department of Physics, Tezpur University, Tezpur 784028, Assam, India
[2]Inter University Accelerator Centre (IUAC), Aruna Asaf Ali Marg, New Delhi 110067, India

Nanocomposites of Reduced graphene oxide (rGO) and Poly (3,4-ethylenedioxythiophene): Polystyrene sulfonate (PEDOT:PSS) nanocomposites have been synthesized via *in situ* polymerization technique. The synthesized nanocomposite films have been implanted with Xe^+ ions at different fluences of 3.3×10^{14}, 3.3×10^{15} and 3.3×10^{16} ions cm^{-2}. FESEM images show the growth of carbon rich clusters in floral pattern at the fluence 3.3×10^{16} ions cm^{-2}. Raman spectra reveal the annealing of the nanocomposite at lower fluence of 3.3×10^{14} ions cm^{-2} and then increase in disorder parameter with further increase in ion fluence. The rGO/PEDOT:PSS hybrid nanocomposite implanted with 3.3×10^{16} ions cm^{-2} Xe^+ ions exhibits slightly different CV pattern with increase in fluence and at the fluence of 3.3×10^{16} ions cm^{-2}, drastic change in CV pattern is observed with lower oxidation potential (0.54 V) and higher anodic current density (48 mA cm^{-2}). The gradual change in CV pattern with fluence can be attributed to the gradual structural changes due to: (i) degassing, where the functional groups present in the nanocomposites transform to 'pre-carbon' structures, (ii) growth of carbon-rich clusters and formation of C=C bond network, (iii) the carbon clusters aggregate to form quasi-continuous carbonaceous layer and (iv) at the highest fluence i.e. 3.3×10^{16} ions cm^{-2}, the carbonaceous layer transforms to graphite like material [1]. 3.3×10^{16} ions cm^{-2} ion irradiated nanocomposite electrode exhibits enhanced cyclic stability of 93% as compared to the pristine one at 800th cycles.

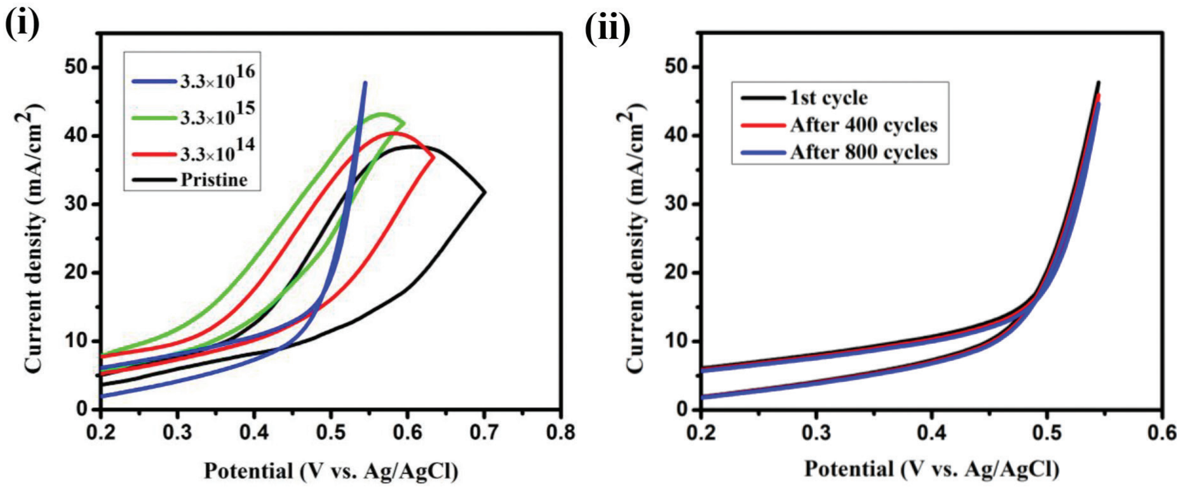

Figure: Cyclic voltammograms of pristine and irradiated rGO/PEDOT:PSS/ITO electrodes with different ion fluences in (i) presence of 0.5 M methanol containing 0.5 M NaOH solution at scan rate 50 mVs^{-1}.
(ii) cyclic stability of rGO/PEDOT:PSS/ITO electrode irradiated with 3.3×10^{16} ions cm^{-2} at a scan rate of 50 mVs^{-1}.

REFERENCES:

[1] V.N. Popok Rev. Adv. Mater. Sci 30 (2012) 1.

5.2.24 Ion irradiation study of Au-C_{60} nanocomposite thin film

Singhal Rahul*, Sharma Kshipra and Vishnoi Ritu

[1]Department of Physics, Malaviya National Institute of Technology-302017, India.

The interaction of light with metal nanoparticles is pointed out by Gustav Mie in 1908, this interaction results in oscillations of collective charge density confined to metallic nanostructures in resonance with the light field and this phenomena is known as surface plasmons resonance (SPR). Tuning of SPR is an interesting study and can be used in solar cells, sensors etc.

Here, we developed Au-C_{60} nanocomposite thin films using thermal co-evaporation method. Then ion irradiation was performed on the developed nanocomposite thin films at different fluences. After irradiating the films, we investigated the modifications occurred in the optical and structural properties of the films at different fluences.

The developed nanocomposite thin films were irradiated with swift heavy Au ions carrying energy of 120 MeV at various fluences using Pelletron accelerator at IUAC, New Delhi. The nanocomposite thin films were exposed to irradiation for an estimated time for each fluence. The films were irradiated at following fluences; 1e12, 3e12, 6e12, 1e13 and 3e13. The electronic (Se) and nuclear energy loss (Sn) for 120 MeV Au ions in Au-C_{60} nanocomposite film were estimated by SRIM 2013 program. After irradiating the films, we studied the modifications taken place in the optical, structural and electrical properties. In order to investigate the optical property, structural property, chemical property and electrical property, we used UV-visible spectroscopy, raman spectroscopy, XPS and I-V measurements and we obtained blue shift of ~117 nm in SPR wavelength. In this study, we got very interesting results which can be further used in the applications of sensors and solar cells.

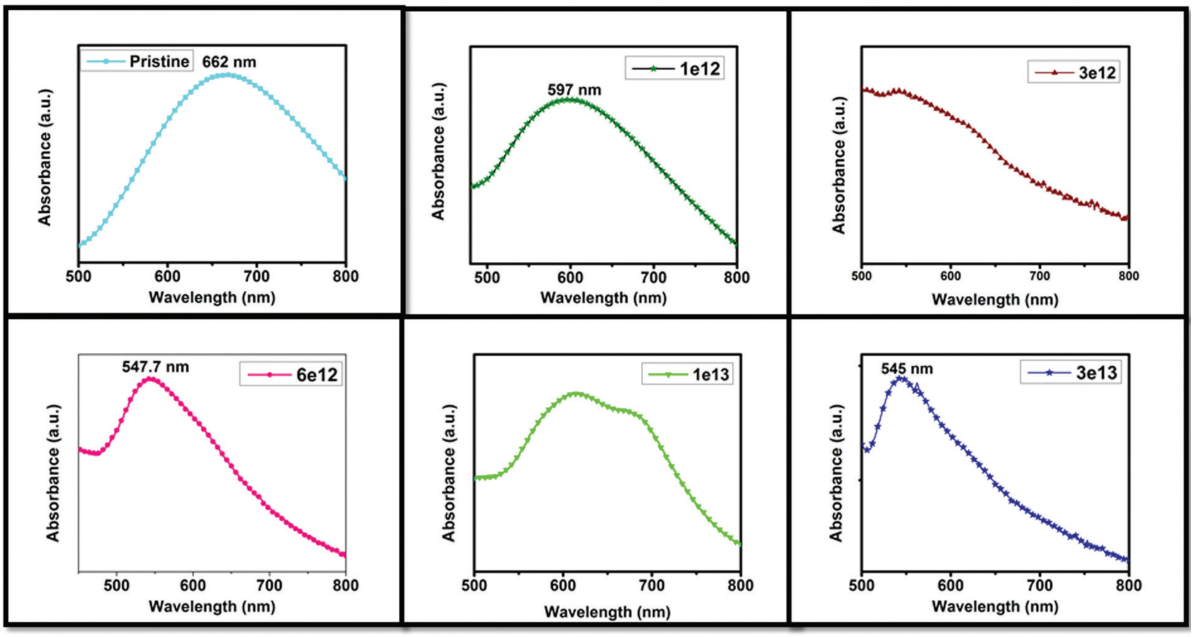

Fig.1. UV-visible absorption spectra of Au-C_{60} nanocomposite thin films at different fluences

5.2.25 Thermoelectric Properties of Fe Ion Implanted $CoSb_3$ Thin Films

Anha Masarrat[1,2], Anuradha Bhogra[1], Ramcharan Meena[1], Manju Bala[3], Ranveer Singh[4], Vineet Barwal[5], Chung-Li Dong[6], Chi- Liang Chen[7], T. Som[4], Ashish Kumar[1], A. Niazi[2] and K. Asokan[1*]

[1]Inter University Accelerator Centre, Aruna Asaf Ali Marg, New Delhi-110067, India
[2]Department of Physics, Jamia Millia Islamia University, New Delhi-110025, India
[3]Department of Physics, Delhi University, New Delhi-110007, India
[4]Institute of Physics, Bhubaneswar - 751005, India
[5]Department of Physics, Indian Institute of Technology Delhi, New Delhi-110016, India
[6]Research Center for X-ray Science, Department of Physics, Tamkang University, Tamsui, Taiwan 251
[7]National Synchrotron Radiation Research Centre, Hsinchu, Taiwan

In the present study, thin films of $CoSb_3$ phase were deposited on Si (100) substrates by pulsed laser deposition (PLD) using a polycrystalline target of $CoSb_3$. These films were implanted by 120 keV Fe-ions with three different fluences: 1×10^{15}, 2.5×10^{15} and 5×10^{15} ions/cm^2. All these films were well characterized for structural, electrical properties including Seebeck Coefficient, S, and electronic structures.

Figure. 1 shows the S for the Fe ion implanted $CoSb_3$ thin films. Inset shows the XRD pattern of the samples before and after annealing.

The S is found to vary with the fluences for a temperature range of 300 K to 420 K and found to be highest, i.e., 254 μV/K at 420 K for the film implanted with 1×10^{15} ions/cm^2. There is change of sign of S from negative for pristine film to positive for Fe implanted samples. X-ray absorption measurements confirm that Fe ions occupy the Co site in the cubic frame of the skutterudite and exist in 3+ oxidation state in this structure [1-3]. Our study shows that the Fe ion is implanted in $CoSb_3$ in Fe^{3+} state and Co ions are in divalent state. It is also found that the S of Fe ion implanted sample is around three times higher than that of Fe doped bulk sample.

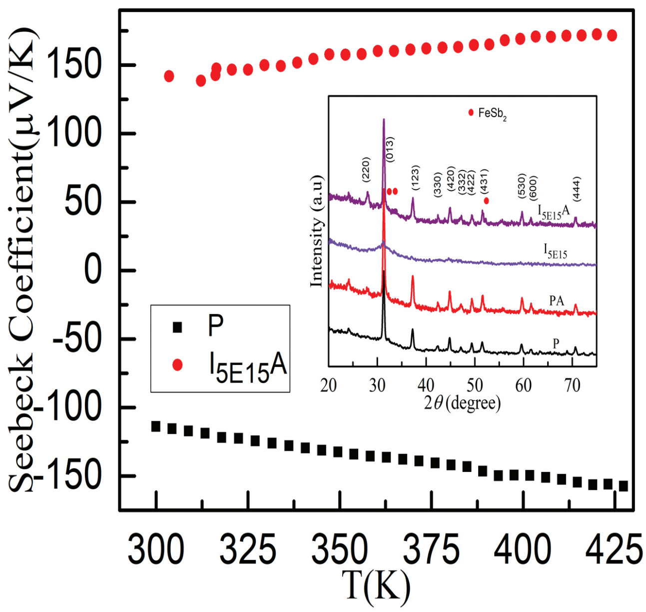

FIGURE 1. XRD pattern of pristine and post-irradiated TiO2/STO bilayer

REFERENCES:

[1] Yang, J., Meisner, G. P., Morelli, D. T. & Uher, C. Iron valence in skutterudites : Transport and magnetic properties of Co 1-x Fe x Sb 3. Phys. Rev. B 63, 1–11 (2000).

[2] Caillat, T., Borshchevsky, A. & Fleurial, J. -P. Properties of single crystalline semiconducting $CoSb_3$. J. Appl. Phys. 80, 4442–4449 (1996).

[3] Bala, M. et al. Evolution of nanostructured single-phase $CoSb_3$ thin films by low-energy ion beam induced mixing and their thermoelectric performance Manju. Phys. Chem. Chem. Phys. 19, 24886–24895 (2017).

5.2.26 Enhancement of thermoelectric properties of $TiO_2/SrTiO_3$ bilayer after Ar ion irradiation

Anuradha Bhogra[1*], Anha Masarrat[1], Ramcharan Meena[1], Dilruba Hasina[2], T. Som[2] and K.Asokan[1]

[1]Inter-University Accelerator Centre, ArunaAsaf Ali Marg, New Delhi-110067, INDIA
[2]Institute of Physics, Bhubaneswar - 751005, INDIA

TiO_2/STO bilayer was deposited on silicon substrate by PLD. The film was grown by ablation of STO bulk ceramic target at energy density of 4.2 J/cm^2 and target was rotated to ensure uniform deposition. The substrate temperature was kept at 700 °C and Ar gas was introduced at a pressure of 20 mTorr using mass flow controller. The thickness of each layer was kept 50 nm. Further, this film was irradiated by using 1 MeV Ar ion beam at a fluence of 1×10^{16} ion/cm^2 using Low Energy Ion Beam Facility (LEIBF) at Inter University Accelerator Centre (IUAC), New Delhi.

Figure 1 shows the XRD spectra of bilayer before irradiation and after irradiation. The pristine bilayer showed the mixed phases of TiO_2 and STO. The peaks in XRD spectra could be assigned to brookite and anatase TiO_2 and cubic STO. After irradiation, poor crystallinity was observed. Figure 1(b) shows the vacancies produced due to Ar irradiation calculated from TRIM simulations.

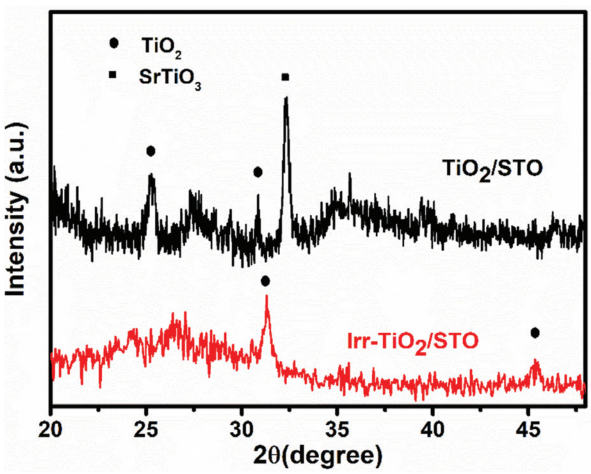

FIGURE 1. XRD pattern of pristine and post-irradiated TiO_2/STO bilayer

Figure 2 shows the variation of resistivity with temperature in the range of 300 to 420 K. Before irradiation, the sample was very much insulating (~$10^{12}\Omega$) to measure with the two probe measurements. After irradiation, resistivity drastically reduced to $1.5\times10^{-4}\Omega$-m and show semiconducting behavior with temperature. This change in resistivity can be attributed to the Ar irradiation induced oxygen vacancies in TiO_2/STO bilayer. For a comparison, the resistivity measurements have been tried for the 1 MeV Ar irradiated STO films deposited on silicon but resistance was very high to measure. This indicates that interface between TiO_2 and STO layer plays a role in enhancing the conductivity of the sample. It is expected that oxygen deficient TiO_2 film after irradiation may take out oxide ions from the STO layer and electrons get confined within interface layer.

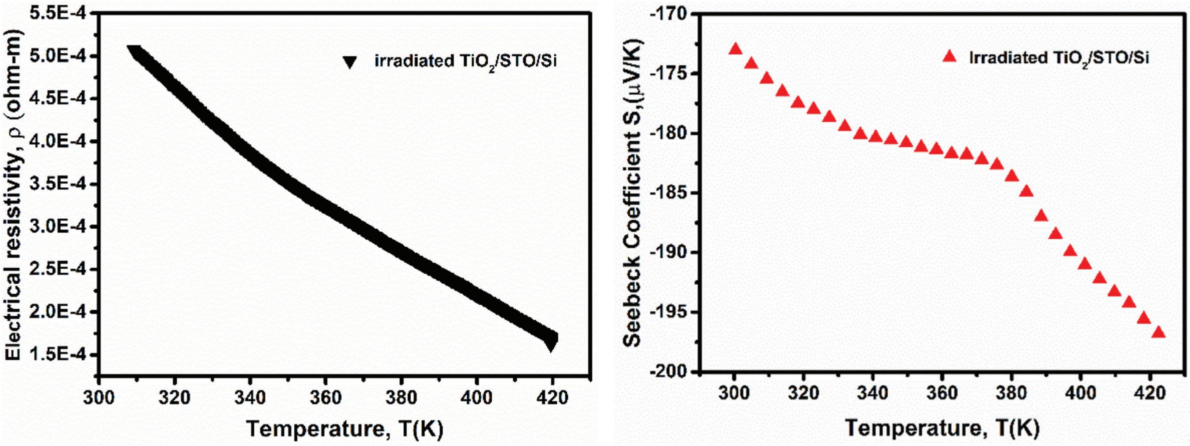

FIGURE 1. XRD pattern of pristine and post-irradiated TiO_2/STO bilayer

The temperature dependence of Seebeck coefficient is shown in figure. The magnitude increases with the temperature and shows semiconducting behavior. At 300 K the Seebeck coefficient reached 173 μV/K which is ~2.8 times larger than the bulk $SrTi_{0.98}Nb_{0.2}O_3$ (61 μV/K).

The TiO_2/STO bilayer was successfully deposited on silicon substrate by PLD. Further, this bilayer was irradiated by 1 MeV Ar ion beam. The XRD spectra recorded reveal the mixed phases of TiO_2 and STO before irradiation and decreased crystallinity after irradiation. The XAS measurements demonstrated the shifting of absorption spectrum to lower energy indicating the presence of oxygen vacancies. This is further observed in thermoelectric measurements where resistivity is dramatically reduced and Seebeck coefficient enhanced after Ar irradiation.

REFERENCES

[1] K. Szot, W. Speier, G. Bihlmayer and R.Waser, Nat Mater**5**, 312-320 (2006).
[2] H. Wang and C.Wang, Journal of Materiomics**2**, 225-236 (2016).
[3] S. A. Hayward and E. K. H. Salje, Phase Transitions **68**, 501-522 (1999).
[4] H. Ohta and K. Koumoto,Nature Materials**6**, 129-134 (2004).
[5] C. H. Chen and M.Hong, Applied Physics Letters**52**, 841-843 (1988).
[6] V. S. Lusavardi and A. Teplyakov, Surface Science **397**, 237-250 (1998).
[7] T. Teranishi and Y. Inada, Journal of American Ceramic Society **96**, 2852-2856 (2013).

5.2.27 Studies to understand the influence of morphology on semiconductor/electrolyte interface in photoelectrochemical splitting of water

Asha Kumari[1], Saif Khan[2], Vibha Rani Satsangi[3], Rohit Shrivastav[1], Rama Kant[4] and Sahab Dass[1*]

[1]Department of Chemistry, Faculty of Science, Dayalbagh Educational Institute, Dayalbagh, Agra,282005, India
[2]Inter-University Accelerator Center, New Delhi, Delhi -110067
[3]Department of Physics & Computer Science, Faculty of Science, Dayalbagh Educational Institute, Dayalbagh, Agra 282005, India
[4]Department of Chemistry, University of Delhi, Delhi, 110007, India

Nanostructured thin films of ZnO prepared by RF sputtering technique were successfully irradiated by low energy (100 KeV) Ar^+ ion beam at an incidence angle of 0°, 40° and 60°. Morphological modifications induced in the films due to ion beam irradiation were quantitatively characterized by Power Spectral Density analysis. Therefore, value of surface microscopic features viz. fractal dimension (D_H), lower (l) and upper cut off length scale (L) were calculated for the pristine and the irradiated samples. The samples were further studied for their photoelectrochemical (PEC) performance for water splitting. A correlation in the PEC performance and morphological surface features was established. It was found that the sample irradiated at 40° angle at the fluence of 5 x 10^{16} ions/cm^2 was found to possess maximum fractal dimension of 2.72, lower and upper cut off length scale of 3.16 nm and 63.00 nm respectively. This sample exhibited maximum photocurrent density of 3.19 mA/cm^2 at 1.23 V/RHE.

Experimental Details

Nanostructured thin films of ZnO were prepared by RF sputtering technique. These films were then subjected to low energy (100 KeV) ion beam irradiation conducted at LEIBF Facility, Inter University Accelerator Centre (IUAC), New Delhi. Irradiation of the films was performed at three different angles viz. 0° i.e. the normal angle of incidence, 40° and 60°, each irradiated at three different fluences 1 x 10^{16} ions/cm^2, 5 x 10^{16} ions/cm^2 and 1 x 10^{17} ions/cm^2. All the pristine and the irradiated films were characterized for thickness measurement (Surface profilometer), surface morphology (Field Emission Scanning Electron Microscopy, FE-SEM) and roughness measurement (Atomic Force Microscopy, AFM). Electrodes of the thin films were prepared and were subjected to electrochemical and photoelectrochemical treatment using a 300W Xenon arc lamp (Newport, RI, USA) with an intensity of 300 mW/cm^2.

Surface morphology analysis

Field-Emission Scanning Electron Microscope (FE-SEM) images of all the samples before and after irradiation is shown in Figure 1. FE-SEM image of Pristine ZnO film shows (Figure 1(A)) that preparation of the samples using RF sputtering technique resulted in the formation of nanopyramidal particles. A homogeneous and uniform deposition can be seen with densely packed particles. It could be concluded that lower fluences in all the angles of incidence caused sharpening or changing of morphology from nanopyramids to nanopspheres while highest fluence of 1x10^{17}ions/cm^2 resulted in complete distortion of the nanoparticles.

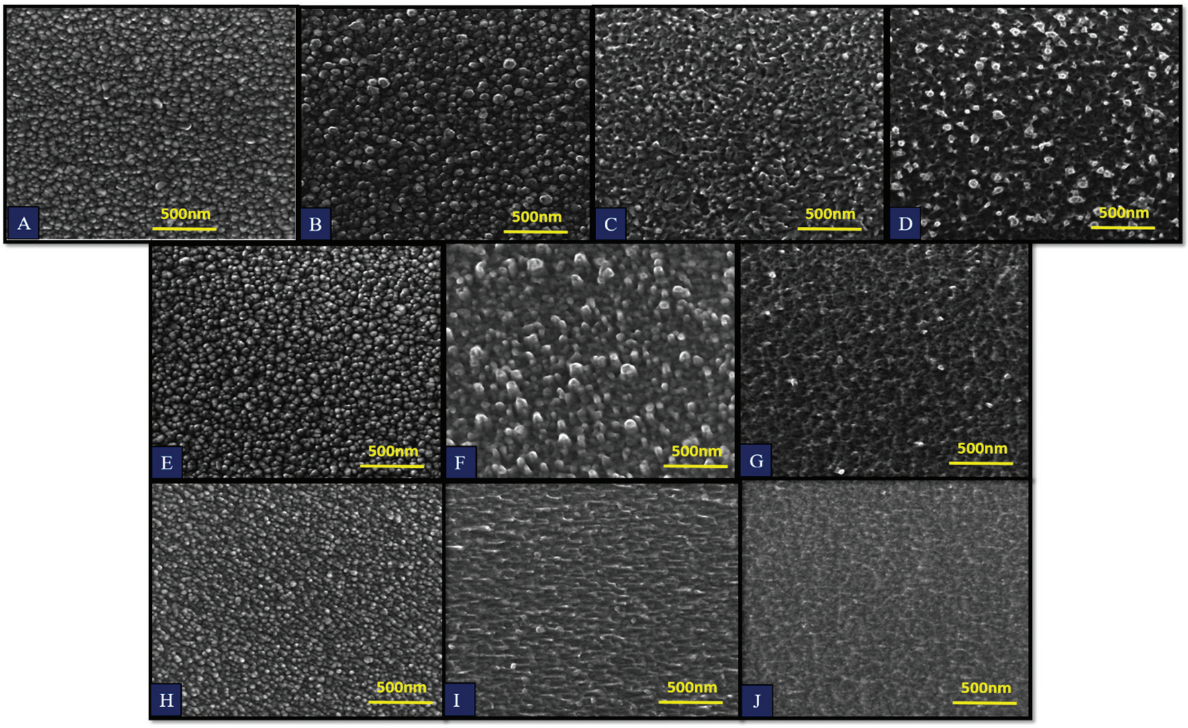

Figure 1. FE-SEM images of (A) Pristine ZnO, samples irradiated at (B) 0°, 1x10^{16} ions/cm^2, (C) 0°, 5x10^{16} ions/cm^2, (D) 0°, 1x10^{17} ions/cm^2, (E) 40°, 1x10^{16} ions/cm^2, (F) 40°, 5x10^{16} ions/cm^2, (G) 40°, 1x10^{17} ions/cm^2, (H) 60°, 1x10^{16} ions/cm^2, (I) 60°, 5x10^{16} ions/cm^2, (J) 60°, 1x10^{17} ions/cm^2

Atomic force microscopy analysis

AFM images of thin films were recorded to investigate their surface topography. As evident from the AFM images, a uniform and dense deposition of nanoparticles can be seen. All the images and structural pattern matches closely with the corresponding FE-SEM images of pristine and irradiated samples. ZnO films irradiated with angle of 40° appear rougher than the films irradiated at 0° and 60° This could be due to decrease in the cystallinity and deterioration of nanopyramids as revealed from XRD and FESEM results. It could be concluded that ZnO thin films irradiated with low energy ion beams (100 KeV) incidented at an angle of 40° enhances the nanoparticles morphology and surface topography.

Power Spectral Density (PSD) analysis

Power Spectral Density analysis was carried out for all the films before and after low energy ion beam irradiation treatment to determine the values of morphological parameters viz. l, L and D_H [1,2] as shown in Fig2.

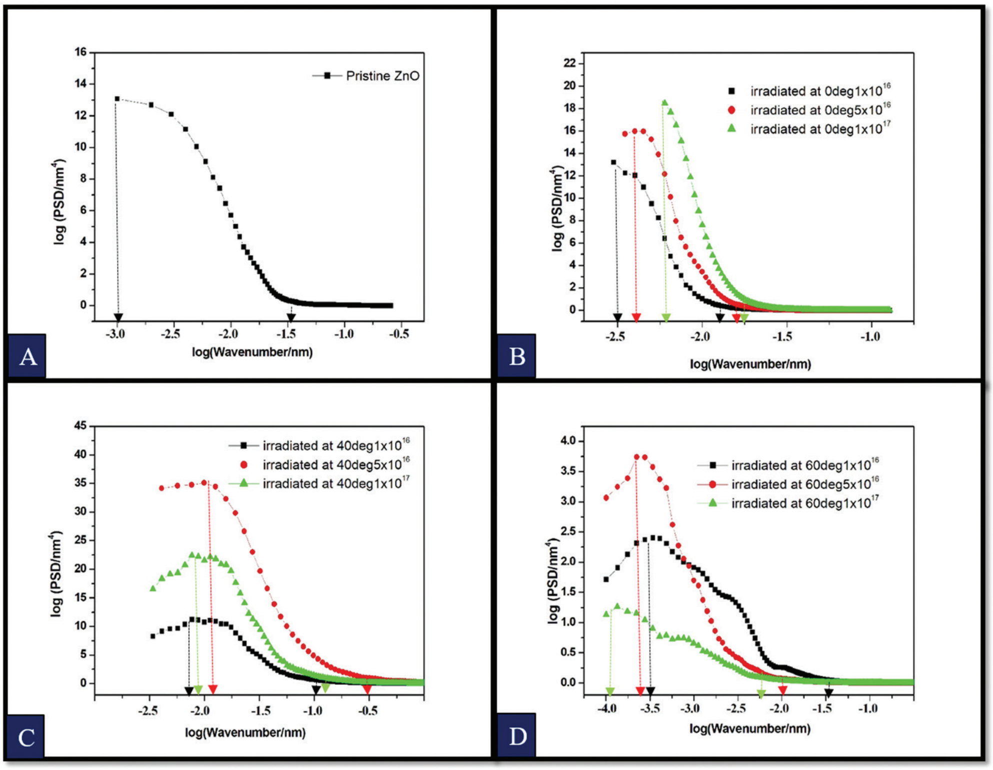

Figure 2. Power spectrum of (A) Pristine ZnO, samples irradiated at (B) 0°, (C) 40°and (D) 60°

Photoelectrochemical Studies

Photoelectrochemical density plots are shown in Figure 3. It is clearly evident from the figure that photocurrent density increases with the increase in the angle of irradiation and fluence up to 40°. Highest photocurrent density of 3.19 mA/cm^2 was obtained in case of the sample irradiated at the fluence of 5 x 10^{16} $ions/cm^2$.

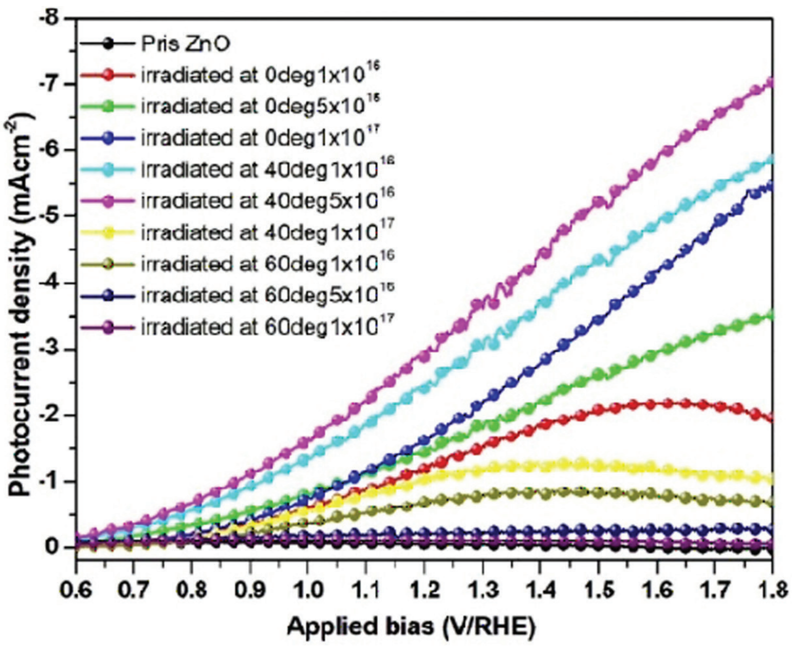

Figure 3. Photocurrent density curves under constant illumination for all ZnO samples in 0.1 M NaOH electrolyte

REFERENCES

[1] S. Dhillon, and R. Kant, Appl. Surf. Sci. 282 (2013), 105

[2] K. Asha et al, J. Power Sources, 432 (2019), 38

5.2.28 Ion implantation induced tunable resistive switching property of HfO_2 thin films

Dilruba Hasina[1], Sudheer[1], Rupam Mandal[1,2] and Tapobrata Som[1]

[1]SUNAG Laboratory, Institute of Physics, Bhubaneswar, Odisha-751005, India.
[2]Homi Bhabha National Institute, Training School Complex, Anushakti Nagar, Mumbai 400085, India

Towards developing next generation scalable HfO_2-based resistive switching (RS) memory devices, the efficacy of 30 keV Au--ion implantation to achieve tunable resistive switcging property at a threshold fluence of 1×10^{16} ions cm^{-2} and at ambient temperature is presented. The RS behaviour of as-grown and ion implantation films are confirmed by conductive atomic force microscopy (cAFM) technique. The different fluence of Au ions is used to tune the number density of defects per unit volume which becomes useful in the tuning of resistive switching properties. X-ray diffraction shows that both as-grown and implanted HfO_2 films are amorphous in nature, whereas atomic force microscopic studies show that all films are granular in nature and RMS roughness increases with increasing ion fluence. To investigate the variation in work function of ion implanted HfO_2 thin films at different fluences, Kelvin probe force microscopic studies are underway.

Experimental Details

As-grown HfO_2 films were implanted by 30 keV Au- ions at room temperature at incident angles of 0˚ and 45˚ with series of ion fluences in the range of 0.05-1×10^{16} ions cm^{-2}. The Au-ions were obtained from low energy ion beam facility (LEIBF) at IUAC, New Delhi. The Faraday cup was used to monitor the beam current (up to 2.4 μA). We maintained a working pressure of the scattering chamber is at 5×10^{-6} mbar for all fluences. The projected range and the atomic concentration ratio of Hf and O at the HfO_2 surface as a function of the fluence were simulated by the TRIDYN simulation code. X-ray diffraction studies were carries out to identify the crystalline nature of HfO_2 films, whereas atomic force microscopy-based studies were performed to study the morphology, roughness, and nanoscale transport property of HfO_2 films before and after Au-ion implantation. To investigate the variation in work function of ion implanted HfO_2 thin films at different fluences, Kelvin probe force microscopic studies are underway. Further to this, x-ray photoelectron spectroscopic measurements were performed to study the composition and nature of chemical bonds in the films.

Results and Discussion

HfO_2 films were grown by RF magnetron sputtering technique by applying 100 W power and a commercially available target (99.99% purity) and Si substrates coated with different back contacts. It is known that the crystallinity plays an important role in determining the electrical properties of a thin film. Thus, the XRD measurements of all HfO_2 films are carried out under similar conditions (eg., scan speed, scan rate, slit width) and presented in Figure 1. XRD data reveal that as-grown HfO_2 films are amorphous and remain so even after ion implantation.

For investigation on the resistive switching (RS) behavior of HfO_2 films before and after implantation, detailed I-V measurements have been carried out by cAFM using standard two-terminal devices (Ti/HfO_2/Pt). The local I-V characteristics of the Rs device fabricated under the fluence of 1×10^{16} ions cm^{-2} (ion immpalatation angle: 45˚) is depicted in Figure 2(a). However, no RS behavior is observed for the as-grown (current map not shown) and ion irradiated samples up to a fluence of 5×10^{15} ions cm^{-2} even after applying a sweeping voltage of ±10V. However, a distinct local RS behavior has been observed within an applied bias of ±2V for a fluence of 1×10^{16} ions cm^{-2} with SET and RESET voltages are 1.92 V and 0.76 V, respectively. Figure 2(b) shows the cAFM image of the top HfO2 layer having a fluence of 1×10^{16} ions cm^{-2} using +2 V tip bias.

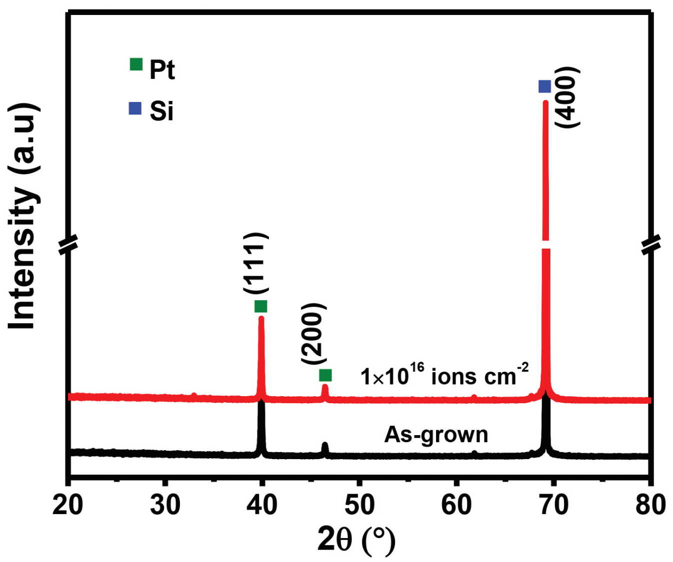

Figure 1. XRD spectra of as-grown and implanted HfO_2 films.

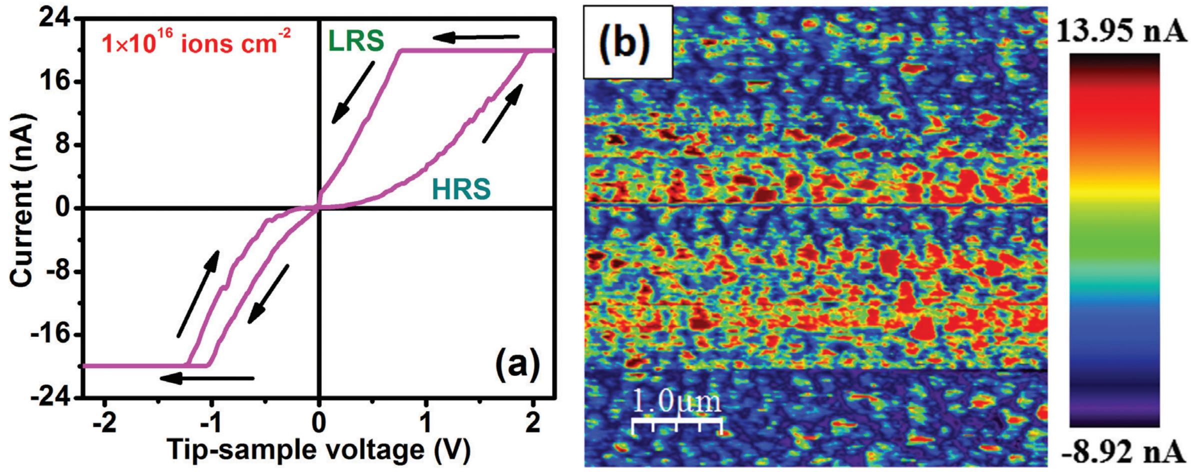

Figure 3. Power spectrum of (A) Pristine ZnO, samples irradiated at (B) 0°, (C) 40°and (D) 60°

X-ray photoelectron spectroscopic measurements show increasing degree of oxygen vacancies in the films with fluence. KPFM measurements are underway to probe implantation-mediated change in the work function of the films to correlate with the observed RS behavior of the films.

5.2.29 Study on the room temperature photoluminescence property of Al implanted ZnO nano rods

Amaresh Das[1], Debdulal Kabiraj[2] and Durga Basak[1]

[1]School of Physical Sciences, Indian Association for the Cultivation of Science, Kolkata-700032, India
[2]Inter-University Accelerator Centre Aruna Asaf Ali Marg, New Delhi-110067, India

We present a detailed study on the effect of Al ion implantation in the room temperature (RT) photoluminescence (PL) properties of ZnO nanorods (NRs). Irrespective of growth technique, Pl spectrum of ZnO shows two peaks, one in the ultraviolet region due to near band edge emission (NBE) and one broad peak in the visible region due to defect levels (DL) within the band gap. When ZnO NRs array film is implanted with Al ions, an by 1.4 times in the ratio of INBE / IDL has been observed for the ZnO NRs implanted with a 5×10^{13} ions/cm^2 fluencies of Al ions. Beyond 5×10^{13} ions/cm^2 , the ratio is decreased with an increase in the Al dose, though it is always higher than that of the pristine sample up to a Al dose of 1×10^{15} ions/cm^2. Finally, a 0.87 times drop in the ratio is observed for the highest dose (1×10^{16} ions/cm^2) Al implanted sample.

Experimental details:

ZnO NRs were grown on glass substrates by aqueous chemical growth (ACG) method.[1] The cleaned glass substrates were spin coated by 0.1 M solution of zinc acetate ($Zn(CH_3COOH)_2$) to obtain seed layer of ZnO and then immersed into a mixed aqueous solution of $(CH_3COO)_2Zn\cdot2H_2O$ and hexamethylenetetramine ($(CH_2)_6N_4$) in a beaker. The beaker containing the precursor and the substrate was kept at 80 °C for growing ZnO NRs and after growth, the substrates were removed from the solution, rinsed in de-ionized water and dried. The as grown ZnO NRs were implanted with 100 keV Al ions having various doses ranging from 1 x 10^{13} to 1 x 10^{16} ions/cm^2 at IUAC, New Delhi using the LEIBF facility. After Al implantation, the implanted ZnO NRs were annealed in Ar ambient at 450 °C for 60 min. The nomenclature of the Al implanted samples according to the dose are as follows: Al/ZnO113 (1 x 10^{13} ions/cm^2), Al/ZnO513 (5 x 10^{13} ions/cm^2), Al/ZnO114 (1 x 10^{14} ions/cm^2), Al/ZnO115 (1 x 10^{15} ions/cm^2), Al/ZnO116 (1 x 10^{16} ions/cm^2. The implanted NRs were characterized using Xray diffractometry (XRD), field emission scanning electron microscopy (FESEM), transmission electron microscopy (TEM), high resolution transmission electron microscopy (HRTEM), RT PL, X-ray photoelectron spectroscopy (XPS), techniques.

Results and discussion:

The XRD patterns of the pristine and ZnO NRs implanted with different doses of Al and Ar show the presence of (100), (002), (101), (102), (103) and (110) peaks of hexagonal wurtzite ZnO (JCPDS card No. 36-1451). The (002) diffraction peak is the strongest among all peaks, implying the growth of NRs along <002> direction. It has been observed that the (002) peak position of the Al implanted ZnO NRs shifts towards the lower 2θ value as compared to the pristine ZnO NRs indicating an existence of the tensile stress.[2] The values of the lattice parameter (c) and full with at half maxima (FWHM) of (002) peak have been observed to be increased as doses of Al is increased.

To understand the microstructure of the Al implanted ZnO NRs at various doses, the SEM, measurement was performed. As seen in top view FESEM images, the hexagonal ZnO NRs have been grown vertically on the seeded glass substrate, which is at par with the XRD results. After implantation with Al, the rod-like structure of ZnO NRs has been maintained. However, for higher dose Al implanted NRs (Al/ZnO116) tips of the NRs have been modified slightly. The morphological changes due to Al implantation have been again examined by HRTEM analysis. The lattice fringes are clearly observed in the HRTEM image for pristine sample, which indicates that the pristine ZnO NRs are free of extended defects such as dislocations, stacking faults, defect clusters etc.[3] The HRTEM image of lower Al implanted NRs is similar to that of pristine, indicating to the complete recovery of implantation induced structural damages due to annealing at 450 ºC. At higher dose of Al, the stacking fault arises due to the distorted lattice arrangement of (0002) planes.

Figure 2a shows the RT PL spectra of pristine and some representative Al implanted samples. All the samples show the strong NBE emission in UV region and a broad emission in the visible. As implanted samples show emission intensities lower than the pristine sample. For implanted and post-implantation annealed samples, the PL properties are highly improved.

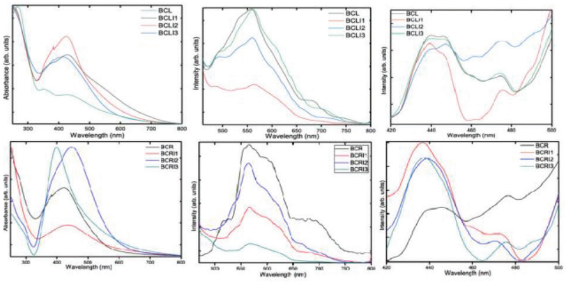

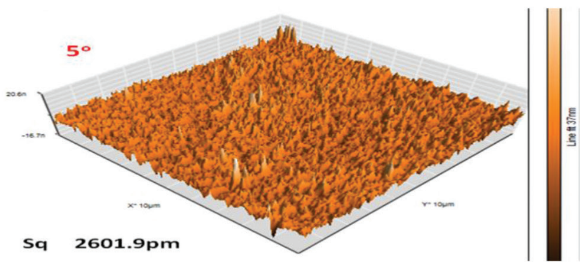

Figure 2a shows that I_{NBE} is maximum for 1 x 10^{13} ions/cm^2 Al implanted NRs. The highly enhanced I_{NBE} for lower dose can be assigned to a recovery of the lattice damages by the annealing treatment, which is supported by our HRTEM results. With increase in the Al dose, extended defects appear,[3] which act as non-radiative recombination centers results reducing PL emission at higher Al dose. However, a blue shift of is found in the NBE peak position for the higher dose (1x 10^{16} ions/cm^2) of Al implanted NRs. Similar to I_{NBE}, the intensity of DL emission is also increased at lower dose and then is gradually decreased for higher dose (The inset of Figure 2a). The DL emission center is seen to be shifted towards higher energy side (~2.4 eV) as compared to the pristine one, which means the visible emission shifts from yellow-orange to green one. V_{Zn} type of defects have been well accepted to be responsible for the green emissios.[4-5] As dose increases, the net effect of V_{Zn} in green emission is expected to be decreased. The creation of radiative recombination path is also a factor for reduction in the PL emissions. The ratio of INBE / IDL has been calculated as summarized by the bar diagram in Figure 2b. It is observed that the value for the pristine sample is 54, while the value is highly enhanced for a lower doses of 1x 10^{13} ions/cm^2 Al implantations to 73. As the dose increases, the INBE /IDL decreases gradually and for 1 x10^{16} ions/cm^2 it becomes 47.

Further study of excitation power dependence of PL spectra confirms that the Al related donor bound excitons are responsible for the radiative recombinations and enhancement in the I_{NBE} / I_{DE} ratio at lower Al dose. At higher Al dose, the extended defects forms act as the non radiative recombination centers, and as a result, the INBE is reduced.

To confirm the presence of Al inside ZnO, XPS measurements were also carried out for Al/ZnO1[16] sample. The observed peak with a binding energy around 74.37 eV confirms the successful substitution of Zn^{2+} ions by Al^{3+} ions in the ZnO lattice of Al/ZnO116 sampless.[6-7] Detailed analyses of the O 1s peak provide support of the formation surface defects.

Conclusions:

In, summary, we demonstrate the effect of Al ion implantation on the RT PL properties of ZnO NRs. The formation of neutral Al donor bound excitonic recombination centers is responsible for PL enhancement for the lower dose Al implanted samples. This Work has been communicated and is under review at Applied Surface Science, 2019.

REFERENCES:

[1] M. Mahanti, T. Ghosh and D. Basak, Nanoscale, 2011, 3, 4427-4433.

[2] F. Mouzaia, D. Djouadi, A. Chelouche and L. Hammiche, Cham, 2018.

[3] L. D. Yao, D. Weissenberger, M. Durrschnabel, D. Gerthsen, I. Tischer, M. Wiedenmann, M. Feneberg, A. Reiser and K. Thonke, J. Appl. Phys., 2009, 105.
[4] F. Fabbri, M. Villani, A. Catellani, A. Calzolari, G. Cicero, D. Calestani, G. Calestani, A. Zappettini, B. Dierre, T. Sekiguchi and G. Salviati, Sci Rep, 2014, 4.
[5] D. C. Reynolds, D. C. Look and B. Jogai, J. Appl. Phys., 2001, 89, 6189-6191.
[6] T. N. Sky, K. M. Johansen, V. Venkatachalapathy, B. G. Svensson, and L. Vines, Physical Review B, 2018, 98, 245204.
[7] H. Lee, K. Sivashanmugan, C. Y. Kao and J. D. Liao, Jpn. J. Appl. Phys., 2017, 56.

5.2.30 Tuning of PMA in trilayer films by ion irradiation technique

A. K. Sahoo[1], A. Talapatra[1,2], J. A. Chelvane[3], and J. Mohanty[1]

[1]Nanomagnetism and Microscopy Laboratory, Department of Physics, Indian Institute of Technology Hyderabad, Kandi, Sangareddy, 502285, Telangana, India
[2]Department of Electrical and Computer Engineering, National University of Singapore, 117576 Singapore
[3]Advanced Magnetics Laboratory, Defence Metallurgical Research Laboratory, Kanchanbagh, Hyderabad 500058, India

Tuning of perpendicular magnetic anisotropy (PMA) of the material systems is a keen interest of scientific communities as well as industries. Trilayer magnetic films are irradiated by Ar^+ ions with two different energies viz. 50 and 100 KeV at 300K. It is observed that as energy in- creases, PMA abruptly decreases. Magnetic domains, which was observed in as-deposited film, became deteriorated at 50 and 100 KeV. Roughness and defects of the irradiated samples are progressively increased as energy is increased.

Experimental Details

Trilayer film [TbFe(100nm)/ GdFe(50nm)/ TbFe(100nm)] was prepared on the Si <100> wafer by e-beam evaporation technique. Ar^+ ions were used for irradiations in this case. Film was irradiated with two different energies, 50 and 100 KeV, at constant ion fluence of 10^{14} ions/cm^2. Samples are kept perpendicular to ion fluxes.

Magnetic films exhibiting PMA, have a great importance towards data storage device and read/write heads because of its thermal stability, high coercivity, and large data storage capacity (nearly 1 Tb/in^2). PMA can be tuned by varying film compositions, growth conditions (variation in deposition pressure, and substrate temperature), and external treatments (like thermal annealing, ion implantations, and ion irradiations etc.). Ion irradiations can induce changes in structural, magnetic, and morphological properties of films [1]. TbFe(100nm)/ GdFe(50nm)/ TbFe(100nm) film was irradiated in order to observe the modification in magnetic domains and PMA.

Atomic force microscopy (AFM) [Fig. 1(a)] and corresponding magnetic force microscopy (MFM) [fig. 1(b)] images of the as de- posited and irradiated films are shown in Fig. 1. It is observed that irradiated films show slightly higher roughness as compared to the as-deposited film. As-deposited film has roughness of around 1 nm whereas, irradiated films have roughness around 1.5 nm. Fig. 1(b) (left) represents MFM image of The as-deposited film. This image contains two distinct contrasts, red and yellow colors. Yellow color represents up-magnetization, whereas red color represents down-magnetization for the out-of-plane magnetized domains. One can clearly observe the patch-kind of domains are present in the as-deposited film. These magnetic domains form in order to minimize the magnetostatic energy of the system. As the film is irradiated with 50 KeV and 100 KeV energies, magnetic domains became deteriorated severely. Middle and right images of Fig. 1(b) represent MFM images of 50 and 100 KeV, respectively. The magnetic phase contrast of irradiated MFM images (0.4degree) are weaker compared to as deposited MFM image (1deg). Further in-depth characterization followed by micromagnetic modeling can provide more details on tuning of PMA of the films as a result of ion irradiation.

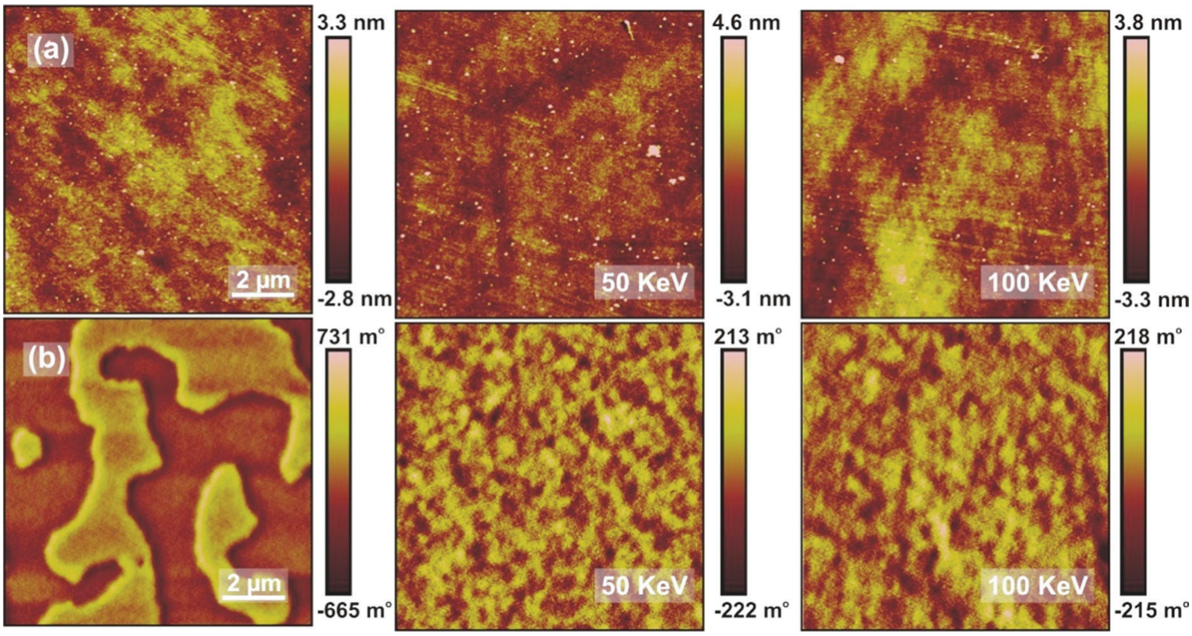

Figure 1: (a) Topography images of as-deposited TbFe(100nm)/ GdFe(50nm)/ TbFe(100nm) film (left), at 50 KeV (middle), and at 100 KeV (right) (b) Corresponding MFM images of the film. MFM images are free from topographic influences.

REFERENCE:

[1] Pawanpreet Kaur, K.K. Sharma, Rabia Pandit, R.J.Choudhary, and Ravi Kumar, Journal of Magnetism and Magnetic Materials, 398 (2016) 220-22.

5.2.31 Enhancement of exchange bias in Ni-NiO bilayer films implanted with Cu ions

Lisha Raghavan[1], Sunil Ojha[1] and D Kanjilal[1]

[1]Inter University Accelerator Centre, New Delhi.

Exchange bias refers to the shift in hysteresis loop of a ferromagnet (FM) in contact with an antiferromagnet (AFM) on cooling below the Neel temperature of the AFM. These kinds of exchange coupled systems are an integral part of magnetic tunnel junctions and spin valves [1]. Exchange bias has been observed in bilayer films, core shell structure, nanotubes, nanoparticulates and so on [2-4]. Exchange bias depends on various factors like FM-AFM thickness, interface, crystallinity etc. and can be tuned by various methods. Defect creation and doping the layers with non magnetic ions has been proven as a suitable way to tune exchange bias [5]. Doping the layers can be done effectively using ion implantation as the energy can be chosen judiciously to dope at the required depths.

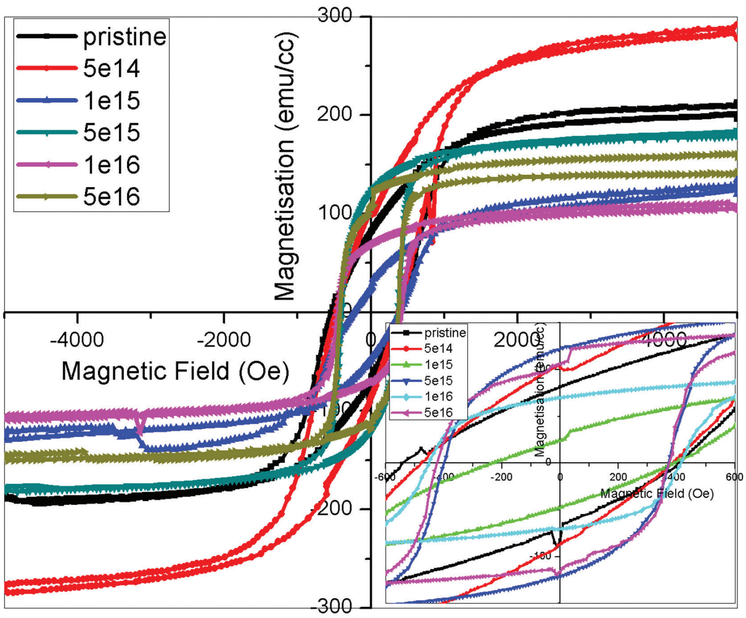

Figure1. Hysteresis loop of Ni-NiO films at 10 K

In the present work Ni films were prepared by thermal evaporation and annealed at 400ºC for 1 hour to form the NiO layer. The film thickness was measured by Rutherford Backscattering Spectrometry (RBS) and found to be 100 nm thick NiO and 40 nm thick Ni layer. 100 keV Cu ions were implanted in the films and their range in NiO was 42 nm. That is 100 keV Cu ions get implanted in NiO layer. The films were implanted with various fluences ranging from 5e14 to 5e16 ions/cm^2. Hysteresis loop were measured after cooling the system from 300K to 10 K in the presence of 1.5 T magnetic fields. It was observed that the pristine film exhibited an exchange field of -72 Oe. On irradiation the exchange field increased and at a fluence of 1e15 maximum value of +72 Oe was obtained. The exchange bias shifted to positive value on ion implantation. On further increase of ion fluence exchange field decreased and again shifts to negative values.

The exchange bias was tuned effectively by Cu ion implantation.

REFERENCES:

[1] J. Nogués, J. Sort, V. Langlais, V. Skumryev, S. Suriñach, J.S. Muñoz, and M.D. Baró, Phys. Rep. 422 (2005) 65.

[2] A. Roy, J.A. De Toro, V.S. Amaral, P. Muniz, J.M. Riveiro, J.M.F. Ferreira, J. Appl. Phys. 115 (2015) 073901

[3] H.L. Chaghouri, F. Tuna, P.N. Santhosh, and P.J. Thomas, Solid State Comm. 230, (2016) 11

[4] T. Yu, Z.W. Zhang, Y.H. Xu, Y. Liu, W.J. Li, Y. Nie, X. Zhang, and G. Xiang, J. Magn. Magn. Mater. 429 (2017) 74

[5] P. Miltényi, M. Gierlings, M. Bamming, U. May, G. Güntherodt, J. Nogués, M. Gruyters, C. Leighton, and I.K. Schuller, Appl. Phys. Lett. 75, (1999) 2304

[6] A.Mougin, T. Mewes, M. Jung, D. Engel, A. Ehresmann, H. Schmoranzer, J. Fassbender, and B. Hillebrands, Phys. Rev. B 63 (2001) 060409-1.

5.2.32 Effect of alpha irradiation on transition metals free and transition metals-containing high-level nuclear waste base glasses

Prince Rautiyal[1*], Pawan K. Kulriya[3], Ruth Edge[2], Laura Leay[2], Alan H. Jones[1] and Paul A. Bingham[1]

[1]Materials and Engineering Research Institute, Sheffield Hallam University, Sheffield, UK,
[2]Dalton Cumbrian Facility, University of Manchester, Cumbria, UK,
[3]Inter-University Accelerator Centre, New Delhi, India.

Performance assessment of high-level radioactive waste (HLW) glasses against radiation damage is of crucial importance to ensure safe and economic disposal over geological disposal periods (tens of thousands to a million years) [1]. This work aims to study alpha irradiation effects in simple glasses using mainly EPR spectroscopy (electron paramagnetic resonance), UV-Vis IR optical absorption spectroscopy and Raman spectroscopy. Alpha irradiation induced defects in two international glasses with and without transition metals namely UK-MW lithium-sodium borosilicate and Indian sodium-barium borosilicate which are being used as immobilization glass matrices for HLW by the UK and India, will be reported. This report presents methodologies and the work underway to achieve the aims of the study.

Experimental Details

Sample prep: All the glasses were prepared using melt-quenched method and annealed below glass transition temperature. Glasses were then cut into small thin samples of thickness ~1mm using a diamond precision cutter. They were then polished using SiC sheets up to grit size of 1000 (approximate size of 8.4 micron).

Irradiations at IUAC: Glasses were irradiated at Inter university accelerator center, Delhi, India using low energy ion beam facility (LEIBF) with a He^{2+} of 650 KeV to simulate the damage from alpha particles. Indian and UK-MW base glasses with and without dopants were irradiated with four different doses; 1x 10^{15}, 1x 10^{16}, 5 x 10^{16} and 1 x 10^{17} ions per square cm.

Raman spectroscopy: Raman spectra on pristine and irradiated samples were acquired using a depolarized 532nm excitation laser wavelength on a Thermo Scientific DXR2 Raman imaging microscope.

Optical absorption spectroscopy: UV-Vis IR optical spectroscopic measurements were done on the pristine and irradiated samples to observe the irradiation-induced absorption bands.

EPR spectroscopy: First derivative continuous wave powdered EPR spectra will be recorded for all the pristine and irradiated glasses at room temperature using an X-band, frequency of 9.6 GHz, EPR Bruker spectrometer [2].

REFERENCES:

[1] R. Ewing, W. Weber and F. Clinard, "Radiation effects in nuclear waste forms for high-level radioactive waste", Progress in Nuclear Energy, vol. 29, no. 2, pp. 63-127, 1995.

[2] M. Mohapatra, R. Kadam, R. Mishra, C. Kaushik, B. Tomar and S. Godbole, "Gamma Radiation-Induced Changes in Trombay Nuclear Waste Glass Containing Iron", International Journal of Applied Glass Science, vol. 4, no. 1, pp. 53-60, 2012.

5.2.33 Mimicking neutron irradiation impact on insulating materials by SHI and low energy ion beam

Sejal Shah

ITER-India, Institute for Plasma Research, Bhat, Gandhinagar, 382428, India

Collaborators:

1. Sunil Kumar, A. Chakraborty. ITER-India, Inst. for Plasma Research, Bhat, Gandhinagar
2. I. Sulania, F. Singh. IUAC, New Delhi
3. V. Sathe, V. Reddy. IUC, Indore

The present study is undertaken to investigate low energy ion beam effect on Al_2O_3. Due to limitation of neutron sources for long operational period and limited fluxes, ion beam is used as surrogate techniques for neutron irradiation. Damage calculations at different fluences for ion beam are carried out using TRIM. 300 keV Ar^{6+} ion beam is used for present study for the fluence ranging from 5×10^{11} ions/cm^2 to 1×10^{16} ions/cm^2. Impact of radiation on structural material properties is studied using different characterization techniques such as Raman, PL, XRD and AFM. Raman analysis shows defect density increase after irradiation at lower fluences where defect annealing at higher fluence. GIXRD data shows the defect creation at lower fluence up to 1×10^{14} ions/cm^2 whereas at higher fluence re-crystallization starts. Re-crystallization/annealing are explained by beam current heating of material. XRD study confirms no sign of amorphization even at highest fluence 1×10^{16} ions/cm^2 used for the irradiation. The results are further validated by Raman and PL study. Overall results confirm the structural integrity of the material for the applied radiation level.

Reference:

1. “Structural investigation of low energy ion irradiated Al_2O_3” Sunil Kumar, Sejal Shah, I. Sulania, F. Singh, A. Chakraborty, J. of Ceramic International.
2. “Radiation Impact on Ceramic materials Intended for Nuclear Reactor Applications” Sejal Shah, Sunil Kumar, S. Vala, R. Kumar, M. Abhangi, I. Sulania, F. Singh and A. Chakraborty.. Presently under review at Publication committee of ITER-India and soon will be submitted to IEEE Transaction on Plasma Science.

5.2.34 Oxide heterostructures on ion-implanted $SrTiO_3$

Ojha Shashank[1], Patel Ranjan[1], Kumar Siddharth[1], Mandal Prithwijit[1], Ojha Sunil[2], Devrani[2], K. Asokan[2] and Middey Srimanta[1]

[1]Department of Physics, Indian Institute of Science, Bangalore-560012, India.
[2]Inter-University Accelerator Centre, New Delhi-110067, India.

Utilizing the spin degrees of freedom is the basic idea for spin-based electronics, where, it is not the electron’s charge but the electron’s spin that carries information and offers opportunities for a new generation of devices with new functionalities[1]. Discovery of two-dimensional electron gas (2-DEG) at oxide interfaces has attracted huge attention in the recent years and is believed to play a pivotal role in realization of next generation oxide-based electronics[2]. In spite of various attempts to realize magnetic 2-DEG at oxide interfaces, creating and manipulating spin polarized 2-DEG at complex oxide interfaces has remained an experimental challenge so far. In the past, much of the attention has been paid to the interface between $LaAlO_3$ and $SrTiO_3$ (LAO/STO). Emergent magnetism at LAO/STO interface is very weak and the microscopic origin of ferromagnetism[3] at LAO/STO is highly debated. Alternatively, ferromagnetic layers have been used to induce the spin-polarization in 2DEGs but room temperature ferromagnetic 2-DEG remains elusive so far.

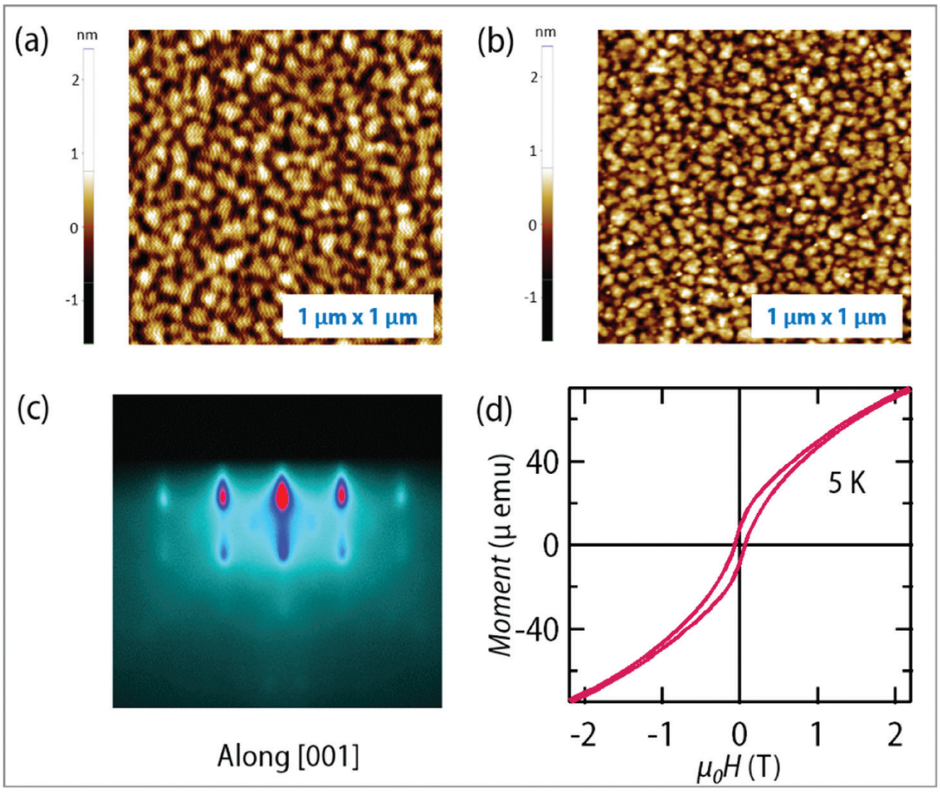

Figure 1: (a) AFM image of implanted substrate after annealing. (b) AFM image, (c) RHEED image along [001] direction (d) M vs magnetic field for 5 u.c. γ-Al_2O_3 film on 5% Co:STO (001).

In order to realize magnetic 2-DEG, we are combining two very different techniques: ion implantation and thin film growth. To introduce magnetic moment, various doses of Co ions have been introduced in single crystalline STO substrates by negative ion beam implantation technique in low energy negative ion beam facility of IUAC. These implanted substrates were post annealed in N_2 gas to restore the crystallinity of the substrate. Fig. 1(a) shows the AFM image of the substrate after annealing. The single crystallinity was confirmed by reflection high energy electron diffraction (RHEED). 4 nm of Al_2O_3 was grown on such Co-implanted STO substrates by pulsed laser deposition in Indian Institute of Science. The AFM image (Fig. 1(b)) and RHEED pattern (Fig. 1(c)) testify the success of the epitaxial growth. Magnetization vs field measurement reveals that this film is indeed ferromagnetic (Fig. 1(d)). However, the film does not exhibit metallic behavior. Optimization of growth conditions to achieve 2-DEG on these implanted substrates is under progress.

REFERENCES:

[1] I. Zutic et al., Rev. Mod. Phys. **76,** 2 (2004).
[2] E. Lesne et al., Nat. Mater. **15,** 1261 (2016).
[3] A. Brinkman et al., Nat. Mater. **6,** 493 (2007).

5.2.35 Low Ion Beam Induced Joining of Strontium Manganate ($SrMno_3$) Nanowires and their Surface Modification in Various Nanodevices Application

Manoj K Rajbhar and Shyamal Chatterjee*

School of Basic Sciences, IIT Bhubaneswar, Odisha-752050, India.

The focal point of our work is to comprehend the effect of ion irradiation treatment on $SrMno_3$ nanowires in network form, especially on their surface properties and in addition the potential outcomes and constraints to tune these properties. We have studied the joining/welding of mesh of nanowires with increase ion source energy at 50 keV, and 80 keV and the dynamics of controlling the wetting properties of fluids on nanostructured surfaces by varying the ion fluences of 5×10^{15}, 8×10^{15}, 1×10^{16}, 2×10^{16}, and 3×10^{16} ions/cm^{-2} respectively, which covered the whole conceivable range of entire wetting (from the superhydrophilic to superhydrophobic). This type of unique control on wettability is achieved by varying the ion energy and fluence. The change in wetting behaviour has vast application in different areas of interest, particularly in microfluidics, as a Laban-a-chip in making nanodevices, chemical micro reactors, microelectronics to control the thermal property, communication based on optical property, drag deliveries, self-cleaning mechanism etc as well as many modern well developed other areas [1]. We will mainly concentrate on the most recent advances in the synthesis of metal nanowires, specifically of $SrMnO_3$ (a perovskite) nanowires, and in addition their properties and a few applications[2]. These nanowires are basically intriguing from the perspective of their wetting properties, which emphatically rely upon the nanowires size and shape. The wetting properties are established relation between the surface property interaction of nanomaterials with incident ion irradiation at different ion energy (varying from 3 keV to 100 keV) and various fluences. Here we also discuss the bending and welding (joining) of Strontium Manganite ($SrMnO_3$) nanowires at the large scale, induced by N^+ ion irradiation at different ion energies and various ion fluences [3]. Transmission electron microscopy (TEM) and field emission scanning electron microscopy (FESEM) studies pointed out interesting structural modifications and joining of the randomly orientated nanowires induced by ion irradiation. The Ion energy above 50 keV having different ion fluences clearly show the joining between two adjacent nanowire in a very large scale, this large scale random bending and joining of the nanowires, at higher energy and higher fluences shows different type of shape of the junction [4].

Thin/ Thick film of $SrMnO_3$ sample are prepared by spin coating and drop casting the liquid sample which is well stirred ultra-sonicated mixture of few milligram $SrMnO_3$ n powder in highly pure 10 ml ethanol bought from Sigma Aldrich, on preheated (~50°C) highly conducting n-type (100 oriented) silicon substrate. The ion irradiation experiments for low ion beam energy were done at energies 50 keV, 80 keV, and 100 Kev for argon (Ar^+) are performed in the Low Energy Ion Beam Radiation Facility at Inter University Accelerator Centre (IUAC, New Delhi), for various ion fluence of 5×10^{15}, 8×10^{15}, 1×10^{16}, 2×10^{16}, and 3×10^{16} ions.cm^{-2}. Sessile contact angles measurements of water droplet (deionized (DI) water (18 M-cm, Millipore)) on both pristine and irradiated $SrMnO_3$ samples were done at ambient temperature (Room temperature) with drop volume of 08 μL using a contact angle measurement unit (Model No. OCA15EC).

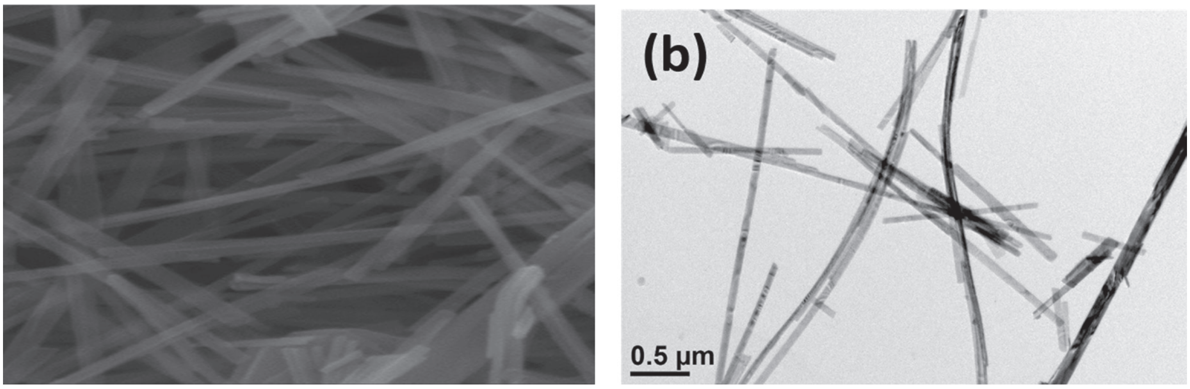

Figure 1. (a) FESEM image, (b) HRTEM image of pristine $SrMnO_3$ nanowires.

The as-synthesized nanowires are usually straight and well separated and uniformly spread on silicon substrate. Figure 1. (a) shows the plan view FESEM image and (b) the HRTEM image of the pristine $SrMnO_3$ nanowires, which shows diameters close to 60 nm as estimated by the histogram plot of pristine sample. The high magnification HRTEM image shows that nanowires are completely straight in length and uniform in diameter along the growth direction (012) which is confirmed by the selected area electron diffraction (SAED) pattern (not shown here).

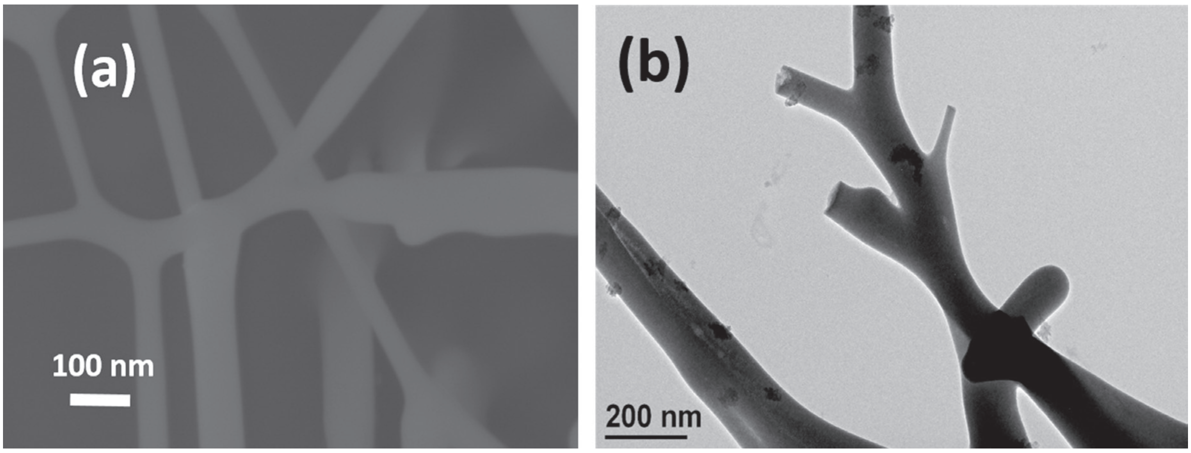

Figure 2. (a) Plan view FESEM image, (b) HRTEM image of joined $SrMnO_3$ nanowires by irradiating it at ion energy 50 keV and at a fluence of 3×10^{16} ions.cm^{-2}.

When we increase the ion energy from initial 3 keV for N^+ ions to 50 keV, 80 keV and 100 keV N^+ ions large scale joining and welding of the nanowires observed which lead to the various type of shape formation of junction such as 'X', 'T','V', 'Y' etc. (Fig 2).The wetting nature of ion modified nanowire assembly is under progress.

REFERENCES:

[1] T. N. Krupenkin, J. A. Taylor, T. M. Schneider, and S. Yang, "From rolling ball to complete wetting: the dynamic tuning of liquids on nanostructured surfaces," Langmuir, vol. 20, no. 10, pp. 3824–3827, 2004.

[2] M. Yoshimura, W. L. Suchanek, T. Watanabe, and B. Sakurai, "In situ fabrication of SrTiO3–BaTiO3 layered thin films by hydrothermal-electrochemical technique," J. Eur. Ceram. Soc., vol. 19, no. 6–7, pp. 1353–1359, 1999.

[3] S. Dhal, S. Chatterjee, S. Sarkar, L. C. Tribedi, R. Bapat, and P. Ayyub, "Nano-welding and junction formation in hydrogen titanate nanowires by low-energy nitrogen ion irradiation," Nanotechnology, vol. 26, no. 23, p. 235601, 2015.

[4] M. K. Rajbhar et al., "Joining of two different ceramic nanomaterials for bottom-up fabrication of heterojunction devices," Appl. Surf. Sci., 2019.

5.2.36 Effect of Low energy N^+ ion implantation in brownmillerite $Ca_2Fe_2O_5$

Durga Sankar Vavilapalli[1], Shubra Singh[1] and K. Asokan[2]

[1]Crystal Growth Centre, Anna University, Chennai-600025,India
[2]Inter-University Accelerator Centre, New Delhi-110067, India. Email: shubra6@gmail.com

It is a well-established fact that material properties can be successfully tailored by using ion implantation technique. Low energy ion bombardment on the metal oxides result in controlled ion - doping or implantation which alter the structural, optical, electrical and magnetic properties. Multifunctional brownmillerite $Ca_2Fe_2O_5$ (CFO) is promising material for energy and environmentalapplications such as fuel cells, batteries, H_2 production and CO_2 capturing etc. owing to their oxygen deficiency, catalytic and mixed ionic electronic conduction (MIEC) properties [1-5]. Brownmillerite structured CFO consists of alternate layers of FeO_6 and FeO_4polyhedra as shown in Figure1. The oxygen vacancies in these compounds are distributed orderly in the two-dimensional FeO_4 tetrahedral layer. Nitrogen (N) substitution in FeO_{4-x} may lead to changes in optical properties by narrowing its bandgap, owing to the lower electronegativity of N than O. Nitrogen substitution can also affect the electrical and magnetic properties of CFO. Keeping in mind, the above mentioned aspects and possibilities, by Nitrogen substitution, we attempted N- ion implantation on CFO bulk films for the first time. Structural and optical properties as implanted films were analyzed.

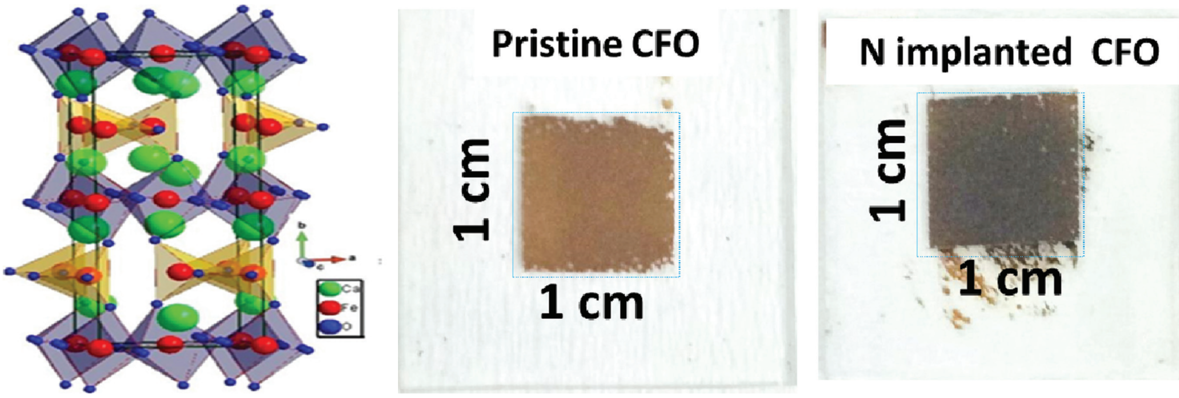

Figure 1 (left) Crystal structure of $Ca_2Fe_2O_5$ with alternate tetrahedra and octahedra layers (right) images of pristine and implanted films

Experimental Details :

Polycrystalline single phase $Ca_2Fe_2O_5$ was prepared by chemical route method [5] and then CFO bulk films were fabricated using Doctor blade method on glass substrate. As coated films annealed in furnace at 300 ºC for 3 hr.These CFO films were then implanted with 1 MeV of N^+ ion beam with a beam current of 1 µA using low energy ion beam facility (LEIBF). The implantation was performed at three ion fluences 10^{14}, 10^{15} and 10^{16} ions per cm^2.

Results and discussion :

X-ray diffraction (XRD) measurements were performed to investigate the effect of N ion implantation on the crystal structureand the nature of crystallinity of CFO films. No additional diffraction peaks corresponding to other phases are detected. This is attributed to the fact that N ionsare incorporated completely into the host lattice site instead ofoccupying some interstitial positions.Figure 1 also shows the image of pristine and N implanted CFO films, the N implanted CFO colour changed due to incorporation of N ions. Nitrogen (N) doping/ substitution in CFO is expected to change the optical properties by narrowing its bandgap due to the lower electronegativity of N as compared to Oxygen.

Conclusion :

CFO films were fabricated using a conventional doctor blade method. The N ions were successful implanted on CFO films with various fluencies successfully. The effect of N ion implantation on CFO films has been examined. The implantation of N ions into CFO significantly decreases the band gap.

REFERENCES:

[1] Baijnath, P. Tiwari, S. Basu, Cobalt and molybdenum co-doped Ca2Fe2O5 cathode for solid oxide fuel cell, International Journal of Hydrogen Energy, 44 (2019) 10059-10070.

[2] S. Dhankhar, P. Tiwari, K. Baskar, S. Basu, S. Singh, Effect of low Cobalt doping on morphology and properties of calcium ferrite and its application as cathode in Solid Oxide Fuel Cell, Current Applied Physics, 17 (2017) 467-473.

[3] S. Dhankhar, S.S. Menon, B. Gupta, K. Baskar, S. Singh, Electrochemical performance of brownmillerite calcium ferrite for application as supercapacitor, AIP Conference Proceedings, 1832 (2017) 080050.

[4] M. Ismail, W. Liu, M.S.C. Chan, M.T. Dunstan, S.A. Scott, Synthesis, Application, and Carbonation Behavior of Ca2Fe2O5 for Chemical Looping H2 Production, Energy & Fuels, 30 (2016) 6220-6232.

[5] K. Gupta, S. Singh, M.S. Ramachandra Rao, Fast, reversible CO2 capture in nanostructured Brownmillerite CaFeO2.5, Nano Energy, 11 (2015) 146-153.

5.2.37 X-Ray Diffraction study of metal ion implanted $BiVO_4$ thin films

P. Sundara Venkatesh[1], M. Ganeshbabu[1], G. Paulraj[2], K. Jeganathan [2] and K. Asokan [3]

[1]Department of Physics, Sri S. Ramasamy Naidu Memorial College, Sattur - 626203, Tamilnadu, India
[2]Centre for Nanoscience and Nanotechnology, Department of Physics, Bharathidasan University, Tiruchirappalli-620024, Tamilnadu, India.
[3]Inter-University Accelerator Centre, New Delhi-110067, India.

Herein, we report the dislocation density and peak shift of the ion implanted Bismuth Vanadate ($BiVO_4$) thin films. $BiVO_4$ thin films were prepared by a simple spin coating technique. After that, the low energy Copper, Nickel and Cobalt ions were implanted on the $BiVO_4$ films with optimum fluency rate. The implanted samples were characterized by X-Ray diffraction (XRD) analysis.

Introduction:

Doping of impurity atoms into a semiconductor material is a traditional way to enhance the physical, chemical and electrical properties [1]. Making composite and heterojunction formation is often used to tailor structural and optical behaviors of the nanomaterials and thin films. But, the distribution of dopant in the host material by chemical process is still not satisfactory. Ion implantation is a promising physical approach to achieve uniform distribution of doping material with great extend.

In this context, we report the structural properties of the BiVO4 thin films with different metal ion implantations at optimum fluency range. $BiVO_4$ is identified as a n-type semiconductor material having ~2.4 eV band gap. Due its narrow band gap nature, it is extensively investigated in the field of visible light photocatalysis and Photoelectrochemical (PEC) systems. The major problem arises when it is used alone are poor charge transportation, high charge recombination and slow hole kinetics of oxygen evolution [2]. In order to overcome this problem we have planned to introduce some metal ions on $BiVO_4$ thin films by ion implantation method.

Simple and cost effective spin coating technique was used to fabricate BiVO4 thin films. Cu and Co ions of 60 keV and Ni ions of 120 keV were implanted on BiVO4 thin films with 5 X 10^{15} ions/cm^2 fluency rate at Inter University Accelerator Centre (IUAC), New Delhi, India.

Results and Discussion:

X-ray Diffraction patterns of the ion implanted $BiVO_4$ thin films were depicted in the given below figure. XRD patterns of the all samples closely matched with JCPDS Cord no: 00-014-0688. This represents the monoclinic phase of $BiVO_4$. As compared to the bare $BiVO_4$ thin films, the dominant (121) peak was shifted to the higher angle side. This may be attributed to the incorporation of ions on the host matrix. The average grain size and dislocation density calibrated from William's and Hall plot. The result obtained from W-H plot is given in the following table.

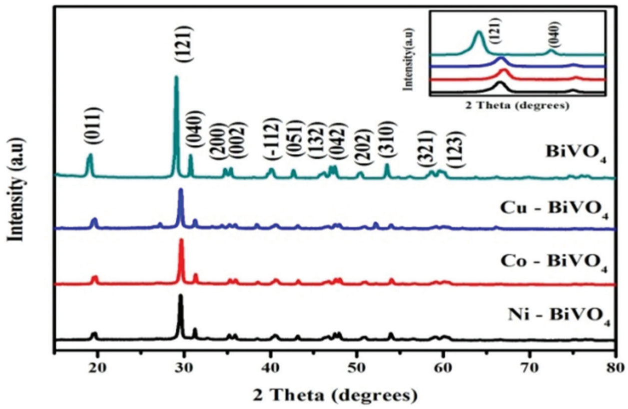

Fig-1 : X-ray Diffraction spectra of pristine and metal ion implanted films

Table-1 :

Sample name	Grain size (nm)	Dislocation density (lines/m^2)
$BiVO_4$	30.80	10.5×10^{14}
Cu-$BiVO_4$	21.65	21.3×10^{14}
Co-$BiVO_4$	22.35	20.0×10^{14}
Ni-$BiVO_4$	26.70	14.02×10^{14}

Crystallite size and dislocation density of the pristine and metal ion implanted films

Conclusion:

XRD patterns of the bare and implanted samples showed that the monoclinic structure of $BiVO_4$. The right angle peak shifts in XRD pattern and dislocation density confirms the defects in the irradiated samples.

REFERENCES:

[1] J. Wallentin & M.T. Borgstrom, Journal of Materials Research, 26 (2011) 2142-2156.

[2] G. Park, H. Kim, H. Kim et al., Nanoscale Adv., 3 (2019) 799-806.

[3] B. Paul, J. S. Sagu, et al., Chem. Vap. Deposition 20(2014), 1–5.

5.2.38 Raman investigation of N implanted ZnO: Defects, disorder and recovery

A Mondal[1], S Pal[2], A Sarkar[3], T. S Bhattacharya[4], S Pal[5], A Singha[4], S. K Ray[6], P Kumar[7], D Kanjilal[7] and D Jana[1,*]

[1]Department of Physics, University of Calcutta, 92 , Acharya Prafulla Chandra Road, Kolkata 700009, India.
[2]Department of Physics, School of Natural Sciences,Shiv Nadar University, NH 91, Tehsil Dadri, Gautam Buddha Nagar, Uttar Pradesh – 201314.
[3]Department of Physics, Bangabasi Morning College, 19 Rajkumar Chakraborty Sarani, Kolkata 700009, India.
[4]Department of Physics, Bose Institute, 93/1, Acharya Prafulla Chandra Road, Kolkata 700009, India.
[5]Department of Physics, Indian Institute of Technology, Kharagpur 721302, India.
[6]S. N. Bose National Centre for Basic Sciences, JD Block, Sector-III, Salt Lake City, Kolkata - 700 106, India.
[7]Inter University Accelerator Centre, Post Box 10502, Aruna Asaf Ali Marg, New Delhi 110067, India.
[*]Email: djphy@caluniv.ac.in

Understanding defects, disorder and doping due to N implantation in ZnO is one of the most debated issues for the last few years. In the present work, a comprehensive investigation has been carried out using Raman, photoluminescence (PL) spectroscopy and grazing-incidence X-ray diffraction on 50 keV N ions implanted granular ZnO with different fluence (~ up to 6.5% atomic concentration) along with post-implantation annealing. Raman investigation suggests that 275, 510, 643, 857 cm^{-1} modes are directly related to nitrogen. Additionally, VZn may have some role in stabilizing 275 cm^{-1} mode. The broadening (or tailing) of E_2^{low} mode is related to vibration of distorted Zn sublattice, may be a product of ion implantation generated defect cluster like VZn-VO. The distortion starts to reduce with annealing at elevated temperatures. Direct correlation between 555 cm^{-1} Raman mode and the tailing of E_2^{low} mode have been found. More defect clustering is vivid from the reduced PL of the ZnO samples with increasing implantation fluence. So, tailing of E_2^{low} Raman mode, increasing intensity of 555 cm^{-1} mode and non radiative defect centers are of common origin. Both the ratios E_1(2LO)/E_1(LO) and E_2^{high} /E_1(LO) both can be used as parameters to measure the defective nature of ZnO after ion implantation/ irradiation. Low temperature PL (selected samples) suggests absence of shallow acceptor states, although negative thermal quenching above 250 K has been observed (implantation fluence 1×10^{16} ions/ cm^2 and annealed at 500 ºC) which can be a signature of deep acceptors.

Experimental Details

Polycrystalline ZnO (99.99% pure, Sigma-Aldrich, Germany) powder in pellet forms has been annealed in a Muffle furnace at 500 ºC for four hours to make samples unwanted organic and H2O free. Annealed samples have been implanted by 50 keV nitrogen ion beam at LEIBF facility in IUAC, New Delhi, India with fluences varying from 10^{12} to 10^{17} ions/cm^2. Furthermore, samples implanted with 10^{16} ions/cm^2 nitrogen ion beam have been further annealed with different temperature (200, 250, 300, 400, 500 and 600 ºC) for 4 hour at ambient air to study the recovery of defects with annealing temperatures.

Raman spectra (RS) have been measured by Lab RAM HR Jovin Yvon Raman set-up equipped with Peltier cold CCD detector having 488 nm Argon laser as an excitation source. Both room and low temperature PL properties of all samples have been recorded using 325 nm laser source with output power 45mW and a TRIAX 320 monochromator was fitted with a cooled Hamamatsu R928 photomultiplier detector. Grazing-incidence X-ray diffraction (GIXRD) measurements has been performed (model: Bruker, D8 Discover) to understand the structural evolution of the implanted layers. Here, the X-ray incidence angle has been kept at 1º to ensure the probe region of the X-ray to be confined within the implanted region.

Results and Discussion:

Figure 1 (a) and (b) depicts the Raman spectra of implanted and post-implanted annealed samples. In the following section, we intend to discuss few key features of Raman spectra in disordered ZnO. From the comparative study of two Raman spectra whose 580 cm^{-1} peak area or height is more or less same it is unambiguous that 275 510, 643, 857 cm^{-1} are related to nitrogen. This is not true for 555 cm^{-1} Raman mode. Rather this Raman mode scales with the disorder which is responsible for the broad tailing of E_2^{high}. Figure 1 (c) depicts that the variation is almost linear. Hence, 555 cm^{-1} Raman mode is indeed related to disorder. Zeng et. al have proposed [1] that typical defects like IZn residing at the interface of Zn/ZnO interface are responsible for 555 cm^{-1} Raman mode. Such kind of defects can be generated due to grain fragmentation during ion irradiation. In our opinion, the distorted Zn sub-lattice vibration gives rise to such tailing of E_2^{low}. The same distortion exists at the fragmented grain interface and/thus distortion generated IZns are also likely to be present there. It is generally understood that 580 cm^{-1} peak intensity scales with the concentration of VOs in ZnO, if we assign the 2.42 eV room temperature PL (RTPL) emission with the VO in ZnO, a correlation is expected which, however, is not found (not shown). Further, it is well known that the intensity ratio of E_1(2LO) and E_1(LO) is an important parameter in ZnO [2] and other semiconductors [3,4] which indicates the spatial extent (average) of coherently scattering regions (CSR) as probed by Raman spectroscopy. So, the ratio of E_1(2LO)/E_1(LO) is closely related with the disorder present in the material. In the same graph (Figure 1 (d)) both intensity ratio of E_1(2LO)/E_1(LO) and E_2^{high} /E_1(LO) have been plotted. If this ratio with fluence is plotted in a log-log scale, almost a linear variation is observed in the whole fluence regime studied here. The uncanny similarity can be understood from the exponential decay fitting (not shown) of of E_1(2LO)/E_1(LO) and area under E_2^{high}. The thermal activation energy of E_1(2LO)/E_1(LO) and area under E_2^{high} turn out to be nearly same. Low activation energy of disorder recovery is representative of the increase of length scale of CSR, mostly found in nanocrystalline materials [5,6]. Similarity in activation energies manifests the fact they share common origin and both the parameters (i.e. E_1(2LO)/E_1(LO) and E_2^{high} /E_1(LO)) can be used to assess the extent of damage due to implantation/irradiation. As the implantation fluence increases the ratio decreases gradually while the ratio increases with annealing temperature.

In conjunction to RTPL findings (not shown), it is evident that defects responsible for the tailing of E_2^{low} mode are mostly non-radiative in nature. The recovery of band edge emission starts above 250 ºC annealing temperature. As manifested by Raman findings, the implanted ZnO gradually recovers with increasing annealing temperature with full recovery at 600 ºC. It is clear that RTPL from ZnO is sensitive to particular type of defects whereas Raman signal probes overall disorder in the sample.

Low temperature PL (LTPL) spectra of un-implanted, implanted samples (with fluences 1E16, 1E17) and post-implanted annealed samples (annealed at 500 ºC and 600 ºC) at near band emission (NBE) mainly dominated by 3.313 eV emission are mostly assigned as free electron transition to localized acceptor states (not shown). Compared to un-implanted sample, the DBX emission is suppressed in all the measured PL spectra of other samples. It can be understood that N implantation inhibits the emission from shallow donors which is indeed interesting. However, no identifiable signature of shallow acceptor bound emission has been noticed in the LTPL spectra of any of the samples. In cases of post-implanted 500 ºC annealed sample, temperature dependent PL spectra exhibits negative thermal quenching (NTQ) above 250 K which can be a signature of deep acceptors. This responsible defect is generated as a combined effect of N implantation and subsequent annealing. Thus, transforming such deep acceptors to shallower one in ZnO is still as a challenge.

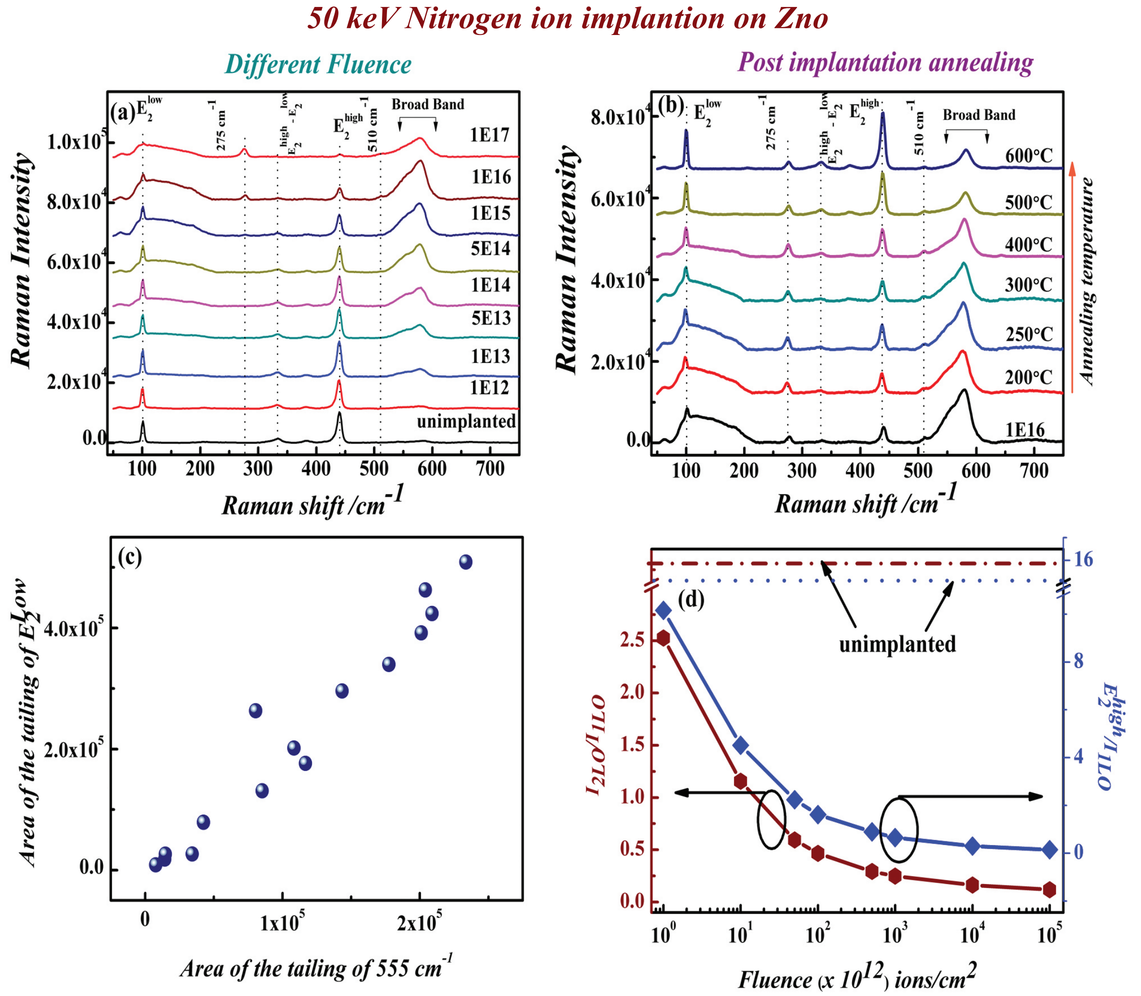

Figure 1: (a) Room temperature Raman spectra of (a) N- implanted at different fluences (b) post-annealed N-implanted (c) variation of area of the tailing of E_2^{low} (100 cm^{-1}) with area under 555 cm^{-1} mode (d) variation of E_1(2LO)/E1(LO) and E2high/E1(LO) with fluences.

REFERENCES:

[1] H. Zeng, X. Ningab and X. Liab, Phys. Chem. Chem. Phys.17 (2015) 19637.

[2] H. M. Cheng, K. F. Lin, H. C. Hsu and W. F. Hsieh, Appl. Phys. Lett. 88 (2006) 261909.

[3] J. Li, J. Ye, F. Ren, D. Tang, Y. Yang, K. Tang, S. Gu, R. Zhang and Y. Zheng, Sci. Rep. 7 (2017) 44399.

[4] D. Paramanik and S. Varma, J. Appl. Phys. 101 (2007) 023528.

[5] X. H. Huang, C. Zhang, C. B. Tay, T. Venkatesan, S. J. Chua, Appl. Phys. Lett. 102 (2013) 111106.

[6] S. Shukla, S. Seal, R. Vij, S. Bandyopadhyay, Nano Lett. 3 (2003) 397.

5.2.39 Development of Ion Beam Modified Self- Cleaning Zno Thin Films for Improved Antimicrobial Efficacy Against Multidrug Resistant Bacteria

Subhavna Juneja[1], Prof. Prasenjit Sen[2] and Dr. Jaydeep Bhattacharya[1]

[1]School of Biotechnology, Jawaharlal Nehru University, New Delhi-110067
[2]School of Physical Science, Jawaharlal Nehru University, New Delhi-110067

Metal oxides are excellent antimicrobial agents with restricted applicability. Limited optical responsiveness, poor adhesion and mechanical strength are its major drawbacks. Plasmonic nanocomposites address these issues to a certain extent however, they have adverse effects in probability of self-recombination, complex surface passivation protocols and controlled functionalization. Thus, manipulating metal oxide matrix at atomic level through implant technology offers to be a good alternative as it is controlled and forms no self-recombination centres.

Experimental Details

In this work, we irradiated previously synthesized zinc oxide nanocomposites with different metallic and gaseous sources for their application as an improved antimicrobial agent. The sources used were Au, Ar and N (Low energy beams).

Results:

Preliminary results obtained from antimicrobial assay indicate similar activity as to control. No significant change in killing efficiency of irradiated and non-irradiated samples was observed. The killing efficiency estimated is approx. ~ 97% in 2 hours. However, these results have been performed only once thereby drawing a firm conclusion is difficult and requires some more experiment to affirm its statistical significance. We'll repeat the implant in the next phase and shall continue to perform the biological measurements. The work has been done in collaboration and discussion with Dr. Asokan.

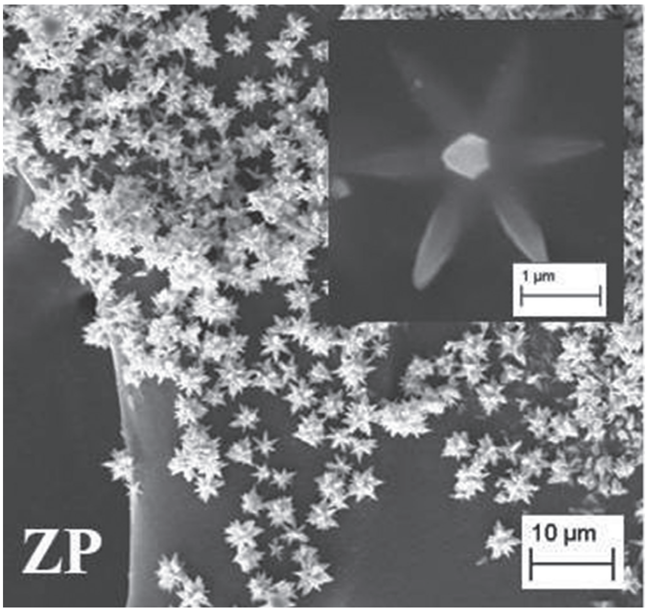

Figure 1: SEM micrograph of the chemically synthesized zinc oxide nanostructures implanted with different ions.

5.2.40 Impact of Space Radiation on stability of medicines flown to spacecraft

Dhara Bhayani[1], Saif Khan[2] and Priti Mehta[1*]

[1]Institute of Pharmacy, Nirma University, Ahmedabad, Gujarat-382481, India.
[2]Inter-University Accelerator Centre, Aruna Asaf Ali Marg, New Delhi 110067, India.

The drugs are inevitable part of healthcare system. Stability of medicines assures its safety and efficacy. The changes in drug product stability can risk a patient safety by formation of toxic degradation product or deliver a lower dose than expected. Exposure of the drugs to space radiations during space missions can lead to alteration in stability of the medicines. Among various space radiations, one of the component – Heavy ion radiation causes damaging effects on the exposed material. So, evaluation of their effects on the drug stability is essential.

We have exposed drugs and their tablet formulations to ^{56}Fe irradiation (^{56}Fe, 100 MeV with 50 cGy, 1 Gy, 10 Gy and 50 Gy doses at RT). Their stability was evaluated post radiation exposure using various analytical techniques such as Fourier-Transform Infrared spectroscopy (FTIR) and High-Performance Liquid Chromatographic (HPLC) method. The physical changes were evaluated using organoleptic evaluation. The results of the study showed that the drugs were stable to ^{56}Fe irradiation at the selected doses.

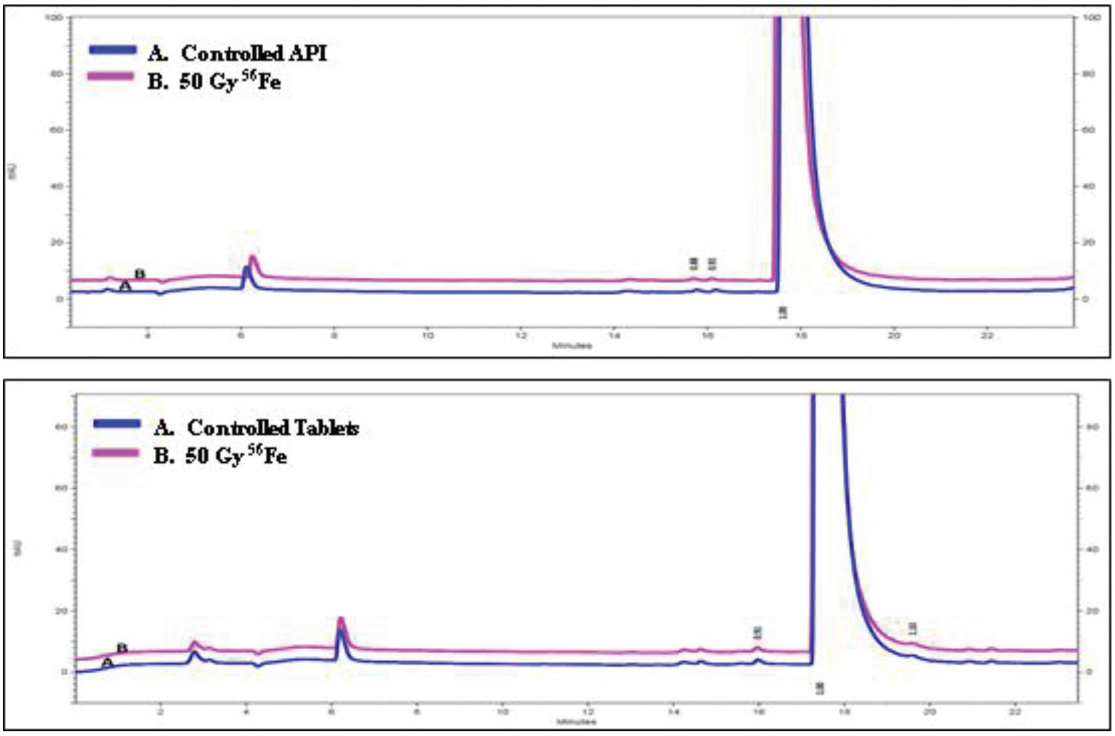

Figure 1 Stability of amlodipine API and tablets after ^{56}Fe irradiation

Experimental Details

API and tables of amlodipine were exposed to ^{56}Fe irradiation (^{56}Fe, 100 MeV with 50 cGy, 1 Gy, 10 Gy and 50 Gy doses at RT). Post radiation exposure samples were analysed for their physicochemical by organopletic evaluation, FTIR and HPLC analysis.

Results

No colour changes were observed in the ^{56}Fe irradiated API or tablet samples. No changes were observed in the recorded FTIR spectra for controlled and irradiated samples. The HPLC chromatograms of API and tablets of each drug irradiated by ^{56}Fe radiation exhibited no additional peak compare to control samples, as well as the peak areas of the peak remained unchanged. These results indicated that drugs were chemically stable to these radiations at selected doses.

We have published one article from this study in a reputed journal: ·
Bhayani, Dhara, Haladhara Naik, T. Newton Nathaniel, Saif Khan, and Priti Mehta. "Simulated space radiation: Investigating ionizing radiation effects on the stability of amlodipine besylate API and tablets." European Journal of Pharmaceutical Sciences (2019): 104982. (Impact factor: 3.5; publication house: Elsevier)

REFERENCES:

[1] Mehta, Priti, and Dhara Bhayani. J. Pharm. Biomed. Anal. 136 (2017): 111-119.
[2] B. Du, V. Daniels, Z. Vaksman, J. Boyd, C. Crady, L. Putcha. AAPS J. 13 (2011) 299–308.
[3] M.C. Chuong, D. Prasad, B. LeDuc, B. Du, L. Putcha. J. Pharm. Biomed. Anal. 55 (2011) 1197–1200.
[4] Wotring, Virginia E. AAPS J. 18(2016): 210-216.

5.2.41 Reversible phase transformation phenomenon in titanium dioxide films: evidence beyond interface-nucleation and dissolution-precipitation kinetics

Subodh K. Gautam[1,2], Jitendra Singh[1], D. K. Shukla[3], E. Pippel[4], P. Poddar[2] and Fouran Singh[1]

[1]Materials Science Group, Inter-University Accelerator Centre, Aruna Asaf Ali Marg, New Delhi, India-110 067
[2]Physical & Materials Chemistry Division, CSIR-National Chemical laboratory, Pune 411008, India.
[3]UGC-DAE Consortium for Scientific Research, University Campus, Khandwa Road, Indore 452017, India
[4]Max Planck Institute of Microstructure Physics, Weinberg 2, D-06120 Halle, Germany

Understanding of thermodynamic stability and phase control of nano-crystalline materials is more important because their device applications response and physio-chemical properties are heavily affected with the changes in crystallite size, stoichiometry and lattice parameters by impurity doping, thermal annealing and ion irradiation [1, 2]. In this study, the reversible PT in nano-crystalline TiO_2 thin films and the thermal stability of nano-sized rutile and anatase crystallites were studied at annealing temperature range from 532 K to 1323 K. The mechanism and factors affecting the phase stability and transformations are understood by the kinetics of phonon dynamics and electronic structure modification using micro-Raman and near edge X-ray absorption fine structure spectroscopy (NEXAFS), respectively. In present work, ion beam sputtered rutile TiO_2 films on silicon substrate are used. Initially, the crystalline rutile films were amorphized using the 120 MeV Ag-ions irradiation at IUAC, New Delhi. *In situ* isothermal annealing study is carried out at 523 K and shows rapid nucleation of anatase phase occurs from amorphous structure with three dimensional growths of anatase NCs. This phenomenon is well explained using Johnson–Mehl–Avrami-Kolmogorov (JMAK) model of nucleation and growth kinetics [3]. In Fig. (a), annealing at low temperature range 523 K - 673 K, shows transformation into rutile phase and follows the interface-nucleation mechanism [1]. At moderate annealing temperature from 623 K to 973 K, results show decrease in rutile weight fraction and reversible PT of nano-sized rutile TiO_2 to anatase NCs. The decrease in rutile weight fraction is related to thermodynamic un-stability of rutile NCs and lattice stress-induced dissolution of small rutile NCs into anatase phase [4]. However, annealing at higher temperature (1123 K - 1323 K) induces the growth of anatase NCs and their natural transform into rutile phase follow the well-known dissolution–precipitation mechanism. Fig. (b) shows the normalized NEXAFS spectra of Ti $L_{3,2}$-edges for the modification of local electronic structural at different annealing temperatures. Thus, overall PT kinetics at different temperature range is well understood by invoking in three step mechanism: I) early stage (523 K - 673 K), anatase-to-rutile transformation is dominated by interface-nucleation, II) then intermediate stage (673 K - 973 K), reversible rutile-to-anatase PT and, III) at later stages at high temperatures, anatase-to-rutile PT is controlled by dissolution–precipitation mechanism. Therefore, present, investigations may encourage new research in similar functional oxide materials and their potential device applications utilizing the reversible transition. For details, see the article **[Subodh K. Gautam *et al.* Acta Materialia 146 (2018) 253-264].**

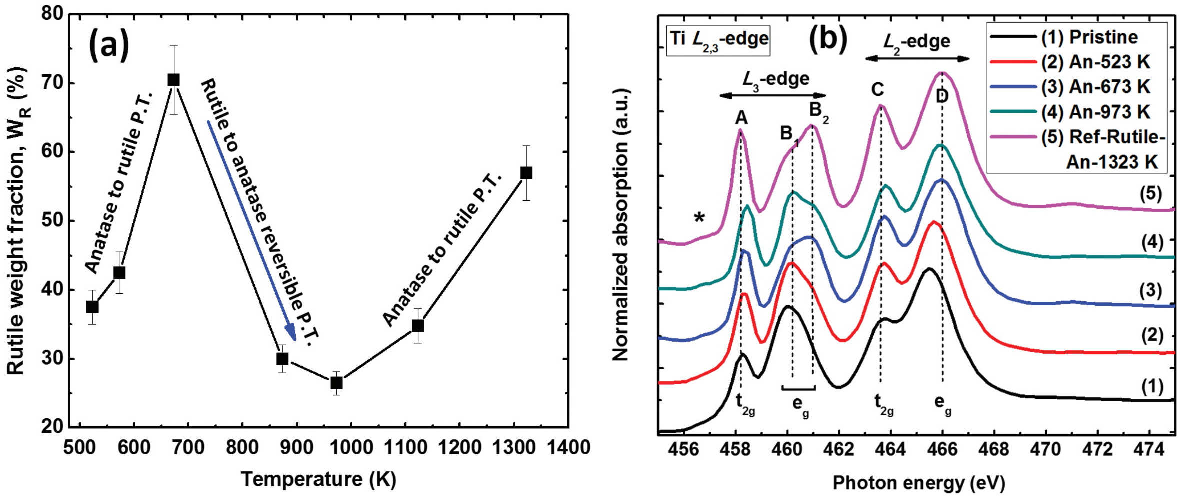

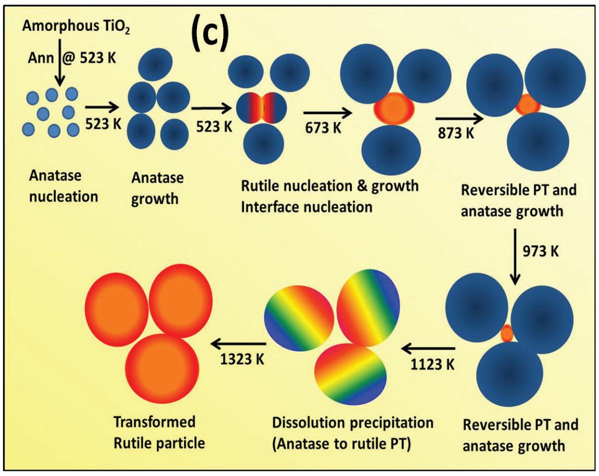

Figure: (a) Response of rutile weight fraction calculated from X-Ray diffraction data analysis and (b) normalized NEXAFS spectra of Ti $L_{3,2}$-edges for the information of local electronic structural modification during PT between anatase and rutile phases as a function of annealing temperature. (c) Schematic diagram shows the re-crystallization of amorphous to anatase phase and overall three step PT mechanisms at different annealing temperatures.

REFERENCES:

[1] H. Zhang *et al.,* Chem. Rev. **114** (2014) 9613–9644.
[2] S.K. Gautam *et al.,* J. Appl. Phys. **115** (2014) 143504
[3] M.C. Weinberg *et al.,* J. Non. Cryst. Solids. **219** (1997) 89–99
[4] K. Wu *et al.,* Appl. Phys. Lett. **91** (2007) 101903

5.2.42 Effect on Structural, Optical and Electrical Properties of Mg Doping on ZnO Nanorods Thin Films

Vishnu V. Kutwade[1], Ketan P. Gattu[2], Makrand E. Sonawane[1], Fouran Singh[3] and Ramphal Sharma[1,2*]

[1]Department of Physics, Dr. Babasaheb Ambedkar Marathwada University Aurangabad, (MS)-431004 India.
[2]Department of Nanotechnology, Dr. Babasaheb Ambedkar Marathwada University Aurangabad, (MS)-431004 India.
[3]Inter-University Accelerator Centre, New Delhi-110067, India.

Pure and (10% and 20%) Mg doped ZnO nanorods thin films have been successfully grown over glass substrate using simple cost effective chemical bath deposition method. The structural, optical and electrical properties of the synthesized materials have been studied using XRD, Raman, UV-Vis spectroscopy and I-V characteristics. The structural properties revealed the formation of MgO phase for 20% Mg doping. This formation of MgO phase had a significant effect on optical and electrical properties of the ZnO nanorods thin films, the optical band gap showed an increase of 0.46 eV with 20% Mg doping, while the electrical properties showed a decrease in resistance after Mg doping

There has been a great deal of interest in ZnO due to its potential applications in gas sensors, optical waveguides, surface acoustic devices and piezoelectric transducers. The intrinsic ZnO thin films are n-type semiconductors with high resistivity. Mg-doped ZnO is considered as the most suitable material for light emitting devices because it efficiently absorbs the near UV (330–400 nm) and emits a broad spectrum covering almost the whole visible region. In order to obtain a wider band gap, Mg doping content in ZnO thin film needs to be higher, at the same time the structure of Mg-doped ZnO thin films should retain wurtzite structure. Hence, different growth techniques are needed to synthesize Mg-doped ZnO thin films. Considering the advantages of chemical synthesis over physical methods and with an aim of mixing materials/sources atomic level so that the materials are close enough to form thermodynamic equilibrium, we have chosen chemical synthesis in our present work. The ZnMgO 1-D nanorods have been grown on the glass substrate using a single step chemical approach.

Experimental Details

Synthesis of ZnMgO 1-D nanorods and Cu2S thin films:

Fig.1. shows a schematic for the synthesis of ZnO and Mg-doped ZnO NR thin film using single-step chemical bath deposition technique on a glass slides. Initially, the glass slides were kept in chromic acid for 1.30 hr. at 80 °C and then subsequently washed with deionized water (DI) and laboline detergent. This cleaning of the substrate is important to step in the deposition process to obtain uniform thin film and achieve better adhesion and stoichiometry. The obtained films were yellowish white in color with uniform deposition over the entire surface of the substrate. The films were washed with deionised water to remove weakly bonded atoms on the surface and dried subsequently.

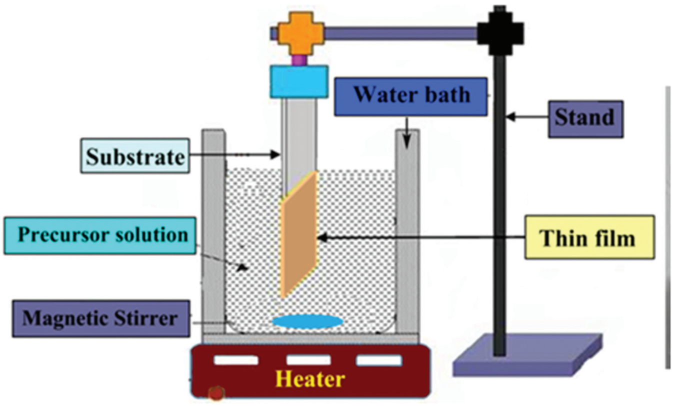

Figure.1 Schematic of a chemical bath deposition

Results and discussion:

Fig. 2a Shows the XRD patterns of ZnO: x% Mg (x= 10, 20). the intensity of the (002) peak decreases and (100) & (101) peaks intensity increases slightly, with a very low broadening at increasing Mg concentrations. This suggests that the incorporation of Mg in the ZnO structure does not substantially affect the crystallinity of the films due to the less difference in ionic radii of Mg (0.57Å) atoms and Zn (0.60 Å) atoms. Fig 2 (d1, d2) shows the SEM micrographs of Pure ZnO and Mg doped ZnO thin films which confirms the 1-D nanorods structures of ZnO thin films.

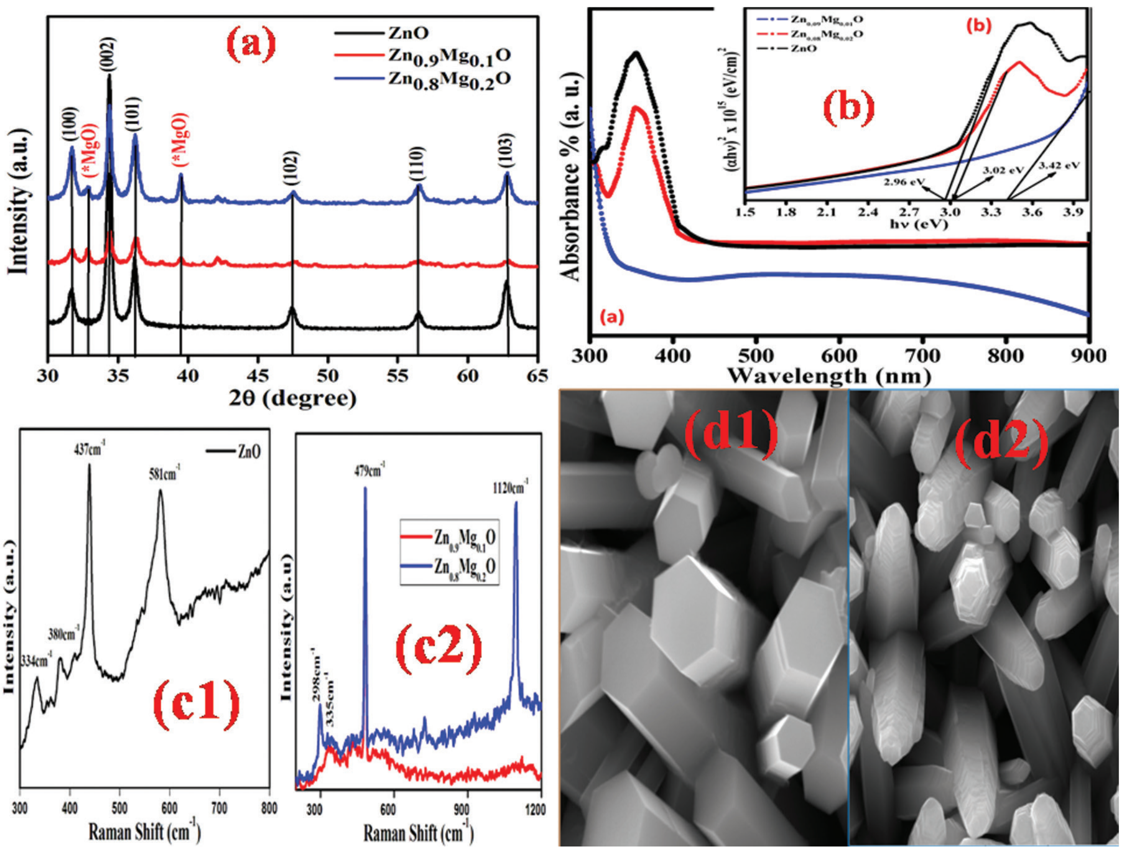

Fig 2 (a) X-ray diffraction patterns of ZnO and Mg (10% & 20%) Doped ZnO NRs thin films; (b) UV-Vis spectra of ZnO and Mg Doped ZnO NRs thin films; (c1) Raman spectra of pure ZnO and (c2) & (c3) Raman spectra of Mg-doped ZnO; (d1) Top view of SEM image of ZnO and (d2) Mg Doped ZnO NRs thin films

The UV–Vis absorption spectra obtained for ZnO and Mg-doped ZnO NRs thin film deposited on a glass substrate is shown in Fig. 2(b). The absorbance spectra show UV cut off at around 350–380 nm, due to the photoexcitation of electrons from valence to conduction band.

The bandgap of the as-grown ZnO and ZnMgO NRs thin film was calculated by extrapolating the plot of $(\alpha h\nu)^2$ vs hν using the Tauc's relation. The bandgap obtained for the ZnO and Mg (10% & 20%)-doped NRs thin films are 2.96eV and 3.02eV & 3.42eV respectively. A Raman spectrum of ZnO sample gives a sharp and dominant peak at 438 cm^{-1} assigns to the Raman active E2 (high) mode, which corresponds to hexagonal wurtzite phase of ZnO as shown in fig 2(c1). Also, three small peaks at 334cm^{-1}, 380cm-1 and 581cm^{-1} were observed. which are assigned to multiple phonon processes, A1 (TO) and E1 (LO), respectively. However, the E2 (high) mode for Mg-doped ZnO nanoparticles thin films has been blue shifted to 481cm-1 compared to ZnO thin films. Mg (10% & 20%) doping into ZnO crystal lattice, which incites the tensile strain within the wurtzite hexagonal Mg-ZnO nanorods structure. In fig 2 (c2) extra peaks at 298cm^{-1}, 335cm^{-1}, and 1120cm^{-1} observed, which shows the formation of MgO phase and the distinguished peak spectra was influenced by the 1LO band is observed at ~1120cm^{-1}. Intensity of 1LO peak increases with increase in concentration of Magnesium (Mg).

Photoluminescence spectra of pure ZnO and Mg-doped ZnO nanorods measured at room temperature with an excitation wavelength of 450 nm. Figure 4 (a) shows the spectra, three bands emission can be observed in both pure ZnO and Mg-doped ZnO thin films, one in the UV region namely near band edge (NBE) emission and another two in the visible region namely deep level (DLE) emission. The PL spectra of the prepared samples from which near-band-edge (NBE) emission band at around ~389 nm observed for all the doped and undoped samples along with the other luminescence bands. The emissions of ZnO nanostructures may consist of LO-phonon (~581 cm-1) replicas occur with a separation of the LO-phonon energy (~71 meV) from NBE. The origin of the emission band observed at around 454 nm is attributed to the presence of zinc vacancies. The broad emission band at around ~561 nm is assigned to oxygen vacancies. This broad emission is enhanced after Mg (10% & 20%) doping due to the increase in defects concentration.

We can see in PL spectra some deep level defects are observed which is due to zinc and oxygen vacancies.

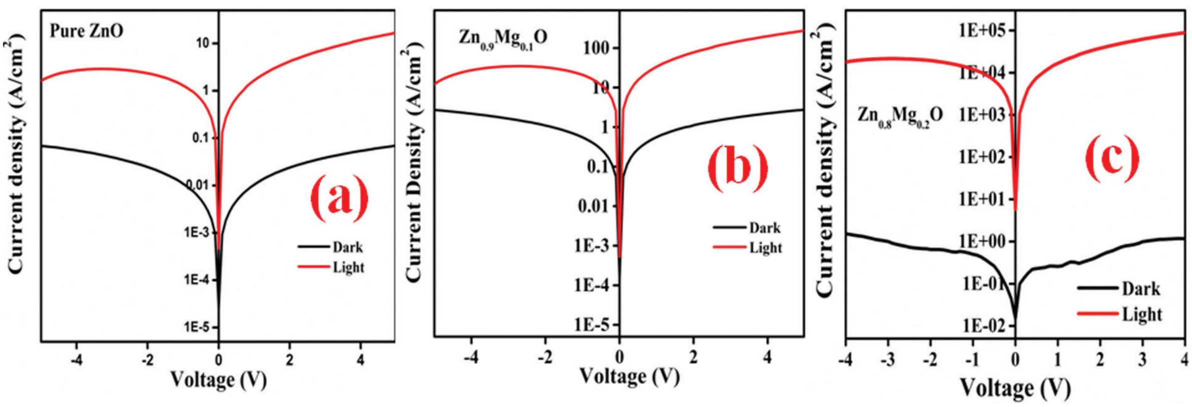

Fig. 3 J-V characteristics of (a) pure ZnO (b) $Zn_{0.9}Mg_{0.1}O$ and (c)$Zn_{0.8}Mg_{0.2}O$ thin films

From Fig. 3 we can clearly see the drastic increase in current density after illumination of light. below in Table1.

This change in resistance after light exposure demonstrates that the films are suitable for visible light photosensor. Also, from the nanorod structure has been reported to have a trapping mechanism for photoconduction. Due to the high surface-to-volume ratio the presence of a high density of hole-trap states at the nanorod surface, drastically affects the transport and photoconduction properties. In dark, a low-conductivity depletion layer is formed near the surface due to the adsorption of oxygen molecules on the oxide surface which captures the free electrons present in the n-type oxide semiconductor. Upon illumination with photon energy above Eg (bandgap energy), electron-hole pairs are photo generated; holes travel to the surface and discharge the negatively charge adsorbed oxygen ions and as a result, oxygen is desorbed from the surface. The unpaired electrons are either collected at the anode or recombine with holes generated when oxygen molecules are adsorbed and ionised at the surface. This hole-trapping mechanism through oxygen adsorption and desorption in nanorods is dominant due to the high density of trap states as a result of dangling bonds at the surface and the surface zinc vacancies enhancing the nanorod photo response.

Acknowledgment

One of the authors Vishnu V. Kutwade is thankfull to IUAC New Delhi for financial support and Dept. of Physics, Dr. B.A.M. University for providing laboratory facilities.

REFERENCES:

[1] MS Alam, U Manzoor, M Mujahid, AS Bhatti, Journal of Sensors, (2016)
[2] M Amin, NA Shah, AS Bhatti, MA Malik, Crystengcomm **16**, 6080-6088 (2014)
[3] SD Senol, C Boyraz, E Ozugurlu, A Gungor, L Arda, Crystal Research and Technology **54,** (2019)
[4] DC Agarwal, F Singh, D Kabiraj, et al., Journal of Physics D: Applied Physics **41,** 045305 (2008)
[5] N Winkler, S Edinger, W Kautek, T Dimopoulos, Journal of Materials Science **53,** 5159-5171 (2018)
[6] E Vinoth, S Gowrishankar, N Gopalakrishnan, Applied Physics a-Materials Science & Processing **124,** (2018)
[7] D-A Dive, D-N Huse, K Gattu, R Sharma, Soft Chemical Growth of Zn 0.8 Mg 0.2 S One Dimensional Nanorod Thin films for Efficient Visible Light Photosensor. (2017)
[8] PFH Inbaraj, JJ Prince, Journal of Materials Science: Materials in Electronics **29,** 935-943 (2018)
[9] ZY Jiang, KR Zhu, ZQ Lin, SW Jin, G Li, Rare Metals **37,** 881-885 (2018)
[10] E Muchuweni, TS Sathiaraj, H Nyakotyo, Heliyon **3,** e00285 (2017)
[11] M Arshad, MM Ansari, AS Ahmed, et al., Journal of Luminescence **161,** 275-280 (2015)
[12] NCS Selvam, S Narayanan, LJ Kennedy, JJ Vijaya, Journal of Environmental Sciences-China **25,** 2157-2167 (2013)
[13] L Umaralikhan, MJM Jaffar, Journal of Materials Science-Materials in Electronics **28,** 7677-7685 (2017)
[14] M Wang, J Yi, S Yang, et al., Applied Surface Science **382,** 217-224 (2016)
[15] C Soci, A Zhang, B Xiang, et al., Nano Letters **7,** 1003-1009 (2007)
[16] SK Mishra, RK Srivastava, SG Prakash, RS Yadav, AC Panday Opto-Electronics Review, (2010)
[17] YK Frodason, KM Johansen, TS Bjørheim, BG Svensson, A Alkauskas, Physical Review B **95,** 094105 (2017)

5.3 RADIATION BIOLOGY

5.3.1 Signaling pathways of activation and secretion of Matrix Metalloproteinases from human lung carcinoma cells after irradiation with carbon ion beam

Dey Payel[1], Chowdhury Priyanka[1], Ghosh Sourav[1], Sarma Asitikantha[2] and Ghosh Utpal[1*]

[1]Department Of Biochemistry & Biophysics, University of Kalyani, Kalyani, Nadia, West Bengal, PIN- 741235
[2]Inter-University Accelerator Center, New Delhi, Delhi -110067

Lung malignancy is the foremost cause of cancer-related deaths globally and most of the lung tumours are inoperable and only choice is radio or chemotherapy. Majority of death occurs due to highly metastatic nature of lung cancer [1] [2]. Matrix metalloproteinases (MMPs) are key element in metastasis and their expression is extremely high in lung tumours compared with non-malignant lung tissue [3]. MMPs are zinc-dependent proteases, involved in the degradation of extracellular matrix [4]. Low LET photon radiation, in contrast to carbon ion radiation, can enhance the metastatic nature of cancer cells by increasing the expression and activities of MMPs leading to great difficulties in radiotherapy using gamma or X-rays [5]. Signaling pathways of activation and secretion of MMPs is not clear yet. It is reported that gamma irradiation induces p38/Akt and PI3K/Akt signaling pathways which can modulate MMP-2 expression [6]. We checked EGFR/Akt/p38/ERK signaling pathways associated with activation of MMP-2 and MMP-9 in highly metastatic lung carcinoma A549 cells after irradiation with carbon ion beam in present and absence of PARP-1 inhibitor.

Results:

Cell survival assay:

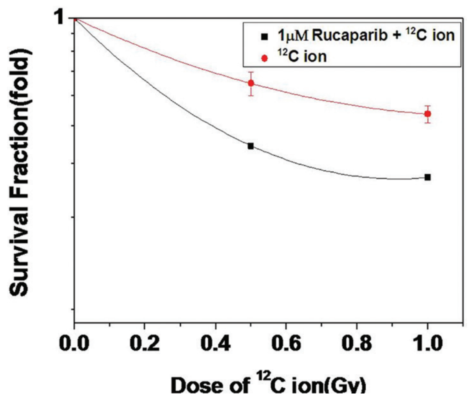

Fig1: Surviving fraction (SF) graph of A549 cell after treatment with PARP-1 inhibitor rucaparib in combination with ^{12}C ion exposure (0-1Gy). combined rucaparib and ^{12}C ion exposure synergistically reduced cell survival.

Immunofluorescence assay:

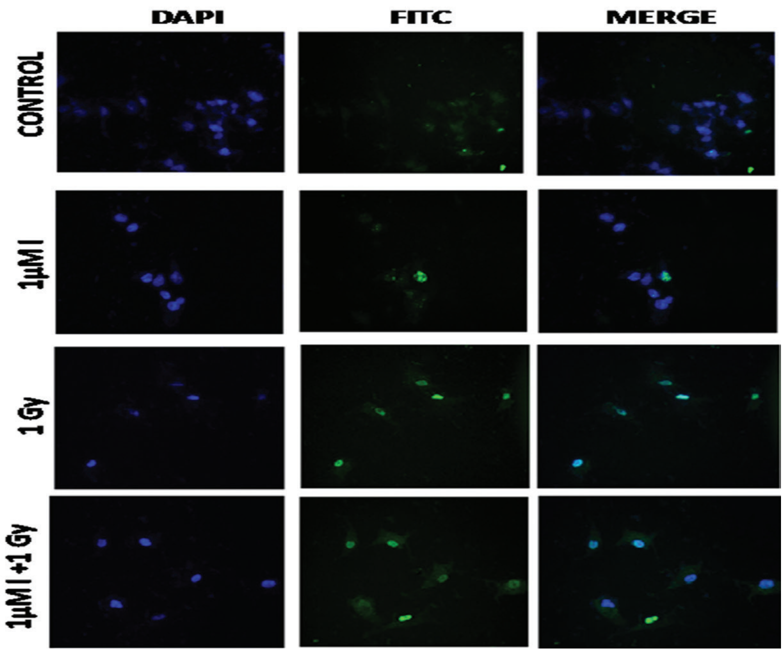

Fig2. Represents increased γ-H2AX foci formation after irradiation with ^{12}C ion in combination with PARP-1 inhibitor.

Expression of EGFR/Akt/p38/ERK involved in the transcriptional regulation of MMP-2 and MMP-9 by western blot:

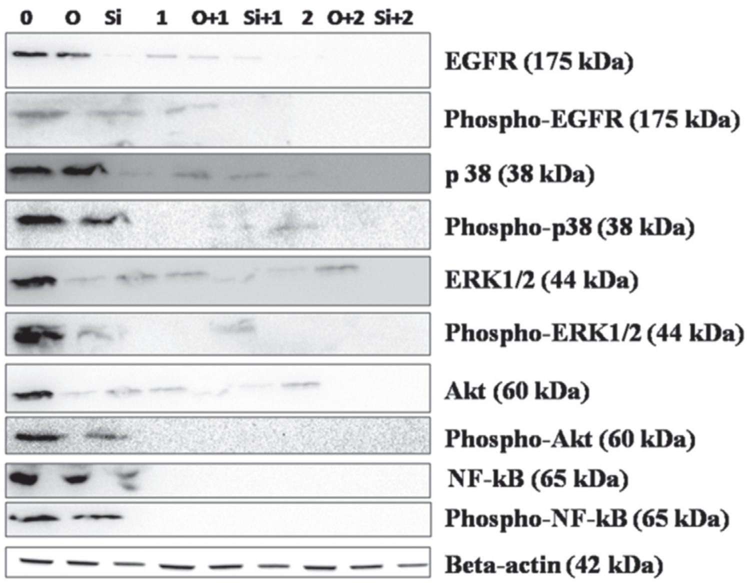

Fig 3: Expression and phosphorylation status of the signaling molecules involved in DDR pathway. Lanes from left- control, olaparib, siPARP-1, 1Gy, olaparib+1Gy, siPARP-1+1Gy, 2Gy, olaparib+2Gy, siPARP-1+2Gy. Here olaparib concentration is 2 μM. All the represented blots are part of the same gel. The number of images from the same blots are developed using anti rabbit and anti mouse secondary HRP conjugated antibodies and by stripping the same blot.

REFERENCES:

[1] Mehlen, Patrick, A. Puisieux.Nature reviews cancer 6.6 (2006): 449.
[2] Minn, A.J., *et al.* Nature 436.7050 (2005): 518.
[3] McCawley, L.J.,L.M. Matrisian. Molecular medicine today 6.4 (2000): 149-156.
[4] D. Nezza, L.A., *et al.* Cancer 94.5 (2002): 1466-1475.
[5] C. Alexander, LC Lin, S. Wen, H.Yan, and W. Hsi. Radiat Oncol. 2017 Aug 15;12(1):132.
[6] Cho, J. Hyun, *et al.* Tumor Biology 37.6 (2016): 7315-7325.
[7] A. Ghorai, N.P. Bhattacharyya, A. Sarma & U. Ghosh. Scientifica. 2014 (2014) 1-10.

5.4 ACCELERATOR MASS SPECTROMETRY

5.4.1 Cosmogenic Radio Nuclides (^{10}Be) In The Laterites of Goa: Impact On Exposure Dating

Achyuthan, H[1], Viegas, A[2], and Dessai, A.G[2].

[1]Institute for ocean Management, Anna University, Chennai 600025
[2]Department of Geology, Goa University, Panjim.

Cosmogenic Radio Nuclides (^{10}Be) In the Laterites of Goa: Impact On Exposure Dating: The project work was carried out since its commencement. Literature reviews on the laterites of Goa have been collected and studied and is updated.

a. Two field trips around Goa at different elevations from the coast were carried out since the second month of the commencement of the project work. Laterite and ferricrete profiles were litho profiled and strategic selection of sampling sites were marked both in the maps and in the filed note. Laterite samples were collected for cosmogenic radionuclide studies and ^{10}Be dating.

b. Over 70 good samples were collected during the field visits. XRF analyses of the samples and XRD analyses of the laterite samples have been carried out. Results have been obtained.

c. Samples processing for the ^{10}Be analyses have to be carried out at IUAC during June 2019.

d. ^{10}Be AMS measurements yet to be performed using accelerator mass spectrometer at IUAC, New Delhi.

Radiocarbons dating of 30 lake samples also have been carried out in February 2019 at the Inter-University Accelerator Centre, New Delhi.

5.4.2 Carbon dynamics in the Ganga basin: implications to the sources, processes and carbon reservoirs

Chinmaya Maharana[1], Pankaj Kumar[1], Rajesh Agnihotri[2], Rajveer Sharma[1], Sanjay Singh[2], J.K.Tripathi[3], Sunil Ojha[1] and Sundeep Chopra[1],

[1]Inter-University Accelerator Centre, New Delhi, India
[2]Birbal Sahni Institute of Paleosciences, Lucknow, India
[3]Jawaharlal Nehru University, New Delhi, India

Objective: The objectives of the present study are i) To elucidate the sources and processes controlling occurrence, distribution and fate of carbon in the Ganga basin ii) To determine the $\Delta^{14}C$ value and ^{14}C age (C-14 dating) of POC to elucidate the sources and age of the organic carbon reservoirs in the Ganga basin.

Methodology: Field work was carried out (March & April 2018) to collect overbank and channel sediment samples from the Ganga river including its tributaries from the Himalaya and Peninsula. Collected sediments were then dried in oven followed by grinding in agate mortar and homogenization. Total particulate carbon (TPC) in the unleached and particulate organic carbon (POC) in the leached (with 0.5M HCl) fractions were measured for the overbank and channel sediment samples by taking few milligrams of sediments in tin capsule and their subsequent analysis by an Elementar carbon analyser at IUAC. Thereafter, the particulate organic fraction was subjected to graphitization using Automated Graphitisation Equipment (AGE) followed by their measurement for ^{14}C by AMS.

Results:

pMC (percent modern carbon) and Libby age for the measured river overbank sediments (Delta 13C = -25)

River	pMC value	Libby age
Ganga river	39.463±0.518 to 86.899±0.450	7469±106 to 1128±41
Himalayan rivers	49.267±0.273 to 91.619±0.466	5686±44 to 703±40
Peninsular rivers	67.301± 0.364 to 87.300± 0.359	3180± 43 to 1091± 33

Note: The data analysis/supportive data generation is in progress.

5.4.3 AMS Dating of samples from Excavations at Uren, District Lakhisarai, Bihar (2016-18)

Bhattacharya Goutami[1] and Kumar Pankaj[2]

[1]Archaeological Survey of India, Excavation Branch III, Patna 800001, India
[2]Inter University Accelerator Centre, New Delhi 110067, India

The modern village of Uren (Urain), 25°10'3"N; 86°13'11"E, falls within Surajgarha Block of District Lakhisarai, Bihar. Excavations were carried out at the site by Excavation Branch III, Patna of the Archaeological Survey of India for two field seasons – 2016-17 and 2017-18 under the direction of the first author. Excavations at the site revealed a complete unbroken sequence of cultures starting with the proto-historic Black-and-Red Ware (henceforth BRW) using culture (around the 2nd millennium BCE) and ending with a flourishing Buddhist establishment during the Pala period (12th century CE). It was possible to visualize the growth and development of a settlement throughout the course of its history. As such Uren represented a microcosm of the ascent of human society through time and space.

It was decided to layout trenches for excavation in all the four directions of the mound and also in the central high part so that the spread of the ancient settlement through space and time could be ascertained. In total 8 trenches were laid in the specified areas and all of them were dug till the natural soil to get a complete cultural sequence at all the sites. The trench URN III laid in the Garh area of the village (highest point) proved to be the most rewarding as well as complex. It emerged as the index trench for the entire site since it revealed a complete, undisturbed and unbroken sequence from the BRW associated rural settlement to the Pala period. It was extremely rich, both in structural remains as well as in antiquities and pottery traditions. The entire cultural deposit of 14.48m above the natural soil was divided into 16 occupational layers. These 16 archaeological horizons were clubbed into 6 cultural periods. Periods I, II and III were named after their dominant pottery traditions which were the main and widely used cultural markers – Black and Red Ware (BRW) associated rural settlement; Black Slipped Ware (BSW) associated rural settlement and the Northern Black Polished Ware culure (NBPW). Periods IV, V and VI were designated after the known political dynasties of this region – Sunga-Kushana, Gupta and, Post-Gupta and Pala periods. As excavation progressed, it soon became apparent that this area of the mound saw regular and intense structural activity from the Sunga-Kushana period onwards. Majority of samples for dating were collected from this trench so that the individual cultural deposits could be dated sequentially and corroborated with those from other excavated trenches. In addition, trench URN V laid to the south of the Uren Hill gave evidence of primary iron smelting activity with no identifiable cultural markers for possible chrono-cultural affiliation. Only one sample could be had from this trench and was crucial for dating the beginning of iron working at the site.

The following table gives the list of samples along with their date range and corresponding cultural affiliation:

Sl. No.	Sample Name	Sample ID	Trench No. and Depth	Radiocarbon Age (BP)	Cal. Age (95.4% Probability) Range and Median	Cultural horizon/ Remarks
1.	URN IIIA/ 1-13.90	IUACD# 18C2181	URN III / 13.90m BS	2956 ± 32	**1261 BC - 1055 BC 1167 BC**	**All these dates correspond to layer 16 (lowermost deposit). These dates belong to Period I designated as BRW associated rural settlement**
2.	URN IIIA/ 2-13.55	IUACD# 18C2182	URN III / 13.55m BS	2901 ± 36	**1213 BC - 996 BC 1087 BC**	
3.	URN IIIA/ 3-13.25	IUACD# 18C2183	URN III / 13.25m BS	2972 ± 40	**1373 BC - 1051 BC 1189 BC**	
4.	URN IIIA/ 4-12.65	IUACD# 18C2184	URN III / 12.65m BS	2966 ± 37	**1287 BC - 1050 BC 1168 BC**	
5.	URN IIIA/ 5-12.00	IUACD# 18C2185	URN III / 12.00m BS	3039 ± 37	**1410 BC - 1135 BC 1295 BC**	
6.	URN IIIA/ 6-11.20	IUACD# 18C2186	URN III / 11.20m BS	2945 ± 43	**1269 BC - 1014 BC 1152 BC**	

7.	URN IIIA/ 8-9.60	IUACD# 18C2188	URN III / 9.60m BS	2853 ± 46	**1192 BC - 904 BC 1021 BC**	**Period II Black Slipped Ware (BSW) associated rural settlement**
8.	URN IIIA/ 9-9.15	IUACD# 18C2189	URN III / 9.15m BS	2511 ± 34	**792 BC - 540 BC 641 BC**	**Period III Northern Black Polished Ware (NBPW) cultural horizon**
9.	URN IIIA/ 10-8.75	IUACD# 18C2190	URN III / 8.75m BS	2688 ± 36	**905 BC - 801 BC 843 BC**	
10.	URN IIIA/ 11-8.50	IUACD# 18C2191	URN III / 8.50m BS	2481 ± 34	**776 BC - 431 BC 631 BC**	
11.	URN IIIA/ 12-7.00	IUACD# 18C2192	URN III / 7.00m BS	2386 ± 40	**746 BC - 387 BC 473 BC**	
12.	URN IIIA/ 13-6.75	IUACD# 18C2193	URN III / 6.75m BS	2163 ± 37	**361 BC - 99 BC 227 BC**	
13.	URN V/ 14-0.78	IUACD# 18C2194	URN V / 0.78m BS	2643 ± 31	**895 BC - 787 BC 812 BC**	**Period III Iron working site**
14.	URN IV/ 16-3.10	IUACD# 18C2196	URN IV / 3.10m BS	1914 ± 34	**6 AD - 211 AD 90 AD**	**Period IV Sunga-Kushana period**
15.	URN IIC/ 17-1.86	IUACD# 18C2197	URN II C / 1.86m BS	2187 ± 28	**360 BC - 176 BC 290 BC**	**Period III NBPW Period**
16.	URN IB/ 18-1.75	IUACD# 18C2198	URN I B / 1.75m BS	2224 ± 34	**381 BC - 203 BC 280 BC**	**Period III NBPW Period**
17.	URN IB/ 19-AAII	IUACD# 18C2199	URN I B	2159 ± 39	**361 BC - 64 BC 216 BC**	**Period IV Sunga-Kushana period**

Authors are thankful to IUAC for extending AMS facility, under Geochronology project funded by Ministry of Earth Sciences, Govt. of India

5.4.4 Brief Report on Bharati Huda Excavation, Odisha with AMS Dates

Dibishada B. Garnayak [1], S. Chopra[2], Pankaj Kumar[2] and R. Sharma[2]

[1]Archaeological Survey of India, Excavation Branch –IV, Bhubaneswar and
[2]Inter University Accelerator Center, New Delhi

The archaeological mound Bharati Huda (20º 06'47''N 86º 05'10'' MSL.11mt), is located in the left bank of river Prachi, 20km away from the Bay of Bengal in Jallarpur village of Niali *tehsil* in Cuttack District and at a distance of 50km from Bhubaneswar, the capital city of Odisha. The site is situated in between river Prachi and rivulet Tanala on its left and right banks respectively which is quite significant for early human settlement. Presently the site is known for its historic antiquities from Chalcolithic period to Iron Age. The region where the site is located has a remark in the map of eastern India for its cultural and religious landscape. The river Prachi gets its name from the word *prachina* meaning ancient. The existing folklore considers river to be a reincarnation of mythical river Saraswati and also references about the river found in *Markandeya Purana, Kapila Samhita, Prachi Mahatmya* and in *Odia Mahabharat.* Tradition and legend link various places of the valley with the Ramayana and the Mahabharata. The valley is studded with religious shrines, ancient forts, *mathas,* monastery and archaeological mounds. The rich and diverse cultural heritage shows that suitable climate for the growth, development, and popularity of various religious sects and culture existed in the valley from the early time.

In the year 2017-18 the excavation work was conducted at Bharati Huda site by Excavation Branch-IV of Archaeological Survey of India under the direction of the first author. During the survey Bharati Huda archaeological mound was found significant and more potential in nature in comparison to most of the sites documented in the valley.

The geology of the area is dominated by the Early Holocene sediments of alluvial origin under a deltaic environment and is one of the youngest marine horizons. The flood plain landscape has been formed out of the deposition of the alluvial sediments of the river Mahanadi around 3000-6000 BCE (Mahalik 2006). The silty clay deposits, moderate to low energy wind, flood plains became a source for agriculture, mangrove forest and biodiversity which attracted the human population to settle over it by c.1500 BCE. The surrounding soil of the archaeological site is of Alfisols (the deltaic alluvial soils) these soils are generally deficient in P2O5 and N2. The K2O are fairly adequate, and pH varies between 6 and 7 (The soil pH value of the archaeological mound varies from 6-8) and has been observed that these soils support paddy crops. This observation is true as corroborated with the present agricultural practices. The excavation also revealed plant remains of domesticated variety of rice, *kulith,* green gram, black gram, lentil and Jute. Thus, the fertile track attracted the pre-historic man for dwelling and settling in this landscape from time to time. The area around the site is highly fertile and supports *dhan/*paddy *(Oryza sativa); surjyamukhi/sun-flower (Helianthus annuus); mug/green-gram (Phaseolus mungo); sarisha/mustard (Sinapis nigra); akshu/sugarcane (Saccharum officinarum)* and other crop round the year due to the canal irrigation. Coconut *(Cocos nucffera)* and pan/betel-leaf *(Chavica betle)* plantations constitute a major economic crop of the area. The climate of the area is characterized by hot humid summers and well distributed rains of the south-west monsoon which supports the semi-evergreen types of natural vegetations. Relative humidity is generally high throughout the year and winds are fairly strong. The average annual rainfall in the area is 1448 mm (Odisha district Gazetteers: Cuttack, 2016).

The existing mound Bharati Huda measures approximately 46215 sq.mts having heights of 4mts from the surrounding landscape. The excavation at the site was carried out to know the chrono-cultural sequence of the site, to correlate the habitational deposit with other known Chalcolithic sites of Odisha in particular and that of eastern and central India in general and to see whether the site has continuous human habitation from prehistoric time to early historic period. According to the availability and suitability of land 750 sq mt area was selected for under taking excavation in 30 quadrants in three pockets within the site, out of which only three quadrants have encountered natural strata having 5mt of habitational deposits divisible into 7 to 8 layers, and divisible in to three cultural phases viz, Early Chaclolithic, Mature Chalcolithic and Iron Age from bottom to top. Among the three quadrants, Trench ZA6/III have been consider as the index trench of the site due to its location at the highest elevation and having maximum cultural deposits.

Trench ZA6/III

This trench lies on the western part of the mound and digging up to a maximum depth of 6mts below surface revealed 8 habitational layers above the natural soil. The details of the layers described below are from bottom to top.

Radiocarbon dating

The Charcoal samples have been collected from stratified layers (3), (4), (5) and (7) by taking proper procedure and were dated by using AMS radiocarbon technique at IUAC, New Delhi. Radiocarbon ages were calibrated using Oxcal software and median ages are utilized in this report.

Layer (9) is gray in colour (2.5Y 5/1 on the basis of Munsell soil colour book) having pH value 6.5, fine in texture sticky in nature, bereft of artifacts and human activity and treated as natural layer.

Layer (8) above the natural soil is dark gray in colour (2.5Y 4/1) pH value 6.5, fine in texture sticky in nature, composed of tiny potsherds of red ware, burnt clay lumps and considered as the first habitational layer dated to early phase of Chalcolithic culture. It was the period when for the first time human beings were migrated to the region and occupied the valley and continued to survive till date.

Layer (7) is grayish brown in colour (2.5Y 5/2) pH value 7, fine in texture semi-compact in nature contains charcoal sample which is dated to 1404 BCE (C^{14} sample ID- IUACD#18C2180) and ceramic assemblage of Red Ware, Red Slipped ware, Chocolate slipped/tan red ware and Grey/Black ware, cord impressed ware, perforated ware, charred bones and burnt patches along with ash.

Layer (6) is dark grayish brown in colour (10YR 4/2) pH value 6, medium to fine in texture semi compact to loose in nature contains charred and un-charred bones, a lonely piece of stone chisel, burnt clay lumps suggesting existence of wattle and daub house, ceramic assemblage of Red Ware, Red Slipped, Chocolate slipped/tan red ware, cord impressed ware, perforated ware, Grey/Black ware and in the upper level evidence of yellow colour mud structure was noticed.

Layer (5) is significant as for the first time Black and Red ware and painted pottery appeared in this layer which has been dated to 1269 BCE (C^{14} sample ID- IUACD#18C2177). It is brown in colour (10YR 5/3) pH value 6, medium to fine in texture compact to loose in nature contains charcoal, ash patches, burnt clay nodules, charred and un-charred bones, antiquities made of bone and stone and potsherds of Red ware, Red slipped ware, Chocolate slipped/Tan red ware, cord impressed ware, perforated ware, Black ware and Black-and-Red ware. In this layer a circular structure made of yellow clay was noticed. A dump in the eastern section of the quadrant containing ash, charcoal pieces, potsherds and charred bone was encountered. The evidence of domesticated rice and jute fiber was also noticed for the first time. It seems that new craft specialization emerged this time or a new ethnic group came in contact with the inhabitants.

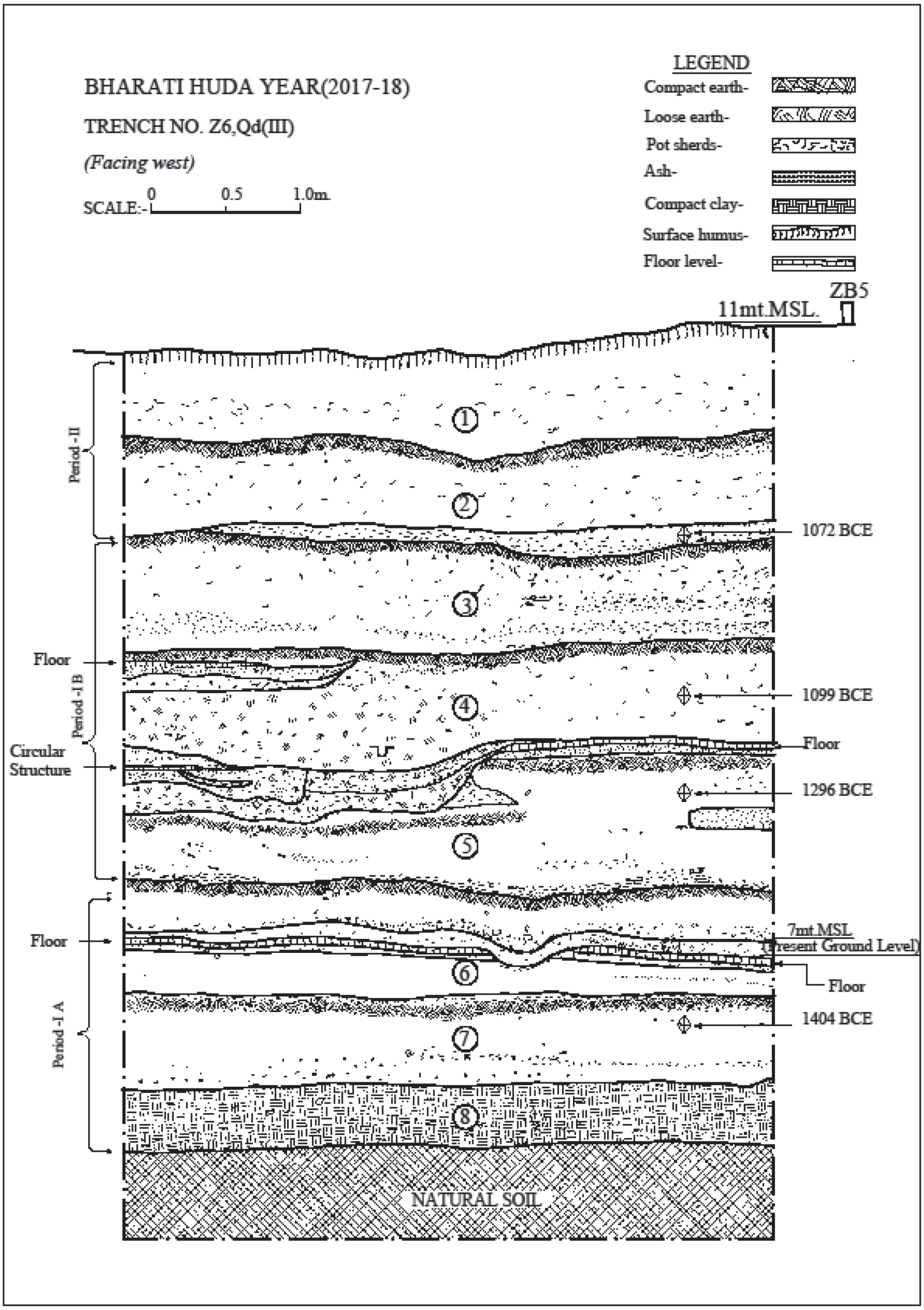

Layer (4) is light yellowish brown in colour (2.5Y 6/3) pH value 6.5 medium to fine in texture, loose in nature contains similar material culture as in layer (5), except the miniature pot in red ware which was found for the first time in this cultural level, variety of bone tools appeared in this period. The AMS date of charcoal sample collected from this layer has been dated to 1099 BCE (C^{14} sample ID- IUACD#18C2176). And within the painted pottery a lonely specimens of Sun motif in a chocolate slipped pottery found from the layer which indirectly gives light on nature worship in the valley.

Layer (3) found to be the last phase of the Chalcolithic period is gray in colour (2.5Y 5/1) pH value 6, medium texture semi compact to compact in nature contains ceramic assemblage of Red Ware in Red Slipped ware Chocolate slipped/tan red ware Grey/Black ware, cord impressed ware, perforated ware Black and Red ware and charcoal, ash patches, burnt clay nodules, charred and un-charred bones, maximum number of antiquities found from the layer assigned to 1072 BCE (C^{14} sample ID- IUACD#18C2175) are made of bone followed by stone, terracotta and a copper fish hook. The findings of toy cart wheel, shark tooth proves their acutancey in both land routes and water routs.

Layer (2) deposit is marked with the presence of iron having continuation of earlier cultural features except the occurrence of pre-firing painted pottery on dull red ware. It is light brownish gray in colour (10YR 6/2) pH value 6; medium texture compact in nature. The evidence of Iron and copper objects in this strata suggested their expanding subsistence zone during this period which can be dated to Iron Age.

Layer (1) is light brownish gray in colour (2.5Y 6/2) pH value 6.5, medium texture compact in nature contains tangible material remains in form of maximum number of Red Ware pottery in comparison to other ware like Red Slipped ware, Grey/Black ware, perforated ware and bereft of Chocolate slipped ware; burnt clay nodules, charred and un-charred bones and materials from Iron age as well as early historical inclusion is noticed in this layer.

Thus the index trench yielded 8 occupational layer, where layer 8 to 6 throw light on the incipient Chalcolithic cultural activities termed as early Chalcolithic followed by a mature phase of the culture as evidenced from the technical advancement noticed in the ceramic assemblage viz., the introduction of Black and Red ware, ochre colour painted potter on chocolate slipped ware in Layer 5 to 3. Not only in technology but also in belief system there was a change as noticed from the Sun motifs painted pottery retrieved from layer 4 which indicates about the nature worship among the inhabitants. The top 2 layers are different from the lower layers with the presence of Iron and copper. The habitation covered a long span of time as known from the 5mts habitational deposit and C^{14} dates provided by IUAC.

Acknowledgements

I am grateful to the Director General and Director (Exploration and Excavation) of Archaeological Survey of India, New Delhi for granting the permission to excavate Bharati Huda archaeological site. I am also thankful to Inter University Accelerator Center, New Delhi for extending AMS facility under Geochronology project [MoES/ P.O.(Seismic)8(09)-Geochron/2012] for providing C14 dates to the site. I am also thankful to Sanjay Panda, Ashis Ranjan Sahoo, Umakanta Bhoi - Assistant Archaeologists and Suvendu Kumar Khuntia-Surveyor Gr.I, Bibhuti Bhusan Badamali-Draughtsman Gr.I, Rabindra Nath Sahoo-Photographer Gr.I, Surath Kumar Bhoi-Store keeper and other staffs for their involvement and to the villagers of Jalarpur for their cooperation and support during the excavation work.

References

[1] Mahalik, N.K. 2006. A study of the morphological features and Bore hole cuttings in understanding the evolution and geological process in Mahanadi Delta, East coast of India, *Journal Geological society of India* Vol.67:595-603 (May 2006).

5.4.5 Estimation of beryllium from Polar Regions and lake sediments - Paleo-Oceanographic implications

Nayak G. N.[1], Choudhary Shabnam[2], Chopra Sundeep[3] and Pankaj Kumar[3]

[1]CSIR Emeritus Scientist, Marine Science, School of Earth, Ocean and Atmosphere Science, Goa University, Goa 403 206, India
[2]Ministry of Earth Science, Govt. of India, New Delhi, India
[3]IUAC, New Delhi

BERYLLIUM ESTIMATION

Surface and core sediment samples were collected from lakes, fjords and bays from Arctic and Antarctic regions and stored at -20ºC. Later, sediment sample collected from lakes and bay from Antarctica was chemically processed for Be analysis at Inter University Accelerator Centre (IUAC), New Delhi. Fe-Mn oxide fraction was extracted following the sequential extraction procedure for the speciation of trace metals (Tessier et al., 1979) [1] as this method have been found efficient to extract 10Be (meteoric) as compared to other methods.

METHODOLOGY

A portion of each subsample was powdered and homogenized in an agate pestle and mortar. 1 g of sediment sample was taken in a centrifuge tube and treated with 20 ml 0.04M hydroxylamine hydrochloride ($NH_2OH.HCl$) in 25% (v/v) acetic acid (HOAc) mixture for 6 hrs at 90ºC, and run with 400 rpm with continuous agitation (Tessier et al., 1979) [1]. The supernatant was removed after centrifugation, and dried completely on the hot plate. Then, the dried extract was dissolved in 10 ml of 1N HCl (Non-Calibrated). 1 ml of this solution was removed and kept for ^{9}Be analysis by ICPMS. Remaining 9 ml of solution was spiked with (.2 ml) ^{9}Be carrier solution (NIST SRM-3105a) and dried on the hot plate. Further, the extract was dissolved in 1 ml 6N HCl and passed through Anion column and the residue was collected in Teflon beakers and dried completely. Further, it was dissolved in 0.2 M H_2SO_4 + 2% H_2O_2 and passed through cation column. This residue was collected and mixed with 5-8 drops of 8M HNO3 and dried completely and precipitated with the help of NH3. The supernatant was removed with the help of centrifugation and precipitate (BeOH) was collected in quartz vials. The quartz vials containing BeOH precipitate were kept in a furnace with step heating up to 900°C to convert precipitate BeOH to BeO. After drying, the BeO powder was loaded to the cathode tube mixed with Nb powder in a ratio of 1:3 and will be analysed for $^{10}Be/^{9}Be$ ratio using an Accelerator Mass Spectrometry (AMS).

DISTRIBUTION OF ^{9}Be IN SEDIMENTS

Along the Prydz Bay, in the surface sediment samples ^{9}Be content fluctuated in a range between 17.62 ppb at station P2 and 166.64 at station P6. Overall, ^{9}Be showed an increasing trend with increasing water depth (31-140 m) away from the coast (P1-P7) similar to that of silt and clay as finer grain size provides large surface area for the adsorption of authigenic ^{9}Be. In Larsemann Hills, East Antarctica ^{9}Be concentration was high (average 122.91 ppb) in core L-8 and low in core L-10 (66.97 ppb). While in Schirmacher Oasis, East Antarctica ^{9}Be concentration was high in core L-6 (average 105.74 ppb) and low in core V-1 (average 70.69 ppb). However, ^{9}Be concentration is lower in core L-8, L-10, L-12, GL-1, V-1 and L-6 as compared to the average crustal values (~2ppm). From all the six cores studied, it is observed that silt has high scavenging efficiency of ^{9}Be as compared to the clay. Clay has tendency to form aggregates which have faster sinking rates. These aggregates provide less surface area for the adsorption of ^{9}Be suggesting high scavenging efficiency of silt as compared to the clays (Simon et al., 2016)[2]. Be also showed good association with Ti supporting lithogenic source.

REFERENCES:

[1] A. Tessier, P.G. Campbell, and M. Bisson, Analytical chem. 51(7)(1979) 844-851.
[2] Q. Simon, N. Thouveny, D.L Bourles, L. Nuttin, C. Hillaire-Marcel, and G. St-Onge, Quarter. Sci. Rev. 140 (2016)142-162.

5.4.6 Beryllium concentration, clay minerals and metals in sediments in reconstruction of paleo-climate

Nayak G. N.[1*], Kangane Janhavi[1], Chopra Sundeep[2] and Pankaj Kumar[2]

[1]Marine Science, School of Earth, Ocean and Atmosphere Science, Goa University, Goa 403 206, India
[2]IUAC, New Delhi
[*]CSIR Emeritus Scientist

OBJECTIVES

To study clay minerals, selected metals, ^{10}Be and ^{9}Be concentration in sediment cores and use them to reconstruct paleoclimate
and
To understand sediment size and composition control on concentrations of 10Be and 9Be and also to understand the degree of paleo weathering using 10Be/9Be to support the climate studies.

RESEARCH WORK CARRIED OUT

Two cores, namely, GC 13 and GC 16 which were collected from Bay of Bengal (onboard SK 308) were analysed for sediment components, while the core GC 13 was further analysed for clay minerals and metals (Fe, Mn, Al, Ti, Pb and Zn) to achieve the project objectives. Sediment component profile of core GC 13 represented cyclicity in the depositional environment.

WORKSHOP ATTENDED

To understand the principle and working of Accelerator Mass Spectrometer (AMS) and also sample processing national workshop on "Isotopes in Earth, Ocean and Atmospheric Sciences" conducted by IUAC and NIO held at CSIR-National Institute of Oceanography (NIO), Goa from 18 – 20 February 2019 was attended.

5.4.7 Palaeoclimatic Reconstruction of Changme Khangpu Glacier, Upper Tista Basin, Eastern Himalaya, India

Manasi Debnath[1], Hiambok Jones Syiemlieh[1], Milap Chand Sharma[2] and Pankaj Kumar[3]

[1]Department of Geography, North-Eastern Hill University, Shillong, Meghalaya 793022, India
[2]Centre for the Study of Regional Development, School of Social Sciences, Jawaharlal Nehru University, New Delhi 110067, India
[3]AMS & Pelletron Group, Inter- University Accelerator Centre, New Delhi 110067, India

The Changme Khangpu (CK) glacier in Sikkim Himalaya has been taken to study the palaeoclimate through the proxy of glacial landforms and glacigenic sediment assemblages. The main axis of CK valley trends N-S and modern glacier restricted at an altitude between 5900 and 4810 m a.s.l. (27.9583 N, 88.6844 E). Lack of previous studies, spectacular preserved landforms and some catastrophic natural events in this valley captivated the attention and raised the importance to portrait the glacial geomorphology and reconstruct the palaeoclimate of this monsoon dominated valley.

The work related to the palaeoclimate reconstruction is supported by the geomorphology, sedimentology, geochemistry, and geochronology. Here, we have used SRTM DEM, Sentinel-2A satellite imageries, GPS, sedimentological analysis and field techniques to portrait the glacial and glacigenic sediment assemblages. The ^{14}C isotope AMS dates of glacio-fluvial and glacio-lacustrine deposition are used to place the observed phases of climate in a common chronological ground. The ^{14}C isotopic measurements of sediment samples have been done in the 500 kV Pelletron AMS. The sediment samples were acquired from the 5 different locations and landforms in the Changme Khangpu basin of North Sikkim Himalaya. Our detailed reconstructed geomorphology supports the sample bearing landforms were developed under the deglacial warmer phases. Four glacial phases have been identified by the prominent latero-frontal moraines and group of hummocky moraines during the field survey, mapping and sedimentological analysis. The deglacial sedimentation in a form of rhythmite archive has been dated back to 31.47 ± 0.15 Ka CalBP situated at 1.7 km from the present glacier snout. The younger talus scree, debris fan are the major paraglacial features are overlying the palaeo-rhythmites and enhancing the modification of primary sedimentation, and hence demarcate the deglaciation phase (Church and Ryder, 1972). This result helps to draw the relative timing of the glacial Phase I and Phase II i.e. before 31.47 ± 0.15 Ka CalBP. Sediment-chronological analysis of glacio-fluvial archive from a trench that is situated within the Phase II limit portrait the oscillating nature of palaeo-climate from 14.053 ± 0.168 to 3.447 ± 0.06 Ka CalBP. The geochemistry also supported the oscillating nature of palaeo-environment that has been identified through the analysis of major elements (SiO2, Al2O3, TiO2, Fe2O3, MnO, MgO, CaO, Na2O, K2O, and P2O5) on the same vertical profile. The elemental analysis was carried out using the XRF facility at IUAC. An inverted age of relatively modern sedimentation has been recognized through the 14C AMS dating that supports the model of the paraglacial slope processes, which is continuously modifying the primary deposited materials (Ballantyne, 2002). The rock samples from the moraines have been collected and processed for extracting the quartz mineral. Samples are ready for 10Be and 26Al dating to reconstruct the absolute age of the glacial phases.

Bibliography:

Ballantyne, C.K., 2002. Paraglacial geomorphology. Quat. Sci. Rev. 21, 1935.
Church, M., Ryder, J.M., 1972. Paraglacial sedimentation: A consideration of fluvial processes conditioned by glaciation. Bull. Geol. Soc. Am. 83, 3059–3072. https://doi.org/10.1130/0016-7606(1972)83[3059:PSACOF]

5.4.8 Investigation of Saraswati paleochannels and associated Indus Valley Civilization in context of drainage evolution and paleoclimate

Naresh Chandra Pant[1], Apoorva Alok[1], Pankaj Kumar[2] and S.Chopra[2]

[1]Department of Geology, University of Delhi, Delhi-110007
[2]Inter-University Accelerator Centre, New Delhi -110067

Introduction and background

Geographical spread of the Indus Valley civilization from NE Afganistan to Pakistan and NW India from 5000-1300 BC (Kenoyer, 1977), its evolution and demise have interesting geological implications as the archaeological remains of the settlements are spatially associated with the past and present basins of the Indus river. It being a dominantly agriculture based civilization, the twin resources of water and soil of significance in settlements and their evolution. The third major factor is that of the influence of change in the climate during Holocene epoch (last 11,700 years).

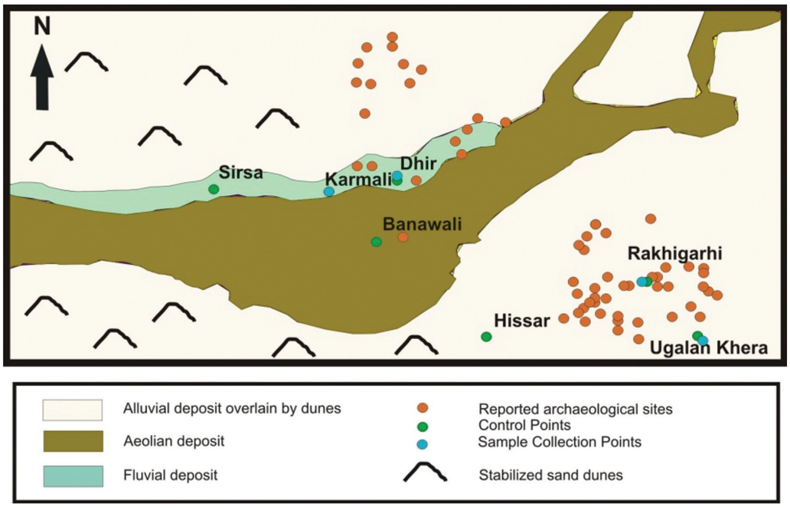

Fig. 5.4.6: Map depicting the sites from where samples were collected.

Our earlier work (Saini et al., 2005, 2009) has described the architecture of palaeochannels in the plains of Haryana and adjacent Rajasthan and had also constrained the three fluvial events starting from >30000years. A climate change in Holocene was also described leading to a reduction in precipitation in Holocene and it coincided with certain changes in the Indus valley civilizations. The ages of these events was mainly constrained by Optically Stimulated Luminescence chronology.

A study was mounted in collaboration with IUAC nearly a year ago to establish the climate change-civilization context with greater precision for Harappan settlements in the main paleochannel as well as newly described tributaries arrived at after a remote sensing and field based hydrological-geological study (Mehdi et al. 2014). In the course of this work we had also collected evidence to demonstrate the higher Himalayan (glacier water) sourcing of the paleo-river commonly referred as river Saraswati (unpublished data).

In the present work samples were collected from existing palaeochannel as well as from a well knownHarappan site at Rakhigarhi (Figure below) to understand the evolution of the mature Harappan phase and to link it to the geological processes operative at that time.

Work reported during previous report

The work carried out so far includes two field campaigns, logging of the geological and cultural mounds, sampling in Rakhigarhi (three archaeological mounds), a geological flood plain succession overlain by archeological mound at Dhir village and aeolian samples (to characterize aridity), generation of ~20 AMS radiocarbon ages, XRD analysis of ~30 samples (mainly for clay mineral content to characterize soil), SEM and sedimentological analysis.

Initial results indicate following:

1. A river (Saraswati?) flowed during Holocene in the now defunct paleochannel and it had atleast two major additional tributaries (Mehdi et al. 2014).

2. The sourcing of sediments in this continued to be from Higher Himalayas during Holocene (Zircon U-Pb unpublished data).

3. A reworking is indicated after 4100 before present (BP) and it is likely to coincide with the 4200-3800 BP rapid climate global climate change event (unpublished data).

4. The soil generally lacked the high cation exchange capacity clay minerals (CEC) thus leading to shifting cultivation and therefore continued relocation of settlements.

Work done since last report

An extensive field work was undertaken where we traversed from the base of Shivaliks to India-Pakistan border along the course of proposed river in search of crucial geological as well as archaeological samples. Samples were collected from paleochannels as well as interfluve to understand the characteristic of deposits of streams proposed by Mehdi et al. 2016. Samples were collected and are under processing.

Results and Discussion

1. The grain size analysis of the collected samples suggest variable flow regime in different layers of deposited sediment in present day channel near India-Pakistan border.

2. The sample collected from geoarchaeological mound in the paleochannel near Dhir shows the succession of clay, silty clay and sand. Floating charcoal pieces are present at several layers which were subjected to AMS radiocarbon geochronology. Sedimentological, heavy mineral and quartz microtexture studies were also carried out.As the samples are from the most prominent paleochannel which was likely to have been active till the end phase of the river, youngest ages of the fluvial activity were expected to be recovered from this site. The lower level sample of the geological component of the succession has indicated an age of C^{14} 2782 $\pm$ 43 years BP while the youngest age of 2030 $\pm$ 45yrs BP is from near the middle of the cultural succession. This is overlain by brownish silty clay from which an age of >20000 year BP has been recorded from charcoal which is not known from this area and needs to be further investigated. Since this succession is within the flood plain of the now defunct river, the older ages were interpreted to be reworking during flooding. However, this interpretation required validation and for that OSL sampling was carried out in joint traverses with the Geological Survey of India. The hypothesis was that if the river was flooded at ~2000 BP, it should be validated by younger than this OSL ages of the associated quartz grains. Two samples from the bottom of this succession gave and age range of 1.4 -1.1 ka (errors of $\pm$ 0.1 ka).

3. At Rakhigarhi, several archaeological mounds are present at this site with exposed sections of upto ~10 m. Clay, silty clay, ash and pottery rich layers constitute the major units of these mounds. AMS radiocarbon dates indicate the reign of habitation in these sites beginning during pre-Harappan time (>5250 yrs BP), flourishing during Early Harappan phase and a depleted occupation during Mature Harappan time (e.g. RGR2). Presence of a remobilized older age in mound RGR4 over a sequentially layered cultural mound may suggest reworking of older carbon material possibly during a flooding event (high precipitation).

4. Clay mineralogy of different layers suggest a relatively colder period between 5000 and 4800 BP, which is also evident by grain size parameters.

5. Absence of sand and sandy-silt deposits in other mounds of Rakhigarhi suggests the presence of a channel near the group of mounds at Rakhigarhi, proving the hypothesis proposed by Mehdi et al. and Kar et al.

Future Work:
1. A research publication is under preparation using all these inferences.
2. XRD and XRF of samples obtained from recent field campaign is to be completed.

5.4.9 Cosmogenic Radionuclide dating of glacial deposits of Thajiwas valley of Kashmir Himalaya

Omar Jaan[1], Reyaz Dar[1], Shakil Romshoo[1], Pankaj Kumar[2], Jitendar Pattanaik[3] and Soumaya Prakash Dal[2]

[1]Department of Earth Sciences, University of Kashmir, 190006
[2]Inter University Accelerator center (IUAC) New-Delhi 110067
[3]Center for Geography and Geology, Central University Punjab 151001

In the present study, glacial-geomorphic landforms of the Thajiwas glacial valley, which provide vital information about the impact of glacial advance and retreat on the geomorphology, were mapped from remote sensing data supported by extensive fieldwork. Morphology, shape and location of terminal and lateral moraine ridges were used to establish the palaeo-glacial extents, glacial volume and the number of glacial advances of the Thajiwas glacier. During the fieldwork, 15 moraine samples were collected from seven different locations to estimate the timing of the last glacial maximum. The samples of Quartz grains were processed for the ^{10}Be and ^{26}Al cosmogenic radionuclide dating.

Mapping and sampling:

The glacial geomorphic features were mapped using the high-resolution satellite data supported by the fieldwork and GPS surveys [1,2]. Vestiges of recently deposited recessional moraines of minor advances reflect the response of the glacier to the regional climate change3. The change in the glacier surface area shows that the glacier has receded from 47.4 km^2 during last glacial maximum to 3.60 km^2 at present. The greater rock excavation during glacial maximum and the concomitant head ward expansion of the glacial valley at the expense of cirque retreat has driven the drainage divide southward, thereby limiting the topographic relief. Well-preserved terminal and lateral moraines samples were collected in the Thajiwas valley, which provide evidence of the last three glacial advances[4].

Sampling Processing details

Different apparatus used for sample processing were washed with Milli-Q (deionized) water . The following steps were followed for the separation of the ^{10}Be and ^{26}Al. Quartz sample was added to the PFA wide-mouth bottle and MQ water was poured into it up to the mark of 500ml for leaching process. 5ml of Hydrofluoric acid was added to the sample and shook regularly after every 30 minutes for 72 hours. Then, the water was drained out from the sample before being transferred to oven for drying. After drying, 20-30 grams of the purified quartz were subjected to digestion process. The samples were transferred into the Teflon beakers and 20ml of HF acid (Double Distilled) was added to each sample. The beakers were put on the hotplate and heated to the temperature of ~110 to 125º C. 5-10 ml of HNO_3 was added to the sample. The samples were dried completely after the digestion. About 10ml of 1N HCl was added to each sample to dissolve it completely. The part of the sample was transferred to the 10ml bottles for the AMS studies. 0.1 ml of ^9Be carrier was added to the sample, the process is called spiking. The sample was thereafter transferred onto the hotplate and heated to the temp of 100-110º C. The anion and cation column separation was carried out using the Bio rad resin column. The samples of Quartz grains were processed for ^{10}Be and ^{26}Al samples and collected during the process and dried completely. The samples were then dissolved using the MQ and transferred to centrifuge tubes. Few ml of NH3 solution was added to the sample, shook and kept undisturbed for 12-15 hours to let ^{10}Be and ^{26}Al precipitate completely. The excess liquid at the surface was drained out and the sample were transferred to the quartz vials and heated in a furnace at a temp of 300º C for 12 hours.

REFERENCES

[1] Dunlop, P., Clark, C.D., 2006. The morphological characteristics of ribbed moraine. Quat. Sci. Rev. 25 (13), 1668-1691.

[2] Clark, C.D., 1997. Reconstructing the evolutionary dynamics of palaeo-ice sheets using multi-temporal evidence, remote sensing and GIS. Quat. Sci. Rev. 16 (9), 1067-1092.

[3] Porter, S.C., 1989. Some geological implications of average Quaternary glacial conditions. Quat. Res. 32 (3), 245e261.

[4] Dar, R. A., Jaan, O., Murtaza, K. O., & Romshoo, S. A. (2017). Glacial-geomorphic study of the Thajwas glacier valley, Kashmir Himalayas, India. Quaternary International, 444, 157-171

5.4.10 Radiocarbon ^{14}C dating of sub-surface sediment samples using Accelerator Mass Spectrometry (AMS)

Parveen Uzma[1], Sreekesh S[1], Pankaj Kumar[2] and S. Chopra[2]

[1]Centre for the study of Regional Development, Jawaharlal Nehru, New Delhi-110067, India.
[2]Inter-University Accelerator Centre, New Delhi-110067, India.

We have measured the absolute ages of subsurface sediments deposits along the Lower Baitarani Basin, East Coast of India using Accelerator Mass Spectrometry (AMS) facility at IUAC. The samples have been obtained from eight locations and subsurface sediment facies have been determined based on colour and textural variability. The facies with carbon content above 0.5 % have been considered for radiocarbon ^{14}C dating. The radiocarbon ages along with geochemical proxies have revealed the depositional environment and climate during the Holocene period in Lower Baitarani region.

OBJECTIVE

The major objective of this work is to analyze the chronology of sediment deposition along the lower reaches of Baitarani Basin up to the depth of 1000 cm. It is also aimed to draw inferences about the past climate based on geochemical proxies and absolute dating.

RESEARCH OUTPUT

Radiocarbon (^{14}C) ages of four samples were determined using AMS through 500 kV Pelletron' 5 accelerator (Vahila et al., 2016). The uncalibrated radiocarbon dates were converted into the calendar ages using OxCal 4.3 (Bronk and Lee, 2013) (Figure 1).

In the mixing zone active floodplain (MS1), beach ridges (MS2), paleochannels (MS3 and MS4) were recognized, and samples were collected by bore-welling at these locations (Figure 2). The samples recovered from the riverine zone could not be dated yet as permission for dating only 12 samples was granted using the AMS facility. Rest of the samples will be dated in the current session.

Samples for ^{14}C dating were collected from MS1 site at the depth of 800 cm, 350 cm and 30 cm providing age ranges (2σ date range) of 1740-1541, 1415-1296 and 961-769 cal yr BP respectively. From MS2 location, samples from 750 cm, 550 cm, and 250 cm depth were recovered giving dates of 7764-7595, 7759-7575 and 4766-4615 cal yr BP (2σ date range). From MS3 site, samples from the depth of 1000 cm, 760 cm, 600 cm, and 450 cm yielded radiocarbon ages of 7790-7610, 7634-7469, 6283-6095 and 2851-2738 cal yr BP (2σ date range). From MS4, ^{14}C samples were obtained from 1000 cm and 700 cm depth providing dates of 7792-7608 and 2441-2301 cal yr BP (2σ date range).

The chronology constructed for the landforms located in the mixing zone has shown remarkable variation in their depositional environment. The present analysis has suggested the occurrence of a relatively humid episode around 7800 cal yr BP followed by a drier phase around 6000 cal yr BP. Another episode of elevated humidity has been marked around 2700 cal yr BP. The humid and arid episodes have also been reported during the Holocene in other parts of the Indian subcontinent (Alappat et al., 2015; Narayana et al., 2017; Babeesh et al., 2019).

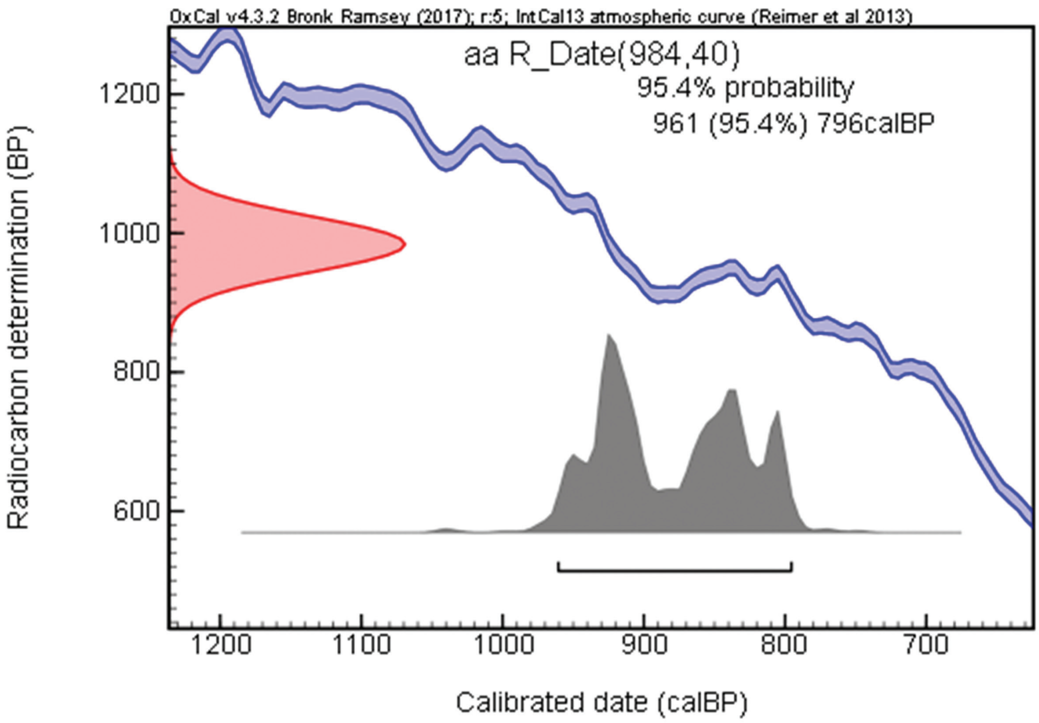

Figure 1 Calibration of radiocarbon dates using OxCal 4.3

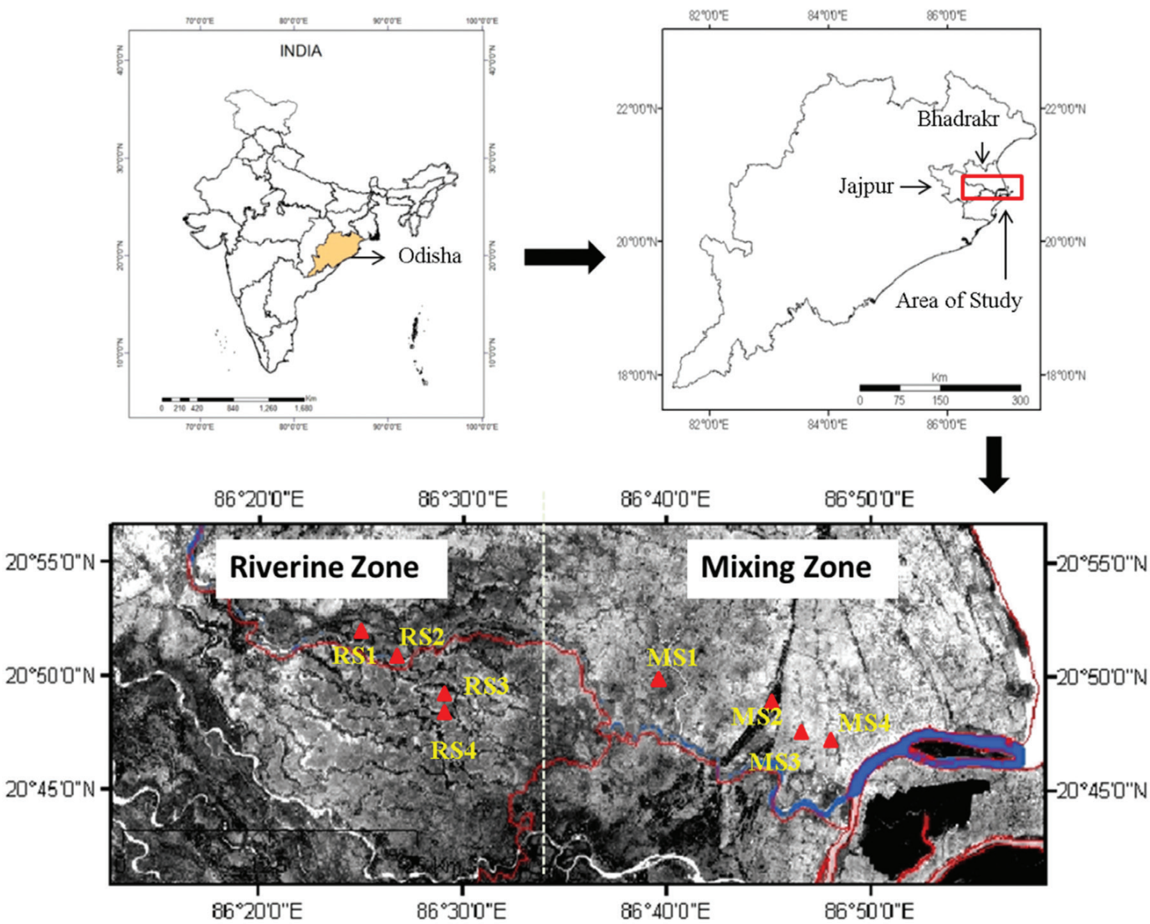

Figure 2 Area of study and sample collection sites

REFERENCES:

[1] Alappat, L., Frechen, M., Sree Kumar, S., Suresh Babu, D.S., Ravur, R., Tsukamot, S. Geomorphology, 245, 73-86 (2015).

[2] Babeesh, C., Achyuthan, H., Resmi, M.R., Nautiyal., C.M., Shah, R.A. Quaternary International, 507, 156-171 (2019).

[3] Bronk, R.C., Lee, S. Radiocarbon, 55, 720-730 (2013).

[4] Narayana A.C., Prakash V., Gautam P.K., Tripathi S. Quaternary International, 443 (3), 115-123 (2017).

[5] Vahila, M.N., Kumar, P., Bhogale, A., Chopra, S., Shinde, V., Jadhav, N., Shastri, R. Current Science, 3 (1), 27-28 (2016).

5.4.11 Radiocarbon dating of soil from Kaziranga National Park, India

Pramit Kumar Deb Burman[1]*, Supriyo Chakraborty[1], Dipankar Sarma[2], Pankaj Kumar[3] and Rajveer Sharma[3]

[1]Centre for Climate Change Research, Indian Institute of Tropical Meteorology, Pune - 411008
[2]Department of Environmental Sciences, Tezpur University, Tezpur - 784028
[3]Inter-University Accelerator Center, New Delhi, Delhi – 110067
*Corresponding author. e-mail: pramit.cat@tropmet.res.in

The terrestrial ecosystems are the largest sink of atmospheric CO_2 with a global sinking strength of 3.1 ± 0.9 GtC y-1 [1]. The soil organic matter (SOM) turnover time is an important parameter for inferring about the soil mixing and nutrient dynamics of any ecosystem that is used as an input parameter for calculating its productivity using the terrestrial biosphere models [2]. In the present proposal (btr62120) we aim to estimate the land carbon pools at the Kazirana National Park (KNP), Tezpur, Assam as part of the research objectives of the MetFlux-India project by the Ministry of Earth Sciences (MoES), the Government of India [3].

The Accelerator Mass Spectrometry (AMS) is a widely used technique for estimating the radiocarbon (C^{14}) age of different archaeological, geological, and biological samples and known for its precision [4]. The C^{14} dating of the soil samples from three different locations in KNP was carried out using the AMS facility at IUAC, Delhi. These samples were collected in April, 2017 and preserved carefully from possible degradation/contaminations. The samples were pre-processed at the wet chemistry laboratory following the standard acid-base-acid protocol [5] in March 2018 and subsequently analyzed for 14C at the IUAC AMS facility, New Delhi in June 2018.

According to the preliminary results the top soil at KNP, up to a depth of a few tens of centimeters is well mixed and has a higher percentage of modern carbon (pMC). Additionally the radiocarbon age of the soil increases with depth suggesting that the top soil is probably better-mixed than the deeply buried layers.

However, these findings are yet to be cross-checked against the supporting measurements. The carbon isotopic fractionation is an important parameter that affects the accuracy of the AMS C^{14} dating technique [6]. As recommended, we are presently in the process of measuring C^{13}/C^{12} ratio using the Isotopic Ratio Mass Spectrometer (IRMS) at IITM, Pune that can be used for an independent recalibration and recalculation of the radiocarbon dates. Additionally, various other soil parameters such as the nutrients, micronutrients, texture, bulk density etc. are being analysed for more information on the soil formation process etc. We plan to supplement our study with the similar measurements being done for the other ecosystems in the MetFlux-India network.

References

[1] C.Le Quéré R.M.Andrew J.G.Candell S.Sitch J.I.Korsbakken G.P.Peters A.C.Manning T.A.Boden P.P.Tans R.A.Houghton R.A.Keeling & others. Earth Syst. Sci. Data 8 (2016) 605-649

[2] D.B.Clark L.M.Mercado S.Sitch C.D.Jones N.Gedney M.J.Best M.Pryor G.G.Rooney R.L.H.Essery E.Blyth O.Boucher R.J.Harding C.Huntingford & P.M.Cox. Geosci. Model Dev. 4 (2011) 701-722

[3] P.K.Deb Burman D.Sarma M.Williams A.Karipot & S.Chakraborty J. Earth Syst. Sci. 126:99 (2017) 1-17

[4] L.K.Fifield Rep. Prog. Phys. 62 (1999) 1223-1274

[5] R.Sharma G.R.Umapathy P.Kumar S.Ojha S.Gargari R.J.Joshi Nuclear Inst. and Methods in Physics Research B. NA (2018) 1-7

[6] L.Calcagnile G.Quarta & M.D'Elia App. Radiat. Isot. 62 (2005) 623-629

5.4.12 Holocene Climatic changes based on multiproxy data from fluvial and lacustrine archives of eastern margin of Little Rann of Kachchh, Western India

Rachna Raj[1], Tripathi J. K[1], Sharma, A[2], Phartiyal B[2], Sridhar A[3], Pankaj Kumar[4] and Chamyal L. S[3]

[1]School of Environmental Sciences, Jawaharlal Nehru University, New Delhi-110067
[2]Birbal Sahni Institute of Palaeosciences, Lucknow-226007
[3]Department of Geology, Faculty of Science, The M. S. University of Baroda, Vadodara-390002
[4]Inter-University Accelerator Centre, New Delhi-110067

Introduction: A multiproxy studies involving palynology, phytoliths, clay mineralogy, magnetic mineralogy, carbon isotopic studies, geochemistry, granulometric analysis and the chronological studies of the lake and abandoned channels that will add meaningfully to the gap of knowledge which exists from the climatically sensitive region lying in the transitional climatic zones, semi-arid south to arid north, showing better sensitivity to even minor changes in temperature and precipitation. Being located in the northern part of the mainland Gujarat, the lakes and abandoned channels are ideal to document and assess the Holocene precipitation related changes for the regional correlation as well as to evaluate climate culture relationships.

Objective: To generate multiproxy data of the core sediments and to determine absolute ages (^{14}C) of the events identified by multi-proxy studies.

Methodology: Based on maps, satellite images and field reconnaissance coring site was identified from which Holocene climate fluctuation records was generated using multiproxy studies. Because of the semi-arid to arid climate in this region there are a limited number of archives that encompass the entire Holocene. Interpretation of data in relation to the data from in and around the study area shall be done and absolute dates shall be provided to the climatic events reflected in geochemical, mineral magnetism, palynological, sedimentological and phytolith data. Overlapping of data generated by the studies to that of regional and global events shall be undertaken to understand the Holocene palaeoclimatic changes evolution of the western India.

Data Generated:

^{14}C analysis of the samples

S. No.	Sample Name	Sample ID	pMC value	Radiocarbon Age (BP)	Median Calibrated age	Ages in BP	Depth (cm)
1.	LR_3_2	IUACD# 18C2153	81.665 ± 0.395	1627 ± 38	425 AD	**1525**	4
2.	LR_3_12	IUACD# 18C2154	70.910 ± 0.289	2761 ± 32	903BC	**2853**	24
3.	LR_3_28	IUACD# 18C2155	69.844 ± 0.284	2883 ± 32	1062 BC	**3012**	56
4.	LR_3_45	IUACD# 18C2156	62.423 ± 0.236	3785 ± 30	2215BC	**4165**	90
5.	LR_3_60	IUACD# 18C2157	56.218 ± 0.259	4626 ± 37	3456 BC	**5406**	120
6.	LR_3_106	IUACD# 18C2158	64.079 ± 0.283	3575 ± 35	1928 BC	**3878**	212
7.8.	LR_3_138	IUACD# 18C2159	55.197 ± 0.275	4773 ± 40	3568 BC	**5518**	276
9.	LR_3_173	IUACD# 18C2160	12.932 ± 0.097	16431 ± 60	17876 BC	**19826**	346
10.	LR_3_202	IUACD# 18C2161	17.767 ± 0.123	13879 ± 55	14865 BC	**16815**	404
11.	LR_3_220	IUACD# 18C2162	23.422 ± 0.133	11659 ± 45	11544 BC	**13494**	440
12.	LR_3_265	IUACD# 18C2164	13.080 ± 0.114	16339 ± 70	17776 BC	**19726**	530
13.	LR_3_270	IUACD# 18C2165	14.888 ± 0.126	15299 ± 68	16625 BC	**18575**	540
14.	LR_3_300	IUACD# 18C2166	19.594 ± 0.142	13093 ± 58	13758 BC	**15708**	600
15.	LR_3_326	IUACD# 18C2167	21.794 ± 0.149	12238 ± 55	12192 BC	**14142**	652
16.	LR_3_337	IUACD# 18C2168	11.602 ± 0.086	17303 ± 60	18916 BC	**20866**	674
17.	LR_3_351	IUACD# 18C2169	12.087 ± 0.098	16973 ± 65	18524 BC	**20474**	702
18.	LR_3_364	IUACD# 18C2170	21.463 ± 0.145	12361 ± 54	12438 BC	**14388**	728
19.	LR_3_370	IUACD# 18C2171	17.927 ± 0.126	13807 ± 56	14755 BC	**16705**	740
	LR_3_375	IUACD# 18C2172	11.758 ± 0.093	17196 ± 64	18790 BC	**20740**	750

Expected outcome: The Holocene climatic changes with absolute numbers from the arid regions of Gujarat has been done. Other proxy data is also generated, although some of the supportive data generation is under process. The detailed interpretation is under progress for a regional/global correlation of the various climatic events and to evaluate climate culture relationships.

5.4.13 Fossil fuel derived CO_2 estimation across India using radiocarbon measurement of annual crop plants

Rajveer Sharma, Pankaj Kumar, Sunil Ojha, Satinath Gargari and Sundeep Chopra

Inter University Accelerator Centre, New Delhi, India

At present, one of the most burning issues of the world is global warming. Main contributors to global warming are greenhouse gases, such as CO_2, CH_4, N_2O etc. Among all greenhouse gases, CO_2 is the largest contributor to the Earth's carbon cycle and climate change. The pre-industrial level of atmospheric CO_2, 278 ppm, reached up to a value of 403 ppm in 2017 [1]. This increase is primarily because of emissions from combustion of fossil fuels and from cement production, deforestation and other land-use changes. How much of the increased atmospheric CO_2 is derived from the combustion of fossil fuel emissions? It is an important question for the researchers and government policy makers. Radiocarbon (^{14}C, half-life of 5730 years) can be used as a tracer to answer this question because fossil fuels do not contain radiocarbon. Several such studies have been carried out in all parts of world including USA [2-3], Europe [4-6], China [7-8], Korea [9].

In present study, we have also traced fossil fuel derived CO_2 in the atmosphere across different parts of India using radiocarbon measurement of annual crop plants. Annual crop plants utilize atmospheric CO_2 for photosynthesis during their growing period. Radiocarbon measurements of these plants materials provide isotopic composition of atmospheric CO_2 utilized during their growing period. Crop plant samples (wheat, rice etc) were collected from 25 locations from different parts of India in the year 2017 and 2018. Samples were dried, grinded, pre-treated with acid and then graphitized using automated graphitization equipment (AGE) at graphitization laboratory in IUAC. AMS ^{14}C measurements of these graphitized samples were performed using XCAMS system at IUAC [10]. $\Delta^{14}C$ value for each sample was calculated from $^{14}C/^{12}C$ as described in [11]. Fossil fuel derived CO_2 mole fractions for each location were calculated using these $\Delta^{14}C$ values.

REFERENCES:

[1] WMO Greenhouse Gas Bulletine, No. 13, published on 30 October, 2017.

[2] Hsueh, D. Y., N. Y. Krakauer, J. T. Randerson, X. M. Xu, S. E. Trumbore, and J. R. Southon (2007), Regional patterns of radiocarbon and fossil fuel-derived CO_2 in surface air across North America, Geophys. Res. Lett., 34, L02816.

[3] Heather D. Graven, Thomas P. Guilderson, Ralph F. Keeling, Observations of radiocarbon in CO_2 at La Jolla, California, USA 1992-2007: Analysis of the long-term trend, Journal of Geophysical Research: Atmospheres, 2012, 117, D2302

[4] D. Bozhinova, M. Combe, S. W. L. Palstra, H. A. J. Meijer, M. C. Krol, W. Peters, The importance of crop growth modeling to interpret the Δ14CO2signature of annual plants, Global Biogeochemical Cycles, 2013, 27, 3, 792.

[5] D Bozhinova, SWL Palstra, MK van der Molen, MC Krol, HAJ Meijer, Three years of $^{14}\Delta CO_2$ observations from Maize Leaves in Netherlands and Western Europe, Radiocarbon 58, 3, 459-478.

[6] Levin, I., Kromer, B., Schmidt, M., Sartorius, H., 2003. A novel approach for independent budgeting of fossil fuel CO2over Europe by $^{14}CO_2$ observations. Geo-phys. Res. Lett. 30, 23, 2194.

[7] Zhenchuan Niu, Weijian Zhou, Xiaoshan Zhang, Sen Wang, Dongxia Zhang, Xuefeng Lu, Peng Cheng, Shugang Wu, Xiaohu Xiong, Hua Du, Yunchong Fu, The spatial distribution of fossil fuel CO_2 traced by $\Delta^{14}C$ in the leaves of gingko (Ginkgo biloba L.) in Beijing City, China, Environmental Science and Pollution Research, 2016, 23, 1, 556.

[8] Weijian Zhou, Shugang Wu, Wenwen Huo, Xiaohu Xiong, Peng Cheng, Xuefeng Lu, Zhenchuan Niu, Tracing fossil fuel CO_2 using $\Delta^{14}C$ in Xi'an City, China, Atmospheric Environment, 2014, 94, 538-545

[9] H. Park, W. Hong, X. Xu, G. Park, K.S. Sung, Kilho Sung, Jong-geol Lee, T. Nakanishi, Hyo-Seok Park, The distribution of $\Delta^{14}C$ in Korea from 2010 to 2013, Nuclear Instruments and Methods in Physics Research Section B: Beam Interactions with Materials and Atoms, 2015, 361, 609

[10] Rajveer Sharma, G.R. Umapathy, Pankaj Kumar, Sunil Ojha, Satinath Gargari, Rajan Joshi, Sundeep Chopra and Dinakar Kanjilal, AMS and upcoming geochronology facility at Inter University Accelerator Centre (IUAC), New Delhi, India, (2018) Nucl. Instr. Meth. B, 438, 124 – 130.

[11] Stuiver, M., Polach, H.A., 1977. Discussion: reporting of ^{14}C data. Radiocarbon 19, 355-363.

5.4.14 Chronology of the Iron Age Site of Ambal, Nagapattinam District, Tamil Nadu

V. Selvakumar[1], Kumar Pankaj[2], C.M. Jaseera[3] and K. Mathivanan[4]

[1]Department of Maritime History and Marine Archaeology, Tamil University, Thanjavur-613010, India.
[2]Scientist- E, AMS & Pelletron Group, Inter- University Accelerator Centre, Delhi 110067
[3]Department of Epigraphy and Archaeology, Tamil University, Thanjavur-613010, India.

The Iron Age-Historical site of Ambal (Lat.10.9482178; Long.79.7035146) located in Nagapattinam district of Tamil Nadu (Fig. 1) and excavations were undertaken in the season of 2015-16. Four organic samples were dated from the site of Ambal in Nagapattinam district of Tamil Nadu using the AMS radiocarbon facility at IUAC. The samples were selected from relatively undisturbed contexts, and to cover all the trenches excavated at the site and to understand the overall chronology of the sites.

Results of the analyses

The measured values and the radiocarbon ages are presented in Table 1.

Table 1 Radiocarbon dates of the samples from Ambal

Sample No/Trench	Context and Depth	IUAC Lab ID	pMC value	Radiocarbon Age (BP)
ABL 1	Trench I 024b, 230 cm	IUACD#18C1822	89.448± 0.322	895± 29
ABL 2 (CHARCOAL)	Trench II 019, B4 190-195	IUACD#18C1823	76.237± 0.334	2179± 35
ABL 3 (CHARCOAL)	Trench III 015, 125 cm	IUACD#18C1824	94.343± 0.349	467 ± 29
ABL 4 (JOB's TEAR SEED)	Trench II, 021, 186-205 cm	IUACD#18C1825	58.691± 0.258	4280 ± 35

Sample - ABL 2 019 B4 190-195 cm:

The sample from ABL Trench II Locus 019 from the depth of 190-195 cm has given a date of 2179± 35. This date reveals 158 cal BC for the sediment. This dating suggests that the settlement of Ambal had developed into a regular habitation by the second century BCE. The houses of this period were made of perishable material and the site witnessed agrarian activities.

Sample from ABL 1

The charcoal sample from the Trench ABL 1 revealed that Locus 024 at a depth of 024b has materials of medieval period which can be placed in the 12th and 13th century CE. This evidence is important and goes with the date of the temple and inscriptions which are found at this settlement. Currently this area is not under occupation and this date suggests that this area had residential complexes as early as 11 and 13 centuries.

Sample from ABL III

The trench ABL III revealed occupation of the site in the later medieval period around 15th century CE. The inscriptions reveal that the settlement had a *nagaram* or a commercial complex with industrial activities. Evidence of copper smelting and possibly gold working was found in this trench in the form of crucibles and fragments of gold. The excavation context matches with the date obtained from AMS. It suggests that in the pre-colonial period the settlement was brisk and there existed industrial activities. Perhaps these activities were abandoned in the colonial period, when new settlements came up on the coastal areas.

Dating of Job's Tear Seeds

A few job's tear seeds were dated sample ABL 4 (from Trench ABL II) and these seeds gave a very early date of early third millennium BCE which does not match with the dating of the context. It appears that the seeds, which were older, might have reached the sedimentary context at a later date. This cannot be ascertained without dating more such samples from the site.

Discussions

The four samples dated from the site of Ambal reveal that the site of Ambal was occupied continuously from second century BCE. These dates are in tune with the archaeological materials such as ceramics and other materials. The settlement of Ambal had established itself as an agrarian settlement as early as second century BCE. However, there is one-meter thick deposit beneath the sediment that produced the date of second century BCE and samples from the lower loci could reveal about the beginning of the Iron Age at this site. More radiocarbon dating is necessary at this site, to understand the beginning of occupation.

Acknowledgements

The authors would like to acknowledge the technical and financial support offered by Inter- University Accelerator Centre and University Grants commission for the research. Authors are thankful to IUAC for extending AMS facility, under Geochronology project funded by Ministry of Earth Sciences Govt of India. We would like to thank Dr Sundeep Chopra, Scientist-H, IUAC for the support.

REFERENCES:

[1] V. Selvakumar et al. Puratattva 46 (2016): 168-174.

[2] J. H. McGuire, D. J. Land, J. G. Brennan, and G. Basbas, Phys. Rev. A 19, 2180 (1979).

5.4.15 Holocene climatic and monsoonal variation: Benthic foraminifera records from Krishna-Godavari and Mahanadi Basins, Bay of Bengal

Mohanty Satabdi[1], Bhaumik Ajoy Kumar[1] and Pankaj Kumar[2]

[1]Department of Applied Geology, IIT (ISM) Dhanbad, Jharkhand, India
[2]Inter-University Accelerator Centre, New Delhi-110067, India.

AMS ^{14}C dating plays a significant role in paleoclimatic study as it provides the time frame to the climatic events in absolute value which is helpful in global correlation. The objective of the study is to obtain radiocarbon dates of mixed foraminifera i.e. both benthic and planktic foraminifera for the global paleoclimatic interpretation.

EXPERIMENTAL DETAILS

We have analyzed benthic and planktic foraminiferal (>125 µm) AMS ^{14}C dating using the foraminiferal calcitic test from 10 samples collected from the sediment cores 15A-1H-1 and 15A-1H-2. Total 8-10 µg of carbonate sample was weighed for the analysis of each sample. Samples were pre-treated and graphitized before radiocarbon measurement.

PRETREATMENT

Foraminiferal samples were oxidized with 15% H2O2 in an ultrasonic bath for 5–15 min and then rinsed with Milli-Q water and oven-dried. Careful handling of the sample was required in case of small samples of less than 10µg carbonate. Samples were crushed using an appropriate method to increase the surface area for chemical pre-treatment.

GRAPHITIZATION

For graphitization, automated graphitization equipment (AGE) coupled with elemental analyzer is used developed by Ionplus AG and ETH, Zurich [1]. The pre-treated foraminifera was put in 4 ml septum sealed vial and flushed with helium (100 ml/min) for 5 min by using a double-walled needle. For the decomposition of carbonate, 0.5 ml H3PO4 was added to the vial with a syringe and then heated at 75° C for at least 30 min. The purified CO2 flushed with helium (100 ml/min) via a water trap of phosphorus pentoxide to a trap containing zeolite in AGE [2]. Trapped CO2 is transferred by thermal expansion into a tube or reactor filled with iron powder. CO2 is reduced by H2 gas on the surface of iron powder at 580°C. Graphite is formed and water vapours are removed with the help of Peltier coolers. After that, the resulting graphite was pressed into cathode capsules and placed in a cathode wheel of the ion source of accelerator for radiocarbon measurements at IUAC.

Table 1: Graphitization log

Sample Name	Mass/mg	CO2/µg	COH2/mbar	T /°C	P/mbar	Time/min
19C2373	12.0	1019	1850	580	153	120
19C2374	5.33	511	938	580	119	120
19C2375	6.2	566	1044	580	144	120
19C2376	4.87	425	776	580	83	120
19C2379	5.0	441	812	580	108	120
19C2383	2.0	221	406	580	73	120
19C2385	3.38	294	554	580	101	120
19C2386	4.8	496	902	580	131	120
19C2387	3.0	224	423	580	92	120
19C2388	5.38	359	652	580	95	120

Table 2: ^{14}C AMS age (2σ) determinations of foraminifera from the Krishna-Godavari basin.

Sample ID	pMC value	Radiocarbon Age (BP)	Calibrated (BP) age ranges	Modelled age ranges (BP)
19C2373	87.688 ± 0.887	1055 ± 81	500-764	846-1058
19C2374	79.643 ± 1.005	1828 ± 102	1178-1607	970-1190
19C2375	79.990 ± 0.857	1793 ± 86	1178-1530	1021-1240
19C2376	80.158 ± 1.142	1776 ± 115	1080-1585	1087-1307
19C2379	76.753 ± 0.973	2125 ± 102	1473-1964	1850-2066
19C2383	72.017 ± 0.612	2636 ± 68	2121-2542	2181-2355
19C2385	67.824 ± 0.752	3118 ± 89	2728-3140	2421-2561
19C2386	69.669 ± 0.806	2903 ± 93	2376-2862	2498-2628
19C2387	72.931 ± 0.783	2535 ± 86	1970- 2412	2644- 2747
19C2388	66.429 ± 0.719	3285 ± 87	2882- 3342	2720- 2847

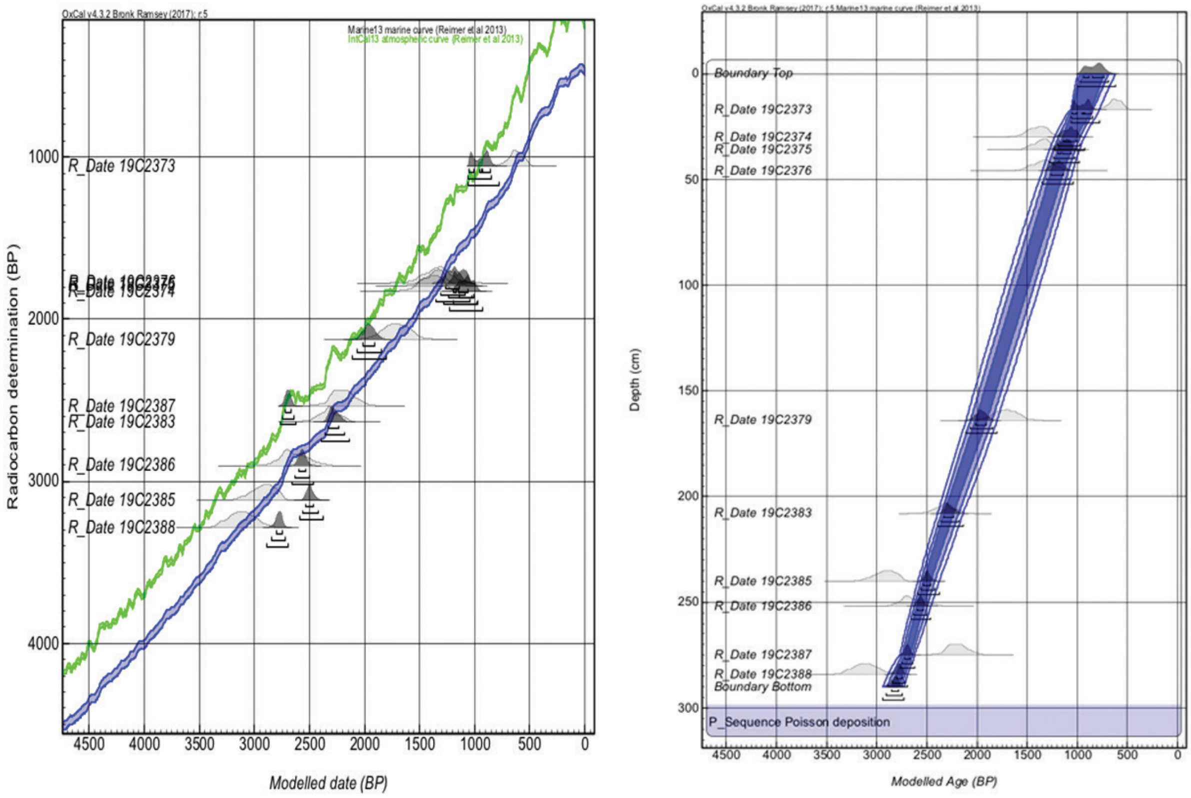

(a) (b)

Fig.1 Shows (a) Obtained ^{14}C Ages and (b) Age-Depth modelled using OxCal 4.3 (Ramsey 2017) [3]

We are still working on the data interpretation part and wait for other proxies data so that we can correlate different climatic events. Supportive data analysis and documentation is in progress that will be summarised for future publications.

REFERENCE:

[1] Wacker, L., Lippold, J., Molnár, M. and Schulz, H., 2013. Towards radiocarbon dating of single foraminifera with a gas ion source. Nuclear Instruments and Methods in Physics Research Section B: Beam Interactions with Materials and Atoms, 294, pp.307-310.

[2] Ruff, M., Szidat, S., Gäggeler, H.W., Suter, M., Synal, H.A. and Wacker, L., 2010. Gaseous radiocarbon measurements of small samples. Nuclear Instruments and Methods in Physics Research Section B: Beam Interactions with Materials and Atoms, 268(7-8), pp.790-794.

[3] Ramsey, C.B., 2017. Methods for summarizing radiocarbon datasets. Radiocarbon, 59(6), pp.1809-1833.

5.4.16 AMS Dating of bones from the Late Pleistocene fossiliferous horizons in the Manjra Valley, District Latur, Maharashtra

Sathe Vijay[1], Chakraborty Prateek[1], Kumar Pankaj[2] and Sharma Rajveer[2]

[1]Department of AIHC & Archaeology, Deccan College Postgraduate & Research Institute, Deemed University, Pune 411006, India.,
[2]Inter-University Accelerator Centre, New Delhi-110067, India.

The present work was carried out by the Department of AIHC & Archaeology, Deccan College Postgraduate & Research Institute Deemed University, Pune in conjunction with the AMS and Pelletron Group, IUAC in the first half of March 2019. The focus of this work was to establish a procedure through which reliable AMS dating of fossil bone and teeth could be carried out, using the material from sites in the Manjra Valley (dist. Latur, Maharashtra) as a case study.

The Manjra River valley is one of the richest fossil site complexes in the Indian subcontinent, and has yielded almost complete evidence of a full food chain structure from apex predator to scavengers. Establishing a clear chronology of this site is essential, since it will allow the finds to be put into a clear chronological context with respect to the appearance and disappearance of several key fauna. Moreover, accurate dating of the site will also allow a clearer analysis of the environmental and climatic data available, allowing further reconstruction of Late Pleistocene environments during the Middle Palaeolithic in Peninsular India.

Due to the low organic content in fossilized tissue, AMS dating has generally been considered inaccurate or error-prone. However, not many efforts have been made using the dental collagen powder from fossilized teeth, which are generally much more resistant to breakdown and decomposition thanks to the protection of the tooth enamel. In the present study, collagen was obtained from the molar teeth of large vertebrates, by drilling into the enamel-dentine junction.

The samples were then subjected to two different processes of AMS dating. The first batch was processed using the standard method, and did not yield measurable amounts of organic carbon. Therefore, larger amounts of sample were taken for the second batch, which were processed as per the recommendations of Cherkinsky 20091, which recommends the treatment of fossil collagen powder using acetic acid for better preservation of organic carbon.

There has been a success in processing the bone samples using method described by Alex Cherkinsky and we have graphitized samples. As explained in the Cherkinsky paper, we intend to compare it with collagen. Currently collagen extraction is in process. Once the collagen extraction is completed, we will graphite collagen and compare it. The work is in progress and hence the actual results in terms of dates are awaited.

REFERENCES.

[1] Cherkinsky, Alexander 2009. Can we get a good radiocarbon age from “bad bone”? Determining the reliability of Radiocarbon Age from Bioapatite. Radiocarbon 51 (2), 647-655.

5.5 ATOMIC PHYSICS

5.5.1 Setting up of EDXRF system using bremsstrahlung from transmission type X-ray generator

Soumya Chatterjee[1], Tapan Nandi[2] and Debasis Mitra[1]

[1]Department of Physics, University of Kalyani, West Bengal-741235, India
[2]Inter University Accelerator center, Aruna Asaf Ali Marg, NewDelhi-110067, India

In various scientific fields like geological sciences, biological sciences and environmental studies, the elemental analysis holds an important role for users. In comparison to other elemental analysis techniques like PIXE, NAA, Energy-Dispersive X-ray Fluorescence (EDXRF) [1] makes a huge impact as its use is less costly than other techniques as well assimple in handling. EDXRF system consists of an x-ray source (radioactiveor x-ray tube), x-ray detector and a data acquisition system. Two methods are available: alpha coefficient method and Fundamental Parameter method (FPM)[1]. In alpha coefficient method there is a need of only ratio (R_i) of intensity of a line for an elementpresent in the sample to that from a standard. Different standardsare required for a single sample. Making of these standards are time consuming and costlier too. For FPM, either one can use monochromatic primary radiation coming directly from radioactive source or fluorescence radiation from secondary source due to incidence of broadprimary spectrumfrom x-ray tube [2]. Sample x-rays are then detected byan x-ray detector. By using a suitable peak fitting program one can find the intensities of different diagram lines which are originating from different elements. Using those line intensities, elemental concentrations can be calculated with the help of some atomic parameters such as photo-ionization cross-section, fluorescence yields, Coster-Kronig transitions and detector efficiency. No standard is required for this technique and hence one single run is enough to determine the elemental concentrations of the sample. Now a day's very small size x-ray generatoroperated by a stable power source like a car battery is commercially available. Here we have shown how the bremsstrahlung spectrum can be used as an exciter for the sample to determine the elemental composition.We have used a small transmission type portable x-ray generator of Amptek (Mini-X), having 4W power with maximum operating voltage of 50kV. X-rays are detected by using a Silicon Pin detector. Absolute efficiency of the detector obtained at IUAC and shown in Figure 1 have been used in this experiment. Figure 2 shows the bremsstrahlung spectra from the tube for operating voltage 20kV, 25kV and 30kV and compared with the simulated one [3]. Experimentally detected bremsstrahlung spectrum matched very well with the simulated one.

For a mono-chromatic incident x-ray beam, elemental analysis can be done by using the following equation [3]

$$Ii = [(I_0\, d\omega)/\, 4\pi\, \mathrm{Sin}\, (\Psi_1)]\, [\sigma_i\, \omega_i\, f_i]\, A_i\, \varepsilon_i\, C_i\, (1+H_i)$$

Where I_0 is for incident flux, ω is for solid angle subtended by detector at target, Ψ_1 denotes entrance angle, σ_i, ω_i and f_i serves the purpose for photo-ionisation cross-section for primary radiation, fluorescence yield and fraction of radiation of considered x-ray line for i^{th} element respectively. A_i is the absorption correction not only for the primary X-rays but also for the fluorescent X-rays inside the target. ε_i is the detector efficiency for fluorescent radiation, H_i is for inter-element enhancement factor and C_i is for relative concentration for i^{th} element of the sample. I_i can be found by calculating the area for K-alpha of each sample. A computer program is written to calculate the concentrations with an arbitrary initial set of values following the condition $\sum C_i=1$. After each set of calculation, the newly calculated concentrations have to be normalized. But to use this equation we have to deal with mono-chromatic x-ray beam. To convert our bremsstrahlung to mono-chromatic x-ray we have to divide our whole spectrum into large number of energy slices so that each energy slice can be treated as monochromatic source of x-ray beam. And the fluorescent lines generated for each of such energy slices can be calculated using above equation. To get the total fluorescent X-rays we have to add up all the contributions from each of these slices which is used to obtain the final result.

To demonstrate the technique, we have taken a one-rupee coin of year 2000, which is exposed to the bremsstrahlung radiation from the x-ray tube operating at 25 KeV. Typical spectrum coming from the coin is detected by the silicon PIN detector and is shown in Figure 3. The concentration calculated in this technique using theoretically generated bremsstrahlung spectra, which is perfectly matched with the experimental one, as shown in table 1 along with the earlier results [4].

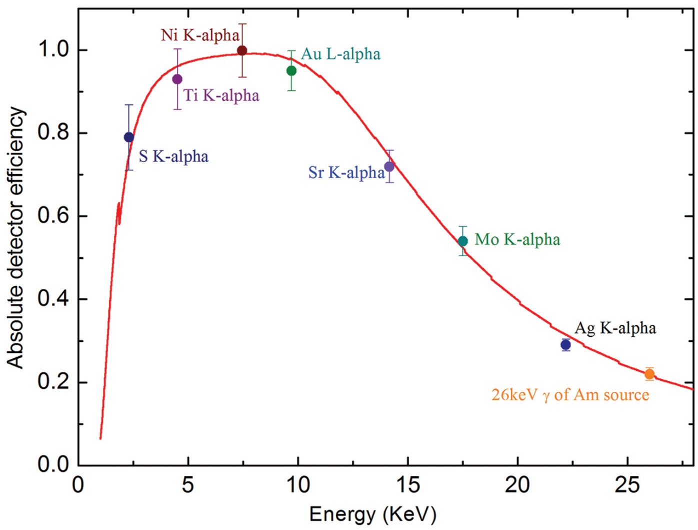

Fig. 1: Absolute efficiency of detector

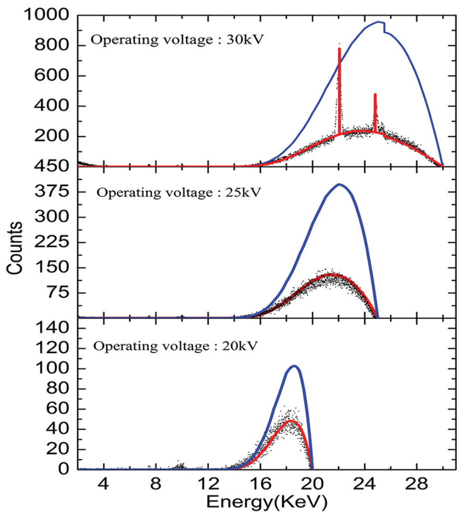

Fig. 2: Experimental (dotted), simulated coming from x-ray generator (blue line), simulated after inclusion of efficiency of x-ray detector (red line) bremsstrahlung spectrum.

REFERENCES
[1] Principles of Quantitative X-ray Fluorescence Analysis (Heyden and Son Ltd,1982).
[2] A.C. Mandal, M. Sarkar, D. Bhattacharya, Eur. Phys. J. AP17 (2002) 81.
[3] A.C. Mandal, S. Santra, D. Mitra, M. Sarkar, D. Bhattacharya, Nucl. Inst. & Meth. B **197** (2002) 179.
[4] A.C. Mandal, S. Santra, D. Mitra, M. Sarkar, D. Bhattacharya, Current Science **85** (2003) 134.

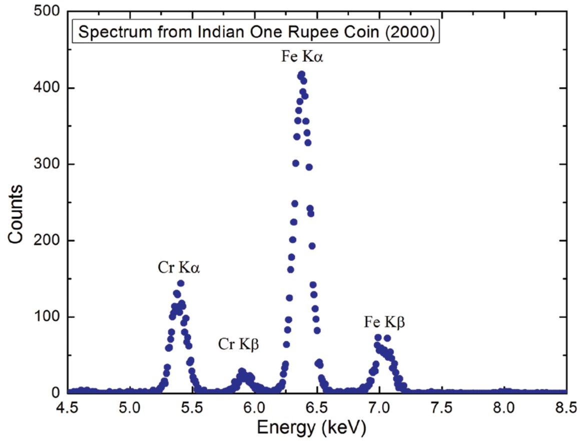

Fig. 3: X ray spectrum obtained from one-rupee coin using 25k operating voltage of the x-ray generator.

Table 1: Elemental concentration of one-rupee coin

Elements	Earlier Result [4]	Present result
Cr	16.8	17.2
Fe	83.2	82.8

5.5.2 Relativistic atomic structure calculations of helium-like ions for odd Z 3d-elements:

Gajendra Singh[1], A.K. Singh[1] and T. Nandi[2]

[1]USICT, GGSIPU, New Delhi - 110078, India.
[2]Inter University Accelerator Centre, Aruna Asaf Ali Marg, New Delhi-110067, India.

We have applied systematically enlarged Multiconfiguration Dirac-Fock (MCDF) wavefunctions [1] with the inclusion of finite nuclear size effects, Breit interactions and quantum electrodynamic corrections to evaluate relativistic atomic structure data of He-like ions for odd Z 3d-elements. Computed energy levels, transition probabilities, oscillator strength and selected x-ray wavelengths are compared with available experimental data. Special emphasis is given on forbidden transition rate, isotopic shift and hyperfine structure calculations as they are of potential interest in astrophysics. An attempt is made to report accurate hyperfine splitting constants to theoretically estimate hyperfine transitions and compared them with available experimental values.

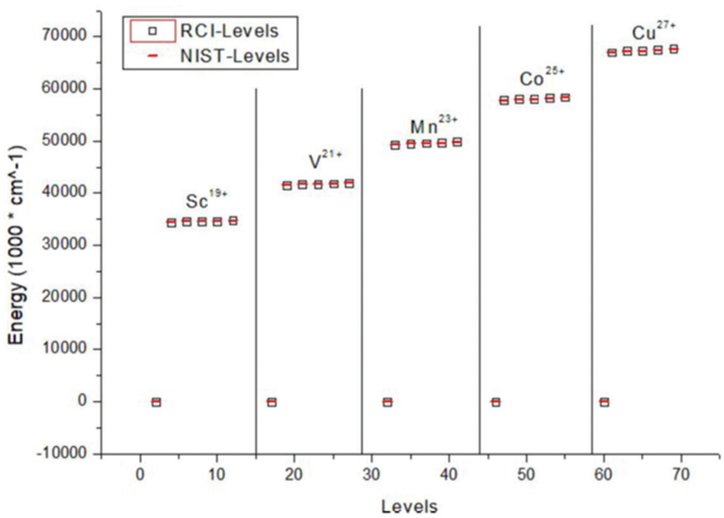

Fig.1: Comparison of the computed energy levels with the NIST energy levels of the ions under study.

Data obtained in above computations for level energies and transition rates for E1, M1 and M2 are in accordance with the NIST database as shown in Fig. 1. At present isotopic shifts and hyperfine coupling-constants are of high demand for determining nuclear quadrupole moment and hyperfine structure from experiments. Further, hyperfine data are also useful to construct fine structure levels to improve plasma diagnostics. We believe that the present work especially isotopic shift and hyperfine structure calculations will be useful to global modelling of extrasolar objects [2].

REFERENCES

[1] P. Jonsson, G. Gaigalas, J. Bieron, C.F. Fischer and I. Grant, Computer Physics Communications **184,** 2197 (2013).

[2] J.U.Ness and N.S. Brickhouse et. al. The Astrophysical Journal **598,** 1277 (2003).

5.5.3 Nuclear orbiting resonances in atomic phenomena

T. Nandi[1], Yash Kuma[2], Prashant Sharma[3], Adya P. Mishra[4], D. Mitra[5], Gajendra Singh[6], Nishchal R. Dwivedi[7], Sudhir R. Jain[7], and A.S. Kheifets[8]

[1]IUAC, JNU New Campus, Aruna Asaf Ali Marg, New Delhi 110067.
[2]Dipartimento di Fisica "Galileo Galilei", Università di Padova, I-35131 Padova, Italy.
[3]Department of Particle Physics and Astrophysics, Weizmann Institute of Science, Rehovot 76100, ISRAEL.
[4]Atomic & Molecular Physics Division, BARC, Trombay, Mumbai - 400 085.
[5]Department of Physics, Kalyani University, Kalyani, Nadia, West Bengal-741235.
[6]USICT, GGSIPU, New Delhi – 110078.
[7]Nuclear Physics Division, BARC, Trombay, Mumbai - 400 085, India.
[8]Research School of Physics, The Australian National University, Canberra, Australian Capital Territory 0200, Australia.

Nuclear orbiting resonances have been studied in the past for various nuclear reactions. However, experiments are carried out only at energies much greater than the fusion barrier energy [1]. In a recent work yet to be published [2], we demonstrate that the nuclear orbiting can occur even at the sub-barrier energies. Even though the dinuclear orbiting cross-section at these energies is an order of magnitude higher than the Coulomb excitation cross-sections, no study has been yet conducted using any nuclear techniques. The target and projectile nuclei in the dinuclear complex are so close that higher nuclear charge is felt by the orbital electrons. By incorporating this fact into a simple model, we have determined the orbiting duration for the dinuclear complex. Interestingly, these values are found to be within a factor of three larger than that of the predictions made by the nucleon exchange code HICOL [3]. Nuclear recoil induced shake off ionization explains well only the enhanced ionization [4], whereas the present mechanism of dinuclear orbiting explains both the enhanced ionization and anomalously large angle scattering. Another interesting fact is that the difference between the resonance energy and interaction barrier gives us the orbiting energy. It means the interaction barrier is revealed to be the point from where the nuclear force starts acting. Hence, interaction barrier radius can be a good measure of the range of the nuclear force. We have also tried to unravel the possible origin of the short time scale of the orbiting complex. It is the Coulomb excitation process, which diminishes the orbiting energy considerably within a few zeptoseconds so that the orbiting complex breaks into the incoming channels. We have proposed the multi photon exchange as a single virtual photon, which is responsible not only for the Coulomb excitation, but also for the atomic excitation. The excitation in a system with a vacancy in the K-shell can lead to autoionization, which does not occur instantly, rather it goes through Wigner-Smith time delay [5] of the order of a few hundreds of as. Hence, the orbiting induced ionization triggered in nuclear time scale (zs) transfers the phenomenon occurring in atomic time scale (as) so that one can measure the x-ray emissions. This process enables us to explain the longstanding discrepancy between the measured values of fission time scales by the nuclear and atomic techniques. Formation of the dinuclear orbiting complexes at sub-barrier energies thus exhibits an intriguing research area in the interface of atomic and nuclear physics.

REFERENCES

[1] Amlan Ray, Nucl. Phys. A **787,** (2007) 499.

[2] T. Nandi, Yash Kumar, Prashant Sharma, Adya P. Mishra, D. Mitra, Gajendra Singh, Nishchal R. Dwivedi, Sudhir R. Jain, and A.S. Kheifets, to be submitted soon.

[3] H. Feldmeier, Repts. Prog. Phys. **50,** (1987) 915.

[4] Prashant Sharma and T. Nandi, Phys. Rev. Lett., **119,** (2017) 203401.

[5] M. Schultze et. al., Science **328,** (2010) 1658.

5.5.4 Unusual charge exchange by swift heavy ions at solid surfaces

Tapan Nandi[1], Prashant Sharma[2] and Pravin Kumar[1]

[1]Inter University Accelerator Centre, Aruna Asaf Ali Marg, New Delhi - 110067, INDIA
[2]Department of Particle Physics and Astrophysics, Weizmann Institute of Science, Rehovot 76100, ISRAEL.

The electromagnetic methods for charge state analysis providean integral measure of the charge changing processes in the bulk and chargeexchange phenomenon at the exit surface of the foil (q^t_m) [1]. However, disentanglingthese two contributions are essential for many applications, e.g., x-ray emission of many astrophysical objects, the infrared emission bands from range of environments in the galaxies, accelerator physics, ion energy losses in solids, cancer therapy and ionization by heavy ions, and the surface modifications innanoscales. Accordingly, we have employed the x-ray spectroscopy techniqueto measure the mean charge states of swift heavy ions evolved due to the chargechanging process only in the bulk (q^b_m) if measured using Kα x-ray peak [2] and the mean charge state in the bulk plus radiative contribution if measured using radiative electron capture peak [3]. We find that the meancharge states so measured by the two methods are very different, because x-ray technique takes account of qbm, whereas q^t_m is deduced by the electromagnetic analyser; the qbm being higher than q^t_m. Theoretical predictions of q^b_m are made using a simple model if the target electrons form a Fermi-gas, withwhich the swift heavy ions interact. For a series of measurements with severalions (z = 22-35) in the energy range 1.5-3.0 MeV/u, a very good agreement isseen between the present experiments and theory [4]. The qt¬m values of the ions as measured by electromagnetic methods are also evaluated accurately by an improvedformula. The q^b_m - q^t_m is a measure of the net charge exchange contribution responsible at the exit surface of the foil. Very surprisingly, for 1 MeV/u uranium ions, up to 37 electrons per event can participate in charge exchange process at thesurface of the carbon foils [3]. In order to validate such findings in a more convincing manner, we are developing an experimental technique capable of measuring directly the charge exchange contribution at the solid surface. Further, we are in the process of establishing a method in fabricating a special type of solid foil that can avoid the charge exchange effect at the exit surface. It implies that we will get qbm from the entire foil instead of q^t_m, which means this method will give us much higher charge state from this special foil. Markedly, this technique will boost up the beam energy of the heavy ions (z>30) with existing accelerators with any budget.

REFERENCES

[1] K. Shima, T. Ishihara, T. Miyoshi, T. Mikumo, Phys. Rev, A **28**, (1983) 2162.

[2] P. Sharma and T. Nandi, Phys. Lett. A **380**, (2016) 182.

[3] P. Sharma and T. Nandi, Phys. Rev. Accl. Beams **22**, (2019) 034501.

[4] T. Nandi, P. Sharma and P. Kumar, to be submitted.

5.5.5 L-shell ionization cross sections of Ta, Pt, Th, and U by Si ions

C. Montanari[1], A. Mendez[1], D. Mitnik[1], M. Oswal[2], S. Kumar[2], U. Singh[3], G. Singh[4], K.P. Singh[2], D. Mehta[2], D. Mitra[5] and T. Nandi[6]

[1]Instituto de Astronomía y Física del Espacio, CONICET and Universidad de Buenos Aires - Buenos Aires (Argentina)
[2]Department of Physics, Panjab University, Chandigarh (India)
[3]The Marian Smoluchowski Institute of Physics, Jagiellonian University, Kraków (Poland)
[4]Department of Physics, Punjabi University, Patiala, Punjab (India)
[5]Department of Physics, University of Kalyani, West Bengal-741235, India
[6]University Accelerator Centre, Aruna Asaf Ali Marg, New Delhi-110067 (India)

Accurate determination of the x-ray production cross sections is important because of their wide use in atomic and molecular physics, and non-destructive elemental analysis of materials. Reliable values of L-shell ionization cross sections are included in the extended particle induced x-ray emission technique (PIXE) [1]. In this opportunity we will present a theoretical experimental study of the L-shell ionization of relativistic targets. The measurements of x-ray production cross sections by (84-140 MeV) Si^{+q} ions (q=8; 12), were held at the Inter-University Accelerator Centre, New Delhi. Multiple-hole fluorescence and Coster-Kronig yields were used to obtain the Li ionization cross sections (i = 1-3) from the measured x-ray production cross sections Lℓ, Lα, and Lβ, Lη, and Lγ [2]. The present experimental values are compared with full theoretical calculations by means of the shellwise local plasma approximation (SLPA) [2]. This model uses the quantum dielectric formalism to obtain the total ionization cross sections from an initial ground state. The wave functions and binding energies of the different targets were obtained by solving the fully relativistic Dirac equation using the HULLAC code package [3]. These calculations are based on first-order perturbation theory with a central field, including Breit interaction and quantum electrodynamics corrections. The new experimental data and the SLPA results for the ionization cross sections of the Li subshells are also compared with the known ECUSAR and ESPSSR [4], which are semi-empirical approximations. The agreement between the SLPA values and the experimental is rather good, also with the ECUSAR. Interestingly, the cross sections are found to be almost independent of the charge state of the Si ions, and not the outgoing charge state of the ion. This is important because the mean charge state plays a decisive role in the multiple ionization during the ion-solid collisions.

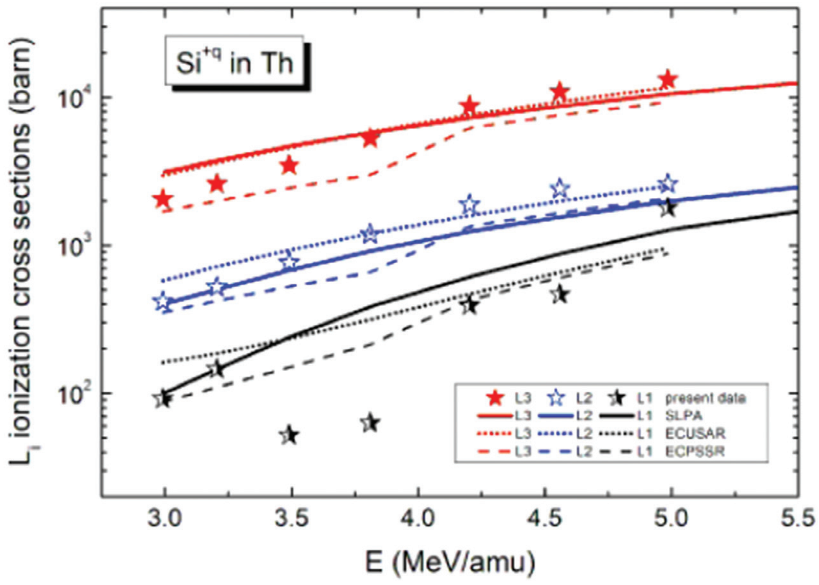

Fig 1: Measured L sub-shell ionization cross sections are compared various theoretical calculations.

REFERENCES

[1] M. Antoszewska-Moneta *et al,* Eur. Phys. J. D. **69,** (2015) 77.
[2] M. Oswal *et al,* Nucl. Instrum. Meth. Phys. Res. B **416,** (2018) 110.
[3] A. Bar-Shalom, M. Klapisch, J. Oreg, J. Quant. Spectrosc. Radiat. Transf. **71,** (2001) 169.
[4] G. Lapicki, Nucl. Instrum. Meth. Phys. Res. B **318,** (2014) 6.

5.5.6 Measurements of M X-ray relative intensities for ^{70}Yb, ^{82}Pb and ^{83}Bi induced by Low energy Carbon ions

Shehla[1], Ajay Kumar[2], Anil Kumar[1], D. K. Swami[3] and Sanjiv Puri[1]

[1]Department of Basic and Applied Sciences, Punjabi University, Patiala-147002, India
[2]Nuclear Physics Division, Bhabha Atomic Research Centre, Trombay, Mumbai - 400085, India
[3]Inter University Accelerator Center, Aruna Asaf Ali Marg, New Delhi-110067, India

In the present work, the intensity ratios, I_{MK} / I_{MN} (exp) (k = ξ, β, γ) for $_{70}$Yb, $_{82}$Pb and $_{83}$Bi induced by the C^{q+} (q = 4, 5) ions having energies in the range 800-1500 keV have been measured. These measurements were performed with the C^{q+}(q = 4, 5) ions accelerated using the Low Energy Ion Beam Facility (LEIBF) at the Inter University Accelerator Center (IUAC), New Delhi, India [1, 2].The targets mounted on a stainless steel holder (diameter 10 mm) were placed at 90° to the beam direction on a multiple target holder ladder. The pressure inside the chamber was kept at ~2×10^{-6} mbar. Targets of $_{70}$Yb, $_{82}$Pb and $_{83}$Bi having thickness ranging 36-150 μg/cm^2 prepared by vacuum evaporation on a 10 μg/cm^2 thick carbon backing have been used in the present measurements. The x-ray spectra from different targets were recorded with a Silicon Drift detector (SDD) (FWHM = 133 eV at 5.9 keV, 8μm Be window) placed at 45° angle to the incident beam direction outside the vacuum chamber. The intensity ratios, I_{MK} / I_{MN} (Exp) (k = ξ, β, γ), for a specific element induced by carbon ions have been evaluated using the relation explained elsewhere [3, 4]. These intensity ratios have been compared with those calculated using the ECPSSR model based carbon ion induced M_j (j=1-5) sub-shell ionization cross sections [5], the x-ray emission rates based on the Dirac-Fock (DF) model [6], two sets of the fluorescence and Coster-Kronig yields based on the non-relativistic Hermann-Skillman potential calculations [7] and those based on the relativistic Dirac-Hartree-Slater model [8]. Significant differences observed between the measured and calculated ratios have been attributed to multiple ionization induced effects in the investigated elements by the incident carbon ions.

REFERENCES

[1] D.Kanjilal, T.Madhu, G.Rodrigues, U.K.Rao, C.P.Safvan, A.Roy, Ind. J. Pure Appl. Phys. **39,** (2001) 25.
[2] P. Kumar, G. Rodrigues, U.K. Rao, C.P. Safvan, D. Kanjilal, A. Roy, Pramana-Journal of Physics **59,** (2002) 805
[3] Shehla, Ajay Kumar, C. Bagdia, Anil Kumar, D. Misra, Sanjiv Puri, L.C. Tribedi, Nucl. Instrum. Meth. Phys. Res. B **399,** (2017) 74.
[4] Shehla, Sanjiv Puri, Radiat. Phys. and Chem. **127,** (2016) 194.
[5] Z. Liu and S. Cipolla, Comput. Phys. Commun. **97,** (1996) 315; 176, (2007) 157; 180, (2009) 1716; 182, (2011) 243.
[6] Sanjiv Puri, At. Data Nucl. Data Tables **93,** (2007) 730 and references therein.
[7] E.J. McGuire, Phys. Rev. A **5,** (1972) 1043.
[8] Yogeshwar Chauhan, Sanjiv Puri, At. Data Nucl. Data Tables **94,** (2008) 38.

5.5.7 Exploring the accurate nuclear potential

D. K. Swami[1], Yash Kumar[2] and T. Nandi[1]

[1]Inter University Accelerator Centre, Aruna Asaf Ali Marg, New Delhi- 110067, India.
[2]Dipartimento di Fisica "Galileo Galilei", Universit`a di Padova, I-35131 Padova, Italy

We have formulated two empirical models, one for fusion barrier and another for interaction barrier heights using the experimental values available in the literature. The present study is restricted to the fusion and interaction barriers for the reactions in the regime 8≤ z ≤278 and 59≤z ≤313, respectively, where $z=\frac{(Z_p Z_t)}{A_p^{\frac{1}{3}}+A_t^{\frac{1}{3}}}$. The fusion barriers so obtained have been compared with various model predictions such as Bass potential [1,2], Christenson and Winther [3], Broglia and Winther [4], Aage Winther [5], Siwek-Wilczyńska and J.Wilczyński [6], Skyrme energy density function model [7], and the Sao Paulo optical potential [8] along with experimental results. The Broglia and Winther model is found to be the best. Further, to examine its predictability, the Broglia and Winther model parameters are used in the CCFULL code to obtain the total fusion cross sections and compared with the experimental values. The comparison shows good agreements at the energies above the fusion barriers (Fig.1), but below the barriers the predictions for some reactions show a departure from the experimental results because of the damping of quantum vibration in the reaction partners near the touching point that causes hindrance to fusion deep below the barrier (Fig. 2). A small variation of the value of radius parameter in Woods-Saxon potential turns the agreement good. Thus, this model can be useful for planning experiments, especially if one is aiming for super heavy elements. Similarly, current interaction barrier heights have also been compared with the Bass potential model [1,2] predictions and found a reasonable agreement. Nevertheless, the present model is chosen for further use as it is based on the experiments. We believe the current interaction barrier model prediction will be a good starting point for future quasi-elastic scattering experiments. Whereas both the Broglia and Winther model and our interaction barrier model will have practical implications in carrying out physics research near the Coulomb barrier [9].

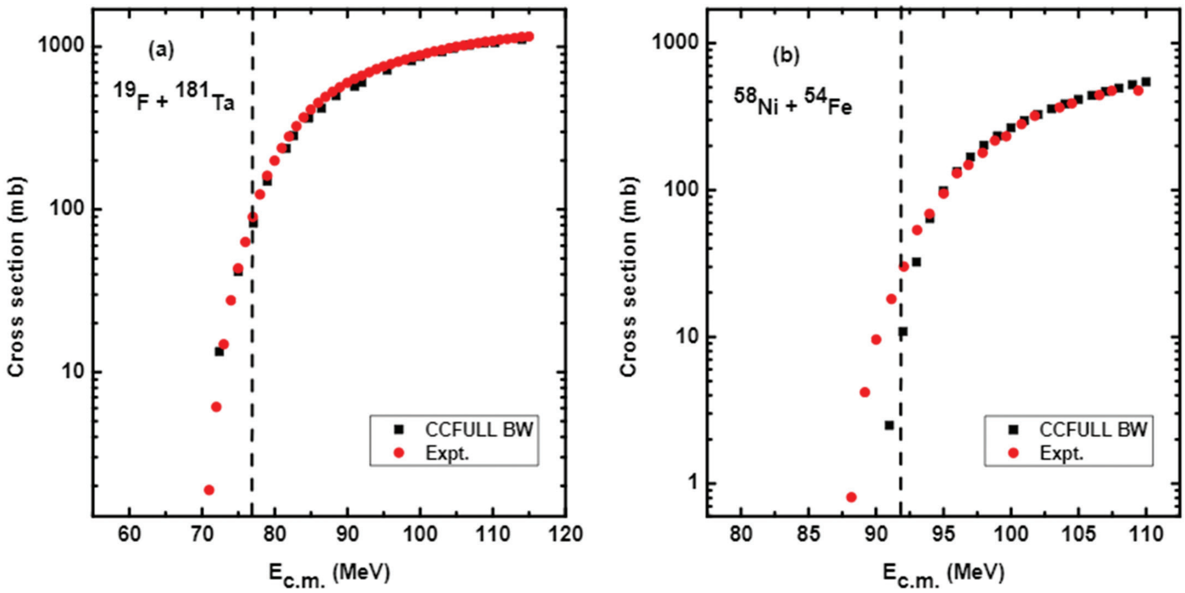

Fig 1: Comparison of total fusion cross section as a function of Ecm between the experimental and CCFULL calculation using Broglia and Winther parameters for the systems of $^{19}F+^{181}Ta$ (a) and $^{58}Ni+^{54}Fe$ (b). The dashed vertical line indicates the fusion barrier height for the corresponding reaction

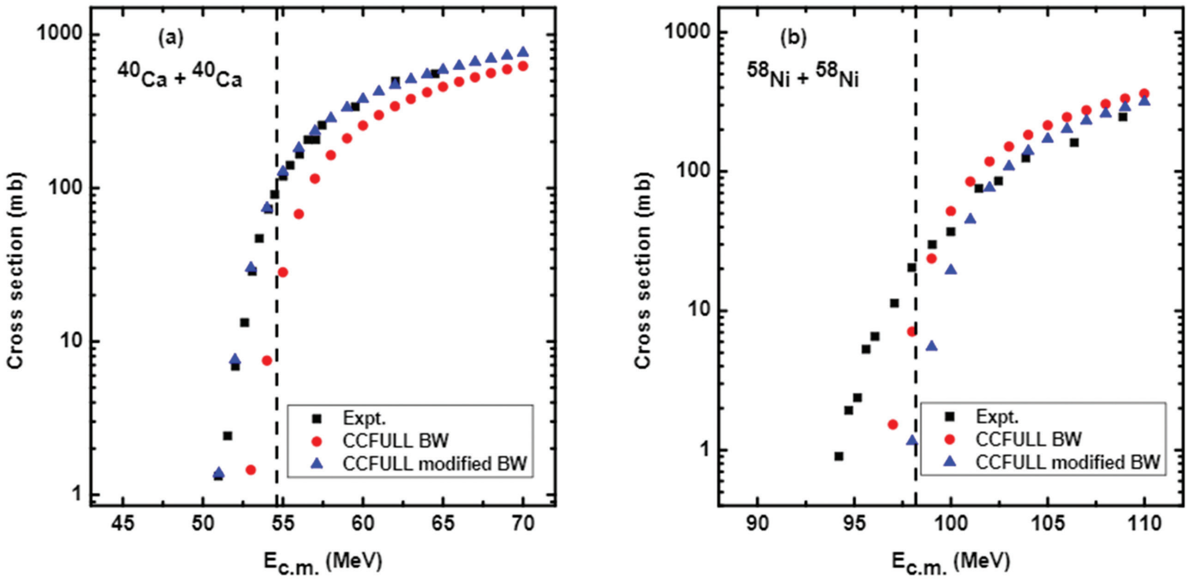

Fig. 2: Comparison of total fusion cross section (mb) as a function of Ecm between the experimental and CCFULL calculation using Broglia and Winther parameters for the systems of $^{40}Ca+^{40}Ca$ (a) and $^{58}Ni+^{58}Ni$ (b). Notice that the Broglia and Winther parameter r0 does not result in agreement with the experimental values. Good concurrence is found by changing r0 from 1.19 to 1.24 fm for $^{40}Ca+^{40}Ca$ and from 1.205 to 1.19 fm for $^{58}Ni+^{58}Ni$. The dashed vertical line indicates the fusion barrier height for the corresponding reaction.

REFERENCES

[1] R. Bass, Nucl. Phys. A **231,** 45 (1974).
[2] R Bass, Phys. Lett. **47,** 139 (1973).
[3] P. R. Christensen and A. Winther, Phys. Lett. 65B, **19** (1976).
[4] W. Reisdorf, J.Phys. G: Nucl. Part.Phys. **20,** 1297 (1994).
[5] A. Winther, Nucl. Phys. A **594,** 203 (1995).
[6] K. Siwek-Wilczy˜nska, J. Wilczy˜nski, Phys. Rev. C **69,** 024611 (2004).
[7] V. Zanganeh, M. Mirzaei and N. Wang, Commun. Theor Phys. **64,** 177 (2015).
[8] A. S. Freitas et al., Braz J Phys **46,**120 (2016).
[9] P. Sharma and T. Nandi, Phys. Rev. Lett. **119,** 203401 (2017).

5.5.8 X-Ray spectroscopy of highly charged slow ions with solids

C. V. Ahmad[1,2,] R. Gupta[1,2], K. Chakraborty[1,2], D. K. Swami[3] and P. Verma[1*]

[1]Department of Physics, Kalindi College, East Patel Nagar, University of Delhi, New-Delhi 110008
[2]Department of Physics and Astrophysics, University of Delhi, New-Delhi 110007
[3]Inter University Accelerator Centre, Aruna Asaf Ali Marg, New Delhi-110067

The M-Shell production cross sections of heavy elements by impact of heavy ion (Xenon) of energy 3-5 MeV have been measured. Strong coulombic field of heavy ions while interacting with target atoms remove various electrons simultaneously from the target atoms. This results into the shift of position and broadening of x-ray peaks emitted from the target during collision [1]. Further, in quasi adiabatic region there is formation of molecular-orbitals between the collision partners which results in emission of non-characteristics x-rays called as Molecular Orbital X-Rays [2-4].

$_{54}Xe^{q+}$ ions (q = 12,14 and 17), obtained from the 10 GHz ECR ion source of Low Energy Ion Beam Facility (LEIBF) at Inter University Accelerator Center (IUAC), New Delhi, were used to bombard solid targets of atomic number ranging between $70 \leq Z_2 \leq 82$ of thickness 360 μg/cm^2 as measure Rutherford back scattering method. These targets were kept in the center of the vacuum chamber mounted on target ladder at 45° with respect to beam direction. The x-rays were recorded by two silicon drift x-ray detectors mounted at 45° and 90° with respect to the incoming beam. They were kept outside the vacuum chamber by specially designed reentry cups. The x-rays before reaching the active volume of the detector passed through mylar foil, air gap and beryllium window of the detector. The detectors had resolution of 120 eV @ 5.9 keV. The ion beam current was monitored intermittently by the collection of charge on Faraday cup placed at 180°with respect to incoming beam. For accurate measurement of the current an electron suppressor was used for suppressing the secondary electrons. The suppressor was kept over the collision center by applying an optimized voltage of -300V. Another Faraday cup was also used for counting the number of outgoing projectiles.

The M X-Ray spectrum obtained in the experiment has complex structure and is not fully resolved by the detector used. Recorded (left) and fitted (right) spectra of 3 MeV Xe^{12+} on Au have been shown in Figure 1.

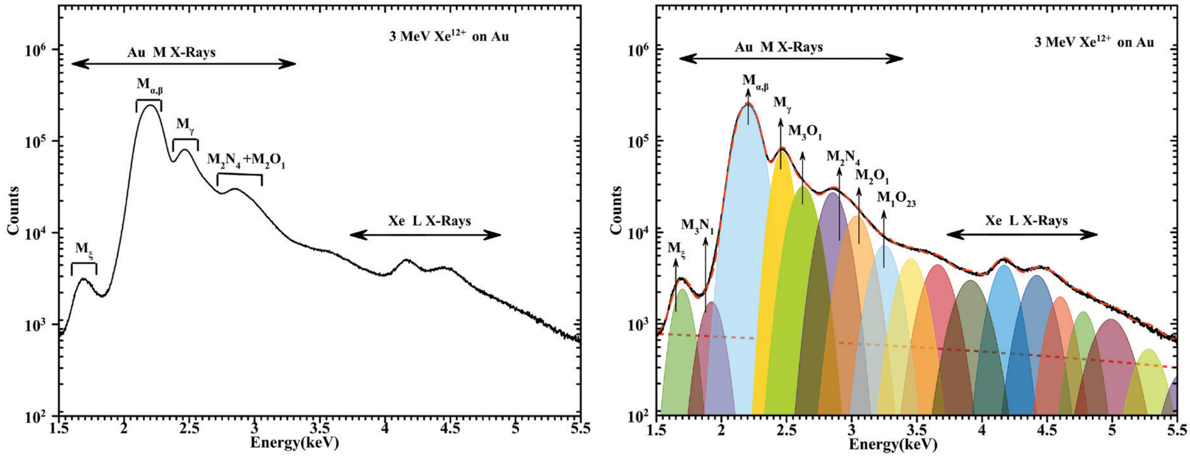

Figure 1: Measured X-Ray spectrum of Au excited by 3 MeV Xe^{12+} ion {recorded (left) and fitted (right) gaussian profiles}.

The target M x-rays showed higher intensities as compared to projectile Xe L X-Rays. This unusually high emission of target M x-rays indicates that a mechanism in addition to electron capture and Coulomb ionization is taking place during the collisions. Moreover, the target intensity ratios were also higher when compared with the theoretically calculated values. This indicates occurrence of multiple ionization of the target atoms during collisions. Measured production and ionization cross sections have been obtained. Theories have been found to underestimate the experimental cross-sections.

REFERENCES

[1] D. Banaś *et al.,* Nucl. Instrum. Meth. Phys. Res. Sect. B **195** (2002) 233.
[2] H. O. Lutz, *et al.,* J. Phys. B **9** (1976) 6.
[3] W. Lichten, J. Phys. Chem. **84** (2002) 2102.
[4] Verma P *et al.,* J. Phys. Conf. Ser. **875** (2017) 092029.

5.5.9 Inferring X-rays at small inter-atomic distances using molecular orbital approach

P Verma[1], R Gupta[1,2], C V Ahmad[1,2], K Chakraborty[1,2], A Rani[2], D. K. Swami[3], G Sharma[4], S.K. Saini[3], P Barua[3], D Mitra[5], S Mandal[2] and T Nandi[3]

[1]Department of Physics, Kalindi College, University of Delhi, East Patel Nagar, New Delhi-110008.
[2]Department of Physics and Astrophysics, University of Delhi, New Delhi-110007.
[3]Inter University Accelerator Centre, Aruna Asaf Ali Marg, New Delhi-110067.
[4]Department of Physics, Government Engineering College, Ajmer, Rajasthan-305001.
[5]Department of Physics, University of Kalyani, Kalyani, Nadia, West Bengal-741235.

In close, adiabatic heavy ion-heavy atom collisions, inner - shell vacancies are produced for collision velocities smaller than the orbital velocities of the target electrons [1]. In such cases, as the inter-nuclear distance decreases, a transient quasi-molecule with a united atomic atom $Z_{UA}=Z_1+Z_2$ (subscript 1 for projectile and 2 for target) is formed. If Z_1 and Z_2 are such that $Z_{UA}\geq 100$, super heavy elements with atomic numbers beyond that of any stable element known can be investigated.

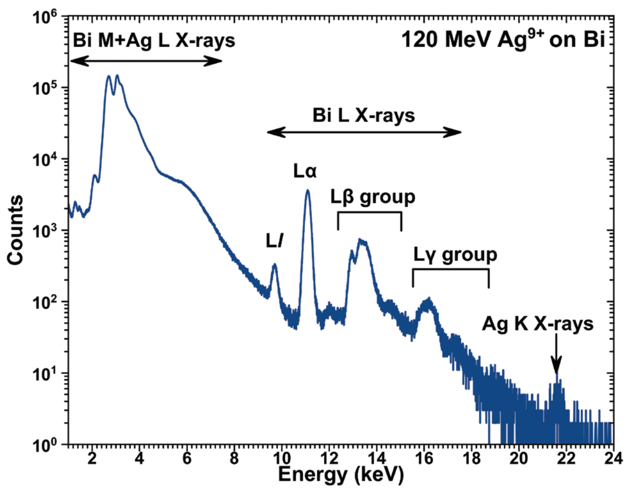

Figure 1: X-ray spectrum of 120 MeV Ag^{9+} ions on 120 μg/cm² Bi with C backing.

Investigation of inner shell ionization of super heavy systems with $120 \leq Z_{UA} \leq 130$ have been performed in the Atomic Physics beam line in beam hall II using the Pelletron facility at IUAC. The super heavy systems were achieved by close adiabatic collisions of 0.65-1.2 MeV/u Ag^{q+} (5 ≤

$q \leq 9$) ions with target foils of $73 \leq Z_2 \leq 83$ of various thicknesses. The collision induced inner shell processes have been studied by measuring x-rays from both collision partners using KETEK SDD detector kept at +135º port of experimental chamber, keeping the target ladder aligned perpendicular to the beam axis (see Figure 1).

For detection of scattered particles, 3 SBD detectors were installed inside the experimental chamber at ±30° and +150°. For beam collimation to 3 mm diameter, a penetrable cylindrical Faraday cup has been designed, fabricated at IUAC workshop and installed at beam entry. The collimator along with its holder was made of SS with length and internal diameter as 60 and 30 mm, respectively. It has three circular collimators of diameter 4, 5 and 3 mm placed consecutively from beam entry side towards chambers centre. It is capable of beam current measurement. A target ladder with 3 columns which can hold 15 target positions simultaneously has been fabricated at IUAC's workshop. It is made of a 2 mm thick SS plate with dimensions 140x80 mm^2.

For correct peak identification in both x-ray and SBD spectra, calibration of the detectors was performed with radioactive sources. The x-ray detector was calibrated using Am-241, Fe-55 and Co-57 radioactive sources covering the energy range from 3 keV to 25 keV. This range pertained to both target and projectile x-rays. Similarly, the SBD detectors were calibrated using Am-241 which is also an alpha source emitting alpha particles of energy 5.5 MeV. Detailed measurements of projectile energy as well as target thickness have been performed. Preliminary analysis has yielded observations such as presence of spectator vacancies [2] giving evidence of multiple ionization of target [3]. The inner shell couplings and vacancy transfer mechanisms are being studied using correlation diagrams which require molecular orbital approach.

REFERENCES

[1] Mokler P H et al X-Ray Production in Heavy Ion-Atom Collisions. In: Sellin I.A. (eds) Structure and Collisions of Ions and Atoms. Topics in Current Physics, vol 5. Springer, Berlin, Heidelberg (1978).

[2] Verma P et al Phys. Scr. **61,** (2000) 335.

[3] Banas D et al Nucl. Instr. Meth. B **154,** (1999) 247 and J. Phys. B: At. Mol. Phys. **33,** (2000) L793.

5.5.10 Evidence of circular Rydberg states in beam-foil experiments: role of surface wake field

Gaurav Sharma[1], Nitin K. Puri[1], Pravin Kumar[2] and T. Nandi[2]

[1]Dept. of Applied Physics, Delhi Technological University, Bawana road, New Delhi 110042, India
[2]Inter University Accelerator Centre, Aruna Asaf Ali Marg, New Delhi 110067, India
[3]Department of Physics, Government Engineering College, Ajmer, Rajasthan-305001.

We have theoretically analyzed the experimental data of 125 MeV fully stripped as well as H-like sulfur ions passing through carbon foils [1] in the light of the fact that the ETACHA code represents well the charge state distribution of the projectile ions in the bulk of the target foil. Though the Rydberg states in the fast-ion foil collisions are formed in the last layers at the exit surface, the production of the projectile Rydberg states in the H-like ions exhibits a pronounce target thickness dependence because surface wake field (SWF) varies with the foil thickness [2]. Both the ions are found to contribute in the formation of circular Rydberg states (CRS) irrespective of the specific incident charge state used. The CRS formation probability (R) shows a saturation in the CRS formation after a certain thickness (Fig.1). The saturation in the value of R in the case of S^{16+} incident ion is relatively faster (about 32 $\mu g/cm^2$) than that in case of the S^{15+} ion incidence (about 55 $\mu g/cm^2$). The transfer probability of having the CRS from the high Rydberg states (HRS) depends on the magnitude of the SWF, which is smaller for the lower foil thickness and larger for higher foil thickness before the saturation. Therefore, the probability of having the CRS from the HRS is expected to be smaller for the lower foil thickness than that of the higher foil thickness. Thus, we observe the lower yield of the Ly-α x-ray for the lower foil thickness. For the low thick foil, the CRS formation is mainly due to capture in comparison to excitation, whereas, both the processes have equal contribution in the higher foil thickness. For the formation of CRS by the influence of SWF an excitation model is developed (Fig.2). The contribution arising only from the SWF is considered in developing the model. As per the present model, the low |m| HRS are formed by the Stark switching process in the last layers and HRS states so formed are transformed to the CRS by the single multiphoton process while passing through the SWF. This transformation occurs with a high probability in the experiment [1] as seen by other methods [3]. The present findings provide an important connection between atomic physics and condensed matter physics. Further, an interesting role of the solid state effects [4] such as the SWF [2] on populating the CRS is evidenced. The detail explanations can be seen in our recent work [5].

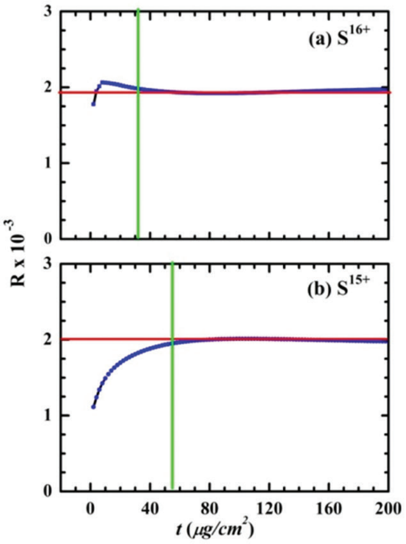

FIG. 1. Relative CRS formation probability: the ratio R, as defined in the text, is plotted as a function of carbon foil thickness (t) for incident ions (a) S^{16+} and (b) S^{15+}. Red lines represent the saturated value of R and green lines represent the thickness where the saturation is reached.

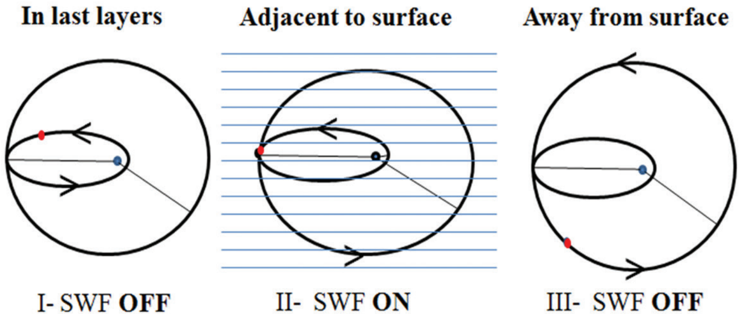

FIG. 2. Excitation model for CRS at the foil surface: I. HRS is formed at the foil surface in the absence of SWF and in the presence of BWF, II. HRS is promoted to CRS in the presence of SWF only, and III. CRS lasts as per its mean lifetime in the field-free regions. The red dot indicates orbiting electron and black dot the nucleus of the ion. The electron will remain in the circular state as the ion exits the SWF.

REFERENCES

[1] H.-D. Betz, D. Roschenthaler, and J. Rothermel, Phys. Rev. Lett. **50,** 34 (1983).
[2] T. Nandi *et. al.,* Phys. Rev. Lett. **110,** 163203 (2013).
[3] R. G. Hullet and D. Kleppner, Phys. Rev. Lett. **51,** 1430 (1983).
[4] C. O. Reinhold et al., J. Phys. B At. Mol. Phys. **33,** L111 (2000).
[5] G. Sharma, N.K. Puri, P. Kumar, and T. Nandi, Euro. Phys. Lett. **120,** 63002 (2017).

6. ACADEMIC ACTIVITIES

6.1 BEAM UTILIZATION BY USERS

6.1.1 LEIBF (Positive and Negative Ion) Beam Time Utilization and Experiments Performed (April, 2018 to March, 2019)

Users	No. of Shifts used (1 Shift =8Hrs.)	Project in	
		Materials Science	Atomic Physics
A. Universities/Colleges			
Amity University, Noida	3	1	
Anna University, Chennai	4	1	
Bharathiar University, Coimbatore	6	1	
Central University of Jammu, Jammu	6	1	
Chitkara University, Solan	15		1
Cochin University of Science & Technology, Kochi	6	1	
Deenbandhu Chhotu Ram University of Science and Technology, Murthal	6	1	
Guru Gobind Singh Indraprastha University, Delhi	11	1	
Guru Nanak Dev University, Amritsar	7	2	
Gurudas College, Kolkata	6	1	
Jamia Millia Islamia University, New Delhi	2	1	
Jawaharlal Nehru University, Delhi	12	3	
Kalindi College, New Delhi	9		1
Madurai Kamaraj University, Madurai	6	1	
Punjabi University, Patiala	9		1
Rashtrasant Tukadoji Maharaj Nagpur University, Nagpur	9	2	
Sheffield Hallam University, Sheffield	6	1	
Tezpur University, Tezpur	7	1	
University and Petroleum & Energy Studies, Dehradun	3	1	
University of Calcutta, Kolkata	6	1	
University of Delhi, New Delhi	3	1	
University of Mysore, Mysuru	3	1	
B. Institutions			
Amrita Vishwa Vidyapeetham, Bangaluru	6	1	
Dayalbagh Educational Institute, Agra	6	1	
Indian Association for the Cultivation of Science, Kolkata	2	1	
Indian Institute of Science, Bengaluru	7	2	
Indian Institute of Science Education and Research Mohali, Mohali	2	1	
Indian Institute of Technology Bhubaneswar, Khordha	9	2	
Indian Institute of Technology Madras, Chennai	4	1	
Indian Institute of Technology Hyderabad, Sangareddy	5	1	
Institute of Physics, Bhubaneswar	20	2	
Institute for Plasma Research, Gandhinagar	3	1	
Inter-University Accelerator Centre, New Delhi	34	8	2

Users	No. of Shifts used (1 Shift =8Hrs.)	Project in	
		Materials Science	Atomic Physics
Malaviya National Institute of Technology Jaipur, Jaipur	3	1	
Solid State Physics Laboratory, DRDO, New Delhi	8	3	
S.N. Bose National Centre for Basic Sciences, Kolkata	6	1	
Facility Test	2	1	
TOTAL	**262**	**50**	**5**

6.1.2 Pelletron Beam Time Utilization and Experiments Performed (April, 2018 to March, 2019)

Users	No. of Shifts Used (1 Shift= 8 Hrs.)	Project in				
		Nuclear Physics	Materials Science	Radiation Biology	Atomic Physics	AMS
A.Universities/Colleges						
Aligarh Muslim University, Aligarh	36	2	1			
Amity University, Noida	5		2	1		
Andhra University, Visakhapatnam	15	1				
Anna University, Chennai	30					1
Banaras Hindu University, Varanasi	44	3				
Bharathiar University, Coimbatore	3		1			
Birla College of Arts, Science and Commerce, Kalyan	3		1			
Central University of Jharkhand, Ranchi	18	1				
Central University of Kerala, Kasaragod	15	1				
Central University of Punjab, Bathinda	3		1			
Central University of Rajasthan, Ajmer	9		2			
Deccan College Post-Graduate and Research Institute, Pune	34					2
Delhi Technological University, Delhi	14					1
Devi Ahilya Vishwavidyalaya, Indore	6		1			
Dr. Babasaheb Ambedkar Marathwada University, Aurangabad	6		2			
Doon University, Dehradun	6		2			
D.A.V. College, Amritsar	3		1			
Gauhati University, Guwahati	15	1				
Gautam Buddha University, Greater Noida	1		1			
Goa University, Plateau	4					1
Govind Ballabh Pant Univ. of Agriculture and Technology, Pantnagar	3		1			

Users	No. of Shifts Used (1 Shift= 8 Hrs.)	Project in				
		Nuclear Physics	Materials Science	Radiation Biology	Atomic Physics	AMS
Gujarat University, Ahmedabad	3		1			
Guru Ghasidas Vishwavidyalaya, Bilaspur	3		1			
Guru Gobind Singh Indraprastha University, Delhi	10		3			
Guru Nanak Dev University, Amritsar	7		2			
Himachal Pradesh University, Shimla	18	1				
Jamia Millia Islamia University, New Delhi	2		1			
Jawaharlal Nehru University, Delhi	31		1			2
Karnataka University, Dharwad	16	1				
Kalindi College, New Delhi	18				1	
Kanya Mahavidyalaya, Jalandhar	3		1			
Kongunadu Arts & Science College, Coimbatore	3		1			
Kyoto University, Kyoto	6		1			
Mangalore University, Mangaluru	30					1
Nirma University, Ahmedabad	3		1			
North-Eastern Hill University, Shillong	40					1
Panjab University, Chandigarh	24	1				
Rashtrasant Tukadoji Maharaj Nagpur University, Nagpur	3		1			
Shiv Nadar University, Greater Noida	3		1			
Sikkim University, Gangtok	3		1			
Tamil University, Thanjavur	7					1
The Maharaja Sayajirao University of Baroda, Vadodara	18	1	1			
Tripura University, Suryamaninagar	3		1			
University College of Engineering, Arni	3		1			
University of Calicut, Kerala	12	1				
University of Delhi, New Delhi	43	1	2			2
University of Hyderabad, Hyderabad	5		1			
University of Kalyani, Kalyani	3			2		
University of Kashmir, Srinagar	6					1
University of Mysore, Mysuru	3		1			
Visvesvaraya Technological University, Belgaum	3		1			

Users	No. of Shifts Used (1 Shift= 8 Hrs.)	Project in				
		Nuclear Physics	Materials Science	Radiation Biology	Atomic Physics	AMS
B. Institutions						
Archaeological Survey of India, Bhubaneswar	8					1
Archaeological Survey of India, Patna	20					1
Bhabha Atomic Research Centre, Mumbai	3		1			
Birbal Sahni Institute of Palaeobotany, Lucknow	20					1
Dr. B.R. Ambedkar National Institute of Technology, Jalandhar	3		1			
Indian Institute of Science Education and Research Mohali, Mohali	2		1			
Indian Institute of Technology Jodhpur, Jodhpur	3		1			
Indian Institute of Technology Kharagpur, Kharagpur	2		1			
Indian Institute of Technology Roorkee, Roorkee	49	1				2
Indian Institute of Technology Ropar, Rupnagar	18	1				
Indian Institute of Technology (ISM), Dhanbad	20					1
Indian Space Research Organisation, Bengaluru	18		1			
Indira Gandhi Centre for Atomic Research, Kalpakkam	3		1			
Inter-University Accelerator Centre, New Delhi	94	2	4			2
Kalinga Institute of Industrial Technology, Bhubaneswar	3		1			
Malaviya National Institute of Technology Jaipur, Jaipur	11		3			
National Institute of Oceanography, Dona Paula	34					2
National Institute of Technology, Srinagar	3		1			
Saha Institute of Nuclear Physics, Kolkata	21	1				
Sant Longowal Institute of Engineering & Technology, Sangrur	5		1			
UGC-DAE-CSR, Kolkata	30	2				
Visva-Bharati, Santiniketan	48	3				
Wadia Institute of Himalayan Geology, Dehradun	45					1
C. Facility Tests	**9**	**2**			**1**	
TOTAL	**1077**	**27**	**57**	**3**	**2**	**24**

6.1.3 List of Users

The following list includes Universities/Colleges/Institutions that have used the IUAC Pelletron facility (once or more) since 1991.

(A) UNIVERSITIES – (131)

1.	Acharya Nagarjuna University	Guntur (Andhra Pradesh)
2.	Alagappa University	Karaikudi (Tamil Nadu)
3.	Aligarh Muslim University	Aligarh (Uttar Pradesh)
4.	Amity University	Noida (Uttar Pradesh)
5.	Andhra University	Visakhapatnam (Andhra Pradesh)
6.	Anna University	Chennai (Tamil Nadu)
7.	Assam University	Silchar (Assam)
8.	Babasaheb Bhimrao Ambedkar University	Lucknow (Uttar Pradesh)
9.	Banaras Hindu University, Varanasi (formerly Central Hindu College)	Varanasi (Uttar Pradesh)
10.	Bangalore University	Bangalore (Karnataka)
11.	Berhampur University	Berhampur (Odisha)
12.	Bharathiar University	Coimbatore (Tamil Nadu)
13.	Bharathidasan University	Tiruchirappalli (Tamil Nadu)
14.	Central University of Haryana	Mahendragarh (Haryana)
15.	Central University of Jammu	Jammu (Jammu and Kashmir)
16.	Central University of Jharkhand	Ranchi (Jharkhand)
17.	Central University of Kerala	Kasaragod (Kerala)
18.	Central University of Punjab	Bathinda (Punjab)
19.	Central University of Rajasthan	Ajmer (Rajasthan)
20.	Central University of South Bihar	Gaya (Bihar)
21.	Chaudhary Charan Singh University, Meerut (formerly Meerut University)	Meerut (Uttar Pradesh)
22.	Chaudhary Devi Lal University	Sirsa (Haryana)
23.	Chitkara University	Solan (Himachal Pradesh)
24.	Cochin University of Science & Technology	Kochi (Kerala)
25.	Darmstadt University of Technology	Darmstadt (Germany)
26.	Deenbandhu Chhotu Ram University Of Science And Technology (formerly Chhotu Ram State College of Engineering)	Murthal (Haryana)
27.	Delhi Technological University (formerly Delhi College of Engineering)	Delhi
28.	Devi Ahilya Vishwavidyalaya	Indore (Madhya Pradesh)

29.	Dr. Babasaheb Ambedkar Marathwada University	Aurangabad (Maharashtra)
30.	Dr. Bhimrao Ambedkar University (formerly Agra University)	Agra (Uttar Pradesh)
31.	Doon University	Dehradun (Uttarakhand)
32.	Gauhati University	Guwahati (Assam)
33.	Gautam Buddha University	Greater Noida (Uttar Pradesh)
34.	Goa University	Plateau (Goa)
35.	Govind Ballabh Pant University of Agriculture and Technology	Pantnagar (Uttarakhand)
36.	Gujarat Technological University	Ahmedabad (Gujarat)
37.	Gujarat University	Ahmedabad (Gujarat)
38.	Gulbarga University	Gulbarga (Karnataka)
39.	Guru Ghasidas Vishwavidyalaya	Bilaspur (Chhattisgarh)
40.	Guru Gobind Singh Indraprastha University (formerly Indraprastha University)	Delhi (Delhi)
41.	Guru Jambheshwar University of Science & Technology	Hisar (Haryana)
42.	Guru Nanak Dev University	Amritsar (Punjab)
43.	Hemwati Nandan Bahuguna Garhwal University	Srinagar (Uttarakhand)
44.	Himachal Pradesh University	Shimla (Himachal Pradesh)
45.	Indira Gandhi National Open University	New Delhi (Delhi)
46.	Indira Gandhi University Meerpur	Meerpur (Haryana)
47.	I.K. Gujral Punjab Technical University (formerly Punjab Technical University)	Kapurthala (Punjab)
48.	Jai Prakash Vishwavidyalaya	Chhapra (Bihar)
49.	Jamia Millia Islamia University	New Delhi (Delhi)
50.	Jawaharlal Nehru University	Delhi (Delhi)
51.	Karnataka University	Dharwad (Karnataka)
52.	Kiel University	Kiel (Germany)
53.	Kolhan University	Chaibasa (Jharkhand)
54.	Kurukshetra University	Kurukshetra (Haryana)
55.	Kuvempu University, Shankaraghatta	Shimoga (Karnataka)
56.	Kyoto University	Kyoto (Japan)
57.	K.R. Mangalam University	Gurgaon (Haryana)
58.	Ludwig-Maximilians-Universität München	Munich (Germany)
59.	Madurai Kamaraj University	Madurai (Tamil Nadu)
60.	Maharaja Krishnakumarsinhji Bhavnagar University (formerly Bhavnagar University)	Bhavnagar (Gujarat)
61.	Maharshi Dayanand University	Rohtak (Haryana)

62.	Maharishi Markandeshwar University	Mullana (Haryana)
63.	Mahatma Gandhi University	Kottayam (Kerala)
64.	Mahatma Jyotiba Phule Rohilkhand University	Bareilly (Uttar Pradesh)
65.	Manav Rachna International Institute of Research and Studies (formerly Manav Rachna International University)	Faridabad (Haryana)
66.	Mangalore University	Mangaluru (Karnataka)
67.	Manipur University	Imphal (Manipur)
68.	Manonmaniam Sundaranar University	Tirunelveli (Tamil Nadu)
69.	Marwadi University	Rajkot (Gujarat)
70.	Mohanlal Sukhadia University (also called University of Udaipur)	Udaipur (Rajasthan)
71.	Nirma University	Ahmedabad (Gujarat)
72.	North Carolina State University	Raleigh (USA)
73.	North-Eastern Hill University	Shillong (Meghalaya)
74.	North Maharashtra University (renamed as Kavayitri Bahinabai Chaudhari North Maharashtra University)	Jalgaon (Maharashtra)
75.	North Orissa University	Baripada (Odisha)
76.	Odisha University of Agriculture and Technology	Bhubaneswar (Odisha)
77.	Osaka University	Osaka (Japan)
78.	Osmania University	Hyderabad (Telangana)
79.	Panjab University	Chandigarh (Punjab)
80.	Patna University	Patna (Bihar)
81.	Periyar University	Salem (Tamil Nadu)
82.	Pondicherry University	Pondicherry (Pondicherry)
83.	Punjab Agricultural University	Ludhiana (Punjab)
84.	Punjabi University	Patiala (Punjab)
85.	Rani Durgavati Vishwavidyalaya (also known as University of Jabalpur)	Jabalpur (Madhya Pradesh)
86.	Rashtrasant Tukadoji Maharaj Nagpur University (formerly Nagpur University)	Nagpur (Maharashtra)
87.	Ravenshaw University	Cuttack (Odisha)
88.	Sabanci University	Tuzla/İstanbul (Turkey)
89.	Saint Petersburg Polytechnic University	Russia (Russia)
90.	Saurashtra University	Rajkot (Gujarat)
91.	Savitribai Phule Pune University (formerly University of Pune)	Pune (Maharashtra)
92.	Sharda University	Greater Noida (Uttar Pradesh)
93.	Sheffield Hallam University	Sheffield (UK)

94.	Shiv Nadar University	Greater Noida (Uttar Pradesh)
95.	Shivaji University	Kolhapur (Maharashtra)
96.	Shri Mata Vaishno Devi University	Katra (Jammu and Kashmir)
97.	Sikkim University	Gangtok (Sikkim)
98.	Sri Krishnadevaraya University	Anantapur (Andhra Pradesh)
99.	Tamil University	Thanjavur (Tamil Nadu)
100.	Tezpur University	Tezpur (Assam)
101.	The Maharaja Sayajirao University of Baroda	Vadodara (Gujarat)
102.	The NorthCap University, (formerly ITM University)	Gurgaon (Haryana)
103.	The University of Burdwan	Bardhaman (West Bengal)
104.	The University of Sheffield	Sheffield (UK)
105.	Tilka Manjhi Bhagalpur University (formerly Bhagalpur University)	Bhagalpur (Bihar)
106.	Tripura University	Suryamaninagar (Tripura)
107.	Tumkur University	Tumkur (Karnataka)
108.	University and Petroleum & Energy Studies	Dehradun (Uttarakhand)
109.	University of Allahabad	Prayagraj (Uttar Pradesh)
110.	University of Calcutta	Kolkata (West Bengal)
111.	University of Calicut	Kerala (Kerala)
112.	University of Delhi	New Delhi (Delhi)
113.	University of Hyderabad	Hyderabad (Telangana)
114.	University of Kalyani	Kalyani (West Bengal)
115.	University of Kashmir	Srinagar (Jammu and Kashmir)
116.	University of Lucknow	Lucknow (Uttar Pradesh)
117.	University of Madras	Chennai (Tamil Nadu)
118.	University of Maryland	Maryland (USA)
119.	University of Mumbai (known earlier as University of Bombay)	Mumbai (Maharashtra)
120.	University of Mysore	Mysuru (Karnataka)
121.	University of Notre Dame	Notre Dame (USA)
122.	University of Padova	Padova (Italy)
123.	University of Rajasthan	Jaipur (Rajasthan)
124.	University of Stuttgart	Stuttgart (Germany)
125.	University of Surrey	Guildford (UK)
126.	Heavy Ion Laboratory, University of Warsaw	Poland (Poland)
127.	Utkal University (also known as Vani Vihar)	Bhubaneswar (Odisha)
128.	Vikram University	Ujjain (Madhya Pradesh)

129.	Visva-Bharati University	Bolpur (West Bengal)
130.	Visvesvaraya Technological University	Belgaum (Karnataka)
131.	Maulana Abul Kalam Azad University of Technology (formerly West Bengal University of Technology)	Kolkata (West Bengal)

(B) COLLEGES – (74)

1.	Aligarh College of Engineering and Technology	Aligarh (Uttar Pradesh)
2.	Anand International College of Engineering	Jaipur (Rajasthan)
3.	Ananda Mohan College	Kolkata (West Bengal)
4.	Armed Forces Medical College	Pune (Maharashtra)
5.	Bareilly College	Bareilly (Uttar Pradesh)
6.	Beant College of Engineering & Technology	Gurdaspur (Punjab)
7.	Bharatiya Jain Sanghatana's Arts, Science and Commerce College	Pune (Maharashtra)
8.	Bhiwandi College	Mumbai (Maharashtra)
9.	Birla College of Arts, Science and Commerce	Kalyan (Maharashtra)
10.	B.N.N. College	Bhiwandi (Maharashtra)
11.	Deen Dayal Upadhyaya College	New Delhi (Delhi)
12.	Doodhsakhar Mahavidyalaya	Kolhapur (Maharashtra)
13.	Dum Dum Motijheel College	South Dum Dum (West Bengal)
14.	D.A.V. College	Amritsar (Punjab)
15.	D.A.V. College	Jalandhar (Punjab)
16.	D.A.V. College	Kanpur (Uttar Pradesh)
17.	D.A.V. College	Mumbai (Maharashtra)
18.	D.B.S. (P.G.) College	Dehradun (Uttarakhand)
19.	Ewing Christian College	Prayagraj (Uttar Pradesh)
20.	Gandhi Faiz-E-Aam College	Shahjahanpur (Uttar Pradesh)
21.	Goalpara College	Assam (Assam)
22.	Government Arts College	Rajahmundry (Andhra Pradesh)
23.	Government College	Ajmer (Rajasthan)
24.	Government College	Kota (Rajasthan)
25.	Government College	Mahendragarh (Haryana)
26.	Guru Nanak Girls College	Ludhiana (Punjab)
27.	Gurudas College	Kolkata (West Bengal)
28.	Iswar Chandra Vidyasagar College (formerly Belonia College)	Belonia (Tripura)

29.	Jai Hind College	Mumbai (Maharashtra)
30.	Kalindi College	New Delhi (Delhi)
31.	Kandi Raj College	Kandi (West Bengal)
32.	Kanya Mahavidyalaya	Jalandhar (Punjab)
33.	Kishinchand Chellaram College	Mumbai (Maharashtra)
34.	Kongunadu Arts & Science College	Coimbatore (Tamil Nadu)
35.	Koshi College	Khagaria (Bihar)
36.	Krishnath College	Baharampur (West Bengal)
37.	K.J. Somaiya College of Science & Commerce	Mumbai (Maharashtra)
38.	Lalbaba College	Howrah (West Bengal)
39.	Maharajah's Post Graduate College	Vizianagaram (Andhra Pradesh)
40.	Maharani Shri Jaya College	Bharatpur (Rajasthan)
41.	Mahila Vidyalaya PG College	Lucknow (Uttar Pradesh)
42.	Marwari College	Ranchi (Jharkhand)
43.	M.M.H. College	Ghaziabad (Uttar Pradesh)
44.	Nayagarh College	Nayagarh (Odisha)
45.	Nizam College	Hyderabad (Telangana)
46.	N.S.A.M. College	Mangaluru (Karnataka)
47.	Poornaprajna College and Post Graduate Centre, Udupi	Udupi (Karnataka)
48.	Punjab Engineering College	Chandigarh (Chandgarh)
49.	Raja Balwant Singh College (formerly known as Balwant Rajput College)	Agra (Uttar Pradesh)
50.	R.D. & D.J. College	Munger (Bihar)
51.	R.P.G. College	Ratnagiri (Maharashtra)
52.	Sanatan Dharma College	Ambala Cantt (Haryana)
53.	School of Physical Sciences	Nanded (Maharashtra)
54.	School of Physical Sciences	New Delhi (Delhi)
55.	School of Technology & Applied Sciences	Kochi (Kerala)
56.	Sharnbasveshwar College of Science	Gulbarga (Karnataka)
57.	Shri Varshney College	Aligarh (Uttar Pradesh)
58.	Smt. Chandibai Himathmal Mansukhani College	Thane (Maharashtra)
59.	Sree Narayana College	Kollam (Kerala)
60.	Sri Bhuvanendra College	Karkala (Karnataka)
61.	Sri S. Ramasamy Naidu Memorial College	Sattur (Tamil Nadu)
62.	Sri Venkateswara College	New Delhi (Delhi)
63.	St. Edmund's College	Shillong (Meghalaya)

64.	St. Xavier's College	Kolkata (West Bengal)
65.	St. Xavier's College	Mumbai (Maharashtra)
66.	Swami Shraddhanand College	New Delhi (Delhi)
67.	S.D.M. College	Mysuru (Karnataka)
68.	S.D.M. College	Uijre (Karnataka)
69.	S.S. Jain Subodh P.G. (Autonomous) College	Jaipur (Rajasthan)
70.	University College of Engineering (a constituent College of Anna University)	Arni (Tamil Nadu)
71.	University College of Science & Technology	Kolkata (West Bengal)
72.	Vaish College of Education	Rohtak (Haryana)
73.	Vardhaman College	Bijnor (Uttar Pradesh)
74.	Zakir Husain Delhi College	Delhi (New Delhi)

(C) OTHER INSTITUTIONS – (118)

1.	All India Council For Technical Education	New Delhi (Delhi)
2.	All India Institute of Medical Sciences	New Delhi (Delhi)
3.	Amity Institute of Nanotechnology	Noida (Uttar Pradesh)
4.	Amity School of Engineering & Technology	New Delhi (Delhi)
5.	Amrita School of Engineering (Amrita School of Engineering is an engineering institution, part of Amrita Vishwa Vidyapeetham)	Bangaluru (Karnataka)
6.	Amrita Vishwa Vidyapeetham,	Bangaluru (Karnataka)
7.	Archaeological Survey of India	Agra (Uttar Pradesh)
8.	Archaeological Survey of India	Bhubaneswar (Odisha)
9.	Archaeological Survey of India	Janpath (Delhi)
10.	Archaeological Survey of India	Patna (Bihar)
11.	Archaeological Survey of India	Red Fort Complex (Delhi)
12.	Archaeological Survey of India	Vadodara (Gujarat)
13.	Atal Bihari Vajpayee Indian Institute of Information Technology and Management	Gwalior (Madhya Pradesh)
14.	AFM/XPS Laboratory	Bhubaneswar (Odisha)
15.	Bangabasi Morning College	Kolkata (West Bengal)
16.	Bhabha Atomic Research Centre	Mumbai (Maharashtra)
17.	Birbal Sahni Institute of Palaeobotany	Lucknow (Uttar Pradesh)
18.	Birla Institute of Technology	Mesra (Jharkhand)

19.	Bose Institute	Kolkata (West Bengal)
20.	Calcutta Institute of Engineering and Management	Kolkata (West Bengal)
21.	Central Electronics Engineering Research Institute	Pilani (Rajasthan)
22.	Centre for Cellular and Molecular Biology	Hyderabad (Telangana)
23.	Centre de Sciences Nucléaires et de Sciences de la Matière	France
24.	Centre for Superconductivity Research	USA
25.	CSIR-Institute of Minerals and Materials Technology (Formerly Regional Research Laboratory)	Bhubaneswar (Odisha)
26.	Dayalbagh Educational Institute	Agra (Uttar Pradesh)
27.	Deccan College Post-Graduate and Research Institute	Pune (Maharashtra)
28.	Defence Laboratory	Jodhpur (Rajasthan)
29.	Defence Metallurgical Research Laboratory	Hyderabad (Telangana)
30.	Defence Research & Development Organization	Dehradun (Uttarakhand)
31.	Dr. B.R. Ambedkar National Institute of Technology (formerly Regional Engineering College Jalandhar)	Jalandhar (Punjab)
32.	Flerov Laboratory of Nuclear Reactions JINR	Russia
33.	Genetic Institute of Manufacturing Technology	Singapore (Singapore)
34.	GSI Helmholtzzentrum für Schwerionenforschung GmbH	Darmstadt (Germany)
35.	Harcourt Butler Technological Institute	Kanpur (Uttar Pradesh)
36.	Homi Bhabha National Institute	Kolkata (West Bengal)
37.	Indian Association for the Cultivation of Science	Kolkata (West Bengal)
38.	Indian Institute of Engineering Science and Technology	Howrah (West Bengal)
39.	Indian Institute of Information Technology (Formerly Bengal Engineering and Science University, Shibpur)	Allahabad (Uttar Pradesh)
40.	Indian Institute of Information Technology Design & Manufacturing Jabalpur	Jabalpur, Madhya Pradesh
41.	Indian Institute of Science	Bengaluru (Karnataka)
42.	Indian Institute of Science Education and Research Kolkata	Mohanpur (West Bengal)
43.	Indian Institute of Science Education and Research Mohali	Mohali (Punjab)
44.	Indian Institute of Space Science and Technology	Valiamala (Kerala)
45.	Indian Institute of Technology Gandhinagar	Gandhinagar (Gujarat)
46.	Indian Institute of Technology Jodhpur	Jodhpur (Rajasthan)
47.	Indian Institute of Technology Kanpur	Kanpur (Uttar Pradesh)
48.	Indian Institute of Technology Kharagpur	Kharagpur (West Bengal)
49.	Indian Institute of Technology Roorkee	Roorkee (Uttarakhand)
50.	Indian Institute of Technology Ropar	Rupnagar (Punjab)
51.	Indian Institute of Technology (BHU)	Varanasi (Uttar Pradesh)

52.	Indian Institute of Technology Bhubaneswar	Khordha (Odisha)
53.	Indian Institute of Technology Bombay	Mumbai (Maharashtra)
54.	Indian Institute of Technology Delhi	New Delhi (Delhi)
55.	Indian Institute of Technology Hyderabad	Sangareddy (Telangana)
56.	Indian Institute of Technology (ISM) (formerly known as Indian School of Mines)	Dhanbad (Jharkhand)
57.	Indian Institute of Technology Madras	Chennai (Tamil Nadu)
58.	Indian Institute of Tropical Meteorology	Pune (Maharashtra)
59.	Indian Space Research Organisation	Bengaluru (Karnataka)
60.	Indira Gandhi Centre for Atomic Research	Kalpakkam (Tamil Nadu)
61.	Institute for Plasma Research	Gandhinagar (Gujarat)
62.	Institute of Basic Science	Agra (Uttar Pradesh)
63.	Institute of Energy and Climate Research, Forschungszentrum Jülich	Jülich (Germany)
64.	Institute of Materials Science	Bhubaneswar (Odisha)
65.	Institute of Nuclear Medicine & Allied Sciences	New Delhi (Delhi)
66.	Institute of Physics	Bhubaneswar (Odisha)
67.	International Centre for Genetic Engineering and Biotechnology	New Delhi (Delhi)
68.	INFN Legnaro National Laboratory (LNL)	Legnaro (Italy)
69.	IUC-DAEF, Calcutta Centre	Kolkata (West Bengal)
70.	IUC-DAEF, Indore Centre	Indore (Madhya Pradesh)
71.	Jawaharlal Nehru Centre For Advanced Scientific Research	Bengaluru (Karnataka)
72.	Jaypee Institute of Information Technology	Noida (Uttar Pradesh)
73.	Joint Institute for Nuclear Research	Dubna (Russia)
74.	Kalinga Institute of Industrial Technology	Bhubaneswar (Odisha)
75.	Malaviya National Institute of Technology Jaipur	Jaipur (Rajasthan)
76.	Massachusetts Institute of Technology	Cambridge (USA)
77.	Maulana Azad National Institute of Technology (also known as National Institute of Technology)	Bhopal (Madhya Pradesh)
78.	Ministry of Defence (R & D Orgn)	Delhi
79.	Motilal Nehru National Institute of Technology (formerly Motilal Nehru Regional Engineering College)	Allahabad (Uttar Pradesh)
80.	Nanocrystals Technology	USA
81.	National Institute of Material Sciences	Japan
82.	National Institute of Oceanography	Dona Paula (Goa)
83.	National Institute of Science Education and Research	Pune (Maharashtra)
84.	National Institute of Science Education and Research Bhubaneswar	Khurda (Odisha)

85.	National Institute of Technology	Silchar (Assam)
86.	National Institute of Technology	Tiruchirappalli (Tamil Nadu)
87.	National Institute of Technology Hamirpur	Hamirpur (Himachal Pradesh)
88.	National Institute of Technology Kurukshetra	Kurukshetra (Haryana)
89.	National Institute of Technology Rourkela	Rourkela (Odisha)
90.	National Institute of Technology Srinagar	Srinagar (Jammu and Kashmir)
91.	National Museum	New Delhi (Delhi)
92.	National Physical Laboratory	New Delhi (Delhi)
93.	NCCCM/BARC	Hyderabad (Telangana)
94.	NCSR	France
95.	Oak Ridge National Laboratory	USA
96.	Physical Research Laboratory	Ahmedabad (Gujarat)
97.	P.E.S. Institute of Technology	Bengaluru (Karnataka)
98.	Raja Ramanna Centre for Advanced Technology	Indore (Madhya Pradesh)
99.	Research Centre Imarat, DRDO	Hyderabad (Telangana)
100.	Saha Institute of Nuclear Physics	Kolkata (West Bengal)
101.	Sant Longowal Institute of Engineering & Technology	Sangrur (Punjab)
102.	Semi-Conductor Laboratory	Mohali (Punjab)
103.	Shree Devi Institute of Technology	Mangaluru (Karnataka)
104.	Solid State Physics Laboratory, DRDO	New Delhi (Delhi)
105.	S.N. Bose National Centre for Basic Sciences	Kolkata (West Bengal)
106.	SUNAG Laboratory, Institute of Physics	Bhubaneswar (Odisha)
107.	Tata Institute of Fundamental Research	Mumbai (Maharashtra)
108.	Thapar Institute of Engineering & Technology (Thapar University)	Patiala (Punjab)
109.	The Institute of Science	MumbaI (Maharashtra)
110.	The National Academy of Sciences	Prayagraj (Uttar Pradesh)
111.	The National Centre for Polar and Ocean Research (formerly known as the National Centre for Antarctic and Ocean Research)	Goa
112.	UGC-DAE-Consortium For Scientific Research	Indore (Madhya Pradesh)
113.	UGC-DAE-Consortium For Scientific Research	Kolkata (West Bengal)
114.	UM-DAC Centre for Excellence in Basic Sciences	Mumbai (Maharashtra)
115.	Variable Energy Cyclotron Centre	Kolkata (West Bengal)
116.	Vidya Prasarak Mandal's Polytechnic	Thane (Maharashtra)
117.	Visva-Bharati	Santiniketan (West Bengal)
118.	Wadia Institute of Himalayan Geology	Dehradun (Uttarakhand)

6.2 STUDENT PROGRAMMES

6.2.1 IUAC Summer Programme 2018 for B.Sc. (Physics) Students

The B.Sc(Physics)Summer Students Programme which is being held annually in IUAC, was organized and held at IUAC in the last year during the period June 04th-29th, 2018. A total of 270 applications from 24 states/ union territories were received through the online portal. In order to limit the total number of projects which were subjected to availability of IUAC resource personnel to guide the students in their respective areas of specialization and availability of accommodation in IUAC hostel and guest house, a criterion point with a cut-off value of 90 % was selected to restrict the number of selected candidates to ~ 15. Location of the current affiliation (college/university/institution) was considered for determining each candidate's representation from a particular state/union territory. Effectively 14 students joined and were assigned various projects related to Materials Science, Atomic and Molecular Physics, Nuclear Physics, Accelerator Mass Spectrometry and Accelerator Physics. Special lectures by experts from various disciplines were organized to cater to the students, a wide area of research possibilities. All students have successfully completed their projects and it has benefitted both IUAC and the students.

Summer Students, 2018

6.2.2 M. Sc. Orientation Programme

R Mehta

Inter-University Accelerator Centre (IUAC) conducts M. Sc. Orientation Programme to encourage interested students to supplement their knowledge and to motivate them to continue their career in science. This programme has been envisaged to provide hands-on training in fields associated with accelerator / ion beam based research to selected M. Sc. students by way of short projects. The duration of M. Sc. Orientation programme is three weeks. It is open throughout the year. Student can apply for this programme based on their convenient time. Applications can be submitted online only. This flexibility allows the students to choose the project period without hampering their main study course. Following students participated in this programe.

S.No.	Name	Affiliation
1	Ayushi Tyagi	JMI, New Delhi
1	Ms Queena Dhiman	H P University, Shimla
2	Udit Gupta	H N B University
3	Ms Uzma |kthar	J M I University
4	Ms Monika Semwal	Banasthali Vidyapith
5	Mr Tanmay Singhvi	Sir Padampat Singhania University
6	Ms. Rajni Rawat	Pt. L. M. S Government post graduate college Rishikesh DEHRADUN

S.No.	Name	Affiliation
7	Mr. Agrim Jetwani	Sri Venkateswara College, University of Delhi
8	Ms Sneha Chaudhary	IIT Roorkee
9	Ms Sajal N T	Department of Physics, Cochin University of Science and Technology
10	Mr. Robin Dahiya	Jamia Millia Islamia University
11	Mr Vimal Narayan Sahoo	Pondicherry Central University
12	Ms Jyotirmayee Acharya	Pondicherry Central University

Details of this programme can be accessed at: http://www.iuac.res.in/sc/msc/index.html

Online Application Portal: http://www.iuac.res.in/indico/event/mscop

6.2.3 PhD Teaching Programme

P. N. Prakash and S. Muralithar

IUAC offers a 16 credit course work conforming to UGC guidelines for the PhD students pursuing research using energetic ion beams. The course work is spread over two semesters. The first semester, held during August-December, offers courses in Advanced Classical & Quantum Mechanics, Experimental Physics, and Accelerator Physics, while the second semester, held during January-May, offers courses in Advanced Condensed Matter Physics, Advanced Nuclear Physics, and Research Methodology. All the courses, except Research Methodology, are of 3 credit points each. The course on Research Methodology, which includes the course on Computational Techniques, is a 4 credit points course.

During the last academic year the PhD teaching programme continued to receive excellent response from students across the country. About a month before the semester commences, a poster giving details of the course modules, schedule, etc. is uploaded on the IUAC website. The printed version of the poster is also sent to the physics departments of various universities and colleges for inviting applications from research scholars and interested faculty members. Accommodation and TA/DA is provided to the selected participants (around 10-15). The details of the course modules offered in semester-I and semester-II during the academic year 2018-19 are given in the following.

A new dedicated lecture hall for conducting classes for the PhD students was setup during this academic year. The aesthetically designed lecture hall is equipped with modern facilities such as an integrated digital podium, ultra-short throw projector which can convert the projection white screen into a smart board, a recording camera with face recognition feature, document reader, audio system, additional camera for holding a web conference, provision for conducting interactive classes in up to 3 additional remote classrooms, large size lacquered glass board, etc. The lecture hall can accommodate 40 students and has desk and chair type sitting arrangement. Power points are provided on each desk for charging laptops. A photograph of the new lecture hall is shown below.

The new lecture hall setup for conducting classes for PhD students.

6.2.4 Teaching Laboratory Activities

Ajith Kumar B P. & V V V Satyanarayana

As a part of IUAC's outreach program, we continue to develop computer interfaced science experiments and train teachers in modern experimental data acquisition and analysis methods. A general purpose computer interface named ExpEYES-17 (Experiments for Young Engineers and Scientists) was released this year under PHOENIX project at IUAC. It is meant to be a tool for learning by exploration, suitable for high school classes and above. The teacher training program is conducted twice a year at IUAC and the one day workshops at colleges/universities all over India. During this year we have conducted two One-Week Training Programs for college teachers at IUAC. One Day Workshops were conducted at PRS University Raipur, Carmel College Goa and IIT Kanpur.

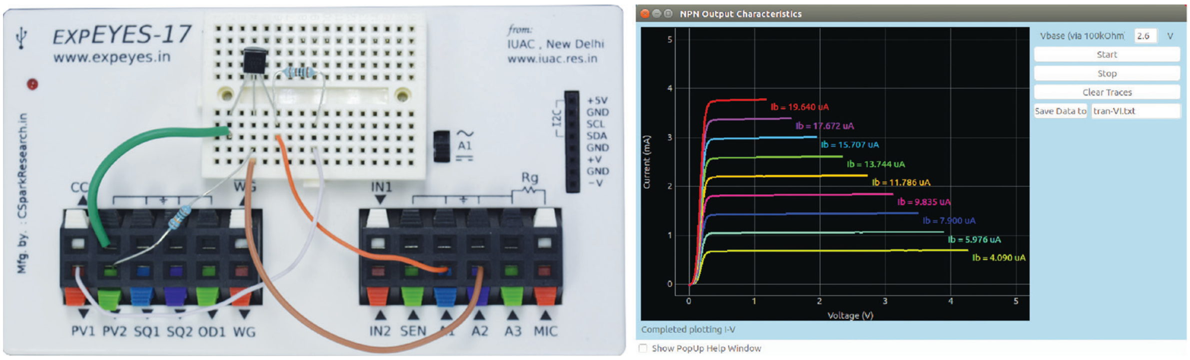

Transistor Output Characteristics experiment using expEYES-17

Six days training Program (3 April to 5 May 2018) at IUAC

6.3 LIBRARY ACTIVITIES

Priyambada Nayak

Salient features

Working hours: Round the clock, all days of the week

Total Books: ~2900 (broadly covering the subjects Nuclear Physics, Materials

	Science,Nanotechnology, Electronics, Computer Science, Radio-biology, Radiation Physics, Vacuum Instrumentation, Cryogenics, Atomic Physics, Mathematical Physics, Quantum Mechanics, Astrophysics etc.
Current E-Journals:	> 2500
Bound Journals:	~8500
Laboratory Reports:	~900 (from nearly 50 labs)
Reprints/Photocopies:	~700
Newsletters, House magazines etc.	50
Databooks, Manuals etc.:	~550
Ph.D. Thesis:	170
Clientele:	Apart from IUAC staff and students, the library is consulted by students, teaching and research staff from over 100 academic and research institutions in different parts of the country.

The technical reports and technicals memos of various projects carried out at IUAC are also compiled and kept in the library for reference purpose. Web-based OPAC and library cataloging software package "KOHA" has been used for the computerization of library documents. Apart from the current online journals, Journal archives (AIP, IOP, APS, ACS, Science Direct, Springer, Science, Nature) are also being subscribed by the library. **"Turn-it-in",** the originality check software is being used to prevent plagiarism. **"Web of Science"** is being subscribed by the library and used by the scholars for citation analysis and other purposes. The library is a member of UGC-INFONET Consortium and more than 2500 journals are being accessed on-line through these facilities. The library is open round the clock. Hence, automatic monitoring system has been installed.

6.4 ACADEMIC ACTIVITIES HELD IN 2018-19

30 April-5 May, 2018	**Training Programme on Computer interfaced Science Experiments** (Contact Person: Ajith Kumar B.P./ V.V.V. Satyanarayana)
7-18 May, 2018	**School on Accelerator Science & Technology** (Contact Person: Rajeev Mehta)
4-29 June, 2018	**Summer Programme for B.Sc. (Physics) Students** (Contact Person: G.O. Rodrigues)
5-7 July, 2018	**Users Workshop**
8 July, 2018	**64th AUC Meeting**
12-18 July, 2018	**International School on Ion Beams in Energy Materials** (Contact Person: P.K. Kulriya/ Fouran Singh)
13-14, 16 August, 2018	**IUAC Academic Workshop** (Contact Person: P. Sugathan)
20 August, 2018	**PhD Programme : Fall Semeser starts** (Contact Person: P.N. Prakash)
7 September, 2018	**Acquaintance Programme at Lucknow University, Lucknow** (Contact Person: R.P. Singh)
24-29 September, 2018	**Training Programme on Computer Interfaced Science Experiments** (Contact Person: Ajith Kumar B.P./ V.V.V. Satyanarayana)

3-7 October, 2018	**International School on Ion Beams in Materials Science** (Contact Person: I. Sulania/ A. Pripathi)
9-12 October, 2018	**International Conference on Ion Beams in Materials Engineering and Characterization** (Contact Person: S.A. Khan/ A. Tripathi)
29 October, 2018	**Acquaintance Programme at Central University of Kerala, Kasaragod** (Contact Person: Subir Nath)
12-16 November, 2018	**School on Modern Techniques in Nuclear Structure Studies** (Contact Person: R.P. Singh/ S. Muralithar)
16-18 December, 2018	**Users Workshop**
19 December, 2018	**Foundation Day Programme & 65th AUC Meeting**
21 January, 2019	**Ph. D. Programme: Winter Semester starts** (Contact Person: S. Muralithar)
13-16 February, 2019	**Asian Committee for Future Accelerators (ACFA) Meeting and Asian Forum for Accelerators and Detectors (AFAD) Workshop** (Contact Person: S. Ghosh)
18-20 February, 2019	**National Workshop on Isotopes in Earth, Ocean and Atmospheric Sciences at CSIR-NIO, Goa** (Contact Persons: S. Chopra and R. Saraswat (NIO))
26-27 February, 2019	**IUAC Academic Workshop** (Contact Person: P. Sugathan)
28 February, 2019	**National Science Day** (Contact Person: Saif A. Khan)
6-7 March, 2019	**Group Presentations on AY/FY 2018-19 and plans for AY/FY 2019-20** (Contact Person: N. Madhavan)
14-15 March, 2019	**Workshop on Disruptive Technologies** (Contact Persons: S. Mookerjee)

6.5 FORTHCOMING EVENTS: 2019

25 April, 2019	**IUAC Acquaintance Programme at Rajiv Gandhi Central University, Itanagar** (Contact Person: R.P. Singh)
29 April-4 May, 2019	**Training Programme on Computer Interfaced Science Experiments** (Contact Person: B.P. Ajith Kumar)
3-28 June, 2019	**Summer Programme for B.Sc. (Physics) Students** (Contact Person: G.O. Rodrigues)
5-7 July, 2019	**Users' Workshop**
8 July, 2019	**66th AUC Meeting**
15-20 July, 2019	**School on Nuclear Reactions** (Contact Persons: S. Nath and K. S. Golda)
29 July, 2019	**IUAC Acquaintance Programme at DDU University, Gorakhpur** (Contact Person: N. Madhavan)

19 August, 2019	**Ph. D. Programme: Monsoon Semester starts** (Contact Person: S. Muralithar)
21-23 August, 2019	**IUAC Academic Workshop** (Contact Person: P. Sugathan)
10-14 September, 2019	**School on Ion Beams in Materials Science** (Contact Person: K. Asokan)
17-18 September, 2019	**Workshop on Results from recent INGA Campaign and Future Perspectives** (Contact Persons: R.P. Singh and S. Muralithar
30 Sept.-5 Oct., 2019	**Training Programme on Computer Interfaced Science Experiments** (Contact Person: V.V.V. Satyanarayana)
15-19 October, 2019	**International Conference on Nanostructuring with Ion Beams at IGCAR, Kalpakkam** (Contact Persons: A. Tripathi and B.K. Panigrahi (IGCAR))
21 October, 2019	**IUAC Acquaintance Programme at Kanchi Mamunivar Centre for Postgraduate Studies, Pondicherry** (Contact Person: P. Sugathan)
1-15 November, 2019	**School and Workshop on Detectors** (Contact Person: A. Jhingan and Archana Sharma (CERN)
11 November, 2019	**IUAC Acquaintance Programme at Patna University, Patna** (Contact Person: P.N. Prakash)
18-21 November, 2019	**Indian Particle Accelerator Conference - InPAC-2019** (Contact Person: R. Mehta)
26-29 November, 2019	**In Silico Quantum Modeling Studies** (Contact Person: S. Mookerjee)
16-18 December, 2019	**Users' Workshop**
19 December, 2019	**Foundation Day Programme & 67th AUC Meeting**

6.6 LIST OF PH.D AWARDEES

The following scholars have completed the Ph.D thesis work during 2018-19

- **Prashant Sharma. Thesis title:** "Study of Atomic phenomena associated with highly charged ions produced during nuclear reactions".
- **Arkaprava Das. Thesis title:** "Study of phase transformations in Cadmium oxide based thin films and nanocomposites for optoelectronic applications".

6.7 LIST OF PUBLICATIONS IN THE YEAR 2018-19

A. NUCLEAR PHYSICS

1. **Fission like events in the $^{14}N+^{181}Ta$ system,** V. R. Sharma, R. Kumar, S. Mukherjee, E. F. Aguilera, M. Shuaib, P. P. Singh, A. Yadav, R. Dubey, S. Appannababu, J. C. Morales-Rivera, S. Kumar, B. P. Singh and R. Prasad, *Phys. Rev. C* ***99,*** *034617 (2019).*
2. **Evaporation residue cross-section measurements for $^{16}O+^{203,205}Tl$,** J. Gehlot, A. M. Vinodkumar, N. Madhavan, S. Nath, A. Jhingan, T. Varughese, T. Banerjee, A. Shamlath, P. V. Laveen, M. Shareef, P. Jisha, P. Sandya Devi, G. N. Jyothi, M. M. Hosamani, I. Mazumdar, V. I. Chepigin, M. L. Chelnokov, A. V. Yeremin, A. K. Sinha and B. R. S. Babu, *Phys. Rev. C* ***99,*** *034615 (2019).*
3. **Systematic study of incomplete-fusion dynamics below 8 MeV/nucleon energy,** H. Kumar, S. A. Tali, M. Afjal Ansari, D. Singh, R. Ali, A. Ali, S. Parashari, P. K. Giri, S. B. Linda, R. Kumar, R. P. Singh and S. Muralithar, *Phys. Rev. C* ***99,*** *034610 (2019).*

4. **Measurement of incomplete fusion cross sections in ^{6,7}Li+^{238}U reactions,** A. Pal, S. Santra, D. Chattopadhyay, A. Kundu, A. Jhingan, P. Sugathan, B. K. Nayak, A. Saxena and S. Kailas, *Phys. Rev. C* ***99,*** *024620 (2019).*
5. **Nuclear dissipation at high excitation energy and angular momenta in reaction forming ^{227}Np,** M. Shareef, E. Prasad, A. Jhingan, N. Saneesh, K. S. Golda, A. M. Vinodkumar, M. Kumar, A. Shamlath, P. V. Laveen, A. C. Visakh, M. M. Hosamani, S. K. Duggi, P. Sandya Devi, G. N. Jyothi, A. Tejaswi, P. N. Patil, J. Sadhukhan, P. Sugathan, A. Chatterjee and S. Pal, *Phys. Rev. C* ***99,*** *024618 (2019).*
6. **Mass and isotopic yield distributions of fission-like events in the ^{19}F+^{169}Tm system at low energies,** M. Shuaib, V. R. Sharma, A. Yadav, S. Thakur, M. K. Sharma, I. Majeed, M. Kumar, P. P. Singh, D. P. Singh, R. Kumar, R. P. Singh, S. Muralithar, B. P. Singh and R. Prasad, *Phys. Rev. C* ***99,*** *024617 (2019).*
7. **Detailed statistical model analysis of observables from fusion-fission reactions,** T. Banerjee, S. Nath and S. Pal, *Phys .Rev. C* ***99,*** *024610 (2019).*
8. **Sub-barrier fusion in the ^{37}Cl+^{130}Te system, R. N. Sahoo, M. Kaushik,** A. Sood, P. Kumar, A. Sharma, S. Thakur, P. P. Singh, P. K. Raina, M. M. Shaikh, R. Biswas, A. Yadav, J. Gehlot, S. Nath, N. Madhavan, V. Srivastava, M. K. Sharma, B. P. Singh, R. Prasad, A. Rani, A. Banerjee, U. Gupta, N. K. Deb and B. J. Roy, *Phys. Rev. C* ***99,*** *024607 (2019).*
9. **Insights into the low energy incomplete fusion,** R. N. Sahoo, M. Kaushik, A. Sood, P. Kumar, V. R. Sharma, A. Yadav, P. P. Singh, M. K. Sharma, R. Kumar, B. P. Singh, S. Aydin and R. Prasad, *Nucl. Phys. A* ***983,*** *145 (2019).*
10. **Shell-model description in ^{99}Rh and systematics of odd-A Rh isotopes,** S. Kumar, S. Sihotra, V. Singh, J. Rather, M. Kaur, J. Goswamy, N. Singh, D. Mehta, T. Trivedi, R. P. Singh, S. Muralithar and R. Palit, Acta. *Phys. Pol. B* ***50,*** *159 (2019).*
11. **Abrupt phase change of the core rotation in the ^{143}Sm nucleus,** S. Rajbanshi, R. Raut, H. Pai, S. Ali, A. Goswami, G. Gangopadhyay, S. Bhattacharyya, G. Mukherjee, S. Muralithar, R. P. Singh, M. Kumar Raju, P. Singh and R. K. Bhowmik, *Phys. Lett. B* ***782,*** *143 (2018).*
12. **Extremely asymmetric shears band in ^{143}Sm,** S. Rajbanshi, R. Raut, H. Pai, S. Ali, A. Goswami, S. Bhattacharyya, G. Mukherjee, R. K. Bhowmik, S. Muralithar, R. P. Singh, G. Gangopadhyay, M. Kumar Raju and P. Singh, *Phys. Rev. C* ***98,*** *061304 (2018).*
13. **Incomplete fusion in ^{16}O+^{89}Y reactions at energies of ≈ 7 MeV/nucleon,** M. Gull, K. Kumar, S. Ali, T. Ahmad, S. Dutt, I. A. Rizvi, A. Agarwal and R. Kumar, *Phys. Rev. C* ***98,*** *034603 (2018).*
14. **Systematic study of ^{192,202,206,210}Po compound nuclei using neutron multiplicity as a probe,** R. Mahajan, B. R. Behera, M. Thakur, G. Kaur, P. Sharma, K. Kapoor, A. Kumar, P. Sugathan, A. Jhingan, A. Chatterjee, N. Saneesh, A. Yadav, R. Dubey, N. Kumar, H. Singh, A. Saxena and S. Pal, *Phys. Rev. C* ***98,*** *034601 (2018).*
15. **Mass distributions of fission fragments from nuclei populated by multi nucleon transfer or incomplete fusion channels in ^{6,7}Li+^{238}U reactions,** A. Pal, S. Santra, D. Chattopadhyay, A. Kundu, A. Jhingan, P. Sugathan, N. Saneesh, M. Kumar, N. L. Singh, A. Yadav, C. Yadav, R. Dubey, K. Kapoor, K. Rani, H. Arora, A. C. Visakh, D. Kaur, B. K. Nayak, A. Saxena, S. Kailas and K. H. Schmidt, *Phys. Rev. C* ***98,*** *031601 (2018).*
16. **Measurement of mass-gated neutron multiplicity for the ^{48}Ti+^{208}Pb reaction at 57.4 MeV excitation energy,** M. Thakur, B. R. Behera, R. Mahajan, G. Kaur, P. Sharma, K. Kapoor, K. Rani, P. Sugathan, A. Jhingan, N. Saneesh, R. Dubey, A. Yadav, A. Chatterjee, M. B. Chatterjee, N. Kumar, S. Mandal, S. K. Duggi, A. Saxena, S. Kailas and S. Pal, *Phys. Rev. C* ***98,*** *014606 (2018).*
17. **Coexistence of principal and tilted axis rotation in ^{110}Ag,** B. Das, P. Datta, S. Chattopadhyay, S. Roy, R. Raut, R. K. Bhowmik, A. Goswami, H. C. Jain, R. Kumar, S. Muralithar, D. Negi, S. Pal, R. Palit and R. P. Singh, *Phys. Rev. C* ***98,*** *014326 (2018).*
18. **Effects of projectile break-up on fusion cross sections at energies near and above the Coulomb barrier: A case of incomplete fusion,** M. Shuaib, V. R. Sharma, A. Yadav, M. K. Sharma, P. P. Singh, D. P. Singh, R. Kumar, R. P. Singh, S. Muralithar, B. P. Singh and R. Prasad, *Phys. Rev. C* ***98,*** *014605 (2018).*
19. **Measurement of excitation functions of evaporation residues in the ^{16}O+^{124}Sn reaction and investigation of the dependence of incomplete fusion dynamics on entrance channel parameters,** D. Singh, S. B. Linda, P. K. Giri, A. Mahato, R. Tripathi, H. Kumar, S. A. Tali, S. Parashari, A. Ali, Ra. Dubey, M. Afzal Ansari, R. Kumar, S. Muralithar and R. P. Singh, *Phys. Rev. C* ***97,*** *064610 (2018).*
20. **Role of input angular momentum and target deformation on the incomplete-fusion dynamics in the ^{16}O+^{154}Sm system at ELab = 6.1 MeV/nucleon,** D. Singh, S. B. Linda, P. K. Giri, A. Mahato, R. Tripathi, H. Kumar, M. Afzal Ansari, N. P. M. Sathik, R. Ali, R. Kumar, S. Muralithar and R. P. Singh, *Phys. Rev. C* ***97,*** *064604 (2018).*

21. **Rotational band on a three-quasineutron isomer in ^{127}Xe,** S. Chakraborty, H. P. Sharma, S. S. Tiwary, C. Majumder, P. Banerjee, S. Ganguly, S. Rai, Pragati, S. Modi, P. Arumugam, Mayank, S. Kumar, R. Palit, A. Kumar, S. S. Bhattacharjee, R. P. Singh and S. Muralithar, *Phys. Rev. C* ***97,*** *054311 (2018);* Erratum *Phys. Rev. C* ***98,*** *059902 (2018).*
22. **Parity doublet structures in doubly-odd ^{216}Fr, Pragati,** A. Y. Deo, S. K. Tandel, S. S. Bhattacharjee, S. Chakraborty, S. Rai, S. G. Wahid, S. Kumar, S. Muralithar, R. P. Singh, I. Bala, R. Garg and A. K. Jain, *Phys. Rev. C* ***97,*** *044309 (2018).*
23. **Investigation of fusion hindrance in a soft asymmetric system deep below the barrier,** M. M. Shaikh, S. Nath, J. Gehlot, T. Banerjee, I. Mukul, R. Dubey, A. Shamlath, P. V. Laveen, M. Shareef, A. Jhingan, N. Madhavan, T. Rajbongshi, P. Jisha, G. N. Jyothi, A. Tejaswi, R. N. Sahoo, A. Rani, *J. Phys. G: Nucl. Part. Phys.* ***45,*** *095103 (2018).*
24. **High spin states in ^{63}Cu,** S. Rai, B. Mukherjee, U. S. Ghosh, A. Biswas, A. Chakraborty, A. K. Mondal, S. Chakraborty, G. Mukherjee, I. Bala and R. P. Singh, *Eur. Phys. J. A* ***54,*** *84 (2018).*

B. MATERIALS SCIENCE

1. **100keV H^+ ion irradiation of as-deposited Al-doped ZnO thin films: An interest in tailoring surface morphology for sensor applications,** S. K. Sahoo, S. Mangal, D. K. Mishra, U. P. Singh, and P. Kumar, *Surf. Interface Anal.* ***50,*** *705 (2018).*
2. **500 keV Ar^{2+} ion irradiation induced anatase to brookite phase transformation and ferromagnetism at room temperature in TiO_2 thin films,** B. Bharati, N. C. Mishra, D. Kanjilal, and C. Rath, *Appl. Surf. Sci.* ***428,*** *723 (2018).*
3. **A facile strategy to synthesize a novel and green nanocomposite based on gum Salai guggal - Investigation of antimicrobial activity,** A. K. Sharma, B. S. Kaith, B. Gupta, U. Shanker, and S. P. Lochab, *Mater. Chem. Phys.* ***219,*** *129 (2018).*
4. **An insight to origin of ferromagnetism in ZnO and N implanted ZnO thin films: Experimental and DFT approach,** P. Kumar, H. K. Malik, A. Ghosh, R. Thangavel, and K. Asokan, *J. Alloy. Compd.* ***768,*** *323 (2018).*
5. **Anisotropic super-paramagnetism in cobalt implanted rutile-TiO_2 single crystals,** S. R. Joshi, B. Padmanabhan, A. Chanda, N. Shukla, V. K. Malik, D. Kanjila, and S. Varma, *J. Magn. Magn. Mater.* ***465,*** *122 (2018).*
6. **Annealing of deep level defects in GaAs nanostructures by ion beam irradiation,** O. Mangla, S. Roy, S. Annapoorni, and K. Asokan, *Mater. Lett.* ***217,*** *231 (2018).*
7. **Antifungal efficacy of Au@ carbon dots nanoconjugates against opportunistic fungal pathogen,** Candida albicans, E. Priyadarshini, K. Rawat, T. Prasad, and H. B. Bohidar, *Colloid Surf. B-Biointerfaces* ***163,*** *355 (2018).*
8. **Antimicrobial and biocompatibility of highly fluorescent ZnSe core and ZnSe@ZnS core-shell quantum dots,** I. A. Mir, H. Alam, E. Priyadarshini, R. Meena, K. Rawat, P. Rajamani, M. S. Rizvi, and H. B. Bohidar, *J. Nanopart. Res.* ***20,*** *11, 174 (2018).*
9. **Bandgap Tunable AgInS based Quantum Dots for High Contrast Cell Imaging with Enhanced Photodynamic and Antifungal Applications,** I. A. Mir, V. S. Radhakrishanan, K. Rawat, T. Prasad, and H. B. Bohidar, *Sci Rep* ***8,*** *12, 9322 (2018).*
10. **$BaSO_4$:Eu as an energy independent thermoluminescent radiation dosimeter for gamma rays and C^{6+} ion beam,** K. Sharma, S. Bahl, B. Singh, P. Kumar, S. P. Lochab, and A. Pandey, *Radiat. Phys. Chem.* ***145,*** *64 (2018).*
11. **Broadband strip-line ferromagnetic resonance spectroscopy of soft magnetic CoFeTaZr patterned thin films,** S. Gupta, D. Kumar, T. L. Jin, R. Nongjai, K. Asokan, A. Ghosh, M. Aparnadevi, P. Suri, and S. N. Piramanayagam, *AIP Adv.* ***8,*** *6, 056125 (2018).*
12. **Carbon doping controlled thermoluminescent defect centers in nanoporous alumina for ion beam dosimetry,** S. Bhowmick, S. Pal, D. Das, V. K. Singh, S. A. Khan, R. Hubner, S. R. Barman, D. Kanjilal, and A. Kanjila, *J. Appl. Phys.* ***124,*** *6, 134902 (2018).*
13. **Clustered vacancies in ZnO: chemical aspects and consequences on physical properties, S. Pal, N. Gogurla,** A. Das, S. S. Singha, P. Kumar, D. Kanjilal, A. Singha, S. Chattopadhyay, D. Jana, and A. Sarkar, *J. Phys. D-Appl. Phys.* ***51,*** *12, 105107 (2018).*
14. **Combined effect of oxygen annealing and La-doping in broadening the phase transition of $Ba(Zr_{0.2}Ti_{0.8})O_3$ ceramics,** R. Kumar, K. Asokan, S. Patnaik, and B. Birajdar, *J. Alloy. Compd.* ***737,*** *561 (2018).*

15. **Comparative studies on thermoluminescence glow curves of calcium oxide nanophosphor irradiated with various ionizing radiations,** K. R. Nagabhushana, D. Prakash, F. Singh, S. H. Tatumi, R. R. Rocca, and S. Watanabe, *J. Alloy. Compd. **735,** 1949 (2018).*
16. **Conductivity and dielectric studies of Li^{3+}-irradiated PVP-based polymer electrolytes,** D. Singh, D. Kanjilal, G. V. S. Laxmi, P. K. Singh, S. K. Tomar, and B. Bhattacharya, *High Perform. Polym. **30,** 978 (2018).*
17. **Controlling room temperature ferromagnetism and band gap in ZnO nanostructured thin films by varying angle of implantation,** R. V. Hariwal, H. K. Malik, A. Negi, and A. Kandasami, *RSC Adv. **8,** 6278 (2018).*
18. **Correlated PL, TL and EPR study in gamma-rays and C^{6+} ion beam irradiated $CaMg_2(SO_4)_3$:Dy^{3+} triple sulphate phosphor,** S. Tamboli, R. M. Kadam, B. Rajeswari, B. Singh, and S. J. Dhoble, *J. Lumines. **203,** 267 (2018).*
19. **Design optimisation of C ion implantation of alpha-Al_2O_3 for medical dosimetry,** M. Agarwal, S. K. Garg, K. Asokan, S. Thulkar, S. Chander, M. K. Dalai, and P. Kumar, *Mater. Des. **153,** 317 (2018).*
20. **Design, development, and testing of a thermopower measurement system by studying the electron transport properties on indium and nitrogen co-doped sputtered ZnO films,** S. K. Kedia, A. Singh, and S. Chaudhary, *Measurement **117,** 49 (2018).*
21. **Detailed optical analysis of 100 MeV Ni^{7+} ion irradiated WO_3 thin films using Surface Plasmon Resonance,** S. Sharma, A. Paliwal, M. Tomar, F. Singh, N. K. Puri, and V. Gupta, *Radiat. Phys. Chem. **153,** 51 (2018).*
22. **Dewetting induced Au-Ge composite nanodot evolution in SiO_2,** D. P. Datta, A. Chettah, V. Siva, D. Kanjilal, and P. K. Sahoo, *Appl. Surf. Sci. **428,** 676 (2018).*
23. **Dimethylglyoxime modified swift heavy oxygen ions irradiated polyaniline/single walled carbon nanotubes composite electrode for detection of cobalt ions,** H. K. Patil, M. A. Deshmukh, G. A. Bodkhe, S. M. Shirsat, K. Asokan, and M. D. Shirsat, *Mater. Res. Express **5,** 8, 065048 (2018).*
24. **Dosimetric properties of ZrO_2 and ZrO_2:Sm^{3+} exposed to beta rays,** H. S. Lokesha, N. Chauhan, K. R. Nagabhushana, and F. Singh, *Ceram. Int. **44,** 18871 (2018).*
25. **Effect of 120 MeV Au^{9+} ion irradiation on the structure and surface morphology of ZnO/NiO heterojunction,** P. K. Das, R. Biswal, R. J. Choudhary, V. Sathe, V. Ganesan, S. A. Khan, N. C. Mishra, and P. Mallick, *Surf. Interface Anal. **50,** 954 (2018).*
26. **Effect of carbon ion-beam irradiation on graphene oxide film,** C. Tyagi, S. A. Khan, S. Ojha, D. K. Avasthi, and A. Tripathi, *Vacuum **154,** 259 (2018).*
27. **Effect of gamma irradiation on AlInGaN/AlN/GaN heterostructures grown by MOCVD,** S. Pradeep, R. Loganathan, S. Surender, K. Prabakaran, K. Asokan, and K. Baskar, *Superlattices Microstruct. **120,** 40 (2018).*
28. **Effect of low energy (keV) ion irradiation on structural, optical and morphological properties of SnO_2-TiO_2 nanocomposite thin films,** V. Kumar, M. K. Jaiswal, R. Gupta, J. Ram, I. Sulania, S. Ojha, X. Sun, N. Koratkar, and R. Kumar, *J. Mater. Sci.-Mater. Electron. **29,** 13328 (2018).*
29. **Effect of nitridation temperature on formation and properties of GaN nanowall networks on sapphire (0001) grown by laser MBE,** C. Ramesh, P. Tyagi, B. S. Yadav, S. Ojha, K. K. Maurya, M. S. Kumar, and S. S. Kushvaha, *Mater. Sci. Eng. B-Adv. Funct. Solid-State Mater. **231,** 105 (2018).*
30. **Effects of gamma-ray irradiation on the optical properties of amorphous $Se_{100-x}Hg_x$ thin films,** S. Ahmad, S. Islam, M. Nasir, K. Asokan, and M. Zulfequar, *J. Phys. Chem. Solids **117,** 122 (2018).*
31. **Effects of high-energy ion-beam irradiation on structural and optical properties of $(Mg_{0.95}Co_{0.05})$ TiO3 thin films,** T. S. Kumar, A. Vinod, M. S. Rathore, A. P. Pathak, F. Singh, D. Pamu, and N. S. Rao, *Radiat. Eff. Defects Solids **173,** 128 (2018).*
32. **Electrical relaxation and conduction mechanisms in iron doped barium strontium titanate,** A. Kaur, L. Singh, and K. Asokan, *Ceram. Int. **44,** 3751 (2018).*
33. **Electronic excitation induced defect dynamics in HfO_2 based MOS devices investigated by in-situ electrical measurements,** N. Manikanthababu, S. Vajandar, N. Arun, A. P. Pathak, K. Asokan, T. Osipowicz, T. Basu, and S. Rao, *Appl. Phys. Lett. **112,** 5, 131601 (2018).*
34. **Electronic excitation induced modifications in the ferroelectric polarization of $BiFeO_3$ thin films,** A. Ravalia, B. Kataria, S. Katba, S. Jethva, M. Vagadia, K. Asokan, S. Gautam, K. H. Chae, and D. G. Kuberkar, *Vacuum **155,** 572 (2018).*
35. **Electronic structure of Cr doped Fe_3O_4 thin films by X-ray absorption near-edge structure spectroscopy,** C. L. Chen, C. L. Dong, K. Asokan, G. Chern, and C. L. Chang, *Solid State Commun. **272,** 48 (2018).*

36. **Electronic structure of Ln_2O_2Te (Ln = La, Sm and Gd) by X-ray absorption spectroscopy,** S. Gautam, K. H. Chae, J. Llanos, O. Pena, and K. Asokan, *Vacuum* ***158,*** *39 (2018).*
37. **Energetic ion-induced modification of embedded Au nanoparticles size: a three-dimensional kinetic lattice Monte Carlo study,** S. A. Khan, D. K. Avasthi, and S. Hooda, *Appl. Phys. A-Mater. Sci. Process.* ***124,*** *9, 351 (2018).*
38. **Engineering bright fluorescent nitrogen-vacancy (NV) nano-diamonds: Role of low-energy ion-irradiation parameters,** R. Kumar, P. Pandit, P. Pal, S. R. Dhakate, R. P. Pant, R. Kumar, D. K. Avasthi, and D. K. Singh, *AIP Adv.* ***8,*** *18, 085023 (2018).*
39. **Engineering of electronic properties of single layer graphene by swift heavy ion irradiation,** S. Kumar, A. Kumar, A. Tripathi, C. Tyagi, and D. K. Avasthi, *J. Appl. Phys.* ***123,*** *7, 161533 (2018).*
40. **Enhanced electrical conductivity in Xe ion irradiated CNT based transparent conducting electrode on PET substrate,** Surbhi, V. Sharma, S. Singh, P. Garg, K. Asokan, and K. Sachdev, *Mater. Res. Express* ***5,*** *10, 025037 (2018).*
41. **Enhanced magnetic behaviour and cell proliferation of gamma irradiated dual metal ions co-doped hydroxyapatite - poly(methyl methacrylate) composite films,** J. R. Ramya, K. T. Arul, P. Sathiamurthi, K. Asokan, N. R. Singh, and S. N. Kalkura, *React. Funct. Polym.* ***123,*** *34 (2018).*
42. **Enhanced visible light photodegradation activity of RhB/MB from aqueous solution using nanosized novel Fe-Cd co-modified ZnO, D. Neena,** K. K. Kondamareddy, H. Bin, D. Z. Lu, P. Kumar, R. K. Dwivedi, V. O. Pelenovich, X. Z. Zhao, W. Gao, and D. J. Fu, *Sci Rep* ***8,*** *12, 10691 (2018).*
43. **Enhancement of magnetostrictive properties of Galfenol thin films,** L. R. Nivedita, P. Manivel, R. Pandian, S. Murugesan, N. A. Morley, K. Asokan, and R. T. R. Kumar, *J. Magn. Magn. Mater.* ***451,*** *300 (2018).*
44. **Enhancement of third-order nonlinear optical properties of HMTA stabilized pure and doped ZnS nanoparticles and their electronic structures,** K. V. Anand, G. Vinitha, S. Gautam, K. H. Chae, R. Mohan, K. Asokan, T. R. Ravindran, and R. Jayavel, *J. Nonlinear Opt. Phys. Mater.* ***27,*** *15, 1850016 (2018).*
45. **Evidence of Ion-Beam-Induced Annealing in Graphene Oxide Films Using in Situ X-Ray Diffraction and Spectroscopy Techniques,** C. Tyagi, S. A. Khan, I. Sulania, R. Meena, D. K. Avasthi, and A. Tripathi, *J. Phys. Chem. C* ***122,*** *9632 (2018).*
46. **Evolution of Visible Photocatalytic Properties of Cu-Doped CeO_2 Nanoparticles: Role of Cu^{2+}-Mediated Oxygen Vacancies and the Mixed-Valence States of Ce Ions,** K. S. Ranjith, C. L. Dong, Y. R. Lu, Y. C. Huang, C. L. Chen, P. Saravanan, K. Asokan, and R. T. R. Kumar, *ACS Sustain. Chem. Eng.* ***6,*** *8536 (2018).*
47. **Formation of Anisotropic Nanostructures on Rutile TiO_2(110) Surfaces and Their Photo-Absorption Properties,** V. Solanki, S. R. Joshi, I. Mishra, D. Kanjilal, and S. Varma, *Metall. Mater. Trans. A-Phys. Metall. Mater. Sci.* ***49A,*** *3117 (2018).*
48. **Formation of graphitic and diamond-like carbon by low energy carbon ion implantation on c plane sapphire substrate,** S. Pradeep, S. Surender, K. Prabakaran, M. Jayasakthi, S. Singh, K. Asokan, and K. Baskar, *Thin Solid Films* ***649,*** *12 (2018).*
49. **Gold -graphene oxide nanocomposites for enzyme-less glucose monitoring,** C. Tyagi, G. Lakshmi, V. Jaiswal, D. K. Avasthi, and A. Tripathi, *Biomed. Phys. Eng. Express* ***4,*** *11, Unsp 065002 (2018).*
50. **Grain fragmentation and phase transformations in hafnium oxide induced by swift heavy ion irradiation,** M. Dhanunjaya, D. K. Avasthi, A. P. Pathak, S. A. Khan, and S. Rao, *Appl. Phys. A-Mater. Sci. Process.* ***124,*** *10, 587 (2018).*
51. **High spin state driven magnetism and thermoelectricity in Mn doped topological insulator Bi_2Se_3,** V. K. Maurya, C. L. Dong, C. L. Chen, K. Asokan, and S. Patnaik, *J. Magn. Magn. Mater.* ***456,*** *1 (2018).*
52. **Highly selective and reversible NO_2 gas sensor using vertically aligned MoS2 flake networks,** R. Kumar, P. K. Kulriya, M. Mishra, F. Singh, G. Gupta, and M. Kumar, *Nanotechnology* ***29,*** *9, 464001 (2018).*
53. **Hydrogen loss and its improved retention in hydrogen plasma treated a-SiN_x:H films: ERDA study with 100 MeV Ag^{7+} ions,** R. K. Bommali, S. Ghosh, S. A. Khan, and P. Srivastava, *Nucl. Instrum. Methods Phys. Res. Sect. B-Beam Interact. Mater. Atoms* ***423,*** *16 (2018).*
54. **Identification of swift heavy ion induced defects in Pt/n-GaN Schottky diodes by in-situ deep level transient spectroscopy,** A. Kumar, J. Dhillon, S. Verma, P. Kumar, K. Asokan, and D. Kanjilal, *Semicond. Sci. Technol.* ***33,*** *6, 085008 (2018).*

55. **Imidazolium based ionic liquid induced DNA gelation at remarkably low concentration,** P. K. Pandey, K. Rawat, V. K. Aswal, J. Kohlbrecher, and H. B. Bohidar, *Colloid Surf. A-Physicochem. Eng. Asp.* ***538,*** *184 (2018).*
56. **Impact of substrate bias and dielectrics on the performance parameters of symmetric lateral bipolar transistor on SiGe-OI for mixed signal applications,** L. B. Devi, K. Singh, and A. Srivastava, *Microelectron. J.* ***81,*** *28 (2018).*
57. **Impedance spectroscopic study on microwave sintered (1-x) $Na_{0.5}Bi_{0.5}TiO_{3-x}$ $BaTiO_3$ ceramics,** H. S. Mohanty, A. Kumar, B. Sahoo, P. K. Kurliya, and D. K. Pradhan, *J. Mater. Sci.-Mater. Electron.* ***29,*** *6966 (2018).*
58. **Improved deep ultraviolet light photosensitivity of nanocomposite ZnO-Ag films deposited with substrate heating,** V. V. S. Kumar, *Mater. Res. Express* ***5,*** *10, 096203 (2018).*
59. **Improvement in crystallinity of ZnO and Zn_2SiO_4 phases by rf sputter deposition; effect of substrate bias,** V. V. S. Kumar and M. K. Sharma, *Vacuum* ***157,*** *72 (2018).*
60. **Influence of 100 keV Ar^+ implantation on electrical and optical properties of TiO_2/Ag/TiO_2 multilayer films,** S. Singh, V. Sharma, D. Saini, S. Shekhawat, K. Asokan, and K. Sachdev, *Mater. Sci. Semicond. Process* ***75,*** *18 (2018).*
61. **Influence of deposition rate on the structural, optical and electrical properties of electron beam evaporated SnO_2 thin films for transparent conducting electrode applications,** N. Kumar, B. Joshi, and K. Asokan, *J. Semicond.* ***39,*** *7, 083002 (2018).*
62. **Influence of post-deposition annealing on structural, optical and transport properties of nanocomposite ZnO-Ag thin films,** V. V. S. Kumar and D. Kanjilal, *Mater. Sci. Semicond. Process* ***81,*** *22 (2018).*
63. **Influence of thermal annealing and radiation enhanced diffusion processes on surface plasmon resonance of gold implanted dielectric matrices,** K. D. Devi, S. Ojha, and F. Singh, *Radiat. Phys. Chem.* ***144,*** *141 (2018).*
64. **In-situ transport and microstructural evolution in GaN Schottky diodes and epilayers exposed to swift heavy ion irradiation,** A. Kumar, R. Singh, P. Kumar, U. B. Singh, K. Asokan, P. A. Karaseov, A. I. Titov, and D. Kanjilal, *J. Appl. Phys.* ***123,*** *6, 161539 (2018).*
65. **Interface and transport properties of gamma irradiated Au/n-GaP Schottky diode,** N. Shiwakoti, A. Bobby, K. Asokan, and B. Antony, *Mater. Sci. Semicond. Process* ***74,*** *1 (2018).*
66. **Investigation of C-60 and C-70 fullerenes under low energy ion impact,** R. Singhal, J. Bhardwaj, R. Vishnoi, A. Sharma, G. D. Sharma, and D. Kanjilal, *J. Mater. Sci.-Mater. Electron.* ***29,*** *14762 (2018).*
67. **Investigation of graphene oxide-hydrogen interaction using in-situ X-ray diffraction studies,** C. Tyagi, P. K. Kulriya, S. Ojha, D. K. Avasthi, and A. Tripathi, *Int. J. Hydrog. Energy* ***43,*** *13339 (2018).*
68. **Investigation of ionic conduction in PEO-PVDF based blend polymer electrolytes,** S. K. Patla, R. Ray, K. Asokan, and S. Karmakar, *J. Appl. Phys.* ***123,*** *11, 125102 (2018).*
69. **In-vitro dosimetry of radioactive patches incorporating Rhenium-188 for local radionuclide therapy,** P. Gupta, S. P. Lochab, G. P. Bandopadhyaya, and C. S. Bal, *Eur. J. Nucl. Med. Mol. Imaging* ***45,*** *S245 (2018).*
70. **Ion beam assisted fortification of photoconduction and photosensitivity,** P. Kumar, N. Saxena, F. Singh, and V. Gupta, *Sens. Actuator A-Phys.* ***279,*** *343 (2018).*
71. **Ion-beam-induced ferromagnetism in Ca-doped $LaMnO_3$ thin films grown on Si (100),** K. Sultan, S. A. ul Islam, Z. Habib, M. Ikram, and K. Asokan, *Radiat. Eff. Defects Solids* ***173,*** *184 (2018).*
72. **Low energy nitrogen ion beam implanted tungsten trioxide thin films modified indium tin oxide electrode based acetylcholine sensor,** A. C. Anithaa, K. Asokan, and C. Sekar, *J. Taiwan Inst. Chem. Eng.* ***84,*** *11 (2018).*
73. **Magnetic and electronic structures of Co ion implanted CeO_2 thin films, P. Kumar,** B. Ahmad, F. Chand, and K. Asokan, *Appl. Surf. Sci.* ***452,*** *217 (2018).*
74. **Magneto-dielectric studies on multiferroic composites of Pr doped $CoFe_2O_4$ and Yb doped $PbZrTiO_3$,** R. Samad, M. U. D. Rather, K. Asokan, and B. Want, *J. Alloy. Compd.* ***744,*** *453 (2018).*
75. **Material engineering to fabricate rare earth erbium thin films for exploring nuclear energy sources,** A. Banerjee, S. R. Abhilash, G. R. Umapathy, D. Kabiraj, S. Ojha, and S. Mandal, *Nucl. Instrum. Methods Phys. Res. Sect. A-Accel. Spectrom. Dect. Assoc. Equip.* ***887,*** *34 (2018).*
76. **Mechanistic insights into the interaction between energetic oxygen ions and nanosized $ZnFe_2O_4$: XAS-XMCD investigations,** J. P. Singh, B. Kaur, A. Sharma, S. H. Kim, S. Gautam, R. C. Srivastava, N. Goyal, W. C. Lim, H. J. Lin, J. M. Chen, K. Asokan, D. Kanjilal, S. O. Won, I. J. Lee, and K. H. Chae, *Phys. Chem. Chem. Phys.* ***20,*** *12084 (2018).*

77. **Microstructural and surface morphological studies on Co doped ZnS diluted magnetic semiconductor thin films,** S. P. Patel, J. C. Pivin, G. Maity, R. P. Yadav, R. Chandra, D. Kanjilal, and L. Kumar, *J. Mater. Sci.-Mater. Electron.* ***29,*** *13541 (2018).*

78. **Mixing ratio dependent complex coacervation versus bicontinuous gelation of pectin with in situ formed zein nanoparticles,** P. Kaushik, K. Rawat, V. K. Aswal, J. Kohlbrecher, and H. B. Bohidar, *Soft Matter* ***14,*** *6463 (2018).*

79. **Modelling of Pinning-Depinning Reversal Mechanism in Ion-Irradiated Co/Al_2O_3 Thin Films,** R. Goyal, R. Gupta, A. Negi, K. Asokan, D. Kanjilal, S. Lamba, and S. Annapoorni, *Phys. Status Solidi A-Appl. Mat.* ***215,*** *8, 1800141 (2018).*

80. **Modification in the transport and morphological properties of solid polymer electrolyte system by low-energy ion irradiation,** H. Manjunatha, R. Damle, K. Pravin, and G. N. Kumaraswamy, *Ionics* ***24,*** *3027 (2018).*

81. **Modification of Structural and Magnetic Properties of Masked Co-Pt Films Induced by High-Energy Ion Implantation,** D. Kumar, S. Gupta, T. L. Jin, R. Nongjai, K. Asokan, and S. N. Piramanayagam, *IEEE Magn. Lett.* ***9,*** *5, 4500305 (2018).*

82. **Modifications in structural, optical and electrical properties of epitaxial graphene on SiC due to 100 MeV silver ion irradiation,** P. D. Kaushik, A. Aziz, A. M. Siddiqui, G. Greczynski, M. J. Jafari, G. Lakshmi, D. K. Avasthi, M. Syvajarvi, and G. R. Yazdi, *Mater. Sci. Semicond. Process* ***74,*** *122 (2018).*

83. **Morphological investigations on the growth of defect-rich Bi_2Te_3 nanorods and their thermoelectric properties,** M. Sinduja, S. Amirthapandian, P. Jegadeesan, P. Magudapathy, and K. Asokan, *Crystengcomm* ***20,*** *4810 (2018).*

84. **Multifunctional hybrid diode: Study of photoresponse, high responsivity, and charge injection mechanisms,** J. Singh, R. G. Singh, S. K. Gautam, and F. Singh, *J. Appl. Phys.* ***123,*** *10, 174503 (2018).*

85. **Nanocrystalline SnO_2 formation by oxygen ion implantation in tin thin films,** V. Kondkar, D. Rukade, D. Kanjilal, and V. Bhattacharyya, *Mater. Res. Express* ***5,*** *7, 035015 (2018).*

86. **NTO/Ag/NTO multilayer transparent conducting electrodes for photovoltaic applications tuned by low energy ion implantation,** S. Singh, V. Sharma, K. Asokan, and K. Sachdev, *Sol. Energy* ***173,*** *651 (2018).*

87. **n-ZnO/p-Si heterojunction nanodiodes based sensor for monitoring UV radiation,** P. D. Sahare, S. Kumar, S. Kumar, and F. Singh, *Sens. Actuator A-Phys.* ***279,*** *351 (2018).*

88. **Observation of Kondo behavior in the single crystals of Mn-doped Bi_2Se_3 topological insulator,** R. R. Urkude, A. Sagdeo, R. Rawat, R. J. Choudhary, K. Asokan, S. Ojha, and U. A. Palikundwar, *AIP Adv.* ***8,*** *11, 045315 (2018).*

89. **On the study of the C^{6+} ion beam and gamma-ray induced effect on structural and luminescence properties of Eu doped $LiNaSO_4$: explanation of TSL mechanism using PL,** TL and EPR study, K. K. Gupta, R. M. Kadam, N. S. Dhoble, S. P. Lochab, and S. J. Dhoble, *Phys. Chem. Chem. Phys.* ***20,*** *1540 (2018).*

90. **Optical properties of Cu-C-70 nanocomposite under low energy ion irradiation,** R. Singhal, S. Gupta, R. Vishnoi, S. Aggarwal, G. D. Sharma, A. Sharma, and S. Ojha, *Mater. Res. Express* ***5,*** *13, 035044 (2018).*

91. **Origin of magnetic properties in carbon implanted ZnO nanowires,** Y. F. Wang, Y. C. Shao, S. H. Hsieh, Y. K. Chang, P. H. Yeh, H. C. Hsueh, J. W. Chiou, H. T. Wang, S. C. Ray, H. M. Tsai, C. W. Pao, C. H. Chen, H. J. Lin, J. F. Lee, C. T. Wu, J. J. Wu, Y. M. Chang, K. Asokan, K. H. Chae, T. Ohigashi, Y. Takagi, T. Yokoyama, N. Kosugi, and W. F. Pong, *Sci Rep* ***8,*** *13, 7758 (2018).*

92. **Oxygen mediated phase transformation in room temperature grown TiO_2 thin films with enhanced photocatalytic activity,** D. Banerjee, A. Barman, S. Deshmukh, C. P. Saini, G. Maity, S. K. Pradhan, M. Gupta, D. M. Phase, S. S. Roy, and A. Kanjilal, *Appl. Phys. Lett.* ***113,*** *5, 084103 (2018).*

93. **Photoluminescence, thermoluminescence and defect centres in Y_2O_3 and Y_2O_3:Tb^{3+} under 100 MeV swift Ni^{8+} ion beam irradiation,** N. J. Shivaramu, B. N. Lakshminarasappa, F. Singh, E. Coetsee, and H. C. Swart, *Mater. Res. Bull.* ***102,*** *62 (2018).*

94. **Photoluminescence, thermoluminescence glow curve and emission characteristics of Y_2O_3:Er^{3+} nanophosphor,** N. J. Shivaramu, B. N. Lakshminarasappa, K. R. Nagabhushana, H. C. Swart, and F. Singh, *Spectroc. Acta Pt. A-Molec. Biomolec. Spectr.* ***189,*** *349 (2018).*

95. **Preparation and characterization of indium chalcogenide thin films: A material for phase change memory,** M. Pandian, P. Matheswaran, B. Gokul, R. Sathyamoorthy, and K. Asokan, *Appl. Surf. Sci.* ***449,*** *55 (2018).*

96. **Probing the impact of energetic argon ions on the structural properties of ZnO:Al/TiO_2 heterostructures,** C. P. Saini, A. Barman, N. Kumar, R. Cours, S. Joulie, V. Serin, A. Claverie, A. K. Sinha, D. Kanjilal, and A. Kanjilal, *J. Appl. Phys.* ***124,*** *7, 155305 (2018).*

97. **Radiation stability of CBD grown nanocrystalline CdS films against ion beam irradiation for solar cell applications,** N. Saxena, P. Kumar, V. Gupta, and D. Kanjilal, *J. Mater. Sci.-Mater. Electron.* ***29,*** *11013 (2018).*

98. **Raman spectroscopic analysis on Li, N and (Li,N) implanted ZnO,** A. Mondal, S. Pal, A. Sarkar, T. S. Bhattacharya, A. Das, N. Gogurla, S. K. Ray, P. Kumar, D. Kanjilal, K. D. Devi, A. Singha, S. Chattopadhyay, and D. Jana, *Mater. Sci. Semicond. Process* ***80,*** *111 (2018).*

99. **Raman spectroscopic study of He ion implanted 4H and 6H-SiC,** A. A. Ali, J. Kumar, V. Ramakrishnan, and K. Asokan, *Mater. Lett.* ***213,*** *208 (2018).*

100. **Reinforcement of polyaniline and poly-(o-toluidine) with SWNTs and tuning of their physicochemical properties by heavy ion beams,** H. K. Patil, M. A. Deshmukh, G. A. Bodkhe, S. M. Shirsat, K. Asokan, and M. D. Shirsat, *Appl. Phys. A-Mater. Sci. Process.* ***124,*** *11, 491 (2018).*

101. **Remarkable effect of halogenation of aromatic compounds on efficiency of nanowire formation through polymerization/crosslinking by high-energy single particle irradiation,** A. Horio, T. Sakurai, K. Kayama, G. Lakshmi, D. K. Avasthi, M. Sugimoto, T. Yamaki, A. Chiba, Y. Saito, and S. Seki, *Radiat. Phys. Chem.* ***142,*** *100 (2018).*

102. **Resistive switching behavior in oxygen ion irradiated TiO_{2-x} films,** A. Barman, C. P. Saini, P. K. Sarkar, G. Bhattacharjee, G. Bhattacharya, S. Srivastava, B. Satpati, D. Kanjilal, S. K. Ghosh, S. Dhar, and A. Kanjilal, *J. Phys. D-Appl. Phys.* ***51,*** *7, 065306 (2018).*

103. **Reversible phase transformation phenomenon in titanium dioxide films: Evidence beyond interface-nucleation and dissolution-precipitation kinetics,** S. K. Gautam, J. Singh, D. K. Shukla, E. Pippel, P. Poddar, and F. Singh, *Acta Mater.* ***146,*** *253 (2018).*

104. **Self-Stabilized Carbon-L1(0) FePt Nanoparticles for Heated Dot Recording Media,** R. Medwal, S. Gautam, S. Gupta, K. H. Chae, K. Asokan, G. R. Deen, R. S. Rawat, R. S. Katiyar, and S. Annapoorni, *IEEE Magn. Lett.* ***9,*** *5, 5504105 (2018).*

105. **Structural and thermoelectric properties of Se doped In_2Te_3 thin films,** P. Mannu, M. Palanisamy, G. Bangaru, S. Ramakrishnan, M. Ramcharan, and A. Kandasami, *AIP Adv.* ***8,*** *11, 115015 (2018).*

106. **Structural phase transformation and modification of optical absorption of SHI induced nanostructured CdS films,** P. K. Mochahari, F. Singh, and K. C. Sarma, *J. Mater. Sci.-Mater. Electron.* ***29,*** *582 (2018).*

107. **Structural response of Nd-stabilized zirconia and its composite under extreme conditions of swift heavy ion irradiation,** C. Nandi, V. Grover, P. K. Kulriya, A. K. Poswal, A. Prakash, K. B. Khan, D. K. Avasthi, and A. K. Tyagi, *J. Nucl. Mater.* ***499,*** *216 (2018).*

108. **Structural, dielectric and ferroelectric properties of rare earth substituted lead zirconate titanate,** R. Samad, M. U. D. Rather, K. Asokan, and B. Want, *J. Mater. Sci.-Mater. Electron.* ***29,*** *4226 (2018).*

109. **Structural, electrical and magnetic properties of multiferroic $BiFeO_3$-$SrTiO_3$ composites,** T. Murtaza, J. Ali, M. S. Khan, and K. Asokan, *J. Mater. Sci.-Mater. Electron.* ***29,*** *2110 (2018).*

110. **Structural, electrical and magnetic properties of multiferroic $NdFeO_3$-$SrTiO_3$ composites,** T. Murtaza, M. S. Khan, J. Ali, T. Hussain, and K. Asokan, *J. Mater. Sci.-Mater. Electron.* ***29,*** *18573 (2018).*

111. **Structural, optical and electrical properties of $In_2(Te_{1-x}Se_x)_3$ thin films,** M. Pandian, P. Matheswaran, B. Gokul, R. Sathyamoorthy, and K. Asokan, *Vacuum* ***147,*** *107 (2018).*

112. **Structural, optical and photoelectrical properties of thermally annealed amorphous $In_{15}Sb_{15}Se_{70}$ chalcogenide films,** S. Sharma, R. Sharma, P. Kumar, R. Thangaraj, K. Asokan, and M. Mian, *Appl. Phys. A-Mater. Sci. Process.* ***124,*** *9, 357 (2018).*

113. **Surface structuring in polypropylene using Ar^+ beam sputtering: Pattern transition from ripples to dot nanostructures,** M. Goyal, S. Aggarwal, A. Sharma, and S. Ojha, *Appl. Surf. Sci.* ***439,*** *380 (2018).*

114 **Synthesis of OSL nanophosphor $Li_3B_7O_{12}$:Mn and its dosimetric properties,** M. Agarwal, K. Asokan, S. K. Garg, E. Dhamija, and P. Kumar, *J. Radiol. Prot.* ***38,*** *1311 (2018).*

115. **Tailoring optical properties of TiO_2-Cr co-sputtered films using swift heavy ions,** R. Gupta, S. Sen, D. M. Phase, D. K. Avasthi, and A. Gupta, *Appl. Surf. Sci.* ***440,*** *403 (2018).*

116. **Tailoring the structural and magnetic properties of masked CoPt thin films using ion implantation,** D. Kumar, S. Gupta, T. Jin, R. Nongjai, K. Asokan, and S. N. Piramanayagam, *AIP Adv.* ***8,*** *5, 056504 (2018).*

117. **Temperature-dependent OSL properties of nano-phosphors $LiAlO_2$:C and alpha-Al_2O_3:C,** M. Agarwal, S. K. Garg, K. Asokan, and P. Kumar, *Appl. Surf. Sci.* ***444,*** *819 (2018).*

118. **The Effect of Low Energy Nitrogen Ion Implantation on Graphene Nanosheets,** M. Mishra, S. Alwarappan, D. Kanjilal, and T. Mohanty, *Electron. Mater. Lett.* ***14,*** *488 (2018).*

119. **The effect of Ti^{+} ion implantation on the anatase-rutile phase transformation and resistive switching properties of TiO_2 thin films,** A. Manna, A. Barman, S. R. Joshi, B. Satpati, P. Dash, A. Chattaraj, S. K. Srivastava, P. K. Sahoo, A. Kanjilal, D. Kanjilal, and S. Varma, *J. Appl. Phys.* ***124,*** *10, 155303 (2018).*

120. **The effects of high-energy ion irradiations on the I-V characteristics of silicon NPN transistors,** A. P. G. Prakash, M. N. Bharathi, V. N. Hegde, T. M. Pradeep, N. Pushpa, and A. Tripathi, *Radiat. Eff. Defects Solids* ***173,*** *683 (2018).*

121. **Thermal annealing and transient electronic excitations induced interfacial and magnetic effects on Pt/Co/Pt trilayer,** N. Sehdev, R. Medwal, R. Malik, A. Kandasami, D. Kanjilal, and S. Annapoorni, *Nucl. Instrum. Methods Phys. Res. Sect. B-Beam Interact. Mater. Atoms* ***420,*** *50 (2018).*

122. **Thermoluminescence properties of 100MeV Si^{7+} ion-irradiated Al_2O_3, S. S. Reddy,** K. R. Nagabhushana, and F. Singh, *Radiat. Eff. Defects Solids* ***173,*** *504 (2018).*

123. **Three-dimensional hybrid silicon nanostructures for surface enhanced Raman spectroscopy based molecular detection,** V. S. Vendamani, S. Rao, S. V. Rao, D. Kanjilal, and A. P. Pathak, *J. Appl. Phys.* ***123,*** *8, 014301 (2018).*

124. **TL/OSL properties of beta irradiated Al_2O_3:Tm^{3+} phosphor synthesized by microwave combustion method,** S. S. Reddy, N. Chauhan, K. R. Nagabhushana, and F. Singh, *Mater. Res. Bull.* ***104,*** *236 (2018).*

125. **Topographic evolution and scaling study of ZnO (0001) single crystal after, low-energy atom beam irradiation,** V. Solanki, D. Kabiraj, D. K. Avasthi, and S. Varma, *Nucl. Instrum. Methods Phys. Res. Sect. B-Beam Interact. Mater. Atoms* ***434,*** *56 (2018).*

126. **Universal Validity of Einstein Relation and Size-Dependent Viscosity and Surface-Active Characteristics of Nanofluids,** A. Sukumaran, K. Das, K. Rawat, and H. B. Bohidar, *Int. J. Nanosci.* ***17,*** *7, 1850006 (2018).*

127. **Zener diode behavior of nitrogen-doped graphene quantum dots,** J. Nag, K. Rawat, K. Asokan, D. Kanjilal, and H. B. Bohidar, *Physica E* ***104,*** *36 (2018).*

C. OTHERS

1. **Radio frequency planar coil based on-chip probe for portable nuclear magnetic resonance,** Manish Gupta, C. P. Safvan, Kundan Singh, D. K. Lobiyal, Preeti Yadav and Shailja Singh, *IEEE Sensors Journal 19, 2500 (2019).*

2. **Power-law decay of doubly ionized ethylene,** K. Takahashi, K. Yokokawa, A. Mizumura, J. Matsumoto, H. Shiromaru, H. Kumar, P. Bhatt and C. P. Safvan, *Phys. Rev. A 98, 062708 (2018).*

3. **Plasmon excitation and subsequent isomerization dynamics in naphthalene and azulene under fast proton interaction,** M. V. Vinitha, P. K. Najeeb, A. Kala, P. Bhatt, C. P. Safvan, S. Vig and U. Kadhane, *J. Chem. Phys. 149, 194303 (2018).*

4. **Experimental investigations of plasma instabilities by Fourier analysis in an Electron cyclotron resonance ion source,** Sarvesh Kumar, Jyotsna Sharma, Prashant Sharma, Shatendra Sharma, Yaduvansh Mathur, Devendra Sharma and Manish K. Kashyap, *Phys. Rev. Accel. Beams 21, 093402 (2018).*

5. **Anisotropy in multiple ionisation of CO by ion collisions at intermediate interaction strengths,** Deepak Sharma, Bhas Bapat, Pragya Bhatt and C. P. Safvan, *J. Phys. B: At. Mol. Opt. Phys. 51, 195202 (2018).*

6. **Multiparticle time-domain analysis of coherent undulator radiation,** Vipul Joshi and Subhendu Ghosh, *Phys. Rev. Accel. Beams 22, 020702 (2019).*

7. **Theoretical and simulation study of 'Comb' electron beam and THz generation,** V. Joshi, U. Lehnert, J. Karmakar, N. Kumar, B. Karmakar, S. Tripathi, A. Aryshev, S. Ghosh, J. Urakawa, R. K. Bhandari and D. Kanjilal, *Nucl. Instrum. Methods A 913, 28 (2019).*

8. **Disentangling the bulk and exit surface contribution on projectile-charge-state evolution,** Prashant Sharma and Tapan Nandi, *Phys. Rev. Accel. Beams 22, 034501 (2019).*

9. **Present status of theoretical understanding of charge changing processes at low beam energies,** Deepak Swami and T. Nandi, *Radiation Physics and Chemistry 153, 120 (2018).*

6.8 LIST OF SEMINARS CONDUCTED IN THE YEAR 2018-19

S.No.	Date	Title	Name & Affiliation
1.	29/05/2018	Production & Applications of Radioisotopes at RIKEN RI Beam Factory	Prof. Hiromitsu Haba, Nishina Centre for Accelerator-Based Science. RIKEN, Wako, Saitama 351-0198, Japan
2.	06-06-2018	Accelerators for Science and Society	Dr. S. Kailas, Bhabha Atomic Research Centre & UM-DAE Centre for Excellence in Baasic Sciences, Mumbai
3.	11-07-2018	Superconducting MRI Project	Dr. Soumen Kar, IUAC, N. Delhi
4.	20-07-2018	Detectors and Detection Techniques for a Dark Mater Search Experiment: An Indian Initiative	Prof. Satyajit Saha SINP, Kolkata
5.	10-08-2018	Tera Hertz (THz) sources and detectors using modified bulk, surface and antenna structures	Prof. S.S. Prabhu TIFR, Mumbai
6.	05-09-2018	Application of Thz Spectroscopy to Study Biologically Important Phenomena	Prof. Rajib Kr. Mitra, S.N. Bose National Centre for Basic Science, Salt Lake, Kolkata
7.	17-10-2018	Risk Assessment and Life Management of Nuclear Plant Systems	Prof. Mahesh Pandey NSERC-UNENE Industrial Research Chair, University of Waterloo, Waterloo, Ontario, Canada
8.	08-11-2018	Supernova Footprint on the Doorstep	Dr. Gunther Korshinek Accelerator Mass Spectrometry Group Technical University Munich, Garching, Germany
9.	22-11-2018	Penning Trap Physics at an Accelerator Facility"	Prof. Manuel Vogel GSI, Darmstadt, Germany
10.	26-12-2018	Facility for Rare Isotope Beams	Dr. Jiban Jyoti Das, Michigan State University, USA
11.	22-01-2019	Some Applications of 14C and 129I using AMS	Prof. A.J. Timothy Jull Arizona University, Tucson, USA
12.	07-02-2019	Prevention of Sexual Harassment at Workplace Act 2013	Mrs. Kuljit Kaur, All India Womens"s Conference, New Delhi. Designation: Hon) Member Incharge.
13.	08-02-2019	Why must Universities in 21st Century Engage in Scientific Research:An Interactive Discussion!	Prof. Yoginder Pal Chugh Fellow, National Academy of Inventors and Professor Emeritus and Visiting Professor, Southern Illinois University, Carbondale, Illinois, USA
14.	21-02-2019	Models for the description of Track Formation	Prof. M. Toulemonde,CIMAP (CEA, CNRS, Ensicaen Univ. Caen, 14070 Caen, France)

S.No.	Date	Title	Name & Affiliation
15.	22-02-2019	Material Transformation: Interaction between Nuclear, Electronic and Potential Energy Deposition	Prof. M. Toulemonde, CIMAP (CEA, CNRS, ENSICAEN, Univ. Caen, 14070 Caen, France)
16.	01-03-2019	Digital system for multi-parametric analysis in physics application	Carlo Tintori (CAEN SpA - Chief of Front-End Division)
17.	08-03-2019	General Awareness about Women's Health	Dr. Meera Chawla, Gynaecologist Dr. Chawla Clinic B-10, Vasant Kunj, New Delhi
18.	19-03-2019	Photons for Food and Medicine	Prof. Rangacharyulu Chary, University of Saskatchewan, Canada
19.	25-03-2019	An introduction to the work of the Cockcroft Institute	Prof. Peter Ratoff, Director Cockcroft Institute, Daresbury, UK
20.	25-04-2019	Chirality, Wobbling and Chirals Wobblers	Prof. Umesh Garg, Prof. Of Physics, Univ. Of Notre Dame, USA
21.	29/04/2019	Symmetry Breaking of CP- Can it explain our pressure in the country	Prof. Natarajan P., DOP and Astrophysics, Univ. Of Delhi

6.9 SCHOOLS, WORKSHOPS, ACQUAINTANCE PROGRAMMMES, FOUNDATION DAY & NATIONAL SCIENCE DAY CELEBRATIONS

School on Accelerator Science and Technology - 2018 (SAST-2018)

Rajeev Mehta

Introduction:

Inter-University Accelerator Centre (IUAC) hosted a School on Accelerator Science & Technology during May 7-18, 2018 under the sponsorship of Department of Science & Technology (DST). This school was third in the series of DST sponsored accelerator school. The aim of the school was to provide educational opportunities for young scientists, engineers, faculty members, post-doctoral fellows and research scholars in this important and advanced field of research and development (R&D) and to encourage them to contribute effectively in this challenging area of R&D

This school gave an overview and status of the existing accelerator system and also explored the possibilities of the upcoming facilities. The school covered basic physics and technologies related to the accelerators. Series of lectures were delivered by experts from various prestigious accelerator based research institutes in India. There were interactive classroom tutorials sessions, special review talks by eminent scientists and engineers on some of the advance topics related to the accelerators. During hands-on experiments session participants were exposed to some of the technologies and equipment related to accelerators.

The school was offered to graduate, postgraduate students, junior researchers and young scientists etc. from all over the India who are highly motivated to pursue their carrier in accelerator science and technology.

Programme Schedule:

The school duration was two weeks starting from 7 May 2018. The program had intensive lectures, tutorials and hands on experiments on the wide range of technologies that form the base of the particle accelerator technology. School covered the areas like Beam Dynamics, RF Accelerator (Linear & Circular), Operational Aspect of Accelerator, Ion Sources, Vacuum, Instrumentations, High Power Devices, Radiation Safety etc. The overall program had 62 sessions

- 38 Lectures
- 10 Special Review Talks and talks on major Indian projects
- 6 Tutorials
- 4 Hands on Experiments of 2 hours each (total 8 sessions)

"Hands on Experiments" was another feature that gave the participants an exposure to some of the technologies of accelerator physics. Following experiments were performed:

1) Leak Detection Techniques
2) Operational Aspects of Turbo Pump
3) Low level RF Measurement Techniques: Bead Pull & Q Measurement
4) High Power RF Test of Cavity

Interactive tutorial sessions were held, where participants were divided into four groups and were asked to solve the problem on the board. Marking system was introduced and the winner group was facilitated in the concluding session.

Participants Detail:

All major accelerator based laboratory, Institutes & Universities in India were asked to nominate upto three participants for this school. The applications were invited online through website of the school. We received overwhelming response to the school. 20 participants were selected to attend the school. Total 38 participants attended the school.

Financial Aid:

The school was fully funded by Department of Science & Technology (DST). All the participants, speakers were provided with local hospitality and accommodation by the school Organizers. Selected participants were provided with travel assistance by 3rd AC train fare.

Excursion Trip & Special Dinners:

An excursion trip was organized for the participants. The excursion trip was free for all the participants. During this trip participants visited Akshardham Temple

International School on Ion Beams In Materials Science (IBMS) 2018

Chairman: Ambuj Tripathi
Convener: Indra Sulania

This school is a regular feature on every year's calendar of events of IUAC, which is held mostly to cater to the academic interest of research students. This year's school was held from 3-7, October, 2018 and convened by Dr Indra Sulania in the able guidance of Dr A Triapthi. More than 50 participants gained knowledge through the lectures delivered by renowned scientists and professors working in this field from India (8 speakers) and abroad (5 speakers). It provided a platform to PhD students from India and abroad to hear to lectures of researchers and academicians from top Institutes and Universities, from all over the world, who works mostly with ion beams. Hands on training was also provided for the usage of key software such as SRIM, RUMP, SIMNRA etc.

Inaguration of the IBMS 2018 with dignitaries on the dais.

Participants of IBMS 2018

International School on Ion Beams in Energy Materials

P. K. Kulriya & Fouran Singh

An International school on ion beams in energy materials was organized from July 12-18th, 2018 in the seminar hall at IUAC. The 12 eminent resource persons from the national institutes and universities like IIT/D, BARC Mumbai, IPR Gandhi Nagar, NPL Delhi, NCL Pune, IGCAR Kalpakkam, University of Delhi, LNMIIT Jaipur, BHU Varanasi including IUAC New Delhi were invited to deliver the lectures. Though, there are various types of energy materials, however this school was mainly focused on the light-harvesting materials/devices, materials for nuclear reactor applications and thermoelectric materials. The school was attended by 38 PhD scholars and young faculties from various universities across the country and 25 candidates from IUAC. The school was inaugurated by the Director IUAC, followed by the keynote address by Professor R. K. Bhandari (former Director VECC Kolkata and Raja Ramanna Fellow) on the structural materials for nuclear applications. The visit to various facilities at IUAC was also arranged during the school. Photograph of the workshop is shown below.

Modern techniques of ♑-ray spectroscopy for nuclear structure studies

Five day school on “Modern techniques of ♑-ray spectroscopy for nuclear structure studies”was held at our Center from 12th November in 2018. About 30 Ph.D. Students from different universities and national institutes attended this school. The talks covered range of topics in gamma ray spectroscopy by experts in the field. About ten faculties from different institutes gave lectures in this school. The topics covered in this school ranged from basic techniques to contemporary in gamma ray spectroscopy, lifetime measurements, linear polarisation of γ-rays, g-factor measurement techniques and gamma ray tracking. The young researchers using Indian National Gamma Array (INGA) benefited as they could use these techniques in the data reduction and interpretation.

IUAC Acquaitance Workshop at Lucknow University

A one day IUAC acquaintance workshop was held at Department of Physics, Lucknow university on 19th September 2018. More than 100 people participated in this workshop. The participants included faculties of Lucknow university, research scholars and M.Sc. students from Lucknow university and neighbouring colleges. Prof. Pallavi Jha, head of the physics department, gave a brief introduction of Physics department. Dr. R. P. Singh gave an overview of the accelerator programs at IUAC. He then gave detailed talk on research in the areas of nuclear structure and nuclear reactions with INGA, NAND, HIRA and HyRA setups. Dr. Pawan Kulriya gave a detailed description of reaserch in the area of material science using heavy ion beams and associated facilities at IUAC. Prof. Balak Das of university of Lucknow gave a brief summary of the research programs being carried out by his group using IUAC setups. The workshop ended with an discussion and interactive session with the faculties and students.

IUAC acquaintance workshop at physics department Lucknow university.

IUAC Acquaintance Programme at the Central University of Kerala, Kasaragod on October 29, 2018





IUAC Acquaintance Programme and One Day National Workshop on Accelerator Based Science Research were conducted at the Department of Physics, Central University of Kerala (CUK), Kasaragod on October 29, 2018. Dr. E. Prasad from CUK was the local convener of the Programme which was attended by more than one hundred and fifty participants from CUK and other colleges and universities of Kerala, Tamil Nadu and Karnataka. Dr. S. Nath and Dr. A. Tripathi talked about the available experimental facilities and the research programmes pursued at IUAC. Prof. K. M. Varier and Prof. A. M. Vinodkumar from Calicut University (CU) delivered lectures based on their works in nuclear reactions carried out using the experimental facilities of IUAC. Dr. Senoy Thomas from Cochin University of Science and Technology (CUSAT) talked about his works in materials science performed in collaboration with IUAC. Prof. B. R. S. Babu from CU and Dr. Rhine Kumar from CUSAT presented their recent results in theoretical nuclear physics. Queries of the participants about the research opportunities and procedures to submit research proposals at IUAC were answered in an open session at the end of the day.

International workshop on 10th. Asian Forum on Accelerators and Detectors (AFAD) at IUAC (Feb. 14-15, 2019)

Asian Forum for Accelerator and Detectors (AFAD), regulated by Asian Committee of Future Accelerator (ACFA), has been created to promote collaboration among universities, research institutes and industries in Asia and Oceania. This Workshop is being held annually since about ten years and was organised in China, Korea, Japan, Australia, Russia, Taiwan, etc. The major focus of the Forum is dedicated to the fields of accelerators, detectors and related technologies as well as their applications which are being developed in the research institutes and universities. The 10th Asian Forum for Accelerators and Detectors “AFAD2019” was organized in the newly inaugurated Maharshi Kanad Auditorium of Inter University Accelerator Center, New Delhi during February, 14-15, 2019. The key topics discussed during the Workshop were:

- Accelerated and related technologies for photon science
- Detector technology development
- Accelerator Technologies for medical and industrial application
- Innovative acceleration techniques
- Accelerator and related technologies for hadron science
- Network and Computing
- Cryogenic, Cryomodule and Superconductivity for Accelerators

The workshop was by invitation only. About 80 participants from China, Japan, Korea, Taiwan, Russia and Australia and about 100 Indian participants had participated in the workshop. During the two day’s workshop of AFAD2019, there were 8 Plenary talks, 120 talks in the seven parallel session and 7 Summary talks. The picture of the Inauguration session and the participants of AFAD2019 are shown in figure 1 and 2.

Figure 1. Inauguration ceremony

Figure 2. Participants of AFAD2019

National Workshop on Isotopes in Earth, Ocean and Atmospheric Sciences, held at NIO Goa during Feb 18-20, 2019

Under the mandate of geochronology project IUAC organizes national workshop on a regular basis to generate awareness about the available and upcoming instruments under geochronology project. This year workshop was organized in collaboration with National Institute of Oceanography (NIO), Goa to make aware the researchers majorly from Goa region as well as from other part of country. The theme of the workshop was kept on “Isotopes in Earth, Ocean and Atmospheric Sciences” and workshop dates were decided during February 18-20, 2019.

In response to the advertisement a total of 280 (180 outstation and 100 local) applications were received for the participation in the workshop. However, due to limited accommodation availability at NIO Guest house, only 85 outstation participants were shortlisted based on their research interest and academic credentials. Participation from all the universities, gender and geographical representation was also kept in mind while short listing the participants. All the local applicants were allowed to participate in the workshop. All together 185 participants (96 PhD students, 65 faculties, scientists, research associates and postdoctoral fellows, and 24 invited speakers) from the countrywide 22 different universities and 25 institutes participated in the workshop. The total outstation participants were 85 and the female to male participant ratio was 1/3. The event hosted 8 plenary sessions, 2 brainstorming sessions and 2 poster sessions. In total, 25 invited plenary lectures were delivered by invited speakers and 5 posters about the research facilities at IUAC were presented.

Invited speakers were from IUAC, NIO, University of Kashmir, BHU, IIT Kaharagpur, University of Delhi, PRL, Ahmedabad, WIHG Dehradun, NCPOR, Goa, IISER Bhopal, NGRI Hyderabad, Colorado University, IISER Kolkata and IISER Pune.

The major outcomes of the workshop are as below.

Outcomes

- Most of the participants and speakers suggested organizing this kind of workshop on a regular basis (yearly) at different locations of the country.
- Awareness among the research community about IUAC and its research facilities is generated.
- Some of the students showed their desire to utilize AMS and other geochronology facilities at IUAC and came to know about the procedure for it.
- The interaction among the students and resource persons clarified their doubts. Students got some new ideas about the research.

Group Photograph of the workshop participants

29th FOUNDATION DAY PROGRAMME

P.N. Prakash

The 29th Foundation Day function of IUAC was held on December 19, 2018 in the auditorium of National Institute of Plant Genome Research. The Foundation Day lecture titled, “Adventures of a Particle Physicist and Why you should care!”, was delivered by Dr. Archana Sharma, Principal Physicist & Project Manager, CMS Muon GEM Upgrade, CERN, Geneva, Switzerland. Prof. D.P. Singh, Hon’ble Chairman, UGC, presided over the function. Director, IUAC presented a status report on the activities of the Centre during the past one year. Prof. D.P. Singh delivered the presidential remarks. As in the past years, science students of classes XI and XII from nearby schools were invited to attend the programme. After attending the lecture in the morning, in the post-lunch session they were taken on a tour to show the particle accelerators and experimental facilities in IUAC. In addition, some interesting experiments to demonstrate basic physics concepts were shown to them. Around 17 schools participated in the function with each school sending 4 students accompanied by a science teacher.

Clockwise from top left:
(i) (R to L) Prof. D.P. Singh, Hon’ble Chairman, UGC, Dr. Archana Sharma,
29th Foundation Day speaker and Dr P.N. Prakash, Convener
(ii) Dr. Archana Sharma and Prof. D.P. Singh on the dais,
(iii) Dr Archana Sharma delivering the 29th Foundation Day Lecture,
(iv) Dr Archana Sharma being honoured by Prof. Avinash Chandra Pandey, Director, IUAC.

National Science Day Programme

A one day workshop on the occasion of National Science Day was organized in the Maharshi Kanad Auditorium of IUAC on 28th February 2019. A total number of 215 teachers and students of B. Sc. (Physics) of 14 colleges/ universities of NCR participated in the workshop. IUAC’s director Prof. A. C. Pandey opened the proceedings with an opening remark. The guest speaker, Prof. Ajoy Ghatak (Professor Meghnad Saha Fellow, The National Academy of Sciences, India) briefly discussed the significance of Einstein’s famous equation $E = mc^2$ and explained how light was created. He also presented a very simple derivation of that equation.

Prof. A. Ghatak addressing the participants

Participants and resource persons in the Maharshi Kanad Auditorium of IUAC during the National Science Day programme.

Mr. S. Ojha (IUAC) described the Accelerator Mass Spectrometry and its applications to the participants while Dr. N. Madhavan (IUAC) motivated the students to work in experimental nuclear physics by listing the exciting aspects of the field. In the post lunch session, the convenor, Dr. S. A. Khan (IUAC), thanked the participants for visiting IUAC and the resource persons for their help in organizing the workshop. Thereafter, the participants toured few of the experimental facilities in the centre. They were also shown the experimental demonstrations setup in the auditorium by the resource persons from IUAC. The workshop concluded with the distribution of the certificates to the participants.

IUAC Sports and Cultural Committee

Soumen Kar, Sudarshan Sharma, ET Subramaniam, Asiti Sharma, VVV Satyanarayana, Mohan Nishal, Rajesh Hariwal and Indu Bala.

Independence Day and Republic Day Celebration

Independence day was celebrated at IUAC by organizing competition among children on various topics like "on the spot painting", elocution, acting, and debate. Similarly, The Republic Day was also celebrated by organizing sports competitions among the children and residents of the campus.

(a)

(b)

Figure 1. (a) Prof. A.C.Pandey, Director IUAC hoisting the National Flag on 26th January 2019, (b) the sports event organized on 26th January 2019

Independence day was celebrated at IUAC by organizing competition among children on various topics like "on the spot painting", elocution, acting, and debate. Similarly, The Republic Day was also celebrated by organizing sports competitions among the children and residents of the campus.

International Yoga Day Celebration

The Sports and Cultural Committee of IUAC organized a yoga awareness camp to celebrate the International Yoga Day on June 21, 2018. About 70 people participated in the yoga awareness camp under the guidance of yoga experts from Sivananda Yoga Vedanta Centre, New Delhi

Community Lighting on Diwali

Figure 2. Community lighting on Diwali at IUAC campus.

To encourage the cracker-free Diwali celebration, IUAC Sports and Cultural committee organized a Community Lighting Ceremony at the football ground of the IUAC campus. Almost 250 residents participated in the celebration by lighting the diyas and candles.

Annual Cultural Program "Spandan"

Figure 3. The annual cultural program: SPANDAN-2018 at IUAC campus.

The annual cultural festival "SPANDAN" of IUAC for the year 2018 was organized by the Sports & Cultural Committee on 17th November 2018. About 70 children supported by the elders, participated in the event adorned by various regional dances, songs, instrumental music, skit, and drama. IUAC employees and students presented a Hindi drama " Pappu ki Parriksha" based on Fritz Karinthy's Refund.

Sports Flooring for Badminton Court

(a)

(b)

Fig. 4. (a) Inauguration of the renovated badminton court by Prof. A.C.Pandey, Director, IUAC, (b) the renovated badminton court at IUAC campus.

The badminton court was renovated by laying tiles-based sports flooring on the existing concrete court.

Installation of Outdoor Gym

Fig. 5. Newly installed outdoor gym items at the IUAC campus.

An outdoor gym has been installed at the IUAC campus. About fifteen number of various outdoor gym items have been installed inside the IUAC campus.

APPENDIX – I

COMMITTEES

A. THE COUNCIL

Prof. D.P. Singh
(President, GC-IUAC)
Chairman
University Grants Commission
Bahadur Shah Zafar Marg
New Delhi – 110 002

Dr. Srikumar Banerjee – Chairman (G.B.-IUAC)
DAE Homi Bhabha Chair Professor
Bhabha Atomic Research Centre
Central Complex, Trombay
Mumbai 400 085

Dr. Bhushan Patwardhan
Vice Chairman
University Grants Commission
Bahadur Shah Zafar Marg
New Delhi – 110 002

Prof. Rajnish Jain
Secretary
University Grants Commission
Bahadur Shah Zafar Marg
New Delhi – 110 002

Prof. M. Jagadesh Kumar
Vice Chancellor
Jawaharlal Nehru University
New Delhi – 110 067

Prof. R.C. Kuhad
Vice Chancellor
Central University of Haryana
Mahendragarh – 123 031

Prof. Vir Singh
Department of Physics
Indian Institute of Technology-Roorkee
Roorkee – 247 667

Dr. D.K. Aswal
Director
National Physical Laboraory
Dr KS Krishnan Marg, South Patel Nagar, Pusa, New Delhi, Delhi 110012

Prof. Dinesh Kumar
Vice Chancellor
YMCA University of Science and Technology
Faridabad – 121 006
(Haryana)

Prof. D.G. Kuberkar
Department of Physics
Saurashtra University
Rajkot – 360 005
(Gujarat)

Prof. V.K. Jain
Vice Chancellor
Tezpur University
Napaam, Tezpur Sontipur
Assam – 784 028

Prof. Sanjay V. Deshmukh
Department of Life Sciences
University of Mumbai
M.G. Road, Fort
Mumbai – 400 032

Dr. K.S. Rangappa
Distinguished Professor
Institution of Excellence
Vijnana Bhavan
University of Mysore
Manasgangotri, Mysore – 570 006

Dr. Sundeep Chopra
Scientist-H
Inter-University Accelerator Centre
New Delhi – 110 067

Yet to be nominated
from GOI

Prof. V. Ramgopal Rao
Director
Indian Institute of Technology-Delhi
Hauz Khas
New Delhi – 110 016

Prof. Ashutosh Sharma
Secretary
Dept. of Science & Technology
New Mehrauli Road
New Delhi – 110 016

Shri K.N. Vyas
Secretary
Department of Atomic Energy
Anushakti Bhawan
Chhatrapati Shivaji Mahraj Marg
Mumbai – 400 039

Dr. Shekhar C. Mande
Director General
Council of Scientific & Industrial Research
Anusandhan Bhavan, 2, Rafi Marg
New Delhi – 110 001

Prof. A. Damodaram
Vice Chancellor
Sri Venkateswara University
Sri Padmavati Mahila Visvavidyalayam Tirupati
Andhra Pradesh – 517502

Prof. Yogesh Singh
Director
Netaji Subhas Institute of Technology
New Delhi – 110 078

Dr. Ajit K.Sinha
Director
UGC-DAE Consortium for Scientific Research
University Campus, Khandwa Road,
Indore - 452017

Prof. Shyam Sundar Patnaik
Vice Chancellor
Biju Patnaik University of Technology
Chhend Colony, Rourkela
Odisha - 769015

Prof. R.C. Kuhad
Vice Chancellor
Central University of Haryana
Mahendragarh (Haryana)

Prof. Sanjay Deshmukh
Vice Chancellor
University of Mumbai
M.G. Road, Fort
Mumbai – 400 032

Prof. Gautam Bhattacharya
Fellow, Indian Academy of Sciences & National Academy of Science
Saha Institute of Nuclear Physics
Kolkata – 700 064

Prof. Alok Chakrabarti
Accelerator Physics Group
Variable Energy Cyclotron Centre
Department of Atomic Energy
Kolkata – 700 064

Prof. Avinash Chandra Pandey
Director
Inter-University Accelerator Centre
New Delhi – 110 067

B. GOVERNING BOARD

Dr. Srikumar Banerjee
Chairman - G.B.
DAE Homi Bhabha Chair Professor
Bhabha Atomic Research Centre
Central Complex, Trombay
Mumbai – 400 085

Dr. Bhushan Patwardhan
Vice Chairman
University Grants Commission
Bahadur Shah Zafar Marg
New Delhi – 110 002

Prof. Rajnish Jain
Secretary
University Grants Commission
Bahadur Shah Zafar Marg
New Delhi – 110 002

Prof. M. Jagadesh Kumar
Vice Chancellor
Jawaharlal Nehru University
New Delhi – 110 067

Dr. D.K. Aswal
Director
National Physical Laboraory
Dr KS Krishnan Marg, South Patel Nagar, Pusa, New Delhi, Delhi 110012

Prof. Dinesh Kumar
Vice Chancellor
YMCA University of Science & Technology
Faridabad – 121 006

Prof. Sanjay V. Deshmukh
Department of Life Science
University of Mumbai
M.G. Road, Fort
Mumbai – 400 032

Prof. Vir Singh
Department of Physics
Indian Institute of Technology - Roorkee
Roorkee – 247 667

Prof. D.G. Kuberkar
Department of Physics
Saurashtra University
Rajkot – 360 005
(Gujarat)

Prof. R.C. Kuhad
Vice Chancellor
Central University of Haryana
Mahendragarh – 123 031
(Haryana)

Prof. V. Ramgopal Rao
Director
Indian Institute of Technology-Delhi
Hauz Khas
New Delhi – 110 016

Prof. Avinash Chandra Pandey
Director
Inter-University Accelerator Centre
New Delhi – 110 067

Dr. K.S. Rangappa
Distinguished Professor
Institution of Excellence
Vijnana Bhavan
University of Mysore
Manasgangotri
Mysore – 570 006

Prof. V.K. Jain
Vice Chancellor
Tezpur University
Napaam, Sonitpur
Assam - 784 028

Dr. Sundeep Chopra
Scientist – H
Inter-University Accelerator Centre
New Delhi – 110 067

C. FINANCE COMMITTEE

Dr. Srikumar Banerjee
Chairman-G.B.
DAE Homi Bhabha Chair Professor
Bhabha Atomic Research Centre
Central Complex, Trombay
Mumbai – 400 085

Prof. Rajnish Jain
Secretary
University Grants Commission
Bahadurshah Zafar Marg
New Delhi-110002

Dr. P.K. Thakur
Financial Advisor
University Grants Commission
Bahadurshah Zafar Marg
New Delhi-110002

Dr. Manju Singh
Joint Secretary & Head-IUC Bureau
University Grants Commission
Bahadurshah Zafar Marg
New Delhi-110002

Prof. D.G. Kuberkar
Department of Physics
Saurashtra University
Rajkot – 360 005
(Gujarat)

Dr. N. Madhavan
Scientist – H
Inter-University Accelerator Centre
New Delhi – 110 067

Mr. Jose N.J.
Administrative Officer (F&A)
(Non Member Secretary)
Inter-University Accelerator Centre
New Delhi – 110067

Dr. Fouran Singh
Inter-University Accelerator Centre
New Delhi – 110 067

Dr. B. Hari Gopal
Science & Engineering Research Board
A Staturoty Body of DST
5&5A Lower Ground Floor
Vasant Square Mall
Plot -A Community Centre
Vasant Kunj, New Delhi – 110 070

Prof. Avinash Chandra Pandey
Director
Inter-University Accelerator Centre
New Delhi – 110 067

D. ACCELERATOR USERS COMMITTEE

Prof. D.G. Kuberkar
Department of Physics
Saurashtra University
Rajkot – 360 005
(Gujarat)

Prof. Bivash Ranjan Behra
Assistant Professor
Department of Physics
University of Panjab
Chandigarh – 160 014

Dr. Shyam Kumar
Dean, Faculty of Sicence
Kurukshetra University
Kurukshetra – 136 119

Prof. Pralay Maiti
School of Material Science And Technology
Indian Institute of Technology-BHU
Banaras Hindu University
Varanasi – 221 005

Prof. D.C. Kothari
Department of Physics
University of Mumbai
Kalina, Santacruz East
Mumabi – 400 098

Prof. Gautam Gangopadhyay
Associate Professor
University of Calcutta
Senate House, 87/1, College Street
Kolkata – 700 073

Prof. Vandana Nanal
Department of Nuclear & Atomic Physics
Tata Institute of Fundamental Research
Homi Bhabha Road
Navy Nagar, Colaba
Mumbai – 400 005

Prof. Shashi K. Dhiman
Professor & Chairman
Department of Physics
Himachal Pradesh University
Gyan-Path, Summer Hill
Shimla – 171 005

Dr. Rajdeep Chatterjee
Associate Professor
Indian Institute of Technology – Roorkee
Roorkee – 247 667

Prof. T. Som
Institute of Physics
P.O.L Sainik School
Bhubaneswar – 751 005
Odhisa

Prof. Avinash Chandra Pandey
Director
IUAC

Dr. S.Chopra
Scientist – H
IUAC

E. SCIENTIFIC ADVISORY COMMITTEE

Members

Dr. Javed Sheikh
Department of Physics
Hazratbal
Srinagar – 190 006
(J&K)

Dr. D.C. Kothari
Department of Physics
University of Mumbai
Vidyanagari, Kalina
Santacruz (E)
Mumbai – 400 098

Prof. D.G. Kuberkar
Department of Physics
Saurashtra University
Saurashtra University Campus
Rajkot – 360 005
Gujarat

Prof. Vinay Gupta
Department of Physics
University of Delhi
Delhi – 110 007

Prof. Raghav Verma
Department of Physics
IIT Bombay
Powai
Mumbai – 400 076

Dr. Alok Chakrabarty
Department of Physics
Variable Energy Crystal Centre
1AF, Bidhannagar
Kolkata – 700 004

Dr. B.P. Ajith Kumar
Scientist
IUAC

Associated Members

Dr. P.D. Gupta
Raja Ramanna Centre for Advance Technology
P.O. CAT
Indore – 452 013 (M.P.)

Dr. A.K. Grover
Vice Chancellor
Punjab University
Sector – 14
Chandigarh – 160 014

Prof. Hans-Arno-Synal
ETH Zurich
Labor f. Ionestrahiphysik (LIP)
HPK H 33
Otto - Stern – weg 5
8093 Zurich

Prof. T.Venky Venkatesan
Director-NUSNNI
Non Core Engineering
Block A, EA, Level 4, Room No. 27
Faculty of Engineering
National University of Singapore
Singapore 117581

Prof. ALAHARI Navin
Grand Accelerateur National d'Jons Lourds
Bd Henri Bacqueral
BP 55 027 – 14076
CAEN Cedex 05, France

Dr. Robert Laxdal
TRIUMF
4004, Wesbrook Mall
Vancouver, BC V6T 2A3
Canada

Prof. Avinash C. Pandey
Chairman - Director
IUAC

APPENDIX-II

April 2018 March 2019

IUAC PERSONNEL

DIRECTOR

Prof. Avinash Chandra Pandey

SCIENTISTS

Dr. T.S. Datta	Dr. Tapan K. Nandi	Dr.(Mrs.) Indra Sulania
Dr. Sundeep Chopra	Dr. Akhil Jhingan	Dr. Rajesh V. Hariwal
Dr. P.N. Prakash	Mr. Sunil Ojha	Dr. Sarvesh Kumar
Dr. S. Murlithar	Dr. Soumen Kar	Ms. Indu Bala
Dr. Ajith Kumar B.P.	Dr. Fouran Singh	Mr. Joydeep Karmakar
Dr. N. Madhavan	Dr. Rakesh Kumar	Mr. Rajveer Sharma
Dr. P. Sugathan	Dr. Subir Nath	Mr. Kedarmal
Dr. Subhendu Ghosh	Mr. Ashutosh Pandey	Mr. Saneesh N
Dr. Ambuj Tripathi	Dr. Praveen Kumar	Mr. Sanjay Kumar Kedia
Dr. G.O. Rodrigues	Mrs. K. Devrani Devi	Mr. Ram Charan Meena
Mr. Abhijit Sarkar	Dr. C.P. Safvan	Mr. Deepak Kumar Swamy
Mr. Rajeev Mehta	Dr. Saif Ahmad Khan	Mr. Bappa Karmakar
Dr. Asiti Sarma	Mrs. K.S. Golda	Mr. Mohit Kumar
Dr. D. Kabiraj	Mr. Abhishek Rai	Mr. G.R. Umapathy
Dr. R.P. Singh	Mr. Sugam Kumar	Mr. Ambuj Mishra
Mr. Debashish Sen	Dr. Pankaj Kumar	Mr. Abhishek Kumar
Dr. K. Asokan	Dr. Pawan Kumar Kulriya	Ms. Gonika
Dr. V.V.V. Siva Kumar	Mrs. P.S. Lakshmy	Ms. Deeksha Khandelwal
Dr. Bhuban Kumar Sahu	Mr. Jagdish Ghelot	Ms. Madhuri
Mr. Anup Choudhary	Mr. Padmanava Patra	Mr. Yashraj

ENGINEERS & TECHNICAL PERSONNEL

Mr. M.K. Gupta
Dr. Piyush Gupta
Mr. K.K. Soni
Dr. Sumit Mookherjee
Mr. Kundan Singh
Mrs. Ruby Shanthi
Mrs. Kusum Rani
Mr. Rajan Joshi
Mr. U.G. Naik
Mr. S. Venkataramanan
Mr. Satinath Gargari
Mr. Joby Antony
Mr. Bishamber Kumar
Mr. A.J. Malyadri
Mr. Raj Kumar
Mr. E.T. Subramaniam
Mr. Rajeev Ahuja
Mr. Pradeep Barua
Mr. Rajesh Kumar
Mr. Santosh Kumar Sahu
Mr. Rajesh Nirdoshi
Mr. Ashish Sharma
Mr. S. Bhatnagar
Mr. U. Koteshwara Rao
Mr. Rajpal Sharma
Mr. Mukesh Sota
Mr. R.N. Dutt
Mr. S.S.K. Sonti
Mr. G.K. Choudhary
Mr. Manoj Kumar
Mr. S.K. Saini
Mr. Suresh Babu M.V.
Mr. Thomas Varughese
Mrs. Arti Gupta
Mr. Ashok Kothari
Mr. V.P. Patel
Mrs. P. Nayak
Mr. S.K. Suman
Mr. D.K. Mathuria
Ms. Mamta Jain
Mr. Kishore Kumar Mistri
Mr. V.V.V Satyanarayana
Mr. Abhilash S.R.
Mr. Birendra Kumar
Mr. M. Archunan
Mr. Yaduvansh Mathur
Mr. B.B. Choudhary
Mr. Mukesh Kumar
Mr. Parmanand Singh
Mr. Radhakishan Gurjar
Mr. Deepak Kumar Munda
Mr. Chandrapal
Mr. Harshwardhan
Mr. Davinder K. Prabhakar
Mr. Prem Kumar Verma

TECHNICIANS

Mr. Jagdish Prasad
Mr. Rakesh Kumar
Mr. Pranav Singh
Mr. M.P. Singh
Mr. Mohan Nishal
Mr. Jaswant Singh
Mr. Suraj Kumar
Mr. N.S. Panwar
Mr. Gaurav Rathuri

ADMINISTRATIVE STAFF

Mr. Bishwambhar Datt
Mr. K. Murali
Mr. M.B. Joseph
Mrs. Ranju Rishi
Mr. N.J. Jose
Mrs. Usha Kataria
Mr. Satyavan
Mr. M.R. Ramasubramaniam
Mrs. Manvinder Kaur
Mr. Sohan Singh
Mr. N.P. Ponnappan
Mr. Sudershan Sharma
Mr. Prakash S. Kumbhare
Mr. Swaroop Kr. Maurya
Mrs. Bindu Xaxa
Mr. Pethan Shanmugam
Mr. R.N. Dhyani
Mr. Rajendra Prasad
Mr. Rahul Sahni
Ms. Manisha Rani
Mr. Paras Nath
Ms. Nishtha Saxena
Mr. Bharat Sharma
Mr. Jay Prakash
Mr. Subhash Chandra
Mr. Shubham Kumar
Mr. Harish Diwakar
Mr. Raj Kumar Verma
Mrs. Chanderkala
Mr. Piyush Verma

DRIVERS

Mr. Madan Lal
Mr. Kailash Kumar
Mr. M. Samantra

RESEARCH SCHOLARS

Mr. Hemant Jatav
Ms. Himanshi Gupta
Mr. Divya Arora
Mr. Abid Hussain
Mr. Jitendra Singh
Mr. Ishitaq Ahmed
Mr. Arkaprava Das
Mr. Vipul Joshi
Mr. Kasuhik Katre
Ms. Chetna Tyagi
Mr. Rohan Biswas
Mr. Sushil Kumar
Ms. Anuradha
Mr. Saurabh Kumar Sharma
Ms. Anusmita Chakravorty

RESEARCH ASSOCIATE

Dr. Chandrabhan Yadav
Dr. Narender Kumar
Dr. Gurpreet Kaur
Dr. Vijay Raj Sharma
Dr. Soumya Prakash Dal
Dr. Chetan Prakash Saini
Dr. Vishal Srivastava
Dr. Soumendu S. Bhattacharjee
Dr. Anamika Parihari
Dr. Md. Moin Shaikh
Dr. Trivedi Priyankaben

PRINCIPAL INVESTIGATOR- DST PROJECT (YOUNG SCIENTISTS)

Dr. Abhishek Yadav
Dr. Chinmaya Maharana
Dr. V.S. Vendamani

DST-INSPIRE FACULTY

Dr. V.S. Vendamani
Dr. Chinmaya Maharana

DST-INSPIRE FACULTY

Dr. Ashish Kumar
Dr. Pragya Bhatt
Dr. Kamla Rawat
Dr. Budhi Singh
Dr. Pramod Kumar

DS KOTHARI POST DOCTORAL FELLOW

Dr. Sumit Tripathi

Dr. Rakesh Kumar

Dr. Lisha Raghavan

UGC POST DOCTORAL FELLOW FOR WOMEN

Dr. Razia Nongjal

IMRI-SAMEER-MEITY PROJECT (TSD)

Dr. R.G. Sharma

Mr. Sankar Ram T

Mr. Navneet Kumar Suman

GITA-DST PROJECT

Ms. Anha Masarrat

CPRI – IUAC (TSD)

Ms. Reetu Bharti

APPENDIX - III

LIST OF USERS 2018-19

HEAVY ION RADIATION BIOLOGY

Ankamwar Balaprasad G.
Department of Chemistry
SP Pune University
Ganeshkhind, Pin Code-411 007.

NUCLEAR PHYSICS

Appannababu S.
Department of Nuclear Physics
Andhra University
Waltair, Visakhapatnam
Andhrapradesh, Pin Code-530 003.

Banerjee Tathagata
Saha Institute of Nuclear Physics
1/AF, Bidhannagar, Kolkata
West Bengal-700 064.

Behera Bivash Ranjan
Department of Physics
Panjab University, Sector-14
Chandigarh-160 014.

Bhati A.K.
Department of Physics
Panjab University
Chandigarh-160 014.

Chamoli S.K.
Department of Physics & Astrophysics
Delhi University, Delhi-110 007.

Deo Ajay Y.
Department of Physics
Indian Institute of Technology Roorkee
Roorkee, Uttrakhand-247667

Mukherjee Gopal
Variable Energy Cyclotron Centre
1/AF Bidhan Nagar, Kolkata
Pin Code-700 064.

Ghosh Tilak Kumar
Variable Energy Cyclotron Centre
1/AF, Bidhan Nagar, Kolkata
Pin Code-700 064.

Kumar Ajay
Department of Physics
Banaras Hindu University
Varanasi, Pin Code-221 005.

Kumar Ashok
Department of Physics
Panjab University
Chandigarh, Pin Code-160 014.

Kumar Vinod
Department of Physics
University of Lucknow
Pin Code-226 007.

Maiti Moumita
Department of Physics
IIT Roorkee
Roorkee- 247 667 Uttrakhand.

Mandal Samit Kr.
Department of Physics and Astrophysics
University of Delhi
Delhi-110 007.

Tandel Sujit
UM-DAE Centre for Excellence in Basic Sciences
University of Mumbai
Kalina, Santacruz(East), Mumbai
Pin Code-400 098.

Prasad E.
Department of Physics
School of Physical Sciences
Central University of Kerala
Thejaswini Hills, Periye
Pin Code-671 316.

Trivedi Tarkeshwar
Pure and Applied Physics
Guru Ghasidas Vishwavidyalaya
Bilaspur, Pin Code-495 009.

Singh Pushpendra P.
Department of Physics
Indian Institute of Technology Ropar
Rupnagar-140 001, Punjab.

Vinodkumar A.M.
Department of Physics
Calicut University
Kerala-673 635.

MATERIALS SCIENCE

Abdelhak Chettah
Department of Physics
University 20 Aout 1955- Skikda
Rue Mouloud Bouaffar
House No12, Ramdane Djamel 21425
Skikda, Algeria, Pin Code-21300.

Awasthi Kamlendra
Department of Physics
Malaviya National Institute of Technology
JLN Road, Jaipur-302 017, Rajasthan.

Amekura Hiroshi
Photon and Ion Beam Physics Group
National Institute for Materials Science
3-13 Sakura, Tsukuba
Ibaraki 305-0003, Japan.

Bajpai P.K.
Department of Pure & Applied Physics
Guru Ghasidas Vishwavidyalaya
Koni, Bilaspur (C.G.)-495 009.

Arora Sunil Kumar
Centre for Nanoscience & Nanotechnology
Block II, South Campus
Panjab University, Chandigarh
Pin Code-160 014.

Banerjee Aritra
Department of Physics
University of Calcutta
92, Acharya Prafulla Chandra Road
Kolkata, Pin Code-700 009.

Avasthi D.K.
Amity Institute of Nanotechnology
Noida, Pin Code-201 313.

Bhattacharya Bhaskar
Department of Physics
MMV, Banaras Hindu University
Varanasi, Pin Code-221 005.

Choudhary Ram Janay
UGC DAE Consortium for Scientific Research
University Campus, Khandwa Road
Indore, Pin Code-452 001.

Giri Rajiv
Centre of Material Science
University of Allahabad
Allahabad, Pin Code-211 002.

Das Pradip
Department of Pure and Applied Physics
Guru Ghasidas University
Koni, Bilaspur, Pin Code-495 009.

Gupta Rajeev K.
Department of Physics
University of Petroleum and Energy Studies
via Prem Nagar, Bidholi
Dehradun-248 001, Uttrakhand.

Das Ratan
Department of Physics
Tripura University
Suryamaninagar, Agartala
Tripura (West), Pin Code-799 022.

Gupta Ratnesh
School of Instrumentation
Devi Ahilya Vishwavidyalaya
Khandwa Road, Indore
Pin Code-452 001.

Dehiya Brijnandan
Deptt. of Material Science & Nanotechnology
DCR University of Science and Technology
Murthal, Haryana, Pin Code-131 039.

Dhoble Sanjay J.
Department of Physics
Rashtrasant Tukadoji Maharaj Nagpur University
Nagpur-440 033 (Maharashtra).

Dixit Abhisek
Room No. 402-D, Block-II
IIT Delhi, Hauz Khas
Delhi-110 016.

Ghosh Santanu
Department of Physics
Indian Institute of Technology Delhi
Hauz Khas, New Delhi-110 016.

Keshri Sunita
Department of Physics
Birla Institute of Technology
Mesra, Ranchi, Jharkhand
Pin Code-835 215.

Khan G.R.
Department of Physics
NIT Srinagar
Jammu and Kashmir-190 006.

Khanuja Manika
Jamia Millia Islamia University
Jamia Nagar, Okhla
Delhi 110 025.

Kumar Pawan
Department of Physics & Astronomy
NIT Rourkela, Pin Code-769 008.

Kumar Pratik
Medical Physics Unit
IRCH, AIIMS
New Delhi-110 029.

Kumar Raavi Sai Santosh
Indian Institute of Technology, Hyderabad
Kandi, Sangareddy, Medak Dist.
Telangana, Pin Code-502 285.

Kumar Rajesh
University School of Basic and Applied Sciences
Guru Gobind Singh Indraprastha University
Dwarka Sector-16-C, New Delhi-110 078.

Islam S.S.
Centre for Nanoscience and Nanotechnology
Jamia Millia Islamia, Jamia Nagar
New Delhi-110 025.

Jeyachandran Yekkoni L.
Department of Physics
Bharathiar University
Marudhamalai Road, Coimbatore
Pin Code-641 046.

Joshi Utpal Shashikant
Department of Physics
School of Sciences
Gujarat University
Ahmedabad-380 009.

Kaur Navjeet
PG Department of Physics
Mata Gujri College
Sri Fatehgarh Sahib-140 406, Punjab.

Mallick Pravanjan
North Orissa University
Takatpur, Baripada-757 003 (Odisha).

Mir Feroz Ahmad
Department of Physics
Baba Gulam Shah Badshah University
Rajouri, Jammu and Kashmir
Pin Code-185 231.

Mishra Naresh Chandra
Department of Physics
Utkal University
Bhubaneswar, Pin Code-751 004.

Nair Lekha
Department of Physics
Jamia Millia Islamia
New Delhi-110 025.

Prakash G. Vijaya
Department of Physics
Indian Institute of Technology Delhi
Pin Code-110 016.

Prakash Jai
Department of Physics
Aligarh Muslim University
Aligarh (UP), Pin Code-202 002.

Prakash Rajiv
School of Materials Science and Technology
Indian Institute of Technology
Banaras Hindu University
Varanasi, Pin Code-221 005.

Mahajan Aman
Department of Physics
Guru Nanak Dev University
Amritsar, Punjab-143 005.

Rajendrakumar R.T.
Department of Nanoscience and Technology
Bharathiar University, Coimbatore
Tamil Nadu, Pin Code-641 046.

Rangra Vir Singh
Department of Physics
HP University, Shimla
Pin Code-177 005 (HP).

Rao S.V.S. Nageswara
School of Physics
University of Hyderabad
Hyderabad-500 046.

Ravalia Ashish B.
Department of Nanoscience
and Advanced Materials
Saurashtra University
Rajkot-360 005.

Sahare P.D.
Department of Physics & Astrophysics
University of Delhi
Delhi-110 007.

Sahoo Pratap Kumar
NISER Bhubaneswar
SPS, NISER, Jatni, Khordha
Bhubaneswar, Odisha, Pin Code-752 050.

Saini Richa
Department of Physics
Gurukul Kangri University
Haridwar-249 404.

Singh Shubra
Crystal Growth Centre
Anna University
Guindy, Chennai
Tamil Nadu-600 025.

Singh Vaishali
BFR-303, USBAS
GGS Indraprashtha University
New Delhi-110 078.

Rahman Faiyazur
Department of Physics
Aligarh Muslim University
Aligarh-202 002.

Sarkar Anindya
Bangabasi Morning College
(Under University of Calcutta)
19, Rajkumar Chakraborty Sarani
Kolkata, Pin Code-700 009.

Shah N.A.
Department of Physics
Saurashtra University
Rajkot, Gujarat
Pin Code-360 005.

Sharma Aditya
Department of Physics
Manav Rachna University
Sector-43, Aravalli Hills
Delhi-Surajkund Road
Faridabad-121 004, (Haryana).

Sharma Himani
School of Physical Sciences
Doon University Dehradun
Pin Code-248 012.

Sheet Goutam
Indian Institute of Science Education
and Research Mohali
Academic Block -1, Sec-81, SAS Nagar
Knowledge City, PO-Manauli
IISER Mohali, Punjab-140 306.

Singh Abhinav Pratap
Department of Physics
Dr. B.R. Ambedkar National Inst. of Tech
Byepass G T Road, Jalandhar
Pin Code-144 011.

Singh Devinder Paul
Department of Physics
Guru Nanak Dev University
Amritsar, Punjab, Pin Code-143 005.

Tanna Ashish R.
Department of Physics
School of Science
RK University
Kasturbadham (Tramba)
Rajkot-360 020 Gujarat.

Verma Shammi
Reliability & Quality Assurance Division
Semi-Conductor Laboratory
Department of Space
Sector-72, Mohali-160 071, Punjab.

Singh Vijay Raj
Department of Physics
Central University of Kashmir
Transit Campus, Near G.B. Pant Hospital
Srinagar-190 004 (J&K).

Srivastava Pankaj
Department of Physics
IIT Delhi, Hauz Khas
New Delhi-110 016.

Sultan Khalid
Department of Physics
Central University of Kashmir
Nowgam Campus-III J&K-190 015.

Vishwakarma Prakash Nath
Department of Physics and Astronomy
National Institute of Technology Rourkela
Dist.-Sundargarh, Odisha-769 008.

Wadhwa Shikha
Amity Institute of Nanotechnology
Amity University
Uttar Pradesh, Pin Code-201 313.

Yogita
Department of Physics
MCM DAV College for Women
Sector-36A, Chandigarh-160 036.

ACCELERATOR MASS SPECTROMETRY

Bhattacharya Goutami
Archaeological Survey of India
Excavation Branch III, Block No.704
7th Floor Lok Nayak Bhawan
Frazer Road, Dak Bunglow Chowk
Patna-800 001 (Bihar).

Bhaumik Ajoy Kumar
Applied Geology
IIT (ISM) Dhanbad
Pin Code-826 004 (Jharkhand).

Iyer Sridhar D
Geological Oceanography Division
CSIR-National Institute of Oceanography
Dona Paula Goa, Pin Code-403 004.

Manjunatha B.R.
Department of Marine Geology
Mangalore University
Mangalagangothri, D.K. District
Pin Code-574 199.

Maurya D.M.
Department of Geology
The M.S. University of Baroda
Vadodara-390 002, Gujarat.

Nathan D. Senthil
Department of Earth Sciences
Pondicherry University
Pondicherry-605 014.

Garnayak Dibishada B.
Archaeological Survey of India
Excavation Branch-IV
Puratattva Bhawan (Ground Floor)
Samantarapur, Bhubaneshwar
Odisha, Pin Code-751 002.

Gupta Anil Kumar
Department of Geology and Geophysics
Indian Institute of Technology Kharagpur
Kharagpur, Pin Code-721 302.

Ramkumar Mu.
Department of Geology
Periyar University
Salem, Pin Code-636 011.

Rawat Suman Lata
Wadia Institute of Himalayan Geology
33, G.M.S. Road, Dehradun
Pin Code-248 001.

Sarkar Anindya
Department of Geology and Geophysics
IIT Kharagpur, West Midnapore
West Bengal, Pin Code-721 302.

Sathe Vijay
Department of Ancient Indian History
Culture and Archaeology
Deccan College Postgraduate & Research Inst.
Deemed to be University Pune
Pin Code-411 006.

N Nihildas
Excavation Branch-I
Archaeological Survey of India
Puratattava Bhavan, First Floor, Seminary Hills
Nagpur, Pin Code-440 006.

Phartiyal Binita
Birbal Sahni Institute of Palaeosciences
53, University Road, Lucknow, UP.
Pin Code-227 007.

Raj Rachna
School of Environmental Sciences
Jawaharlal Nehru University
New Delhi-110 067.

Sreekesh S.
Centre for the Study of Regional Development
School of Social Sciences
Jawaharlal Nehru University
New Delhi-110 067.

Shekhar Shashank
Room No.-121
Department of Geology
University of Delhi
Delhi-110 007.

Singh Pramod
Department of Earth Sciences
School of Physical
Chemical and Applied Sciences
Pondicherry University, Kalapet
Pondicherry, Pin Code-605 014

Singh Neelratan
School of Environmental Sciences
Jawaharlal Nehru University
New Delhi, Pin Code-110 067.

Tripathi. Jayant K
Lab No. 013, School of Environmental Sciences
Jawahrlal Nehru University
New Delhi-110 067.

ATOMIC PHYSICS

Bapat Bhas
Indian Institute of
Science Education & Research
Pashan,Pune-411 008.

Puri Sanjiv
Department of Basic and
Applied Sciences
Punjabi University
Patiala, Pin Code-147 002.

Verma Punita
Department of Physics
Kalindi College, East Patel Nagar
University of Delhi, Delhi-110 007.

LOW ENERGY ION BEAM FACILITY

Ahmed Arham Shareef
Department of Physics
Aligarh Muslim University, Aligarh
Pin Code-202 002.

Avasthi D.K.
Amity Institute of Nanotechnology
Noida, Pin Code-201 313.

Awasthi Kamlendra
Department of Physics
Malaviya National Institute of Technology
JLN Road, Jaipur-302 017, Rajasthan.

Banerjee Aritra
Department of Physics
University of Calcutta
92, Acharya Prafulla Chandra Road
Kolkata, Pin Code-700 009.

Bhattacharya Bhaskar
Department of Physics
MMV, Banaras Hindu University
Varanasi, Pin Code-221 005.

Chand Prakash
Department of Physics
National Institute of Technology
Kurukshetra, Haryana
Pin Code-136 119.

Bajpai P.K.
Department of Pure & Applied Physics
Guru Ghasidas Vishwavidyalaya
Koni, Bilaspur (C.G.)-495 009.

Das Pradip
Department of Pure and Applied Physics
Guru Ghasidas University
Koni, Bilaspur, Pin Code-495 009.

Datta Debi Prasad
Basic Sciences and Humanities Department
Silicon Institute of Technology
Silicon Hills, Patia, Bhubaneswar
Pin Code-751 024.

Dhaka Rajendra S.
IIT Delhi, Hauz Khas
New Delhi-110 016.

Dhar Sankar
Head , Dept. of Physics
School of Natural Sciences
Shiv Nadar University
Dadri, Gautam Budh Nagar
Pin Code-201 314.

Dhiman Rajnish
Room No. 304
Department of Physics & Astronomical Science
Central University of Himachal Pradesh
Dharamshala, TAB Shahpur
District Kangra, Pin Code-176 206.

Dhoble Sanjay J.
Department of Physics
Rashtrasant Tukadoji Maharaj Nagpur University
Nagpur-440 033 (Maharashtra).

Goel Lokesh
Homi Bhabha National Institute
Materials Science Division
2-319-S, 2nd Floor
Modlab-D, BARC, Trombay
Mumbai, Pin Code-400 085

Kelkar Aditya H.
Department of Physics
Indian Institute of Technology Kanpur
Kanpur-208 016.

Kumar G. Ramesh
Department of Physics
University College of Engineering Arni
(A Constituent College of Anna University Chennai)
Arni to Devikapuram Road, Thatchur
Arni -632 326 (Tamil Nadu).

Chatterjee Shyamal
Room 120, School of Basic Sciences
IIT Bhubaneswar, Jatni
Khordha, Odisha, Pin Code-752 050.

Gokul B.
Department of Physics
Kongunadu Arts and Science College
Coimbatore -641 029.

Islam S.S.
Centre for Nanoscience and Nanotechnology
Jamia Millia Islamia
Jamia Nagar, New Delhi-110 025.

Jain Utkarsh
Amity Institute of Nanotechnology
J2, Room No-308, 3rd Floor
Amity University
Noida-201 313.

Jana Debnarayan
Department of Physics
University of Calcutta
92, A.P.C Road, Kolkata-700 009.

Jeyachandran Yekkoni L.
Department of Physics
Bharathiar University
Marudhamalai Road, Coimbatore
Pin Code-641 046.

Junaid M.
Department of Physics
Cochin University of Science and Technology
Kochi-22, Kerala.

Karn Ranjeet Kumar
Department of Physics
Kolhan University
Chaibasa, Jharkhand
Pin Code-833 202.

Matheswaran P.
Department of Physics
Kongunadu Arts and Science College
Coimbatore-641 029.

Middey Srimanta
Department of Physics
Indian Institute of Science
Bengaluru-560 012.

Kumar Manoj
High Pressure Physics Lab
Department of Physics
Malaviya National Institute of Technology
Jaipur, Pin Code-302 017.

Kumar Raavi Sai Santosh
Indian Institute of Technology, Hyderabad
Kandi, Sangareddy, Medak Dist., Telangana
Pin Code-502 285.

Kumar Ramesh
Department of Physics
Guru Jambheshwar University of Sc. & Tech.
Hisar, Haryana-125 001.

Kumar Shyam
Department of Physics
Kurukshetra University
Kurukshetra, Pin Code-136 119.

Kumar Pratik
Medical Physics Unit
IRCH, AIIMS
New Delhi-110 029.

Prakash Jai
Department of Physics
AMU, Aligarh
U.P., Pin Code-202 002.

Puri Sanjiv
Department of Basic and Applied Sciences
Punjabi University
Patiala, Pin Code-147 002.

Rahman Faiyazur
Department of Physics
Aligarh Muslim University
Aligarh-202 002.

Rajendrakumar R.T.
Department of Nanoscience and Technology
Bharathiar University, Coimbatore
Tamil Nadu, Pin Code-641 046.

Rao M.S. Ramachandra
Department of Physics
IIT Madras, Chennai-600 036.

Mitra Debais
Department of Physics
University of Kalyani
Kalyani, Nadia, West Bengal
Pin Code-741 235.

Mohanty Tanuja
School of Physical Sciences
JNU, New Delhi-110 067.

Muthuraaman B.
Department of Energy
University of Madras
Guindy Campus, Chennai
Tamilnadu, Pin Code-600 025.

Nelamarri Srinivasa Rao
Department of Physics
Malaviya National Institute of Technology Jaipur
JLN Marg, Jaipur-302 017, Rajasthan.

Prakash G. Vijaya
Department of Physics
Indian Institute of technology Delhi
Pin Code-110 016.

Ryu Ho Jin
Department of Nuclear and Quantum Engineering
Korea Advanced Institute of Science and Technology
291 Daehak-ro, Yuseong-gu
34141 Daejeon, South Korea.

Sahoo Pratap Kumar
NISER Bhubaneswar
SPS, NISER, Jatni
Khordha, Bhubaneswar
Odisha, Pin Code-752 050.

Saini Richa
Department of Physics
Gurukul Kangri University
Haridwar-249 404.

Sarkar Anindya
Bangabasi Morning College
(Under University of Calcutta)
19, Rajkumar Chakraborty Sarani
Kolkata, Pin Code-700 009.

Sharma Aditya
Department of Physics
Manav Rachna University
Sector-43, Aravalli Hills
Delhi-Surajkund Road
Faridabad-121 004 (Haryana).

Rao S.V.S. Nageswara
School of Physics
University of Hyderabad
Hyderabad-500 046.

Raychaudhuri Arup Kumar
S.N. Bose National Centre for Basic Sciences
JD Block, Sector-III, Salt Lake
Kolkata-700 106.

Singh Abhinav Pratap
Department of Physics
Dr. B.R. Ambedkar National Inst. of Technology
Byepass GT Road, Jalandhar
Pin Code-144 011.

Singh Devinder Paul
Department of Physics
Guru Nanak Dev University
Amritsar, Punjab, Pin Code-143 005.

Singh Shubra
Crystal Growth Centre
Anna University, Guindy
Chennai, Tamil Nadu-600 025.

Singhal Rahul
Department of Physics
JLN Marg, Malviya Nagar
Jaipur-302 017, Rajasthan.

Som Tapobrata
Institute of Physics
Sachivalaya Marg
Bhubaneswar, Pin Code-751 005.

Srivastava R.C.
Department of Physics
G.B. Pant University of Ag. & Tech. Pantnagar
Uttarakhand, Pin Code-263 145.

Sharma Himani
School of Physical Sciences
Doon University Dehradun
Pin Code-248 012.

Sharma Shatendra K.
Jawahar Lal Nehru University
New Mehrauli Road
Delhi-110 067.

Tiwari M.K.
Indus Accelerator Complex
Indus Synchrotron Utilisation Division
Raja Ramanna Centre for Advanced Technology
Indore-452 013 (M.P).

Vashisht Garima
Room No. 78
Department of Physics and Astrophysics
University of Delhi
Pin Code-110 007.

Verma Punita
Department of Physics
Kalindi College
University of Delhi-110 007.

Vishwakarma Prakash Nath
Department of Physics and Astronomy
National Institute of technology Rourkela
Dist.-Sundargarh, Odisha-769 008.

Yogita
Department of Physics
MCM DAV College for Women
Sector-36A, Chandigarh-160 036.

Zulfequar Mohammad
Department of Physics
Jamia Millia Islamia
New Delhi-110 025.